

Development of tomato genotypes
with enhanced xanthophyll content in
ripe fruit

Elzbieta Rapacz

This thesis was submitted for the degree of Doctor of Philosophy at Royal
Holloway University of London, September 2019

Declaration of Authorship

I, Elzbieta Rapacz, hereby declare that the work presented in this thesis is the original work of the author unless otherwise stated. Original material used in the creation of this thesis has not been previously submitted either in part or whole for a degree of any description from any institution.

Date: 19th, September 2019

Abstract

Zeaxanthin is a high-value carotenoid used as a food supplement and a colourant in foods and animal feed in order to improve the flavour and appearance of the products. Its nutraceutical value is derived from its role in lowering the risk of developing certain age-related eye conditions, particularly age-related macular degeneration (AMD), which has been concluded from large clinical trials. The present limited availability of plant renewable sources for zeaxanthin and its complex chemical synthesis, has encouraged engineering of the existing biosynthetic pathways in plants to create new biosources of zeaxanthin and related xanthophylls.

A good plant-based candidate for a novel source of zeaxanthin is tomato. The ripe fruit of tomato accumulate high amounts of the red pigment lycopene from which zeaxanthin can be derived. Even though the tomato genome encodes all functional enzymes of the carotenoid biosynthetic pathway necessary for the synthesis of zeaxanthin, the tomato fruit only accumulate trace amounts of this compound. Previously, a tomato line accumulating high levels of β -carotene, a carotenoid compound derived from lycopene, has been identified. Zeaxanthin can be generated from β -carotene in a series of two hydroxylation steps catalysed by β -carotene hydroxylase. Through an introduction of an additional copy of tomato β -carotene hydroxylase into the high β -carotene background, a new line accumulating zeaxanthin in its ripe fruit has been generated. Although, the levels of zeaxanthin in this new tomato line were too low to consider it a novel plant source, it was shown that the *de novo* synthesis and accumulation of previously unencountered xanthophylls in tomato fruit is possible to achieve.

A strategy for the enhancement of zeaxanthin content was developed in which the generated line was crossed with the *high-pigment 3 (hp3)* tomato mutant in order to reduce epoxidation of zeaxanthin into violaxanthin. This led to a 26-fold improvement in the fruit zeaxanthin content which was high enough to provide the daily recommended dose of zeaxanthin in one fruit serving. Thus, a potential new, renewable tomato source of zeaxanthin has been generated.

With the use of the new gene editing technology CRISPR/Cas9, alternative mutations in the gene encoding zeaxanthin epoxidase were generated with the potential to use the novel variants for further enhancement of zeaxanthin content.

Acknowledgements

This PhD offered me a great opportunity to deepen my knowledge in the subject, train my practical skills and also to share my knowledge during presentations and conference meetings. It also allowed me to meet great scientists from all over the world who share a similar passion for science.

This would not have been possible without my supervisor Prof. Paul Fraser. I would like to thank him for his support, commitment and encouragement. His understanding and a great sense of humour kept me positive and motivated.

I am grateful to my co-supervisors Drs Genny Enfissi and Marilise Nogueira for providing the initial material on which this study was based, their invaluable input into this work and advice throughout. I greatly appreciate the great advice and feedback regarding my written work I received from Professor Peter Bramley. I would like to also thank Professor Joseph Hirschberg from Hebrew University of Jerusalem for providing seeds of the *hp3* tomato line. Many thanks to the members of the lab, the technical and post-doctoral staff as well as my fellow PhD students, for teaching me new experimental techniques and for just simply making the work enjoyable.

I also gratefully acknowledge the funding received towards my PhD from the Biotechnology and Biological Sciences Research Council.

Finally, I would like to thank my family. I am very grateful to my parents for always encouraging me to pursue my dreams. Most importantly, I would like to thank my fiancée Mateusz for his patience, kindness and all his invaluable help I received throughout the time of my PhD degree.

I truly believe that this experience will help me to grow as a scientist and also a better person. Thank you all.

Ela

Table of Contents

Declaration of Authorship.....	2
Abstract.....	3
Acknowledgements.....	4
Table of Contents.....	5
List of Figures.....	12
List of Tables.....	19
Abbreviations.....	21
Chapter I: Introduction.....	24
1.1 Characterisation of carotenoids.....	25
1.1.1 Structure and function.....	25
1.1.2 Nomenclature.....	28
1.1.3 Biosynthesis.....	30
1.1.4 Xanthophyll cycle.....	36
1.1.5 Carotenoid deposition and storage.....	38
1.1.6 Market value and uses of carotenoids.....	39
1.2 Age-related macular degeneration (AMD).....	41
1.2.1 Description, aetiology and current treatments.....	41
1.2.2 Prevalence of AMD.....	44
1.2.3 Financial burden of AMD.....	44
1.2.4 Macular pigments – lutein and zeaxanthin.....	45
1.2.5 Evidence for involvement of zeaxanthin in prevention against AMD.....	48
1.3 Zeaxanthin – characterisation and sources.....	52
1.3.1 General characterisation.....	52
1.3.2 Sources of zeaxanthin.....	53
1.3.2.1 Food sources.....	54
1.3.2.2 Non-food sources.....	56
1.3.2.2.1 Microbial sources.....	56
1.3.2.2.2 Plant sources.....	63
1.3.2.3 Synthetic zeaxanthin.....	66
1.4 Enhancing content of carotenoids in plants.....	70
1.4.1 Conventional plant breeding approaches.....	70
1.4.2 Genetic engineering.....	72
1.5 Aims and objectives.....	75
1.5.1 Identification and characterisation of xanthophyll-accumulating tomato.....	76
1.5.2 Optimisation of zeaxanthin production.....	77
1.5.3 CRISPR/Cas9-mediated editing of <i>ZEP</i>	77

Chapter II: Materials and Methods.....	79
2.1 Plant cultivation and material collection	80
2.1.1 Tomato varieties	80
2.1.2 Seed germination and glasshouse growth conditions	83
2.1.3 Cross-pollination of tomato lines.....	83
2.1.4 Material collection and storage	85
2.1.5 Seed separation and sterilisation.....	85
2.1.6 General characterisation of tomato leaf and fruit organs	86
2.1.6.1 Photosynthetic performance (F_v/F_m)	86
2.1.6.2 Fruit firmness	86
2.1.6.3 Transmission electron microscopy (TEM) of tomato pericarp	87
2.2 Bacterial, fungal and plant tissue cultures.....	87
2.2.1 Bacterial cultures	87
2.2.1.1 Maintenance of bacterial cultures.....	87
2.2.1.1.1 Growth media	87
2.2.1.1.2 Antibiotics used for bacterial selection	88
2.2.1.1.3 Preparation of glycerol stocks.....	88
2.2.1.1.4 Streaking bacteria from glycerol stocks.....	89
2.2.1.1.5 Cultivation of bacteria in liquid cultures.....	89
2.2.1.2 Preparation of competent cells	89
2.2.1.2.1 Preparation of chemically competent <i>Escherichia coli</i>	89
2.2.1.2.2 Preparation of heat-shock amenable <i>Agrobacterium tumefaciens</i>	90
2.2.1.3 Bacterial transformation.....	90
2.2.1.3.1 Heat-shock transformation of chemically competent <i>E. coli</i>	90
2.2.1.3.2 Analysis of transformation efficiency	91
2.2.1.3.3 Heat shock transformation of <i>A. tumefaciens</i>	91
2.2.2 Fungal cultures.....	92
2.2.2.1 Growth media preparation	92
2.2.2.2 Culture propagation, collection and storage	92
2.2.3 Plant tissue cultures	92
2.2.3.1 Growth media	92
2.2.3.2 Stable transformation of tomato.....	93
2.2.3.2.1 <i>Agrobacterium</i> cultures	93
2.2.3.2.2 Seed germination.....	94
2.2.3.2.3 <i>Agrobacterium</i> -mediated plant transformation.....	94
2.2.3.2.4 Regeneration.....	94
2.2.3.2.5 Rooting.....	95

2.3 Extraction and analysis of nucleic acids.....	95
2.3.1 Extraction of nucleic acids	95
2.3.1.1 Extraction of plasmids from bacteria.....	95
2.3.1.2 Extraction of plant genomic DNA.....	95
2.3.1.2.1 Spin-column based purification	95
2.3.1.2.2 96-well plate-based purification	96
2.3.1.3 Extraction of RNA.....	96
2.3.2 Quantification of nucleic acids.....	97
2.3.3 Agarose gel electrophoresis.....	97
2.3.4 Sequencing.....	98
2.3.4.1 DNA sequencing.....	98
2.3.4.2 RNA sequencing (RNA-Seq).....	99
2.3.4.2.1 Sample preparation	99
2.3.4.2.2 Quality control, sequencing and data analysis	99
2.3.4.2.3 Identification of candidate genes	100
2.3.5 Polymerase chain reaction (PCR).....	101
2.3.5.1 Genotyping of the segregating populations	103
2.3.5.1.1 Identification of transgenic <i>CrtR-b2</i> and <i>S. galapagense</i> <i>CYC-B</i> allele.....	103
2.3.5.1.2 Identification of the mutated allele of <i>ZEP</i> in the <i>hp3</i> line.....	103
2.3.5.2 Screening of AC primary transformants (T_0).....	103
2.3.5.2.1 Verification of level 2 Golden-Gate constructs.....	103
2.3.5.2.2 Identification of CRISPR/Cas9 edited plants	104
2.3.5.2.3 Analysis of CRISPR/Cas9 off-targets.....	104
2.3.5.3 Two-step PCR to amplify single guide RNA (sgRNA) scaffolds.....	105
2.3.5.4 Synthesis of the Southern blot hybridisation probe.....	106
2.3.5.5 Primer design and preparation	106
2.3.5.6 Purification of PCR products	107
2.3.6 High Resolution Melt (HRM).....	107
2.3.7 Determination of a gene copy number.....	108
2.3.7.1 Segregation test	109
2.3.7.2 Southern blotting.....	109
2.3.7.2.1 Solutions and buffers	109
2.3.7.2.2 DNA transfer	110
2.3.7.2.3 Crosslinking and hybridisation.....	110
2.3.7.2.4 Washing and chemiluminescent detection	111
2.3.7.2.5 Data analysis	111
2.3.7.3 Real-time quantitative PCR (RT-qPCR).....	111

2.3.7.3.1 Preparation of plasmid templates	112
2.3.7.3.2 Real-time amplification.....	112
2.3.7.3.3 Data analysis	113
2.4 Construction and verification of vectors.....	113
2.4.1 Molecular cloning.....	113
2.4.1.1 TOPO cloning.....	113
2.4.1.2 Golden-Gate cloning	114
2.4.1.2.1 Assembly of level 1 vectors.....	114
2.4.1.2.2 Assembly of level 2 binary vectors.....	115
2.4.2 Restriction enzyme digestion.....	116
2.4.2.1 Digestion of plant genomic DNA.....	116
2.4.2.2 Verification of Golden-Gate vectors	116
2.4.2.3 Verification of level 1 and 2 constructs	117
2.5 CRISPR/Cas9 targeting of zeaxanthin epoxidase (<i>ZEP</i>)	119
2.5.1 Designing single guide RNAs (sgRNAs).....	119
2.5.2 Construction of vectors.....	122
2.5.3 Stable transformation of tomatoes	122
2.5.4 Analysis of transformed tomato plants	122
2.6 Extraction and analysis of metabolites	123
2.6.1 Extraction of carotenoids and chlorophylls	123
2.6.1.1 Preparation of the freeze-dried material.....	123
2.6.1.2 Methanol-chloroform extraction of pigments.....	123
2.6.2 Sample analysis on the HPLC and UPLC systems	124
2.6.2.1 Sample preparation	124
2.6.2.2 High-performance liquid chromatography (HPLC)	125
2.6.2.3 Ultra-performance liquid chromatography (UPLC).....	126
2.6.2.4 Quantitative data pre-processing	126
2.6.3 Extraction and purification of standards	129
2.6.3.1 Extraction of standards	129
2.6.3.1.1 Phytoene	129
2.6.3.1.2 Lycopene	130
2.6.3.1.3 Violaxanthin	130
2.6.3.2 Standards purification by column chromatography	131
2.6.3.2.1 Alumina gravity column	131
2.6.3.2.2 Flash chromatography	132
2.6.3.3 Quality assessment of the in-house prepared carotenoid standards.....	132
2.6.4 Chromatographic quantification of plant-derived compounds.....	135

2.6.4.1	Quantification of isoprenoid, chlorophyll and α -tocopherol standards.....	135
2.6.4.1.1	Quantification of isoprenoids and α -tocopherol	135
2.6.4.1.2	Quantification of chlorophylls	136
2.6.4.2	Generation of standard curves on the HPLC system	137
2.6.4.2.1	Determination of coefficients.....	137
2.6.4.2.2	Quantification of compounds	138
2.6.5	Thin-layer chromatography (TLC)	138
2.6.5.1	Purification of phytoene	139
2.6.5.2	Analysis of xanthophylls.....	139
2.6.6	Gas chromatography – mass spectrometry (GC-MS)	140
2.6.6.1	Plant material.....	140
2.6.6.2	Sample extraction	140
2.6.6.3	Sample derivatisation	141
2.6.6.4	GC-MS analysis.....	141
2.6.6.5	Data analysis	141
2.6.7	Solid-phase microextraction (SPME).....	142
2.6.7.1	Sample preparation	142
2.6.7.2	SPME	143
2.6.7.3	Data analysis	144
2.6.8	Sub-chromoplast fractionation	144
2.6.8.1	Plant material.....	145
2.6.8.2	Extraction and gradient buffers	145
2.6.8.3	Chromoplast extraction	145
2.6.8.4	Separation of sub-chromoplast compartments with sucrose gradient.....	146
2.6.8.5	Fraction collection and analysis	146
2.7	Data analysis	146
2.7.1	Descriptive statistics	146
2.7.2	Inferential statistics.....	146
Chapter III: Characterisation of tomato lines overexpressing <i>CYC-B</i> and <i>CrtR-b2</i>		147
3.1	Introduction	148
3.2	Results.....	150
3.2.1	Preparation of calibration curves for carotenoid quantification.....	150
3.2.2	Screening of F ₁ population and isolation of xanthophyll-accumulating line	152
3.2.3	Screening of F ₂ segregating population	157
3.2.4	Phenotypic characterisation of F ₂ population lines	162
3.2.5	Leaf pigment analysis of F ₂ population lines.....	162
3.2.6	Effect of saponification on leaf pigment extraction	166

3.2.7 Fruit pigment analysis of F ₂ population lines.....	169
3.2.8 Identification of zeaxanthin on different platforms	172
3.2.9 Analysis of gene combinations in leaves and fruit of F ₂ population lines.....	174
3.2.10 Sub-chromoplast fractionation of F ₂ population lines.....	177
3.2.11 Analysis of primary metabolites of F ₂ population lines	181
3.2.12 Volatile compounds analysis of F ₂ population lines.....	185
3.2.13 Ripening series of the selected F ₂ population lines	189
3.2.14 Analysis of fruit firmness of the selected F ₂ population lines.....	193
3.2.15 Transmission electron microscopy of the selected F ₂ population lines.....	193
3.2.16 Transcriptome analysis of the selected F ₂ population lines	195
3.3 Discussion.....	200
3.3.1 Selection of the reference line.....	200
3.3.2 RT-qPCR as a screening method for determining zygosity	201
3.3.3 Silencing of the hydroxylase in a homozygous state	204
3.3.4 HPLC as an analytical and quantitative technique.....	206
3.3.5 Accumulation of xanthophylls in ripe tomato fruit	207
3.3.6 Identification of candidate genes	212
3.3.7 Proposal of a regulatory mechanism	216
3.3.8 Calculation of fruit weight providing the recommended dose of zeaxanthin	217
Chapter IV: Generation and characterisation of zeaxanthin-accumulating tomato lines	218
4.1 Introduction	219
4.2 Results.....	220
4.2.1 Introduction of the <i>hp3</i> allele into the U/0; B/B and U/0; B/+ lines.....	220
4.2.2 High Resolution Melt analysis to identify the <i>hp3</i> allele	222
4.2.3 Phenotypic characterisation of the selected lines.....	224
4.2.4 Leaf pigment analysis of the selected lines	226
4.2.5 Fruit pigment analysis of the selected lines.....	230
4.2.6 Analysis of gene combinations in leaves and fruit.....	234
4.2.7 Flower pigment analysis of the selected lines	236
4.2.8 Sub-chromoplast fractionation of the selected lines.....	240
4.2.9 Photosynthetic performance	240
4.2.10 Analysis of primary metabolites of the selected lines	243
4.2.11 Volatile compounds analysis of the selected lines	248
4.2.12 Comparison with existing food sources of zeaxanthin	252
4.3 Discussion.....	253
4.3.1 Generation of a new, renewable source of zeaxanthin.....	253
4.3.2 HRM as a screening method	253

4.3.3 Accumulation of zeaxanthin in ripe tomato fruit.....	254
4.3.4 Possible limits to zeaxanthin accumulation	257
4.3.5 Photosynthetic performance	262
Chapter V: CRISPR/Cas9-targeted editing of zeaxanthin epoxidase.....	264
5.1 Introduction	265
5.2 Results.....	265
5.2.1 Selection of target sequences within <i>ZEP</i>	265
5.2.2 Assembly and verification of CRISPR/Cas9 expression cassettes	270
5.2.3 Screening of AC primary transformants (T ₀)	275
5.2.4 General characterisation of T ₀ plants	281
5.2.5 Pigment analysis of leaf and fruit tissues.....	287
5.2.6 <i>In silico</i> modelling of novel alleles of <i>ZEP</i>	292
5.3 Discussion.....	297
5.3.1 CRISPR/Cas9 editing generates chimeric plants	297
5.3.2 A novel, exon 6-truncated allele of <i>ZEP</i> mimics the <i>hp3</i> phenotype.....	301
5.3.3 Summary of <i>ZEP</i> activity.....	303
Chapter VI: General discussion	306
6.1 Summary and key points.....	307
6.2 Industrial relevance.....	308
6.3 Future directions and recommendations	309
6.4 Issues and alternative approaches.....	311
Appendices.....	313
7.1 Appendix 1	314
7.2 Appendix 2	345
7.3 Appendix 3	346
Reference List.....	350

List of Figures

Figure 1.1.	<i>Joining of isoprene units to form carotenoids.</i>	25
Figure 1.2.	<i>Carotenoid nomenclature is based on the carbon ‘carotene’ skeleton.</i>	29
Figure 1.3.	<i>Summary of the MVA and MEP pathways in higher plants leading to the production of carotenoids and other IPP-derived secondary metabolites.</i>	31
Figure 1.4.	<i>Formation of DMAPP and IPP in the MEP pathway.</i>	32
Figure 1.5.	<i>Synthesis of phytoene from DMAPP and IPP.</i>	33
Figure 1.6.	<i>Synthesis of lycopene from phytoene in higher plants.</i>	34
Figure 1.7.	<i>Synthesis of carotenoids from lycopene.</i>	35
Figure 1.8.	<i>Summary of the xanthophyll cycle in higher plants.</i>	37
Figure 1.9.	<i>Summary of the structural changes that take place during chloroplast to chromoplast transition (from Bian et al., 2011).</i>	39
Figure 1.10.	<i>Page of print (left) and a group of faces (right) as seen in a conventional photograph (A), at one moment in time (B) and as a simulated view through the eyes of a person with a blind spot in the centre of their visual field like in the case of AMD (C).</i>	41
Figure 1.11.	<i>Stages of AMD showing the interior surface of the eye (left) and the corresponding optical coherence tomography images of the relevant retinal ultrastructure.</i>	43
Figure 1.12.	<i>(A) Cross-section through a primate retina focused at the macula photographed in white light (top) and blue light (bottom). (B) Distribution of total macular pigments across the retina.</i>	46
Figure 1.13.	<i>Chemical structures of lutein, zeaxanthin and meso-zeaxanthin.</i>	47
Figure 1.14.	<i>Chemical structures of zeaxanthin isomers (C₄₀H₅₆O₂).</i>	53
Figure 1.15.	<i>Wild type rice grains (left) compared to the first (middle) and second (right) generations of Golden Rice.</i>	74
Figure 1.16.	<i>Placement of the major objectives within the simplified carotenoid biosynthetic pathway.</i>	78
Figure 2.1.	<i>Outline of the crossing strategy.</i>	81
Figure 2.2.	<i>UV-Vis spectra of the compounds identified and quantified on the HPLC system.</i>	127
Figure 2.3.	<i>UV-Vis spectra of the compounds identified on the UPLC system.</i>	128
Figure 2.4.	<i>Outlines of the procedures used to obtain standards of lycopene (A), phytoene (B) and violaxanthin (C).</i>	134
Figure 3.1.	<i>Strategy used to create lines overexpressing CrtR-b2 and CYC-B.</i>	149
Figure 3.2.	<i>Identification of lycopene (A), phytoene (B) and violaxanthin (C).</i>	150
Figure 3.3.	<i>Screening of the parental tomato lines (U/U and B/B) and the F₁ hybrids for the presence of the Cauliflower Mosaic Virus 35S (35S) promoter and Solanum galapagense CYC-B (pS.g) allele (A) and S. lycopersicum CYC-B allele (B). (C) Mature fruit of the F₁ hybrids. (D) Side-by-side comparison of the mature fruit of hybrid 1 and hybrid 2. (E) Cross-sections of the mature fruit of hybrid 1 and hybrid 3.</i>	152

Figure 3.4.	<i>HPLC analysis of the pigments from the fruit (A), leaf (B) and saponified leaf (C) extracts of the indicated tomato lines at 450 nm.</i>	154
Figure 3.5.	<i>(A) Screening of the F₂ segregating population against the reference genotypes (MM, U/U, B/B) for the presence of CaMV 35S (35S) promoter, S. galapagense CYC-B allele (pS.g) and S. lycopersicum CYC-B allele (pS.l). (B) Southern blot analysis of selected F₂ plants (PL0051, PL0057 and PL0064). (C) Screening of the F₁ progeny of the plant from the F₂ population (PL0051) crossed with the hp3 line for the presence of the 35S-CrtR-b2 fragment (35S-C), S. galapagense CYC-B (pS.g) and S. lycopersicum CYC-B (pS.l).</i>	158
Figure 3.6.	<i>(A) Cloning of the CaMV 35S and PDS fragments into TOPO vectors was verified by PCR. (B) Determination of transgene zygosity by RT-qPCR. (C) The presence of transgenic CrtR-b2 in a homozygous state was associated with the appearance of leaf variegations which were already apparent at the cotyledon stage (2 weeks; red boxes) and clearly visible at later stages (1 and 2 months red boxes and inset, respectively).</i>	161
Figure 3.7.	<i>Side-by-side comparison of the fruit (A) and leaf (B) phenotypes of the indicated tomato lines of the F₂ population.</i>	163
Figure 3.8.	<i>(A) HPLC chromatograms of saponified leaf extracts of the indicated F₂ population lines. (B) Quantification of isoprenoids and chlorophylls from the non-saponified leaf extracts of the F₂ population lines.</i>	164
Figure 3.9.	<i>Comparison of carotenoids obtained from unsaponified (black bars) and saponified (grey bars) leaf extracts of the F₂ lines.</i>	168
Figure 3.10.	<i>(A) HPLC chromatograms of mature fruit extracts of the indicated F₂ population lines. (B) Quantification of isoprenoids and α-tocopherol from mature fruit of the F₂ population lines.</i>	171
Figure 3.11.	<i>(A) Quantification of zeaxanthin from mature fruit of the U/O; B/B (grey bars) and U/O; B/+ (black bars) lines on the HPLC system. (B) Fruit extracts from F₂ population lines (Azygous and U/O; B/B) were resolved on a TLC plate against the zeaxanthin standard. (C) HPLC analysis of the extracted bands.</i>	173
Figure 3.12.	<i>Effects of different gene combinations on leaf (A) and fruit (B) pigment profiles.</i>	175
Figure 3.13.	<i>Sequestration of carotenoids and α-tocopherol in sub-plastidial compartments of the Azygous, U/O; B/B and U/O; B/+ fruit.</i>	178
Figure 3.14.	<i>Sequestration of carotenoids and α-tocopherol in sub-plastidial compartments of the Azygous, U/U; B/B and U/U; B/+ fruit.</i>	179
Figure 3.15.	<i>Principal component analysis (PCA) of the metabolites identified by GC-MS analysis of polar and non-polar extracts from ripe fruit of the indicated lines.</i>	181
Figure 3.16.	<i>Heat map comparison of the 65 metabolites found to be significantly different between the five F₂ lines.</i>	182
Figure 3.17.	<i>Changes in fruit metabolites of the U/O; B/B line compared to the Az reference line displayed over schematic biochemical pathways.</i>	184
Figure 3.18.	<i>Principal component analysis (PCA) of the volatile compounds detected by SPME analysis of mature fruit of the indicated tomato lines.</i>	185

Figure 3.19.	<i>Heat map comparison of the 92 volatile compounds found to be significantly different between the five F₂ lines.</i>	186
Figure 3.20.	<i>Changes in fruit VOCs of the U/O; B/B line compared to the Az line displayed over schematic biochemical pathways.</i>	188
Figure 3.21.	<i>Representative phenotypes of fruit of the Azygous, U/O; B/B and U/O; B/+ lines collected at the indicated stages of development.</i>	189
Figure 3.22.	<i>Changes in the amounts of isoprenoids and chlorophylls during fruit ripening of the Azygous (Az), U/O; B/B and U/O; B/+ lines.</i>	190
Figure 3.23.	<i>Mature fruit of the U/O; B/B line are significantly firmer than mature fruit of the Azygous line.</i>	193
Figure 3.24.	<i>TEM micrographs of chromoplast from ripe fruit of the Azygous (A) and U/O; B/B line (B).</i>	194
Figure 3.25.	<i>(A) Density plot of log₁₀-transformed expression values (FPKM+1) of the 34 878 protein coding genes in the Azygous (red) and U/O; B/B (blue) lines. (B) Scatter plot of log₁₀-transformed FPKM+1 values of the U/O; B/B line against Azygous. (C) Volcano plot of the differentially expressed genes in the U/O; B/B line compared to Azygous.</i>	196
Figure 3.26.	<i>Summary of the differentially expressed genes between the U/O; B/B line and the Azygous reference line.</i>	198
Figure 3.27.	<i>Summary of the interactions between carotenoids, VOCs and fatty acids.</i>	216
Figure 4.1.	<i>(A) Strategy used to create triple crosses. (B) 8-day-old seedlings of the F₂ triple crosses germinated on MS media supplemented with kanamycin.</i>	221
Figure 4.2.	<i>(A) Sequenced ZEP^{WT/WT}, ZEP^{hp3/hp3} and ZEP^{WT/hp3} allele fragments amplified from the F₂ U/O; B/B line, hp3 lines and F₁ U/O; B/+, hp3/+ hybrid, respectively. (B) Specificity of the HRM primers was confirmed across a range of temperatures. (C) Normalised melt curves (left) of the three fragments allowed to identify the C to T transition between the two homoduplexes (green and violet) and heteroduplex (blue). (D) Auto-calling of unknown genotypes of the F₂ triple cross population based on the reference genotypes (shaded).</i>	223
Figure 4.3.	<i>Side-by-side comparison of the fruit (A) and flower (B) phenotypes of the indicated tomato lines.</i>	225
Figure 4.4.	<i>(A) HPLC chromatograms of saponified leaf extracts of the indicated lines. (B) Quantification of isoprenoids and chlorophylls from the non-saponified leaf extracts of the hp3 line and the indicated triple crosses.</i>	227
Figure 4.5.	<i>Comparison of non-saponified leaf extracts of the F₃ population Azygous (N = 7) and U/O; B/B (N = 10) lines against the hp3 (N = 6) and F₂ U/O; B/B; hp3/hp3 lines (N = 3).</i>	229
Figure 4.6.	<i>(A) HPLC chromatograms of ripe fruit extracts of the indicated tomato lines. (B) Quantification of isoprenoids and α-tocopherol from ripe fruit of the hp3 line and the indicated triple crosses.</i>	232
Figure 4.7.	<i>Comparison of ripe fruit extracts of the F₃ population Azygous (N = 3) and U/O; B/B (N = 3) lines against the hp3 (N = 3) and F₂ U/O; B/B; hp3/hp3 lines (N = 3).</i>	233
Figure 4.8.	<i>Effects of different gene combination on leaf (A) and fruit (B) pigment profiles.</i>	235

Figure 4.9.	<i>Pigment profiles of non-saponified (A) and saponified (B) extracts from flowers of the indicated lines. (C) Quantification of carotenoids from the flowers of the indicated lines.</i>	237
Figure 4.10.	<i>Sequestration of carotenoids and α-tocopherol in sub-plastidial compartment of the Az, U/0; B/B and U/0; B/B; hp3/hp3 fruit.</i>	241
Figure 4.11.	<i>Comparison of photosystem II (PSII) efficiency between the indicated lines.</i>	242
Figure 4.12.	<i>Plots of the F_v/F_m ratios of the indicated tomato lines against their corresponding ratios of total chlorophyll to total carotenoids (CHL:CAR) (A) and total chlorophyll to zeaxanthin (CHL:ZEA) (B).</i>	243
Figure 4.13.	<i>Principal component analysis (PCA) of the metabolites identified by GC-MS analysis of polar and non-polar extracts from ripe fruit of the indicated lines.</i>	244
Figure 4.14.	<i>Heat map comparison of the 93 metabolites found to be significantly different between the five lines.</i>	245
Figure 4.15.	<i>Changes in fruit metabolites of the U/0; B/B; hp3/hp3 line compared to the hp3 control displayed over schematic biochemical pathways.</i>	247
Figure 4.16.	<i>Principal component analysis (PCA) of the volatile compounds detected by SPME analysis of ripe fruit of the indicated tomato lines.</i>	248
Figure 4.17.	<i>Heat map comparison of the 98 volatile compounds found to be significantly different between the five lines.</i>	249
Figure 4.18.	<i>Changes in fruit VOCs of the U/0; B/B; hp3/hp3 line compared to the hp3 control displayed over schematic biochemical pathways.</i>	251
Figure 4.19.	<i>(A) HPLC chromatograms of saponified leaf extracts from spinach, kale and the U/0; B/B; hp3/hp3 line at 450 nm. (B) Comparison between the carotenoid levels in the unsaponified leaf extracts of spinach (N = 3), kale (N = 3) and the U/0; B/B; hp3/hp3 line (N = 3).</i>	252
Figure 5.1.	<i>(A) The predicted 3D structure of ZEP with 63% of the residues modelled at more than 90% confidence. (B) the predicted topology of the transmembrane domain (helix, S1) of ZEP.</i>	266
Figure 5.2.	<i>(A) Pocket detection (red) in ZEP indicating possible locations of the active sites. (B) Prediction of functional and/or phenotypic effects of missense mutations occurring at the given amino acid residues. (C) Predicted effects of mutations at the residue 142 (glutamic acid). Mutational sensitivity of alanine at the position 137 (D) and threonine at the position 365 (E) displayed against predicted pockets (highlighted in red).</i>	267
Figure 5.3.	<i>(A) Position of ZEP within the tomato genome. (B) Position of exons (grey rectangles) within ZEP. Sequences of the 20 nucleotide-long Cas9 target sites in exon 6 (C) and exon 1 (D) with the corresponding amino acid sequences.</i>	268
Figure 5.4.	<i>In silico prediction of secondary structures of sgRNAs targeting exon 6 (A) and exon 1 (C) using CONTRAfold inference engine based on calculating base-pairing probabilities. In silico prediction of minimum free energy (MFE) secondary structures of sgRNAs targeting exon 6 (B) and exon 1 (D) based on the provided constraint.</i>	269

- Figure 5.5.** (A) PCR amplification of the sgRNA scaffolds targeting the exon 6 and exon 1 of ZEP. (B) Restriction enzyme digests of the empty (E) and fully assembled level 1 plasmids (I – VII) with Bpil (top) and NotI/Sfil (bottom). (C) EcoRV restriction enzyme digests of the fully assembled level 2 plasmids (I – VI) compared against the empty (E) undigested (U) and single digested (S) level 2 vectors. 272
- Figure 5.6.** Alignment of the sequenced level 1 constructs harbouring guides targeting the exon 6 (A) and exon 1 (B) against their respective templates. 273
- Figure 5.7.** MAFFT alignment of the forward and reverse sequenced level 2 constructs at their right (A) and left (B) borders, respectively. 274
- Figure 5.8.** Plasmid maps of the level 1 (A) and level 2 (B) constructs assembled using the Golden-Gate cloning strategy. 275
- Figure 5.9.** (A) Amplification of the hCas9 and NPTII fragments from the assembled level 2 constructs. (B) Amplification of the hCas9, NPTII, exon 1 and exon 6 fragments from an untransformed AC control plant. 276
- Figure 5.10.** (A) Screening for the presence of the hCas9 and NPTII fragment from AC tomato plants transformed with pICSL4723::zepE6 targeting the exon 6. (B) Amplification of the exon 6 fragments from the plants positive for hCas9 and NPTII screened in (A). (C) Sequencing of the exon 6 fragments from (B). 278
- Figure 5.11.** Comparison of fruit (A) and flower (B) phenotypes of CRISPR/Cas9 edited plants targeted at the exon 1 (ID 12.7.1) and the exon 6 (all except ID 12.7.1). 283
- Figure 5.12.** Photosystem II efficiency of the screened AC transformants (black, N = 1) against control lines: Az (blue; N = 7) and hp3 (red, N = 6). 284
- Figure 5.13.** (A) Amplification of CRISPR/Cas9 off-target sites from the plant (ID 12.6.8) harbouring a biallelic mutation in the exon 6 of ZEP. (B) MAFFT alignment of sequenced off-target sites against their respective templates. 285-286
- Figure 5.14.** (A) Comparison of fruit pigments and α -tocopherol of the selected T_0 plants against the hp3 line. (B) Total fruit carotenoid levels (CAR, α -tocopherol not included) of the tomato plants from (A). 288
- Figure 5.15.** (A) HPLC chromatograms of saponified leaf extract of the AC control, the hp3 tomato line and the T_0 plant ID 12.6.8 harbouring a biallelic mutation of ZEP. (B) Quantification of the major pigments from saponified leaf extracts of the three plants analysed above. 290
- Figure 5.16.** (A) Predicted 3D structure of the wild type (WT) allele of ZEP. The predicted 3D models of the two novel alleles of ZEP resulting from the 2 bp (B) and 16 bp (C) deletions of the DNA. 293
- Figure 5.17.** (A) Predicted 3D structure of the wild type (WT) allele of ZEP. The predicted 3D models of the two novel alleles of ZEP resulting from the 1 bp (B) and the 8 bp (C) deletions in the DNA. 294
- Figure 5.18.** (A) Two ligand clusters were identified within the structure of WT ZEP. (B) and (C) A single, FAD-binding ligand cluster was identified in both truncated at the exon 6 alleles of ZEP. (D) and (E) Three ligand clusters were identified within the structure of the truncated at the exon 1 alleles of ZEP. 295

Figure 5.19.	<i>(A) Predicted 3D structure of the hp3 allele of ZEP with 58% of the residues modelled at more than 90% confidence. (B) Two ligand clusters were identified within the structure of the hp3 allele of ZEP.</i>	296
Figure 5.20.	<i>Targeting phytoene desaturase, PDS in tomato may generate T₀ plants of varying levels and sites of editing here clearly expressed by the albino phenotype.</i>	297
Figure 5.21.	<i>Summary of ZEP activity at the thylakoid membrane of the chloroplast.</i>	305
Figure 6.1.	<i>Summary of the conclusions of Chapters III – V.</i>	307
Supplementary Figure 1.1.	<i>Standard curves of the selected isoprenoid compounds generated on the HPLC system (A – J) at the indicated light wavelengths [nm].</i>	315- 316
Supplementary Figure 1.2.	<i>UPLC was used to confirm the presence of compounds in the fruit (A), leaf (B) and saponified leaf (C) extracts of the indicated lines at 450 nm.</i>	317
Supplementary Figure 1.3.	<i>Comparison of leaf carotenoid extracts of the indicated tomato lines without (black bars) and following (grey bars) saponification.</i>	318
Supplementary Figure 1.4.	<i>(A) PCR screen of the F₂ plants used in Southern blotting for the presence of CaMV 35S (35S), S. galapagense CYC-B (pS.g) and S. lycopersicum CYC-B (pS.l) against the reference genotypes. (B) Comparison of the 35S-CrtR-b2 DIG-dUTP labelled probe (35S-C^{DIG-dUTP}) against the unlabelled 35S-CrtR-b2 fragment (35S-C). (C) Verification of the quality of genomic DNA of the plants selected from the F₂ population and used in Southern blot. (D) Separation of genomic DNA used in Southern blot analysis following its digestion with HindIII. (E) Full screen of the F₁ progeny of the selected F₂ plants crossed with the hp3 line for the 35S-CrtR-b2 fragment indicating the presence of transgenic CrtR-b2.</i>	319
Supplementary Figure 1.5.	<i>MAFFT alignment of the PDS (top) and CaMV 35S (bottom) fragments cloned into their respective TOPO vectors.</i>	320
Supplementary Figure 1.6.	<i>(A) Assessment of the integrity of total RNA on agarose gel. (B) Electropherograms of the samples provide information on the level of RNA degradation.</i>	320
Supplementary Figure 1.7.	<i>Comparison of the height of the F₂ population plants assigned to the Azygous (A) and the U/0; B/B line (B).</i>	344
Supplementary Figure 2.1.	<i>The F₂ U/0; B/B line, hp3 line and F₁ U/0; B/+; hp3/+ hybrid were used to amplify the 350 bp-long fragment of the exon 1 of ZEP, spanning the region where the missense mutation in the hp3 line occurred.</i>	345
Supplementary Figure 2.2.	<i>Preparation of the instrument for the use in the measurement of Photosystem II efficiency.</i>	345
Supplementary Figure 3.1.	<i>Restriction digest of plasmids used to construct level 1 and 2 vectors.</i>	346

- Supplementary Figure 3.2.** *E. coli* transformed with pICH47751::zepE6 (left) and pICH47751::zepE1 (right) constructs. 346
- Supplementary Figure 3.3.** Plasmid maps of the fully assembled level 1 (left) and level 2 (right) constructs. 347
- Supplementary Figure 3.4.** (A) Verification of *Agrobacterium tumefaciens* LBA4404 cultures transformed with the level 2 binary plasmids harbouring the CRISPR/Cas9 expression cassettes targeting either exon 6 or exon1 of ZEP and intended for the use in tomato stable transformation. (B) Early stage tissue culture transformation plates of the tomato leaf explants unexposed to bacterial suspension (AC control) and exposed to the suspension of bacteria transformed with the level 2 binary constructs (either pICSL4723::sgRNA_zepE6 or pICSL4723::sgRNA_zepE1). 348
- Supplementary Figure 3.5.** (A) Screening for the presence of the hCas9 and NPTII fragments from AC tomato plants transformed with pICSL4723::zepE1 targeting exon 1. (B) Amplification of the exon 1 fragments from the plants screened in (A). 349
- Supplementary Figure 3.6.** Screening of a group of AC plants transformed with pICSL4723::zepE6 targeting exon 6 amongst which the plant harbouring a biallelic edit of ZEP (plant identifier 12.6.8, indicated with an asterisk (*)) was first identified. 349
- Supplementary Figure 3.7.** The flower trusses collected from the same CRISPR/Cas9 edited tomato plant (9.6.1). 349

List of Tables

Table 2.1.	<i>Tomato varieties used in this study.</i>	82
Table 2.2.	<i>List of tomato populations grown between 2015 and 2018.</i>	84
Table 2.3.	<i>Antibiotics used for selection.</i>	88
Table 2.4.	<i>General cycling conditions used in the genotyping of tomato populations.</i>	101
Table 2.5.	<i>Primer sequences and their parameters for the use in PCR.</i>	102
Table 2.6.	<i>Primers used to amplify sgRNA_zepE6 off-target (OT) sites.</i>	105
Table 2.7.	<i>Cycling conditions used for the amplification of sgRNA scaffolds with specific 20-bp-long guide targets.</i>	106
Table 2.8.	<i>Conditions used for the amplification of the 100 bp fragment of ZEP used in HRM analysis.</i>	108
Table 2.9.	<i>Amplification conditions used in two-step RT-qPCR.</i>	113
Table 2.10.	<i>Conditions used for the digestion-ligation assembly of level 1 plasmids.</i>	114
Table 2.11.	<i>Plasmids used in the assembly of the level 2 CRISPR/Cas9 expression cassettes.</i>	118
Table 2.12.	<i>Top 20 off-targets for the guide targeting exon 1.</i>	120
Table 2.13.	<i>Top 20 off-targets for the guide targeting exon 6.</i>	121
Table 2.14.	<i>List of compounds used for the preparation of standard curves.</i>	135
Table 3.1.	<i>Quantification of isoprenoids and chlorophylls from the fruit and non-saponified leaf extracts of the indicated tomato lines.</i>	155
Table 3.2.	<i>χ^2 goodness of fit test allowed to conclude that the segregation of transgenic CrtR-b2 at the U locus was occurring in the manner as expected, given the zygosity of the maternal F_2 plant ($\chi^2 = 0.2$, $d_f = 4$, $P = 0.995$).</i>	160
Table 3.3.	<i>List of carotenoid-related genes found to be differentially expressed in the U/O; B/B line compared to the Azygous reference line as analysed by RNA-Seq.</i>	199
Table 5.1.	<i>Predicted sizes of fragments generated through in silico restriction enzyme digests of the assembled constructs with the specified enzymes.</i>	270
Table 5.2.	<i>Efficiency of the Golden-Gate assembly of the level 1 and level 2 vectors calculated as a ratio of the number of white clones to the total number of all clones for each of the designed guides.</i>	271
Table 5.3.	<i>Types and frequencies of mutations in hCas9/NPTII-positive transformants targeted at the exon 6.</i>	279
Table 5.4.	<i>Types and frequencies of mutations in hCas9-positive transformants targeted at the exon 1.</i>	279
Table 5.5.	<i>Quantification of isoprenoids and chlorophylls from the non-saponified leaf extracts of the indicated T_0 transformants, the AC control and the hp3 line.</i>	291

Supplementary Table 1.1.	<i>Summary of the coefficients (a and b) used in quantification of isoprenoids and chlorophylls at the specified light wavelengths (nm).</i>	317
Supplementary Table 1.2.	<i>Summary of the quality of RNA samples used in preparation of the cDNA library for sequencing.</i>	321
Supplementary Table 1.3.	<i>List of significantly upregulated genes in the U/0; B/B line with over a 2.83-fold increase compared to the Azygous reference line.</i>	322- 339
Supplementary Table 1.4.	<i>List of significantly downregulated genes in the U/0; B/B line with over a 2.83-fold decrease compared to the Azygous reference line.</i>	340- 343

Abbreviations

16L/8D	16 hours of light and 8 hours of dark
¹ Chl*	Singlet excited state chlorophyll
³ Car*	Triplet excited state carotenoid
³ Chl*	Triplet excited state chlorophyll
ABA	Abscisic acid
AC	Ailsa Craig
AMD	Age-related macular degeneration
AREDS	Age-Related Eye Disease Study
ASGs	Acyl sterol glycosides
Az	Azygous
bn	Billion
bp	Base pairs
bp.	Boiling point
CAGR	Compound annual growth rate
CaMV	Cauliflower mosaic virus
CAR	Carotenoids
CAREDS	Carotenoids in Age-Related Eye Disease Study
Cas9	CRISPR-associated protein 9
CCDs	Carotenoid cleavage dioxygenases
CCS	Capsanthin/capsorubin synthase
CDP-ME	4-(cytidine 5'-diphospho)-2-C-methyl-D-erythritol
CDP-MEP	2-phospho-4-(cytidine 5'-diphospho)-2-C-methyl-D-erythritol
CHL	Chlorophyll
CMK	4-(cytidine 5'-diphospho)-2-C-methyl-D-erythritol kinase
CRISPR	Clustered regularly interspaced short palindromic repeats
CRTI	Phytoene desaturase from bacteria and fungi
CRTISO	Carotene <i>cis-trans</i> isomerase
CrtR-b	β-carotene hydroxylase
CrtR-e	ε-ring hydroxylase
CYC-B	Lycopene β-cyclases, chromoplastic
DCW	Dry cell weight
DHA	Dehydroascorbate
DMAPP	Dimethylallyl diphosphate
DMSO	Dimethyl sulfoxide
DW	Dry weight
DXP	1-deoxy-D-xylulose 5-phosphate
DXR	1-deoxy-D-xylulose 5-phosphate reductoisomerase
DXS	1-deoxy-D-xylulose 5-phosphate synthase
EDCCS	Eye Disease Case-Control Study Group
ee	Enantiomeric excess
EET	Excitation energy transfer
EFSA	European Food Safety Authority
ElgM	Elongation media
EMS	Ethyl methanesulfonate
ERF	Ethylene Response Factor
FAD	Flavin adenine dinucleotide
FPKM	Fragments per kilobase of transcript per million mapped reads
FPP	Farnesyl pyrophosphate

FW	Fresh weight
G3P	Glyceraldehyde 3-phosphate
GAs	Gibberellins
GC-MS	Gas chromatography-mass spectrometry
GGPP	Geranylgeranyl diphosphate
GGPS	Geranylgeranyl diphosphate synthase
GMO	Genetically modified organism
GPP	Geranyl pyrophosphate
GPS	Geranyl diphosphate synthase
GRAS	Generally recognised as safe
HDR	1-hydroxy-2-methyl-2-(<i>E</i>)-butenyl 4-diphosphate reductase
HDS	1-hydroxy-2-methyl-2-(<i>E</i>)-butenyl 4-diphosphate synthase
HMBPP	1-hydroxy-2-methyl-2-(<i>E</i>)-butenyl 4-phosphate
<i>hp3</i>	<i>High-pigment 3</i>
HPLC	High-performance liquid chromatography
HRM	High Resolution Melt
IAA	Indole-3-acetic acid
IDI	Isopentenyl-diphosphate isomerase
IM	Immature green
IPP	Isopentenyl diphosphate
IUB	International Union of Biochemistry
IUPAC	International Union of Pure and Applied Chemistry
LB	Lysogeny broth
LCY-B	Lycopene β -cyclase
LCY-E	Lycopene ϵ -cyclase
LHCs	Light-harvesting complexes
M	Million
MAFFT	Multiple alignment using fast Fourier transform
MAS	Marker assisted selection
MCS	2-C-methyl-D-erythritol 2,4-cyclodiphosphate synthase
MCT	2-C-methyl-D-erythritol 4-phosphate cytidyl transferase
ME-cPP	2-C-methyl-D-erythritol 2,4-cyclodiphosphate
MEP	2-C-methyl-D-erythritol 4-phosphate
MG	Mature green
MM	Moneymaker
MPOD	Macular pigment optical density
MS	Murashige and Skoog medium
MVA	Mevalonate
NADPH	Nicotinamide adenine dinucleotide phosphate
NCED	9- <i>cis</i> -epoxycarotenoid dioxygenase
NPQ	Non-photochemical quenching
NPTII	Neomycin phosphotransferase II enzyme
NXS	Neoxanthin synthase
OD	Optical density
OT	Off-target
PAM	Protospacer adjacent motif
PAR	Photosynthetically active radiation
PCA	Principal component analysis
PCR	Polymerase chain reaction

PDS	Phytoene desaturase
POLA	Pathologies Oculaires Liées à l'Age study
ppb	Parts per billion
ppm	Parts per million
PPPP	Pre-phytoene diphosphate
PSI	Photosystem I
PSII	Photosystem II
PSY	Phytoene synthase
QC	Quality control
R	Ripe
RgM1	Regeneration media 1
RgM2	Regeneration media 2
RgM3	Regeneration media 3
RIL	Recombinant inbred line
RNA-Seq	RNA sequencing
ROS	Reactive oxygen species
RPM	Revolutions per minute
RT	Retention time
RtM	Rooting media
RT-qPCR	Real-time quantitative PCR
S ₁	Singlet excited state
SD	Standard deviation
SGAs	Steroidal glycoalkaloids
sgRNA	Single guide RNA
SGs	Sterol glycosides
SNP	Single nuclear polymorphism
SOB	Super optimal broth
SOC	Super optimal broth with catabolite repression
SPME	Solid phase microextraction
T	Turning
T _a	Annealing temperature
TCA	Tricarboxylic acid
TEM	Transition electron microscopy
Temp.	Temperature
TILLING	Targeting Induced Local Lesions in Genomes
TLC	Thin layer chromatography
UPLC	Ultra-performance liquid chromatography
v/v	Volume per volume
v/w	Volume per weight
VDE	Violaxanthin de-epoxidase
VOCs	Volatile organic compounds
VVM	Volumes per minute
w/v	Weight per volume
w/w	Weight per weight
WT	Wild type
ZEA	Zeaxanthin
ZEP	Zeaxanthin epoxidase
ZDS	ζ-carotene desaturase
ZISO	ζ-carotene <i>cis-trans</i> isomerase

Chapter I: Introduction

1.1 Characterisation of carotenoids

1.1.1 Structure and function

Carotenoids are natural pigments belonging to the tetraterpene (C_{40}) class of organic compounds. They are almost exclusively synthesised by photosynthetic organisms (plants and algae), but also by some bacteria and certain fungi. Carotenoids are responsible for the characteristic yellow, orange or red colours of many vegetables, flowers and fruit. Animals are unable to synthesise carotenoids with the noteworthy exception of some herbivorous insect, such as aphids and spider mites, which have acquired the ability to produce carotenoids *de novo* through horizontal gene transfer from fungi (Altincicek *et al.*, 2012). Therefore, most animals must rely on their diet in order to acquire these compounds.

Currently, there are 1 117 naturally occurring carotenoid compounds (Yabuzaki, 2017), which, based on their structures, can be classified into three groups: carotenes, carotenoids and xanthophylls. Carotenes, such as lycopene, phytoene and phytofluene, are acyclic tetraterpenes. Carotenoids, such as α -carotene and β -carotene, contain cyclic rings. Xanthophylls additionally contain oxygen in the form of hydroxyl- (lutein and zeaxanthin), epoxide- (antheraxanthin, violaxanthin and neoxanthin), methoxy- (spirilloxanthin) or keto- (astaxanthin and echinenone) groups attached to their carbon skeleton or, more commonly, the end-rings. The carotenoid carbon skeleton is derived from eight C_5H_8 isoprene units (Figure 1.1A) joined together head-to-tail (1-4 link; Figure 1.1B) to form a $C_{40}H_{64}$ tetraterpene compound. In the middle of the molecule,

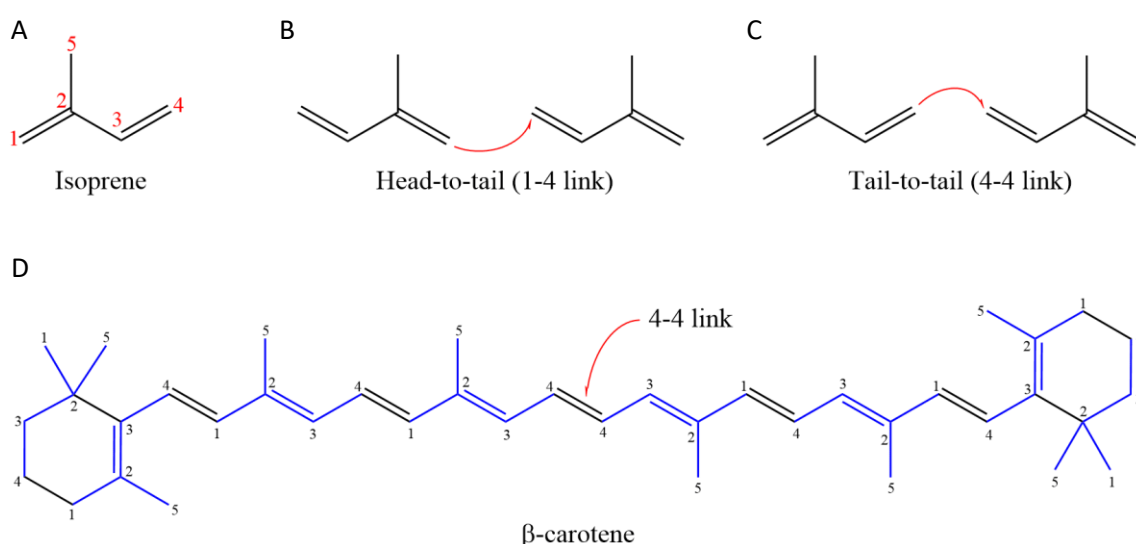


Figure 1.1. Joining of isoprene units to form carotenoids. **(A)** Numbering of carbon atoms in a single isoprene unit. Carbon 1 corresponds to the head, carbon 4 – tail. **(B)** Joining of two isoprene units in a head-to-tail fashion. The bond is formed between carbon 1 of the first unit and carbon 4 of the next one. Two isoprene units form a monoterpene. **(C)** Tail-to-tail joining of two isoprene units. **(D)** Example of joining of eight isoprene units (blue) to form a molecule of β -carotene. Two isoprene units cyclise at each end to form closed rings. The units are joined by the 1-4 link except in the middle where the 4-4 link is formed. Carbon atoms of the isoprene units are numbered.

however, the isoprene units are inverted and joined tail-to-tail (4-4 link; Figure 1.1C), giving the polyene chain a centre of symmetry (Gross, 1991; Figure 1.1D). Modifications to this basic carbon skeleton give rise to the great variety of carotenoids found in nature. Some carotenes, including lycopene, phytoene and phytofluene, have only linear polyene chain structures. In other carotenoids, either one or both ends of the molecule are cyclised to form closed hydrocarbon rings (Figure 1.1D). The rings can be present at one end of the molecule only, as in torulene, or both ends, as in α - and β -carotene. The type of the end group determines the nature of the carotenoid. As tetraterpenes are hydrocarbons, not all carotenoid compounds can be classified as such. Xanthophylls contain oxygen and therefore, are considered to be tetraterpenoids, which are tetraterpene derivatives. Xanthophylls, similarly to some carotenes also contain one or two end rings, however these are often modified with oxygen-containing functional groups. Some xanthophylls, such as citranaxanthin, contain unmodified end-rings with oxygen attached to the polyene chain instead. Carotenoid polyene chains contain between 9 and 13 double bonds forming long conjugated systems. These alternating single and double bonds are responsible for the yellow, orange and red colours of carotenoids as their absorption spectra are shifted towards longer light wavelengths in the range of 450 to 550 nm, which correspond to violet to green light (Fieser, 1950; Gross, 1991; Hashimoto *et al.*, 2018).

Carotenoids perform several important functions in plants, algae, bacteria, fungi and also animals (Cazzonelli, 2011). It is the structure of carotenoids that in fact specifically imparts their biological and physiological functions. In many plants, carotenoids provide bright pigmentation to flowers and fruit which helps to attract pollinators and promotes seed dispersal. Indeed, it is the extent of the conjugated system as well as the presence of the functional groups contained in carotenoid molecules that determine the colour of these compounds. In photosynthetic organisms, carotenoids, such as lutein, neoxanthin, violaxanthin and zeaxanthin, serve as accessory pigments which are important components of the light-harvesting complexes (LHCs), also referred to as the antenna complexes. LHCs are arrays of proteins and photosynthetic pigments which surround the reaction centre of the photosystem. Carotenoids capture light in the regions in which the chlorophylls absorb less efficiently, therefore widening the spectrum of light that can be utilised in photosynthesis (Hashimoto *et al.*, 2018). Following light capture by accessory pigments, the energy is shuttled by excitation energy transfer (EET) to the chlorophyll molecules within the reaction centre in order to drive the reactions of photosynthesis. This singlet-singlet energy transfer is facilitated by the conjugated systems of alternating double bonds within carotenoid molecules (Gradinaru *et al.*, 2000; Holt *et al.*, 2003). The role of carotenoids within LHCs is not limited to light capture only. In fact, they are essential for the assembly and stability of photosystems. In cyanobacteria, lack of carotenoids reduces photosystem I (PSI) oligomerisation and stops photosystem II (PSII) formation (Tóth *et al.*, 2015).

Arabidopsis thaliana no xanthophylls (nox) mutant was found to be depleted in LHC subunits and to have impaired efficiencies of non-photochemical quenching (NPQ) and photosynthetic electron transfer. The phenotype has particularly affected PSI due to decreased translation and stability of its two major subunits, PsaA and PsaB (Dall'Osto *et al.*, 2013).

Within the LHCs, carotenoids also provide protection against photoinhibition and light-induced damage to the photosynthetic apparatus. Molecular oxygen is released as a by-product of photosynthesis, making the photosynthetic organisms prone to forming reactive oxygen species (ROS), which cause oxidative damage to the membranes and proteins of the cell. As the light intensity reaching the photosystems increases, so does the levels of singlet excited state chlorophyll ($^1\text{Chl}^*$), which can transition by intersystem crossing into long-living triplet excited state ($^3\text{Chl}^*$). Due to its longer lifetime, $^3\text{Chl}^*$ has a greater chance to interact with molecular oxygen and readily reacts with it forming singlet oxygen, which further increases ROS formation (Robinson, 1963; Pinnola *et al.*, 2016). Carotenoids provide photoprotection by quenching $^3\text{Chl}^*$ through triplet-triplet energy transfer conducted by Dexter exchange mechanism which generates carotenoid triplet excited states ($^3\text{Car}^*$) which rapidly decay to ground states (Kvíčalová *et al.*, 2016). Additionally, carotenoids are at least partially responsible for quenching $^1\text{Chl}^*$ preventing its transition into $^3\text{Chl}^*$ (Beddard *et al.*, 1977; Naqvi *et al.*, 1997; Chen *et al.*, 2017). The excess energy is dissipated by carotenoids in form of heat by the mechanism known as the non-photochemical quenching (NPQ) which is achieved through molecular vibrations (Niyogi *et al.*, 1998). The process behind this is a form of light-dependent and enzyme-controlled NPQ known as the xanthophyll cycle (Demmig-Adams *et al.*, 1996; Jahns & Holzwarth, 2012). The excess energy within the LHCs is thermally dissipated before it reaches the reaction centre preventing the formation of $^3\text{Chl}^*$ and subsequently, ROS. The xanthophyll cycle is discussed in detail in later sections. However, the xanthophyll cycle is not the sole NPQ mechanism operating in photosynthetic organisms. A separate, zeaxanthin-independent NPQ mechanism related to a decrease in PSII photochemistry has been identified as well (Finazzi *et al.*, 2004). Finally, carotenoids contribute to photoprotection by scavenging the ROS which had already been generated and stopping them from inflicting oxidative damage to membrane lipids and other cellular components (Johnson *et al.*, 2007; Ballottari *et al.*, 2013). Carotenoids are therefore very potent antioxidants, the property which is attributed to their conjugated chromophores.

Some carotenoids serve as precursors for plant hormones and signalling molecules. For example, the xanthophyll neoxanthin is a precursor for the synthesis of plant hormone abscisic acid (ABA) involved in abscission, regulation of plant growth, seed germination and dormancy as well as response to various stresses (Seo & Koshiba, 2002). Mycorradicin, originating from the cleavage of an unknown C_{40} -carotenoid, is thought to promote symbiosis between plant roots

and mycorrhizal fungi (Strack & Fester, 2006; Floss *et al.*, 2008). Strigolactones, such as strigol, are also derived from C₄₀-carotenoids and are potent inhibitors of shoot branching (Gomez-Roldan *et al.*, 2008). Action of carotenoid cleavage dioxygenases (CCDs) on certain carotenoids leads to the production of aroma compounds such as ionones, damascones and damascenones collectively known as rose ketones (Huang *et al.*, 2009).

In animals, carotenoids are responsible for providing vibrant colouration which is often ornamental but commonly is involved in behavioural, reproductive and survival aspects of an animal's life. For instance, female zebra finches, *Taeniopygia guttata*, prefer to mate with males with redder bills, the colour of which is determined by carotenoids (Simons & Verhulst, 2011). In flamingos, the pink colouration of the plumage is also the result of carotenoids acquired through diet. Greater flamingos, *Phoenicopterus roseus*, with more intensely coloured plumage were found to be more attractive mating partners and initiated nesting earlier compared to less coloured individuals (Amat *et al.*, 2010). Some carotenoids directly promote survival of certain organisms depending on environmental conditions. Pea aphids, *Acyrtosiphon pisum*, are one of the few animals capable of carotenoid synthesis (Moran & Jarvik, 2010). Pea aphids display a red-green polymorphism which is determined by the types of carotenoids the organism synthesises. The polymorphisms has a survival role as the red aphids are more likely to be predated on, whereas the green aphids are more likely to be infected with parasites. Therefore, the colour of the aphid provides a survival advantage depending on the presence of the selective pressure (Losey *et al.*, 1997). Carotenoids are also essential for survival of certain microorganisms. Staphyloxanthin, carotenoid responsible for the golden colouration of pathogenic bacterium *Staphylococcus aureus*, is one such example. *S. aureus* mutants deficient in this pigment are less pathogenic as they are more susceptible to oxidative immune attack with ROS by neutrophils which indicates that staphyloxanthin acts as an antioxidative agent (Liu *et al.*, 2005). Finally, carotenoids with provitamin A activity, such as α - and β -carotene, β -cryptoxanthin and γ -carotene, which contain unsubstituted β -ionone rings, are converted to vitamin A in the small intestine with help of the enzyme β,β -carotene-15,15'-oxygenase 1 (BCO1). Vitamin A is important for the embryonic development, growth, reproduction as well as the maintenance of epithelial cells, immune system and good vision (Von Lintig & Vogt, 2004).

1.1.2 Nomenclature

The rules for the nomenclature of carotenoids were set and approved by the International Union of Pure and Applied Chemistry (IUPAC) Commission on the Nomenclature of Organic Chemistry and the International Union of Biochemistry (IUB) Commission on Biochemical Nomenclature (IUPAC Commission on the Nomenclature of Organic Chemistry and the IUPAC-IUB Commission

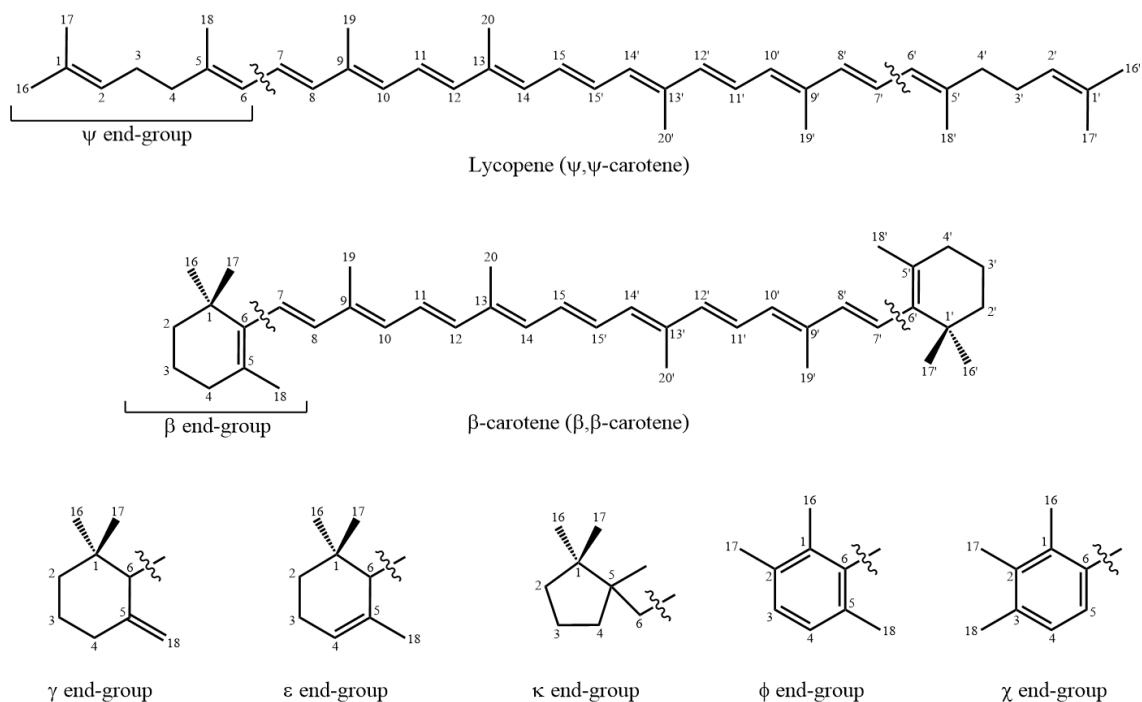


Figure 1.2. Carotenoid nomenclature is based on the carbon ‘carotene’ skeleton. Attachment of specific end groups to this skeleton determines the name and nature of the given compound. Numbering of the carbon atoms in an acyclic carotenoid lycopene and cyclic β -carotene are indicated. The ends of the molecule, either one or both of them, can be substituted with the indicated end-groups which can be further modified to contain functional groups.

on Biochemical Nomenclature, 1975). Since carotenoids are relatively large molecules, their full IUPAC systematic names, which list the types and positions of the bonds as well as the types of the functional groups, are very rarely used. More commonly, their semi-systematic and trivial names are used instead (Britton, 1996). The semi-systematic nomenclature is based on the structure and numbering of the basic ‘carotene’ core. The carbon skeleton can be either linear (acyclic), or, more commonly, contain closed rings at one or both ends of the chain (cyclic). The carbon skeleton is treated as two separate halves, symmetric around the middle. The numbering starts from each end of the molecule towards the middle beginning with number 1 until 15 on the left side and from 1’ to 15’ as moving from the right. Each half is named based on the original compound it was derived from. The end groups are given Greek letters to characterise them (Figure 1.2). Any changes to the end groups, for example the presence of functional groups, is indicated and numbered depending on its position within the ring. For instance, the systematic name of β -carotene (trivial name) is 1,3,3-trimethyl-2-[(1*E*,3*E*,5*E*,7*E*,9*E*,11*E*,13*E*,15*E*,17*E*)-3,7,12,16-tetramethyl-18-(2,6,6-trimethylcyclohexen-1-yl)]o-ctadeca-1,3,5,7,9,11,13,15,17-nonenyl]cyclohexene. More commonly, the semi-systematic name β,β -carotene is used, indicating the presence of two β -end rings (Figure 1.2). In naming xanthophylls, the modifications to the end groups are indicated. Zeaxanthin (trivial name) contains two hydroxylated β -rings at positions 3 and 3’, so its semi-systematic name is β,β -carotene-3,3’-diol. Lutein (trivial name),

a xanthophyll with two hydroxylated end rings at the same positions as zeaxanthin, has a semisynthetic name of β,ϵ -carotene-3,3'-diol.

As seen by the case of zeaxanthin and lutein, the semi-systematic names can already provide enough information on the structural differences between the compounds. The trivial names given to carotenoids are often derived from the original material they came from. This, however, could sometimes result in confusion as the same carotenoid could have more than one trivial name prior to its chemical characterisation. However, trivial names are useful for naming newly discovered carotenoids if the structure of the compound has not yet been determined. Additionally, due to the presence of the conjugated double bonds, some carotenoids appear as different *cis-trans* (*Z-E*) geometrical isomers. In nature however, most carotenoids occur in the all-*trans* forms due to the way their biosynthesis proceeds and these isomeric forms are considered to be more thermodynamically stable than their *cis* counterparts (Aman *et al.*, 2005). Moreover, in some carotenoids the substituted end-group rings introduce chiral centres leading to the *R-S* optical isomerism. Trivial names are used predominantly throughout this work however, where relevant, the different stereoisomers are indicated.

1.1.3 Biosynthesis

The precursors for the biosynthesis of carotenoids, dimethylallyl diphosphate (DMAPP) and its isomer, isopentenyl diphosphate (IPP) are generated through either the cytosol-localised mevalonate (MVA) pathway or the plastid-based MVA-independent pathway known as the 2-C-methyl-D-erythritol 4-phosphate (MEP) pathway. In higher plants and some bacteria, both MVA and MEP pathways operate. In fungi and archaea only the MVA pathway is present, whereas in cyanobacteria and green algae, DMAPP and IPP are generated through the MEP pathway only (Lohr *et al.*, 2012; Pérez-Gil & Rodríguez-Concepción, 2013). In higher plants, both pathways lead to the production of a number of important, IPP-derived secondary metabolites. Dolichols, sesquiterpenes, triterpenes, phytosterols and phytosterol derived plant hormones – brassinosteroids, are produced through the MVA pathway. The MEP pathway provides precursors for the synthesis of isoprene, monoterpenes, diterpenes, plastoquinones, polyprenols, carotenoids and chlorophylls as well as several vitamins, namely vitamin B₁ (thiamine), B₆ (pyridoxal), E (tocopherols) and K₁ (phylloquinones). Several important plant hormones, such as cytokinins and gibberellins, also originate from the MEP pathway. In order to account for the levels of plastid-derived isoprenoids it is understood that IPP, generated by the MVA pathway is transported into the chloroplast (Fraser & Bramley, 2004; Flügge & Gao, 2005). The summary of the two pathways is provided in Figure 1.3. In higher plants, carotenoids are synthesised and localised in plastids, therefore, the MEP pathway is discussed in further detail.

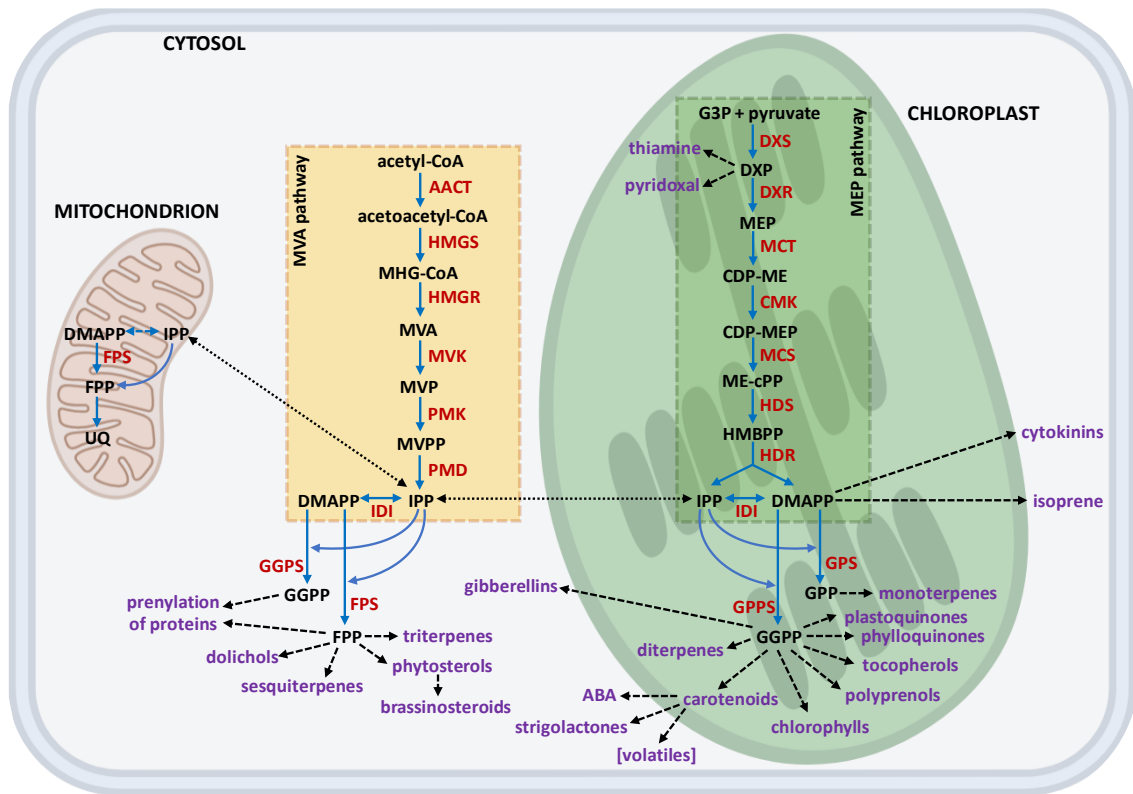


Figure 1.3. Summary of the MVA and MEP pathways in higher plants leading to the production of carotenoids and other IPP-derived secondary metabolites. Compounds and enzymes within the pathways are in black and red, respectively. The derivatives of both pathways are indicated in purple. Substrates of the pathways listed in alphabetical order: ABA – abscisic acid; CDP-ME – 4-(cytidine 5'-diphospho)-2-C-methyl-D-erythritol; CDP-MEP – 2-phospho-4-(cytidine 5'diphospho)-2-C-methyl-D-erythritol; DMAAP – dimethylallyl diphosphate; DXP – 1-deoxy-D-xylulose 5-phosphate; FPP – farnesyl pyrophosphate; G3P – glyceraldehyde 3-phosphate; GGPP – geranylgeranyl diphosphate; GPP – geranyl diphosphate; HMBPP – 1-hydroxy-2-methyl-2-(E)-butenyl 4-phospahte; IPP – isopentenyl diphosphate; ME-cPP – 2-C-methyl-D-erythritol 2,4-cyclodiphosphate; MEP – 2-C-methyl-D-erythritol 4-phosphate; MHG-CoA – 3-hydroxy-3-methylglutaryl CoA; MVA – mevalonic acid; MVP – 5-phosphomevalonate; MVPP – 5-diphosphomevalonate; UQ – ubiquinone. Enzymes operating in the pathways listed in alphabetical order: AACT – acetoacetyl-CoA thiolase; CMK – 4-(cytidine 5'-diphospho)-2-C-methyl-D-erythritol kinase; DXR – 1-deoxy-D-xylulose 5-phosphate reductoisomerase; DXS – 1-deoxy-D-xylulose 5-phosphate synthase; FPS – farnesyl pyrophosphate synthetase; GGPS – geranylgeranyl diphosphate synthase; GPPS – geranyl diphosphate synthase; HDR – 1-hydroxy-2-methyl-2-(E)-butenyl 4-diphosphate reductase; HDS – 1-hydroxy-2-methyl-2-(E)-butenyl 4-diphosphate synthase; HMGR – 3-hydroxy-3-methylglutaryl CoA reductase; HMGS – 3-hydroxy-methylglutaryl CoA synthase; IDI – isopentenyl-diphosphate isomerase; MCS – 2-C-methyl-D-erythritol 2,4-cyclodiphosphate synthase; MCT – 2-C-methyl-D-erythritol 4-phosphate cytidyl transferase; MVK – mevalonate kinase; PMD – phosphomevalonate decarboxylase; PMK – 5-phosphomevalonate kinase. Figure adapted from Akhtar *et al.* (2017) and Tetali (2018).

The MEP pathway begins with the condensation reaction between pyruvate and glyceraldehyde 3-phosphate (G3P) to produce 1-deoxy-D-xylulose 5-phosphate (DXP). This reaction is catalysed by 1-deoxy-D-xylulose 5-phosphate synthase (DXS). Isomerisation and reduction of DXP by 1-deoxy-D-xylulose 5-phosphate reductoisomerase (DXR) produces 2-C-methyl-D-erythritol 4-phosphate (MEP). Evidence suggest that DXS and DXR catalyse the rate-limiting steps of the MEP pathway (Estévez *et al.*, 2001; Carretero-Paulet *et al.*, 2006). MEP is converted by 2-C-methyl-D-erythritol 4-phosphate cytidyl transferase (MCT) to 4-(cytidine 5'-diphospho)-2-C-methyl-D-erythritol (CDP-ME) which is further converted by 4-(cytidine 5'-diphospho)-2-C-

methyl-D-erythritol kinase (CMK) to 2-phospho-4-(cytidine 5'diphospho)-2-C-methyl-D-erythritol (CDP-MEP). 2-C-methyl-D-erythritol 2,4-cyclodiphosphate synthase (MCS) converts CDP-MEP to 2-C-methyl-D-erythritol 2,4-cyclodiphosphate (ME-cPP). Through the action of 1-hydroxy-2-methyl-2-(E)-butenyl 4-diphosphate synthase (HDS), ME-cPP is converted to 1-hydroxy-2-methyl-2-(E)-butenyl 4-phosphate (HMBPP). HMBPP is finally converted to a mixture of IPP and DMAPP at the 5 to 1 ratio. This step is catalysed by 1-hydroxy-2-methyl-2-(E)-butenyl 4-diphosphate reductase (HDR). IPP and DMAPP, the immediate precursors of carotenoids, are interconverted into each other by isopentenyl-diphosphate isomerase (IDI). Figure 1.4 illustrates the steps of IPP and DMAPP synthesis from pyruvate and G3P.

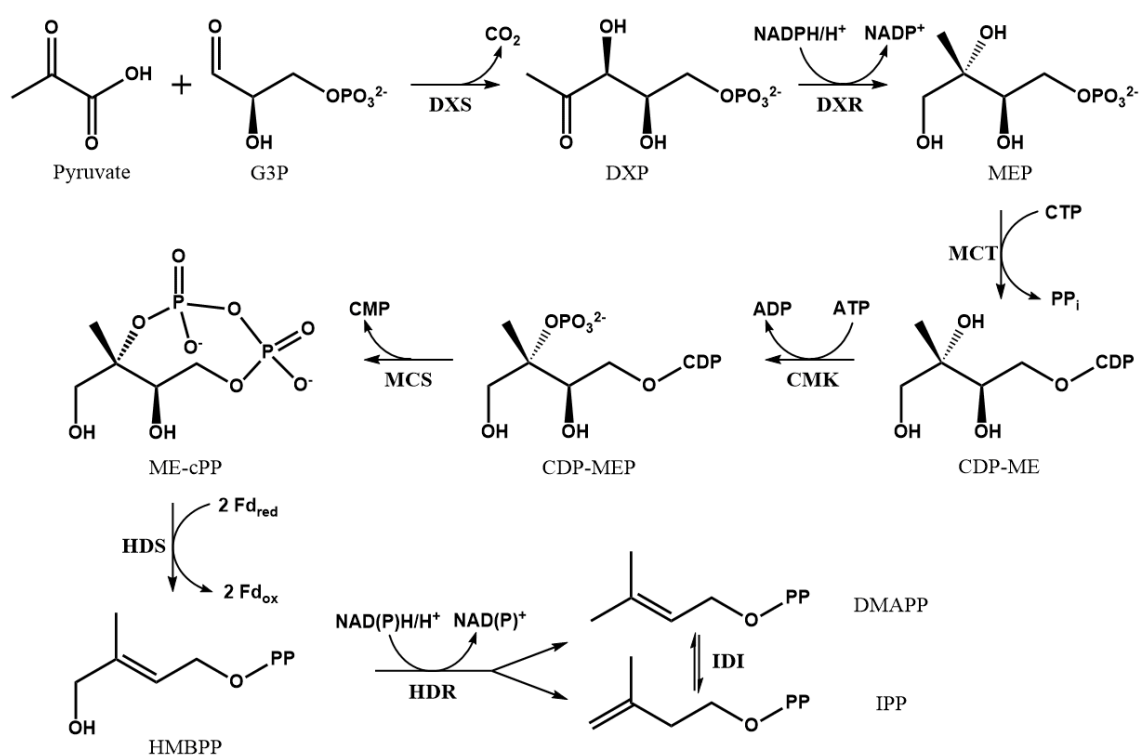


Figure 1.4. Formation of DMAPP and IPP in the MEP pathway. For names of the intermediates and enzymes refer to Figure 1.3. Some cofactors required for the reactions to take place are indicated. CDP – cytidine diphosphate; CMP – cytidine monophosphate; CTP – cytidine triphosphate; Fd_{ox} – oxidised form of ferredoxin; Fd_{red} – reduced form of ferredoxin; PP_i – pyrophosphate. Adapted from Fraser & Bramley (2004) and Qidwai *et al.* (2014).

The initiation of chain elongation (Figure 1.5) starts with isomerisation of IPP to DMAPP and subsequent head-to-tail joining of IPP and DMAPP to generate geranyl pyrophosphate (GPP). GPP, a C_{10} -molecule, is joined with another molecule of IPP to form the C_{15} -compound farnesyl pyrophosphate (FPP). Addition of yet another IPP molecule to FPP yields geranylgeranyl diphosphate (GGPP). GGPP, a C_{20} -compound, is the immediate precursor from which carotenoids are synthesised. Extension of DMAPP with IPP molecules is catalysed by a single enzyme geranylgeranyl diphosphate synthase (GGPS). Another enzyme, geranyl diphosphate synthase (GPS), catalyses joining of IPP and DMAPP to form GPP, however this enzyme is not

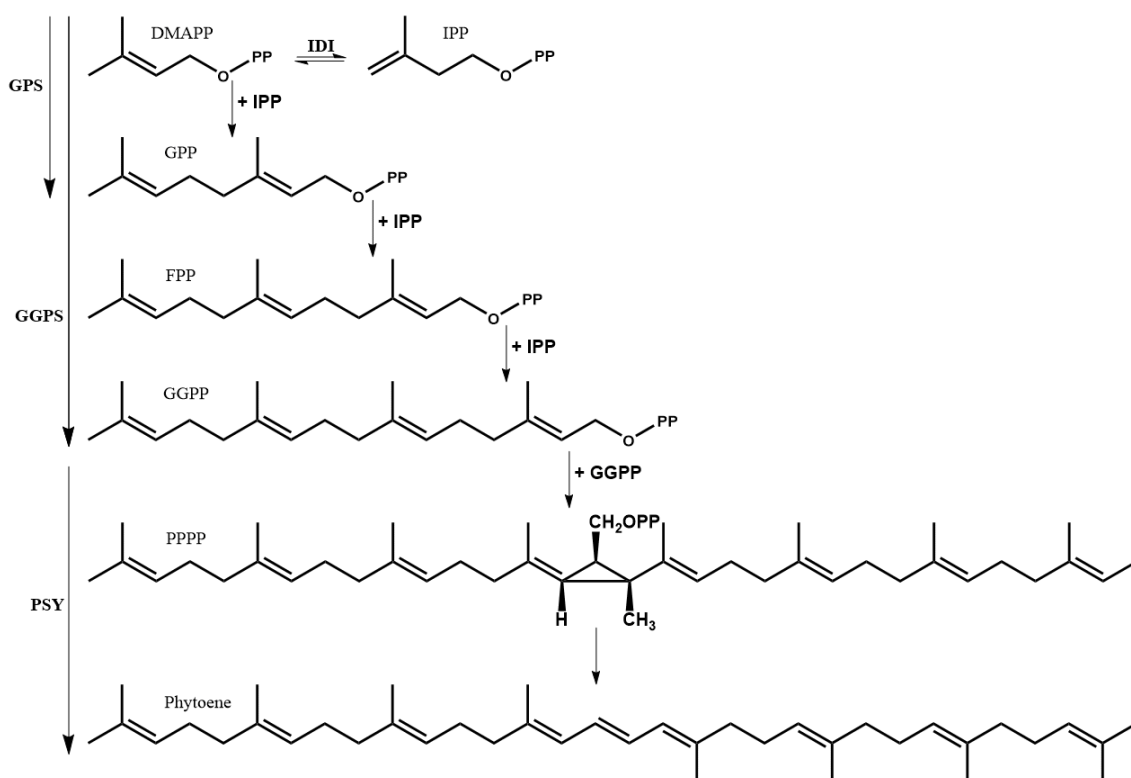


Figure 1.5. Synthesis of phytoene from DMAPP and IPP. Intermediates of the pathway listed in alphabetical order: DMAPP – dimethylallyl diphosphate; FPP – farnesyl diphosphate; GGPP – geranylgeranyl diphosphate; GPP – geranyl diphosphate; IPP – isopentenyl diphosphate; PPPP – pre-phytoene diphosphate. Enzymes listed in the alphabetical order: GGPS – geranylgeranyl diphosphate synthase; GPS – geranyl diphosphate synthase; IDI – isopentenyl-diphosphate isomerase; PSY – phytoene synthase. Reproduced with modifications from Fraser & Bramley (2004).

involved in carotenoid synthesis but instead participates in the biosynthesis of monoterpenes. Phytoene synthase (PSY) catalyses a two-step reaction resulting in the formation of phytoene from two molecules of GGPP. The first step is a head-to-head condensation of two all-*trans* GGPP molecules to form an intermediate pre-phytoene diphosphate (PPPP). The second step involves elimination of the diphosphate group and stereoselective proton abstraction to yield the final, colourless product, phytoene. In most carotenoid-synthesising organisms, including plants, phytoene is predominantly present as the 15-*cis* isomer (Fraser & Bramley, 2004).

Phytoene is converted into the red carotenoid all-*trans* lycopene in a series of desaturation and isomerisation reactions (Figure 1.6). In higher plants and cyanobacteria, the first two steps involve the action of phytoene desaturase (PDS) which introduces two *trans*-double bonds at C₁₁ and C_{11'} to form light yellow ζ-carotene via the colourless intermediate phytofluene. ζ-carotene *cis-trans* isomerase (ZISO) acts on the C₁₅-C_{15'} *cis*-double bond of ζ-carotene changing its configuration to *trans*. Further action of ζ-carotene desaturase (ZDS) on the generated product introduces two *cis*-double bonds at the C₇ and C_{7'} positions leading to the production of the red compound 9,9',7'-tetra-*cis*-lycopene (pro-lycopene) via the intermediate neurosporene. Carotene *cis-trans* isomerase (CRTISO) acts on pro-lycopene to introduce the all-*trans*-

configuration (Fraser & Bramley, 2004; Gemmecker *et al.*, 2015). Interestingly, phytoene desaturase from bacteria and fungi (CRTI) forms all-*trans* lycopene directly from 15-*cis* phytoene by introducing the new double bonds in *trans* configuration (Schaub *et al.*, 2012).

Lycopene is used as the substrate for cyclisation reactions to produce a vast variety of carotenoids (Figure 1.7). It can be either converted to δ -carotene via the action of lycopene ϵ -cyclase (LCY-E) or γ -carotene via the action of lycopene β -cyclase (LCY-B). δ -carotene is further converted by LCY-B into α -carotene containing one ϵ - and one β -ring. Carotenoids containing two ϵ -rings are very rare. One exception is the lettuce, *Lactuca sativa*, which is known to accumulate ϵ,ϵ -carotene generated through the action of LCY-E on δ -carotene (Cunningham & Gantt, 2001). α -carotene can be converted to α -cryptoxanthin by ϵ -ring hydroxylase (CrtR-e) which attaches a hydroxyl group to C₃ of the ϵ -ring. Further hydroxylation of α -cryptoxanthin at C_{3'} of the β -ring produces lutein. This reaction is catalysed by β -carotene hydroxylase (CrtR-b). On the other hand, γ -carotene is converted by LCY-B

to β -carotene by the addition of another β -ring. β -carotene undergoes hydroxylation at either C₃ only or C₃ and C_{3'} to produce β -cryptoxanthin and zeaxanthin, respectively. Hydroxylation of β -carotene is catalysed by CrtR-b. In tomato, two functionally identical lycopene β -cyclases (LCY-B and CYC-B) and β -carotene hydroxylases (CrtR-b1 and CrtR-b2), exhibiting tissue-specific

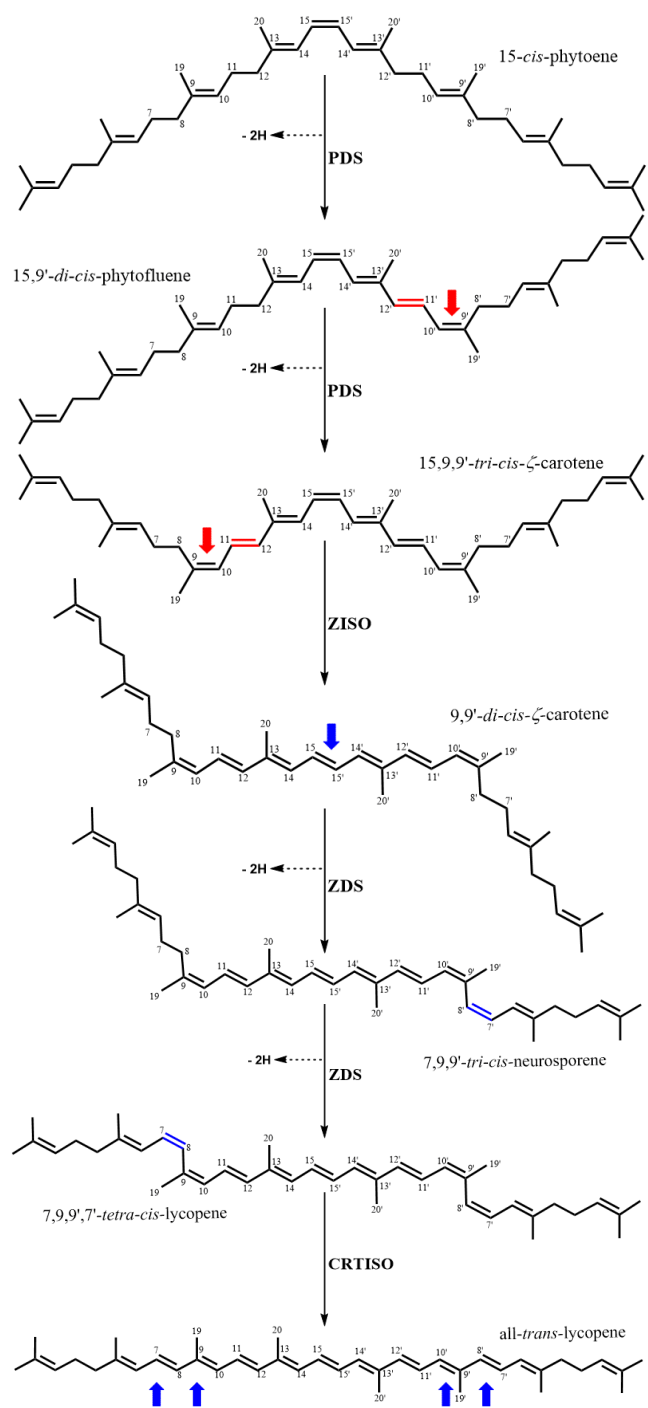


Figure 1.6. Synthesis of lycopene from phytoene in higher plants. Red and blue bonds indicate new double bonds introduced in *trans* and *cis* configurations, respectively. Red and blue arrows indicate *trans-cis* and *cis-trans* transitions, respectively. CRTISO – carotene *cis-trans* isomerase; PDS – phytoene desaturase; ZDS – ζ -carotene desaturase; ZISO – ζ -carotene *cis-trans* isomerase. Reproduced with modifications from Gemmecker *et al.* (2015).

expression, have been isolated. LCY-B and CrtR-b1 are expressed in chloroplasts, so they are limited to the green parts of the plant, whereas CYC-B and CrtR-b2 are chromoplast-specific enzymes expressed in flowers and fruit (Ronen *et al.*, 2000; Galpaz *et al.*, 2006). Zeaxanthin is

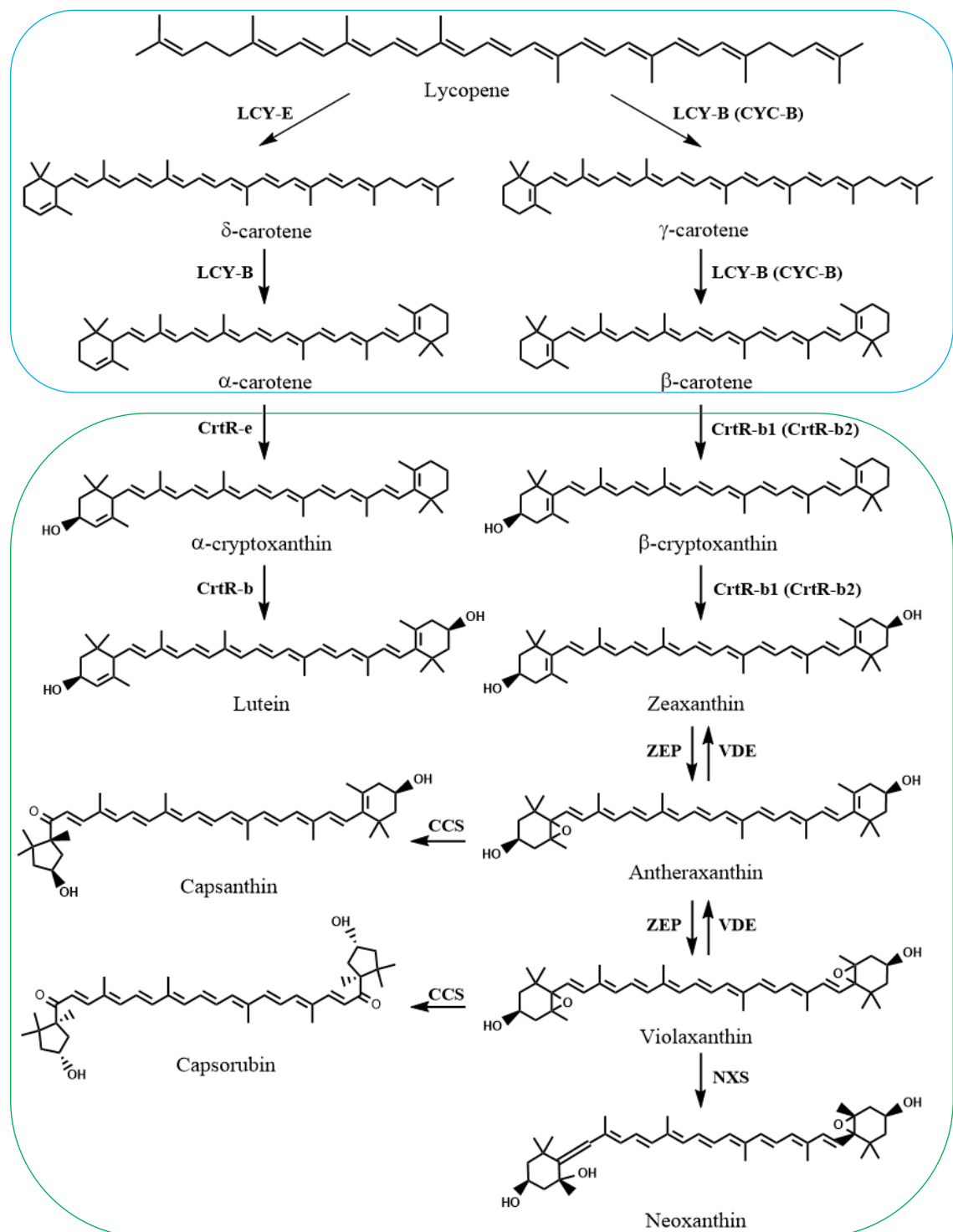


Figure 1.7. Synthesis of carotenoids from lycopene. Carotenes are enclosed by the blue box, xanthophylls – green. Where relevant, the two forms of lycopene β-cyclase and β-carotene hydroxylase are indicated. The conversion of δ-carotene to ε,ε-carotene by the action of LCY-E is not shown. Enzymes listed in alphabetical order: CCS – capsanthin/capsorubin synthase; CrtR-b1 – β-carotene hydroxylase, chloroplast-specific; CrtR-b2 – β-carotene hydroxylase, chromoplast-specific; CrtR-e – ε-ring hydroxylase; CYC-B – lycopene β-cyclase, chromoplast-specific; LCY-B – lycopene β-cyclase, chloroplast-specific; LCY-E – lycopene ε-cyclase; NXS – neoxanthin synthase; VDE – violaxanthin de-epoxidase; ZEP – zeaxanthin epoxidase. Reproduced with modifications from Fraser & Bramley (2004).

further converted to violaxanthin by zeaxanthin epoxidase (ZEP) through a mono-epoxidated intermediate antheraxanthin. Violaxanthin can be de-epoxidated back to zeaxanthin by violaxanthin de-epoxidase (VDE). This conversion of zeaxanthin to violaxanthin and vice versa is known as the xanthophyll cycle. However, violaxanthin can be further metabolised to another xanthophyll, neoxanthin. This is done with help of the enzyme, neoxanthin synthase (NXS). Two red xanthophylls, capsanthin and capsorubin, which are relatively unique to the mature fruit of peppers, are formed from antheraxanthin and violaxanthin, respectively. The enzyme required for this conversion is capsanthin/capsorubin synthase (CCS).

However, the pathway outlined above is not complete. In fact, carotenoids serve as substrates in the synthesis of other secondary metabolites. Neoxanthin is a precursor of the plant hormone ABA. Neoxanthin is believed to undergo isomerisation to its 9-*cis* isomer which is then cleaved by 9-*cis*-epoxycarotenoid dioxygenase (NCED) to xanthoxin. Xanthoxin is oxidised to ABA via the intermediate abscisic aldehyde. The 9-*cis* isomer of violaxanthin can also be cleaved by NCED to yield xanthoxin. However, an isomerase acting upon violaxanthin or neoxanthin has not yet been identified (Nambara & Marion-Poll, 2005). β -carotene gives rise to a group of plant hormones known as strigolactones. The first step involves isomerisation of β -carotene to its 9-*cis* isomer followed by the cleavage with carotenoid cleavage deoxygenase (CCD) to 9-*cis*- β -apo-10'-carotenal. Another CCD cleaves and rearranges this product to carlactone. Carlactone is a precursor for the biosynthesis of strigolactones (Brewer *et al.*, 2016). Carotenoids are also precursors for a number of open chain and cyclic volatile compounds. CCD-mediated oxidative cleavage of lycopene produces lemon-scented 6-methyl-5-hepten-2-one which can be further converted to another volatile compound 6-methyl-5-hepten-2-ol (Zhang *et al.*, 2015). Geranylacetone, a fruity scented compound, is the cleavage product of ζ -carotene (Vogel *et al.*, 2008). β -carotene is a precursor for the formation of β -ionone, β -cyclocitral and β -damascenone. β -cyclocitral is a newly identified regulator which controls root growth by promoting cell division (Dickinson *et al.*, 2019).

1.1.4 Xanthophyll cycle

Under high light irradiance, the xanthophyll cycle, placed within the carotenoid biosynthetic pathway, promotes dissipation of excess excitation energy by the mechanism known as non-photochemical quenching (NPQ). In higher plants, the cycle involves conversion of violaxanthin to zeaxanthin via the mono-epoxidated intermediate antheraxanthin. This reaction is catalysed by violaxanthin de-epoxidase (VDE). VDE is confined to the thylakoid lumen and functions in a pH-dependent manner. When light reaching the photosynthetic tissues is greater than what is required for the saturation of photosynthesis, the proton-motive force across the thylakoid membrane exceeds the ATPase activity leading to the acidification of the thylakoid lumen. This

decrease in pH activates VDE which binds to the thylakoid membrane where violaxanthin is found. In the presence of the VDE cofactor ascorbate, which acts as a reducing agent, violaxanthin is de-epoxidised to zeaxanthin (Jahns *et al.*, 2009). Zeaxanthin quenches the singlet excited state chlorophylls ($^1\text{Chl}^*$) and then dissipates the excess excitation energy within the LHCs as heat, thus preventing generation of reactive oxygen species (ROS). ROS, if not removed, cause oxidative damage to membrane lipids and other cellular components (Niyogi *et al.*, 1998; Müller *et al.*, 2001). When the light intensity decreases, the proton-motive force across the thylakoid membrane slows down, rising the pH inside the thylakoid lumen. This inactivates VDE which dissociates from the membrane back into the lumen. On the stromal side, zeaxanthin epoxidase (ZEP) converts zeaxanthin back to violaxanthin which completes the cycle. This process is summarised in Figure 1.8.

Although, the cycle provides photoprotection to the photosynthetic apparatus against light-induced damage, it is not entirely understood why de-epoxidation of violaxanthin to zeaxanthin is necessary to achieve this. Conversion of violaxanthin to zeaxanthin increases the number of conjugated double bonds from 9 to 11 and generally, increasing the length of chromophore decreases electronic transition energies. Thus, the lowest singlet excited state (S_1) of zeaxanthin might be just at a slightly lower energy level than the lowest chlorophyll states thus facilitating an effective energy transfer from chlorophyll to zeaxanthin. On the opposite, the S_1 state of violaxanthin might be at a slightly higher energy level than the lowest chlorophyll state thus

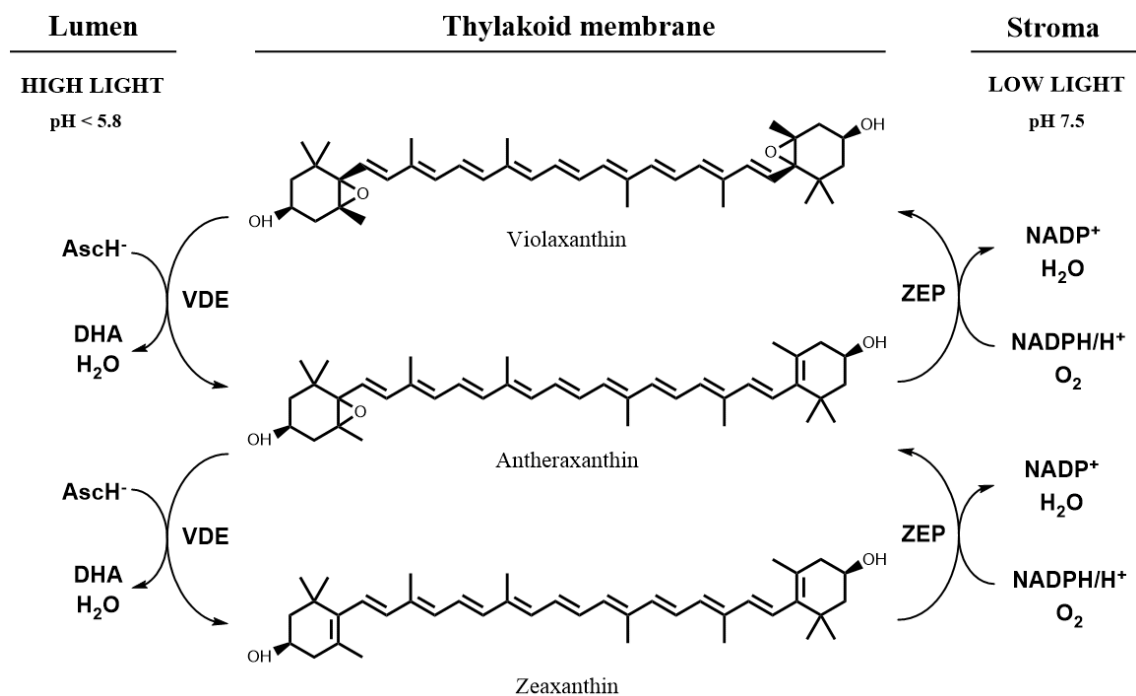


Figure 1.8. Summary of the xanthophyll cycle in higher plants. Conversion of violaxanthin to zeaxanthin takes place under high light irradiance when the pH of the thylakoid lumen drops. AscH⁻ – ascorbate monoanion; DHA – dehydroascorbic acid; VDE – violaxanthin de-epoxidase; ZEP – zeaxanthin epoxidase. Reproduced with modifications from Racsko & Schrader (2012).

being unable to accept energy from the chlorophyll. Instead, violaxanthin, which accumulates under light limiting conditions, might transfer energy to the chlorophyll thus contributing to light capture (Frank *et al.*, 2000). However, this mechanism has not been proven conclusively. A separate experiment concluded that the S_1 states of zeaxanthin and violaxanthin are, in fact, both lower than the lowest chlorophyll states (Polívka *et al.*, 1999). Zeaxanthin is a much stronger quencher of chlorophyll fluorescence than violaxanthin (Avital *et al.*, 2006) but neither of the mechanisms can explain why. It may be possible that the structural differences between zeaxanthin and violaxanthin are more important than the differences between their S_1 state levels (Müller *et al.*, 2001). Further work is necessary to discover the mechanism by which quenching of chlorophyll fluorescence is achieved by zeaxanthin.

1.1.5 Carotenoid deposition and storage

In plants, carotenoids are synthesised and stored within the plastids. Two types of plastids, namely chloroplasts and chromoplasts, are the most relevant in the context of carotenoid biosynthesis and sequestration. In the chloroplast, carotenoids are mainly localised within the thylakoid membranes. Chloroplasts have limited capacity to store carotenoids. This is to ensure that the ratio of carotenoids to chlorophylls is maintained at the levels optimal for efficient photosynthesis and photoprotection (Sun *et al.*, 2018). Chromoplasts are the main carotenoid-containing plastids found in flowers, fruit and roots. They have a greater capacity to store carotenoids than chloroplasts as they do not carry out photosynthesis. Chromoplasts are derived from other plastids including chloroplasts. In fact, fruit ripening, for example in tomato, is marked by chloroplast to chromoplast transition accompanied by a massive carotenoid accumulation (Barsan *et al.*, 2012). The most important structural changes occurring during the transition of chloroplasts to chromoplast involve thylakoid disintegration as well as increase in the number and size of plastoglobuli. The summary of the changes occurring during this process is provided in Figure 1.9. The carotenoid content of chromoplasts varies amongst plant species and even the plant's organs (Sun *et al.*, 2018). Tomato chromoplasts accumulate mainly lycopene crystals (Jeffery *et al.*, 2012). Pepper chromoplasts accumulate carotenoids mostly in esterified forms (Hornero-Méndez & Mínguez-Mosquera, 2000). Esterification of carotenoids reduces their degradation. Moreover, carotenoid esterification is used by many flowers to overproduce and accumulate very high levels of carotenoids in their chromoplasts (Ariizumi *et al.*, 2014).

Animals, which generally do not produce carotenoids, obtain these from the consumed diet. Following ingestion of carotenoid-containing foods, these deposit in various body parts such as the skin, flesh, fat, feathers, beaks and eyes (Britton, 1996; McGraw *et al.*, 2004). Carotenoids are also responsible for the yellow colouration of the egg yolks (Britton, 1996). Orange

discolouration of the skin known as carotenosis, can be caused by excessive dietary or supplementary intake of carotenoids (Takita *et al.*, 2006).

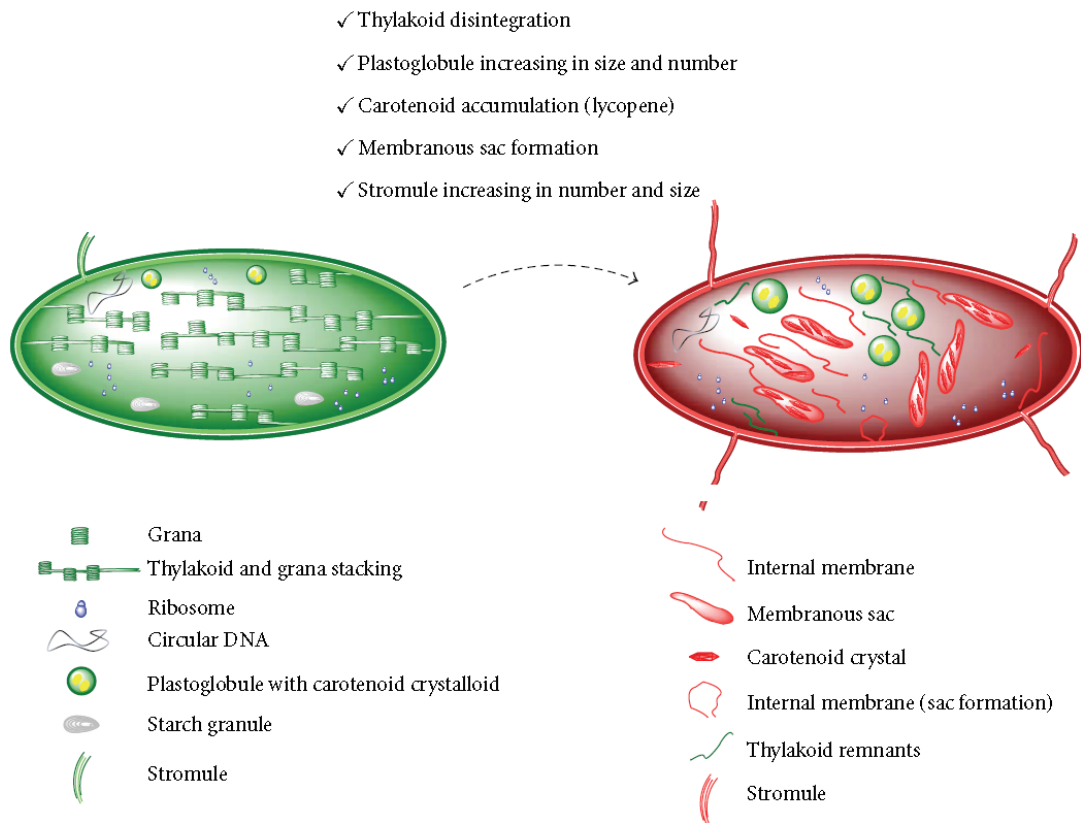


Figure 1.9. Summary of the structural changes that take place during chloroplast to chromoplast transition (from Bian *et al.*, 2011).

1.1.6 Market value and uses of carotenoids

Due to a high commercial and nutraceutical value of carotenoids, the carotenoid biosynthetic pathway has been the focus of extensive research involving bacterial, algal, fungal and plant homologous and heterologous expression systems. The global market for carotenoids was worth 1.4 bn USD in 2016 and, with a compound annual growth rate (CAGR) of 5.7%, it is predicted to reach 2.0 bn USD by 2022.

Although, many carotenoids are present in the environment, only a handful is used commercially. These are: annatto, astaxanthin, β -carotene, β -apo-8'-carotenal (apocarotenal), β -apo-8'-carotenal ester, canthaxanthin, capsanthin, lutein, lycopene and zeaxanthin. Astaxanthin is expected to dominate the global carotenoid production in the next few years. In 2016 astaxanthin accounted for 22% of the global carotenoid production worth of 267.5 M USD. By 2022, the global market for astaxanthin is estimated to be worth 426.9 M USD with CAGR of 8.1% (McWilliams, 2018). In 2016, capsanthin was worth 285.0 M USD, β -carotene – 246.2 M, lutein – 225.0 M, annatto – 170.0 M, lycopene – 107.0 M, canthaxanthin – 72.3 M, zeaxanthin – 45.9 M, β -apo-8'-carotenal – 22.5 M and β -apo-8'-carotenal ester – 5.0 M (McWilliams, 2018).

The price per unit (typically kg) varies greatly depending on the carotenoid itself, the source the carotenoid is obtained from or its mode of production, its purity and the country of its origin. For example, astaxanthin is available at an average price of 1 139 USD kg⁻¹, lutein at a much lower price of 264 USD kg⁻¹, zeaxanthin – 180 USD kg⁻¹, lycopene – 172 USD kg⁻¹, β-carotene – 121 USD kg⁻¹ and annatto for as little as 4.0 USD kg⁻¹ (IndiaMART InterMESH, 2019; Lepro PharmaCompass, 2019). The average price excludes laboratory standards which are sold in small quantities at a much greater purity and, so it follows, at a greater price as well.

The major producers of carotenoids, at the same time their major consumers, are India and China. The rise of India and China as the major producers of carotenoids was possible due to availability of raw materials and cheap labour (McWilliams, 2018). Carotenoids are either obtained by extraction from plant, algal or fungal material, produced by microbial fermentation or chemical synthesis. The use of natural sources to obtain carotenoids is predicted to increase the most in the next few years (McWilliams, 2018). Nevertheless, obtaining carotenoids from plant sources is highly dependent on seasonal and geographic variability. Nowadays, however, most carotenoids are obtained from chemical synthesis with BASF SE (Germany), Hoffman-La Roche (Switzerland), Royal DSM N.V. (The Netherlands), Chr. Hansen A/S (Denmark), FMC Corporation (US), Kemin Industries, Inc. (US) and Cyanotech Corporation (US) being the major producers (Pasarín & Rovinaru, 2018; McWilliams, 2018). Only eight out of all known carotenoids, including five C₄₀-carotenoids and three apocarotenoids are chemically synthesised at a commercial scale due to economic and technological reasons. These are astaxanthin, β-carotene, canthaxanthin, lycopene, zeaxanthin and the three apocarotenoids β-apo-8'-carotenal, ethyl β-apo-8'-carotenoate and citranaxanthin (Mayer & Isler, 1971).

Carotenoids were primarily valued as natural colourants in animal feed as well as food and beverage industries. They are added to animal feed in order to improve the appearance of meat, meat products and fish and to enhance food palatability. Carotenoids are also used in bakery products, other confectionery and occasionally, in cosmetics, mainly due to their antioxidant potential and vitamin A properties (Pasarín & Rovinaru, 2018). However, a growing, complemented by scientific evidence, awareness among consumers about the health benefits of carotenoids, greater emphasis on a healthy lifestyle and rising incidence of various diseases across the globe, has been driving an increase in the use of carotenoids as dietary supplements and nutraceuticals. Carotenoid supplements are taken to prevent deficiency-related disorders, most notably hypovitaminosis A. Other carotenoids, namely lutein and zeaxanthin, have been linked to preventing degenerative eye diseases, with strongest evidence in age-related macular degeneration (AMD) as found by the Age-Related Eye Disease Study, AREDS (Age-Related Eye Disease Study Research Group, 2007) and other studies described in later sections.

1.2 Age-related macular degeneration (AMD)

1.2.1 Description, aetiology and current treatments

Age-Related Macular Degeneration (AMD) is a painless medical condition, characterised by deterioration of the central part of the retina encompassing the central visual field. The central visual field is defined as 10° of the visual angle (Horton Hoyt, 1991a; Horton & Hoyt, 1991b) projecting onto the middle 3 mm of the retina (Wandell, 1995; Valberg, 2005) and ophthalmologically it is described as the *macula lutea*, henceforth, the macula (Provis *et al.*, 2013). AMD usually affects both eyes (Wang *et al.*, 1998) and leads to blurring or loss of the central vision. Although, the macula comprises only about 2% of the entire retinal surface, more than a half of the visual cortex is devoted to processing the information gathered from it (Horton & Hoyt, 1991a; Horton & Hoyt, 1991b). The very middle of the macula is where the *fovea centralis*, henceforth, the fovea is situated. It covers about 3° of the visual field which corresponds to a region of approximately 1 mm in diameter. It is an area deprived of blood



Figure 1.10. Page of print (left) and a group of faces (right) as seen in a conventional photograph (A), at one moment in time (B) and as a simulated view through the eyes of a person with a blind spot in the centre of their visual field like in the case of AMD (C). The top two pictures (A), illustrate the clarity of vision one obtains while scanning the page or the faces in a normal fashion. Middle pictures (B) show the views when fixing the sight at one spot at any one moment which clearly illustrates that the very centre of the visual field is the only place of the sharp, clear vision and even a small deviation from this field makes the recognition of the text or faces very difficult. Bottom pictures (C) illustrate how this central, sharp vision is affected when a person suffers from AMD; reading and recognition of faces becomes impossible. The images appear as such when viewed from a normal reading distance of 36 cm from the text and as standing at the distance of 2.7 m from the people (Marmor & Marmor, 2010).

vessels and because of this, it appears as a depression within the macula. The blood vessels of the fovea have been replaced by densely packed cone cells. Out of all the cones that are found on the entire retinal surface, the majority of them are located within the fovea and their spatial density decreases dramatically the closer one moves towards the peripheral retina. Both, the high density of cones and the lack of blood vessels at the fovea, results in high-resolution visual acuity at this region (Provis *et al.*, 1998).

The vision of a person affected by AMD is often described as a sight obstructed by a black spot in the middle with the rest of the visual field preserved. However, this does not do justice to the devastating effects that AMD has on peoples' ability to see. Although, AMD rarely leads to a complete blindness, the macula is the only place on the entire retina that is responsible for generating sharp vision, important for precise tasks such as face recognition, reading and driving. The further from the macula, the blurrier the object one is looking at becomes. Once the central vision is lost as the consequence of AMD, any remaining visual functions are profoundly affected, severely impinging on the quality of life of a person suffering from AMD (Marmor & Marmor, 2010). A very good approximation of this visual damage is depicted in Figure 1.10.

AMD is classified into early and late stages (Fine *et al.*, 2000) depending on the extent of the visual impairment (Cook *et al.*, 2008). The early stages, when the vision is still well preserved, are characterised by the presence of large drusen (Figure 1.11A) – build-ups of extracellular debris consisting of proteins and lipids between the Bruch's membrane and the retinal pigment epithelium (Bressler *et al.*, 1994). 14% of patients with large drusen will then progress into late AMD, when the vision is severely impaired (Klein *et al.*, 2002). Overall, the people with large drusen are 6 times more likely to progress into late AMD as compared to those not having such depositions (Wang *et al.*, 2003). Late AMD can be further subdivided into wet (neovascular or exudative) and dry (atrophic or nonexudative) forms. The dry form of AMD comprises 80 – 85% while the wet form 15 – 20% of all the late AMD cases (Bonastre *et al.*, 2002). Although, the wet type of AMD is less prevalent than the dry form, wet AMD is responsible for approximately 75% of severe cases of visual impairment (Klein *et al.*, 1997). Late, wet AMD is characterised by choroidal neovascularisation – growth of abnormal and very fragile blood vessels through Bruch's membrane into the sub-retinal pigment epithelium or sub-retinal spaces. These blood vessels leak blood and fluid which build up beneath the retina leading to serous or haemorrhagic detachment of the retinal pigment epithelium (Figure 1.11C). This, if untreated, leads to fibrovascular scarring and permanent loss of the central vision. Due to the character of the condition, wet AMD results in a sudden and profound worsening of the central vision. However, there are treatment options available for wet AMD which involve laser photocoagulation,

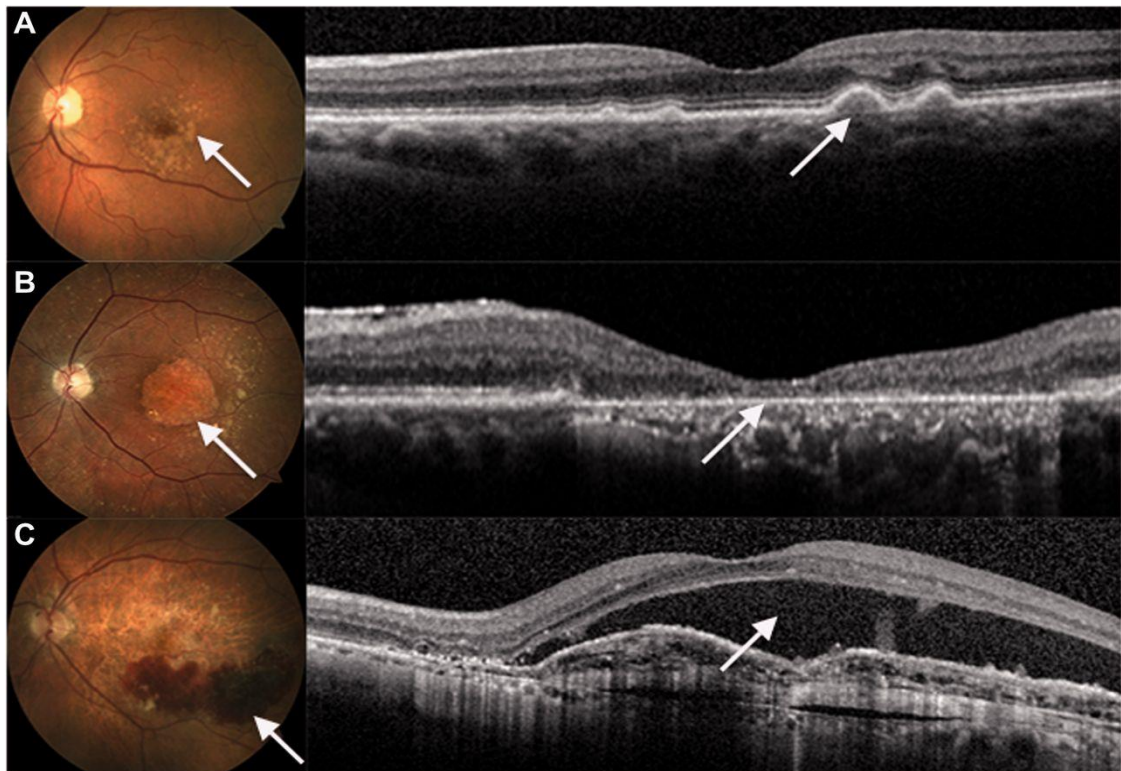


Figure 1.11. Stages of AMD showing the interior surface of the eye (left) and the corresponding optical coherence tomography images of the relevant retinal ultrastructure. **(A)** Moderate AMD with drusen accumulations below the retinal pigment epithelium indicated by the arrows. **(B)** Late, dry AMD with an extensive geographic atrophy lesion at the site of the macula. Loss of photoreceptors is visible as a central retinal thinning, indicated on the right by the arrow. **(C)** Late, wet AMD with an extensive leakage from abnormal blood vessels. The sub-retinal haemorrhage, which led to the detachment of the retinal pigment epithelium from the retina is indicated on the right by the arrow (Broadhead *et al.*, 2015).

photodynamic therapy and the application of anti-VEGF medication (Fine *et al.*, 2000; Cook *et al.*, 2008). These treatments lead to a relative rapid reduction in the accumulated fluids and therefore, can greatly improve the visual acuity. However, once a profound damage takes place, this cannot be reversed. Moreover, only around 30% of patients will benefit from the laser treatment (Bonastre *et al.*, 2002). Late, dry AMD is characterised by the presence of geographic atrophy (Figure 1.11B). The geographic atrophy forms when an extensive patch of photoreceptors on the retina is lost (Holz *et al.*, 2014). Although dry AMD progresses much slower than wet AMD, there is no treatment available for it and it leads to a progressive deterioration of vision and eventually severe its impairment (Fine *et al.*, 2000; Cook *et al.*, 2008).

AMD is an incurable condition and once it develops, it eventually leads to a visual impairment. Currently, there are no treatment options available to reverse the visual loss. Therefore, a lot of research effort focuses on identifying compounds which could prevent the development of AMD in the first place or slow down the worsening of the condition. A lot of the attention has been given to two macular carotenoid pigments: lutein and zeaxanthin. These pigments are responsible for the characteristic yellow colouration from which the name for macula lutea – the yellow spot, originates (Snodderly, 1995).

1.2.2 Prevalence of AMD

Globally, AMD is the fourth leading cause of blindness (0.13%) following cataracts (1.00%), glaucoma (0.34%) and preterm birth complications (0.30%; Resnikoff *et al.*, 2004; Global Burden of Disease Study 2013 Collaborators, 2015) and the leading cause of visual loss in people over the age of 60 (Klein *et al.*, 1999; Mehta, 2015). AMD has been estimated to affect 8.7% of the worldwide population (Wong *et al.*, 2014). The incidence of AMD has a strong, positive correlation with increasing age (Vingerling *et al.*, 1995; Klein *et al.*, 1997; Rudnicka *et al.*, 2015) and therefore, the number of people affected globally is predicted to rise following the exponentially aging populations (Augood *et al.*, 2006). This rise has been estimated from 196 M in 2020 to 288 M by 2040 (Wong *et al.*, 2014). In Britain, the incidence of AMD has been shown to have increased by 30 – 40% in the last 50 years while, on the opposite end, other causes of visual impairment, such as cataracts, glaucoma and optic atrophy have decreased (Evans & Wormald, 1996). The prevalence of AMD is greater amongst the white populations than the black ones (Sommer *et al.*, 1991; Klein *et al.*, 1999; Friedman *et al.*, 2004) and women tend to be more often affected than men (Klein *et al.*, 1995; Klein *et al.*, 1997; Javitt *et al.*, 2003), although not all studies agree with this and report that males and females are affected equally (Vingerling *et al.*, 1995). Interestingly, excluding age, tobacco smoking is the major and most consistently associated risk factor with any form of AMD (Smith *et al.*, 2001).

1.2.3 Financial burden of AMD

The economic burden of AMD has been thoroughly analysed and described (Bonastre *et al.*, 2002; Brown *et al.*, 2005; Schmier *et al.*, 2006; Gupta *et al.*, 2007). The yearly budget impact of AMD in France, Germany, Italy and the United Kingdom was found to be between 51.3 and 101.1 M Euros for France and the UK, respectively with Italy and Germany placing between these two figures (Bonastre *et al.*, 2002). The research conducted by AMD Alliance International, a non-profit organisation comprising the world's leading vision research organisations working to raise the awareness of AMD, led to an estimation of the worldwide cost of the visual impairment as the result of AMD to reach 343 bn USD in 2010 with 255 bn out of this sum attributed to direct health care costs. This number is predicted to increase to 392 bn USD by 2020. Due to the increased life expectancy and greater health care costs in developed countries, AMD contributes to a much bigger proportion of the economic burden there than anywhere else (Access Economics, 2010). The total loss in gross domestic profit in the USA as the result of loss of employment and salary due to AMD, was estimated to reach 29.8 bn USD. The majority of these costs were attributed to patients below the age of 65 due to their higher employment rate as compared to the older population, even though the prevalence of AMD in this group was lower than in people above 65 years of age (Brown *et al.*, 2005).

The quality of life of people affected by AMD is another important factor that has been looked into as well. A mild form of AMD has been reported to decrease the quality of life by 17% as compared to a healthy individual. This compares to a quality of life of a person with symptomatic AIDS. Severe and very severe forms of AMD decreased the life quality by 53% and 60%, respectively. This is a greater reduction of life quality than reported by people undergoing dialysis and similar to this reported by people who underwent a severe stroke that left them in the need of constant nursing care (Brown *et al.*, 2005). Interestingly, the quality of life of AMD affected patients with varying levels of severity, was underestimated by the treating ophthalmologist by 96 – 750% for the same condition (Brown *et al.*, 2005).

1.2.4 Macular pigments – lutein and zeaxanthin

High-performance liquid chromatography (HPLC) was used to determine that lutein and zeaxanthin, both belonging to a group of chemical compounds known as xanthophylls (oxygen-containing carotenoids), were highly concentrated in the human retina (Bone *et al.*, 1988; Bone *et al.*, 1997; Bernstein *et al.*, 2001). This concentration was found to be between 0.1 and 1 mM, which is around 1 000 times greater than in any other tissue in the body (Landrum *et al.*, 1999). The dietary origin of these yellow macular pigments has been demonstrated by Malinow *et al.* (1980). In this study, it was shown that monkeys fed diets deprived of xanthophylls, lacked the characteristic yellow pigmentation of the macula in contrast to the control group which was fed a xanthophyll containing diet. Interestingly, drusen-like bodies were found to be significantly more common on the retinal pigment epithelium of the monkeys in the experimental groups as compared to the controls. Importantly, the presence of zeaxanthin at the macula cannot be attributed to its conversion from violaxanthin or neoxanthin in the body since both of these xanthophylls are present in many of the consumed vegetables as they are important in photosynthesis and plant hormone physiology, but have repeatedly been found to be absent from human plasma and organs (Khachik *et al.*, 1991; Barua & Olson, 2001; Pérez-Gálvez *et al.*, 2003; Asai *et al.*, 2008).

A clear distribution of the macular pigments within the layers of the retina can be seen when the macula is photographed under blue light, the wavelength strongly absorbed by these xanthophylls (Figure 1.12A). However, the distribution of the macular pigments throughout the retina is not uniform. Despite limited dietary sources of zeaxanthin as compared to lutein, zeaxanthin is 2.4 times more concentrated at the fovea than lutein. As the distance from the fovea increases, the concentration of the macular carotenoids falls drastically and the ratio of zeaxanthin to lutein reverses to 1:2 (Figure 1.12B). Interestingly, this change in the ratio of zeaxanthin to lutein across the retina correlates linearly with the changing ratio of cones to rods across the same area. It has been suggested that a selective mechanism of uptake of zeaxanthin

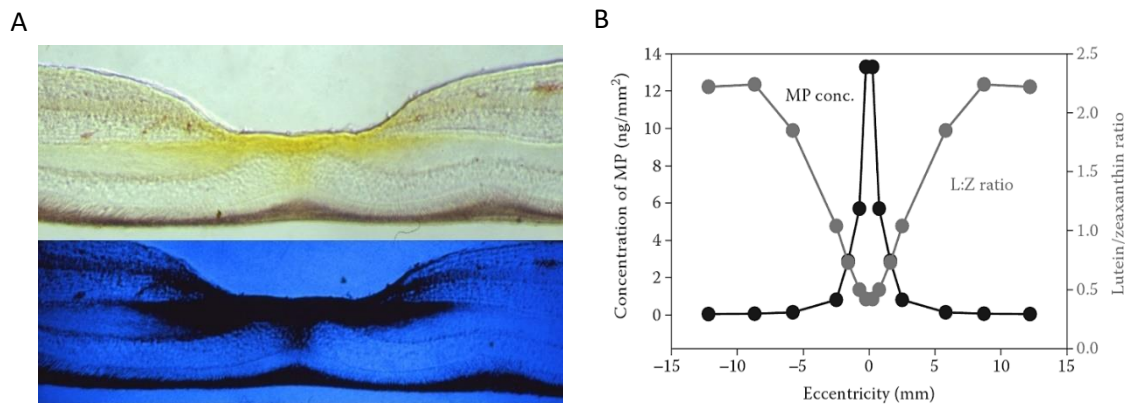


Figure 1.12. (A) Cross-section through a primate retina focused at the macula photographed in white light (top) and blue light (bottom). The extent of the macular pigments in the retinal layers is clearly visible. Macular pigments appear black in the blue light as they absorb very strongly in this part of the spectrum and therefore, appear yellow in colour (Snodderly *et al.*, 1984; Snodderly, 1995). (B) Distribution of total macular pigments across the retina (black line) and the ratio of lutein to zeaxanthin (grey line) across the same area (Landrum *et al.*, 2010).

and lutein by cones and rods, respectively, may be responsible for this correlation (Bone *et al.*, 1988). Moreover, Bone *et al.* (1993) have discovered that around a half of zeaxanthin in the retina is of dietary origin and the remaining half, consist of an uncommon stereoisomer of zeaxanthin, *meso*-zeaxanthin (Figure 1.13). Initially, it was suggested that *meso*-zeaxanthin is derived from retinal lutein through a biochemical conversion at the retina (Bone *et al.*, 1993; Johnson *et al.*, 2005). More recently however, *meso*-zeaxanthin has been identified in certain food products which points to its dietary origin (Prado-Cabrero *et al.*, 2016). Interestingly, the human diet is rich in many other carotenoids which, along with their metabolites, are present both in blood and body tissues in relative high amounts. However, these do not accumulate in the macula similarly to lutein and zeaxanthin and only trace amounts of these have been detected in the retina (Handelman *et al.*, 1992; Khachik *et al.*, 1997a; Khachik *et al.*, 1997b; Yeum *et al.*, 1999). This suggest a selective and active transport of macular pigments from the blood into the specific locations within the retina.

It is still not entirely clear what the role of lutein and zeaxanthin at the retina is. The characteristic chemical structure of the macular xanthophylls, marked by the presence of an extensive system of conjugated double bonds and the hydroxylated rings at both ends of the molecules (Figure 1.13), allows them to absorb high energy light in the blue and UV ranges of the spectrum which could cause a photochemical damage to the delicate structures of the retina (Glickman, 2011). Lutein is oriented in parallel and perpendicular directions with respect to the plane of the cell membrane which makes lutein a much better filter of the blue light than zeaxanthin (Sujak *et al.*, 1999). Zeaxanthin and *meso*-zeaxanthin are found to be at the perpendicular orientation with respect to the cell membranes. However, the structural

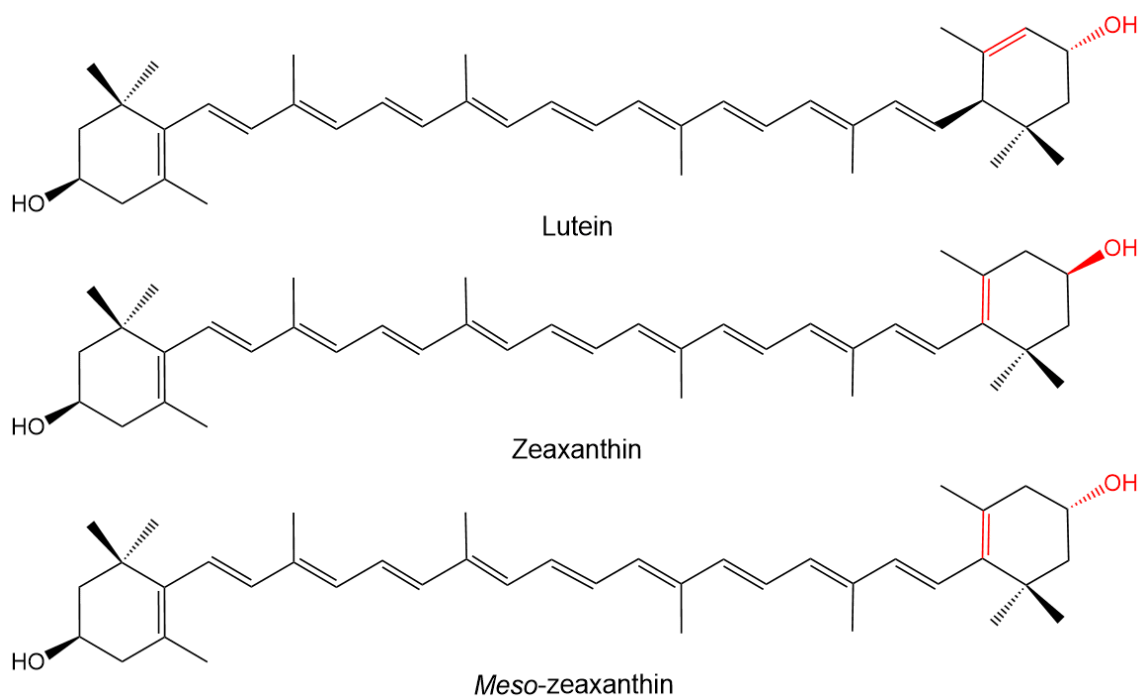


Figure 1.13. Chemical structures of lutein, zeaxanthin and *meso*-zeaxanthin. These C₄₀ structures are derived from joined isoprenoid units, resulting in an assembly of conjugated double bonds allowing the molecules to absorb in the visible spectrum of light. Macular pigments have hydroxyl groups attached at the 3 and 3' carbon positions. Zeaxanthin and *meso*-zeaxanthin contain two β-ring end groups and lutein contains one β- and one ε-ring, which decreases the length of its conjugation chain as compared to the other two pigments. Lutein and zeaxanthin are isomers. Zeaxanthin (3*R*,3'*R*) and *meso*-zeaxanthin (3*R*,3'*S*) are diastereomers and have a different spatial orientation of the hydroxyl group at the C_{3'} chiral carbon atom (Nolan *et al.*, 2013). The OH-group and the double bond that differ between the three molecules are highlighted in red.

differences between these macular pigments (Figure 1.13) along with their orientation, lead to the optimal filtration capacity of blue and UV light at the macula (Billsten *et al.*, 2003). Additionally, UV light can lead to the generation of reactive oxygen species (ROS) which can induce lipid peroxidation of the polyunsaturated fatty acids of the cell membranes. This leads to the destruction of membrane lipids as well as accumulation of end-products of this reaction. The macular pigments contain polyene chains, a readily available source of electrons which can directly quench the generated ROS and thus limit the oxidative damage (Britton 1995a; Sujak *et al.*, 1999; Junghans *et al.*, 2001; Trevithick-Sutton *et al.*, 2006; Pintea *et al.*, 2011). The efficacy of zeaxanthin at quenching ROS is twice of this of lutein and is thought to be a consequence of the extra double bond added to the conjugated system that is provided by the β-ring and which is missing from the ε-ring in lutein (Cantrell *et al.*, 2003). The same conjugated system is also present in *meso*-zeaxanthin (Figure 1.13), however, some evidence suggests that *meso*-zeaxanthin is a more potent antioxidant than zeaxanthin (Bhosale & Bernstein, 2005). Finally, there may be a specific reason as to why the macular pigments appear in this and not in a different combination. In vitro studies with the use of post-mortem human macula and retinal pigment epithelium has showed that exogenously added macular pigments can quench ROS.

The greatest quenching ability in solution was achieved when all three macular pigments were present at the equal 1:1:1 ratio rather than when they were used individually at the same total concentration (Li *et al.*, 2010a).

The evidence gathered above, coupled with the spatial distribution of the macular pigments within the retina, led to hypothesise that the macular pigments are the necessary components for maintaining healthy eyes and proper vision. Bone *et al.* (2003) reported that dietary supplements of lutein and zeaxanthin increase macular pigment density and, following from this, it could be possible that supplementation with lutein and zeaxanthin can prevent, slow down or even improve the course of AMD. Several epidemiological studies have found a negative correlation between the risk of developing AMD and the dietary intake or serum concentration of lutein and zeaxanthin.

1.2.5 Evidence for involvement of zeaxanthin in prevention against AMD

The first published evidence comes from the Eye Disease Case-Control Study Group, EDCCS (1993) on the cohort of 421 patients with the more severe and visually disabling form of AMD known as wet or neovascular AMD compared to the group of 615 healthy controls. The subjects were split into three groups – low, medium and high, depending on the blood levels of total carotenoids but also individual carotenoids, such as lutein with zeaxanthin, β -carotene, α -carotene, cryptoxanthin and lycopene according to the same criteria. Participants belonging to the medium and high blood levels groups for the total carotenoids as well as the medium and high blood levels for all individual carotenoids except lycopene, had substantially reduced risk of developing neovascular AMD as compared to the participants belonging to the low blood levels groups. For combined lutein with zeaxanthin in the medium and high blood levels groups, the odd ratios for developing wet AMD were 0.7 and 0.3, respectively as compared to the low blood levels. Moreover, further analysis of this patients' cohort by Seddon *et al.* (1994) has found that after adjusting for other risk factors for AMD such as smoking, a higher dietary intake of carotenoids correlated with a lower risk of developing AMD. Participants in the highest quantile of carotenoid intake had a 43% reduction in their risk for AMD (odds ratio, 0.57; 95% confidence interval, 0.35 to 0.92; $P = 0.02$) as compared to the participants in the lowest quantile. The increase in carotenoid intake and reduction in the risk of AMD appear to follow a linear correlation trend. Interestingly, the study also showed that within all the carotenoids investigated, combination of lutein with zeaxanthin gave the greatest reduction of 56% in the risk for AMD (odds ratio, 0.43; 95% confidence interval, 0.2 to 0.7; $P < 0.001$).

Another noticeable outcome of the EDCCS study came from the analysis of different types of foods, which were known to be sources of certain carotenoids, the subjects were consuming. One of the richest sources of lutein and zeaxanthin are spinach and collard greens (Sajilata *et*

al., 2008). Consumption of these foods two to four times per week led to a 48% reduction in the risk of AMD as compared to a consumption of less than once a month (odds ratio, 0.52; 95% confidence interval, 0.3 to 0.9). Finally, this study looked at how these results were modified when smoking was taken into account. The study re-confirmed that smoking was a major risk factor for AMD and the current smokers were at a much higher risk than past and non-smokers. A lower risk for AMD with higher intake of lutein and zeaxanthin was seen in all categories of smoking, but the strongest association was in current smokers. This outcome is very important as smoking is one of the major risk factors for both AMD and lung cancer. However, study by Tanvetyanon & Bepler (2008) unexpectedly showed that the risk of lung cancer in current smokers was increased with a high-dose of β -carotene supplementation. As both, β -carotene and lutein with zeaxanthin decrease the risk of AMD, β -carotene supplementation should not be given to current smokers and formulations of lutein with zeaxanthin should be used instead.

Further evidence comes from study by Mares-Perlman *et al.* (2001), where it was investigated how lutein and zeaxanthin intake influenced early and late AMD in people over 40 on a group of 8 222 participants. People in the lower age groups, 40 – 59 were found to have a reduced incidence of pigmentary abnormalities (odds ratio, 0.1; 95% confidence interval, 0.1 to 0.3) when they were assigned to the high lutein and zeaxanthin diet group as compared to the low one. These pigmentary abnormalities are a sign of early AMD and predict the progression into late AMD (Klein *et al.*, 1997). This is a very important observation because appropriate supplementation at this stage could prevent further progression into late AMD. This study also found that people with a high risk of developing late AMD (60 – 79 years of age), had this risk reduced if they were found in high lutein and zeaxanthin diet group (odds ratio, 0.1; 95% confidence interval, 0.0 to 0.9).

Similarly, in a randomised controlled trial by Parisi *et al.* (2008), early stage AMD patients showed improvement in the bioelectric potential of the macula after taking supplements of zeaxanthin and other carotenoids. Snellen *et al.* (2002) found that people with a low intake of lutein/zeaxanthin were at a higher risk of developing AMD than people with a high intake (odds ratio, 2.4; 95% confidence interval, 1.1 to 5.1) which agrees with the previous studies. Gale *et al.* (2003) focused his study on a group of elderly men and women and wanted to investigate what was the relation between the plasma levels of lutein, zeaxanthin and AMD. His cohort consisted of 380 men and women between 66 and 75 years of age. He found that the participants with lower concentrations of zeaxanthin in blood (< 27 nM) were at a 2.2 times greater risk (95% confidence interval, 1.1 to 4.2; *P* for trend = 0.019) of developing AMD than those who had highest levels of this macular pigment in plasma (> 46.3 nM).

Delcourt *et al.* (2006) in the Pathologies Oculaires Liées à l'Age (POLA) study also aimed to investigate the association between AMD and plasma levels of macular pigments but also other carotenoids. HPLC was used to measure plasma levels of carotenoids in 899 participants. The study reported the strongest association between high plasma levels of zeaxanthin and the risk reduction of AMD (odds ratio, 0.07; 95% confidence interval, 0.01 to 0.58; P for trend = 0.005). Plasma levels of combined macular pigments, lutein and zeaxanthin (odds ratio, 0.21; 95% confidence interval, 0.05 to 0.79; P for trend = 0.01) and lutein alone (odds ratio, 0.31; 95% confidence interval, 0.09 to 1.07; P for trend = 0.04) were also showing an association with AMD, although this was weaker than for zeaxanthin alone. Interestingly, unlike the EDCCS study, β -carotene was not found to reduce the risk of AMD.

The Carotenoids in Age-related Eye Disease Study (CAREDS) focused on women between 50 and 79 years of age and the relation between dietary macular pigments and intermediate-age AMD (Moeller *et al.*, 2006). The study found that stable intake of macular carotenoids in women younger than 75 with no previous history of AMD and overall healthy, protected against intermediate AMD (odds ratio, 0.57; 95% confidence interval, 0.34 to 0.59), large drusen and also possibly advanced AMD, although this result was not significant. The strongest inverse association between AMD was observed with a high intake of green vegetables such as spinach and also vegetables in general.

Wu *et al.* (2015) looked at the cohort of 63 443 women and 38 603 men who were followed for a period of 26 years to investigate how intake of carotenoids influenced AMD. Based on a food frequency questionnaire, predicted plasma levels of lutein and zeaxanthin were computed. The study found a 40% risk reduction for advanced AMD in both males and females between the highest predicted and lowest predicted plasma levels of the macular pigments (odds ratio, 0.59; 95% confidence interval, 0.48 to 0.73; P for trend < 0.001). This led to the conclusion that a high intake of macular pigments is associated with a long-term risk reduction of AMD.

The long-term effects of lutein, zeaxanthin and omega-3-LCPUFAs supplementation on optical density of macular pigment in AMD patients (LUTEGA) study (Dawczynski *et al.*, 2013) investigated how long-term supplementation with formulations of lutein and zeaxanthin affected macular pigment optical density (MPOD) in patients with dry form of AMD. This study differed from the ones above as it was a one-year long double-blind, placebo-controlled trial involving 172 patients with dry AMD and randomly assigned to one of the three treatment groups. The three groups included placebo and a single or double dose of 10 mg of lutein, 1 mg of zeaxanthin and 255 mg of concentrated fish oil. After a year of the follow-up MPOD has significantly increased in both groups taking lutein and zeaxanthin (P < 0.001) but there was no difference between the two dosage groups. This showed that the levels of macular pigments in

the retina reached saturation even in people already diagnosed with AMD. Interestingly, another study showed that supplementation with 10 mg of lutein and 2 mg of zeaxanthin did indeed increase the serum levels of lutein and zeaxanthin, but these were significantly lower for people who were diagnosed with AMD than for the healthy controls (Huang *et al.*, 2008).

When analysing the above results, one needs to think laterally. It could be that people with low levels of macular carotenoids in their retinas are more likely to develop AMD, but equally likely, the low levels of lutein and zeaxanthin could be the consequence of this condition. It could also be possible that AMD develops not because not enough lutein and zeaxanthin is provided in the diet but because the process of deposition of macular carotenoids from plasma into the retina becomes disrupted. It has been shown that plasma levels of lutein and zeaxanthin increase in healthy and AMD affected people after a xanthophyll-rich diet is provided. Therefore, the lower than normal concentration of macular pigments in the retinas of AMD affected people (Bone *et al.*, 2001) can be explained by abnormalities in the uptake of lutein and zeaxanthin from the plasma and their subsequent transport into the retina (Wang *et al.*, 2007). The selective retinal capture and accumulation of macular pigments are still poorly understood but the involvement of xanthophyll-binding proteins is becoming more apparent. A thorough review of our current understating of this process is provided elsewhere (Loane *et al.*, 2008; Li *et al.*, 2010b).

Nonetheless, a number of independently carried out studies, including case-control, cohort and prospective studies as well as randomised controlled clinical trials, provide an overall strong evidence that intake of lutein and zeaxanthin, either in form of supplements or derived from their food sources, is important for lowering the risk of AMD. These and other evidence up to August 2012 have been systematically reviewed in the Cochrane Database of Systematic Reviews by Evans & Lawrenson (2012) and in meta-analysis by Ma *et al.* (2012). The overall conclusions indicate that lutein and zeaxanthin do play a role in reducing the risk for AMD. Although, the exact mechanisms for this remains unexplored, the evidence for its existence is substantial. It is also still not unequivocally decided what the recommended dose of lutein and zeaxanthin should be. No adverse effects of taking synthetic zeaxanthin at daily doses between 10 and 30 mg for a period of up to six months by healthy individuals have been reported (EFSA, 2008). The issue of a daily recommended dose of lutein and zeaxanthin was addressed by the Age-Related Eye Disease Study 2, AREDS2 (Age-Related Eye Disease Study 2 Research Group, 2013). They reported that 10 mg of lutein and 2 mg of zeaxanthin taken daily was as good at reducing the risk of AMD as the original AREDS formulation. As the outcome of this study, it is recommended to replace β -carotene with combined lutein and zeaxanthin in smokers and past-smokers as supplements of β -carotene increase incidence of lung cancer in these groups (EDCCS, 1993; AREDS2, 2013).

Moreover, other studies provide evidence that increased intake of zeaxanthin also decreases the risk of developing cataracts and this is positively correlated with higher levels of antioxidants in blood (Vu *et al.*, 2006; Dherani *et al.*, 2008; Moeller *et al.*, 2008; Karppi *et al.*, 2012). However, the health benefits of zeaxanthin are not limited to only eye-related diseases. Additional evidence supports the role of zeaxanthin in the prevention of development of various cancers (Cha *et al.*, 2008) including breast (Zhang *et al.*, 1999) and lung cancer (Voorrips *et al.*, 2000). Furthermore, more evidence implicating the involvement of zeaxanthin in cognitive (Bovier *et al.*, 2014; Vishwanathan *et al.*, 2014) and neuronal (Leung *et al.*, 2004; Zimmer & Hammond, 2007) functions has been emerging.

1.3 Zeaxanthin – characterisation and sources

1.3.1 General characterisation

Zeaxanthin is a solid, lipid-soluble, organic compound belonging to a class of oxygenated carotenoids known as xanthophylls. Like the rest of carotenoids, zeaxanthin has a conjugated double bond system across multiple atoms which is responsible for its orange colour. Zeaxanthin has no vitamin A activity and as a food dye is labelled with the E number E161h. Zeaxanthin is considered to be safe for human consumption. In safety tests no evidence of foetal toxicity or teratogenicity in rats or rabbits, mutagenicity, histopathological changes or adverse effect in primates attributed to zeaxanthin were found. Based on this evidence, an Acceptable Daily Intake (ADI) of zeaxanthin of 53 mg day⁻¹ for a 70 kg adult is considered to lie well within the safety margin (Edwards, 2016). Zeaxanthin, similarly to lutein, is less prone to thermal degradation than antheraxanthin or violaxanthin during cooking such as boiling or frying (Cuéllar-Cepeda *et al.*, 2019) but is susceptible to degradation at higher pressures (Garnett *et al.*, 1998). Zeaxanthin is preferred as a feed additive in order to enhance pigmentation of meat in poultry and fish as it provides more of a natural colour and it deposits evenly in the tissues and egg yolks. Other carotenoid-containing animal feeds, such as alfalfa, cayenne pepper or feeds enriched in canthaxanthin, were found to cause red or purple striations in the flesh or yolk when administered to poultry (Orndorff *et al.*, 1994). Lutein as well as being a less potent colourant than zeaxanthin, when added as a feed additive, may cause the poultry meat and egg yolks to develop a greenish hue (Breithaupt, 2007).

The chemical structure of zeaxanthin (Figure 1.14) has been extensively studied and described in a great detail previously (Bartalucci *et al.*, 2007; Sajilata *et al.*, 2008). In zeaxanthin, the basic tetraterpene skeleton is modified through cyclisation of the isoprenoid units at both ends of the molecule to form β -rings followed by hydroxylation of the β -rings at the non-allylic carbons C₃ and C_{3'}. This modification of the end rings in zeaxanthin introduces chiral centres into the

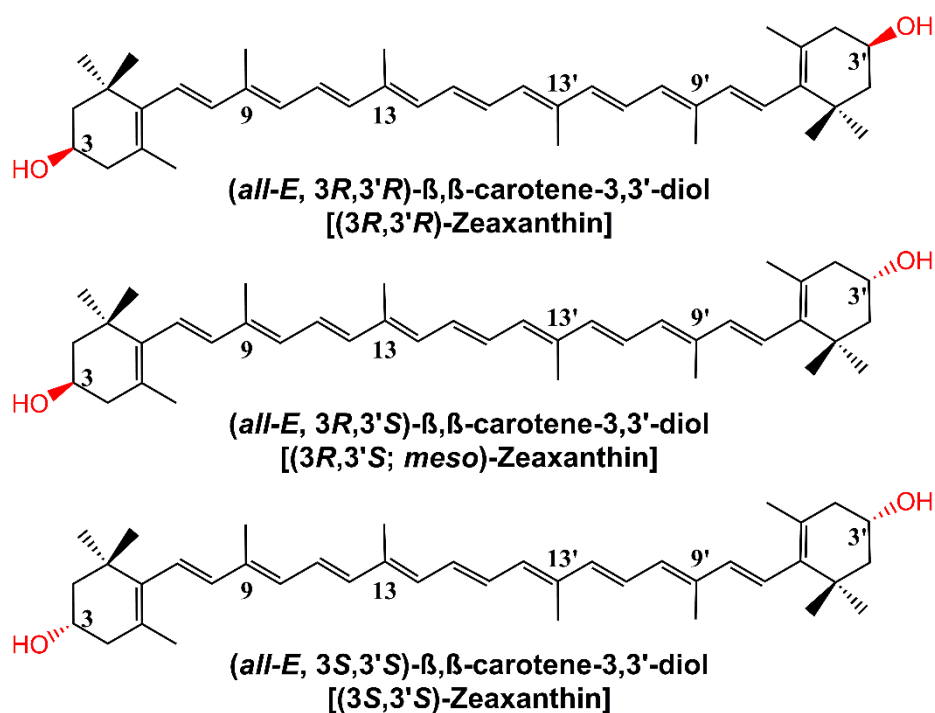


Figure 1.14. Chemical structures of zeaxanthin isomers ($C_{40}H_{56}O_2$). The OH-groups attached to the chiral carbon atoms (C_3 and $C_{3'}$) are highlighted in red (modified from Khachik *et al.*, 2006).

molecule. However, with two chiral centres at carbons C_3 and $C_{3'}$ in each of the end rings, zeaxanthin has only three stereoisomers. This is the consequence of the symmetry of the molecule and the $(3R,3'S)$ and $(3S,3'R)$ stereoisomers are identical (Figure 1.14). The most naturally abundant stereoisomer of zeaxanthin is $(3R,3'R)$ -zeaxanthin and together with *meso*-zeaxanthin are found in the macula (Bone *et al.*, 1993; Khachik *et al.*, 2002). The third stereoisomer, $(3S,3'S)$ -zeaxanthin, has also been found in the macula but in much lower quantities than the other two forms (Bone *et al.*, 1993; Bone *et al.*, 1997; Bernstein *et al.*, 2001). Interestingly, though *meso*-zeaxanthin is rare in nature, it accumulates in large amounts in commercially produced chickens and eggs in Mexico where it is used as a feed additive in order to improve the colour of the poultry meat and egg yolks (Bone *et al.*, 2007).

1.3.2 Sources of zeaxanthin

Both macular pigments, lutein and zeaxanthin, are highly sought after as dietary supplements, therefore it became important to identify food sources rich in these xanthophylls. Based on the results of the Age-Related Eye Disease Study 2, AREDS2 (Age-Related Eye Disease Study 2 Research Group, 2013), the recommendation is to take 10 mg of lutein and 2 mg of zeaxanthin daily, to reduce risk of AMD. As far as lutein is concerned, several lutein-rich renewable sources are available, therefore it is fairly easy to obtain enough of it from the consumed diet (Eisenhauer *et al.*, 2017). On the other hand, the increasing demand for zeaxanthin combined with its limited availability from renewable sources (Eisenhauer *et al.*, 2017) has led to the

development of alternative ways of obtaining this valuable xanthophyll in addition to the natural sources. Commercially available carotenoid supplements, aiming at improving the health of the eye, generally contain significantly higher amounts of lutein compared to zeaxanthin (Sajilata *et al.*, 2008). Zeaxanthin can be obtained synthetically or extracted from non-food sources as well. These approaches include synthetic production of zeaxanthin through Witting reaction and extraction from the flowers of *Tagetes erecta* and *Tagetes patula*, the Mexican and French marigold, respectively. These two methods differ by the amounts and purity of obtained zeaxanthin, generated by-products and contaminants (Stankovic, 2004).

1.3.2.1 Food sources

Zeaxanthin does not accumulate in high quantities in plants unless the plant is under stress or it is exposed to high-intensity light (Rowe, 2014). This is a result of the conversion of violaxanthin to zeaxanthin as a part of the xanthophyll cycle in order to protect the photosynthetic apparatus from photodamage (Latowski *et al.*, 2011). However, under normal light intensity, violaxanthin is further irreversibly metabolised to neoxanthin and then to the hormone abscisic acid, ABA. ABA plays an important role in response to environmental stresses and pathogen interaction throughout the plant's development (Seo & Koshiba, 2002) and controls stomatal resistance (Steuer *et al.*, 1988). Lutein, on the other hand, is the final product on the β/ϵ side of the carotenoid biosynthetic pathway and it does not get converted into further metabolites, therefore, it accumulates in higher amounts than zeaxanthin does. For this reason, lutein is much more easily obtained from diet than zeaxanthin (Eisenhauer *et al.*, 2017). With few exceptions, even the plant sources relatively rich in zeaxanthin, contain much higher levels of lutein (Sommerburg *et al.*, 1998; Holden *et al.*, 1999; Humphries & Khachik, 2003).

Vegetable and fruit food sources containing some amounts of zeaxanthin and rich in lutein include broccoli, Brussels sprouts, cabbage, dark-green leafy vegetables (such as kale and spinach), green beans, mandarins, peas, pumpkins and squash. Plants high in zeaxanthin are scarce but the richest ones are honeydew melons, mangoes, oranges and yellow corn (Holden *et al.*, 1999; Humphries & Khachik, 2003; Eisenhauer *et al.*, 2017). Notably, the best plant source of zeaxanthin is the orange pepper where this xanthophyll accounts for 37% of all carotenoids present (Sommerburg *et al.*, 1998), which is equivalent to $16.7 \mu\text{g g}^{-1}$ FW (Perry *et al.*, 2009). Interestingly, goji berries, the fruit of *Lycium barbarum* or *Lycium chinense* of the Solanaceae family, used in traditional Chinese medicine, contain levels of the zeaxanthin ester, zeaxanthin dipalmitate at close to 0.5 mg g^{-1} FW (Niro *et al.*, 2017). In peppers, free xanthophylls are esterified with fatty acids during fruit ripening and only around 24% of the total xanthophylls are found in the free form (Hornero-Méndez & Mínguez-Mosquera, 2000). Xanthophyll esters may undergo saponification prior to being prepared into specific supplement formulations.

However, the use of zeaxanthin in its esterified form does not seem to impact its bioavailability negatively since zeaxanthin esters are hydrolysed in the small intestine prior to being absorbed (Chitchumroonchokchai & Failla, 2006). In a randomised, single-blind crossover study Breithaupt *et al.* (2004) found that esterified zeaxanthin from the goji berry had, in fact, a significantly enhanced bioavailability compared to the free form.

The only food source of animal origin known to contain high levels of zeaxanthin, is the egg yolk where 35% of all carotenoids, equivalent to $7.6 \mu\text{g g}^{-1}$ FW, is represented by this xanthophyll (Sommerburg *et al.*, 1998; Perry *et al.*, 2009). Zeaxanthin in egg yolks is not of primary origin but the result of the incorporation of the pigments naturally available in the diet or added to the feed (Hammershøj *et al.*, 2010).

The advantage of natural food sources of zeaxanthin, such as fruit and vegetables, over zeaxanthin extracts is that they are renewable and can provide both the nutrient component of the diet as well as the food supplement which would lower the area and costs of the exploitation of the land. A pure fruit or vegetable producer of zeaxanthin offers a great advantage over extracted or synthetic zeaxanthin. The zeaxanthin-containing biomass can be directly or after minimal bioprocessing used as a food colourant or fed directly into the livestock without the need for pigment isolation. Nogueira *et al.* (2017) greatly improved the colour of trout fillets with ketocarotenoids provided in the esterified form in homogenised, freeze-dried tomato powders. In this work, the accumulation of ketocarotenoids in tomato fruit was achieved through transgenesis. Carotenoids contained within such prepared plant biomass are prevented from photochemical or enzymatic oxidation by the surrounding tissue matrix (Britton, 1996). Furthermore, fruit and vegetables are designed to be consumed shortly after their harvest and, with only a few exceptions such as apples, beets, carrots, onions and potatoes, do not undergo extended periods of storage which would lead to their spoilage.

The advantage of consumption of fresh fruit and vegetable products over processed food, is that food processing, including thermal processing, may lead to changes in the isomerisation state of zeaxanthin. The predominant form of zeaxanthin found in fresh fruit and vegetables, resulting from the normal biosynthetic process, similarly to lycopene and lutein, is the all-*trans* form (Sajilata *et al.*, 2008). During thermal food processing, the all-*trans* zeaxanthin changes into its *cis* isomer, which affects the bioavailability and antioxidant properties of zeaxanthin (Schieber & Carle, 2005). It was found that incubation for as little as 10 minutes at 75°C already induced *trans*-to-*cis* isomerisation of zeaxanthin and the magnitude of the conversion doubled at 85°C (Milanowska & Gruszecki, 2005). In canned corn, kale, green peas and spinach as well as microwaved broccoli, the presence of the *cis* isomer of zeaxanthin increased, on average, by

17% compared to the unprocessed fresh vegetables (Updike & Schwartz, 2003). The *trans*-to-*cis* isomerisation also takes place in the presence of light and acids (Sajilata *et al.*, 2008).

The pure crystalline form of zeaxanthin, either obtained by extraction or synthesis, requires specific conditions for its storage, as it becomes degraded in the presence of heat, light and oxygen. Topuz & Ozdemir (2003) reported losses of more than 80% of zeaxanthin from sun-dried paprika. During an 8-day long experiment of drying whole pepper fruit (*Capsicum annuum* L.), zeaxanthin content decreased by almost 30% in the first 24 hours with the final decrease at the end of drying of 51% (Pérez-Gálvez *et al.*, 2004). Another study reported that increasing the storage temperature of powdered pepper fruit from 0 to 20°C, led to a 36% decrease in zeaxanthin levels in the first two months (Kim *et al.*, 2004). Prevention of carotenoid degradation during storage is a subject of ongoing research, however, several methods have been developed including encapsulation and are currently being evaluated with some showing promising results (de Campo *et al.*, 2018). Exposure to light, especially a direct exposure of a carotenoid to sunlight or UV, can induce a conversion into a different geometrical isomer (Britton, 1996). Therefore, handling of carotenoids requires appropriate lighting conditions and shielding during storage. Traces of oxygen in stored carotenoid samples can cause bleaching and generation of artefacts including epoxy-carotenoids and apocarotenals, even if the samples are kept at deep-freezing temperatures (Britton, 1996). The influence of oxygen can be eliminated with the use of a vacuum at the extraction stage and nitrogen or argon atmosphere during storage. However, this increases the costs of storage of synthetic or extracted zeaxanthin. Protection from oxidation can also be achieved by the addition of antioxidants, this however, changes the formulation of the final product and also adds to the final cost of manufacture (Sajilata *et al.*, 2008).

Unfortunately, regardless of the advantages fresh vegetable or fruit sources can offer, a zeaxanthin-rich plant, which could provide high content of this xanthophyll to be able to compete against other methods of zeaxanthin production, has not yet been identified. Therefore, despite the disadvantages of obtaining zeaxanthin through synthesis or extraction, these methods are extensively used and researched to improve the available technologies.

1.3.2.2 Non-food sources

1.3.2.2.1 Microbial sources

Obtaining zeaxanthin from microbial sources has been of great interest due to a potentially high yield and minimal downtime between batches that these methods can offer. However, the majority of carotenoid-producing organisms synthesise either β -carotene or astaxanthin as their major product (Sanchez *et al.*, 2013). Nonetheless, a number of microorganisms, naturally accumulating zeaxanthin, has been identified (Asker *et al.*, 2018; Zhang *et al.*, 2018).

Bacterium *Paracoccus zeaxanthinifaciens* (formerly, *Flavobacterium* sp. strain R-1 512, ATCC 21588; Berry *et al.*, 2003) is possibly one of the best zeaxanthin producers as, under proper fermentation conditions, (3*R*,3'*R*)-zeaxanthin is essentially the only carotenoid that this strain accumulates next to very small amounts of β -cryptoxanthin (Britton *et al.*, 1977; Masetto *et al.*, 2001). This is significant, as purification of zeaxanthin is greatly facilitated because otherwise, zeaxanthin would be very difficult to separate from other xanthophylls. Using mathematical approaches and optimisation algorithms to predict the optimum growth conditions (24.3 g l⁻¹ glucose, 30 g l⁻¹ yeast extract, 0.18 mg l⁻¹ pyridoxine hydrochloride and 8 g l⁻¹ methyl palmitate), Joshi & Singhal (2016), achieved the overall levels of zeaxanthin production in *P. zeaxanthinifaciens* at 11.6 mg l⁻¹ after 72-hour incubation at 30°C on a small scale. Without a particular control of growth conditions, zeaxanthin levels between 10 and 40 mg l⁻¹ were obtained from fermentation of *P. zeaxanthinifaciens* in a medium supplemented with glucose and corn steep liquor on a laboratory scale. However, this yield could be greatly increased up to 335 mg l⁻¹ by reducing the incubation temperature and supplementation with palmitic esters, methionine, pyridoxine and ferrous salts maintained at constant levels throughout the growth (Ninet & Renaut, 1979). Chávez-Parga *et al.* (2012), used a fluidised bed bioreactor with immobilised *P. zeaxanthinifaciens* for the production of zeaxanthin. The highest, ever reported yield reaching 2.96 g l⁻¹ was achieved with the defined medium containing a constant, 2.0 to 1.0 ratio of carbon to nitrogen, air flow of 2.0 vessel volumes per minute (VVM), NaCl of 4.5 g l⁻¹ and pH of 7.2.

Another bacterium accumulating zeaxanthin is non-fastidious, non-pathogenic, Gram-negative *Sphingobacterium multivorum*, formerly known as *Flavobacterium multivorum* (Yabuuchi *et al.*, 1983). In the late logarithmic growth phase, under optimised medium (6.02 mM malic acid, 6.20 mM isocitric acid and 0.02 mM α -ketoglutarate), zeaxanthin represented 95 to 99% of all carotenoids the bacterium stored, which was equivalent to the concentration of 10.7 mg l⁻¹ (Bhosale *et al.*, 2004). Zeaxanthin precursors, β -carotene and β -cryptoxanthin only accumulated in the early logarithmic phase of the bacterial growth.

Another zeaxanthin producer is a Gram-negative, strictly aerobic bacterium belonging to the Flavobacteriaceae family, *Mesoflavibacter zeaxanthinifaciens* TD-ZX30^T (Asker *et al.*, 2007). The reported levels of zeaxanthin in this bacterium were 0.91 mg g⁻¹ of dry cell weight (DCW). In *Formosa* sp. KMW, a marine bacterium also belonging to the Flavobacteriaceae family, zeaxanthin content accounted for 51.4% of the total accumulated carotenoids following a 6-day long incubation in marine broth at high light illumination, pH 7.0, 200 RPM and 37°C. Although the total carotenoid levels were quite low (0.97 mg l⁻¹), the final yield was found to increase with longer incubation times and the presence of agitation and light. Interestingly, absence of sugars

promoted carotenoid accumulation and, contrary to other studies (Alcantara & Sanchez, 1999; Prabhu *et al.*, 2013), addition of the tricarboxylic acid (TCA) cycle intermediates did not improve carotenoid production (Sowmya & Sachindra, 2015).

Several members of the *Muricauda* genus were also identified to accumulate zeaxanthin. A thermophilic bacterium, *Muricauda lutaonensis* strain CC-HSB-11^T, accumulated 3.12 mg l⁻¹ of zeaxanthin following 72 hours culturing in a bioreactor under a constant agitation at 150 RPM, aeration of 1.0 VVM, 40°C and pH 7.4 (Hameed *et al.*, 2011). *M. aquimarina* YUAB-SO-11 accumulated 1.20 mg g⁻¹ DCW of zeaxanthin following a 72-hour long incubation in optimised culture conditions and similarly, *M. olearia* YUAB-SO-45 produced 1.02 mg g⁻¹ DCW after 48 hours at 30°C, pH 7.0 when cultured on a laboratory scale in marine broth. The yield of zeaxanthin was significantly increased when the media were supplemented with glutamic acid to 1.47 and 1.18 mg g⁻¹ DCW in the two strains, respectively (Prabhu *et al.*, 2013). Another member of this genus, *M. flavescens* JCM 11812^T accumulated up to 4.4 mg l⁻¹ of zeaxanthin after 72 hours in marine broth at 32°C (Prabhu *et al.*, 2014).

Gram-negative, strictly aerobic *Siansivirga zeaxanthinifaciens* CC-SAMT-1^T, accumulated zeaxanthin at levels up to 6.5 mg g⁻¹ DCW following a 72-hour long incubation in marine broth at 30°C (Hameed *et al.*, 2012). Sponge-associated bacterium *Sphingomonas natatoria* KODA19-6 accumulated 4.9 mg g⁻¹ DCW zeaxanthin following a 4-day long incubation in modified Zobell medium at 30°C, pH 7.6 and 150 RPM (Thawornwiriyanun *et al.*, 2012).

In addition to bacteria, some microalgae also accumulate zeaxanthin. *Neosporangiococcum*, a green alga, is currently the only FDA-approved (21CFR73.275) generally recognised as safe (GRAS) strain used as a feed additive to enhance the yellow colouration in poultry (Sajilata *et al.*, 2008). In *N. excentricum* zeaxanthin comprises at least 0.65% of the dry algal weight (Liao *et al.*, 1995). *Spirulina*, a blue-green alga, has been listed by FDA as a colour additive exempt from certification for foods (21CFR73.530) and drugs (21CFR73.1530). *S. maxima* was found to contain up to 0.74 mg g⁻¹ DCW of zeaxanthin (Yu *et al.*, 2012) and the daily recommended dose of zeaxanthin could be provided in as little as 2.8 g of dry algal mass. Interestingly, when *Spirulina* was incorporated as a part of the feed in Black Tiger prawn, *Penaeus monodon* culture, a significant enhancement of the carapace colour was achieved, which greatly improved the market quality of the cultured prawns (Liao *et al.*, 1993). The colour enhancement was the result of rapid conversion of zeaxanthin to astaxanthin by the prawns themselves. The same conversion into astaxanthin occurs in goldfish and ornamental carp therefore, zeaxanthin from *Spirulina* is used in their feeds as well (Maoka, 2011). Toyomizu *et al.* (2001) fed male broiler chicks with a diet supplemented with *Spirulina* and found that the yellow colouration of the flesh

was significantly enhanced and positively correlated with increasing amounts of the algae in the feed.

Marine cyanobacterium, *Synechococcus* PCC7942 cultured for 5 hours in BG11 medium supplemented with 30 $\mu\text{g ml}^{-1}$ methionine accumulated 1.7 $\mu\text{g g}^{-1}$ DCW of zeaxanthin which represented 58% of total carotenoids (Schäfer *et al.*, 2006). *Microcystis aeruginosa*, a freshwater cyanobacteria was used in high-speed counter-current chromatography (HSCCC) separation and purification of zeaxanthin (Chen *et al.*, 2005). A one-step separation resulted in the final purity of zeaxanthin extract of 96.2% from the 150 mg of the crude extract and 91.4% recovery. Fresh water green algae *Chlorella pyrenoidosa* accumulated 2.2 mg g^{-1} DCW of zeaxanthin which only accounted for 1.3% of the total carotenoids (Inbaraj *et al.*, 2006). *C. saccharophila* accumulated 11.2 mg g^{-1} DCW of zeaxanthin following an 8-day long incubation at pH 6.5, 20°C and 150 RPM (Singh *et al.*, 2015). This is the highest, native microalgae producer of zeaxanthin reported to date, but this value might be attributed to the optimised extraction method. In cyanobacteria *Acaryochloris marina* MBIC 11017 and *Acaryochloris* sp. strain Awaji, zeaxanthin accounted for 43% and 61%, respectively, of total carotenoids. In cyanobacteria belonging to photosynthetic picoplankton, *Prochlorococcus marinus* strain CCMP 1986, *P. marinus* strain CCMP 1375^T, *P. marinus* strain CCMP 2773 and *Prochlorothrix hollandica* PCC 9006^T zeaxanthin accounted for 92%, 78%, 50% and 68% of total carotenoids, respectively (Takaichi *et al.*, 2012).

Obtaining carotenoids from microbial sources faces a number of challenges. The best producers selected based on laboratory scale experiments may not behave in the same way on the industrial scale. Therefore, optimisation of the strains needs to continue in order to achieve the best yield. This requires a constant monitoring of the growth conditions and quality assessments. Batch to batch variation in the yield of carotenoids may be substantial if unstable strains are used or the growth conditions are altered. The issue of strain stability particularly applies to microorganism engineered to produce higher levels of carotenoids. The oleaginous yeast, *Yarrowia lipolytica* strain CLIB138, modified to accumulate β -carotene through transformation with the genes of the carotenoid biosynthetic pathway (bifunctional lycopene cyclase/phytoene synthase (*carRP*) and phytoene dehydrogenase (*carB*)), was found to lose its initial production capacity when sub-cultured for extensive periods of time. Shortly after the 100th generation, the percentage of the initial production remaining was close to zero (Czajka *et al.*, 2018). The loss of carotenoid production capability was also reported in engineered *E. coli* strains transformed with the genes of the carotenoid biosynthetic pathway from *Erwinia urevudora*. Four out of the 14 *E. coli* strains tested showed unstable expression. This was manifested by sectoring pigmentation of the colonies and growth of unpigmented clones on selective media indicating the presence of the transforming plasmid (Wurtzel *et al.*, 1997).

Furthermore, the appropriate aeration of the microbial culture is essential for its growth and accumulation of carotenoids. Oxygen is crucial for growth of *Flavobacterium* and is a substrate in carotenoid biosynthesis (Masetto *et al.*, 2001; Bhosale *et al.*, 2004). However, it is often the case that the optimal conditions for growth of the culture are not the same as the optimal conditions for the pigment accumulation in that same culture (Han & Mudgett, 1992; Lee *et al.*, 2002). Selecting the optimal conditions, including media and aeration of the fermenter, supporting growth of the biomass and the production of carotenoids is one of the major challenges hindering the widespread use of microbial organisms for the production of pigments on an industrial scale.

Algibacter strain AQP096 and its mutant generated by UV irradiation AQP096 MU016, accumulated 3.47 and 11.41 mg g⁻¹ DCW of zeaxanthin, respectively following 48 hours culturing at 26°C in standard marine broth (Issouf *et al.*, 2012). However, type of the dominant carotenoid produced in *Algibacter* depended on the culture conditions. When imidazole and casamino acid were added to the media containing yeast extract at a high ratio with glucose, lycopene was accumulated instead of zeaxanthin due to inhibition of β -carotene cyclase (Issouf *et al.*, 2012). Sowmya & Sachindra (2015) studied the influence of different amino acids in the culture media on the carotenoid production in *Formosa* sp. KMW. For instance, supplementation with 10 mM asparagine resulted in the highest total carotenoid yield of 103.54 μ g mg⁻¹ of biomass compared to the same concentration of histidine which led to the significant, over two-fold reduction in total carotenoid production measured at 47.06 μ g mg⁻¹ of biomass. Alcantara & Sanchez (1999) studied the influence of 55 mM carbon and 7.5 mM nitrogen sources on the growth and zeaxanthin accumulation in *Flavobacterium* sp. (ATCC 25582). Compared to the highest growth in 1% yeast extract of OD 2.38, the next highest growth of OD 1.82 was supported by sucrose. Zeaxanthin production at the levels of 0.75 μ g ml⁻¹ was highest in the yeast extract while sucrose and D-glucose promoted zeaxanthin production at the same level of 0.15 μ g ml⁻¹. Highest growth of OD 3.74 and OD 2.96, respectively, was achieved with supplementation of L-asparagine and L-glutamine also leading to highest zeaxanthin accumulation of 0.38 and 0.36 μ g ml⁻¹, respectively. Interestingly, addition of 7.5 mM L-asparagine to high-glucose containing medium (above 55 mM) resulted in a steady decrease in zeaxanthin accumulation leaving the biomass production unaffected. Addition of 10 mM oxaloacetate to the medium stimulated growth and zeaxanthin accumulation. Similarly, addition of other TCA cycle intermediates also improved biomass growth and zeaxanthin production, however the intermediates of glycolysis (glucose 6-phosphate and fructose 1,6-diphosphate) did not.

The perceived carotenoid yield is also highly dependent on the method of carotenoid extraction. Conventional extraction methods, such as atmospheric liquid extraction with maceration or

Soxhlet extraction, involve drying and pulverisation of the biomass, digestion of the biomass with an inert organic solvent and finally, filtering and isolation of the desired compound by elution with an inert organic solvent (Kadam *et al.*, 2013). The choice of inert solvent depends on the nature of the molecule to be extracted. Non-polar solvents such as chloroform, diethyl ether, hexane or petroleum ether are used in the extraction of non-polar carotenoids or xanthophyll esters, whereas more polar solvents, like acetone, dichloromethane, ethanol, ethyl acetate, isopropanol, methanol or tetrahydrofuran (THF) are used for polar carotenoids (Saini & Keum, 2018). The conventional methods are generally simple, provide high extraction yield and do not require sophisticated equipment. However, they are time-consuming and require large amounts of solvents increasing the costs of the extraction. Most of the inorganic solvent used are unsustainable and toxic and pose environmental, health and safety hazards (Kadam *et al.*, 2013; Saini & Keum, 2018). Novel extraction technologies include ultrasound-assisted extraction (UAE), supercritical fluid extraction (SFE), microwave-assisted extraction (MAE), enzyme-assisted extraction (EAE) and pressurised liquid extraction (PLE). The novel methods are generally faster, provide high extraction yields and are more environmentally friendly as they require less organic solvents. However, these are generally associated with higher costs due to the requirement of specific instrumentation, may induce thermal degradation or *trans*-to-*cis* isomerisation (MAE) or are not suitable for extraction of polar carotenoids and use with samples containing high amounts of water (SFE). The cost of manufacture, in USD per kilogram of extract, was estimated to be lowest for atmospheric liquid extraction with maceration (13.4 USD kg⁻¹), followed by PLE (29.2 USD kg⁻¹) with Soxhlet being the most expensive (45.1 USD kg⁻¹) for a 0.5 m³ vessel (Cardenas-Toro *et al.*, 2015).

Sowmya & Sachindra (2015) evaluated carotenoid production using *Formosa* sp. KMW and found that the total concentration of carotenoids in the extract, composition of the carotenoids in the extract and amount of the extract itself were depended on the method of extraction. Highest carotenoid concentration in the extract (1.83 µg mg⁻¹ of extract) and highest overall carotenoid yield (0.96 mg l⁻¹) were obtained when vortexing was used as the method of extraction. The greatest yields of carotenoid extract from the biomass were obtained when the cells were disrupted by sonication either using a bath (139.67 µg mg⁻¹ of biomass) or a probe sonicator (148.90 µg mg⁻¹ of biomass). The use of a 30-minute ultrasonication treatment reported by Singh *et al.* (2013) for the carotenoid extraction from *Chlorella saccharophila* cell suspension improved zeaxanthin extraction nearly 40-fold compared to the direct extraction (repeated solvent extraction until the supernatant becomes colourless). However, use of ultrasonication increases energy consumption and the overall cost and time of the procedure. Koo *et al.* (2011) used PLE with either hexane, ethanol or isopropanol for the extraction of zeaxanthin from *Chlorella ellipsoidea* (KMCC C-020). The optimal extraction conditions were

achieved with ethanol after 23.3 minutes at 115.4°C. This is significant as a high yield extraction can be achieved using a food-grade solvent instead of more conventionally used organic solvents of significant toxicity such as acetone, chloroform and hexane. Strati *et al.* (2015) evaluated the use of enzymes in the carotenoid extraction from tomato waste. It was concluded that the use of enzymes improves total carotenoid extraction. Similarly, the use of enzymes for carotenoid extraction from algae *Haematococcus pluvialis* improved the extractability 2.3-fold compared to the situation where no enzymes were used (Machado *et al.*, 2016).

There are other technical challenges associated with the use of microbial cultures, especially in large reaction vessels or open ponds. Contamination of the monoculture with fungi or other species of bacteria or algae can decrease or stop the production of the desired carotenoid or even destroy the entire culture. Contamination is particularly problematic for algal cultures as they can be rapidly overtaken by other, much faster growing microorganisms (Xu *et al.*, 2009). Finally, the generated waste requires appropriate disposal, especially when genetically modified organisms (GMOs) are used. The amount and type of the waste depends on the processing methods but generally, the production of waste is kept to minimum in order to increase the profits. The methods of disposal include the use of microbial waste as a bio-fertiliser if the waste is not GM, burning as a biofuel to provide energy or use as substrate for fermentation (El Shimi & Moustafa, 2016). Generally, the production costs of a microbial biomass are high (Torregrosa-Crespo *et al.*, 2018). However, most likely due to the food matrix effect, zeaxanthin from certain microbial sources, such as *Flavobacterium multivorum* strain ATCC 55238 (Gierhart, 1994) and *Spirulina* (Yu *et al.*, 2012), has up to a 3-fold greater bioavailability than zeaxanthin obtained from marigold or other dietary sources.

Current industrial production of zeaxanthin in microbes involves culture cultivation, harvesting, biomass pre-treatment, solid-liquid extraction and, if required, product purification according to the intended use (Cardoso *et al.*, 2017; Keller *et al.*, 2017). These five steps generally differ depending on the microorganism used and can also be a subject to trade secret or patent protection by individual manufacturers. Culture cultivation can be carried out in open raceways with paddle wheels or closed bioreactors (Keller *et al.*, 2017). Harvesting of the culture is then carried out using centrifugation or membrane filtration. Biomass pre-treatment typically involves drying and milling. Drying is essential in order to reduce weight of the material and the amounts of contaminants which could be co-extracted from the liquid media. Milling, on the other hand, increases the surface area available for contact with the extracting solvents which greatly facilitates the extraction process. If the selected microorganism has a thick cell-wall, which is generally the case, chemical or mechanical cell disruption is typically carried out prior to drying. The biomass prepared in such a way undergoes solvent extraction. Polar solvents,

such as acetone, ethanol or ethyl acetate are used in extraction of zeaxanthin. The biomass typically undergoes repeated re-extractions and the generated extract is then concentrated allowing for solvent recovery (Cardoso *et al.*, 2017). If the selected microorganism produces a mixture of carotenoid products instead of pure zeaxanthin, extractions with solvents of increased polarity can be carried out in order to obtain fractions containing specific products (Keller *et al.*, 2017). Depending on the intended use, the concentrated extract of zeaxanthin may require further purification. If the original material the extract was obtained from was classified as GRAS, further purification is usually not necessary unless higher product concentration is required. Moreover, further purification is not necessary for extracts used as animal feed additives. For the products intended for human consumption, such as supplements, further purification of the zeaxanthin extract is carried out. This is typically achieved by adsorption, chromatography and crystallisation. Finally, specific formulations are prepared for particular applications. This may simply involve addition of antioxidants, such as butylated hydroxytoluene (BHT) or butylated hydroxyanisole (BHA) to the final product or incorporating zeaxanthin into tablets, capsules or emulsions (Cardoso *et al.*, 2017; Saini & Keum, 2018).

1.3.2.2.2 Plant sources

On an industrial scale, marigold is the most commercially relevant, non-food plant source of zeaxanthin and zeaxanthin esters. The petal extract from *Tagetes patula*, *T. erecta*, *T. minuta* and *T. glandulifera* have been approved by FDA (21CFR172.510) for the use as a natural flavouring substance. Additionally, marigold meal (dried and powdered flower petals) and marigold extract from *T. erecta* may be safely used in poultry feed and as colour additives (21CFR73.295). Zeaxanthin from marigold has been given the GRAS status (GRN No. 639) for the use in baby formulations, candies, cereals, dairy products, soups and beverages up to 300 mg per serving.

Obtaining zeaxanthin from marigold requires cultivation of the plant material followed by processing of the generated biomass. Marigold typically flowers within 50 days following sowing (Sivasubramanian & Ganeshkumar, 2004). Compared to microbial sources, cultivation of marigold requires more land and water but less nutrients and energy. Moreover, extraction of zeaxanthin from microorganisms requires disruption of the thick cell walls which further rises energy demands. Therefore, despite all the advantages the microbial sources can offer, extracting zeaxanthin from marigold is easier, faster and cheaper and this is the reason why on a global scale, marigold remains the most relevant zeaxanthin source (Lin *et al.*, 2015).

Following collection of fresh marigolds, the flowers are separated from the receptacles and ensilaged (sprayed) with microorganisms in order to help degradation of the cell walls which enhances the extraction process (Navarrete-Bolaños *et al.*, 2003). Next, water content of the

fresh flowers is reduced by 70 to 75% using a hydraulic press. Further reduction in moisture content down to between 8 and 10% is achieved through drying in hot air using belt, roller or airflow dryers (Sowbhagya *et al.*, 2013). At this point, the flower density reaches about 150 kg m⁻³ (Lin *et al.*, 2015). Pressing is less energy consuming than the subsequent drying and therefore, increasing the efficiency of water removal during pressing may greatly reduce the energy demands. The dried flowers are then ground in a hammer mill to a powder and the marigold meal can either be pelleted into small granules and directly used as a feed additive or extracted with hexane or other suitable solvent (Navarrete-Bolaños *et al.*, 2005; Sowbhagya *et al.*, 2013). After distillation of the solvent at the temperature close to its boiling point, a thick, dark-brown paste called oleoresin is obtained. At this point, oleoresin contains 80 – 120 g kg⁻¹ of xanthophylls comprising mainly fatty acid esters of lutein and zeaxanthin. The oleoresin has a mild smell of marigold but also the characteristic fetid odour resulting from the retting process during ensilaging and therefore, it is not suitable as a food product and may only be added to the poultry forage (Attokaran, 2017). Marigold extract, when used as feed additive for *Coturnix coturnix japonica* laying quail, was found to improved egg quality and egg production performance of the quail (Mirzah & Djulard, 2017). In order to obtain extract of zeaxanthin suitable for human consumption, further processing is required. Fine processing of oleoresins involves saponification with methanolic KOH or NaOH (40% w/v) to liberate free xanthophylls from their fatty acid esters. Removal of fatty acids is carried out by precipitation of fatty ester salts with metallic halogenides such as CaCl₂, ZnCl₂ and MgCl₂ (Rosales & Torres-Cardona, 2006). The precipitate is filtered to separate xanthophyll-rich liquid phase and the accumulated solid forms a cake which is washed over the filter with ethanol or other class 3 solvents until no colouration of the wash-through is produced (Navarrete-Bolaños *et al.*, 2004). The solvent is recovered by evaporation and the remaining xanthophyll crystals are washed with water and alcohol to remove impurities and subsequently dried under vacuum. This procedure generates crystals of up to 70% purity, however these can be purified further up to 97% by re-extraction, re-crystallisation or separation on a silica gel column to obtain individual carotenoids (Lin *et al.*, 2015). The pure product is suitable for human consumption and can be used as a food additive and in supplements (Sowbhagya *et al.*, 2004).

Annual yield of fresh marigold flowers varies from 11 (Sowbhagya *et al.*, 2004) up to 45 t ha⁻¹ (Lin *et al.*, 2015) which roughly equates to 1.5 – 6.0 t ha⁻¹ of petal powder after the removal of receptacles and decreasing the moisture content down to 10% (Lin *et al.*, 2015). Typically, the yield of oleoresin from the dried powder reaches 8 to 10% (equivalent to 0.15 – 0.60 t ha⁻¹ for the 10% oleoresin yield). With the use of improved extraction methods, such as treatment with cellulolytic enzymes, the yield of total xanthophylls up to 29.3 g kg⁻¹ of dry marigold petal (equivalent to 44.0 – 176.0 kg ha⁻¹) can be achieved (Navarrete-Bolaños *et al.*, 2004) as

compared to 11.4 g kg⁻¹ (equivalent to 17.0 – 70.0 kg ha⁻¹) which can be obtained from extractions where no enzymes are used (Delgado-Vargas & Paredes-López, 1997). *Trans*-lutein is the major xanthophyll found in marigold (Hadden *et al.*, 1999; Navarrete-Bolaños *et al.*, 2004) accounting in some varieties for up to 95% of the total carotenoids (Rosales & Torres-Cardona, 2006). However, zeaxanthin-rich marigold varieties are also available where *trans*-zeaxanthin accounts for up to 60% of the total carotenoids (Sethuraman & Madavalappil, 2010). Using these varieties and following the optimised extraction methodology outlined above, the maximum zeaxanthin yield of 26.0 – 106 kg ha⁻¹ can be achieved.

The same technological processes, as used to obtain oleoresins and zeaxanthin from marigold petals, may be directly applied or modified accordingly to suit the processed material, in order to obtain zeaxanthin from other plant food and non-food sources. Potential commercial sources for the preparation of zeaxanthin-containing oleoresins include dried wolfberries (*Lycium barbarum*), Chinese lanterns (*Physalis alkekengi*), orange, red and That Chili peppers (*Capsicum annum*) and sea buckthorn berries (*Hippophae rhamnoides*). Although, the husks and fruit of *P. alkekengi* and wolfberries contain a very high proportion of zeaxanthin compared to other carotenoids (58%, 69% and 89%, respectively), marigold is still the preferred source due to its ease of cultivation, large biomass production and the fact that much greater yields of zeaxanthin can be obtained from the same amount of dried material (Weller & Breithaupt, 2003). For instance, some sources indicate that the calyces of red *Physalis* (*Physalis alkekengi* L.), which are considered an agroindustrial waste (Cicchetti *et al.*, 2018), contain exceptionally high levels of zeaxanthin, including zeaxanthin fatty acid esters, in the range of 8.3 – 10.1 g kg⁻¹ dry weight (DW; Wen *et al.*, 2017) as compared to high-zeaxanthin marigold lines where 1.94 g kg⁻¹ DW of zeaxanthin can be obtained (Sethuraman & Madavalappil, 2010). However, Weller & Breithaupt (2003) reported much lower zeaxanthin content in *Physalis* calyces of 0.55 g kg⁻¹ DW therefore, the final amount might be highly dependent on the cultivation conditions and extraction methods. Moreover, compared to India alone, one of the biggest marigold producers worldwide, where the area of marigold cultivation is estimated to be 34 000 hectares (Singh *et al.*, 2013), in Colombia, the world largest producer of *Physalis*, the cultivation area is estimated at 800 – 1 000 hectares with the fruit output of 15 – 28 t ha⁻¹ (Muniz *et al.*, 2014). Other agroindustrial wastes that may be used to obtain zeaxanthin include distillers dried grains with solubles (DDGS), which are the by-product of the distillation process. DDGS were used to obtain oleoresin following Soxhlet extraction which was subsequently purified by centrifugal partition chromatography to recover close to 0.02 g kg⁻¹ of zeaxanthin and 0.04 g kg⁻¹ of lutein (Li & Engelberth, 2018).

As the marigold extract is intended for animal or human consumption, certain technical and safety aspects of the formula preparation must be followed. For instance, organic solvents, such

as hexane, used to obtain oleoresin, are highly toxic and must not be present in significant amounts in the final product. This is particularly important, if class 2 solvents (dichloromethane, hexane or tetrahydrofuran, for example) are used during recrystallisation rather than the considered to be less toxic, class 3 solvents such as ethanol. The amounts of residual solvents in the final product are strictly limited and so for hexane the concentration limit is 290 parts per million (ppm), dichloromethane – 600 ppm and tetrahydrofuran – 720 ppm (EMA, 2018). Therefore, the manufacture process must ensure that extraction solvent is removed through, for example, vacuum distillation and the limits are adhered to. However, small amounts of the residual solvents may still remain in the final product (Attokaran, 2017). Other aspects to consider include the treatment of marigold petals with commercial hydrolytic enzymes prior to extraction which greatly improves the amounts of obtained xanthophylls, however it also increases the cost of manufacture (Navarrete-Bolaños *et al.*, 2005). An alternative may be to employ enzymes synthesised by microorganism associated with the marigold flowers in order to generate a more cost-effective process (Navarrete-Bolaños *et al.*, 2004; Navarrete-Bolaños *et al.*, 2005). Finally, when prepared for poultry feed, xanthophyll esters in marigold flowers have been reported to be negatively affected during drying, milling and storage. Therefore, in order to stabilise the pigments, antioxidants such as ethoxyquin, can be included during the extraction process or added to the final product (Sowbhagya *et al.*, 2004). However, the use of antioxidants in the manufactured product changes its final formulation, increases the cost of manufacture and, most importantly, certain concerns regarding the safety and possible genotoxic effects of antioxidants have arisen (EFSA FEEDAP Panel, 2015).

1.3.2.3 Synthetic zeaxanthin

Only a small fraction of all industrially available carotenoids is obtained from microbial or plant sources. The great majority of carotenoids is chemically synthesised albeit this is accompanied by high production costs (Pasarín & Rovinaru, 2018). In fact, it was estimated that chemically synthesised carotenoids account for between 76 (McWilliams, 2018) and 90% (Saini & Keum, 2017; Tang *et al.*, 2019) of the total market. Synthetic zeaxanthin has been approved by the European Food Safety Authority (EFSA) to be safe for human consumption in form of food supplements. No adverse effects of taking synthetic zeaxanthin at daily doses of between 10 and 30 mg for a period of up to six months by healthy individuals have been reported (EFSA, 2008). A daily intake of 53 mg of synthetic zeaxanthin by a person of 70 kg of weight, a dose corresponding to 0.75 mg kg⁻¹, was not found to raise any safety concerns (EFSA, 2012).

Synthetic zeaxanthin is a dark orange to red, odourless or slightly scented crystalline powder, majorly present in the *trans*-form (96 to 98%) with minor amounts of *cis*-zeaxanthin (up to 2.0%), parasiloxanthin (up to 0.8%), diatoxanthin (up to 0.2%) and 12'-apo-zeaxanthinal (up to 0.1%;

Stankovic, 2004). Parasiloxanthin is the product of zeaxanthin hydrogenation at positions C₇' and C₈', diatoxanthin is the product of zeaxanthin dehydrogenation at positions C₇' and C₈' and 12'-apo-zeaxanthinal is the product of oxidative cleavage of zeaxanthin at the C₁₁'-C₁₂' double bond. The two major producers of synthetic zeaxanthin are BASF and – following the acquisition of Vitamins & Fine Chemicals division of F. Hoffmann-La Roche & Co. – DSM (Ernst, 2002; Fernandes *et al.*, 2018). Industrially, the total synthesis of zeaxanthin is achieved either with the method developed by BASF based on the Wittig reaction (Wittig & Pommer, 1959) or using the method developed by Hoffmann-La Roche & Co., which is based on the Grignard reaction (Isler *et al.*, 1956).

A double Wittig condensation (C₁₅ + C₁₀ + C₁₅-strategy) between a commercially available, symmetric C₁₀-dialdehyde, corresponding to the central part of the molecule, and two molecules of appropriate C₁₅-phosphonium salts is the most efficient way of building up symmetric, C₄₀-molecules with two identical end groups, such as zeaxanthin. For this reason, the Wittig reaction is the most commonly employed synthesis method. The C₁₅-phosphonium salts are derived from cyclic C₉-ketones, namely ketoisophorone, which are readily available from petroleum-derived products. The Wittig condensation yields the desired all-*trans* isomers as well as mono- and di-*cis* isomers at the newly formed C₁₁-C₁₂ and C₁₁'-C₁₂' disubstituted double bonds. The *cis* isomers are thermally converted into the desired *trans*-form. During the process, the *trans*-isomer crystallises out of the reaction solution of heptane or ethanol and the reaction equilibrium drives the *cis*-to-*trans* conversion.

However, chemical synthesis of zeaxanthin involves additional steps of introducing the chiral centres at the desired configuration to produce the naturally occurring (3*R*,3'*R*)-isomer. This requires generation of an enantiopure C₉-hydroxyketone by introducing the appropriate chirality at the C₄ position (Ernst, 2002). This can be achieved chemically through an enantioselective catalytic hydrogenation (Soukup *et al.*, 1990; Widmer *et al.*, 1990). However, more industrially relevant is a combined, biocatalytic process involving enantioselective fermentative hydrogenation with baker's yeast followed by a catalytic reduction of the C₄ carbonyl group (Leuenberger *et al.*, 1976).

In the first method employing enantioselective catalytic hydrogenation, it is the enol acetate derivative of the ketoisophorone that is used as a substrate and the reaction is catalysed by cationic rhodium diphosphine complexes such as (all-*R*)-EtDuPhOS. The product undergoes methanolysis to remove the acetyl group to produce (*S*)-phorenol and a saturated diketone – a racemic by-product of the reaction. The enantiomeric excess (ee) of (*S*)-phorenol in this reaction is 98% indicating very high purity. (*S*)-phorenol is then converted by a number of steps

into (*R*)-configured C₁₅-phosphonium salt through chain lengthening with C₁-, C₃- and C₂-units (Ernst, 2002).

Alternatively, the introduction of chiral centres can take place by biocatalytic process developed by the Roche group with the use of baker's yeast (Ito *et al.*, 2009). In this process, the C-C double bond of ketoisophorone is reduced to the (*6R*)-configured levodione. The product is catalytically hydrogenated at the sterically less-shielded carbonyl group at C₄ to produce a mixture of (*4R,6R*)-actinol and its (*4S*)-epimer at the 4 to 1 ratio. The epimer is then separated out from the main product by distillation resulting in ee of more than 99.5% (Ernst, 2002). (*4R,6R*)-actinol is then used to make the C₁₅-phosphonium salt either by the C₉ + C₂ + C₄- or C₉ + C₁ + C₃ + C₂-strategy. In the first strategy, a stepwise extension of (*4R,6R*)-actinol is achieved by attaching C₂- and C₄-units corresponding to acetylene and methyl vinyl ketone, respectively. This strategy requires introduction of protective groups on three occasions, which need to be removed to yield the final product. Initially, a protective acetal group is added to resist basic conditions during ethynylation. Next, an acid-stable protective group is introduced which is required for the copper sulfate-catalysed dehydration. Finally, a base-stable protective group is required during the attachment of the C₄-unit and the hydride reduction of propargyl alcohol. Although, this strategy has a high overall yield, the process itself is laborious and unsatisfactory economically and environmentally. The second strategy involves addition of a C₁-unit which is dichloromethyl lithium produced in situ by reacting dichloromethane with butyl lithium. The hydroxyl group of (*4R,6R*)-actinol is deprotonated to the lithium alkoxide and the ketone group is converted to a chlorooxirane. In an elevated temperature, the epoxide ring opens and rearranges to an aldehyde releasing lithium chloride during the process. During aldol condensation, acetone and vinyl Grignard reagent, the C₃- and C₂-units, respectively, are added. After reaction of the product with triphenylphosphane hydrobromide, the oxabicycloheptane system opens to produce C₁₅-phosphonium bromide (Ernst, 2002).

Finally, zeaxanthin can be obtained from isomerisation of lutein, which is of great benefit as this xanthophyll is more abundant in nature and generally easier to obtain, for example from marigold flowers or other food sources. Following lutein purification, excipients, often referred to as 'bulking agents', such as polyoxyethylene glycol (POE) and antioxidants, for example ethoxyquin are added and the isomerisation reaction is allowed to proceed. Under optimised conditions, the achieved yield is 97% (Torres-Cardona & Vizcarra-Gonzales, 2010). In fact, conversion of lutein into *meso*-zeaxanthin requires a change in the position of a single carbon-carbon double bond in the ϵ -ring of lutein. Therefore, conversion of lutein to *meso*-zeaxanthin is readily achieved and although *meso*-zeaxanthin is rare in nature, it is present in significant amounts in chickens and eggs because zeaxanthin is prepared in this form for the use in poultry

feed (Bone *et al.*, 2007). On the other hand, Khachik (2003) obtained a similar yield of 95% in his method describing the conversion of (3*R*,3'*R*,6'*R*)-lutein to (3*R*,3'*R*)-zeaxanthin with *meso*-zeaxanthin being a minor component (5%).

Chemical synthesis allows for a large-scale production, which is the major advantage over other methods used for obtaining zeaxanthin and carotenoids, in general. This is the reason why zeaxanthin obtained by the synthetic route is generally cheaper than zeaxanthin extracts of plant or microbial origin. In fact, the price of synthetic carotenoids stands between 250 and 2 000 USD kg⁻¹, whereas natural carotenoids sell for between 350 and 7 500 USD kg⁻¹ (McWilliams, 2018). Since zeaxanthin is a chiral molecule, some methods of chemical synthesis of zeaxanthin produce a racemic mixture at the ratio of 1:2:1 of the (3*R*, 3'*R*)-, (3*R*, 3'*S*; *meso*)- and (3*S*,3'*S*)-isomers, respectively. As food additives, racemic synthetic carotenoids are cheapest as they do not undergo a difficult and costly separation process into their component enantiomers. However, it was found that the deposition of the racemic zeaxanthin in egg yolks was 25 to 27% lower than that of the *R-R* isomer. Moreover, the rate of carotenoid deposition was found to be the major factor determining the pigmenting efficacy. In fact, carotenoids with higher deposition rate contributed to a greater extent to meat and egg yolk pigmentation than those with lower rates of deposition (Hencken, 1992). Additionally, certain formulations of zeaxanthin require a costly separation of the specific *R-R*, *R-S* and *S-S* stereoisomers, as in case of analytical standards (Garnett *et al.*, 1997). For instance, synthetic zeaxanthin supplied by Cayman Chemical, which is 98% pure and present exclusively as the (3*R*,3'*R*)-isomer (C. Forward, 2019, personal communication, 1st July), is available at 357 USD mg⁻¹. On the other hand, over 95% pure synthetic zeaxanthin supplied by Sigma-Aldrich is available at 497 USD mg⁻¹ even though it is sold in the all-racemic form (V. Kamath, 2019, personal communication, 2nd July).

Finally, a number of technical and safety aspects need to be considered in regard to synthetic zeaxanthin. The most important ones include the reaction efficiency, the final yield of the product and the process of by-product elimination. On top of this, the price of reagents and machinery and the operational costs associated with running and maintenance of the plant need to be factored in. Synthesis of zeaxanthin involves multiple steps with less than 100% efficiency each, resulting in a relatively low final yield of the product (Ernst, 2002). For instance, Loeber *et al.* (1971) developed an eleven-step method in which zeaxanthin was obtained at the final yield of just under 4%. Ruttimann & Mayer (1980) described a seven-step synthesis method of (3*R*,3'*R*)-zeaxanthin with the final yield of 3%. Widmer *et al.* (1990) and subsequently Soukup *et al.* (1990), described eight- and eleven-step processes, respectively of (3*R*,3'*R*)-zeaxanthin synthesis from 6-oxo-isophorone which resulted in the final yields of 27 and 39%, respectively. By-products generated during zeaxanthin synthesis, such as diatoxathin, parasiloxanthin,

C₂₅-zeaxanthaldehyde and the *cis*-isomers of zeaxanthin can be separated from *trans*-zeaxanthin by high-pressure liquid chromatography (HPLC) resulting in over 96% purity (Stankovic, 2004). However, the Wittig reaction yields the difficult to remove by-product of this reaction, triphenylphosphine oxide (TPPO). Removal of TPPO can be achieved by column chromatography, which is particularly tedious on an industrial scale. Other methods of TPPO removal include distillation, direct precipitation, crystallisation, co-crystallisation or conversion into more easily removable species (Batesky *et al.*, 2017). When baker's yeast are used for the preparation of C₉-hydroxyketone, the biocatalyst must be removed from the product. This is generally difficult in conventional fermenters, however immobilisation onto raisins can greatly improve this process (Ernst, 2002).

1.4 Enhancing content of carotenoids in plants

An increasing demand for carotenoids attributed to their health benefits as well as their use in animal and aquaculture feed formulations have stimulated interest in identifying new sources for their production. Generally, carotenoids from renewable plant sources obtained through diet are more appealing to the consumers than synthetic or extracted carotenoids of plant or microbial origin as they are considered to be natural and in fact, identical to the original product identified to have the beneficial effect on health. However, the number of currently available plant sources is unable to meet the market demand for carotenoids. Therefore, many carotenoids are obtained by chemical synthesis and extraction from non-food plant sources and microorganisms. A number of strategies, such as conventional plant breeding and genetic engineering, have been employed to improve the levels of carotenoids in the existing food crops as well as to generate new plant sources of carotenoids through modification of the existing biosynthetic pathways or introduction of entirely new pathways into non-carotenoid accumulating backgrounds.

1.4.1 Conventional plant breeding approaches

Conventional plant breeding methods rely on selecting plants with the desired traits and propagating the chosen phenotypes while removing plants with less desirable characteristics. Alternatively, crossing of different species of the same genus, typically an elite variety (recurrent or recipient parent) with a wild variety (donor parent), followed by repeated backcrossing with the recurrent elite parent can introduce new traits into the desired background. The movement of a part of the genome or a single gene from one species into the gene pool of another through repeated backcrossing with one of the parents is known as introgression. For instance, the introgression of the bottom of chromosome 4 from the green-fruited wild tomato *Solanum habrochaites* (previously *Lycopersicon hirsutum*) LA1777 into the *S. lycopersicum* (previously

L. esculentum) cv. E6203 (TA209) background enhanced lycopene accumulation and the red colouration of the fruit (Monforte *et al.*, 2001). Two independent loci, namely *ecol4.1* and *icol4.2*, affecting fruit colour were identified within the introgressed region. Interestingly, none of the genes known to code for the enzymes involved in carotenoid biosynthesis nor any of the known ripening-related genes were found to map to the identified loci on chromosome 4. Therefore, it was suggested that *ecol4.1* and *icol4.2* could be involved in the regulatory aspects of carotenoid biosynthesis by controlling expression of genes directly involved in lycopene production and accumulation (Monforte *et al.*, 2001).

However, in conventional breeding, selection of the individual plants with the desired traits is not always easy, especially when the phenotype is expressed late in the development. With the advent of molecular biology, marker assisted selection (MAS) became available. MAS relies on a selection of an appropriate molecular marker associated with the desired trait and screening for this marker instead in the breeding population. The marker could be a fragment of DNA such as amplified fragment length polymorphism (AFLP), random amplification of polymorphic DNA (RAPD), restriction fragment length polymorphism (RFLP), single nucleotide polymorphisms (SNPs) or a short tandem repeat (STR) flanking a chromosomal region, known as the quantitative trait locus (QTL), which is associated with the desired trait. A QTL may consist of a single gene or a cluster of genes and can be found on the same or different chromosomes. For example, the 3' transposable element (TE) spanning the region between exon 6 and the 3' untranslated region (3'UTR) of β -carotene hydroxylase 1 (*CrtR-b1*) was used in MAS to identify maize hybrids with up to a 12.6-fold increase in kernel β -carotene levels compared to the recurrent parent (Muthusamy *et al.*, 2014). In tomato, increased lycopene content was found to be associated with a 1.5 centimorgan (cM) region on chromosome 12 introgressed from *S. pimpinellifolium* cultivar LA2093. This region, known as *lyc12.1*, was proposed to be a potential target for MAS (Kinkade & Foolad, 2013).

Mutation breeding, which employs the use of mutagens such as ethyl methanesulfonate (EMS) and dimethyl sulfate (DMS) or radiation in order to introduce changes at the DNA level, is also considered as a conventional breeding method. The EMS-induced *high-pigment 3* (*hp3*) tomato mutant, with a missense mutation in ZEP, was found to accumulate 30% more carotenoids in the mature fruit compared to the wild type (Galpaz *et al.*, 2008). However, mutation breeding does not always cause an increase in carotenoids content. In fact, it very rarely does. For instance, the tomato *white-flower* (*wf*) mutagen-induced mutant, with affected β -carotene hydroxylase 2 (*CrtR-b2*), accumulated 80% less carotenoids in the flower petals compared to the wild type. Interestingly, the carotenoid levels in the leaves and fruit of this plant were not affected (Galpaz *et al.*, 2006).

Another breeding strategy, which takes advantage of mutational breeding, is Targeting Induced Local Lesions in Genomes (TILLING). A selected mutagen, typically EMS, introduces point mutations in a vast seed population. The mutations are consequently screened using high throughput methods at the specific target site and associated with the phenotype. For instance, TILLING was used to identify lycopene ϵ -cyclase (*LCY-E*) gene mutant in durum wheat (*Triticum turgidum* L.ssp. *durum*) with a 75% increase in β -carotene as well as a greater overall carotenoid content in leaves (Richaud *et al.*, 2018). TILLING allowed to identify point mutations in the gene encoding a component of light signal machinery *DET1*, leading to 1.9-fold and 4.5-fold increases in β -carotene and lutein, respectively in ripe tomato fruit (Jones *et al.*, 2012). TILLING method was also used to identify a missense mutation in chromoplast-specific lycopene β -cyclase (*CYC-B*) in tomato which caused a 2.1-fold increase in accumulation of lycopene in fruit (Silletti *et al.*, 2012). Phytoene synthase (*PSY1*), the enzyme catalysing the first committed step of the carotenoid biosynthetic pathway was analysed by TILLING as well. Two mutations of *PSY1* were identified: a premature STOP codon and a base substitution. The nonsense mutation generated a knockout allele resulting in almost complete loss of carotenoids in the ripe fruit except for lutein. The second mutation involved a substitution of a single amino acid. This mutation delayed lycopene and β -carotene accumulation during fruit ripening (Gady *et al.*, 2012).

Conventional plant breeding programs are expensive, laborious and time consuming. Generation of near-isogenic lines (NILs) containing the desired introgression fragments in an otherwise homogeneous background requires repeated backcrossing, sometimes up to the 7th generation. However, if successful, these programs can generate new varieties with enhanced carotenoid content and traits in general. On the other hand, induced plant mutants may not always contain desired mutations. However, they are important tools for studying regulation of carotenoid biosynthesis. They can also be used in breeding as introducing different mutations in a single plant might indeed lead to the accumulation of a desired carotenoid product.

1.4.2 Genetic engineering

In conventional breeding, the pool of available genes is limited in any one species and there is also a lack of control over which traits get to be passed on to the next generation. Even with hybrid breeding, the heterosis effect is progressively reduced in the following generations. Genetic engineering can overcome these restrictions as it allows for transfer of genes between different and sometimes unrelated species, greatly increasing the availability of the desired traits lasting over many generations. Compared to the conventional breeding methods, genetic engineering offers much more versatility in terms of what traits can be introduced or silenced in the selected genetic background. However, overexpression or silencing of a gene might not necessarily lead to the accumulation of the desired product in the plant host. Carotenoids,

similarly to other secondary metabolites, are produced through a complicated biological pathway with many regulatory mechanisms acting at different levels within it. Therefore, a better understanding of the pathway itself and its regulatory mechanisms is required in order to apply certain modification that could potentially lead to an increased production and accumulation of the desired product.

Metabolic engineering uses the tools that genetic engineering offers but additionally studies different metabolic pathways and identifies their rate-limiting and regulatory elements. This information is then used to introduce genetic modifications in a way that optimises or changes flux through the pathway. Engineering of the pathway can be either quantitative or qualitative. Quantitative engineering aims at increasing flux through the pathway in order to accumulate the end product. Qualitative engineering on the other hand, aims to create a new carotenoid pathway or change carotenoid composition in a tissue of interest.

The application of genetic engineering to increase or modify carotenoid content in plants has been successful. Transformation of potato, *Solanum tuberosum* L., with the sense and antisense constructs encoding ZEP, prevented conversion of zeaxanthin to violaxanthin and increased accumulation of this xanthophyll. Levels of zeaxanthin up to 130-fold greater than in the wild type were achieved using this method (Römer *et al.*, 2002). Enfissi *et al.* (2005) generated a transgenic tomato line accumulating 2.4- and 2.2-fold greater levels of phytoene and β -carotene by transforming plants with bacterial 1-deoxy-D-xylulose 5-phosphate synthase (*DXS*) gene. The previous two approaches worked by targeting a gene encoding an enzyme of the carotenoid biosynthetic pathway. Another approach was taken by Lu *et al.* (2018), where they identified a transcription factor from sweet orange, *Citrus sinensis*, binding the promoter of lycopene β -cyclase (*LCY-B*). This transcription factor, *CsMADS6*, was overexpressed in tomato leading to altered carotenoid profiles. Fruit pericarp accumulated higher levels of β -carotene and lower levels of lutein compared to the wild type. Interestingly, the sepals accumulated very high levels of lycopene which is normally absent in this part of the plant. Overexpression of the transcription factor also led to upregulation of genes encoding lycopene β -cyclase (*LCY-B1* and *CYC-B*), phytoene synthase (*PSY*), phytoene desaturase (*PDS*), carotene *cis-trans* isomerase (*CRTISO*) and α - and β -carotene hydroxylases (*CrtR-e* and *CrtR-b*) in tomato fruit. As can be seen from this approach, the introduction of a transcription factor into the pathway has a potential to influence that pathway at multiple levels and alter the carotenoid profile significantly.

Finally, β -carotene production was also achieved in rice grain, which normally does not accumulate carotenoids as it lacks the elements of the carotenoid biosynthetic pathway capable of converting GGPP to lycopene. To fill in this gap, phytoene synthase (*PSY*) from daffodil

(*Narcissus pseudonarcissus*) and phytoene desaturase (*CRTI*) from the soil bacterium *Pantoea ananatis* (previously *Erwinia uredovora*) were placed under the control of the endosperm-specific glutelin 1 (*Gt1*) promoter and transformed into rice (Ye *et al.*, 2000). The combination of these two genes together with endogenously expressed lycopene



Figure 1.15. Wild type rice grains (left) compared to the first (middle) and second (right) generations of Golden Rice. The wild type rice produces β -carotene only in the leaf tissue but not in the endosperm, unlike the Golden Rice which also produces β -carotene in its endosperm giving the rice grain the characteristic yellow/gold colouration (Paine *et al.*, 2005).

isomerase and lycopene β -cyclase in the rice grains, led to the final production of Golden Rice accumulating β -carotene (Figure 1.15). Further work led to the generation of Golden Rice 2, which accumulated up to 23 times more carotenoids than the original variety (Paine *et al.*, 2005). As of 2020, Australia, Canada, New Zealand, Philippines and USA have already affirmed the safety of Golden Rice for consumption, however, its commercial propagation has not yet been approved by the respective governing bodies.

The development of Golden Rice was possible due to the use of biotechnology and metabolic engineering and has a potential to alleviate vitamin A deficiency. However, the use of genetic engineering in plant breeding faces a number of regulatory challenges. GM crops have been grown in the United States, India and China extensively, however, not without opposition. The growth of GM crops in Europe is strictly regulated and requires pre-market authorisation and post-market monitoring. European Food Safety Authority (EFSA) is responsible for the evaluation of each new GM crop and then reports to European Commission which either grants or refuses the authorisation. However, many member states, such as France, Germany, Austria, Greece, Hungary, the Netherlands, Latvia, Lithuania, Luxembourg, Bulgaria, Poland, Denmark, Malta, Slovenia, Italy and Croatia, have banned the growth of GM crops. GM crops also face resentment from the general public as they tend to be perceived by many as something unnatural and dangerous to people and the natural environment. It is quite unlikely that GM crops will be grown extensively in Europe in the near future. However, GM crops intended for animal instead for human consumption do not require the same level of approval and raise fewer concerns. Moreover, the valuable products extracted from GM crops can be used in a variety of markets as long as biochemical and functional equivalence of the compound to the natural one is demonstrated (Food and Agriculture Organization of the United Nations, 2008). An alternative to the use of genetic engineering in generation of crops accumulating valuable compounds could be the use of novel gene editing technologies, such as CRISPR/Cas9. Although still considered a genetic modification, this approach could be more acceptable as once the

modifications have taken place and the desired trait was achieved, the remaining foreign DNA can be lost in the next generations. It was already shown that CRISPR/Cas9 mediated editing of stay green 1 (*SGR1*) gene could increase lycopene accumulation 5.1-fold (Li *et al.*, 2018b). Therefore, the use of genome editing technologies can become a useful tool for the enhancement of carotenoid content.

1.5 Aims and objectives

In light of the presented evidence describing the commercial and health-related importance of zeaxanthin, **the aim of this project is to develop a novel tomato line accumulating zeaxanthin in its ripe fruit.**

Two different strategies will be used to achieve this aim. Firstly, conventional crossing will be carried out in two stages (Chapters III and IV) to combine the genes of interest from three parental lines into a single plant in order to enhance accumulation of zeaxanthin. Originally, these genes were introduced into the respective parental lines either by conventional breeding or genetic engineering. Specifically, each of the parental lines was developed using one of the following: genetic engineering, introgression through repeated backcrossing or mutagenesis. Secondly, the novel genetic editing technology with CRISPR/Cas9 (Chapter V) will be used to target *ZEP* and facilitate zeaxanthin accumulation in tomato plants. This approach may lead to the generation of novel alleles of *ZEP* with potential for their use in future breeding programs. The first strategy is considered to have a lower risk of failure since it involves work with lines of well-established phenotypes. On the other hand, the second strategy is considered to have a higher chance of being unsuccessful. Firstly, because it involves the use of a novel technique in a limited timeframe. Secondly, CRISPR/Cas9-mediated editing of *ZEP* may knockout the gene important for plant photoprotection and hormone metabolism.

To reiterate, zeaxanthin was selected as the target compound due to its limited availability in consumed diet and its known health benefits. The platform selected to carry out the presented work is tomato. There are several reasons for choosing this organism and to use it as a vessel to deliver zeaxanthin. Firstly, tomato is a staple crop which is widely cultivated and popular amongst the consumers. Secondly, the carotenoid biosynthetic pathway of tomato has been elucidated in detail. Most importantly however, tomato accumulates great amounts of lycopene which is the precursor of zeaxanthin and other xanthophylls. Additionally, the work on tomato is facilitated by the fact that its genome has been sequenced and the plant is amenable to genetic manipulation and conventional breeding strategies.

The subsequent sections outline in more detail the activities towards the major objectives that will be carried out in order to achieve the aim of this thesis.

1.5.1 Identification and characterisation of xanthophyll-accumulating tomato

Some work has been done previously on designing a strategy for xanthophyll accumulation in tomato by generating a single-insert hemizygous transgenic U/0 line overexpressing β -carotene hydroxylase (*CrtR-b2*) gene (D'Ambrosio *et al.*, 2011). In the following work, in order to further increase the flux through the pathway and push it towards the production of zeaxanthin, the U/0 line has been crossed with a recombinant inbred line (RIL) characterised by high levels of β -carotene (Nogueira *et al.*, 2017). The high β -carotene content in this line is a consequence of the strong promoter of chromoplast-specific lycopene β -cyclase (*CYC-B*) causing the *CYC-B* gene to be expressed at a very high level. This particular allele of *CYC-B* has been known as the *B* gene prior to its identification (Ronen *et al.*, 2000).

Objective 1: Verification of the above strategy as a means to generate new lines capable of accumulating xanthophylls in their fruit instead of the typically present carotenes.

Activities towards the major objective include:

- Designing an efficient screening method to identify lines with different combinations of the two genes of interest (*CrtR-b2* and *CYC-B*) in the segregating population.
- Characterisation of leaf and fruit pigment profiles of the different lines in order to evaluate the best gene combinations for future breeding programs.
- Assessment of phenotype stability by taking the selected lines to the next generation.
- Analysis and comparison of primary and secondary metabolites in the fruit of the generated lines in order to assess if and how they are affected by changes in the carotenoid profile.
- Profiling of carotenoids derived from fractionated chromoplasts of the generated lines in order to identify sites of xanthophyll deposition at the sub-plastidial level.
- Comparison of the chromoplast ultrastructure of the xanthophyll-accumulating line with the wild type chromoplast in order to assess if and how the chromoplast adapts or responds to the presence of the xanthophylls and to the perturbations in carotenoid composition in general.
- Identification of differentially expressed genes in the xanthophyll-accumulating line. These candidate genes could serve as targets for future work aiming at optimisation of xanthophyll accumulation in tomato and could also provide some insight into the regulatory mechanisms of carotenoid biosynthesis.

The above activities are the subject of Chapter III of this thesis.

1.5.2 Optimisation of zeaxanthin production

Generation of new, renewable plant food sources of zeaxanthin is of particular interest as its beneficial role in supporting eye health has long been established. However, zeaxanthin is not easily obtainable through diet unlike the other macular pigment, lutein because it acts as a precursor for synthesis of other xanthophylls and the plant hormone ABA. Therefore, in order to boost zeaxanthin accumulation in tomato and simultaneously stop it from being metabolised further, the strategy used to increase flux through the carotenoid pathway described in Chapter III will be combined with a metabolic block at the level of ZEP. In order to introduce this block into the pathway, the allele of *ZEP* encoding a defective form of the enzyme will be used. The source of this allele is the *high-pigment 3 (hp3)* tomato mutant (Galpaz *et al.*, 2008).

Objective 2: Optimisation of zeaxanthin accumulation by selecting tomato lines accumulating xanthophylls in their fruit (the outcome of Chapter III) and crossing them with the *hp3* tomato mutant.

Activities towards the major objective include:

- Screening for the presence of *CrtR-b2* and *CYC-B* in the segregating population using the strategy developed in Chapter III in order to identify lines with the desired gene combinations.
- Designing an efficient screening method to identify plants carrying the *hp3* allele of *ZEP*.
- Characterisation of the leaf, fruit and flower pigment profiles of the lines with different combinations of the genes of interest to assess which of them are necessary for zeaxanthin accumulation.
- Analysis and comparison of fruit primary and secondary metabolites of the selected lines to assess if and how they are affected by changes in the carotenoid profile.
- Profiling of carotenoids derived from fractionated chromoplasts of the selected lines in order to identify sites of zeaxanthin deposition at the sub-plastidial level.
- Analysis of the photosynthetic efficiency of the selected lines in context of the pigment composition of the leaf tissue.
- Quantification of zeaxanthin content in the fruit and comparison against the daily recommended dose as well as other known plant sources of zeaxanthin.

The above activities are the subject of Chapter IV of this thesis.

1.5.3 CRISPR/Cas9-mediated editing of *ZEP*

The functionality of *ZEP* seems to be critical for the plant's ability to accumulate zeaxanthin. This was first shown by Thompson *et al.* (2000) when antisense downregulation of *ZEP* caused an

increased accumulation of zeaxanthin in tomato leaves and simultaneously led to a decrease in violaxanthin and neoxanthin contents. Since only two, other than the wild type, alleles of *ZEP* are known, namely *hp3-1* and *hp3-2*, with the latter exhibiting only a weak phenotype, discovery of novel alleles of this gene in tomato is highly anticipated. Currently, this process can be accelerated with CRISPR/Cas9 technology. The use of targeted gene editing systems has a potential to generate a range of alleles or knockouts with new and interesting phenotypes and the novel alleles may contribute to a better understanding of a gene's function. Therefore, generation of novel alleles of *ZEP* may bring about new phenotypes characterised by elevated levels of zeaxanthin and broaden the knowledge about this gene and the enzyme it encodes.

Objective 3: Generation of new alleles of *ZEP* using CRISPR/Cas9.

Activities towards the major objective include:

- Analysis of leaf and fruit pigments of the edited plants in order to identify interesting phenotypes and compare them against the *hp3* mutant.
- Identification of types of mutations that have occurred in the edited plants in order to assess how these correspond to the observed phenotypes.
- Modelling of the novel alleles of *ZEP* and comparison with the *hp3-1* allele.

The above activities are the subject of Chapter V of this thesis.

The placement of the three major objectives within the carotenoid biosynthetic pathway is illustrated in Figure 1.16.

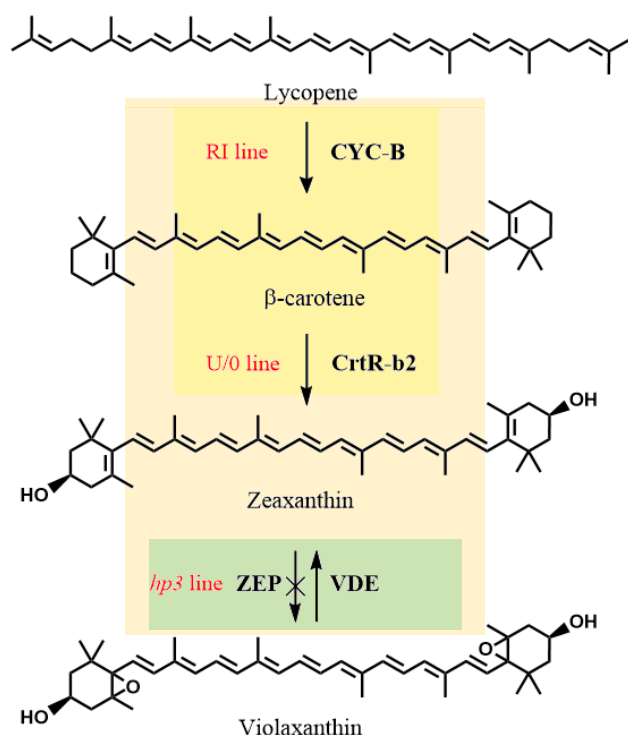


Figure 1.16. Placement of the major objectives within the simplified carotenoid biosynthetic pathway. Objectives 1, 2 and 3 are indicated in yellow, orange and green rectangles, respectively. The names of the parental lines are indicated in red and placed next to the steps of the pathway to which they contribute. For detailed description of the parental lines, refer to Sections 1.5.1 and 1.5.2 above and Section 2.1.1 of Materials and Methods. CrtR-b2 – β -carotene hydroxylase, chromoplast-specific; CYC-B – lycopene β -cyclase, chromoplast-specific; VDE – violaxanthin de-epoxidase; ZEP – zeaxanthin epoxidase.

Chapter II: Materials and Methods

2.1 Plant cultivation and material collection

2.1.1 Tomato varieties

In stable transformation of tomato with CRISPR/Cas9 expression cassettes (2.5.3), the laboratory's own in-house seed stocks of the cultivar Ailsa Craig (AC) were used. The population of AC plants has been sustained through regular sowing and seed collection. Similarly, the cultivar Moneymaker (MM), initially used as a reference phenotype, has been maintained in the laboratory through repeated cultivation. The following varieties were used to generate novel lines by cross-pollination (2.1.3) as outlined in Figure 2.1. The RI variety is a recombinant inbred line derived from the 7th generation backcross (BC7) between the cultivated *Solanum lycopersicum* UC204B (LA4437) and the wild tomato *S. galapagense* (LA0483) and is characterised by high levels of β -carotene in its ripe fruit (Peterson *et al.*, 1991). This phenotype results from introgression of chromoplastic (flower- and fruit-specific) lycopene β -cyclase (*CYC-B*) from chromosome 6 of *S. galapagense* into the UC204B background. This dominant allele of *CYC-B*, which used to be known as the *B* gene prior to its characterisation, is expressed from a strong promoter at high levels from the breaker stage of fruit development onwards (Ronen *et al.*, 2000). The RI line was provided from the Bulgarian collection as a part of the EU-funded collaborative project EUSOL (Maggioni & Spellman, 2001). Prior to this work, the RI line had been crossed with transgenic ZW line expressing fused bacterial β -carotene hydroxylase (*CrtZ*) and ketolase (*CrtW*) from *Brevundimonas* sp. (Nogueira *et al.*, 2017). The fusion gene was lost in later generations producing lines of mixed genetic backgrounds which retained the *B* gene (Figure 2.1). In this work, lines derived from the RI parent are labelled as *B/B* or *B/+* to indicate plants homozygous and heterozygous for *S. galapagense* *CYC-B* allele, respectively. The U/0 tomato is a single-insert hemizygous transgenic line of the cultivar Red Setter background overexpressing endogenous, chromoplast-specific β -carotene hydroxylase 2 (*CrtR-b2*; GenBank Accession no. DQ864755) derived from the cDNA of Red Setter and placed under control of the Cauliflower Mosaic Virus (CaMV) 35S promoter (D'Ambrosio *et al.*, 2011). This line accumulates β -carotene-derived xanthophylls in its ripe fruit. However, when the transgene is present in a homozygous state (U/U), this does not happen. The seeds of the U/U line were kindly provided by Doctors Caterina D'Ambrosio, Adriana Lucia Stigliani and Giovanni Giorio from Metapontum Agrobios, Italy. The *high-pigment 3* (*hp3*) tomato is an EMS-induced mutant of the cultivar M82 background characterised by ABA deficiency, beige flowers and increased total carotenoid content of ripe fruit. The *hp3* phenotype results from a recessive, missense mutation in exon 1 of *ZEP* which is only expressed when both mutated alleles are present (Galpaz *et al.*, 2008). The seeds of the *hp3* tomato were kindly provided by Professor Joseph Hirschberg from the Hebrew University of Jerusalem. A brief description of varieties used in this work is provided in Table 2.1.

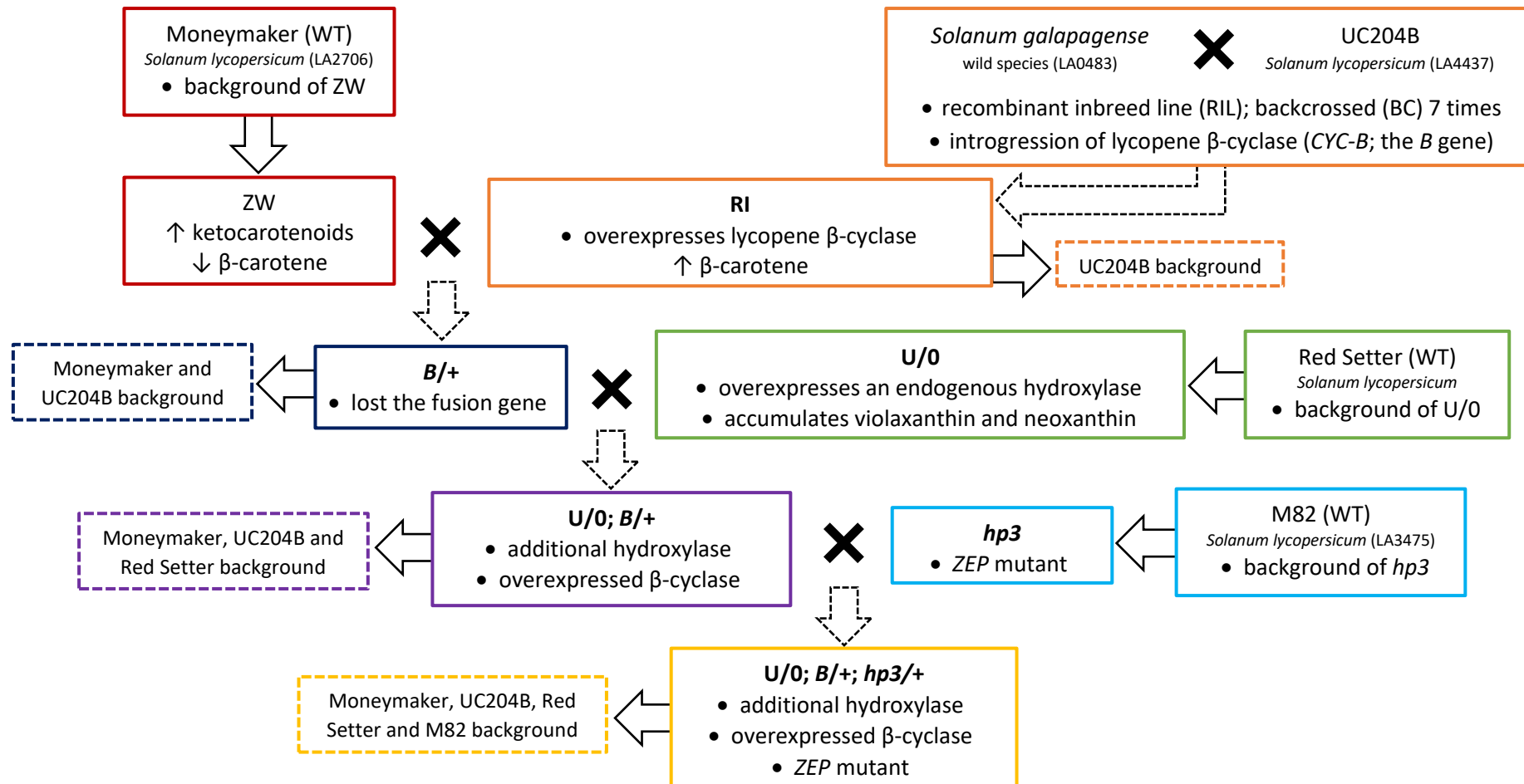


Figure 2.1. Outline of the crossing strategy. The black crosses indicate crossing events with the dashed arrows pointing towards the F₁ hybrids. The full arrows point towards the background of a given tomato line (dashed rectangles) or from the original variety that was modified (full rectangles). Names or genotypes of the relevant varieties are in bold font. Hence, only the genotypes of the first filial generations are provided. Genotypes: '+' – wild type allele at any locus; *B* – *S. galapagense* *CYC-B* allele (dominant); *hp3* – *high-pigment 3* allele of *ZEP* (recessive); *U* – *CrtR-b2* transgene insertion; *0* – lack of transgene insertion. Hence, if written alone, *hp3* refers to the original line described by Galpaz *et al.* (2008).

Table 2.1. Tomato varieties used in this study. The accession numbers are provided by UC Davis Tomato Genetics Resource Center (TGRC); n/a – not applicable.

Variety	Accession	Gene	Description	Background	Reference
Ailsa Craig, AC	LA2838A	n/a	- used in stable transformation of tomato	n/a	n/a
Azygous, Az	n/a	n/a	- transgenic <i>CrtR-b2</i> at the U locus and <i>S. galapagense</i> <i>CYC-B</i> alleles segregated out - reference phenotype	MM, UC204B and Red Setter	n/a
<i>hp3</i>	n/a	zeaxanthin epoxidase, <i>ZEP</i>	- accumulates 30% more carotenoids in the ripe fruit compared to WT M82 - carries two <i>hp3-1</i> alleles of <i>ZEP</i> (substitution of glutamic acid by lysine at position 142 (E142K))	M82	Galpaz <i>et al.</i> , 2008
Moneymaker, MM	LA2706	n/a	- reference phenotype (only initially)	n/a	n/a
RI	n/a	lycopene β -cyclase, <i>CYC-B</i>	- levels of β -carotene in the ripe fruit are 6 times greater than in MM - introgression of chromoplast-specific <i>CYC-B</i> (the <i>B</i> gene) from <i>S. galapagense</i> (LA0483) - phenotype expressed either in homozygous (<i>B/B</i>) or heterozygous (<i>B/+</i>) state	UC204B	Peterson <i>et al.</i> , 1991; Nogueira <i>et al.</i> , 2017
U/0	n/a	β -carotene hydroxylase, <i>CrtR-b2</i>	- overexpression of endogenous, chromoplast-specific <i>CrtR-b2</i> from the U locus under control of the CaMV 35S promoter - transgene expression in homozygous plants (U/U) is lower than in hemizygous (U/0) plants	Red Setter	D'Ambrosio <i>et al.</i> , 2011

2.1.2 Seed germination and glasshouse growth conditions

Sterilised tomato seeds (2.1.5) were germinated on Advance Seed & Modular F2+S compost (Levington, UK) and grown at $26^{\circ}\text{C} \pm 3^{\circ}\text{C}/19^{\circ}\text{C} \pm 3^{\circ}\text{C}$ day/night temperatures and 16 hours of light and 8 hours of dark (16L/8D) photoperiod under supplementary 400 W, 230 V sodium SON-T luminaires (Agrolux, The Netherlands). The minimum irradiance measured at crop-height within the chamber was $160 \mu\text{mol m}^{-2} \text{s}^{-1}$ Photosynthetically Active Radiation (PAR). Plants were potted up with High Nutrient M3 compost (Levington, UK) mixed with the granular systemic insecticide Exemptor® (0.4 g l^{-1} ; Dejex, UK) containing thiacloprid (10% w/w; BHGS Ltd, UK). At fruit set, plants were fed on a weekly basis with Allrounder 20-20-20+TE (Peters Professional, UK) via a D3 Green line (Dosatron, France). The seeds collected from the F₁ hybrid crosses of the U/0; B/+, *hp3*/+ genotype were germinated on nutrient-agar supplemented with kanamycin ($100 \mu\text{g ml}^{-1}$; Sigma) to select for *CrtR-b2* transgenic plants. The composition of the growth media and incubation conditions are described in Section 2.2.3. Seedlings, showing no symptoms of stress from the growth on kanamycin, were transferred to the F2+S compost and then the M3 compost and cultivated in the glasshouse at the conditions described above. Table 2.2 lists the growth seasons and cultivation sites of different tomato populations along the type of material collected and analyses performed on this material.

2.1.3 Cross-pollination of tomato lines

Plants were cross-pollinated in the morning (at 15 to 21°C) to avoid excessive temperatures. Unopened flowers (female parents) were emasculated with tweezers to remove the anther cone and the petals making sure that the pistil remained intact. The pollen was collected from opened or partially opened flowers (male parents) onto a glass slide by tapping the flower with vibrating tweezers. The pollen was transferred to a female flower by touching the stigma with the pollen-covered glass slide. The initial cross between the B/+ variety (the cross between the ZW and the RI line where the fused transgene had been segregated out) and the U/0 line (Figure 2.1) generated the F₁ hybrid population hemizygous for the transgene U locus and heterozygous for the B gene (U/0; B/+ genotype). In the following F₂ population, both genes segregated independently and the plants from which they were lost (0/0; +/+ genotype), were selected as a reference phenotype. In this work, these plants are referred to as Azygous (Az) and, although not indicated, they also carry two WT alleles of *ZEP*. Additionally, the segregation pattern at the transgene U locus was used to establish zygosity of the parental plants (2.3.7.1). For crossing with the *hp3* line, typically plants of the U/U; B/B genotype were selected as female parents to minimise screening steps in subsequent generations. However, due to limited flower availability, some crosses were reciprocal and U/0; B/B plants were also used. Crossings were primarily performed by Mr Mark Levy, a horticulturist at Royal Holloway University of London.

Table 2.2. List of tomato populations grown between 2015 and 2018. For the description of analyses performed, see further text. Refer to Figure 2.1 for the explanation of genotypes. Hence, if written alone, *hp3* refers to the original line described by Galpaz *et al.* (2008). Az – Azygous; L – leaf; Fr – fruit; Fl – flower; n/a – not applicable.

Year	Season	Population	Type of analysis and material collected	Generation	Crossing	Site
2015	Autumn – Winter	U/0; B/+	- L: screening (PCR), pigment (HPLC) - Fr: pigment (HPLC)	F ₁	Selfing	Silwood
2016	Spring – Autumn	U/0; B/B, U/0; B/+ U/U; B/B, U/U; B/+ 0/0; +/+ (Az)	- L: screening (PCR, Southern blot, qPCR), pigment (HPLC) - Fr: pigment (TLC, HPLC), metabolites (GC-MS), volatiles (SPME), transcriptome (RNA-Seq)	F ₂	Crossed with <i>hp3</i>	Bourne/ Chestnut
		<i>hp3</i>	- L: screening (PCR)	n/a	Crossed with F ₂ U/U; B/B or U/0; B/B	
2017	Spring – Autumn	U/0; B/B, U/0; B/+ U/U; B/B, U/U; B/+ 0/0; +/+ (Az)	- L: screening (PCR, qPCR) - Fr: sub-chromoplast fractionation (UPLC), microscopy (TEM), fruit firmness	F ₂		
		<i>hp3</i>	- L: screening (PCR, HRM)	n/a		
		U/0; B/+; <i>hp3</i> /+	- L: screening (PCR, qPCR, HRM)	F ₁		
2017 – 2018	Autumn – Spring	U/0; B/B; <i>hp3</i> / <i>hp3</i> U/0; B/+; <i>hp3</i> / <i>hp3</i> U/U; B/B; <i>hp3</i> / <i>hp3</i> U/U; B/+; <i>hp3</i> / <i>hp3</i>	- L: screening (PCR, HRM), pigment (HPLC), chlorophyll fluorescence - Fr: pigment (HPLC), sub-chromoplast fractionation (UPLC), metabolites (GC-MS), volatiles (SPME) - Fl: pigment (HPLC)	F ₂		Chestnut
		U/0; B/B 0/0; +/+ (Az)	- L: screening, (PCR, HRM), pigment (HPLC), chlorophyll fluorescence - Fr: pigment (HPLC), sub-chromoplast fractionation (UPLC) - Fl: pigment (HPLC)	F ₃		
		<i>hp3</i>	- L: screening, (PCR, HRM), pigment (HPLC), chlorophyll fluorescence - Fr: pigment (HPLC), metabolites (GC-MS), volatiles (SPME) - Fl: pigment (HPLC)	n/a	n/a	
		AC	- Stable transformation of tomato (CRISPR/Cas9 editing) - L: screening (PCR), pigment (HPLC), chlorophyll fluorescence - Fr: pigment (HPLC)	T ₀		

2.1.4 Material collection and storage

For genotyping of tomato lines, young leaves from the growing tip of each plant were collected. This tissue was used directly for genomic DNA extraction (2.3.1.2) or, if not used immediately, snap-frozen in liquid nitrogen and stored at -80°C until required. For extraction of pigments from tomato leaves and flowers, the material was snap-frozen in liquid nitrogen directly after the collection and processed immediately or stored at -80°C until required. Prior to the pigment extraction, the leaf and flower material was freeze-dried overnight on the FreeZone 12L freeze-dry system (Labconco, USA) or the LYOVAC GT2 freeze-dryer (Leybold-Heraeus, Germany) and processed as further described (2.6.1). For leaf tissue analysis, between 10 and 12 of the uppermost mature leaves were collected per plant. For flower analysis, between 12 and 15 of the fully-opened flowers were collected from each plant. The peduncles and sepals of these flowers were discarded, and the petals and anther cones were kept for analysis. Spinach and kale leaf samples were purchased from a local goods supplier and used for pigment extraction. The material was snap-frozen in liquid nitrogen and freeze-dried overnight (spinach) or for 3 days (kale) before being processed as further described (2.6.1). For the analysis of pigments of ripe tomato fruit (2.6.2), polar and non-polar metabolites (2.6.6) as well as volatile compounds (2.6.7), the collected fruit were de-seeded, cut into smaller pieces, snap-frozen in liquid nitrogen and stored at -80°C until required. Additionally, the fruit of *Azygous*, U/0; B/B and U/0; B/+ tomato plants were used for pigment analysis at different ripening stages: immature green (IG), mature green (MG) and turning (T). Prior to the extraction of pigments (2.6.1) and polar and non-polar metabolites (2.6.6), the fruit material was freeze-dried for 3 days. Prior to the analysis of volatile compounds (2.6.7), the snap-frozen tomato fruit tissue was thawed on ice overnight. Typically, at least three fruit at the required developmental stage (IG, MG, T and ripe (R)) were collected per plant and pooled. All analyses were performed on at least three biological samples (plants) or as otherwise indicated, if not enough replicates were available. The collected plant material (flower, leaf and fruit) was photographed using an EOS 750D (W) digital camera (Canon, Japan) and EF-S 18 – 55 mm, f/3.5 – 5.6 IS STM, Ø58 mm zoom lens (Canon).

2.1.5 Seed separation and sterilisation

Tomato seeds were removed from the locular cavity along with some of the jelly-like parenchyma surrounding them and soaked for 2 hours at room temperature (~22°C) in a solution of hydrochloric acid, HCl (18.5% v/v; Fisher Chemical, USA). Next, the seeds were thoroughly rinsed with cold tap water, left to air-dry for 2 days and subsequently stored in paper bags at room temperature in dark and away from moisture. Prior to sowing, the seeds were sterilised in order to comply with the regulations on prevention of the introduction of new plant pathogens such as Tobacco Mosaic Virus (TMV) into the glasshouse. Initially, the seeds were surface

sterilised by soaking in a solution of trisodium phosphate, TSP (10% w/v; VWR, USA) for 20 minutes at room temperature. This was followed by a thorough rinse in running cold water. Further sterilisation was achieved by incubating the seeds at 67°C for 2 days in the SI30H hybridisation oven/shaker (Stuart, UK). The sterilised seeds were germinated as previously described (2.1.2).

2.1.6 General characterisation of tomato leaf and fruit organs

A general characterisation of the selected lines was performed by assessing their photosynthetic performance, fruit firmness and chromoplast ultrastructure.

2.1.6.1 Photosynthetic performance (F_v/F_m)

The ratio of variable (F_v) over maximum (F_m) chlorophyll fluorescence was measured using the Pocket PEA Chlorophyll Fluorimeter (Hansatech Instruments Ltd, UK) and data were extracted with PEA Plus software, version 1.02. The F_v/F_m ratio represents the maximum potential quantum efficiency of Photosystem II (PS II) if all capable reaction centres were open (Kitajima & Butler, 1975). The measurement parameters – time to reach the dark adaptation and the minimal light intensity to fully reduce all reaction centres were established experimentally by performing a light induction curve in the range of 500 – 3 500 $\mu\text{mol m}^{-2} \text{s}^{-1}$ on the dark-adapted Azygous (Az) plants over a course of 5 – 30 minutes. The measurement was carried out on at least three tomato plants from the F_2 population of the U/0; B/B; *hp3/hp3*, U/0; B/+; *hp3/hp3*, U/U; B/B; *hp3/hp3* and U/U; B/+; *hp3/hp3* genotypes, F_3 population of the U/0; B/B and 0/0; +/+ (Az) genotypes, *hp3* line and all T_0 CRISPR/Cas9 edited AC plants (Table 2.2). Three leaves were analysed per plant and the readings were averaged. The tallest and visually healthy-looking leaves were selected from the bottom, middle and top sections of each plant (one leaf per section). Prior to taking the measurement, the leaves were dark-adapted for 20 minutes with clips. The clips were attached to the leaf laminae at positions unobstructed by the veins. The F_v/F_m measurements were obtained with a single saturating light pulse of 627 nm at the intensity of 2 500 $\mu\text{mol m}^{-2} \text{s}^{-1}$. The measurements were taken over a course of one afternoon in cloudless weather with the glasshouse lights turned off.

2.1.6.2 Fruit firmness

Firmness of ripe tomato fruit (breaker + 7 days) was measured with the Analogue HP – FFF Mechanical Hardness Tester (Bareiss Prüfgerätebau GmbH, Germany) fitted with the 0.25 cm^2 Test Anvil. The plants selected for this analysis included the F_2 population Azygous (0/0; +/+) and U/0; B/B lines (Table 2.2). Six plants of each genotype were selected for analysis and the measurements were taken from three fruit per plant. The readings were taken at three, equidistantly spaced points around the tomato equator (the fruit perimeter at its widest).

2.1.6.3 Transmission electron microscopy (TEM) of tomato pericarp

Two plants from the F₂ segregating population were selected for TEM analysis: the line hemizygous for transgenic *CrtR-b2* and homozygous for *S. galapagense CYC-B* (U/0; B/B) and the Azygous (Az) reference line (0/0; +/+), where the transgenic *CrtR-b2* and *S. galapagense CYC-B* segregated out. Ripe and firm fruit were cut into approximately 1 mm³ cubes with a sterile, single-use disposable scalpel. The cubed tissue was immediately placed in vials containing a fixative solution (3% v/v glutaraldehyde, 4% v/v formaldehyde in 0.1 M PIPES buffer) pre-warmed to room temperature (~22°C). The vials were incubated for 1 hour at room temperature and transported to the Biomedical Imaging Unit, Southampton General Hospital at the ambient temperature. The sections for TEM imaging were post-fixed in osmium tetroxide (1% w/v), dehydrated, resin-embedded, sectioned, fixed on a copper mesh and counterstained at the Biomedical Imaging Unit, Southampton. The sections were imaged on a Tecnai T12 Transmission Electron Microscope (Field Electron and Ion Company, USA) with the 120 kV accelerating voltage of the electron beam. Images were acquired with 11 Megapixel TEM Camera MORADA G2 (EMSIS GmbH, Germany).

2.2 Bacterial, fungal and plant tissue cultures

All work involving handling of bacterial, fungal or plant tissue cultures was performed following standard laboratory aseptic techniques. The handling of the cultures was performed in a cell culture hood with laminar flow specifically designated for microbial or plant organisms. The hoods were sterilised with a UV-C germicidal lamp (30 W, 76 µW cm⁻² intensity, 230 V, 50 Hz; Cole-Parmer, USA) prior to and after handling of the material.

2.2.1 Bacterial cultures

Cultures of bacteria, namely *Escherichia coli* and *Agrobacterium tumefaciens*, were used extensively to complement various objectives of this study. The following sections describe the methods of maintenance and handling of the bacterial cultures and their application in stable transformation of tomato and plant screening.

2.2.1.1 Maintenance of bacterial cultures

2.2.1.1.1 Growth media

Lysogeny broth (LB) growth liquid media were prepared by combining tryptone (1% w/v; Sigma, USA), yeast extract (0.5% w/v; Oxoid, UK) and NaCl (170 mM; Sigma) in an appropriate amount of water. LB agar solid media were prepared as above with addition of agar (1.5% w/v; Sigma). The water used in preparation of the media was filtered with the Purite Select Analyst 160 (SUEZ Water, UK) reverse-osmosis (RO) water purification system and is henceforth referred to as double distilled water (ddH₂O). The growth media were sterilised by autoclaving for 20 minutes

at 121°C. LB agar plates were prepared by pouring microwave-melted and cooled LB agar media (typically 30 ml) onto sterile Petri dishes with or without the addition of an antibiotic. The agar was left to solidify in a sterile fume hood or near an open flame before being used. Super Optimal Broth (SOB) media were prepared by first combining tryptone (2% w/v), yeast extract (0.5% w/v), NaCl (10 mM) and KCl (2.5 mM; BDH, UK) in an appropriate amount of ddH₂O and autoclaving. Next, filter-sterilised solutions of MgCl₂ (1 M; anhydrous; Sigma) and MgSO₄ (1 M; anhydrous; Fluka, USA) were added aseptically (each to the final concentration of 10 mM) to complete the preparation of SOB. Super Optimal Broth with Catabolite repression (SOC) media were prepared by additionally adding a filter-sterilised solution of glucose (1 M; Sigma) to SOB (to the final concentration of 20 mM). All filter-sterilised solutions were prepared using a GyroDisc Syr 0.2 µm pore-size filter, CA-PC 30 mm (Orange Scientific, Belgium).

2.2.1.1.2 Antibiotics used for bacterial selection

The list of antibiotics used for selection in bacterial cultures with their corresponding stock and working (final) concentrations as well as the names of solvents the antibiotics were prepared in, is provided in Table 2.3. All antibiotics were purchased from Sigma. The stocks of ampicillin, kanamycin, spectinomycin and streptomycin were filter-sterilised through a GyroDisc Syr 0.2 µm pore-size filter and stored in small aliquots (1.0 ml) at -20°C up to a month. The stock of rifampicin was prepared fresh and protected from light by covering in aluminium foil. For their use with media, an aliquot of the antibiotic was thawed and added aseptically to the appropriate working concentration to the media cooled to approximately 55°C.

Table 2.3. Antibiotics used for selection; ddH₂O – double distilled water; DMSO – dimethyl sulfoxide.

Antibiotic	Solvent	Stock conc. [mg ml ⁻¹]	Working conc. [µg ml ⁻¹]
Rifampicin	DMSO	50	25
Ampicillin	ddH ₂ O	100	100
Streptomycin			
Kanamycin		50	50
Spectinomycin			

2.2.1.1.3 Preparation of glycerol stocks

Stocks of bacterial cultures were prepared following the standard laboratory aseptic techniques. An aliquot of bacterial overnight culture (0.5 ml) was mixed thoroughly with autoclaved solution (0.5 ml) of glycerol (50% v/v; Sigma) in a sterile 2 ml cryotube (Camlab, UK). The tubes were immediately flash-frozen in liquid nitrogen and stored at -80°C.

2.2.1.1.4 Streaking bacteria from glycerol stocks

Bacteria were streaked onto solidified LB agar plates supplemented with antibiotics as required with the use of a sterile, plastic loop and incubated overnight at 37°C for *E. coli* and at 28°C for 2 or 3 days for *Agrobacterium*. While streaking bacteria from their glycerol stocks onto LB agar plates, the vials were kept on a -20°C ice block to prevent repeated freeze-thawing of the cells.

2.2.1.1.5 Cultivation of bacteria in liquid cultures

A single, well separated colony was isolated from the LB agar plate and transferred aseptically into liquid LB or SOB media with the use of a sterile plastic loop or a sterile pipette tip. Overnight liquid cultures were typically prepared in liquid LB media (5 ml) for *E. coli* and liquid SOB media (3 or 5 ml) for *Agrobacterium*. The overnight liquid cultures of transformed bacteria (2.2.1.3) were typically used for preparation of bacterial stocks (2.2.1.1.3) and for plasmid extraction (2.3.1.1). When specified, these small overnight liquid cultures were inoculated into fresh media and propagated into larger liquid cultures (50 or 100 ml; typically, at 1:100 v/v ratio of the inoculant to the media or as otherwise indicated). Larger liquid cultures were typically prepared in liquid LB media (50 ml) for *E. coli* and liquid SOB media (50 or 100 ml) for *Agrobacterium*. Larger liquid cultures were used for the preparation of chemically competent *E. coli* (2.2.1.2.1), amenable to the heat-shock transformation *Agrobacterium* (2.2.1.2.2) and *Agrobacterium* cultures used in the stable transformation of tomato (2.2.3.2). *E. coli* were grown overnight or until the required optical density (OD) at 37°C and 180 RPM. *Agrobacteria* were grown either overnight, for 2 days or until the required OD at 28°C and 120 or 150 RPM as further specified for individual experiments. The liquid cultures were prepared with or without addition of an antibiotic as required. *E. coli* used for the preparation of chemically competent cells (2.2.1.2.1) were propagated without addition of an antibiotic while *Agrobacteria* used for the preparation of cells amenable to the heat-shock transformation (2.2.1.2.2) were propagated in media supplemented with rifampicin and streptomycin. Transformed *E. coli* (2.2.1.3.1) were propagated in media supplemented with the antibiotic to which the resistance was provided by the transforming plasmid. Transformed *Agrobacteria* (2.2.1.3.3) were propagated in media supplemented with rifampicin, streptomycin and kanamycin. The concentrations of antibiotics are listed in Table 2.3. The OD of bacterial cultures (1 ml) was measured using Novaspec™ Plus Visible Spectrophotometer (Amersham Biosciences, UK) in 1.6 ml semi-micro cuvettes 12.5 × 12.5 × 45 mm (Greiner Bio-One, Austria).

2.2.1.2 Preparation of competent cells

2.2.1.2.1 Preparation of chemically competent *Escherichia coli*

E. coli strain DH5α (genotype: F⁻ *endA1 glnV44 thi-1 recA1 relA1 gyrA96 deoR nupG purB20 φ80dlacZΔM15 Δ(lacZYA-argF)U169, hsdR17(r_K⁻m_K⁺), λ⁻) was streaked onto an antibiotic-free LB*

agar plate under aseptic conditions and incubated overnight at 37°C. A single, well separated colony was propagated into liquid LB media (5 ml) without antibiotic selection and incubated overnight at 37°C, 180 RPM. An aliquot of this overnight pre-culture (0.5 ml) was inoculated into fresh antibiotic-free LB liquid media (50 ml; 1:100 v/v ratio of inoculant to media) and grown at 37°C, 180 RPM until reaching the optical density ($OD_{600\text{ nm}}$) of 0.6. The culture was then transferred into two sterile, pre-chilled 50 ml tubes and incubated on ice for 10 minutes. The tubes were centrifuged at 2 700 *g*, 4°C for 10 minutes in a refrigerated 5810 R centrifuge (Eppendorf, Germany) with a swing-bucket rotor A-4-62 (Eppendorf). The supernatant was decanted and the pellet was resuspended in a freshly prepared, ice-cold and filter-sterilised solution of glycerol (10 ml, 10% v/v; Sigma) supplemented with $\text{CaCl}_2 \cdot 2\text{H}_2\text{O}$ (100 mM; Fluka, USA). The solution of glycerol with CaCl_2 was sterilised through a GyroDisc Syr 0.2 μm pore-size filter, CA-PC 30 mm (Orange Scientific, Belgium). The tubes were incubated on ice for further 15 minutes and centrifuged as above. The supernatant was decanted and the pellet was gently resuspended in the sterile, ice-cold solution of glycerol with CaCl_2 (1 ml). The bacterial suspension was aliquoted (100 μl) into pre-chilled and autoclaved 1.5 ml microcentrifuge tubes, snap-frozen in liquid nitrogen and stored at -80°C.

2.2.1.2.2 Preparation of heat-shock amenable *Agrobacterium tumefaciens*

Electrocompetent ElectroMAX™ *A. tumefaciens* strain LBA4404 cells (Invitrogen, USA) were streaked onto an LB plate supplemented with rifampicin (25 $\mu\text{g ml}^{-1}$; Sigma) and streptomycin (100 $\mu\text{g ml}^{-1}$; Sigma) and incubated for 3 days at 28°C. A single, well-separated colony was inoculated into SOB liquid medium (3 ml) supplemented with rifampicin (25 $\mu\text{g ml}^{-1}$) and streptomycin (100 $\mu\text{g ml}^{-1}$) and incubated overnight at 28°C, 150 RPM. An aliquot of the overnight culture (150 μl) was then inoculated into fresh SOB media (100 ml) and grown at 28°C, 150 RPM until a mid-log phase of bacterial growth was reached ($OD_{600\text{ nm}}$ between 0.5 and 1.0). The culture was incubated on ice for 15 minutes, transferred into chilled, sterile tubes and centrifuged for 8 minutes at 2 500 *g* and 4°C. The supernatant was decanted, the pellet was dried in an inverted position for 1 minute and then resuspended in a sterile, ice-cold glycerol solution (1 ml, 10% v/v; Sigma) supplemented with $\text{CaCl}_2 \cdot 2\text{H}_2\text{O}$ (20 mM; Fluka). The bacterial suspension was aliquoted (100 μl) on ice into pre-chilled, sterile 1.5 ml microcentrifuge tubes, snap-frozen in liquid nitrogen and stored at -80°C.

2.2.1.3 Bacterial transformation

2.2.1.3.1 Heat-shock transformation of chemically competent *E. coli*

Transformation of in-house prepared chemically competent DH5 α (2.2.1.2.1) or One Shot® TOP10 (Invitrogen) *E. coli* was performed following the standard laboratory aseptic techniques. Vials of chemically competent *E. coli* were thawed on ice. A specified amount of plasmid or

ligation mixture (not exceeding 10% of the bacterial volume in a vial or as otherwise stated), was added to the bacteria, mixed gently by tapping and incubated on ice for 30 minutes. The cells were heat-shocked at 42°C for 30 seconds for One Shot® TOP10 (Invitrogen) *E. coli* and for 45 seconds for in-house prepared chemically competent DH5α and the vials were immediately placed on ice for 2 minutes. Pre-warmed to room temperature (~22°C) liquid SOC media (250 μl) were added to each vial and the cells were incubated for 1 hour at 225 RPM, 37°C. Aliquots of transformed cells (between 20 and 200 μl) were plated on pre-warmed to 37°C LB agar plates supplemented with appropriate antibiotics. All transformations were prepared along a negative control, where untransformed competent cells were spread on an LB agar plate supplemented with the same antibiotics, and a positive control, where untransformed competent cells were spread on an antibiotic-free plate. Where specified, LB agar plates were coated prior to plating with ChromoMax™ IPTG/X-Gal Solution (100 μl; Fisher BioReagents, USA) for the blue-white screen of positive ligation events. The plates were inverted and incubated overnight at 37°C.

2.2.1.3.2 Analysis of transformation efficiency

Transformation efficiency of the in-house prepared *E. coli* DH5α (2.2.1.2.1) was tested with the pUC19 plasmid (Invitrogen). The plasmid (10 pg) was added to a vial of *E. coli* DH5α (100 μl) and the cells were transformed as described above. Before plating, the transformation mix was diluted (10X) in the LB liquid medium pre-warmed to room temperature (~22°C). An aliquot of the diluted transformation mix (100 μl) was plated onto a pre-warmed to 37°C LB agar plate supplemented with ampicillin (100 μg ml⁻¹). The cells were grown overnight as described above. The transformation efficiency (TE), expressed as the ratio between the number of transformants [colony forming units, CFU] and amount of plasmid used [μg], was calculated using the formula:

$$\frac{\text{No. of colonies}}{10 \text{ pg pUC19}} \times \frac{10^6 \text{ pg}}{\mu\text{g}} \times \frac{\text{TTV}}{\text{PV}} \times 10 = \text{TE}$$

Where: TTV – total transformation volume [μl]

PV – plated volume [μl]

TE – transformation efficiency [CFU μg⁻¹]

2.2.1.3.3 Heat shock transformation of *A. tumefaciens*

Vials of chemically competent *A. tumefaciens* (2.2.1.2.2) were thawed on ice. Plasmid DNA (1 μg) was added to the suspension of *A. tumefaciens* and mixed by gentle tapping. The cells were incubated on ice for 30 minutes then snap-frozen in liquid nitrogen and allowed to thaw for 5 minutes at 37°C. SOB liquid media (0.5 ml) was added to each vial and then incubated for 2 hours at 28°C, 150 RPM. An aliquot of the cell suspension (100 μl) was plated onto LB agar

plates supplemented with rifampicin (25 $\mu\text{g ml}^{-1}$), streptomycin (100 $\mu\text{g ml}^{-1}$) and kanamycin (50 $\mu\text{g ml}^{-1}$) and incubated for 2 days at 28°C.

2.2.2 Fungal cultures

The protocol for cultivation of *Phycomyces blakesleeanus* strain C5, carrying *carB10* mutation resulting in the accumulation of phytoene instead of β -carotene (Meissner & Delbruck, 1968), was described by Cerda-Olmedo (1987) and it is outlined below. The strain (sporangiospores) was kindly provided by Dr Eugenio Alcalde Rodriguez, Postdoctoral Research Assistant at RHUL and used for the preparation of phytoene standard (2.6.3.1.1).

2.2.2.1 Growth media preparation

Standard minimal media (Sutter, 1975) were prepared by combining glucose (2% w/v; Sigma-Aldrich, USA), yeast extract (0.5% w/v; Oxoid, UK), L-asparagine (0.2 % w/v; Sigma-Aldrich), KH_2PO_4 (0.5% w/v; Fisher Scientific, USA), $\text{MgSO}_4 \cdot 7\text{H}_2\text{O}$ (0.05% w/v; BDH, UK), Sutter solution (1% v/v; 100X stock) and calcium solution (1% v/v; 100X stock) in ddH₂O. The Sutter solution (100X) consisted of thiamine hydrochloride (0.3 mM; Sigma-Aldrich), citric acid monohydrate (0.95 mM; Sigma-Aldrich), $\text{Fe}(\text{NO}_3)_3 \cdot 9\text{H}_2\text{O}$ (0.37 mM; Sigma-Aldrich), $\text{ZnSO}_4 \cdot 7\text{H}_2\text{O}$ (0.35 mM; Sigma-Aldrich), $\text{MnSO}_4 \cdot \text{H}_2\text{O}$ (0.18 mM; Sigma-Aldrich), $\text{CuSO}_4 \cdot 5\text{H}_2\text{O}$ (20 μM ; Sigma-Aldrich) and $\text{Na}_2\text{MoO}_4 \cdot 2\text{H}_2\text{O}$ (20 μM ; Sigma-Aldrich) in ddH₂O. The calcium solution (100X) contained $\text{CaCl}_2 \cdot 2\text{H}_2\text{O}$ (19.0 mM; Sigma-Aldrich) in ddH₂O. The solution of glucose with yeast extract was autoclaved separately from the solution of L-asparagine with the salts and the trace elements.

2.2.2.2 Culture propagation, collection and storage

Phycomyces sporangiospores (500 μl) were combined with autoclaved ddH₂O (100 μl) in a sterile microcentrifuge tube and heat activated for 15 minutes at 55°C. The activated spores (100 μl) were inoculated into two 500 ml Erlenmeyer flasks containing liquid growth media (250 ml) and incubated for 4 days at 22°C under continuous overhead illumination (16 – 20 $\mu\text{mol m}^{-2} \text{s}^{-1}$) and constant agitation at 150 RPM on Type AK100 Orbitec Platform Orbital Shaker (Infors AG, Switzerland). Mycelia (500 ml) were harvested by vacuum filtration through three layers of Whatman® Grade 3MM Chr Chromatography paper (Whatman) with a N035.1.2 diaphragm vacuum pump (KNF Neuberger, Inc., USA), transferred into 50 ml centrifuge tubes, covered with aluminium foil and freeze-dried for two days (Labconco, USA). The dried material was stored away from light at ambient temperature (~22°C) and used for extraction of phytoene (2.6.3.1.1).

2.2.3 Plant tissue cultures

2.2.3.1 Growth media

The sodium hypochlorite (~0.8% v/v) seed surface sterilisation solution consisted of commercial Kleen Off bleach (18% v/v; Jeyes Group Ltd, UK) diluted in sterile ddH₂O with two drops of

TWEEN® 20 (Sigma). The stocks of 2,4-dichlorophenoxyacetic acid, 2,4-D (0.2 mg ml⁻¹; Sigma), acetosyringone (100 mM; Sigma), indole-3-acetic acid, IAA (1 mg ml⁻¹; Sigma), kanamycin (100 mg ml⁻¹; Gibco™, USA), kinetin (0.1 mg ml⁻¹; Sigma), timentin (300 mg ml⁻¹; Duchefa Biochemie, The Netherlands) and *trans*-zeatin riboside (2 mg ml⁻¹; Sigma) were prepared by Mr Kit Liew in ddH₂O and filter-sterilised. The compounds were added aseptically to the required final concentrations to sterile, microwave-melted media cooled to ~55°C. For *Agrobacterium*-mediated transformation (2.2.3.2), the AC seeds were germinated on antibiotic-free half strength MS10 (½MS10) solid media containing Murashige and Skoog (MS) Medium with Gamborg B₅ vitamins (0.22% w/v; Duchefa Biochemie), sucrose (1.0% w/v; molecular biology, ≥ 99.5% GC; Sigma) and Phyto Agar (0.8% w/v; Melford Laboratories Ltd, UK) in ddH₂O. Seeds from the F₁ U/0; B/+, *hp3*/+ crosses (2.1.2) were germinated on ½MS10 media supplemented with kanamycin (100 µg ml⁻¹). The MS30 solid media contained MS Medium with Gamborg B₅ vitamins (0.44% w/v), sucrose (3.0% w/v) and Phyto Agar (0.8% w/v) in ddH₂O. For the transformation of plants (2.2.3.2), the *Agrobacterium* suspension was prepared in MS10 liquid media containing MS Medium with Gamborg B₅ vitamins (0.44% w/v) and sucrose (1.0% w/v). The pH of MS media was adjusted to 5.8 with KOH (1 M; Sigma) using a CD720 WPA pH meter (WPA Linton, UK). All media were autoclaved for 20 minutes at 121°C. The co-cultivation media consisted of MS30 supplemented with 2,4-D (0.2 µg ml⁻¹) and kinetin (0.1 µg ml⁻¹). The regeneration media 1 (RgM1) consisted of MS30 supplemented with *trans*-zeatin riboside (2 µg ml⁻¹), kanamycin (100 µg ml⁻¹) and timentin (300 µg ml⁻¹). The regeneration media 2 (RgM2) consisted of RgM1 supplemented with IAA (0.1 µg ml⁻¹). The regeneration media 3 (RgM3) were prepared similarly to RgM2 but with lowered concentration of *trans*-zeatin riboside (1 µg ml⁻¹). The elongation media (ElgM) consisted of MS30 supplemented with kanamycin (100 µg ml⁻¹) and timentin (300 µg ml⁻¹). The rooting media (RtM) consisted of MS30 solid media supplemented with IAA (1 µg ml⁻¹), kanamycin (100 µg ml⁻¹) and timentin (300 µg ml⁻¹).

2.2.3.2 Stable transformation of tomato

Agrobacterium-mediated stable transformation of tomato is based on the protocol developed by Gupta & Van Eck (2016) with modifications as described below. The developing explants were incubated in a CONVIRON A1000 plant growth chamber (Controlled Environments Ltd, Canada). Small explants were initially cultivated in sterile polystyrene Petri dishes 60 × 15 mm (Sigma-Aldrich, Poole, UK) and subsequently transferred to sterile, disposable 11.4 × 8.6 × 6.4 cm (smaller plantlets) or 11.4 × 8.6 × 10.2 cm (larger plantlets) PETG Phytatray™ vessels (Sigma).

2.2.3.2.1 *Agrobacterium* cultures

Bacteria from *Agrobacterium* stocks were streaked onto LB agar plates supplemented with rifampicin (25 µg ml⁻¹), streptomycin (100 µg ml⁻¹) and kanamycin (50 µg ml⁻¹) and incubated for

3 days at 28°C. A single colony was inoculated into SOB liquid media (5 ml) supplemented with the above antibiotics and incubated overnight at 28°C, 120 RPM. An aliquot of this starting culture (100 µl) was inoculated into fresh SOB liquid media (50 ml; 500:1 volume ratio of SOB to inoculum) supplemented with the antibiotics and incubated at 28°C, 120 RPM until the mid-exponential phase of bacterial growth ($OD_{600\text{ nm}}$ of ~0.4 – 0.5). The *Agrobacterium* culture was centrifuged for 10 minutes at 2 000 g, 4°C and the pellet was resuspended to the $OD_{600\text{ nm}}$ of ~0.5 in sterile MS10 liquid medium. Prior to the transformation, sterile acetosyringone was added to the *Agrobacterium* suspension (to the final concentration of 100 µM).

2.2.3.2.2 Seed germination

S. lycopersicum cultivar Ailsa Craig seeds were surface sterilised by soaking in ethanol AnalaR NORMAPUR® ACS (70% v/v; VWR Chemicals, USA) for 5 minutes. This was then followed by a 10-minute wash in sodium hypochlorite (0.8% v/v) sterilisation solution and a thorough wash in sterile ddH₂O which was repeated several times to remove any residues of the sterilisation solution. The seeds were germinated on ½MS10 solid media (2.2.3.1) and incubated at a constant temperature of $24 \pm 1^\circ\text{C}$ for 4 days in dark followed by 4 days of 16L/8D photoperiod at the light intensity of 80 – 100 µmol m⁻² s⁻¹ PAR.

2.2.3.2.3 *Agrobacterium*-mediated plant transformation

Approximately 2 cm² explants were cut from the cotyledons of 8-day-old seedlings and pre-conditioned for 1 day on co-cultivation MS30 solid media at $24 \pm 1^\circ\text{C}$ under 16L/8D photoperiod at the light intensity of 25 – 40 µmol m⁻² s⁻¹ PAR, with the abaxial surface in contact with the medium. Two drops of the *Agrobacterium* suspension in MS10 liquid media were added onto the surface of each explant and incubated for 10 minutes at room temperature (~22°C). The cotyledon pieces were blotted dry between layers of sterile filter paper and returned to the incubator for 2 days under 16L/8D photoperiod at 25 – 40 µmol m⁻² s⁻¹ PAR. A control tissue culture regeneration experiment was set up along the transformation. The explants in the control experiment were not exposed to the *Agrobacterium* suspension, but otherwise they were cultured on the same media as described further for the transformed explants except that kanamycin was not included.

2.2.3.2.4 Regeneration

The explants were first transferred onto RgM1 MS30 solid media and incubated for 1 week under 16L/8D photoperiod at $24 \pm 1^\circ\text{C}$, 60 – 100 µmol m⁻² s⁻¹ PAR. Following this, the explants were transferred onto RgM2 MS30 solid media and incubated as above for two weeks. The developing calluses were then transferred onto RgM3 MS30 solid media and sub-cultured onto this media every two weeks for the total period of four weeks.

2.2.3.2.5 Rooting

Leaf explants along with the developing calluses were sub-cultured onto ElgM MS30 solid media every 2 weeks until shoots were formed. To induce roots, the shoots were separated from the adhering calluses and transferred onto RtM MS30 solid media. Shoots that rooted in the presence of kanamycin and were showing no signs of bleaching were transferred to the glasshouse for acclimatisation and then soil and cultivated as described earlier (2.1.2).

2.3 Extraction and analysis of nucleic acids

The analysis of nucleic acids (DNA and RNA) was crucial for obtaining information on the studied tomato lines. The following protocols describe the handling and the use of nucleic acids to complement various objectives of this study.

2.3.1 Extraction of nucleic acids

2.3.1.1 Extraction of plasmids from bacteria

Plasmid DNA was extracted from transformed *E. coli* and *Agrobacterium* using the Wizard® Plus SV Minipreps DNA Purification System (Promega). Overnight LB liquid cultures of *Agrobacterium* (5 ml) and *E. coli* (5 ml) were pelleted down by centrifugation for 8 and 10 minutes, respectively at 3 500 RPM, 4°C using a refrigerated 5810 R centrifuge (Eppendorf, Germany) with a swing-bucket rotor A-4-62 (Eppendorf). The supernatant was decanted and the tubes were kept in the inverted position for 10 minutes allowing the pellets to dry. The plasmid DNA was then purified using the centrifugation extraction method as specified in the manufacturer's protocol. The volume of nuclease-free water used to elute plasmid DNA was reduced compared to the original protocol (50 µl) and the elution step was performed twice. The extracted plasmid DNA was kept at -20°C for a long-term storage or at 4°C for a short-term usage.

2.3.1.2 Extraction of plant genomic DNA

Depending on the size of the population screened, two different extraction methods were used: the spin-column method for smaller number of samples or the 96-well plate method for high-throughput DNA extraction.

2.3.1.2.1 Spin-column based purification

Genomic DNA was extracted using the DNeasy Plant Mini Kit (QIAGEN, Germany). Fresh and young tomato leaf material (between 80 and 100 mg) was weighted out into 2 ml safe-lock micro test tubes (Eppendorf, Germany) containing a clean 3 mm tungsten carbide bead (QIAGEN, Germany) and snap-frozen in liquid nitrogen. The frozen material was disrupted at either 50 Hz using TissueLyser LT (QIAGEN) or at 30 Hz using TissueLyser II (QIAGEN). The adapter sets of TissueLyser LT and TissueLyser II were placed at -80°C for 1 hour prior to tissue disruption. The

tissue was homogenised for 1 minute, the tubes containing the material were re-frozen in liquid nitrogen for 20 minutes and the adapters were returned to -80°C before the tissue was disrupted for another minute. The beads were reused after the tissue disruption and first cleaned in dH₂O (20 ml) in a beaker (100 ml), then soaked in a solution of ethanol, AnalaR NORMAPUR® ACS (70% v/v; VWR, USA) and finally rinsed with dH₂O (40 ml) before being dried in an oven. The genomic DNA was then extracted as specified in the protocol. The recommended centrifugation step for 5 minutes at 20 000 *g* was performed. In the instances of a substantial green discolouration of the spin column membrane after the wash with Buffer AW2, an additional wash with ethanol (500 µl, 96 – 100% v/v; VWR) was performed. The flow-through was discarded and the column was centrifuged for 2 minutes at 20 000 *g* to dry the membrane. In the final step, DNA was eluted twice with molecular biology-grade water, DNases/RNases/proteases free (50 µl; VWR). Extracted DNA was used for plant genotyping by PCR (2.3.5.1 – 2 and 2.3.7.3) and Southern blot (2.3.7.2) and kept at -20°C for a long-term storage or at 4°C for a short-term usage.

2.3.1.2.2 96-well plate-based purification

For genotyping of segregating populations, a large-scale genomic DNA extraction from fresh tomato leaf material was carried out using the DNeasy 96 Plant Kit (QIAGEN). Young tomato leaves were collected and the material (50 mg) was placed in each of the collection microtubes containing a clean 3 mm tungsten carbide bead (QIAGEN, Germany). The leaf material was disrupted at 30 Hz using TissueLyser II (Qiagen) and the genomic DNA was extracted as specified in the manufacturer's protocol. All centrifugation steps were performed using a refrigerated 5804R centrifuge (Eppendorf) with a swing-bucket A-2-DWP rotor and the deep well plate carriers (Eppendorf). The plates were centrifuged at the maximum for this rotor speed of 3 700 RPM instead of the recommended speed of 6 000 RPM indicated in the protocol. Therefore, the centrifugation times stated in the protocol were increased by 50% to compensate for the lower than required rotor speed. Genomic DNA was eluted twice with Buffer AE (50 µl) and kept at -20°C for a long-term storage or at 4°C for a short-term usage.

2.3.1.3 Extraction of RNA

Tomato fruit used to obtain total RNA were stored at -80°C prior to extraction. A pooled material from three fruit at the turning stage of development was used per biological sample. The frozen material was prevented from thawing during all stages of its handling by storing it in liquid nitrogen until the first addition of the buffer. The material was homogenised at 30 Hz for 1.5 minutes using TissueLyser II (QIAGEN) and 10 ml stainless steel gridding jars (QIAGEN). The jars were cooled in liquid nitrogen prior to use. RNA was extracted from finely grinded tomato powder (100 mg) using the RNeasy Plant Mini Kit (QIAGEN). The solution of 2-mercaptoethanol, β-ME (Sigma-Aldrich, USA) in Buffer RLT was prepared at the specified concentration (10 µl of

β -ME per 1.0 ml of RLT) prior to the extraction and used in the procedure. The optional step of the on-column digestion with DNase I was performed using the RNase-Free DNase Set (QIAGEN). The stock of DNase I (2.7 Kunitz units μl^{-1} of RNase free water) was prepared as specified in the manufacturer's protocol. An aliquot of the DNase I stock (10 μl , 27 Kunitz units) was combined with Buffer RDD (80 μl) and the digestion step was performed as specified in the protocol at ambient temperature ($\sim 22^\circ\text{C}$) for 15 minutes. Following the washes in Buffer RPE (500 μl), the optional centrifugation step for 1 minute in a fresh 2 ml collection tube to dry the membrane was carried out. RNA was eluted twice with nuclease-free water (30 μl) and stored at -80°C until required.

2.3.2 Quantification of nucleic acids

The concentration of DNA and RNA samples was measured with NanoDrop® ND-1000 Spectrophotometer (Thermo Fisher Scientific, USA). The spectrophotometer was blanked with the same medium as the nucleic acids were eluted with. An aliquot of each sample (2 μl) was used to quantify the concentration of genomic and plasmid DNA as well as RNA using the conversion factor of 50 (DNA-50) and 40 (RNA-40) for DNA and RNA, respectively.

2.3.3 Agarose gel electrophoresis

The extracted nucleic acids (DNA and RNA; 2.3.1), the products of PCR amplifications (2.3.5) and restriction enzyme digestions (2.4.2) were separated according to their sizes by electrophoresis on agarose gels of specified concentrations. Prior to the analysis of RNA, the electrophoresis tank and casting trays were cleaned thoroughly with Distel™ Surface Disinfectant (Tristel Solutions Limited, UK), ddH₂O and ethanol (70% v/v; VWR, USA) to remove contaminating RNases. The undigested genomic DNA used in Southern blotting (2.3.1.2), the RNA samples (2.3.1.3) and the products of PCR amplifications (2.3.5.1 – 2) and restriction enzyme digestions (2.4.2.2 – 3) were resolved on 1% (w/v) molecular-grade agarose gels (Bioline Reagents Ltd, UK). For the resolution of sgRNAs (2.3.5.3) and digested genomic DNA used in Southern blotting (2.4.2.1), 2% (w/v) and thin 0.9% (w/v) agarose gels were used, respectively. All gels were prepared by melting the appropriate amount of agarose in 1X Tris-acetate-EDTA (TAE) buffer in a microwave oven. The melted agar was cooled to $\sim 60^\circ\text{C}$, stained with 1X GelRed® Nucleic Acid Gel Stain (10 000X concentrate in water; Biotium, USA) for the visualisation of nucleic acids, poured into casting trays and allowed to settle. The 0.9% (w/v) agarose gel was stained post-electrophoresis by a gentle, 25-minute long agitation in a solution of GelRed® (500 ml; 33 000X diluted) while shielded from light. The TAE buffer was prepared at the 50X stock concentration consisting of ethylenediaminetetraacetic acid (EDTA; 50 mM, pH 8.0; Sigma-Aldrich), Trizma® (Tris base; 2.0 M; Sigma-Aldrich), analytical reagent-grade (ARG) glacial acetic acid (1.0 M; Fisher Scientific, USA) in ddH₂O and pH ~ 8.3 . 1X TAE buffer (1.0 mM EDTA, 40 mM Trizma®, 20 mM

glacial acetic acid) was obtained from its 50X stock by preparing a 1:49 dilution in ddH₂O. The nucleic acids to be analysed were combined with the 6X Blue/Orange Loading Dye (1X final concentration; Promega, UK) prior to loading onto the gel. For standard analysis of nucleic acids according to their sizes, an aliquot of the original product was loaded onto the gel (typically 10 or 15 µl of DNA and 5 µl of RNA). For the use in subsequent cloning (2.4.1) or sequencing (2.3.4), if the PCR product was to be gel purified, the whole reaction volume was loaded onto the gel (typically 30 or 50 µl), or if the PCR product was to be directly purified from its reaction, a small aliquot of the reaction (typically 2.0 µl) was used. The samples of nucleic acids were run along molecular-weight size markers and appropriate controls. The DNA ladders were prepared according to their manufacturers' instructions and loaded onto the gel (5 µl) along the samples. PCR amplicons (2.3.5) were resolved against 100 bp DNA ladder (Promega, UK) or Quick-Load® Purple 100 bp DNA Ladder (NEB, USA). The extracted RNA samples (2.3.1.3) and digested plasmids (2.4.2.2 – 3) were separated on the gel against GeneRuler 1 kb Plus DNA Ladder (Thermo Fisher Scientific). The digested DNA used in Southern blotting (2.4.2.1) was compared against the λ DNA/*Hind*III Marker (Promega, USA). The gels were run in 1X TAE buffer with either PowerPac™ HC High-Current Power Supply (250 V, 3.0 A, 300 W; Bio-Rad Laboratories, USA) in a HU13 Midi horizontal gel unit (Scie-Plas Ltd, USA) or the RunOne™ Electrophoresis Unit with Time Control, 100 – 120V (Embi Tec Inc., USA) at 100 V for 20 – 45 minutes (undigested total DNA 2.3.1.2; RNA samples, 2.3.1.3; PCR products, 2.3.5) or 1 – 2 hours (restriction enzyme digests, 2.4.2.2 – 3). The digested DNA used in Southern blot (2.4.2.1) was resolved at 25 V for ~6 hours. The agarose gels were visualised using Gel imaging U:Genius³ visualiser (Syngene, UK).

2.3.4 Sequencing

2.3.4.1 DNA sequencing

The samples (PCR products (2.3.5) or plasmids (2.3.1.1)) were prepared according to the specification set by the provider of the service and sequenced at Eurofins Genomics, Germany. The 35S-TOPO and *PDS*-TOPO plasmids used for the generation of standard curves in RT-qPCR (2.3.7.3) were sequences with the T7 forward (T7_F) primer: taatacagactcactataggg. In order to identify the mutated allele of *ZEP* (2.3.5.1.2), exon 1 amplicons from plants of the +/+, *hp3/hp3* and *hp3/+* genotypes were sequenced with the *hp3_E1* primer pair (Table 2.5). Level 1 and 2 plasmids (2.4.1.2) were sequences with the forward (Level 1_F), gaacctgtggtggcatgcacatac and reverse (Level 1_R), ctggtggcaggatatattgtggtg primers. The PCR fragments of exon 1 and exon 6 of *ZEP* amplified from the AC stable transformants (2.3.5.2.2) and subsequently cloned into TOPO vectors (2.4.1.1) were sequenced with their respective forward primers: *zepE1_F* and *zepE6_F* (Table 2.5). The PCR fragments of the off-targets (OTs; 2.3.5.2.3) were sequenced with their respective forward and reverse primers (Table 2.6). The sequences were aligned at

benchling.com using multiple alignment with fast Fourier transform (MAFFT) algorithm (Katoh & Standley, 2013) and the default alignment parameters.

2.3.4.2 RNA sequencing (RNA-Seq)

2.3.4.2.1 Sample preparation

Genotypes used in RNA-Seq analysis were selected from the F₂ segregating population and included the Azygous (Az) reference line, where the transgenic *CrtR-b2* and *S. galapagense* *CYC-B* have segregated out (0/0; +/+) and the line hemizygous for transgenic *CrtR-b2* and homozygous for *S. galapagense* *CYC-B* (U/0; B/B). The fruit were collected at the turning stage of development, deseeded, diced, snap-frozen in liquid nitrogen and stored at -80°C. Three fruit were collected per plant and three tomato plants were analysed per line. RNA was extracted (2.3.1.3), quantified (2.3.2) and its quality was assessed by gel electrophoresis (2.3.3). The RNA samples (5.0 µg) were combined with RNAsable® LD (20.0 µl; Biomatrix, USA) in sterile, 1.5 ml Eppendorf tubes and mixed by gentle pipetting. The samples were dried for 1.5 hours in the Genevac EZ-2 Mk2 Plus Centrifugal Evaporator (Genevac, UK) at the aqueous drying setting. The dried samples were stored in a plastic bag with a desiccant packet, heat-sealed inside a Barrier Foil Ziplock aluminium Pouche (Agar Scientific Ltd, UK) using Vacuum Sealer V.100® (Lava, Germany) and stored at room temperature until their shipment.

2.3.4.2.2 Quality control, sequencing and data analysis

Quality assessment of the RNA samples and their sequencing were performed at IGA Technology Services (IGATS), Italy. The quality of RNA was assessed on LabChip® GX Touch™ Nucleic Acid Analyzer (PerkinElmer, USA) operated by LabChip GX Software, version 3.1.935.0. Only good quality RNA samples, with RNA Integrity Numbers (RINs) above 7, were used as an input for cDNA library preparation. Prior to cDNA synthesis, the RNA samples were filtered for the polyadenylated tails using poly-T oligomers attached to magnetic beads to enrich for mRNA. Single-end sequencing was carried out on the NextSeq™ 500 Sequencing System (Illumina, Inc., USA). The CASAVA 1.8.2 version of the Illumina pipeline was used to process raw data (base calling, demultiplexing and trimming). The transcript sequences were mapped to FastaQ files using Sanger/Illumina 1.9 encoding (Phred+33). Between 21 934 305 and 35 846 072 of 100 bp sequence reads were processed from the samples analysed. No sequences were flagged for poor quality (post-trimming). Quality control checks of the starting library material and the run were assessed through FastQC analysis. All samples were determined to be of good quality based on the generated FastQC report modules (data available on request). The Tuxedo suite of tools (Trapnell *et al.*, 2012) was followed to align the reads on the reference genome (Bowtie and TopHat2 with default parameters), assemble transcripts to the reference annotation and execute their relative abundances in the samples (Cufflinks with default parameters), perform

mapping statistics (RSeqQC; statistics on the transcriptome alignment metrics, read distribution, 'strandness' of the reads and coverage over the gene body) and to identify differentially expressed genes (Cuffdiff with default geometric normalisation). Alignment metrics were used to assess quality of the alignment of the libraries. Between 81.2 – 83.1% of the reads were uniquely mapped to the reference genome across the samples with 5.7 – 6.4% of the reads being aligned more than once (data available on request). *S. lycopersicum* cultivar Heinz 1706 build SL3.0 reference genome (GenBank assembly accession: GCA_000188115.3) with ITAG3.10 annotation was used in the RNA-Seq analysis. Data processing, up to the point of differential expression analysis inclusive, was performed by Dr Vera Vendramin at IGATS.

2.3.4.2.3 Identification of candidate genes

The normalised estimation of gene expression was reported as the Fragments Per Kilobase of transcript per Million mapped reads (FPKM) value. FPKM values are obtained by normalising the number of reads mapped to a given gene to its length and the sequencing depth of the sample. The FPKM values of the 34 878 protein coding genes from the two lines were \log_{10} -transformed and displayed on density and scatter plots. A density plot represents a distribution of the FPKM values across the individual samples whereas a scatter plot provides a visual comparison of gene level variation between the two lines. To account for the FPKM values of 0, which by definition are undefined following a logarithmic transformation, a constant value of 1 was added to all FPKM values (FPKM+1) prior to the transformation. A simple linear regression analysis between the $\log_{10}(\text{FPKM}+1)$ values of the two lines was carried out and displayed as a straight line together with the coefficient of determination (R^2) on the \log_{10} -transformed FPKM+1 scatter plot of the transgenic U/O; B/B line against the Azygous. Additionally, a rough differential expression analysis was performed by calculating a fold change between the FPKM+1 gene values of the transgenic line compared to the Azygous. Points corresponding to the genes with greater than a 2-fold increase or decrease in the transgenic line were coloured green and red, respectively. Gene-level differential expression was performed by testing differences in the summed FPKM values of transcripts sharing the same gene annotation. The FPKM value of each of the annotated genes in the transgenic line was compared to its corresponding FPKM value in the reference line to calculate a fold change (FC) in gene expression level. The FC values for the annotated genes were \log_2 -transformed and plotted against their corresponding negative- \log_{10} -transformed p -values to generate a volcano plot. For clarity of display, genes with p -values equal to 1 as well as genes with infinite $\log_2\text{FC}$ in expression levels and all non-significant genes with absolute (abs) $\log_2\text{FC} > 10$ were not included, resulting in 18 978 genes being displayed on the final volcano plot. RStudio version 1.1.456 (R Core Team, 2018), an integrated development environment for R software application and 'ggplot2' (Wickham, 2016), 'ggthemes' (Arnold, 2019), 'plyr' (Wickham, 2011), 'dplyr' (Wickham *et al.*, 2018), 'readx1' (Wickham & Bryan, 2018)

and 'ggpmisc' (Aphalo, 2016) R packages were used to generate the plots. Differentially expressed genes in the transgenic line were only considered significant if their corresponding *q*-value was smaller than 0.05 (corresponding *p*-value < 0.00185). Using this criterium, 654 genes from the volcano plot were found to be significantly different in the transgenic line. Additionally, 44 genes with an infinite log₂FC in the transgenic line were also identified giving the total of 698 significantly altered genes. To narrow down the number of identified genes to a manageable number and to identify the genes with the greatest absolute changes, only genes with *P* < 0.001 (equivalent *Q* < 0.033365) and an absolute log₂FC > 1.5, corresponding to a factual absolute 2^{1.5}-fold change (~2.83-fold increase or decrease) were included in the final analysis. These criteria led to the inclusion of 247 differentially expressed genes from the volcano plot. Additionally, 39 genes with an infinite log₂FC were identified to match the same criteria giving the total of 286 genes of interest. These genes were grouped according to their functionality.

2.3.5 Polymerase chain reaction (PCR)

The majority of PCR amplifications were carried out using PuReTaq Ready-To-Go PCR Beads (GE Healthcare, UK), except for the synthesis of the single guide RNAs (sgRNAs) and the hybridisation probe used in Southern blotting, which are described separately. The reactions were incubated in T100™ (Bio-Rad, USA) or Veriti™ Thermal Cyclers (Applied Biosystems, USA) at the general conditions specified in Table 2.4. The specific amplification conditions and the sequences of the primers are provided in Tables 2.5 and 2.6. Each reaction consisted of genomic (100 – 200 ng) or plasmid DNA (10 – 50 ng), forward and reverse primers (0.4 μM of each) and DNases/RNases/proteases free molecular biology-grade water (to the total of 25 μl; VWR, USA). The control reactions were prepared alongside. Non-template control reactions, which lacked the genomic or plasmid DNA, were prepared to ensure that the primer stocks and water were not contaminated. The PCR products were verified by agarose gel electrophoresis (2.3.3) and/or sequencing (2.3.4.1) with some of the PCR amplicons used in subsequent cloning (2.4.1).

Table 2.4. General cycling conditions used in the genotyping of tomato populations. The variable (var.) values are provided in Tables 2.5 and 2.6.

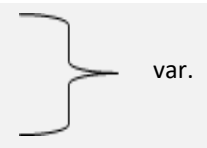
Cycling step	Time	Temp. [°C]	No. of cycles
Initial denaturation	5 min	95	1
Denaturation	30 sec	94	
Annealing	30 sec	var.	
Elongation	var.	72	
Final elongation	5 min	72	1

Table 2.5. Primer sequences and their parameters for the use in PCR. Forward primers are listed first. The variable (var.) information for OT1 – 14 is provided in Table 2.6. Alternative names for the amplified fragments are provided in the brackets next to the corresponding primer. Hence, if written alone, *hp3* refers to the original line described by Galpaz *et al.* (2008). Double crosses refer to the lines segregating for transgenic *CrtR-b2* at the U locus and *S. galapagense* *CYC-B* allele. Triple crosses refer to the lines segregating for transgenic *CrtR-b2* at the U locus, *S. galapagense* *CYC-B* allele and the *hp3* allele of *ZEP*; bp – base pairs; OT – off-target; T_a – annealing temperature.

Name	Primer Pair	Size [bp]	Plants screened	Description	T _a [°C]	Elongation [sec]	No. of cycles
<i>PDS</i>	ctaggttcttgctgccttgg ccaacttttggcaatgctt	148	n/a	- verification of <i>PDS</i> -TOPO vector - establishing zygosity of <i>CrtR-b2</i>	50	30	30
CaMV 35S (35S)	gtctttacggcgagttctgt tatggacgattcaaggcttct	139	double crosses	- screening for transgenic <i>CrtR-b2</i> - preparation of 35S-TOPO vector - establishing zygosity of <i>CrtR-b2</i>			
35S- <i>CrtR-b2</i> (35S-C)	cccactatccttcgcaagac ggactgagaaacgggttatg	147	<i>hp3</i> and triple crosses	- screening for transgenic <i>CrtR-b2</i> - Southern blot hybridisation probe	55		
p <i>S.gala</i> <i>CYC-B</i> (p <i>S.g</i>)	cacttgataactagagttgggttc tgtagtcagtgcatggacgg	199	<i>hp3</i> , double crosses and triple crosses	- screening for <i>S. galapagense</i> <i>CYC-B</i> allele			
p <i>S.lyco</i> <i>CYC-B</i> (p <i>S.l</i>)	ccaactattttatcacttgataactaac tttccaatcccagtcca	552		- screening for <i>S. lycopersicum</i> <i>CYC-B</i> allele			
<i>hp3_E1</i>	ttctgaggagggtggtatccc ggtaggttagtgttcttgg	350		- verification of <i>ZEP</i> allele			
<i>hCas9</i>	agactatcactccctggaacttcg atcttcttgagctgtttcacggtaac	290		- verification of level 2 constructs - verification of CRISPR/Cas9 cassette integration	57		
<i>NPTII</i>	atggttgaacaagatggattgcac tcagaagaactcgtcaagaaggcg	795	T ₀ AC stable transformants	- screening for editions in <i>ZEP</i> exon 1	56	40	35
<i>zepE1</i>	tgggttctgaggagggtggtat tgctgaagctccagttactct	460		- screening for editions in <i>ZEP</i> exon 6	55		
<i>zepE6</i>	aggaacgttcagtggttaca tgccactatgatgctcaagaggt	441		- screening of sgRNA_ <i>zepE6</i> off-targets	var.		
OT1 – 14	var. (Table 2.6)	var.					

2.3.5.1 Genotyping of the segregating populations

2.3.5.1.1 Identification of transgenic *CrtR-b2* and *S. galapagense* *CYC-B* allele

Genomic DNA was extracted from leaf tissue as described previously (2.3.1.2) and used for screening of tomato populations segregating for the genes of interest. End-point PCR was used to detect the presence of the transgenic copy of β -carotene hydroxylase (*CrtR-b2*) by amplifying the Cauliflower Mosaic Virus (CaMV) 35S promoter (CaMV 35S) fragment or alternatively, in the segregating tomato populations crossed with the *hp3* variety, the joined region between CaMV 35S and *CrtR-b2* (35S-*CrtR-b2*). The presence of *S. galapagense* or *S. lycopersicum* *CYC-B* alleles was verified through the amplification of the *S. galapagense* (pS.gala *CYC-B*) or *S. lycopersicum* *CYC-B* (pS.lyco *CYC-B*) promoter fragments, respectively. Parental tomato lines were used as positive and negative controls for the amplification of the fragments of interest. Primers CaMV 35S (35S), pS.gala *CYC-B* (pS.g) and pS.lyco *CYC-B* (pS.l) were designed and kindly provided by Dr Eugenia M.A. Enfissi and the primer 35S-*CrtR-b2* (35S-C) was designed and kindly provided by Ms Esther Lewis.

2.3.5.1.2 Identification of the mutated allele of *ZEP* in the *hp3* line

In the original EMS mutagenesis experiment (Galpaz *et al.*, 2008), two variants of the zeaxanthin epoxidase (*ZEP*) allele were isolated. To establish which variant of the *ZEP* allele was present in the variety used in this study, the fragment of zeaxanthin epoxidase gene was amplified with the *hp3_E1* primer pair, covering the region of exon 1 where the two different mutations occurred. The genomic DNA used as a template was isolated from the original *hp3* variety for the positive identification of the variant – homozygous mutant (*hp3/hp3*). The wild type (WT) allele was amplified from the genomic DNA extracted from the F₂ population plants of the U/0; B/B genotype – homozygous WT (+/+). The genomic DNA extracted from the F₁ population plants of the U/0; B/+; *hp3*/+ genotype was used for the amplification of both alleles – heterozygous (*hp3*/+). The amplicons of the three zygotic combinations were sequenced (2.3.4.1) and used in cross-validation of the High Resolution Melt (HRM) experiment (2.3.6).

2.3.5.2 Screening of AC primary transformants (T₀)

2.3.5.2.1 Verification of level 2 Golden-Gate constructs

Following the transformation of LBA4404 *A. tumefaciens* (2.2.1.3.3) with the level 2 binary vectors (pICSL4723::*zepE1* and pICSL4723::*zepE6*), the plasmids were extracted (2.3.1.1), digested (2.4.2.2 – 3) and additionally used as PCR templates to confirm the presence of the necessary components of the CRISPR/Cas9 expression cassettes. The reactions were set up as described above using PuReTaq Ready-To-Go PCR Beads. The presence of the 165-bp long sgRNA scaffolds within the constructs was verified with the same sets of primers as used for the initial generation of the fragments (2.3.5.3) and the same cycling condition as specified in Table 2.7.

The presence of the *hCas9* and neomycin phosphotransferase II (*NPTII*) fragments was verified with the sets of primers and conditions listed in Tables 2.4 and 2.5. *A. tumefaciens* strains, confirmed to contain the properly assembled level 2 binary vectors, were used for the stable transformation of tomato (2.2.3.2).

2.3.5.2.2 Identification of CRISPR/Cas9 edited plants

DNA was extracted from primary transformants (T_0) as previously described (2.3.1.2). Initially, the plants were screened for the presence of *hCas9* and *NPTII* fragments to identify positive integration events of the CRISPR/Cas9 expression cassette into the plant's genome. The primaries positive for both fragments were subsequently screened for the presence of editions within the sgRNA-targeted regions. The exon 1 and exon 6 fragments of *ZEP* were amplified with *zepE1* and *zepE6* primers, respectively. The amplicons were verified on agarose gel (2.3.3) and sequenced (2.3.4.1). The primaries, whose sequencing of the PCR amplicons produced collapsed reads or overlapping chromatograms, were identified as positively edited and analysed further to establish the types and frequencies of the mutations. The edited regions of exon 1 and exon 6 were amplified as above, and the amplicons were cloned into TOPO vectors for sequencing (2.4.1.1). The genomic DNA extracted from untransformed AC plants, regenerated through the tissue culture in the same conditions as the primaries, was used as the negative control for the amplification of the *hCas9* and *NPTII* fragments as well as to obtain the wild-type fragments of exon 1 and exon 6. The level 2 binary plasmids, harbouring the CRISPR/Cas9 expression cassettes used in the stable transformation of tomato (*pICSL4723::zepE1* and *pICSL4723::zepE6*), were used as positive controls for the amplification of the *hCas9* and *NPTII* fragments.

2.3.5.2.3 Analysis of CRISPR/Cas9 off-targets

A single plant, successfully edited at both alleles of *ZEP* (a biallelic mutation), was selected for the analysis of the off-target activity of sgRNA_*zepE6* (*pICSL4723::zepE6*). In this plant, none of the fragments amplified across the exon 6 region of *ZEP* and cloned into TOPO vectors (2.4.1.1) were identified to contain the WT allele of *ZEP*. The list of the top 20 off-targets (OTs) for the sgRNA_*zepE6* guide (Table 2.13; 2.5.1) was obtained at crispr.hzau.edu.cn/CRISPR2/ with the use of CRISPR-P v 2.0 (Lei *et al.*, 2014; Ding *et al.*, 2016; Liu *et al.*, 2017) and 14 most significant OTs were selected for sequencing (Table 2.6). At the time of analysis (7th April 2018), version SL3.0 of the tomato genome has not yet been released to the public domain (build SL3.0 available from 18th April 2018 at NCBI), therefore the OTs were based on the older build SL2.50. However, version SL3.0 has already been available internally at IGATS and hence, used in the RNA-Seq analysis (2.3.4.2.2). The sequences of primers flanking the OT sites with their annealing temperatures and sizes of the amplicons, are provided in Table 2.6. The amplified fragments were analysed on agarose gel (2.3.3) and sequenced (2.3.4).

Table 2.6. Primers used to amplify sgRNA_ *zepE6* off-target (OT) sites; bp – base pairs; T_a – annealing temperature.

Name	Forward Primer	Reverse Primer	Size [bp]	T _a [°C]
OT1	ccaatataccccaataaaccacca	attcatgtaataacaaccaagggtc	350	56.0
OT2	tgactgttgagatgaggagc	acttgatggatagcttgagaga	374	56.3
OT3	cttggtgtctgtgtgattggtt	ttggtttcaattgtgggaaaagga	334	55.3
OT4	tgatgtaatccttctctgtggg	aagtgaaaacagtggatgcc	274	56.6
OT5	accaaacgtactgacttatgaga	tgtgagcatcatgaaatccagtg	453	55.3
OT6	atacggggatcacgcgcaaa	tgtatctaccaacattccaccacc	436	58.0
OT7	gcacaggaatgaagaggtatgg	aaggcatagtaggaacaacacca	404	56.6
OT8	tgagctatatcttttgggtagag	gtgtgcctgttttaaggctgaat	307	56.3
OT9	agctaggacctacgggtaca	tctcttgatgatttccttaatggt	416	56.0
OT10	agtgtgaacatatgctgacgaaa	ccccacacccccttttaga	425	56.3
OT11	agccaggatcgcgtaaaaatac	aaaaaccctctgctttgcc	364	54.0
OT12	cgccaccgactgaacctaata	gcctagcgtagaacagacctc	308	57.4
OT13	cctcctccatcggtgagaac	ctcgaccacctaacgcatga	483	57.4
OT14	tctagtttctgagttaaactagcct	gtaggtattctagcacagagtaagt	310	56.0

2.3.5.3 Two-step PCR to amplify single guide RNA (sgRNA) scaffolds

The primers used for generation of the two 165-bp long sgRNA scaffolds, each containing a specific 20-bp long target sequence, were designed according to the criteria set by Liang *et al.* (2016). The sgRNAs specific against the exon 1 (*zepE1*) and exon 6 (*zepE6*) of *ZEP* were amplified using **tg**tggtctcaattgACAGATACAGAGCAATGCATg~~ttttagagctagaaatagcaag~~ and **tg**tggtctcaattgCCTCTTCCCAACTAAAGGTg~~ttttagagctagaaatagcaag~~, forward primers, respectively. The reverse primer for both amplicons was **tg**tggtctcaagcgtaatgccaactttgtac. The capitalised parts of the forward primers correspond to the specific 20 bp targets in the plant genome. The underlined bases in each primer indicate the *BsaI* restriction recognition sites necessary for the Golden-Gate assembly of the CRISPR/Cas9 expression cassettes (2.4.1.2). To account for the *Arabidopsis* U6 (*AtU6*) promoter transcription start site, an additional guanine (in bold lowercase) was added at the beginning of each target sequence. Plasmid pICH86966::AtU6p::sgRNA_ *PDS*, a kind gift from Sophien Kamoun (Addgene plasmid #46966), was used as the template for the amplification of sgRNA scaffolds. PCR was carried out using Phusion® High-Fidelity DNA Polymerase (NEB, USA). Each reaction consisted of 1X Phusion® HF Buffer, dNTPs Solution Mix (200 µM; NEB), forward and reverse primers (0.5 µM of each), the scaffold template (10 ng), polymerase (1.0 U) and molecular biology-grade water (to the total of 50 µl; VWR). The cycling conditions are provided

in Table 2.7. The annealing and elongation steps were combined into a single step due to the high melting temperatures of the primers. The amplified sgRNA scaffolds targeting exon 1 and exon 6 were named sgRNA_zepe1 and sgRNA_zepe6, respectively.

Table 2.7. Cycling conditions used for the amplification of sgRNA scaffolds with specific 20-bp long guide targets.

Cycling step	Time	Temp. [°C]	No. of cycles
Initial denaturation	30 sec	98	1
Denaturation	10 sec	98	30
Annealing + elongation	20 sec	72	
Final elongation	10 min	72	1

2.3.5.4 Synthesis of the Southern blot hybridisation probe

The digoxigenin-11-dUTP (DIG-dUTP) labelled hybridisation probe for detecting transgenic *CrtR-b2* was synthesised with the PCR DIG Probe Synthesis Kit (Roche, Switzerland). The reactions were set up according to the protocol provided by the manufacturer of the kit. The template (10 pg) for the reaction, the plasmid containing a cloned 35S-*CrtR-b2* fragment (35S-*CrtR-b2*-TOPO), was provided by Ms Lewis. The probe was amplified with 35S-*CrtR-b2* primers (used at the final concentration of 1 µM; Table 2.5). The cycling conditions were set as specified in the protocol, except for the annealing temperature which was lowered to 55°C. The amplified products were analysed on agarose gel (2.3.3) and the DIG-labelled 35S-*CrtR-b2* probe was compared to the unlabelled 35S-*CrtR-b2* control fragment to evaluate the efficiency of labelling. The preparation of the Southern blot hybridisation probe was carried out by Ms Lewis.

2.3.5.5 Primer design and preparation

The primers were designed based on the *S. lycopersicum*, cultivar Heinz 1706, SL2.50 reference genome (GenBank assembly accession: GCA_000188115.2) using an online platform at benchling.com. The selectivity and suitability of the primers for the screens were confirmed by Primer-BLAST (Ye *et al.*, 2012) against the non-redundant (nr) database (NCBI Resource Coordinators, 2015) and *S. lycopersicum* reference genome. All primers were synthesised at Eurofins Scientific in Germany (headquarters in Belgium) and provided in a lyophilised form. Upon arrival, the primer vials were centrifuged for 1 minute at 17 000 *g* using Heraeus™ Pico™ 17 Microcentrifuge (Thermo Scientific, USA) to ensure that the powder sedimented to the bottom of each tube. The primers were dissolved with molecular biology-grade water (VWR) to

prepare stock solutions (100 μ M) and stored at -20°C . For the set-up of PCR, working solutions of primers (10 μ M) were prepared to reduce the risk of contamination and to avoid repeated freeze-thawing of the original stocks.

2.3.5.6 Purification of PCR products

PCR products were separated according to their sizes by agarose gel electrophoresis (2.3.3) and either directly purified from their reactions (CaMV 35S fragments for TOPO cloning, 2.3.5.1.1; sgRNA_*zepE1* and sgRNA_*zepE6* scaffolds, 2.3.5.3; sgRNA targeted exon 1 and exon 6 fragments if directly used for sequencing, 2.3.5.2.2) or purified after excision from the agarose gel (CRISPR/Cas9 OTs, 2.3.5.2.3; *hp3* allele fragments, 2.3.5.1.2; sgRNA targeted exon 1 and exon 6 fragments if used for cloning, 2.4.1.1). A direct purification from the PCR reaction was performed if the gel-resolved PCR products were free from unspecific amplifications or excessive primer dimers. If unspecific amplifications or excessive primer dimers were present, the products of the correct sizes were excised from the gel with a sterile scalpel blade. For the excision of the bands of interest, the agarose gels were briefly visualised under either blue light (465 nm) on the SmartBlue™ Blue Light Transilluminator (Accuris Instruments, USA) or under UV light (302 nm) with the 2011 Macrovue Transilluminator (LKB-Produkter AB, Sweden). The nucleic acids were cleaned up with the Wizard® SV Gel and PCR Clean-Up System (Promega) according to the manufacturer's protocol using the centrifugation purification method and a reduced volume of nuclease-free water for elution (30 μ l). The quality and concentration of purified DNA was assessed as described previously (2.3.2). The purified products were used in ligation reactions (2.4.1) or sequencing (2.3.4.1) and were used immediately or stored at -20°C until necessary.

2.3.6 High Resolution Melt (HRM)

The *hp3-1* allele is characterised by a single amino acid change (E150K) in zeaxanthin epoxidase due to a single nucleotide substitution from G to A. To determine the presence of this mutation in the F_2 population segregating for the transgenic *CrtR-b2*, *S. galapagense* *CYC-B* and *hp3* allele, High Resolution Melt (HRM) analysis with pre-amplification was performed. The *hp3* line and the variety of the U/0; B/B genotype were used as positive (homozygous *hp3/hp3*) and negative (homozygous +/+) controls for the mutant allele, respectively. The hemizygous (*hp3*/+) control was selected from the F_1 population of the U/0; B/+; *hp3*/+ genotype. The PCR reactions were set up using QuantiFast SYBR® Green PCR Kit (QIAGEN) and run on the Rotor-Gene Q (QIAGEN) thermal cycler operated by Rotor-Gene Q Software, version 2.3.1.49 (QIAGEN). The genomic DNA was diluted to the same concentration so that an equal volume of the template was added into each reaction tube. Each reaction consisted of Rotor-Gene SYBR Green PCR Master Mix (1X), genomic DNA (25 ng), forward and reverse primers (each at the final concentration of 1 μ M) and RNase-free water (to the total of 20 μ l). To amplify the 100 bp fragment of *ZEP* spanning the

mutation site, the forward *gcagccagcattcataatgtcttc* and reverse *gggacaatatagaggccaataacag* primers were used. Non-template control reactions were included in each run. All reactions were prepared in triplicates. The cycling conditions are given in Table 2.8. The real-time amplification data were acquired to the green channel at the end of the annealing step. For the HRM step, the temperature was increased from 70 to 90°C in 0.1°C increments with a 2-second hold at each increment. The data were acquired automatically to the HRM channel. The gain optimisation was set at the maximum fluorescence level of 70. For the real-time amplification step, optimisation before 1st acquisition was performed with the background fluorescence set between 1 and 3 fluorescence intensity (FI) units.

Table 2.8. Conditions used for the amplification of the 100 bp fragment of *ZEP* used in HRM analysis.

Cycling step	Temp. [°C]	Time	No. of cycles
Hold	95	5 min	1
Denaturation	95	10 sec	40
Annealing	60	20 sec	
Elongation	72	15 sec	
HRM	70 – 90	n/a	n/a

Quantitative real-time amplification data were assessed for the cycle threshold (C_t) values, the end-point fluorescence levels and amplification efficiency prior to the HRM data analysis. The HRM results were displayed as normalised melt plots and difference plots against one of the controls. The unknown genotypes were called automatically by the software based on their degrees of similarity to the difference plots of the control genotype. The auto-called results were assigned confidence values to provide a measure of certainty at which each genotype was allocated. The accuracy of the software in identifying the variations in nucleic acid sequences was cross-validated by performing the HRM analysis on the tomato varieties of the known *ZEP* allele variants and zygosity (+/+, *hp3/hp3* and *hp3/+*) in which the region of a single-nucleotide polymorphism (SNP) has been previously sequenced (2.3.4.1).

2.3.7 Determination of a gene copy number

The end-point PCR results are sufficient to determine the zygosity of *S. galapagense* *CYC-B* in the population segregating for this gene by testing if *S. lycopersicum* *CYC-B* allele is also present (plants heterozygous for *S. galapagense* *CYC-B*; *B/+*) or absent (plants homozygous for *S. galapagense* *CYC-B*; *B/B*). PCR can also be used to select transgenic plants from the segregating population; however, it cannot be used to determine the zygosity of the transgene.

Therefore, the zygosity of transgenic *CrtR-b2* was determined through the segregation test, Southern blot and real-time quantitative PCR (RT-qPCR) analyses as described below.

2.3.7.1 Segregation test

The zygosity of transgenic *CrtR-b2* could not be established through the amplification of the CaMV 35S fragment alone (2.3.5.1.1) in the population segregating for the transgene (Table 2.2, Section 2.1.2). However, in the hybrid F₁ population generated by crossing the *hp3* variety with the F₂ population plants of the U/0; B/B or U/U; B/B genotypes, the transgene is inherited in all of the progeny only if the parental plant is homozygous for the transgene (U/U) and in approximately half of the progeny, if the parental plant is hemizygous for the transgene (U/0). The F₁ populations, originating from different parental transgenic lines, were screened for the presence of the 35S-*CrtR-b2* fragment by PCR as described (2.3.5.1.1). The frequency of transgenic *CrtR-b2* occurrence in the F₁ population was used to infer the zygosity of the transgene in the parental lines (F₂ U/0; B/B or U/U; B/B). Three plants from this F₂ population were selected as calibrators for RT-qPCR. The zygosity of these plants was cross-validated by Southern blot as described below.

2.3.7.2 Southern blotting

2.3.7.2.1 Solutions and buffers

The following solutions and buffers were prepared for Southern blot analysis: denaturation solution (NaOH (0.5 M; Sigma, USA) and NaCl (1.5 M; Sigma)), neutralisation solution (Trizma[®] hydrochloride, Tris-HCl (0.5 M; Sigma) and NaCl (1.5 M) with the pH adjusted to 7.5), 20X saline-sodium citrate, 20X SSC buffer (NaCl (3 M), sodium citrate (300 mM; BDH, UK) with the pH adjusted to 7.0), low stringency buffer (2X SSC and sodium dodecyl sulphate, SDS (0.1% w/v; Sigma)), high stringency buffer (0.1X SSC and SDS (0.1% w/v)), maleic acid buffer (maleic acid (0.1 M; Sigma) and NaCl (0.15 M) with the pH adjusted to 7.5), washing buffer (maleic acid (0.1 M), NaCl (0.15 M), TWEEN[®] 20 (0.3% v/v; Sigma) and the pH adjusted to 7.5), detection buffer (Tris-HCl (0.1 M), NaCl (0.1 M) and pH 9.5). 2X and 0.1X SSC buffers were prepared by diluting 20X SSC with appropriate amounts of ddH₂O. The solutions, buffers and ddH₂O were sterilised by autoclaving. The solution of SDS (10% w/v) was prepared separately and filter sterilised through a GyroDisc Syr 0.2 µm pore-size filter (Orange Scientific). The appropriate volumes of TWEEN[®] 20 and SDS (10% w/v) were added to the specified final concentrations after autoclaving the buffers. The pH was adjusted using CD720 WPA pH meter (WPA Linton, UK). The pre-hybridisation buffer was prepared fresh by dissolving the DIG Easy Hyb[™] Granules (Roche, Switzerland) in sterile ddH₂O (64 ml) and stirring for 5 minutes at 37°C. To prepare the hybridisation buffer, the DIG-dUTP labelled hybridisation probe (21 µl) was denatured by boiling for 5 minutes with molecular biology-grade water (50 µl; VWR), immediately chilled on ice and

mixed with the pre-warmed DIG Easy Hyb™ solution (pre-hybridisation buffer; 7 ml). The DIG-dUTP labelled hybridisation probe against the 35S-*CrtR-b2* fragment was synthesised using PCR (2.3.5.4). The pre-hybridisation/hybridisation and high stringency buffers were pre-heated before the use to 45 and 68°C, respectively. The blocking solution was prepared fresh by preparing a dilution (10X) of the Blocking Reagent stock solution (Roche) in the maleic acid buffer. The antibody solution was prepared fresh by diluting (10 000X) the Anti-Digoxigenin-AP, Fab fragments (Roche) in the blocking solution. The CSPD solution was prepared fresh by diluting (100X) the CSPD ready-to-use stock (Roche) in the detection buffer. Unless otherwise stated, all washes were carried out at room temperature (~22°C). Care was taken not to allow the membrane to dry at any point during pre-hybridisation, hybridisation and detection.

2.3.7.2.2 DNA transfer

Genomic DNA was extracted as described (2.3.1.2) from the U/U (positive transgenic control) and MM (negative WT control) tomato varieties as well as the three F₂ population plants identified through the segregation test (2.3.7.1) and chosen as calibrators for RT-qPCR. The quality of extracted DNA was tested by agarose gel electrophoresis (2.3.3) and quantified (2.3.2). Plant genomic DNA (10 µg) and 35S-*CrtR-b2*-TOPO plasmid (50 pg; positive blotting control) were digested (2.4.2.1) and separated on agarose gel (2.3.3). The gel was washed 2 × 15 minutes in denaturation solution (100 ml) with gentle shaking, rinsed in sterile ddH₂O (100 ml) and agitated again 2 × 15 minutes in neutralisation solution (100 ml). The gel was equilibrated for 20 minutes in 20X SSC (100 ml). The Southern blot transfer assembly was prepared on a glass plate resting on top of a reservoir filled with 20X SSC (300 ml). A strip of Whatman® Grade 3MM Chr Chromatography paper (Whatman, UK), pre-soaked in 20X SSC (100 ml), was placed over the glass plate with its ends submerged into the buffer to form a capillary bridge between the transfer sandwich and the reservoir. Any trapped air bubbles were rolled off using a sterile glass burette. The agarose gel was placed on top the Whatman® paper. A positively charged nylon membrane (Roche) was cut to the shape of the gel and placed atop it. Three additional layers of Whatman® paper were placed on the membrane and the assembly was completed with a stack of paper towels and a weight. DNA was transferred overnight.

2.3.7.2.3 Crosslinking and hybridisation

The blot assembly was taken apart and the wet nylon membrane was placed with the DNA side up on top of a sheet of pre-soaked in 2X SSC (100 ml) Whatman® paper. DNA was bound to the membrane with CL-508.G UV crosslinker (UVItec, UK) at 120 mJ for 1 minute. The membrane was rinsed in sterile ddH₂O (100 ml), air dried and placed on a pre-soaked in 2X SSC (100 ml) mesh sheet. The mesh with the membrane was rolled and placed inside the Hybaid hybridisation tube (Thermo Scientific, USA) filled with 2X SSC (15 ml). The tube was manually turned to unroll

the mesh, the buffer was removed and replaced with the pre-hybridisation buffer (20 ml). The tube was incubated in the SI30H hybridisation oven/shaker (Stuart, UK) for 30 minutes at 45°C and 5 RPM. Following this, the pre-hybridisation buffer was discarded, immediately replaced with the hybridisation buffer (7 ml) and incubated at 45°C, 5 RPM for 16 hours.

2.3.7.2.4 Washing and chemiluminescent detection

The hybridisation buffer was discarded from the Hybaid tube, replaced with the low stringency buffer (100 ml) and incubated 2 × 5 minutes with gentle manual rolling. The low stringency buffer was replaced with the high stringency buffer (100 ml) and incubated 2 × 15 minutes at 68°C, 5 RPM. The membrane was removed from the tube, placed in a container and agitated gently in the washing buffer (100 ml) for 2 minutes. The washing solution was discarded and the membrane was agitated in the blocking solution (100 ml) for 30 minutes. The blocking solution was replaced with the antibody solution (50 ml) and the membrane was incubated for further 30 minutes. The antibody solution was discarded, the membrane was rinsed in sterile ddH₂O (100 ml) and incubated 2 × 15 minutes in the washing buffer (100 ml). The membrane was equilibrated for 3 minutes in the detection buffer (20 ml), placed in a plastic bag, evenly covered with the CSPD solution (4 ml) and incubated for 5 minutes. The excess CSPD solution was removed, the membrane was heat-sealed in the plastic bag and incubated at 37°C for 10 minutes to enhance the luminescence reaction. The plastic bag with the membrane inside was placed in a 20 cm × 25 cm CURIX MR 800 film cassette (Agfa-Gevaert, Belgium) together with a sheet of Lumi-Film Chemiluminescent Detection Film (Roche) and exposed for 1 hour. The film was developed using the CURIX 60 Automatic X-Ray Film Processor (Agfa-Gevaert). The handling of the detection film and its development was performed in the dark room.

2.3.7.2.5 Data analysis

The developed film was scanned to a digital copy and analysed with ImageJ, version 1.51k (Schneider *et al.*, 2012). The software was used to quantify the intensities of the bands produced by the transgene. The obtained absolute values were normalised against the corresponding starting amounts of digested genomic DNA. These normalised ratios obtained for the individual plants were compared against each other and the relative ratios between the plants were used to infer the zygosity of the transgene.

2.3.7.3 Real-time quantitative PCR (RT-qPCR)

Southern blotting is a time-consuming technique and requires large amounts of starting DNA material in order to be carried out. To establish zygosity of transgenic *CrtR-b2* at the U locus in a large population using low amounts of initial DNA, RT-qPCR was performed. The method described by Enfissi *et al.* (2010), based on the absolute concentration of a reference gene of a known copy number – the standard curve method, was selected. A single-copy endogenous

gene – phytoene desaturase, *PDS* (Corona *et al.*, 1996) was chosen as the reference gene. The calibrator, a plant of a known zygosity, was selected based on the segregation test and Southern blot (2.3.7.1 – 2).

2.3.7.3.1 Preparation of plasmid templates

The selected method of gene quantification requires generation of standard curves based on the amplification of short DNA fragments from the known amounts of the template. Two sets of standard curves were generated: one for the reference gene – *PDS* and second, for the gene requiring quantification – transgenic *CrtR-b2*. Similarly to the approach used in end-point PCR (2.3.5.1.1), the presence of the transgenic copy of *CrtR-b2* was identified by PCR for a fragment of the CaMV 35S promoter. The *PDS* and CaMV 35S amplicons were designed to be of similar lengths and were amplified from their respective plasmid templates (2.3.5.1). The *PDS*-TOPO vector and the primers specific for this fragment were designed and kindly provided by Dr Enfissi. The presence of the *PDS* fragment in the TOPO vector was verified by PCR (2.3.5.1). The CaMV 35S fragment was initially amplified by PCR from the genomic DNA of a F_2 population plant of the U/0; B/B genotype and subsequently cloned into the TOPO vector (2.4.1.1). The suitability of *PDS*-TOPO and CaMV 35S-TOPO vectors for their use in RT-qPCR was verified by sequencing (2.3.4.1). The sequences of primers used in preparation of the plasmid templates and the PCR conditions for both fragments are provided in Tables 2.4 and 2.5. The same sets of primers were subsequently used in RT-qPCR.

2.3.7.3.2 Real-time amplification

Genomic DNA was extracted from the U/U (positive control) and MM (negative control) tomato varieties and the F_2 population segregating for the transgene (2.3.1.2). The RT-qPCR reactions were prepared as described for the HRM analysis using the QuantiFast SYBR® Green PCR Kit (QIAGEN; 2.3.6). The *PDS* and the CaMV 35S fragments were amplified in separate reaction tubes during the course of the same experiment to account for the run-to-run variation. For quantification purposes, a 5-point calibration curve was run for each gene concurrently with the experimental samples. The plasmid templates were used at 0.001, 0.01, 0.1, 1.0 and 10 pg per reaction volume. All RT-qPCR reactions were prepared in triplicates and non-template control reactions were included for both primers. The cycling conditions are provided in Table 2.9. Gain optimisation before 1st acquisition was performed for the real-time amplification step with the background fluorescence set between 1 and 3 FI units. A melting-curve analysis was used to verify the specificity of the amplifications and to confirm the absence of contamination. For the melting curve step, the temperature was increased from 60 to 95°C in 1°C increments and a 5-second hold at each step. The gain optimisation before melt on all tubes was set at the maximum fluorescence level of 70. The data were acquired onto the green channel.

Table 2.9. Amplification conditions used in two-step RT-qPCR.

Cycling step	Temp. [°C]	Time	No. of cycles
Hold	95	5 min	1
Denaturation	95	5 sec	40
Annealing + elongation	60	10 sec	
Melting analysis	60 – 95	n/a	n/a

2.3.7.3.3 Data analysis

The data were processed with Rotor-Gene Q 2.3.1.49 (QIAGEN) software. The amplifications of the *PDS* and *CaMV 35S* fragments from the known amounts of the template, were used to generate dose-response curves for each of the gene of interest based on the C_t values calculated by the software. The curves were used to assess the efficiency of the RT-qPCR reactions during each run. The fit of the standard curves to a linear model was assessed by computing the coefficient of determination, R^2 . Only runs of 90 – 110% efficiency producing standard curves with $R^2 \geq 0.98$ were used in subsequent quantifications. The software was used to calculate the absolute concentrations of each gene in the known amount of the starting genomic DNA. The ratios of the absolute concentrations of *PDS* to *CaMV 35S* were normalised against the calibrator to infer the unknown zygosity of the tested genotypes.

2.4 Construction and verification of vectors

2.4.1 Molecular cloning

Plasmid vectors were primarily used for sequencing of PCR products (2.3.4.1) and targeted gene editing with CRISPR/Cas9 (2.5.2). The following sections describe the construction and verification of the vectors used to complement various objectives of this study.

2.4.1.1 TOPO cloning

PCR products were generated with PuReTaq Ready-To-Go PCR Beads (GE Healthcare, UK; 2.3.5). These products or their aliquots were separated by agarose gel electrophoresis (2.3.3) based on size and either gel purified or cleaned up directly from their respective PCR reactions (2.3.5.6). Those PCR products used to generate standard curves for the quantification of a gene copy number in RT-qPCR (2.3.7.3), were cloned into pCR™4-TOPO® TA vector (Invitrogen, USA). The PCR products resulting from the analysis of CRISPR/Cas9 edited plants (2.3.5.2.2) as well as the *35S-CrtR-b2* fragment, which was used as the positive control in the Southern blot experiment (2.3.7.2), were cloned into pCR®2.1-TOPO® vector (Invitrogen). The TOPO ligation reactions were prepared at the 1 to 10 molar ratio of the vector to the insert using TOPO™ TA Cloning™

Kit (Invitrogen). PCR products (between 0.5 and 4.0 μ l) were combined with the salt solution (1.0 μ l), DNases/RNases/proteases free molecular biology-grade water (to the final volume of 5 μ l; VWR) and the TOPO[®] vector (1.0 μ l). The reaction was mixed gently by tapping and incubated at room temperature (~22°C) for 1 hour. The ligation reaction was then placed on ice and used for the transformation of One Shot[®] TOP10 (Invitrogen) or in-house prepared DH5 α chemically-competent *E. coli* cells (2.2.1.3.1).

2.4.1.2 Golden-Gate cloning

The protocol for the Golden-Gate assembly of the plasmids used in the stable transformation of tomato was based on Weber *et al.* (2011) and Belhja *et al.* (2013). The details of the procedure and the reagents used are outlined below.

2.4.1.2.1 Assembly of level 1 vectors

The sgRNA scaffolds, containing 20 bases long sequences targeting either exon 1 (sgRNA_zepE1) or exon 6 (sgRNA_zepE6) of *ZEP*, were amplified with Phusion[®] High-Fidelity DNA Polymerase (NEB, USA; 2.3.5.3). Small aliquots of the PCR products (2.0 μ l) were resolved and verified by agarose gel electrophoresis (2.3.3) based on size. The PCR products were cleaned up directly from their PCR reactions (2.3.5.6). For the digestion-ligation reactions, level 1 acceptor pICH47751 (150 ng; a gift from Sylvestre Marillonnet; Addgene plasmid #48002), plasmid pICSL01009::AtU6p (7.5 ng; a gift from Sophien Kamoun; Addgene plasmid #46968), purified sgRNA scaffold (12 ng; sgRNA_zepE1 or sgRNA_zepE6), Ligase 10X Buffer (1.5 μ l; Promega), Acetylated BSA (75 μ g ml⁻¹; Promega), T4 DNA Ligase (3.0 U; Promega), *Bsal* (5.0 U; NEB) and molecular biology-grade water (to the final volume of 20 μ l) were combined and mixed by gentle pipetting. The reactions were incubated in a T100™ Thermal Cycler (Bio-Rad, USA) under the cycling conditions given in Table 2.10.

Table 2.10. Conditions used for the digestion-ligation assembly of level 1 plasmids.

Cycling step	Time	Temp. [°C]	No. of cycles
Initial incubation	20 sec	37	1
Digestion	3 min	37	26
Annealing/ligation	4 min	16	
Final digestion	5 min	50	1
Enzyme inactivation	5 min	80	1

The completed level 1 assemblies were named pICH47751::AtU6p::sgRNA_zepe1 (pICH47751::zepe1) and pICH47751::AtU6p::sgRNA_zepe6 (pICH47751::zepe6). An aliquot of each digestion-ligation reaction (5 μ l) was used to transform One Shot® TOP10 Chemically Competent *E. coli* (Invitrogen, USA) as previously described (2.2.1.3.1). Colonies were grown overnight at 37°C on ampicillin (100 μ g ml⁻¹; Sigma, USA) LB plates coated with ChromoMax™ IPTG/X-Gal Solution (100 μ l; Fisher BioReagents, USA) for the blue-white screen of positive ligation events. White clones (seven) from each transformation experiment were selected for further analysis and propagated overnight at 37°C, 180 RPM in liquid LB media (5 ml) supplemented with ampicillin (100 μ g ml⁻¹). The plasmids were isolated (2.3.1.1) and verified by restriction enzyme digestion (2.4.2.3) and sequencing (2.3.4.1). Correctly assembled pICH47751::zepe1 and pICH47751::zepe6 level 1 plasmids were used for the construction of level 2 binary vectors.

2.4.1.2.2 Assembly of level 2 binary vectors

Level 2 acceptor pICSL4723 (150 ng; a gift from Mark Youles; Addgene plasmid #48015), pICSL11024 (144 ng; pICH47732::NOSp-NPTII-OCST; a gift from Jonathan D. Jones; Addgene plasmid #51144), pICH47742::2x35S-5'UTR-hCas9(STOP)-NOST (217.5 ng; a gift from Sophien Kamoun; Addgene plasmid #49771), level 2 end-linker pICH41766 (75 ng; a gift from Sylvestre Marillonnet; Addgene plasmid #48018), either pICH47751::zepe1 or pICH47751::zepe6 (105 ng), 10X T4 DNA Ligase Reaction Buffer (1.5 μ l; NEB), Acetylated BSA (75 μ g ml⁻¹; Promega), T4 DNA Ligase (400 U; NEB), *Bpil* (10 U; Thermo Fisher Scientific) and molecular biology-grade water (to the final volume of 20 μ l) were combined together and used for the construction of level 2 binary vectors. The reactions were incubated under the same conditions as those used to assemble the level 1 constructs (Table 2.10) except that the number of digestion-ligation cycles was increased from 26 to 50. An aliquot of each reaction (10 μ l) was used to transform One Shot® TOP10 *E. coli* (Invitrogen; 2.2.1.3.1). Colonies were grown overnight at 37°C on kanamycin (50 μ g ml⁻¹; Sigma) LB agar plates. White clones (six per construct) were selected for further analysis and propagated overnight at 37°C, 180 RPM in liquid LB media (5 ml) supplemented with kanamycin (50 μ g ml⁻¹). Level 2 plasmids were isolated (2.3.1.1) and the constructs were verified by a restriction enzyme digest (2.4.2.3). Plasmids with the correct digestion patterns were sequenced at the left and right borders with the same set of primers as used for sequencing of level 1 vectors (2.3.4.1). The final level 2 assemblies pICSL4723::NOSp-NPTII-OCST::2x35S-5'UTR-hCas9(STOP)-NOST::AtU6p::sgRNA_zepe1 (pICSL4723::zepe1) and pICSL4723::NOSp-NPTII-OCST::2x35S-5'UTR-hCas9(STOP)-NOST::AtU6p::sgRNA_zepe6 (pICSL4723::zepe6) were used for a heat shock transformation of ElectroMAX™ *Agrobacterium tumefaciens* strain LBA4404 (Invitrogen, USA; 2.2.1.3.3).

2.4.2 Restriction enzyme digestion

2.4.2.1 Digestion of plant genomic DNA

DNA was extracted from the U/U (positive control) and MM (negative WT control) tomato varieties and three plants of the F₂ segregating population (one hemizygous and two homozygous for transgenic *CrtR-b2*, as inferred from the segregation test) using DNeasy Plant Mini Kit (QIAGEN, 2.3.1.2.1). If necessary, multiple extractions were carried out from the same plant and the samples were pooled to obtain the required amount of the nucleic acid. Extracted DNA was tested for its concentration and purity (2.3.2). When necessary, the DNA samples were concentrated down using Genevac EZ-2 Mk2 Plus Centrifugal Evaporator (Genevac, UK) at the aqueous drying setting. An enzyme with a high frequency of recognition sites in the DNA predicted to cleave once between the left and the right borders of the insert but not within it, was selected for the restriction digest. Genomic DNA (10 µg), 1X NEBuffer™ 4 (NEB, USA), *HindIII*-HF™ (140 U; NEB) and molecular biology-grade water (to the total of 45 µl; VWR) were combined and the reactions were incubated for 16 hours at 37°C. Digestion of the positive blotting control – 35S-*CrtR-b2*-TOPO plasmid was prepared by combining the plasmid DNA (50 pg) with 1X NEBuffer™ 4, *HindIII*-HF™ (10 U) and molecular biology-grade water (to the total of 20 µl; VWR) and incubated together with the plant DNA samples. The enzymes were inactivated by incubating at 80°C for 20 minutes. The samples were separated by agarose gel electrophoresis (2.3.3).

2.4.2.2 Verification of Golden-Gate vectors

The plasmids used in Golden-Gate cloning (Table 2.11) were purchased from the Addgene plasmid repository (<http://www.addgene.org/>) and provided in form of bacterial stabs. Each plasmid-containing strain was streaked onto a LB agar plate supplemented with an appropriate antibiotic and incubated overnight at 37°C (2.2.1.1). A single clone was picked from the plate and propagated overnight in LB liquid media (5 ml) supplemented with the antibiotic and used for extraction of plasmids (2.3.1.1). Diagnostic digests of the plasmids were carried out with the enzymes listed in Table 2.11 to confirm the suitability of the material for cloning. The enzymes were chosen based on the plasmid maps from Addgene and the sequence provided by the depositor in case of pICSL4723. To predict the patterns and sizes of the fragments, *in silico* digestions were performed online using NEBcutter V2.0 (Vincze *et al.*, 2003). *Asel* and *AatII* enzymes were purchased from NEB (USA) and *BamHI*, *EcoRV*, *NdeI*, *NotI* and *Sall* from Promega (UK). The digests were set up with 1X Buffer D (Promega), Acetylated BSA (100 µg ml⁻¹; Promega), plasmid DNA (1 µg; all plasmids except pICSL01009::AtU6p), restriction enzyme (5 U of each; Promega) and molecular biology-grade water (to the total of 20 µl; VWR) or 1X Buffer 3.1 (NEB), plasmid pICSL01009::AtU6p (1 µg), *Asel/AatII* enzymes (10 U of each) and

molecular biology-grade water (to the total of 50 µl; VWR). Digestion with the *Asel/AatII* enzyme pair was carried out at 37°C for 15 minutes and for the remaining enzymes the incubation was extended to 4 hours. The *Asel/AatII* enzymes were heat inactivated at 80°C for 20 minutes and the remaining enzymes were inactivated for 15 minutes at 65°C. Digestion of each plasmid, except pICSL4723, was accompanied by a mock reaction in which the enzymes were omitted. Additionally, to verify the efficacy of the double digests, each plasmid, except pICSL4723, was linearised by digestion with a single enzyme (first enzyme in the enzyme pair in Table 2.11). The mock reactions and single digests were otherwise set up and incubated as described above. Digested products were analysed on agarose gel (2.3.3).

2.4.2.3 Verification of level 1 and 2 constructs

Following the assembly of the level 1 and 2 vectors (2.4.1.2), the constructs were verified by a restriction enzyme digest. The digestion patterns were predicted *in silico* with NEBcutter V2.0 (Vincze *et al.*, 2003). For each of the assembled level 1 (pICH47751::AtU6p::sgRNA_zepe1 and pICH47751::AtU6p::sgRNA_zepe6) and level 2 (pICSL4723::zepe1 and pICSL4723::zepe6) constructs, seven and six white bacterial clones were chosen for analysis, respectively. The clones were propagated overnight in LB liquid media (5 ml) supplemented with appropriate antibiotics (2.2.1.1) and used for plasmids extractions (2.3.1.1). Level 1 constructs were single-enzyme digested with *Bpil* (*BbsI*; Thermo Fisher Scientific, USA) and double-enzyme digested with *NotI* (Promega) and *Sfil* (NEB). The empty level 1 acceptor, pICH47751, was digested alongside. The digests were set up with 1X Buffer G (Thermo Fisher Scientific), plasmid DNA (400 ng) and *Bpil* (5 U) for the single digests and 1X Buffer D (Promega), Acetylated BSA (100 µg ml⁻¹; Promega), plasmid DNA (400 ng) and *NotI* (10 U) for the double digests with molecular biology-grade water (to the total of 20 µl; VWR). The reactions were incubated at 37°C for 2 hours then the enzymes were inactivated for 20 minutes at 65°C. Following *NotI* inactivation, *Sfil* (20 U) was added to the reaction tubes and incubated for further 30 minutes at 50°C. Level 2 constructs and the empty level 2 vector, pICSL4723, were digested with *EcoRV* (Promega). The reactions were set up as described above for the other Promega restriction enzymes (2.4.2.2) and incubated for 2 hours at 37°C. The mock digest was performed on a successfully assembled level 2 binary vector confirmed by sequencing. The digestion products of level 1 and 2 plasmids were analysed on agarose gel (2.3.3) and vectors with the correct digestion patterns were sequenced (2.3.4.1). Correctly assembled level 2 plasmids were used for transformation of LBA4404 *A. tumefaciens* (2.2.1.3.3) and subsequently used in the stable transformation of tomato (2.2.3.2).

Table 2.11. Plasmids used in the assembly of the level 2 CRISPR/Cas9 expression cassettes. The antibiotic resistance conferred by the plasmids, names of restriction enzymes used in the digestions as well as the expected sizes of the fragments are indicated. Hence, the commas between the numbers in the last column separate fragments of different sizes and are not used to separate thousands; A – ampicillin; K – kanamycin; S – spectinomycin; bp – base pairs.

Addgene ID	Name	Description	Resistance	Enzymes	Fragments [bp]
#48002	pICH47751	- empty level 1 cloning vector			548, 4 420
#49771	pICH47742::2x35S-5'UTR-hCas9(STOP)-NOST	- level 1 hCas9 module (human codon optimised)	A	<i>NotI/BamHI</i>	3 174, 6 449
#51144	pICSL11024 (pICH47732::NOSp-NPTII-OCST)	- confers kanamycin resistance in planta		<i>NotI/NdeI</i>	2 654, 3 589
#46966	pICH86966::AtU6p::sgRNA_PDS	- sgRNA scaffold template		<i>NdeI/SalI</i>	2 197, 4 358
#48015	pICSL4723*	- empty level 2 cloning vector	K	<i>EcoRV</i>	1 649, 3 822, 7 477
#46968	pICSL01009::AtU6p	- <i>Arabidopsis</i> U6 promoter in level 0 vector - places sgRNA under <i>Arabidopsis</i> U6 promoter	S	<i>AscI/AatII</i>	194, 2 129
#48018	pICH41766	- level 2 end-linker		<i>NdeI/SalI</i>	729, 2 589

*The original level 2 cloning vector, pAGM4723 was found to lack a complete overdrive sequence at the right boarder which led to incomplete T-DNA insertion events and increased incidence of vector backbone transfer. The overdrive sequence was amended and the correct plasmid was provided by Mr Mark Youles, The Sainsbury Laboratory, Norwich, UK. Plasmid pICSL4723 was digested alongside the assembled level 2 binary vectors as described in Section 2.4.2.3.

2.5 CRISPR/Cas9 targeting of zeaxanthin epoxidase (*ZEP*)

2.5.1 Designing single guide RNAs (sgRNAs)

In silico prediction and analyses of the wild type (WT) zeaxanthin epoxidase, *ZEP* structure (UniProtKB Accession P93236 (ABA2_SOLLC); Apweiler *et al.*, 2017) and its novel alleles were performed with Phyre2 (Kelley *et al.*, 2015), a web-based protein structure prediction service using intensive modelling mode. Phyre2 was used for mutational analysis of WT *ZEP* using the SuSPect method (Yates *et al.*, 2014) to predict functional or phenotypic effects of missense mutations at particular positions in the sequence. Additionally, pocket detection analysis of WT *ZEP* was performed using fpocket2 (Schmidtke *et al.*, 2010) program in Phyre2. Ligand binding site prediction was performed on the WT and edited *ZEP* protein models generated through Phyre2 using 3DLigandSite (Wass *et al.*, 2010). The 20-bp long guides targeting exon 1 (SL2.50ch02:-5237466..52374686) and exon 6 (SL2.50ch02:+52372505..52372524) of the gene encoding zeaxanthin epoxidase, *ZEP* (*Solyc02g090890.2*; Kersey *et al.*, 2018) were designed based on *S. lycopersicum* cultivar Heinz 1706 reference genome (GCA_000188115.2) using an online platform at benchling.com and selected according to the criteria set by Liang *et al.* (2016). An additional guanine was added to the beginning of the guide to account for the *Arabidopsis* U6 (*AtU6*) promoter transcription start site. The guides were confirmed to be free of *Bsa*I and *Bbs*I (*Bpi*I) restriction sites with NEBcutter V2.0 (Vincze *et al.*, 2003). The on-scores of the guides against exon 1 and exon 6 were 0.645 and 0.480, respectively. Secondary structures of the guides were analysed using an online RNA folding tool at Bioinformatics Web Server for RNA (rtools.cbrc.jp; Hamada *et al.*, 2016) with CONTRAfold inference engine and at *RNAfold* WebServer (<http://rna.tbi.univie.ac.at/cgi-bin/RNAWebSuite/RNAfold.cgi>) using a minimum free energy (MFE) structure prediction and enforcing the constraint pairing pattern of:

.....(((((((.....xxxx.....))))))..((xxxxx)).xxxxx.....xxxx.....xxx.....

Where: x – indicates bases, which must not pair

. – indicates bases with no constraint at all

() – indicates base pairs

The off-target analysis was performed using CRISPR-P v 2.0 at crispr.hzau.edu.cn/CRISPR2/ (Lei *et al.*, 2014; Ding *et al.*, 2016; Liu *et al.*, 2017). The lists of the top 20 off-targets (OTs) for the guides targeting exon 1 (23 OT sites in total) and exon 6 (32 OT sites in total) are provided in Tables 2.12 and 2.13, respectively.

Table 2.12. Top 20 off-targets for the guide targeting exon 1. Underlined bases indicate mismatches; CDS – coding sequence; MMs – mismatches.

Sequence	MMs	Off-score	Locus	Gene	Region	Description
<u>ct</u> agatagagagcaatg <u>t</u> at		0.322	SL2.50ch04:+61385388		Intergenic	
actgata <u>t</u> cgagcaatg <u>t</u> at		0.227	SL2.50ch09:-70291159	<i>Solyc09g090870.2</i>	CDS	DNA mismatch repair protein mutS
<u>t</u> ca <u>t</u> ata <u>c</u> gaagcaatgcat		0.226	SL2.50ch05:-27422203			
actgata <u>t</u> agagaaagcat		0.216	SL2.50ch01:+41092683			
aca <u>t</u> atagaagcaat <u>a</u> cat		0.204	SL2.50ch05:-32750138			
<u>t</u> caaatacaagccatgcat		0.18	SL2.50ch06:+16531181			
acagatg <u>t</u> acagaaatgcat		0.095	SL2.50ch09:+10768222		Intergenic	
acagataca <u>t</u> a <u>t</u> aatg <u>t</u> at		0.088	SL2.50ch10:+12897254			
aca <u>a</u> a <u>a</u> ccagagcaat <u>c</u> cat	4	0.08	SL2.50ch10:-10293691			
a <u>a</u> agataca <u>t</u> a <u>c</u> ccatgcat		0.067	SL2.50ch05:-16946349			
a <u>a</u> a <u>a</u> atacagagaaat <u>c</u> cat		0.059	SL2.50ch03:-32082800			
aca <u>a</u> a <u>a</u> acagagcaaatcat		0.048	SL2.50ch02:+40634097	<i>Solyc02g071140.2</i>	Intron	Ca ²⁺ activated outward rectifying K ⁺ channel 6
aca <u>c</u> atacaagacatgcat		0.041	SL2.50ch08:-24703016			
acatt <u>t</u> aagat <u>t</u> caatgcat		0.033	SL2.50ch09:+49787178		Intergenic	
acaga <u>a</u> ccatagcactgcat		0.022	SL2.50ch08:+51108864			
atgga <u>a</u> acagaggaatgcat		0.017	SL2.50ch06:-38513270	<i>Solyc06g060490.2</i>	CDS	Uncharacterised protein
acaga <u>a</u> acagagccctc <u>c</u> cat		0.013	SL2.50ch11:+1573826	<i>Solyc11g007110.1</i>	CDS	Single-stranded nucleic acid binding R3H protein
a <u>t</u> agatacagagcatagcat		0.043	SL2.50ch11:+21833369		Intergenic	
acagat <u>t</u> caga <u>a</u> cat <u>t</u> gcat	3	0.021	SL2.50ch08:+45953379			
acagatagagat <u>a</u> catgcat	2	0.064	SL2.50ch11:-4458843	<i>Solyc11g011380.1</i>	Intron	Glutamine synthetase

Table 2.13. Top 20 off-targets for the guide targeting exon 6. Underlined bases indicate mismatches; CDS – coding sequence; MMs – mismatches; UTR – untranslated region.

Sequence	MMs	Off-score	Locus	Gene	Region	Description
<u>t</u> atctt <u>a</u> ccaactaaaggt*		0.477	SL2.50ch09:-17919042		Intergenic	
cctct <u>c</u> gcaactaaagat*		0.362	SL2.50ch10:-65200118	<i>Solyc10g086340.1</i>	Intron	ATP binding microtubule motor family protein
<u>t</u> gtctt <u>c</u> ccaacaaaaggt*		0.35	SL2.50ch06:+41766808			
<u>t</u> ctct <u>c</u> caaaccaaggt*		0.223	SL2.50ch11:+24362591		Intergenic	
cctctg <u>c</u> cc <u>t</u> aactgaagga*		0.197	SL2.50ch01:-41607904			
ccttt <u>c</u> ctgaactaaaggt*		0.188	SL2.50ch07:-1248637	<i>Solyc07g006440.1</i>	CDS	Aspartic proteinase nepenthesin-2-like
<u>t</u> ctct <u>c</u> ccatactaaaggt*		0.185	SL2.50ch08:-50731691		Intergenic	
<u>t</u> ct <u>a</u> ttcccaaccaa <u>t</u> gt*		0.16	SL2.50ch09:-6056851	<i>Solyc09g014440.2</i>	Intron	RNAP II C-terminal domain phosphatase-like 2
<u>t</u> cc <u>t</u> ttccca <u>a</u> aa <u>t</u> aaaggt*		0.143	SL2.50ch09:-56835675		Intergenic	
<u>t</u> ca <u>t</u> ttcccaactaa <u>t</u> gt*	4	0.099	SL2.50ch09:+71184815	<i>Solyc09g091990.2</i>	UTR	Receptor like protein kinase S.2
cctctg <u>c</u> cc <u>t</u> a <u>c</u> tgaaggt*		0.092	SL2.50ch08:-65649204	<i>Solyc08g083070.2</i>	CDS	Hop-interacting protein THI002
<u>a</u> ctctg <u>c</u> cc <u>t</u> a <u>c</u> aaaaggt*		0.09	SL2.50ch08:-2673981	<i>Solyc08g008230.2</i>	Intron	Uncharacterised protein
cctttccca <u>a</u> actaaaggt		0.085	SL2.50ch01:+58120791			
cctttccca <u>a</u> actaaaggt		0.085	SL2.50ch01:+58143751		Intergenic	
<u>c</u> tc <u>a</u> tcccaac <u>c</u> aaaggt*		0.056	SL2.50ch06:-42691131	<i>Solyc06g068860.2</i>	Intron	α-mannosidase precursor
cctcatg <u>c</u> ccat <u>c</u> aaaaggt		0.049	SL2.50ch01:+45142491			
cctcat <u>t</u> ccaact <u>t</u> aagga		0.049	SL2.50ch02:-25531628			
cctcatg <u>c</u> ccat <u>c</u> aaaaggt		0.049	SL2.50ch10:-15720616		Intergenic	
cctttccca <u>t</u> ct <u>t</u> aaggt		0.046	SL2.50ch01:-36562824			
cctttccca <u>a</u> tt <u>a</u> at <u>g</u> gt*	3	0.075	SL2.50ch02:+22232460	<i>Solyc02g021230.2</i>	Intron	Uncharacterised protein

* Off-targets analysed by PCR; these are numbered from 1 to 14 as going from top to bottom.

2.5.2 Construction of vectors

In silico assembly of level 1 and 2 vectors was performed at benchling.com. The guides targeting exon 1 (sgRNA_zepe1) and exon 6 (sgRNA_zepe6) were amplified with a high-fidelity polymerase (2.3.5.3) and purified (2.3.5.6). The vectors were constructed using the Golden-Gate cloning protocol (2.4.1.2) and verified by restriction-enzyme digest (2.4.2.3), PCR (2.3.5.2.1) and sequencing (2.3.4.1). Level 2 constructs, pICSL4723::NOSp-NPTII-OCST::2x35S-5'UTR-hCas9(STOP)-NOST::AtU6p::sgRNA_zepe1 (pICSL4723::zepe1) and pICSL4723::NOSp-NPTII-OCST::2x35S-5'UTR-hCas9(STOP)-NOST::AtU6p::sgRNA_zepe6 (pICSL4723::zepe6), were used for transformation of ElectroMAX™ *A. tumefaciens* strain LBA4404 (Invitrogen, USA; 2.2.1.3.3).

2.5.3 Stable transformation of tomatoes

S. lycopersicum cultivar Ailsa Craig was used for *Agrobacterium* mediated stable transformation of tomato (2.2.3.2). 500 explants (approximately 130 plantlets; usually 2 explants per cotyledon) were used per construct. A control tissue culture regeneration experiment with 20 explants was set up along the *Agrobacterium* transformation experiment. The explants in the control experiment were not exposed to *Agrobacterium* but otherwise were cultured in the same way as the transformed explants without kanamycin selection. The rooted shoots were acclimatised, transferred into the soil and grown in the glasshouse at the conditions specified earlier (2.1.2).

2.5.4 Analysis of transformed tomato plants

Positive transformation events were selected based on the presence of the hCas9 and NPTII fragments (2.3.5.2.2). Untransformed plants, regenerated through the tissue culture, were used as negative controls for the presence of these fragments and the level 2 binary plasmids (pICSL4723::zepe1 and pICSL4723::zepe6; 2.4.1.2.2) were used as positive controls. Plants positive for hCas9 and NPTII fragments were tested for the presence of editions in the targeted regions by amplifying exon 1 and exon 6 fragments (2.3.5.2.2). The wild type fragments of both exons were amplified from the untransformed control plants. The PCR amplicons were sequenced with their respective forward PCR primers (2.3.4.1). Plants, identified as edited in the targeted regions by overlapping or collapsed sequencing readouts, were selected for further analysis. To identify the types and frequencies of editions, PCR amplicons spanning the edited sites of either exon 1 or exon 6 were cloned into TOPO plasmids (2.4.1.1) and sequenced (2.3.4.1). Between 10 and 20 clones were analysed per edited plant. The plant identified to have a biallelic edition of the exon 6 and mimicking the *hp3* phenotype was analysed for possible off-target editions. The primers (Table 2.6) flanking the selected off-target (OT) sites (Table 2.13) were designed at benchling.com based on *S. lycopersicum* cultivar Heinz 1706 reference genome (GCA_000188115.2). The OTs to be analysed were selected based on their off-scores and positions within the genome. The OT regions were amplified and sequenced (2.3.5.2.3).

2.6 Extraction and analysis of metabolites

The major objective of this study was to characterise the metabolic profiles of the studied lines. Three different analytical techniques, namely liquid chromatography (HPLC and UPLC; 2.6.2), gas chromatography (GC-MS; 2.6.6) and solid phase microextraction (SPME; 2.6.7) were engaged in order to complement this objective. The methods of extraction and analysis of plants' polar, non-polar as well as volatile metabolites are described in the following sections.

2.6.1 Extraction of carotenoids and chlorophylls

2.6.1.1 Preparation of the freeze-dried material

Snap-frozen or stored at -80°C tomato flower, fruit and leaf material was freeze-dried for one (flower and leaf) or three (fruit) days prior to extraction. Snap-frozen spinach and kale leaves were freeze-dried for one and three days, respectively. The pooled material from at least three tomato fruit, 12 – 15 fully opened flowers and 10 leaves was used per plant in the extractions. The material was homogenised for 3 minutes either at 30 Hz using TissueLyser II (Qiagen) or at 50 Hz using TissueLyser LT (Qiagen) in 2 ml Safe-Lock Micro Test Tubes (Eppendorf, Germany) containing a clean, 5 mm Stainless Steel Bead (Qiagen, Germany). The disrupted material was weighted out into separate 1.5 ml microcentrifuge tubes (Camlab Ltd, UK). Approximately 15 mg of the material was used in the extractions of pigments from leaf and fruit tissues and 10 mg were used in the extractions of pigments from flowers. The weights of the samples were recorded to the tenths of a milligram using a Secura124-1S analytical balance (Sartorius AG, Germany). Extractions of quality control (QC) samples of similar weights to the samples analysed were carried out along the batch extractions. The QCs were prepared for each type of material analysed by combining aliquots of equal weights from all samples analysed in the experiment. Each biological sample was extracted in three technical repeats. One QC sample was extracted per 6 biological samples analysed. The 5 mm beads were reused and cleaned with ddH₂O (20 ml) in a beaker (100 ml) followed by a wash in ethanol, AnalaR NORMAPUR[®] ACS (70% v/v; VWR Chemicals, USA) to remove any residual material and a final wash in ddH₂O (40 ml).

2.6.1.2 Methanol-chloroform extraction of pigments

Extractions of the freeze-dried tissues were carried out at the 1:2 volume ratio of methanol to chloroform. HPLC-grade methanol (250 μl ; Fisher Chemical) was added to the homogenised and weighed-out fruit, flower or leaf samples and vortexed vigorously to remove any clumps. Chloroform (500 μl ; Fisher Chemical) was then added to the samples, vortexed and incubated in dark on ice for 20 minutes. In order to generate phase separation, ddH₂O (250 μl) was added to the samples, vortexed vigorously and centrifuged for 5 minutes at 17 000 g using Heraeus™ Pico™ 17 Microcentrifuge (Thermo Scientific, USA). The bottom (nonpolar) layer was removed

into a fresh 1.5 ml microcentrifuge tube while avoiding transfer of the top (polar) layer. Chloroform (500 µl) was added once more to each sample tube for re-extraction. The samples were vortexed vigorously and centrifuged for 5 minutes as previously. The nonpolar layer was removed once more and pooled with the same phase removed earlier. The polar phases were discarded and nonpolar phases containing carotenoids were dried in the Genevac EZ-2 Mk2 Plus Centrifugal Evaporator (Genevac, UK) at the low boiling point setting and with the lamp turned off. The samples were analysed immediately or stored in sealed tubes under nitrogen gas at -80°C for later analysis (2.6.2).

Following the collection of fractions (1.0 ml or 0.5 ml) from the tomato sub-chromoplast fractionation experiment (2.6.8), the samples were extracted prior to their analysis on the UPLC system (2.6.2.3) similarly to what was described above. In the extractions of 1.0 ml fractions, the amount of methanol used was the same as above (250 µl) and the amount of chloroform was increased (750 µl); in the extractions of 0.5 ml fractions these volumes were halved (to 125 µl and 375 µl, respectively). Water (ddH₂O) was not added during the extractions but otherwise the samples were processed in the same manner as described above.

For the removal of carotenoid esters and chlorophylls from the freeze-dried flower and leaf material, respectively, the samples were saponified prior to the extraction in KOH (6% w/v) in methanol solution (250 µl). Initially, an aqueous solution of KOH (60% w/v; Sigma-Aldrich) was prepared and subsequently diluted (10X) in methanol to obtain the required final concentration. The leaf and flower samples were incubated in dark at 37°C for 1 hour and at 40°C for 3 hours, respectively. Chloroform (500 µl) was then added to each sample and the extraction procedure was carried out as described above for the freeze-dried fruit, flower and leaf samples.

2.6.2 Sample analysis on the HPLC and UPLC systems

2.6.2.1 Sample preparation

The extracted and dried samples of carotenoids and chlorophylls (2.6.1) were dissolved in appropriate amounts of the solvent. These volumes as well as the sample injection volumes were selected experimentally so as the chromatographic output signal would fall within the analytical range of the standard curve (2.6.4.2). For the use in high-performance liquid chromatography (HPLC) analysis, HPLC-grade ethyl acetate (Fisher Chemical, USA) was used to dissolve the extracted fruit samples (typically 80 or 100 µl), saponified and non-saponified flower samples (140 µl) as well as saponified (150 µl) and non-saponified (300 µl) leaf samples. For the use in ultra-performance liquid chromatography (UPLC) analysis, extracted samples were also dissolved in the HPLC-grade ethyl acetate (typically in 30, 60 or 120 µl of the solvent). In order to remove solid particulates which could block the column, the samples were centrifuged at

17 000 *g* and room temperature (~22°C) for 5 minutes prior to the HPLC analysis and for 10 minutes prior to the UPLC analysis using Heraeus™ Pico™ 17 Microcentrifuge (Thermo Scientific). The top layer of each sample (typically around 80% of the original volume) was transferred into a 300 µl glass insert with plastic springs (Sigma, USA) placed in a 1.5 ml screw-top glass vial (Sigma). Care was taken not to disrupt any solid particulates at the bottom of the centrifuged tube. The samples were injected into the HPLC system (typically 10 or 20 µl) or into the UPLC system (typically 3 or 5 µl) for the analysis. The data were processed using Empower™ 2, version 6.1.2154.924 software (Waters® Corporation, USA). Chromatographic traces were extracted at 450 nm for carotenoids and chlorophylls, 286 nm for phytoene and 292 nm for α-tocopherol. The data were stored and processed on configuration 14 LAC/E³²™ acquisition server with RAID1 support (Waters®).

2.6.2.2 High-performance liquid chromatography (HPLC)

The samples extracted from fruit, flowers and leaves were analysed on the Alliance 2695 HPLC System (Waters®) coupled to 996 Photodiode Array Detector (Waters®). The samples were separated on a 5 µm particle size C₃₀-bonded silica-based reverse-phase column (150 × 4.6 mm; YMC CO., Japan) coupled to a compatible 5 µm particle size guard column (4.0 × 20 mm; YMC CO.). The column temperature was set at 25°C and maintained by a column heater/chiller compartment Model 7955 (Jones Chromatography, UK). The samples were kept in the HPLC autosampler compartment at 8°C. The method of sample separation was previously described by Fraser *et al.* (2000). Briefly, the mobile phase consisted of methanol (solvent A), water with methanol mixture (1 to 4 v/v ratio) containing ammonium acetate (0.2% w/v; DBH Chemicals, UK; solvent B) and methyl *tert*-butyl ether, MTBE (solvent C). Solvent B was maintained at a constant level of 5% throughout the 60-minute long run. The gradient was started isocratically at 95% A and 0% C for the first 6 minutes, stepped linearly to 80% A and 15% C within 1 minute and run isocratically at this composition for the next 5 minutes. At 12 minutes, a 20-minute long linear gradient started to the final concentration of 30% A and 65% C. The solvents were run isocratically at their final concentrations for the next 16 minutes. At 48 minutes, the gradient returned to the initial composition of 95% A and 0% C within 2 minutes and was continued isocratically for the remaining 10 minutes of the run to equilibrate the column before the next injection. The flow was maintained at 1 ml min⁻¹. All solvents were of HPLC-grade purity and purchased from Fisher Chemical. Solvent B was prepared prior to the HPLC analysis and filtered through a 0.2 µm pore size hydrophilic polypropylene membrane filter (Ø47 mm; Pall Corporation, USA) using a Laboport UN820.3 FTP vacuum pump (KNF Neuberger, Inc., USA). The detection in the ultraviolet-visible spectral region (UV-Vis) was performed continuously in the range between 220 and 600 nm with a 996 PDA detector (Waters®) with 1 Hz sampling rate and wavelength resolution of 1.2 nm. Identification of compounds was performed by matching their

retention times (RTs) and spectra to the authentic standards as well as to the previously characterised tomato extracts on this HPLC system described by Fraser *et al.* (2007) and Dr Price (unpublished data). The spectra of the compounds identified on the HPLC system are provided in Figure 2.2.

2.6.2.3 Ultra-performance liquid chromatography (UPLC)

The UPLC system was primarily used for analysis of samples extracted from the tomato fruit sub-chromoplast fractionations (2.6.8) and for assessment of sample purity during preparation of carotenoid standards (2.6.3). The samples were analysed on Acquity UPLC system (Waters®) and separated on 1.7 µm particle size Ethylene Bridged Hybrid (BEH) C₁₈ column (2.1 × 100 mm; Waters®) coupled to a VanGuard™ pre-column (2.1 × 5 mm; Waters®). The column was maintained at 30°C and the samples were kept in the autosampler compartment at 8°C. The method of sample separation was previously described by Alcalde & Fraser (2016). Briefly, the mobile phase consisted of water with methanol mixture (1 to 1 v/v ratio; solvent A) and ethyl acetate with acetonitrile mixture (1 to 3 v/v ratio; solvent B). The gradient was started isocratically at 30% A and 70% B for the first 0.5 minutes, stepped linearly to 0.1% A and 99.9% B for the next 3.5 minutes, run isocratically at this final composition for 2 minutes and returned to the initial composition of 30% A and 70% B for the last 2 minutes of the run. The flow rate was maintained at 0.5 ml min⁻¹. The UV-Vis detection was performed continuously in the range between 250 and 600 nm with Acquity UPLC PDA detector (Waters®) with 20 Hz sampling rate and wavelength resolution of 1.2 nm. Identification of compounds was performed by matching their RTs and spectra to the authentic standards as well as to previously characterised tomato extracts on this UPLC system (Nogueira, unpublished data). The spectra of the identified compounds are provided in Figure 2.3.

2.6.2.4 Quantitative data pre-processing

In the analysis on the HPLC system, the chromatographic peak traces were extracted, integrated and processed to obtain the amounts of carotenoids in analysed samples using the standard curve method (2.6.4.2). The amounts of carotenoids were reported in µg per a gram of the dry-weight sample [µg g⁻¹ DW]. The amounts of carotenoids were adjusted to QCs if necessary, to account for the batch-to-batch variation. The technical repeats were examined for repeatability and averaged. The statistical analyses were performed on biological repeats averaged from technical repeats. In the analysis on the UPLC system of the extracted sub-chromoplast fractions (2.6.8.5), the amount of each carotenoid in a fraction was reported as a percentage of its total content in the fractionated sample.

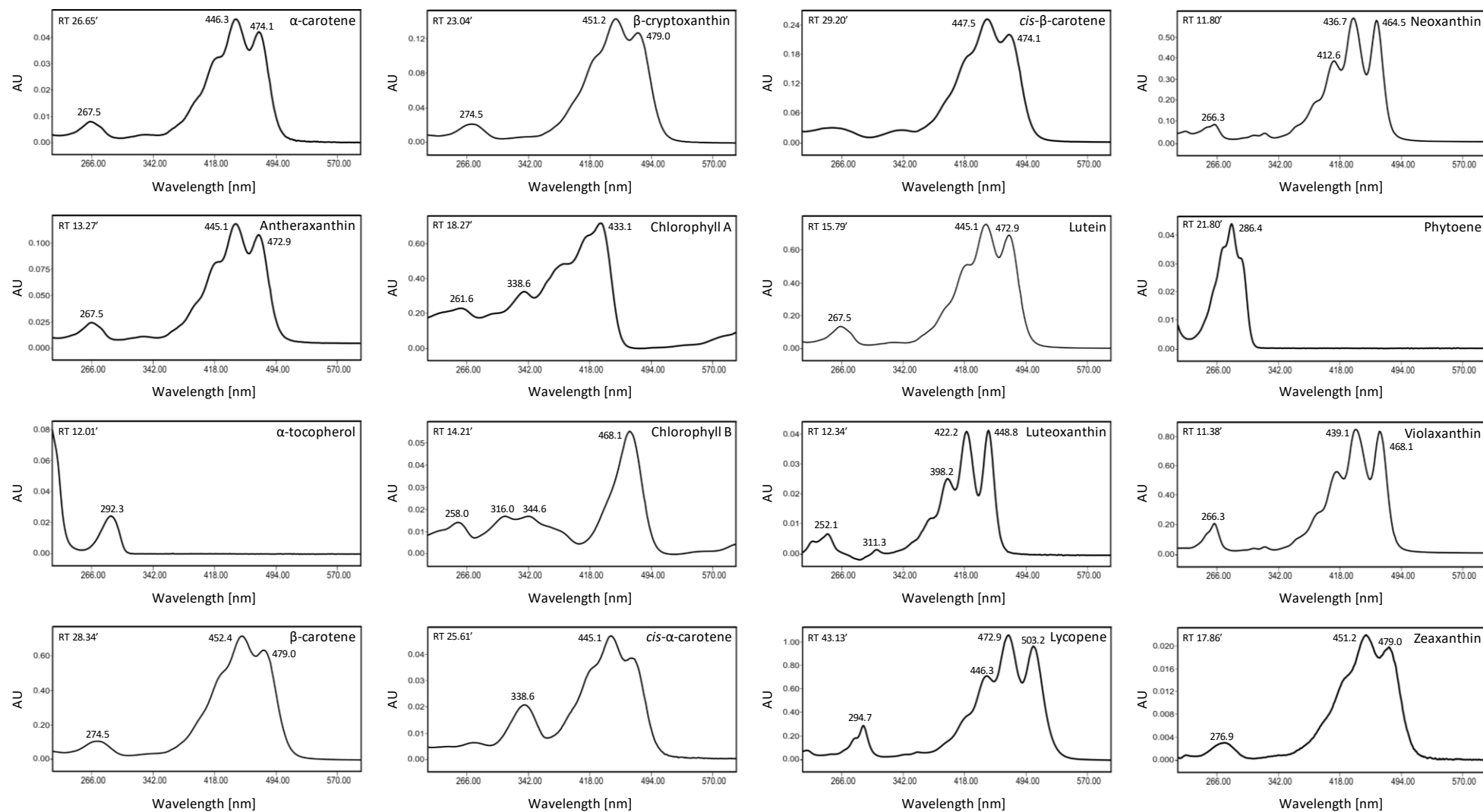


Figure 2.2. UV-Vis spectra of the compounds identified and quantified on the HPLC system. The names of the compounds, their retention times (RT) and peak maxima are indicated on the spectra. The spectra were extracted at 450 nm except α -tocopherol and phytoene whose spectra were extracted at 292 and 286 nm, respectively.

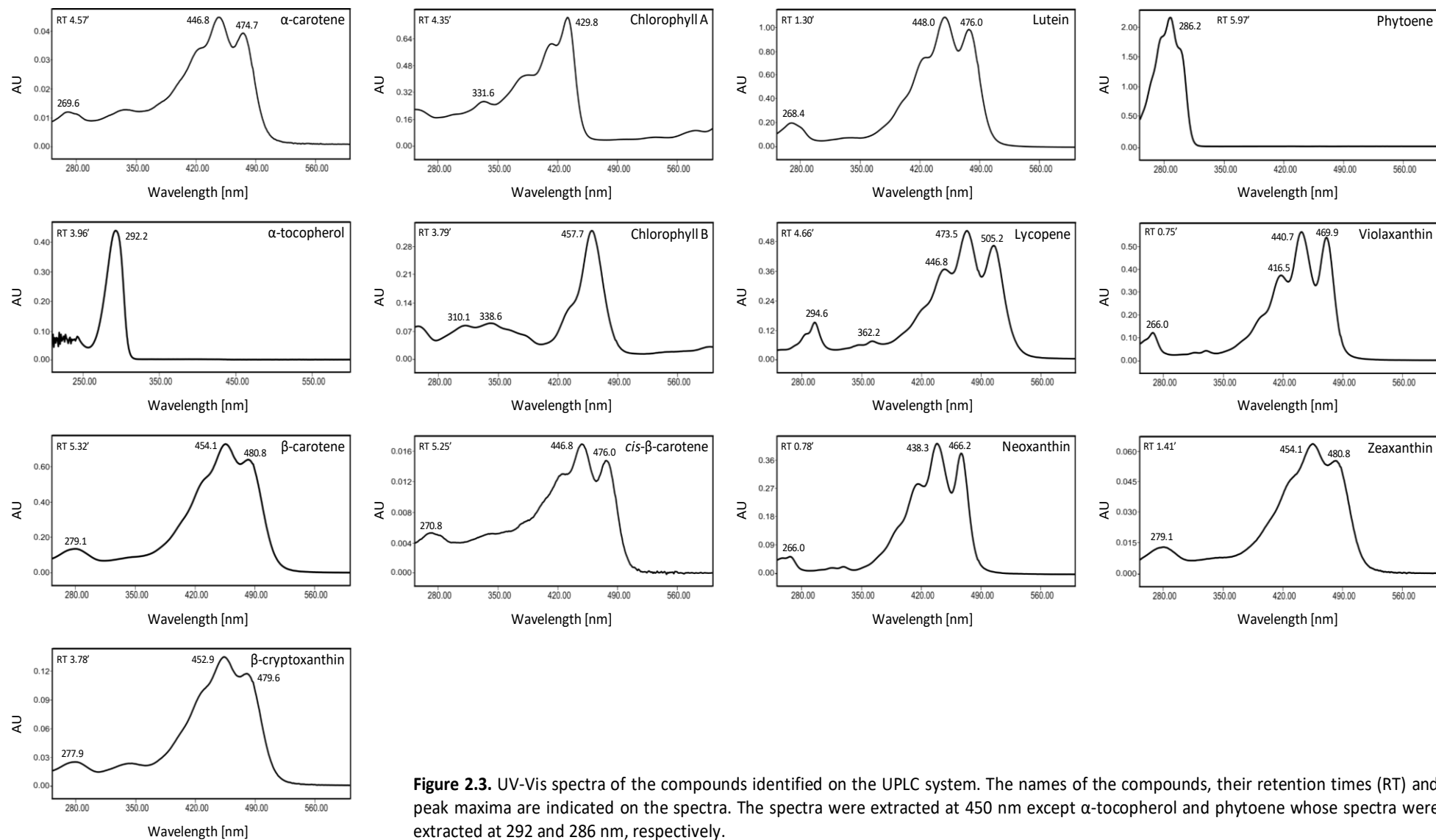


Figure 2.3. UV-Vis spectra of the compounds identified on the UPLC system. The names of the compounds, their retention times (RT) and peak maxima are indicated on the spectra. The spectra were extracted at 450 nm except α -tocopherol and phytoene whose spectra were extracted at 292 and 286 nm, respectively.

2.6.3 Extraction and purification of standards

Liquid chromatography (2.6.2) allows to characterise carotenoid profiles of the studied lines. However, this technique can also be used to quantify amounts of the metabolites in order to better understand changes within the carotenoid pathway that have occurred as the result of introduction of the genes of interest. Quantification of the compounds of interest requires generation of a dose-response curve characteristic for a given compound and the analytical platform. Not all standards were readily available, and the following sections describe the methods of preparation of lycopene, phytoene and violaxanthin standards required for subsequent quantification of these compounds.

2.6.3.1 Extraction of standards

The extraction of phytoene was carried out at 22°C (ambient temperature) whereas lycopene and violaxanthin were extracted at 4°C in a temperature-controlled room (cold room). Crude extracts were transferred into a 1 000 ml Quickfit™ round bottom flask (Fisher Scientific, USA) and evaporated to dryness using Büchi® Rotavapor-R, Type KRvr 65/45 rotary evaporator (ORME Scientific Ltd, UK) attached to a N035.1.2 diaphragm vacuum pump (KNF Neuberger). The round bottom flask was lowered into the water bath so as the lower surface of the glass was just touching the water surface and rotated at 100 RPM. The water bath was maintained at ambient temperature for drying of phytoene extracts and at 36°C for lycopene and violaxanthin extracts. The crude, dry extracts were stored in sealed round bottom flasks at -20°C and subsequently purified by TLC (phytoene; 2.6.5.1), alumina (Al₂O₃) gravity column (phytoene and lycopene; 2.6.3.2.1) or silica gel (SiO₂) flash chromatography (violaxanthin; 2.6.3.2.2). The extractions were carried out in dim light and the sample tubes were wrapped in aluminium foil to reduce their exposure to light.

2.6.3.1.1 Phytoene

Lyophilised *P. blakesleeanus* (4.42 and 2.60 g; 2.2.2.2) mycelia were combined with pure sand (2.5 g; silver, general purpose grade; Fisher Chemical, USA) and grinded manually with a mortar and pestle. Petroleum ether, bp. 40 – 60°C (150 ml, Fisher Chemical) was added to the powdered mixture and the suspension was grinded for 10 minutes. The supernatant was decanted into a glass flask and the sample was re-extracted with petroleum ether (150 ml) until a clear supernatant was obtained. Residual sand was removed from the extract by centrifugation at 4 000 RPM for 10 minutes, 4°C in a refrigerated 5810 R centrifuge (Eppendorf, Germany) with a swing-bucket rotor A-4-62 (Eppendorf). Centrifugation was repeated as necessary to obtain the extract free of sand particulates. The extract was transferred into a round bottom flask and dried on a rotary evaporator. The dried sample was resuspended in methanol (6 ml; Fisher Chemical) and analysed on DU® 800 spectrophotometer (Beckman Coulter) at the original

concentration and at the 1:100 dilution to ensure that the measured absorbance fell within the photometric readout of the machine. The samples were dried under a stream of nitrogen gas and stored at -20°C. To assess the purity of the extracted compound, the 1:100 dilution of the crude fungal extract was resuspended in ethyl acetate (200 µl), further diluted (1:2 and 1:4) to cover a range of photometric readouts and analysed on the UPLC system (2.6.2.3).

2.6.3.1.2 Lycopene

Lycopene was extracted from ripe red tomatoes of AC variety, kindly provided by Mr Jack Gillan. Fresh, whole tomatoes (135 g) were finely chopped (~5 mm² sections), covered in methanol (500 ml; approximately 3:1 volume ratio of solvent to tissue; Fisher Chemical) and homogenised with the upright T25 Basic Homogeniser (IKA®-Werke GmbH & Co. KG, Germany) and a 20 cm long Dispersing Element S25N-18G (IKA®-Werke GmbH & Co. KG). The homogenate was incubated for 10 minutes under aluminium foil. An equal volume of diethyl ether (10% v/v; Acros Organics™, Belgium) in petroleum ether, bp. 40 – 60°C (500 ml) was added to the homogenate, incubated for further 10 minutes and filtered in a fume hood through 3 layers of Whatman® Grade 3MM Chr Chromatography paper (Whatman) with a N035.1.2 diaphragm vacuum pump (KNF Neuberger, Inc.). The remaining solid material was washed with diethyl ether (10% v/v) in petroleum ether (300 ml). The filtrate was split in half and transferred into two 1 000 ml Fisherbrand™ Glass Conical Separating Funnels (Fisher Scientific) rinsed with petroleum ether. The two phases were equalled with diethyl ether (10% v/v) in petroleum ether (50 ml) and ddH₂O (50 ml; to the total of ~750 ml; ¾ of the total volume of the separating funnel). The separatory funnel was inverted and vented by opening the stopcock to release the build-up of gases. The stopcock was closed, the funnel was gently swirled and the pressure was released by opening the stopcock again. The process was repeated until no more vapour was expelled from the tap. The funnels were covered in foil and left to equilibrate for 30 minutes. The stoppers were removed from the funnels and the top layers were collected, pooled into a round bottom flask, dried on a rotary evaporator and stored as described above.

2.6.3.1.3 Violaxanthin

Violaxanthin was separated out from leaves of the F₃ population plants of the U/O; B/B genotype accumulating elevated levels of this xanthophyll. The leaf material (200 g) was soaked in HPLC-grade acetone (1.5 l; Fisher Chemical) for 30 minutes and blended in an 8010ES laboratory blender (Waring Conair, USA). The slurry was vacuum filtered through three layers of muslin cloth (MacCulloch & Wallis, UK) with a N035.1.2 diaphragm vacuum pump. The remaining solid material was washed with diethyl ether (10% v/v) in petroleum ether (750 ml). A saturated solution of NaCl (50% w/v; Sigma-Aldrich, USA) in ddH₂O (500 ml) was added to the filtrate, stirred together and the whole mixture was split into two 1 000 ml Fisherbrand™ Glass Conical

Separating Funnels (Fisher Scientific) and a 2 000 ml Pyrex™ Pear-Shaped Glass Separating Funnel (Fisher Scientific). The funnels were rinsed with petroleum ether prior to use. The funnels were inverted, vented and incubated as described above (2.6.3.1.2). The aqueous salt phases (bottom) were discarded and the top organic phases were pooled into a conical flask. Anhydrous Na₂SO₄ (150 g; Sigma-Aldrich) was added to the organic phase and incubated at -20°C for 2 hours. The supernatant was decanted into a round bottom flask, dried (2.6.3.1.2) and stored at -20°C.

2.6.3.2 Standards purification by column chromatography

2.6.3.2.1 Alumina gravity column

The crude extracts of phytoene (2.6.3.1.1) and lycopene (2.6.3.1.2) were separated on alumina (Al₂O₃) gravity column to remove ergosterol and β-carotene, respectively. ICN Alumina N, Akt. I (10 g; ICN EcoChrom, Germany) was oven baked overnight at 110°C and activated to Grade III by addition of ddH₂O (0.6 ml; 6% v/w) and thorough stirring. Petroleum ether, bp. 40 – 60°C (100 ml; Fisher Chemical, USA) was added to the activated powder to form a slurry and packed into a Synthware™ chromatography column with PTFE stopcock and coarse frit (L 305 mm, I.D. 15 mm; Kemtech America Inc., USA). The column was rinsed with petroleum ether prior to its use. The crude extracts of phytoene (from 4.42 g of dried mycelia) and lycopene (from 135 g of tomato fruit) were dissolved in petroleum ether (2.0 and 1.0 ml, respectively). The extracts were wet-loaded onto the column and flushed with petroleum ether (10 ml). For the elution of phytoene, solvent gradients (30 ml) of diethyl ether (1% and 5% v/v; Acros Organics™) in petroleum ether were used. Lycopene was eluted with solvent gradients (10 ml) of diethyl ether (1%, 2%, 5% and 10% v/v; Acros Organics™) in petroleum ether with a final wash in diethyl ether (10 ml; 100% v/v). A total of 11 phytoene (~5 ml) and 6 lycopene (~10 ml) fractions were collected into 15 ml glass test tubes. The fractions of phytoene (F1 – F11) were dried under a stream of nitrogen gas, re-dissolved in chloroform (1.0 ml; Fisher Chemical), further diluted (1:100) and scanned continuously for absorption between 200 and 800 nm using 1.0 ml synthetic far-UV quartz cuvettes, 200 – 2 500 nm with 1.0 cm light-path width (Hellma, Germany) and a DU® 800 spectrophotometer (Beckman Coulter, USA). The samples were dried under a stream of nitrogen gas and re-dissolved in HPLC-grade ethyl acetate (500 μl), further diluted (1:100 – fractions 1 and 3 – 11; 1:1 000 – fraction 2 only) and analysed on the UPLC system (5 μl injections) as described in Section 2.6.2.3 in order to assess the purity of phytoene following the on-column separation. The remaining samples were dried under a steam of nitrogen and stored at -20°C. Aliquots (1.0 ml) of the lycopene fractions (F1 – F6) were first analysed spectrophotometrically as described above. Fractions 4 and 5 were diluted further (1:100) to fall in the photometric readout of the machine. The fractions were dried under a stream of nitrogen gas, re-dissolved

in ethyl acetate (100 µl), diluted if necessary (1:4 – fraction 4 only) and analysed on the HPLC system (10 µl injections) as described in Section 2.6.2.2 to assess the purity of lycopene following the on-column separation. The remaining fractions were dried under a stream of nitrogen gas and stored at -20°C.

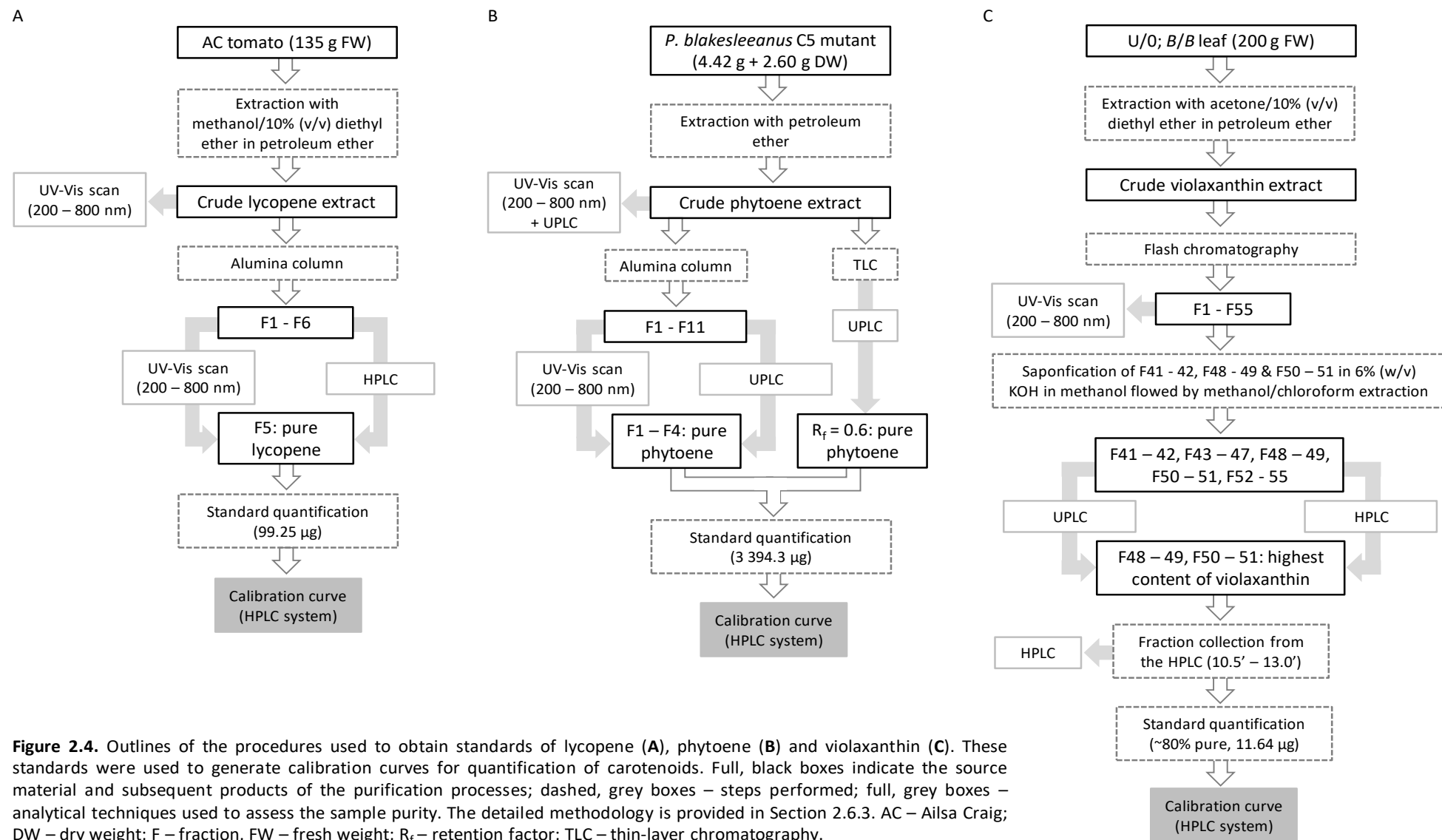
2.6.3.2.2 Flash chromatography

The method for isolation of violaxanthin from the crude leaf extract (2.6.3.1.3) using flash chromatography was followed as previously demonstrated (ChemUCSD, 2011) and is outlined briefly below. The EZSafe® flash-chromatography assembly with a 1 000 ml capacity standard column (O.D. 57 mm × L 508 mm; Sigma-Aldrich, USA) and a GL-45 connector for the solvent reservoir (Sigma-Aldrich) were used in the separation. The column was washed with acetone (Fisher Chemical) prior to its use. A piece of Macherey-Nagel™ Glass Fiber Wadding (Fisher Scientific, USA) was used to plug the bottom of the column and washed through with petroleum ether, bp. 40 – 60°C (50 ml; Fisher Chemical). The column was packed from the Kieselgel 60 Silica Gel 0.040 – 0.063 mm, 230 – 400 mesh ASTM slurry (44 g; Merck Millipore, USA) in petroleum ether (100 ml). Pure sand, silver, general purpose grade (2.0 g; Fisher Chemical) was added on top of the silica. The packed column was washed twice with petroleum ether (100 ml). The crude leaf extract (2.6.3.1.3) was dissolved in petroleum ether (300 ml) and wet-loaded onto the column (50 ml). The remaining extract was dried in Büchi® Rotavapor-R, Type KRvr 65/45 rotary evaporator (ORME Scientific Ltd). Solvent gradients (120 ml) of petroleum ether (100% v/v) and acetone (2%, 8%, 15%, 25%, 50% and 100% v/v) in petroleum ether were run sequentially through the column and fractions (~15 ml; total of 55) were collected into glass test tubes. An aliquot (1.0 ml) of every other fraction was analysed spectrophotometrically using 1.0 ml synthetic far-UV quartz cuvettes (Hellma) on a DU® 800 spectrophotometer (Beckman Coulter). The fractions were pooled together according to their colours (F13 – 15, F26 – 32, F33 – 38, F39 – 40, F41 – 42, F43 – 47, F48 – 49, F50 – 51 and F52 – 55). The pooled fractions were dried under a stream of nitrogen gas and stored at -20°C.

2.6.3.3 Quality assessment of the in-house prepared carotenoid standards

Following the extraction of phytoene, lycopene and violaxanthin (2.6.3.1) and their separation (2.6.3.2), the standards were assessed for their purity. Phytoene, following TLC (2.6.5.1) and alumina column (2.6.3.2.1) separations, was analysed on the UPLC system (2.6.2.3). The TLC extract and alumina fractions (F1 – F4) containing pure phytoene were combined. Lycopene separated on alumina column (2.6.3.2.1) was analysed on the HPLC system (2.6.2.2) and fraction 5 (F5) was identified to contain the pure compound. The pooled fractions (F41 – 42, F48 – 49 and F50 – 51) from the flash chromatography of the leaf extract used to isolate violaxanthin (2.6.3.2.2) were saponified in KOH (6% w/v; Sigma-Aldrich, USA) in methanol

(250 µl; Fisher Chemical, USA) at 37°C for 3 hours. The samples were then extracted with methanol and chloroform as described (2.6.1.2) and dried under a stream of nitrogen gas. The pooled fractions were re-dissolved in ethyl acetate (300 µl) and analysed on the UPLC system (3 µl injections; 2.6.2.3) and the HPLC system (10 µl injections; 2.6.2.2) at the original concentrations (F41 – 55) and at the 1:100 dilution (F43 – 55; HPLC only). F48 – F51 were identified to contain the highest amounts of violaxanthin. However, these fractions were also found to contain other xanthophylls and therefore, required further purification. The only chromatographic method, capable of providing sufficient resolution for xanthophyll separation and readily available at the laboratory, was HPLC. Therefore, F48 – 49 and F50 – 51 were run on the HPLC system (50 µl injections). After passage through the HPLC column, fractions (250 µl; total of 10) with eluting violaxanthin (time points between 10.5' and 13.0') were collected. The first four (F48 – 49) and three (F50 – 51) HPLC-collected fractions were pooled together and dried under a stream of nitrogen gas, re-dissolved in ethyl acetate (300 µl) and reanalysed on the HPLC system (10 µl injections; 2.6.2.2). The final purity of violaxanthin was determined at ~80% (~20% contamination with lutein epoxide). The pooled standards were dried under a stream of nitrogen gas and stored at -20°C until required. The amounts of the in-house prepared standards were quantified as described in Section 2.6.4.1.1. It was determined that 3 394.3 µg, 99.25 µg and 11.64 µg of standards of pure phytoene (from 7.02 g of dry mycelia), pure lycopene (from 135 g of fresh tomato fruit) and ~80% pure violaxanthin (from 200 g of fresh tomato leaf) were obtained from their initial starting materials, respectively. The quantified standards were subsequently used for the preparation of their respective HPLC standard curves (2.6.4.2). Figure 2.4 provides detailed workflows summarising the procedures used to obtain carotenoid standards.



2.6.4 Chromatographic quantification of plant-derived compounds

2.6.4.1 Quantification of isoprenoid, chlorophyll and α -tocopherol standards

The concentrations of the standards used for the generation of dose-response (standard) curves were determined spectroscopically using 1.0 ml synthetic far-UV quartz cuvettes, 200 – 2500 nm with 1.0 cm light-path width (Hellma, Germany) and the DU[®] 800 spectrophotometer (Beckman Coulter, USA) operated by DU 800 UV/Visible Spectrophotometer System and Applications software, version 3.0, build 5. The standard curves were subsequently used in quantification of plant-derived compounds by HPLC.

2.6.4.1.1 Quantification of isoprenoids and α -tocopherol

Dry isoprenoid powders and α -tocopherol oil were fully dissolved in the solvents listed in Table 2.14. An aliquot of the solution (1.0 ml) was withdrawn into a fresh microcentrifuge tube and three separate dilutions of this standard stock were prepared. The absorbances of the diluted standard stocks were measured at the photometric readout specified for the DU[®] 800 spectrophotometer using the wavelengths (λ) provided in Table 2.14. The authentic standards were purchased from Sigma-Aldrich (USA). The in-house standards of lycopene, phytoene and violaxanthin were prepared as described (2.6.3). The in-house prepared standard of neoxanthin was already available in the laboratory and originated from an unknown source. The solvents were purchased from VMR Chemicals (USA; ethanol only) and Fisher Chemical (USA; remaining solvents). The literature references, which were used to obtain the values of the specific absorption coefficients ($A_{1\text{cm}}^{1\%}$) and the wavelengths corresponding to the absorption maxima of the compounds dissolved in the chosen solvents, are provided in Table 2.14.

Table 2.14. List of compounds used for the preparation of standard curves; $A_{1\text{cm}}^{1\%}$ – specific absorption coefficient; A – acetone; E – ethanol; C – chloroform; H – hexane; P – petroleum ether, bp. 40 – 60°C.

Compound	$A_{1\text{cm}}^{1\%}$	λ [nm]	Solvent	Source	Reference
α -tocopherol	72	292	E	Authentic standards	Talwar <i>et al.</i> , 1998
Lutein	2 369	454	C		Craft & Soares, 1992
β -carotene	2 396	465	C		Britton, 1995b
Zeaxanthin	2 340	452	A		
Chlorophyll A	n/a	648 and 666	C	Authentic standards	Wellburn, 1994
Chlorophyll B	n/a		C		
Lycopene	3 450	470	P	In-house prepared standards	Britton, 1995b
Neoxanthin	2 470	438	E		
Phytoene	915	286	H		
Violaxanthin	2 400	442	A		

According to the Beer-Lambert law, the amount of the standard in the solvent, here diluted from the stock solution, can be calculated using the formula (Schiedt & Liaaen-Jensen, 1995):

$$x = \frac{A \times y \times 1\,000}{A_{1\text{ cm}}^{1\%} \times 100}$$

Where: x – weight of the compound in the solvent diluted from the original stock [mg]

A – absorbance

y – sample volume; here always 1 [ml]

$A_{1\text{ cm}}^{1\%}$ – specific absorption coefficient [$\text{g}^{-1}\text{ cm}^{-1}$]

The amount of the standard remaining in the original stock was calculated using the formula:

$$x_{\text{ST}} = x \times \text{DF} \times \text{RF}$$

Where: x_{ST} – weight of the standard remaining in the original stock [mg]

x – weight of the compound in the solvent diluted from the original stock [mg]

DF – the dilution factor

RF – remaining fraction of the original volume after removing the sample for a spectrometric measurement, which is calculated using the formula below:

$$\text{RF} = \frac{1\,000 - y_s}{1\,000}$$

Where: y_s – the total volume removed from the original stock to prepare dilutions [μl]

The standard stocks were shielded from light by covering in aluminium foil, dried down under a stream of nitrogen gas and used immediately for the preparation of standard curves (2.6.4.2).

2.6.4.1.2 Quantification of chlorophylls

Chlorophyll standards were prepared as described above (2.6.4.1.1) using the solvents given in Table 2.14. The amounts of chlorophyll A (Ch_A) and chlorophyll B (Ch_B) in the solvent (1 ml) diluted from the original stock, were calculated using the formulae below:

$$\text{Ch}_A = 10.91 \times A_{666\text{ nm}} - 1.2 \times A_{648\text{ nm}}$$

$$\text{Ch}_B = 16.38 \times A_{648\text{ nm}} - 4.57 \times A_{666\text{ nm}}$$

Where: Ch_A/Ch_B – weight of chlorophyll A or B in the solvent diluted from the original stock [μg]

$A_{666\text{ nm}}$ and $A_{648\text{ nm}}$ – absorbances at 666 and 648 nm, respectively

The amounts of chlorophylls remaining in the original stocks were calculated as above (2.6.4.1.1). Chlorophyll standards were dried as described above and used immediately for the preparation of standard curves on the HPLC system (2.6.4.2).

2.6.4.2 Generation of standard curves on the HPLC system

To generate standard curves on the HPLC system, dried standards of chlorophylls, isoprenoids and α -tocopherol were dissolved in appropriate volumes of HPLC-grade ethyl acetate (Fisher Chemical) to produce stock solutions ($1 \mu\text{g } \mu\text{l}^{-1}$) from which required dilutions of the standards were prepared. Except for violaxanthin, which consisted of a 5-point curve (0.025, 0.050, 0.100, 0.500 and $1.000 \mu\text{g}$), all curves were run across a 10-point range (0.010, 0.025, 0.050, 0.075, 0.100, 0.250, 0.500, 1.000, 1.500 and $2.000 \mu\text{g}$). Each curve was run in triplicate with each injection being made from a separate vial. The method of analysis on the HPLC system was described previously (2.6.2).

2.6.4.2.1 Determination of coefficients

The curves were analysed using Empower™ 2 (Waters®) software at 450 nm for β -carotene, chlorophyll A, chlorophyll B, lutein, lycopene, neoxanthin, violaxanthin and zeaxanthin, at 292 nm for α -tocopherol and at 286 nm for phytoene. Due to lack of analytical standards for some of the compounds of interest, standard curves of zeaxanthin and β -carotene were used for quantification of antheraxanthin and β -cryptoxanthin, respectively. The standard injected into the HPLC system generated a chromatographic peak at a retention time (RT) characteristic for that compound with the area of the peak being proportional to the amount of the standard injected. The standard curves were generated by plotting the averaged peak areas from three separate runs against the corresponding amounts of the standard injected into the system. The fit to the linear model was assessed by calculating the coefficient of determination, R^2 . The consistency between the retention times of the standards was compared across the three runs. For quantification purposes, the standard curves were split into low (0.010 to $0.100 \mu\text{g}$) and high (0.250 and $2.000 \mu\text{g}$) ranges except violaxanthin standard curve, which was used across its entire range (between 0.025 and $1.000 \mu\text{g}$). The generated standard curves could be described with a general equation of the straight line:

$$y = ax + b$$

Where: y – peak area [$\mu\text{V s}$]

a – slope of the line; obtained experimentally

x – amount of the standard [μg]

b – y -axis intercept; obtained experimentally

2.6.4.2.2 Quantification of compounds

The unknown amount of a compound of interest (x_i) in the injected sample was then determined by obtaining the peak area (y_i) for that compound from its chromatographic trace at the same wavelength absorption as was used in the generation of the standard curve for that compound. From rearranging the equation of the standard curve for the compound of interest, the amount of the compound in the HPLC system could be calculated using the formula:

$$x_i = \frac{y_i - b}{a}$$

Where: x_i – amount of the compound injected into the HPLC system in a given sample [μg]

y_i – area underneath the peak of a compound of interest [$\mu\text{V s}$]

b – y-axis intercept characteristic for a given compound

a – slope of the line characteristic for a given compound

The actual amount of the compound of interest in the freeze-dried material used in the extraction, expressed in μg per gram of the dry-weight (DW) powder, was calculated using the formula below:

$$x_a = \frac{x_i \times \frac{V_d}{V_i}}{m} \times 1\,000$$

Where: x_a – the amount of the compound of interest in the analysed sample [$\mu\text{g g}^{-1}$ of DW]

x_i – amount of the compound injected into the HPLC system [μg]

V_d – volume of ethyl acetate used to dissolve the sample [μl]

V_i – volume of sample injected into the HPLC system [μl]

m – mass of the freeze-dried material used in the extraction [mg]

The above calculations were implemented into a VBA Macros equipped spreadsheet using Microsoft Excel 2016, version 16.0.8431.2270 kindly prepared and shared by Mr Mateusz Czarnota, MScEng.

2.6.5 Thin-layer chromatography (TLC)

Separation of compounds by TLC was carried out in an enclosed paper-chromatography glass tank Panglas TLC Chromatank (Shandon Scientific Co. Ltd, UK). The tank was kept inside a fume hood in dim light. The solvents used in the TLC preparation were purchased from Fisher Chemical and the compositions of the mobile phases are described below. Prior to their usage, the TLC plates were covered in aluminium foil and baked in the oven at 110°C for 2 hours. The mobile phases (100 ml) and two 20×30 cm pieces of Whatman® Grade 3MM Chr Chromatography

paper (Whatman) were placed in the glass tank and allowed to equilibrate for 10 minutes. The samples were spotted manually 1 cm apart at the baseline of the TLC plate with a mLINE® mechanical pipette, 1-ch, 0.5 – 10 µl (Sartorius AG, Germany). The baseline was positioned 1 cm away from the edge of the plate. The plate was air-dried in dark for 2 – 3 minutes and immediately placed inside the glass tank for the length of time as specified below. The distance travelled by the solvent (solvent front) was marked and the plates were air-dried in the fume hood for 5 minutes. For each spot separated on the TLC, its retention factor (R_f) value was calculated with the equation:

$$R_f = \frac{R_s}{R_{sf}}$$

Where: R_f – retention factor

R_s – migration distance of substance as measured from the baseline

R_{sf} – migration distance of solvent front as measured from the baseline

2.6.5.1 Purification of phytoene

Phytoene extracted from *P. blakesleeanus* strain C5 (2.60 g; 2.6.3.1.1), containing a substantial proportion of ergosterol, was dissolved in HPLC-grade ethyl acetate (100 µl), spotted (100 µl) on a 20 × 20 cm TLC Silica gel 60 RP-18 F₂₅₄S Aluminium sheet (Merck KGaA, Germany) and separated for 20 minutes. The mobile phase (100 ml) consisted of toluene (3% v/v) in petroleum ether, bp. 40 – 60°C. The spots were visualised using a UVGL-55 Handheld UV Lamp (UVP, USA) mounted on a C-10 Chromato-Vue Viewing Cabinet (UVP). The bands of interest ($R_f = 0.6$) were scratched off the plate and extracted with chloroform (5 × 1.0 ml). The extract was centrifuged at 4 000 RPM for 10 minutes, 4°C in a refrigerated 5810 R centrifuge (Eppendorf, Germany) with a swing-bucket rotor A-4-62 (Eppendorf). The supernatant was transferred into a new, 15 ml tube and dried in the Genevac EZ-2 Mk2 Plus Centrifugal Evaporator (Genevac) at the low boiling point setting and with the lamp turned off. The extract was dissolved in HPLC-grade ethyl acetate (200 µl) and analysed (3.0 µl injections) on the UPLC system (2.6.2.3) to assess purity of the compound.

2.6.5.2 Analysis of xanthophylls

Carotenoids were extracted (2.6.1) from ripe fruit of the F₂ population reference (Az) line and three plants of the U/0; B/B genotype (lines homozygous for *S. galapagense* *CYC-B* allele and hemizygous for transgenic *CrtR-b2*; Table 2.2, Section 2.1.2), dissolved in ethyl acetate (200 µl), spotted (20 µl) on a 20 × 20 cm TLC Silica gel 60 F₂₅₄ Aluminium sheet (Merck KGaA) and separated for 40 minutes. The mobile phase (100 ml) consisted of ethyl acetate (40% v/v) in hexane. Zeaxanthin standard (Sigma-Aldrich), dissolved in HPLC-grade ethyl acetate (1.0 µg µl⁻¹)

was spotted (20 µl) along the analysed samples. The plates with the resolved compounds were photographed and the spots of the R_f values corresponding to the zeaxanthin standard were scratched off the plates, extracted with methanol (3 × 200 µl) and dried under a stream of nitrogen gas. The extracts were dissolved in HPLC-grade ethyl acetate (50 µl) and analysed on the HPLC system (10 µl injections; 2.6.2.2).

2.6.6 Gas chromatography – mass spectrometry (GC-MS)

2.6.6.1 Plant material

Tables 2.1 and 2.2 in Section 2.1 describe lines selected for GC-MS analysis. The total of 10 genotypes (conditions) were chosen: Azygous (Az; 0/0; +/+) and *hp3* reference lines, two lines heterozygous for *S. galapagense* *CYC-B* allele (*B*/+) and either homozygous (*U*/*U*) or hemizygous (*U*/*O*) for transgenic *CrtR-b2*, two lines homozygous for *S. galapagense* *CYC-B* allele (*B*/*B*) and either *U*/*U* or *U*/*O* and four lines homozygous for the *hp3-1* allele of *ZEP* with either of the four zygotic combinations of *S. galapagense* *CYC-B* and transgenic *CrtR-b2* described above. Analyses were performed on six biological replicates (plants) per condition when a sufficient number of replicates was available. Otherwise, the same biological samples were extracted multiple times (technical repeat extractions) to obtain the required number of samples for statistical analysis. The pooled material from at least three ripe tomato fruit was analysed per plant.

2.6.6.2 Sample extraction

Freeze-dried fruit were disrupted (2.6.1.1) and the homogenised tomato powder (~10 mg) was weighed out into 2 ml microcentrifuge tubes (Camlab Ltd, UK). The weights of the samples were recorded to the tenths of a milligram using Secura124-1S analytical balance (Sartorius AG, Germany). HPLC-grade methanol (400 µl; Fisher Chemical, USA) and HPLC-grade water (400 µl; Fisher Chemical) were added to each sample and vortexed. The suspension was incubated at room temperature (~22°C) for 1 hour while being inverted under aluminium foil at 25 RPM on a SB3 bench-top revolting mixer (Stuart Equipment, UK). Chloroform (800 µl; Fisher Chemical) was then added to each sample and vortexed. To achieve phase separation, the samples were centrifuged for 5 minutes at 17 000 *g* using Heraeus™ Pico™ 17 Microcentrifuge (Thermo Scientific). The polar extract (20 µl; upper layer) was transferred into a 300 µl glass insert with plastic springs (Sigma-Aldrich) placed in a 1.5 ml screw-top glass vial (Sigma-Aldrich) and spiked with the internal standard (10 µl), d_4 -succinic acid (1 mg ml⁻¹ in methanol; ISOTEC® Stable Isotopes, USA). The non-polar extract (700 µl; bottom layer) was transferred directly into a glass vial (Sigma-Aldrich) and spiked with the internal standard (10 µl), d_{27} -myristic acid (1 mg ml⁻¹ in chloroform; Cambridge Isotope Laboratories, USA). The internal standards were kindly prepared and shared by Dr Drapal. The samples were dried in the Genevac EZ-2 Mk2 Plus centrifugal evaporator (Genevac, UK) at the aqueous setting for the polar compounds and at the low boiling

point setting for the non-polar compounds with the lamp switched off. The samples were stored at -20°C until derivatisation.

2.6.6.3 Sample derivatisation

Samples were placed on a 40°C heat-block for 5 minutes to clear away water of condensation from the vials following their removal from the freezer. An aliquot (30 µl) of methoxyamine hydrochloride (MEOX; Sigma-Aldrich) solution in pyridine (20 mg ml⁻¹; Sigma-Aldrich) was added to each sample and the vials were incubated at 40°C for 1 hour. N-Methyl-N-trimethylsilyl-trifluoroacetamide (MSTFA; 70 µl; Apollo Scientific, UK) was then added to the samples and the vials were incubated for further 2 hours at 40 °C. The non-polar samples were transferred into glass inserts and placed inside glass vials prior to analysis. The samples were derivatised on the day of analysis.

2.6.6.4 GC-MS analysis

GC-MS analysis was performed using an Agilent 7890A Gas Chromatography (GC) System (Agilent Technologies Inc., USA), equipped with 7683 Series Autosampler (Agilent Technologies Inc.) and 7683B Series Injector (Agilent Technologies Inc.), coupled to an Agilent 5975C Inert Mass Selective Detector (MSD; Agilent Technologies Inc.) and operated by Agilent G1701EA Enhanced MSD Productivity ChemStation software, version E.02.02 (Agilent Technologies Inc.). Samples were analysed in a randomised order and injected (1 µl) in a splitless mode through the injection port maintained at 280°C into a DB-5ms GC column (30 m, 0.25 mm, 0.25 µm; Agilent Technologies Inc.) and separated with a temperature gradient. The septum purge flow was maintained at 3 ml min⁻¹. The GC oven was initially held at 70°C for 3 minutes and then the temperature was raised in 4°C min⁻¹ increments until reaching the maximum temperature of 325°C which was held for 1 minute. Helium (He) was used as a carrier gas at the flow rate of 1.3 ml min⁻¹. The separated compounds entered the MS through a transfer line heated to 250°C. The total run time per sample was 67.75 minutes. The MS source and MS quadrupole were held at 230°C and 150°C, respectively. MS was performed in full scan mode within a mass range of between 50 and 1 000 m/z using 70 eV positive electron impact ionisation (EI). The gain factor was set at 2.0. Retention time locking (RTL) to the internal standard was used.

2.6.6.5 Data analysis

The raw data generated through GC-MS analysis were processed and deconvoluted with Automated Mass Spectral Deconvolution & Identification System (AMDIS), version 2.71.134.27 (Davies, 1998). Based on the in-house compiled library of authentic standards analysed on the same system (Perez-Fons *et al.*, 2014), the metabolites were identified at the Metabolomics Standards Initiative (MSI) level 1 by matching their retention indices (RI) and mass spectra to those of the authentic standards. The metabolites not included in the above library were

compared against the NIST/EPA/NIH Mass Spectral Library database, version 2.0 g, build 2011 (NIST11; Stein *et al.*, 2011) and added to an in-house customised tomato library. The metabolites which were matched with scores of 800 or above to the compounds in the NIST11 database, were assigned the MSI level 2 or level 3 identification. The remaining metabolites with the matching compound scores lower than 800 were identified at the MSI level 4 and labelled as unknowns. The AMDIS-generated output files were sorted using a Python™ IDLE, version 3.4.0 (Rossum, 1995) script, kindly prepared and shared by Mr Herbert Schlechta. The IDLE output file was a matrix of the identified metabolites against their RTs and peak areas for each injected sample. The raw data were exported into Microsoft Excel 2016, version 16.0.8431.2270, analysed with principal component analysis (PCA) in SIMCA version 15.0.0.4783 (Satorius AG, Germany) to identify outliers and normalised against the internal standards and weights of the samples. The chromatographic signals originating from the column bleed or other contaminants, such as derivatisation agents, were excluded from further analysis. The different derivatisation products of the same compound were combined. If the metabolite was detected in more than 60% of the biological or technical replicates (four samples out of six) of a given genotype, the missing values were replaced with the mean value of that metabolite. Otherwise, if the metabolite was missing from 50% or more of the biological or technical replicates, the remaining values were replaced with zeroes. The normalised and processed data sets were re-analysed with PCA to validate the applied changes and used in further statistical analyses. The mean metabolite values were used to calculate the mean ratios \pm standard deviations (SD) between the genotypes of interest and the reference lines (*Azygous* or *hp3*) as indicated. The normalised and processed data were analysed for statistical significance using one-way ANOVA with Fishers Least Significant Difference (LSD) post-hoc test using the online metabolomic data analysis tools available at MetaboAnalyst (Chong *et al.*, 2018). False Discovery Rate (FDR) adjusted *p*-values (FDR < 0.05) were used to identify the statistically significant changes between the metabolites of the selected genotypes and the reference lines and these were plotted as heat maps using MetaboAnalyst. For the selected genotypes, the statistically significant changes between the metabolites were overlaid on biochemical pathway diagrams created with in-house developed BioSynLab® software, version 1.3 (Zervas *et al.*, 2007).

2.6.7 Solid-phase microextraction (SPME)

2.6.7.1 Sample preparation

SPME analysis was carried out on the same genotypes as were used in the GC-MS analysis (the same biological replicates; 2.6.6.1). Deseeded and diced ripe fruit, previously snap-frozen in liquid nitrogen and stored at -80°C, were thawed overnight on ice at 4°C. The fruit were homogenised in a cold room (4°C) with a T25 Basic Homogeniser (IKA®-Werke GmbH & Co. KG,

Germany) and a 20 cm long IKA Dispersing Element S25N-18G (IKA®-Werke GmbH & Co. KG). The suspension (2.0 g) was then pipetted into 20 ml brown screw cap vials, Ø14.7 x 45 mm, thread Ø18 mm (Anatune Ltd, UK). Prior to analysis, aliquots of the external standard (2.0 ml), acetophenone-β,β,β-d₃ (Sigma-Aldrich, USA) in ddH₂O (20 ppb) were prepared via serial dilution, stored at -20°C up to two weeks and thawed on the day of analysis.

2.6.7.2 SPME

Analysis of volatile organic compounds (VOCs) was carried out with an Agilent 7890B Gas Chromatography (GC) System (Agilent Technologies Inc., USA), equipped with MultiPurpose Sampler (MPS, upgraded; GERSTEL, Germany) and sample trays for 32 vials 10/20 ml (VT 32; GERSTEL), coupled to an Agilent 5977B Inert Mass Selective Detector (MSD; Agilent Technologies Inc.) and operated by MassHunter GC/MS Acquisition for GC/MSD, B.07.04.2260, version 6.0.0.0 (Agilent Technologies Inc.). Samples were analysed in a randomised order in six batches. Each batch was initiated with a blank sample (air from the surrounding area where the samples were prepared) followed by an external standard (2.0 ml), fruit samples (2.0 g) and another external standard (2.0 ml). Prior to VOCs analysis, the samples were incubated for 30 minutes in the MPS Agitator/Stirrer AS (GERSTEL) at 60°C and 300 RPM to promote transfer of the VOCs to the headspace. The direction of agitation was altered every 10 seconds with one second pause between the change. The VOCs were extracted by headspace sampling with StableFlex™ SPME Fiber Assembly Divinylbenzene, Carboxen, Polydimethylsiloxane (DVB/CAR/PDMS), needle size 23 ga, d_f 50/30 µm, fiber L 1 cm (Sigma-Aldrich). Prior to its first use, the fibre was conditioned in the front inlet maintained at 270°C for 30 minutes at the penetration depth of 43.0 mm and the split ratio of 200:1 with the purge flow to split vent of 100 ml min⁻¹ and 1-minute solvent delay. During the conditioning, the oven temperature was maintained at 300°C and the column flow rate was set at 2.0 ml min⁻¹. Before running a new batch and after analysis of each sample, the fibre was reconditioned as above for 5 minutes. For extraction of the VOCs from the samples, the fibre was exposed to the headspace for 20 minutes at the vial penetration depth of 25.0 mm during continuous sample agitation. The SPME fibre coating, containing the headspace VOCs, was introduced into the GC injection port maintained at 250°C at 54.0 mm penetration depth and held for 5 minutes for desorption in splitless mode with the septum purge flow set at 3.0 ml min⁻¹ and solvent delay of 3.8 minutes. The injection port was lined with 0.75 mm ID Straight/SPME Inlet Liner (Restek Corporation, USA). The desorbed VOCs were separated on J&W HP-5ms GC Column, 30 m, 0.25 mm, 0.25 µm (Agilent Technologies Inc.) with helium used as a carrier gas at the linear velocity of 1.0 ml min⁻¹. The GC oven was initially maintained at 40°C for 2 minutes, then increased to 120°C at the rate of 5.0°C min⁻¹, kept at this temperature for 2 minutes, increased to 250°C at the rate of 5.0°C min⁻¹, held at this temperature for further 2 minutes and finally increased to 300°C at the rate of 6.0°C min⁻¹ maintaining this temperature

for the remaining 5 minutes of the run. The total run time per sample was 61.33 minutes. The separated compounds entered the MS through a transfer line heated to 250°C. The MS source and MS quadrupole were held at 230°C and 150°C, respectively. MS was performed in normal scan mode within a mass range of between 33 and 550 m/z using 70 eV positive EI and electron-multiplying (EM) gain of 1.0.

2.6.7.3 Data analysis

The raw data generated through SPME analysis were processed and deconvoluted with AMDIS, version 2.71.134.27 software (Davies, 1998). The metabolites were provisionally identified by comparing against the NIST11 database (Stein *et al.*, 2011) and added to the in-house customised library, kindly shared by Ms Lewis. The precursors of the identified VOCs were annotated based on the previously published work (Rambla *et al.*, 2014; Zhang *et al.*, 2015; Radulović *et al.*, 2017; Seo *et al.*, 2018; Kim *et al.*, 2019). The AMDIS-generated output files were sorted using a Python™ IDLE, version 3.4.0 (Rossum, 1995) script as described for the GC data (2.6.6.5). The raw data were exported into Microsoft Excel 2016, version 16.0.8431.2270 and analysed with principal component analysis (PCA) in SIMCA version 15.0.0.4783 (Satorius AG, Germany) to identify outliers. The compounds identified in blank samples were averaged across the runs and subtracted from the experimental samples. Similarly to what was described for GC data (2.6.6.5), the metabolites found in 50% or less of the biological or technical replicates (three or fewer samples) of a given genotype, were replaced with zeroes. If a compound was detected in more than 60% of the biological or technical replicates of a given genotype, the missing values were replaced with the mean value of that metabolite. The processed data were re-analysed with PCA to validate the applied changes and used in further statistical analyses. The peak areas of all metabolites detected in the sample were added up and each metabolite was reported as a percentage of the total area. Mean percentage content of the metabolites \pm relative standard deviation (RSD) were calculated for the genotypes of interest and compared against the reference lines (Az or *hp3*) as indicated. The processed data were analysed for statistical significance using one-way ANOVA with LSD post-hoc test using MetaboAnalyst (Chong *et al.*, 2018). FDR adjusted *p*-values (FDR < 0.05) were used to identify the statistically significant changes between the VOCs of the selected genotypes and the reference lines and these were plotted as heat maps using MetaboAnalyst. For the selected genotypes, the VOCs identified to be altered in the lines of interest were overlaid on metabolic pathway diagrams created in BioSynLab[®] software, version 1.3 (Zervas *et al.*, 2007).

2.6.8 Sub-chromoplast fractionation

The method of sub-chromoplast fractionation was described by Nogueira *et al.* (2016) and is outlined below. Chromoplast extractions were carried out at 4°C in a temperature-controlled

room (cold room). The components in contact with the fractionated tissues, such as the buffers, glassware, centrifugation tubes and rotors, were pre-chilled to 4°C prior to their use.

2.6.8.1 Plant material

The lines selected for sub-chromoplast fractionation are listed in Table 2.2 (Section 2.1). Briefly, the F₂ segregating population was used in experiments 1 and 2 (F#1 and F#2). Five lines were selected from this population: the Az line (F#1 and F#2) and lines of the U/0; B/B (F#1), U/0; B/+ (F#1), U/U; B/B (F#2) and U/U; B/+ (F#2) genotypes. For fractionation experiment 3 (F#3), the F₃ population lines of the Az (0/0; +/+) and U/0; B/B genotypes and the F₂ population line of the U/0; B/B; *hp3/hp3* genotype were used. Fractionations were carried out on pooled fruit material from three plants of the same genotype (condition). Between 6 and 9 firm fruit (2 – 3 per plant) at the ripening stage of breaker + 5 days were collected per condition, washed in ddH₂O, deseeded and cut into ~1 cm² pieces. For each experiment, the fruit were weighed out (130 g), covered in aluminium foil and incubated overnight at 4°C to reduce starch content.

2.6.8.2 Extraction and gradient buffers

The extraction buffer consisted of sucrose (0.4 M), Trizma® (50 mM), EDTA (1.0 mM), dithiothreitol (DTT; 1.0 mM) in ddH₂O and pH adjusted to 7.8 with HCl (32% v/v). The sucrose gradient buffers consisted of varying amounts of sucrose (45%, 38%, 20%, 15% and 5% w/v) with tricine (50 mM), EDTA (2.0 mM), sodium bisulphite (5.0 mM), DTT (2.0 mM) in ddH₂O and pH adjusted to 7.9 with KOH (1.0 M). DTT was added to the buffers shortly prior to their use. All compounds used in the preparation of the buffers were purchased from Sigma-Aldrich (USA).

2.6.8.3 Chromoplast extraction

Cut fruit were placed in an 8010ES laboratory blender (Waring Conair, USA), covered in the extraction buffer (1 to 3 volume ratio of fruit to buffer), soaked for 5 minutes and homogenised twice for 3 seconds. The slurry was filtered through four layers of muslin cloth (MacCulloch & Wallis, UK) and transferred into 500 ml screw-cap Nalgene™ centrifuge bottles (Nalge Nunc International, USA). The bottles were filled to 2/3 of their volume with the extraction buffer, balanced and centrifuged for 10 minutes at 5 000 *g*, 4°C using Sorvall RC-5C centrifuge (Thermo Scientific, USA) and the Fiberlite™ F12-6 x 500 LEX Fixed Angle Rotor (Thermo Scientific). The supernatant was decanted and the pellet was gently resuspended in the extraction buffer using a rod with a rubber end. The mixture of the crude plastid fractions was transferred into 50 ml Nalgene™ round centrifuge tubes (Nalge Nunc International). The tubes were filled to 3/4 of their volume with the extraction buffer, balanced and centrifuged for 10 minutes at 9 000 *g*, 4°C using Sorvall RC-5C centrifuge and the SS-34 Fixed Angle Rotor (Thermo Scientific). The supernatant was discarded and the pellet was resuspended in the sucrose (45% w/v) gradient buffer (8 ml).

The suspension was transferred into a 55 ml Potter-Elvehjem glass mortar (Fisher Scientific, USA) and chromoplasts were broken with 10 strokes of the pestle. The homogenate was transferred back into its original tube and kept on ice until preparation of the gradients.

2.6.8.4 Separation of sub-chromoplast compartments with sucrose gradient

The sucrose (45% w/v) gradient buffer was added to the homogenate of broken chromoplasts (to the final volume of 16 ml). The suspension was mixed thoroughly and split equally (8 ml) into two 38.5 ml thin-wall Ultra-Clear™ centrifuge tubes (Beckman Coulter, USA). Using a plastic Pasteur pipette, a discontinuous gradient was built with sucrose (w/v) buffers in the following order: 38% (6 ml), 20% (6 ml), 15% (4 ml) and 5% (8 ml). Each gradient was prepared in a duplicate and centrifuged at 100 000 *g*, 4°C for 19 hours in the Optima XPN-90 Ultracentrifuge (Beckman Coulter) with the 28 Ti Swinging-Bucket Aluminum Rotor (Beckman Coulter).

2.6.8.5 Fraction collection and analysis

Fractions were collected beneath the meniscus with a needle using a MINIPULS® 3 Peristaltic Pump (Gilson, UK) and an FC 203B Fraction Collector (Gilson). Depending on the genotypes selected, either 1.0 (F#1 and F#2; typically 32 fractions in total) or 0.5 ml fractions (F#3; typically 64 fractions in total) were collected into 2 ml microcentrifuge tubes (Camlab Ltd, UK), stored at -80°C and subsequently extracted (2.6.1.2). Fractions of smaller volumes were collected to achieve a greater resolution of the sucrose gradients. Depending on the genotype, the extracts from the fractions were resuspended in either 30 (F#3), 60 (F#1) or 120 µl (F#2) of HPLC-grade ethyl acetate (Fischer Chemical). Either 3 (F#2) or 5 µl (F#1 and F#3) injects of the extracts were analysed on the UPLC system (2.6.2.3).

2.7 Data analysis

2.7.1 Descriptive statistics

Raw data were processed and presented in form of tables or figures as a mean of the N number of biological replicates ± standard deviation (SD). Statistical analyses were performed on a minimum of three biological replicates unless otherwise indicated. Graphs and tables were prepared in GraphPad Prism version 8.1.1 (GraphPad Software, USA) and Microsoft Excel 2016, version 16.0.8431.2270 (Microsoft Corporation, USA).

2.7.2 Inferential statistics

Data were processed and specific statistical tests were performed in GraphPad Prism and SPSS Statistics 21 (IBM Corporation, USA). Specific statistical tests used for the comparison of the indicated tomato lines are described for each data set in the Results Chapters III – V. Significant results were reported for the probability values (*P*) of 0.05 or lower.

Chapter III: Characterisation of tomato lines overexpressing *CYC-B* and *CrtR-b2*

3.1 Introduction

The role of zeaxanthin in preventing age-related macular degeneration (AMD) has become more evident over the last years. However, food sources high in zeaxanthin are scarce. Therefore, some consumers choose to use supplements which contain extracted or synthetic forms of this carotenoid. Nonetheless, in order to meet consumer expectations and market demand, a new plant source of zeaxanthin is highly anticipated.

Tomato is one of the most important crops in the world in terms of its commercial and dietary value. Tomato fruit is generally recognised as safe and acts as a storage organ for carotenoids, which enables their subsequent testing and quantification. During tomato fruit ripening, its carotenoid content increases around 400 times. Most of this content is represented by the red pigment lycopene. Lycopene is a precursor for the synthesis of some xanthophylls, including zeaxanthin and violaxanthin. However, despite the presence of all elements of the carotenoid biosynthetic pathway needed for synthesis of zeaxanthin and the downstream xanthophylls, the ripe tomato fruit, unlike the green tissues where xanthophylls are abundantly present, only accumulate trace amounts of these compounds (Fraser *et al.*, 1994). Still, the high levels of lycopene present in the ripe tomato fruit represent a pool of the starting material from which zeaxanthin could be derived. Previously, a complex metabolic engineering of the tomato carotenoid biosynthetic pathway led to the accumulation of high-value ketocarotenoids in its fruit. Tomato normally does not produce ketocarotenoids, but the introduction of two additional genes from *Brevundimonas sp.*, namely β -carotene hydroxylase (*CrtZ*) and β -carotene oxygenase (*CrtW*), into a high β -carotene background, led to the production of these compounds (Nogueira *et al.*, 2017). Interestingly, ketocarotenoids in tomato were found mostly in esterified rather than free form. Pepper chromoplasts achieve very high levels of xanthophylls by storing them in an esterified form as well (Hornero-Méndez & Mínguez-Mosquera, 2000).

The successful engineering of tomato plants resulting in accumulation of ketocarotenoids has led to the idea for their potential use in production of other valuable compounds such as zeaxanthin. Therefore, to increase the flux through the carotenoid biosynthetic pathway and push it towards the production of xanthophylls, a tomato line overexpressing chromoplast-specific β -carotene hydroxylase (*CrtR-b2*) gene has been crossed with a recombinant inbred (RI) line accumulating high levels of β -carotene. The tomato lines overexpressing *CrtR-b2* are described as either U/U or U/O to indicate plants homozygous or hemizygous for the transgene, respectively. The high β -carotene content in the RI line results from a high level of expression of chromoplast-specific lycopene β -cyclase (*CYC-B*; the *B* gene) gene driven by its strong promoter during fruit ripening and it is the same line as used by Nogueira *et al.* (2017) for the accumulation of ketocarotenoids. Figure 3.1 outlines how the initial crossing was performed and which genetic

backgrounds contributed to the lines used in this study. In this work, the generated crosses were characterised for their carotenoid content and the lines accumulating xanthophylls in their ripe fruit were identified and propagated to further generations. Sub-chromoplast fractionation was performed to verify if and how the change in carotenoid composition has affected carotenoid sequestration and also to determine in which chromoplast compartments the previously unencountered xanthophylls were being deposited. Since perturbations of carotenoid profiles may lead to changes in the composition of other metabolites, analysis of primary and secondary metabolites was carried out as well. This is important if the newly generated plant producer of carotenoids is intended for human or animal consumption.

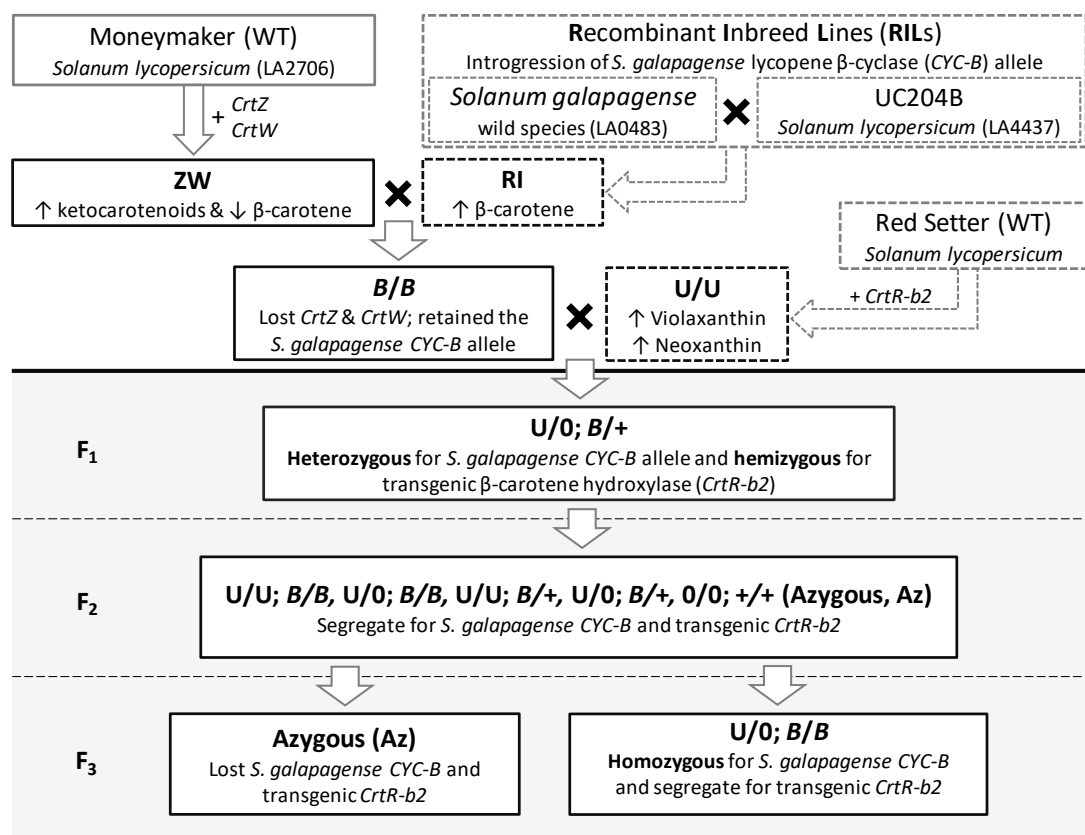


Figure 3.1. Strategy used to create lines overexpressing *Crtr-b2* and *CYC-B*. These lines are also referred to as the double cross. Steps above the black horizontal line were performed by collaborators (dashed boxes and arrows) and other lab members (full boxes and arrows) prior to the presented study (grey background). The F_1 hybrids were produced by crossing the *B/B* line homozygous for *S. galapagense* chromoplast-specific lycopene β -cyclase (*CYC-B*; the *B* gene) with the *U/U* line homozygous for transgenic chromoplast-specific β -carotene hydroxylase (*Crtr-b2*). An F_1 plant with the desired phenotype was advanced to the F_2 generation by self-fertilisation. Two plants from the F_2 population displaying the best characteristics were chosen as parents of the *Az* and *U/0; B/B* lines and advanced by self-fertilisation to the F_3 generation. Plants homozygous or hemizygous for transgenic *Crtr-b2* are referred to as *U/U* or *U/0*, respectively. The boxes indicate individual plants. Genotypes and names of the parental lines are in bold. Only relevant genotypes of the F_2 population (comma-separated) are listed. The backgrounds of the parental lines (*ZW*, *RI* and *U/U*) are in grey boxes. Black crosses indicate crossing events. *CrTZ* and *CrTW* – β -carotene hydroxylase and β -carotene ketolase from *Brevundimonas* sp. (fusion gene).

3.2 Results

3.2.1 Preparation of calibration curves for carotenoid quantification

In order to quantify the absolute amounts of carotenoids accumulated by the new tomato lines, calibration curves had to be prepared on the same platform as was used for the analysis of plant samples. The absolute amounts are required in order to compare the carotenoid levels of the new tomato lines with the existing plant sources of xanthophylls. These are also necessary to

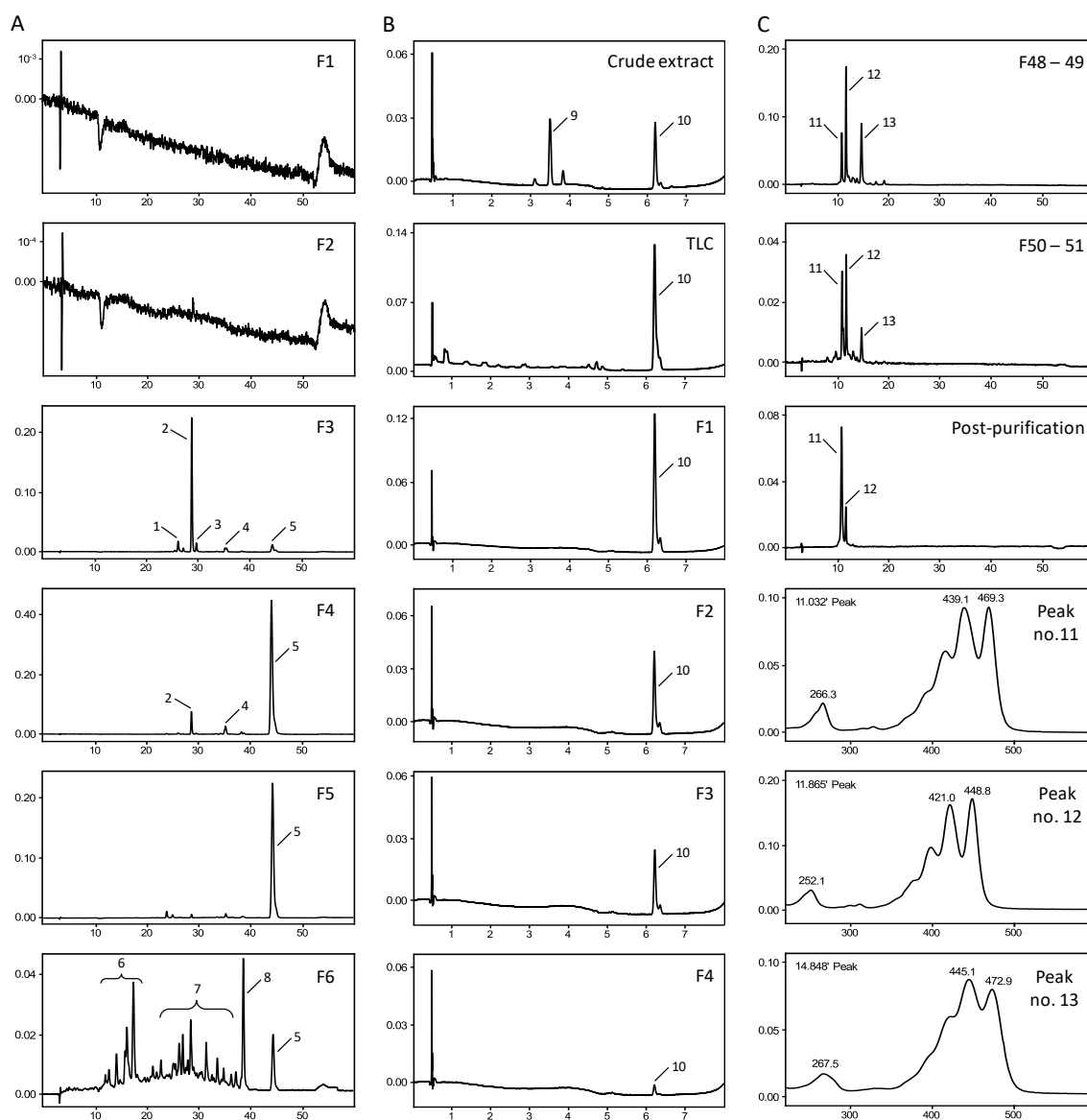


Figure 3.2. Identification of lycopene (A), phytoene (B) and violaxanthin (C). (A) HPLC analysis of alumina fractions 1 – 6 (F1 – F6) from the crude tomato extract at 450 nm. Pure lycopene was found in F5. (B) UPLC analysis of the crude extract from *P. blakesleeanus* C5 mutant (top), followed by the TLC-purified compound of $R_f = 0.6$ (TLC) and alumina-purified fractions (F1 – F4) at 286 nm. Pure phytoene was isolated successfully using both separation techniques. (C) HPLC analysis of flash chromatography fractions obtained from the crude tomato leaf extract and found to contain violaxanthin (F48 – 49 and F50 – 51) at 450 nm. Spectra of the identified compounds (peaks 11 – 13) are shown below. Eluting violaxanthin was collected from the fractions over a course of several HPLC runs and pooled. Following this, violaxanthin was found to constitute the major component (post-purification) and used for the generation of a dose-response curve. 1 – α -carotene, 2 – β -carotene, 3 – *cis*- β -carotene, 4 – γ -carotene, 5 – *trans*-lycopene, 6 – xanthophylls, 7 – fatty acid esters of carotenoids, 8 – *cis*-lycopene, 9 – ergosterol, 10 – phytoene, 11 – violaxanthin, 12 – luteoxanthin, 13 – lutein.

establish the weight of the fresh fruit that needs to be consumed in order to provide a daily recommended amount of a given compound. The dose-response curves (standard curves) for the isoprenoid compounds of interest were prepared using the analytical standards as described in Section 2.6.4 of Materials and Methods.

However, not all standards were readily available and lycopene, phytoene and violaxanthin had to be extracted and purified as described in Section 2.6.3 of Materials and Methods. Following separation of the crude extracts into fractions by alumina column chromatography, flash column chromatography or thin-layer chromatography (TLC), these were analysed by high-performance or ultra-performance liquid chromatography (HPLC or UPLC, respectively). Pure fractions of lycopene (Figure 3.2A; peak no. 5 in fraction no. 5) and phytoene (Figure 3.2B; peak no 10 in the TLC purified extract and fractions no. 1 – 4) were isolated. Purification of violaxanthin turned out to be more challenging. The fractions from the crude leaf extract were found to contain a mixture of three xanthophylls, namely violaxanthin, luteoxanthin and lutein (Figure 3.2C; peaks no. 11 – 13 in fractions no. 48 – 51). Subsequent separation of these fractions by HPLC and collection of the eluate allowed for the elimination of lutein and enrichment for violaxanthin (post-purification peaks no. 10 and 11). However, due to the limited amount of material available and very close elution times of violaxanthin and luteoxanthin, these were not separated further. The final purity of the in-house prepared standard of violaxanthin was close to 80% as calculated by the ratio of the violaxanthin peak area to the total area of all peaks in the sample (data not shown).

The in-house prepared and authentic analytical standards were used for the generation of calibration curves of α -tocopherol, β -carotene, chlorophyll A, chlorophyll B, lutein, lycopene, neoxanthin, phytoene, violaxanthin and zeaxanthin. Each standard curve was prepared on the HPLC system in triplicate (Supplementary Figure 1.1). All ten curves had a coefficient of determination, R^2 greater than 0.996; nine curves had $R^2 > 0.998$ and seven $R^2 > 0.999$. Additionally, shifts in the retention times (RT) of the compounds were assessed within and between the runs. Generally, the RT shifts within the same run were below 10 seconds (violaxanthin – 4 seconds; α -tocopherol – 5 seconds; β -carotene, neoxanthin and phytoene – 6 seconds; chlorophyll B – 7 seconds). However, the within-run RT shifts were larger for chlorophyll A (11 seconds), lutein (17 seconds), zeaxanthin (23 seconds) and lycopene (40 seconds). The RT shifts between the runs were more variable but did not differ by more than 47 seconds as for lycopene, 30 seconds for zeaxanthin, 25 seconds for lutein, 17 seconds for phytoene, 12 seconds for the chlorophylls, 10 seconds for β -carotene, 8 seconds for neoxanthin and violaxanthin and finally 5 seconds for α -tocopherol. However, the characteristic UV-Vis spectra of the compounds (Figure 2.2 in Section 2.6.2.2 of Material and Methods) remained

unchanged within and between the runs (data not shown). Moreover, the order in which the compounds were eluted during HPLC analysis has remained unchanged which, together with the UV-Vis data, allowed for the positive identification of compounds in the analysed samples.

To account for nonlinear absorption of the standards across a range of concentrations, all curves (except violaxanthin) were additionally plotted at the low and high concentration ranges (Supplementary Figure 1.1). These calibration curves were subsequently used for quantification of the compounds in analysed samples. The coefficients of the standard curves are provided in Supplementary Table 1.1 together with the explanation on how they were applied within the two concentration ranges depending on the peak area of the quantified compound.

3.2.2 Screening of F₁ population and isolation of xanthophyll-accumulating line

The crosses between the parental U/U and B/B lines were screened for the genes of interest. The transgenic copy of *CrtR-b2*, passed down from the U/U parent, was identified by amplifying a fragment of the CaMV 35S promoter which drives overexpression of the transgene. The F₁ population was also screened for the presence of *Solanum galapagense* and *S. lycopersicum* alleles of *CYC-B*. Only *S. galapagense* *CYC-B* allele, inherited from the B/B parent, leads to the

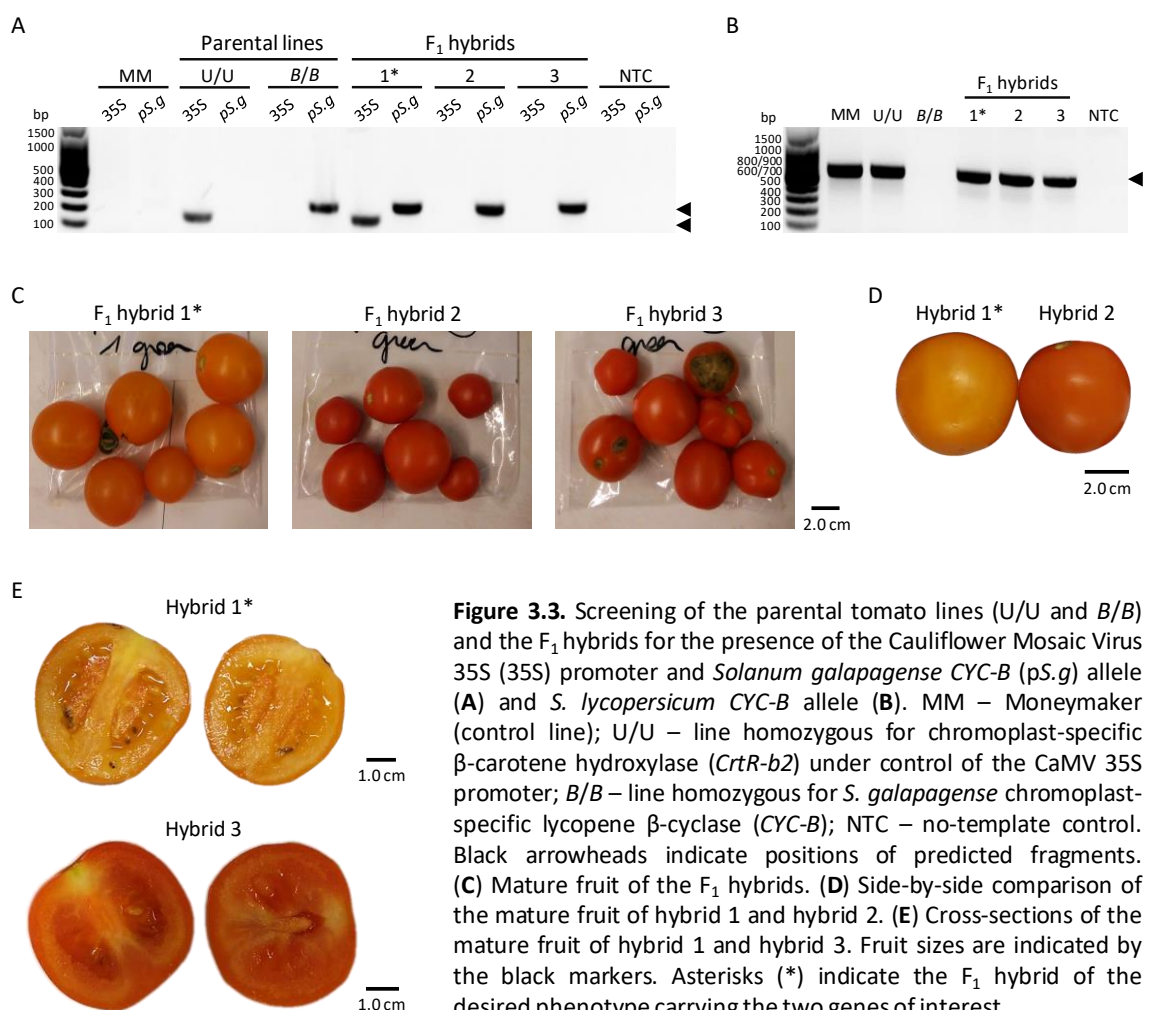


Figure 3.3. Screening of the parental tomato lines (U/U and B/B) and the F₁ hybrids for the presence of the Cauliflower Mosaic Virus 35S (35S) promoter and *Solanum galapagense* *CYC-B* (pS.g) allele (A) and *S. lycopersicum* *CYC-B* allele (B). MM – Moneymaker (control line); U/U – line homozygous for chromoplast-specific β-carotene hydroxylase (*CrtR-b2*) under control of the CaMV 35S promoter; B/B – line homozygous for *S. galapagense* chromoplast-specific lycopene β-cyclase (*CYC-B*); NTC – no-template control. Black arrowheads indicate positions of predicted fragments. (C) Mature fruit of the F₁ hybrids. (D) Side-by-side comparison of the mature fruit of hybrid 1 and hybrid 2. (E) Cross-sections of the mature fruit of hybrid 1 and hybrid 3. Fruit sizes are indicated by the black markers. Asterisks (*) indicate the F₁ hybrid of the desired phenotype carrying the two genes of interest.

accumulation of high levels of β -carotene in fruit as a consequence of *CYC-B* overexpression. The F_1 hybrid no. 1 was identified to contain both genes of interest, whereas the other two F_1 hybrids (no. 2 and 3) were negative for the transgene (Figure 3.3A). In fact, all F_1 hybrids inherited a copy of *S. lycopersicum* *CYC-B* from their U/U parent (Figure 3.3B) and therefore, they were heterozygous for *S. galapagense* *CYC-B* (*B/+* genotype). However, the absence of the transgene in the F_1 hybrids no. 2 and 3 indicates that the U/U parent must have been in fact hemizygous for the transgene rather than homozygous as initially described (M Nogueira 2015, personal communication, 26 October). The comparison of fruit phenotypes of the three F_1 hybrids revealed that only the plant which inherited both genes of interest (hybrid no. 1) displayed a remarkably different colouration of its mature fruit on the outside (Figure 3.3C and D) and on the inside (Figure 3.3E) compared to the other two plants (hybrids no. 2 and 3). The fruit of the F_1 hybrids no. 2 and 3 appeared darker than the F_1 hybrid no. 1 and similar to a typical red tomato. The parental phenotypes (U/U and *B/B*) were not included due to the limited availability of material. However, the mature fruit of the *B/B* parent appeared virtually identical to the mature fruit of the F_1 hybrids no. 2 and 3, whereas the fruit of the U/U parent were red.

In order to qualitatively and quantitatively assess the changes in carotenoid composition between the different lines, the fruit and leaf pigments were extracted from the parental lines, F_1 hybrids and tomato cultivar Moneymaker (MM) and analysed on the HPLC (Figure 3.4) and UPLC (Supplementary Figure 1.2) systems. Both platforms identified the same compounds in the extracts and thus were found suitable for the analysis of this type of material. However, compared to the UPLC, HPLC provided a much better peak resolution and therefore was selected as the method of choice for analysis and absolute quantification of the identified compounds. The cultivar Moneymaker was initially used for comparison as one of the backgrounds, but more importantly, as a popular commercial variety, it provided a point of reference for the other lines.

Analysis of the pigment profiles revealed that the U/U parental line, similarly to the cultivar Moneymaker, accumulated primarily lycopene (peak no. 13) in its fruit (Figure 3.4A). The mature fruit of the *B/B* parental line, similarly to the F_1 hybrids no. 2 and 3, which were found to be negative for the transgenic copy of *CrtR-b2*, accumulated β -carotene (peak no. 9) as the major pigment. The orange fruit of the F_1 hybrid no. 1 were also found to contain β -carotene but unlike any other fruit, they accumulated substantial amounts of xanthophylls, primarily violaxanthin (peak no. 1) and the derivative of violaxanthin – luteoxanthin (peak no. 2). Therefore, the combination of a high β -carotene background as the result of *CYC-B* overexpression with simultaneous overexpression of β -carotene hydroxylase (*CrtR-b2*) modified the carotenoid profile of the mature fruit significantly compared to the parental lines and the commercial variety (Moneymaker) and led to the accumulation of xanthophylls.

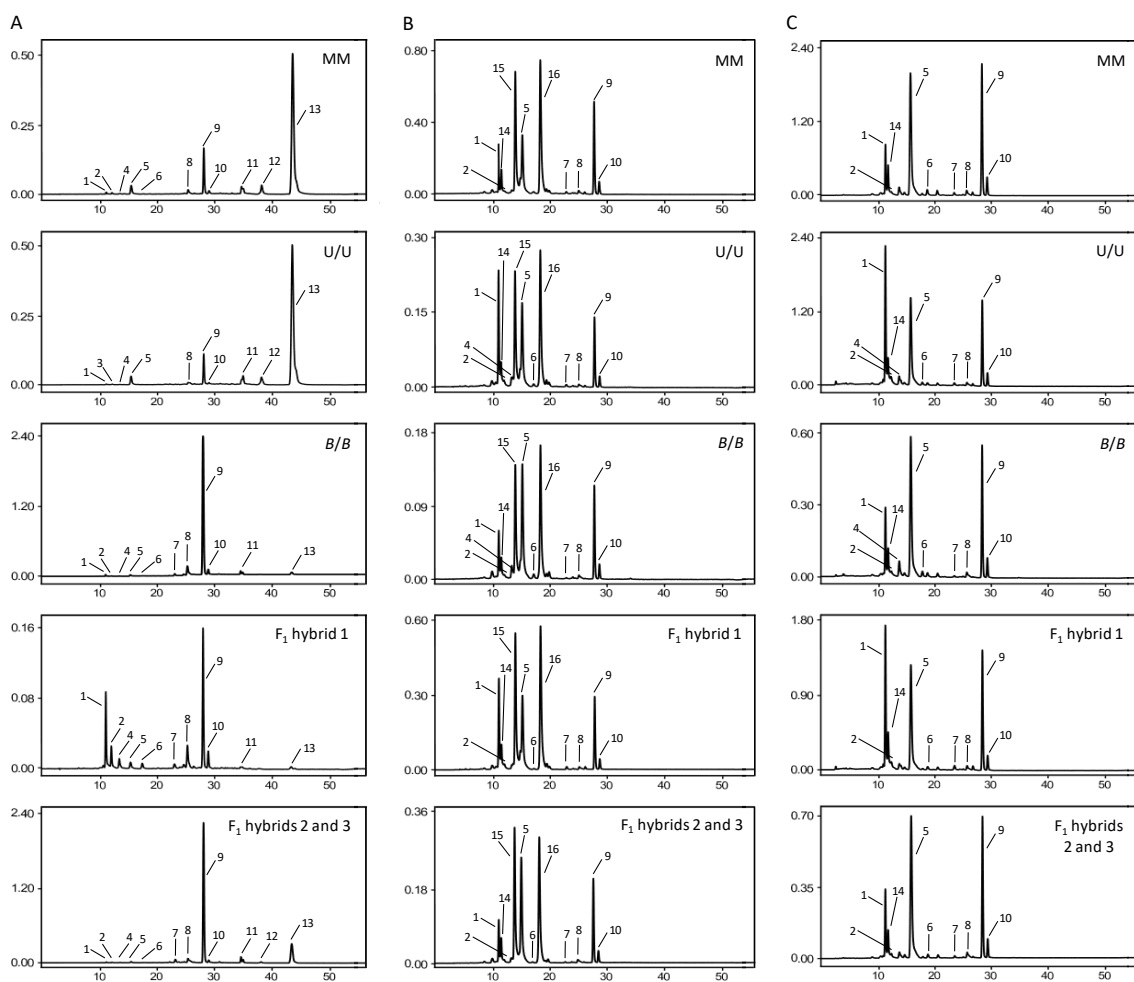


Figure 3.4. HPLC analysis of the pigments from the fruit (A), leaf (B) and saponified leaf (C) extracts of the indicated tomato lines at 450 nm. The areas of the peaks were used to quantify the compounds. Since the pigment profiles of the F₁ hybrids no. 2 and 3 were very similar, only representative chromatograms are shown. 1 – violaxanthin, 2 – luteoxanthin, 3 – violaxanthin derivative, 4 – antheraxanthin, 5 – lutein, 6 – zeaxanthin, 7 – β -carotene 5,6-epoxide, 8 – α -carotene, 9 – β -carotene, 10 – *cis*- β -carotene, 11 – γ -carotene, 12 – *cis*-lycopene, 13 – all-*trans*-lycopene, 14 – neoxanthin, 15 – chlorophyll B, 16 – chlorophyll A; MM – Moneymaker.

Pigments were also extracted from the leaves of the investigated lines and analysed because changes at the carotenoid level might affect the photosynthetic performance of the plant due to modifications of the light-absorbing properties of the tissue (Figure 3.4B). However, in order to simplify the comparison between the lines, the chlorophylls were removed from the samples by saponification prior to the extraction (Figure 3.4C). As seen from the chromatograms of the saponified leaf samples of Moneymaker, the *B/B* parental line and the F₁ hybrids no. 2 and 3, these three lines had very similar pigment profiles with the two major components being lutein (peak no. 5) and β -carotene (peak no. 9). On the other hand, in the leaf profiles of the U/U parent and the F₁ hybrid no. 1, violaxanthin (peak no. 1) appeared to be the major component. Therefore, it seemed that the leaf profiles were predominantly altered in the presence of transgenic *CrtR-b2* and *S. galapagense* *CYC-B* allele had very little effect.

Comparing the HPLC chromatograms allows to assess qualitative changes between the lines; however, these can be used as well to obtain the absolute amounts of carotenoids (Table 3.1).

Table 3.1. Quantification of isoprenoids and chlorophylls from the fruit and non-saponified leaf extracts of the indicated tomato lines. The reported values were used to obtain total carotenoids (CAR; α -tocopherol not included) and total chlorophylls (CHL). The ratios of chlorophyll A to chlorophyll B (Chl A : Chl B) and total chlorophylls to total carotenoids (CHL : CAR) were calculated as well. Since the pigment profiles of the F₁ hybrids no. 2 and 3 were very similar, only hybrid no. 2 is shown. The amounts of the compounds are reported as $\mu\text{g g}^{-1}$ DW. The data are presented as the mean of three technical replicates \pm SD; biological replicates, N = 1; nd – not detected.

Compound	Fruit					Leaf				
	MM	U/U	B/B	F ₁ hybrid 1	F ₁ hybrid 2	MM	U/U	B/B	F ₁ hybrid 1	F ₁ hybrid 2
Violaxanthin	13.5 \pm 1.9	5.5 \pm 1.5	68.4 \pm 1.1	224.2 \pm 8.0	25.6 \pm 3.3	1 710.3 \pm 33.4	2 055.8 \pm 207.4	503.7 \pm 48.0	3 280.9 \pm 406.2	796.5 \pm 47.9
Neoxanthin						1 147.2 \pm 29.6	601.9 \pm 62.1	342.1 \pm 21.0	1 083.7 \pm 65.8	566.0 \pm 1.3
α -tocopherol	99.1 \pm 16.7	132.2 \pm 2.7	107.8 \pm 1.8	127.8 \pm 4.7	151.0 \pm 1.2					
Luteoxanthin	10.9 \pm 1.1	nd	18.2 \pm 1.9	79.8 \pm 3.3	18.4 \pm 2.5	209.5 \pm 12.4	213.4 \pm 37.7	38.7 \pm 6.9	396.4 \pm 29.4	83.7 \pm 25.6
Antheraxanthin	1.0 \pm 0.3	0.3 \pm 0.1	3.2 \pm 1.0	6.5 \pm 0.5	2.2 \pm 0.1	nd	27.4 \pm 3.5	27.5 \pm 2.5	nd	nd
Lutein	23.0 \pm 1.5	25.4 \pm 1.4	17.7 \pm 0.6	5.3 \pm 0.3	11.6 \pm 0.5	814.8 \pm 51.6	435.3 \pm 33.0	356.5 \pm 21.4	821.8 \pm 67.7	585.0 \pm 15.1
Zeaxanthin	0.1 \pm 0.0	nd	1.4 \pm 0.2	3.0 \pm 0.2	0.5 \pm 0.1	10.5 \pm 1.7 [†]	8.7 \pm 0.5	9.6 \pm 1.6	7.4 \pm 0.5	2.9 \pm 1.4
Phytoene	76.1 \pm 4.4	193.4 \pm 3.0	69.6 \pm 1.6	9.2 \pm 0.3	153.7 \pm 8.2	2.3 \pm 0.2	2.6 \pm 0.7	2.1 \pm 0.2	2.7 \pm 0.4	1.9 \pm 0.1
α -carotene	13.1 \pm 0.2	11.9 \pm 0.2	121.2 \pm 16.8	20.4 \pm 0.4	59.0 \pm 20.4	47.5 \pm 2.5	20.6 \pm 2.4	18.4 \pm 2.2	35.0 \pm 1.6	26.6 \pm 1.2
β -carotene	69.2 \pm 6.1	45.6 \pm 6.0	1 567.8 \pm 23.4	62.4 \pm 1.2	1 354.4 \pm 26.1	805.0 \pm 14.5	150.1 \pm 6.4	111.6 \pm 6.0	404.6 \pm 14.5	241.6 \pm 7.8
Lycopene	631.9 \pm 22.3	699.2 \pm 44.0	55.3 \pm 1.0	3.7 \pm 0.1	350.6 \pm 17.5					
Total CAR	838.8 \pm 23.7	981.3 \pm 44.6	1 922.8 \pm 29.0	414.5 \pm 8.8	1 976.0 \pm 38.6	4 747.1 \pm 70.9	3 515.8 \pm 222.3	1 410.2 \pm 57.4	6 032.5 \pm 418.3	2 304.2 \pm 57.0
Chlorophyll A						10 977.6 \pm 677.5	4 418.7 \pm 428.6	2 584.7 \pm 149.9	9 147.4 \pm 534.0	4 165.0 \pm 57.8
Chlorophyll B						2 911.1 \pm 203.1	1 259.1 \pm 199.2	746.6 \pm 89.2	2 691.1 \pm 268.7	1 333.8 \pm 16.8
Total CHL						13 888.7 \pm 707.3	5 677.8 \pm 472.6	3 331.3 \pm 174.4	11 838.5 \pm 597.8	5 498.8 \pm 60.2
Chl A : Chl B						3.8 \pm 0.4	3.5 \pm 0.7	3.5 \pm 0.5	3.4 \pm 0.4	3.1 \pm 0.1
CHL : CAR						2.9 \pm 0.2	1.6 \pm 0.2	2.4 \pm 0.2	2.0 \pm 0.2	2.4 \pm 0.1

[†]Amount obtained from saponified leaf extract of MM since no zeaxanthin was identified in non-saponified samples

In order to quantify the carotenoid and chlorophyll levels in the fruit and leaf tissues, the areas of the peaks were integrated and substituted into the equations of the corresponding calibration curves (Supplementary Table 1.1). The peak areas from the fruit (Figure 3.4A) and non-saponified leaf (Figure 3.4B) samples were used for quantification. Generally, saponified leaf samples were not used throughout this work for quantification of simple matrices such as these presented in Figure 3.4B. This is because saponification seems to affect the amounts of extracted carotenoids (Supplementary Figure 1.3). Generally, the levels of isoprenoids in the saponified samples were decreased compared with the non-saponified extracts, except in case of β -carotene where saponification seemed to have an opposite effect. However, a detailed statistical analysis of these extracts was not possible due to the limited number of biological replicates ($N = 1$). Moreover, saponification removes chlorophylls from the extract and therefore does not allow for their quantification. Nevertheless, saponification is sometimes useful when a strong signal from one peak obstructs a neighbouring peak with a much smaller amplitude. This was seen in case of the Moneymaker leaf extract where zeaxanthin was only identified after the sample was saponified (Figure 3.4C). In the non-saponified leaf extract, the zeaxanthin peak was obstructed by the neighbouring chlorophyll A peak (Figure 3.4B; Supplementary Figure 1.3). Table 3.1 provides the amounts of the isoprenoid compounds and the chlorophylls from the fruit and non-saponified leaf extracts of the analysed lines.

The levels of zeaxanthin were not markedly increased in the orange fruit of the F_1 hybrid no. 1, although they were the highest amongst the plants tested, reaching $3.0 \mu\text{g g}^{-1}$ DW. Similarly, the levels of antheraxanthin, a mono-epoxidated derivative of zeaxanthin, were the highest in this hybrid ($6.5 \mu\text{g g}^{-1}$ DW) albeit they were still relatively low overall. However, the F_1 hybrid no. 1 accumulated the highest amounts of violaxanthin ($224.2 \mu\text{g g}^{-1}$ DW) and luteoxanthin ($79.8 \mu\text{g g}^{-1}$ DW) in its fruit. In fact, the levels of violaxanthin in this plant were 3.3 times higher than in the B/B parent which contained the second highest levels of this xanthophyll ($68.4 \mu\text{g g}^{-1}$ DW). The levels of luteoxanthin were over 4.3 times greater in the fruit of F_1 hybrid no. 1 than the B/B parent and the F_1 hybrid no. 2, which accumulated similar levels of this compound (18.2 and $18.4 \mu\text{g g}^{-1}$ DW, respectively). On the other hand, the levels of lutein, phytoene and lycopene were the lowest in the F_1 hybrid no. 1 (5.3 , 9.2 and $3.7 \mu\text{g g}^{-1}$ DW, respectively). The levels of α - and β -carotene were similar between the fruit of Moneymaker, the U/U parent and the F_1 hybrid no. 1. The B/B parent and F_1 hybrid no. 2 accumulated the highest levels of β -carotene ($1\ 567.8$ and $1\ 354.4 \mu\text{g g}^{-1}$ DW, respectively) and also had the highest total fruit carotenoid content ($1\ 922.8$ and $1\ 976.0 \mu\text{g g}^{-1}$ DW, respectively). The fruit of Moneymaker and the U/U parent had very similar pigment profiles, but the overall carotenoid content was higher in the U/U parent reaching 981.3 as compared with $838.8 \mu\text{g g}^{-1}$ DW in Moneymaker. The total carotenoid levels in the fruit of F_1 hybrid no. 1 were the lowest amongst

the analysed plants, reaching 414.5 $\mu\text{g g}^{-1}$ DW. However, the total xanthophylls comprised 76.9% of the total carotenoids in this plant, which was the highest proportion among the tested fruit. Comparatively, in the mature fruit of Moneymaker, the *B/B* and *U/U* parents as well as the F_1 hybrid no. 2, the xanthophylls comprised less than 6% of the total carotenoid content.

Analysis of leaf pigments is important in the context of the plant's photosynthetic performance. Changing the carotenoid composition may disrupt the ratio of total chlorophylls to accessory pigments, which in turn can modify the absorptive properties of the tissue. Therefore, changes in the leaf pigment profiles must be assessed following modifications to the carotenoid biosynthetic pathway. The F_1 hybrid no. 1, similarly to what was seen in the fruit, accumulated the highest levels of violaxanthin and luteoxanthin in its leaves, reaching 3 280.9 and 396.4 $\mu\text{g g}^{-1}$ DW, respectively. This was almost a 1.6-fold increase in the violaxanthin content compared with the *U/U* parent which accumulated the second highest levels of this xanthophyll (2 055.8 $\mu\text{g g}^{-1}$ DW). However, unlike in its fruit, the F_1 hybrid no. 1 had the highest total leaf carotenoid levels (6 032.5 $\mu\text{g g}^{-1}$ DW). Interestingly, the levels of lutein were also the highest in the leaves of this plant, reaching 821.8 $\mu\text{g g}^{-1}$ DW, whereas in the fruit, they were the lowest. All plants contained some, yet small, amounts of zeaxanthin. Antheraxanthin was only detected in the two parental lines but not in Moneymaker, nor in the F_1 hybrids. The total chlorophyll was the highest in Moneymaker and F_1 hybrid no. 1 (13 888.7 and 11 838.5 $\mu\text{g g}^{-1}$ DW, respectively) followed by the *U/U* parent and hybrid no. 2 (5 677.8 and 5 498.9 $\mu\text{g g}^{-1}$ DW, respectively). The *B/B* parent had the lowest total chlorophyll content (3 331.3 $\mu\text{g g}^{-1}$ DW). Although the plants contained different amounts of the chlorophylls, they all had similar ratios of chlorophyll A to chlorophyll B which lay between 3.1 to 1 (hybrid no. 2) and 3.8 to 1 (Moneymaker). The ratios of total chlorophylls to total carotenoids were greater than 2.0 to 1 in all plants analysed except the *U/U* parent, where this ratio was slightly lower (1.6 to 1).

Due to the exceptionally high content of total xanthophylls in its fruit, the F_1 hybrid no. 1 was advanced to the next generation. Its progeny, the F_2 generation, segregated for the *B* gene and transgenic *CrtR-b2* and required screening prior to the isolation of the genotypes of interest.

3.2.3 Screening of F_2 segregating population

The F_2 segregating population consisting of 185 plants (PL0001 – PL0185) originating from the high-xanthophyll F_1 hybrid no. 1, was screened for the presence of the CaMV 35S promoter and *S. galapagense* and *S. lycopersicum* alleles of *CYC-B* (Figure 3.5A). Lines homozygous (*B/B*) and heterozygous (*B/+*) for *S. galapagense* *CYC-B* allele (the *B* gene) were identified using the PCR screening method. Similarly, the Azygous (*Az*; 0/0; +/- genotype) reference lines were identified by PCR. However, end-point PCR could not be used to distinguish between plants hemizygous and homozygous for transgenic *CrtR-b2* (indicated as *U/_* in Figure 3.5A).

Initially, three F₂ plants (PL0051, PL0057 and PL0064) were selected to carry out Southern blot analysis in order to confirm the number of transgenic inserts. These plants have been previously screened by PCR and confirmed to be positive for the CaMV 35S promoter (Supplementary Figure 1.4A). The probe targeting the joined region between the CaMV 35S promoter and *CrtR-b2* was successfully prepared (Supplementary Figure 1.4B). The genomic DNA extracted from the plants was confirmed to be of good quality as it run as a single band and did not produce smearing on the electrophoresis gel (Supplementary Figure 1.4C). The genomic DNA was digested with *Hind*III (Supplementary Figure 1.4D) and blotted onto a nylon membrane. The probe hybridised with the transgenic copy of *CrtR-b2* (the T-band in Figure 3.5B) present in all plants except the negative control Moneymaker (MM). Additionally, the endogenous copy of *CrtR-b2* (the E-band) was detected by the hybridisation probe in all five plants. The presence of a single transgenic (T) band indicated that the plants contained a single insert of *CrtR-b2*.

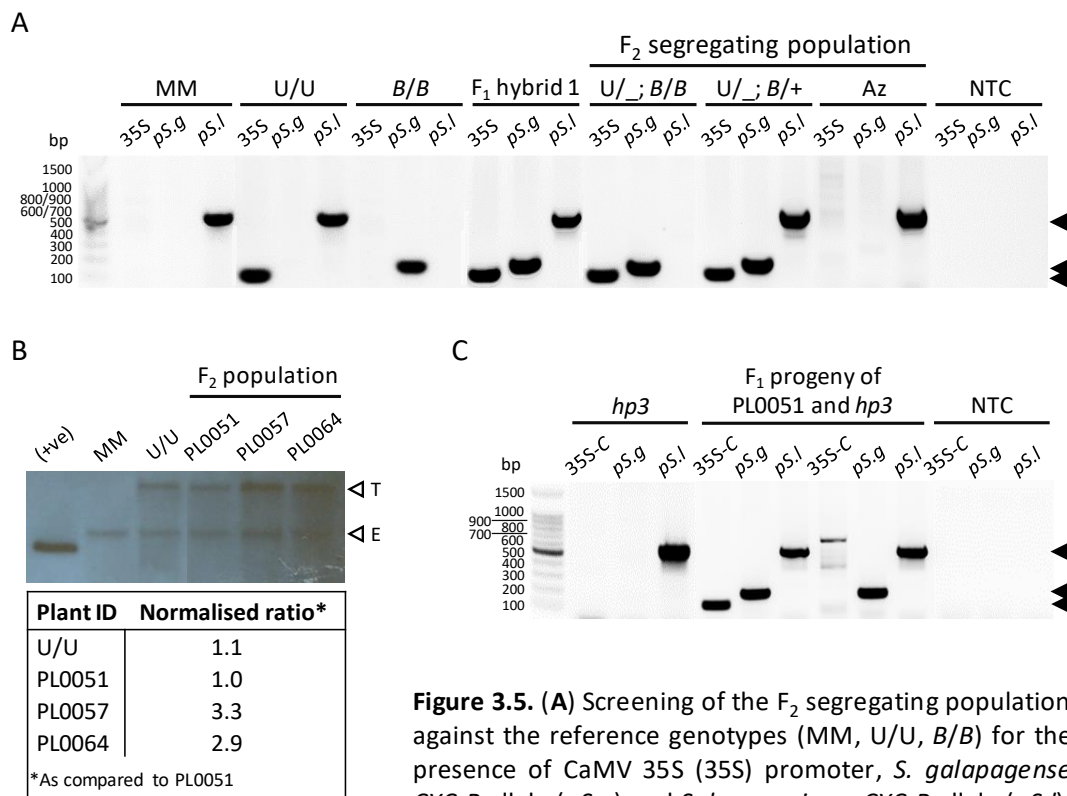


Figure 3.5. (A) Screening of the F₂ segregating population against the reference genotypes (MM, U/U, B/B) for the presence of CaMV 35S (35S) promoter, *S. galapagense* CYC-B allele (pS.g) and *S. lycopersicum* CYC-B allele (pS.l). For the description of reference lines, refer to Figure 3.3.

F₁ hybrid 1 – parent of the F₂ segregating population; U/-; B/B and U/-; B/+ – CaMV 35S-positive plants homozygous and heterozygous for *S. galapagense* CYC-B, respectively; Az – Azygous reference line negative for CaMV 35S and *S. galapagense* CYC-B and homozygous for *S. lycopersicum* CYC-B (0/0; +/+). Only representative genotypes are shown. NTC – no-template control. Black arrowheads indicate positions of predicted fragments. (B) Southern blot analysis of selected F₂ plants (PL0051, PL0057 and PL0064). Empty arrowheads indicate the endogenous (E) and transgenic (T) copies of *CrtR-b2*. Intensity of each T band was normalised against the corresponding amount of DNA and divided by the value obtained for PL0051. (+ve) – 35S-*CrtR-b2*-TOPO, positive blotting control. (C) Screening of the F₁ progeny of the plant from the F₂ population (PL0051) crossed with the *hp3* line for the presence of the 35S-*CrtR-b2* fragment (35S-C), *S. galapagense* CYC-B (pS.g) and *S. lycopersicum* CYC-B (pS.l). Only representative examples of the two possible genotypes are shown.

The transgenic (T) band intensity on the X-ray film could be used to infer the zygosity of *CrtR-b2* (Figure 3.5B). In order to account for unequal gel loading, the signal from each T-band was normalised to the intensity of the corresponding digested DNA used in the blot (Supplementary Figure 1.4D). This allowed to calculate the zygosity of each plant (table in Figure 3.5B). However, the result of the Southern blot was inconclusive, as the parental U/U line, expected to be homozygous for transgenic *CrtR-b2* as indicated by D'Ambrosio *et al.* (2011), was found to be hemizygous instead. Additionally, two F₂ plants (PL0057 and PL0064) appeared to have more than two copies of the transgene at the U locus. In any case, this result was not consistent with the zygosity observed in the parental U/U line and could suggest the presence of chromosomal abnormalities, such as polysomy or polyploidy, in the F₂ plants. However, the appearance of the same chromosomal aberrations in two different plants is rather unlikely and the more plausible explanation is that, although the band intensity could indicate zygosity, this method is not quantitative enough to reliably detect a two-fold difference.

The findings of the Southern blot analysis most likely result from an uneven gel loading and the low quality of the gel used in the normalisation step (Supplementary Figure 1.4D). In order to circumvent this problem, the intensity of the signal produced by the transgenic copy of *CrtR-b2* (the T-band) was compared to the signal intensity produced by the endogenous copy of the gene (the E-band). The ratios of T-band to the E-band were 2.08 for the U/U parent, 0.99 for PL0051, 2.04 for PL0057 and 1.94 for PL0064. This result would suggest that, relatively to each other, the U/U parent and plants PL0057 and PL0064 were homozygous for the transgene, whereas PL0051 was hemizygous. However, this approach was only possible because the endogenous copy of *CrtR-b2* was detected by the hybridisation probe and further validation was required in order to confirm this observation.

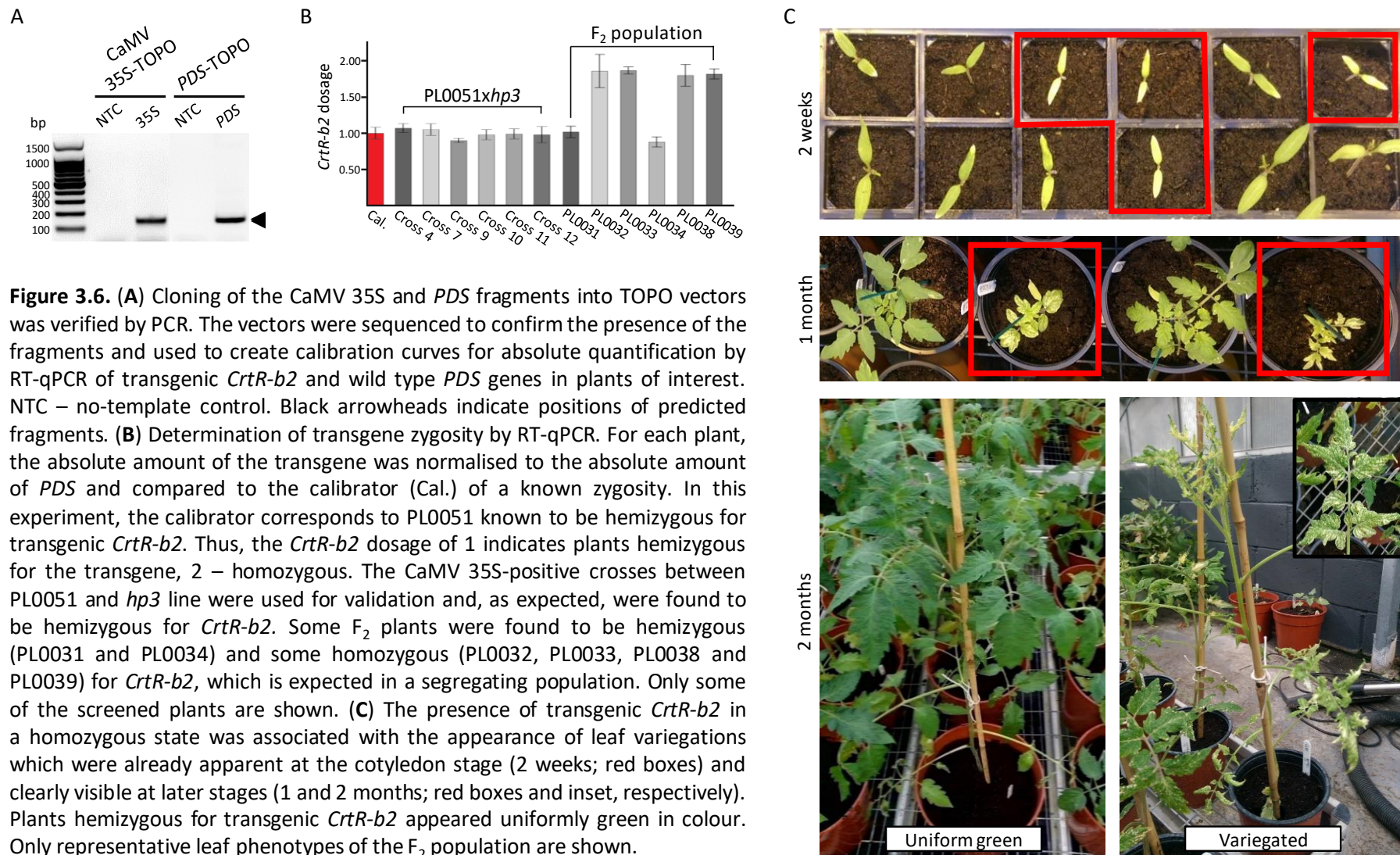
In order to verify the above findings, several plants from the F₂ population (PL0025, PL0051, PL0057, PL0058 and PL0078), including some which were used in the Southern blot experiment, were crossed with the *hp3* tomato variety (a reference line used in Chapters IV and V) to carry out a segregation study (Supplementary Figure 1.4E). The *hp3* line and the resulting crosses were screened similarly to the F₂ segregating population to confirm the suitability of the primers for later screens (Figure 3.5C). The presence of the CaMV 35S promoter was tested with the same primers as used for the generation of the Southern blot hybridisation probe. The segregation pattern of the transgene was then used to establish the zygosity of the parental line. For instance, some of the F₁ progeny of PL0051 and *hp3* line was positive and some negative for the CaMV 35S fragment indicating that the parental PL0051 plant must have been hemizygous for the transgene (Figure 3.5C). The full screen of the selected plants is provided in Supplementary Figure 1.4E. Based on this screen, chi-squared (χ^2) test was carried out to assess whether the

Table 3.2. χ^2 goodness of fit test allowed to conclude that the segregation of transgenic *CrtR-b2* at the U locus was occurring in the manner as expected, given the zygosity of the maternal F_2 plant ($\chi^2 = 0.2$, $d_f = 4$, $P = 0.995$).

F_2 plant (maternal)	F_1 progeny of the F_2 plant crossed with the <i>hp3</i> line		<i>CrtR-b2</i> zygosity of the F_2 plant
	Number of plants positive for CaMV 35S- <i>CrtR-b2</i> fragment	Total number of plants	
PL0025	7	7	Homozygous (U/U)
PL0051	7	14	Hemizygous (U/0)
PL0057	10	10	Homozygous (U/U)
PL0058	5	5	Homozygous (U/U)
PL0078	4	10	Hemizygous (U/0)

segregation pattern followed what was predicted from the genotypes of the parental lines (Table 3.2). The result of the test indicated that the segregation pattern did not differ from what was expected given the genotypes of the parental plants. Based on this test, the maternal plants were characterised for *CrtR-b2* zygosity and used as reference genotypes. The segregation test also allowed to conclude that plants PL0051 and PL0057, used in the Southern blot experiment, were identified correctly as hemizygous and homozygous for the transgene, respectively.

However, the above methods are not suitable for screening of large populations. Segregation tests are lengthy and require extra space for the developing plants. Similarly, Southern blotting is time-consuming, requires large amounts of genomic DNA and provides a low throughput. Therefore, in order to screen the entire F_2 segregating population, real time quantitative PCR (RT-qPCR) was selected as the method of choice. The plants characterised by the Southern blot analysis and the segregation test were used as reference genotypes (calibrators) of a known transgene zygosity. The plasmids with cloned fragments of the CaMV 35S promoter and a gene of a known copy number (phytoene desaturase, *PDS*) were used to generate standard curves for absolute quantification of the two genes (Figure 3.6A). The plasmids were sequenced prior to the analysis to confirm that both vectors contained the correct fragments with no mismatches in the primer annealing regions (Supplementary Figure 1.5). The ratio of CaMV 35S to *PDS* was calculated for each plant and normalised to the calibrator (Figure 3.6B). The method was first validated on the same crosses as used in the segregation test (Supplementary Figure 1.4E). All *hp3* crosses positive for the CaMV 35S promoter were found to be hemizygous for the transgene as expected in the first generation. The U/U parental line used in the Southern blot experiment was found to be homozygous for *CrtR-b2* (data not shown). Interestingly, it was realised that plants homozygous for transgenic *CrtR-b2* displayed a variegated leaf phenotype and stunted growth in early development (Figure 3.6C; two weeks). The phenotypes of plants hemizygous and homozygous for the transgene were clearly distinguishable later in development (one and two months), which greatly facilitated selection of plants with the desired genotypes.



3.2.4 Phenotypic characterisation of F₂ population lines

The screening methods described above were used to classify the plants of the F₂ segregating population according to the absence, presence and zygosity of the genes of interest. The plants which lost *S. galapagense* *CYC-B* and transgenic *CrtR-b2* were selected as a reference phenotype for other lines. These plants are referred to as the Azygous (Az) line of the 0/0; +/+ genotype. The Az line was the only line with intensely red-coloured mature fruit (Figure 3.7A). The mature fruit of the lines hemizygous for transgenic *CrtR-b2* (U/0) and either homozygous (*B/B*) or heterozygous (*B/+*) for *S. galapagense* *CYC-B* were amber-orange. The lines homozygous for transgenic *CrtR-b2* (U/U) and either homozygous (*B/B*) or heterozygous (*B/+*) for *S. galapagense* *CYC-B* also had orange fruit but these appeared darker than the fruit of the other two transgenic lines. Thus, the transgene zygosity seems to determine the intensity of orange colouration of the fruit allowing to distinguish the lines homozygous for the transgene from the hemizygous ones. The leaves of the lines homozygous for transgenic *CrtR-b2*, irrespective of *S. galapagense* *CYC-B* zygosity, displayed a variegated phenotype and could be separated from the other lines which had a uniformly green colouration of their leaves (Figures 3.6C and 3.7B). Subsequently, the fruit and leaf tissues of the five lines were analysed for their pigment content by HPLC.

3.2.5 Leaf pigment analysis of F₂ population lines

The saponified and unsaponified leaf extracts of the Azygous (Az), U/0; *B/B*, U/0; *B/+*, U/U; *B/B* and U/U; *B/+* lines were analysed on the HPLC system. The chromatograms of the saponified extracts showed that the four transgenic lines were different from the Az line (Figure 3.8A). Lutein (peak no. 5) and β -carotene (peak no. 8) were the two major pigments identified in the Az reference line. In the U/0; *B/B* line, violaxanthin (peak no. 1) produced the strongest signal, whereas lutein and β -carotene appeared equally as the next major components. The HPLC trace of the U/0; *B/+* line was more similar to the Az line than the U/0; *B/B* line. However, after lutein, violaxanthin produced the second strongest signal in this line. The chromatographic traces of the U/U; *B/B* and U/U; *B/+* lines were very similar to each other and also were the closest to the pigment profile of the Az reference line. The zeaxanthin peak was not particularly prominent in any of the transgenic lines. However, a small antheraxanthin peak was identified in all of them. Neither zeaxanthin nor antheraxanthin were identified in the Az reference line.

Comparison of the HPLC chromatograms of the saponified leaf extracts is useful to assess the major carotenoid changes. However, quantification by peak integration is necessary to obtain absolute amounts which can subsequently be used for statistical analysis. Quantification of the pigments from the unsaponified leaf extracts of the five lines was carried out. The obtained values were first compared to the Az reference line then all F₂ lines were compared to each other and statistically significant changes in the pigment content were indicated (Figure 3.8B).

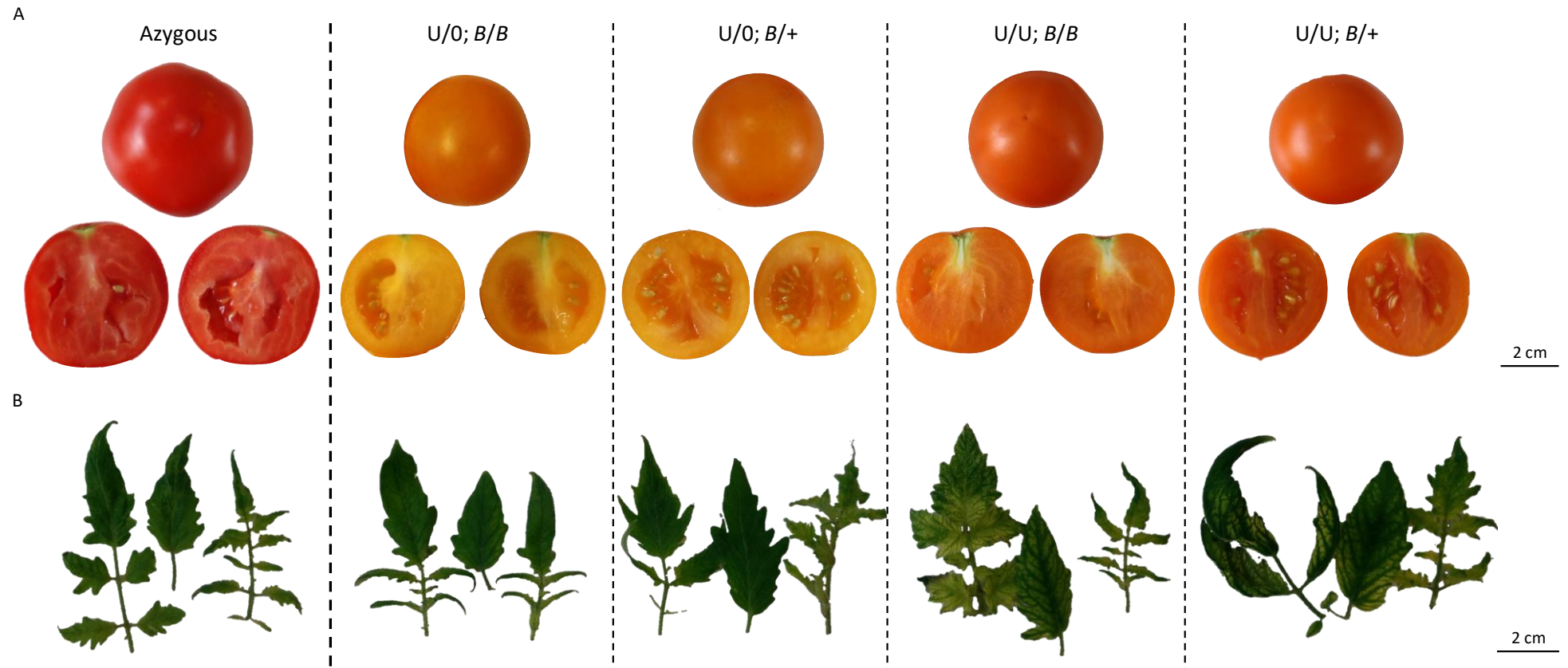
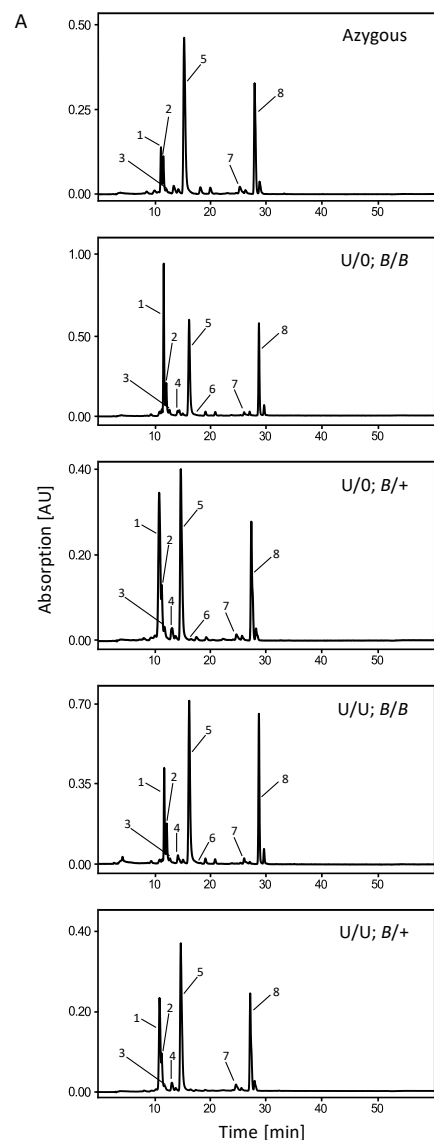


Figure 3.7. Side-by-side comparison of the fruit (A) and leaf (B) phenotypes of the indicated tomato lines of the F₂ population. (A) Compared to the red-coloured fruit of the Azygous line, the other four lines have distinctively orange fruit. The fruit of the lines hemizygous for transgenic *CrtR-b2* (U/0) appear lighter compared with the fruit of the lines homozygous for transgenic *CrtR-b2* (U/U). On the other hand, the shade of orange of the transgenic lines with the same *CrtR-b2* zygosity does not seem to be influenced by the change in *S. galapagense* *CYC-B* (the *B* gene) zygosity. The transgenic fruit also appear smaller than the fruit of the Azygous line. (B) The leaves of the Azygous and U/0 lines are uniformly green, whereas the leaves of the U/U lines are not uniform in appearance. Only subtle areas of discolouration (variegations) are visible on the leaves of the U/U lines due to the poor quality of the photo; hence refer to Figure 3.6C for a clearer comparison.



B

Compound	Leaf						
	U/U	B/B	Azygous	U/O; B/B	U/O; B/+	U/U; B/B	U/U; B/+
Violaxanthin	2 055.8 ± 207.4	503.7 ± 48.0	1 259.0 ± 229.8 ^a	6 340.1 ± 2 012.8 ^c	3 718.3 ± 981.4 ^b	3 401.1 ± 1 274.7 ^b	2 832.0 ± 813.2 ^b
Neoxanthin	601.9 ± 62.1	342.1 ± 21.0	1 498.6 ± 261.8 ^a	2 285.9 ± 727.7 ^b	1 510.4 ± 415.8 ^a	1 729.4 ± 437.1 ^{ab}	1 443.5 ± 219.7 ^a
Luteoxanthin	213.4 ± 37.7	38.7 ± 6.9	511.6 ± 118.2 ^a	1 035.7 ± 414.5 ^b	1 328.7 ± 412.6 ^b	994.5 ± 396.3 ^b	968.9 ± 233.1 ^b
Antheraxanthin	27.4 ± 3.5	27.5 ± 2.5	nd ^a	27.1 ± 32.2 ^{ab}	79.0 ± 26.4 ^c	51.8 ± 47.9 ^{bc}	15.0 ± 27.9 ^{ab}
Lutein	435.3 ± 33.0	356.5 ± 21.4	1 727.9 ± 322.2 ^b	1 727.3 ± 462.8 ^b	1 290.2 ± 360.6 ^a	1 523.5 ± 423.4 ^{ab}	1 332.1 ± 209.7 ^{ab}
Zeaxanthin	8.7 ± 0.5	9.6 ± 1.6	nd ^a	12.7 ± 16.6 ^{ab}	22.0 ± 18.4 ^b	16.8 ± 23.7 ^{ab}	nd ^a
Phytoene	2.6 ± 0.7	2.1 ± 0.2	4.2 ± 0.8 ^a	5.8 ± 1.5 ^{ac}	6.1 ± 1.2 ^{bc}	4.8 ± 1.3 ^{ab}	7.1 ± 2.2 ^c
α-carotene	20.6 ± 2.4	18.4 ± 2.2	62.9 ± 9.7 ^b	41.7 ± 13.9 ^a	45.5 ± 11.4 ^a	50.8 ± 10.8 ^{ab}	49.4 ± 9.9 ^{ab}
β-carotene	150.1 ± 6.4	111.6 ± 6.0	803.9 ± 157.3 ^b	853.4 ± 241.5 ^b	586.2 ± 186.4 ^a	792.9 ± 232.8 ^{ab}	622.5 ± 125.1 ^{ab}
Total CAR	3 515.8 ± 222.3	1 410.2 ± 57.4	5 868.0 ± 1 020.8 ^a	12 329.7 ± 3 496.1 ^c	8 586.4 ± 2 267.9 ^b	8 565.5 ± 2 124.5 ^{ab}	7 270.5 ± 1 284.4 ^{ab}
Chlorophyll A	4 418.7 ± 428.6	2 584.7 ± 149.9	8 470.4 ± 1 578.7 ^a	11 351.1 ± 3 133.4 ^b	6 964.1 ± 2 067.1 ^a	8 646.9 ± 2 568.1 ^{ab}	7 178.4 ± 1 633.5 ^a
Chlorophyll B	1 259.1 ± 199.2	746.6 ± 89.2	3 149.4 ± 536.5 ^{ab}	3 676.6 ± 1 006.8 ^b	2 628.2 ± 763.9 ^a	3 215.4 ± 698.7 ^{ab}	2 694.7 ± 448.4 ^a
Total CHL	5 677.8 ± 472.6	3 331.3 ± 174.4	11 619.8 ± 2 107.9 ^{ab}	15 027.8 ± 4 096.2 ^b	9 592.4 ± 2 819.4 ^a	11 862.3 ± 3 149.0 ^{ab}	9 873.0 ± 2 073.9 ^a
Chl A : Chl B	3.5 ± 0.7	3.5 ± 0.5	2.7 ± 0.1 ^a	3.1 ± 0.3 ^b	2.6 ± 0.2 ^a	2.7 ± 0.4 ^a	2.6 ± 0.3 ^a
CHL : CAR	1.6 ± 0.2	2.4 ± 0.2	2.0 ± 0.1 ^c	1.2 ± 0.1 ^{ab}	1.1 ± 0.1 ^a	1.4 ± 0.3 ^b	1.4 ± 0.2 ^b
N	1	1	12	12	17	8	8

Figure 3.8. (A) HPLC chromatograms of saponified leaf extracts of the indicated F₂ population lines. 1 – violaxanthin, 2 – neoxanthin, 3 – luteoxanthin, 4 – antheraxanthin, 5 – lutein, 6 – zeaxanthin, 7 – α-carotene, 8 – β-carotene. **(B)** Quantification of isoprenoids and chlorophylls from the non-saponified leaf extracts of the F₂ population lines. The reported values were used to obtain total carotenoids (CAR) and total chlorophylls (CHL). The ratios of chlorophyll A to chlorophyll B (Chl A : Chl B) and total chlorophylls to total carotenoids (CHL : CAR) were also calculated. The amounts of the compounds are reported as μg g⁻¹ DW. The data are presented as the mean of N biological replicates ± SD; nd – not detected. The pigments from the four transgenic lines (U/O; B/B, U/O; B/+, U/U; B/B and U/U; B/+) were compared to the Azygous line using one-way ANOVA with Dunnett’s multiple comparison test; green shading indicates significant increases, red – significant decreases. Additionally, multiple comparisons one-way ANOVA with Tukey’s post-hoc test was carried out to compare the F₂ lines to each other; compact letter display was used to indicate homogeneous subsets. Data normality was validated with Shapiro-Wilk test. Significant results are reported for P < 0.05. Parental lines (U/U and B/B) are included for comparison only.

The leaf pigment profiles of the transgenic lines were more similar to the U/U parental line than the B/B parent due to the high levels of violaxanthin and similar ratios of total chlorophylls to total carotenoids in these plants (Figure 3.8B). The violaxanthin content was significantly higher in the leaves of the F₂ transgenic lines than the Az line. The same trend was seen between the F₁ hybrid no. 1 and the parental lines (Table 3.1). Compared with the Az reference line, the largest, 5-fold increase in violaxanthin content was found in the U/0; B/B line and the smallest, 2.2-fold increase in the U/U; B/+ line. Similarly, luteoxanthin was increased in the four transgenic lines but the largest, 2.6-fold rise was recorded in the U/0; B/+ line. Therefore, the increase in violaxanthin content was accompanied by a concurrent, yet not directly proportional, increase in luteoxanthin. For instance, in the U/0; B/B line the levels of violaxanthin were 6.1 times greater than luteoxanthin, whereas in the other F₂ transgenic lines, the differences between the levels of violaxanthin and luteoxanthin were smaller (between 2.8- and 3.4-fold). Interestingly, compared with the Az line, neoxanthin was only significantly increased in the U/0; B/B line. This is interesting since luteoxanthin and neoxanthin are both derivatives of violaxanthin, yet higher levels of violaxanthin in the leaves are not necessarily accompanied by proportionally elevated levels of neoxanthin and luteoxanthin.

The pigments of the xanthophyll cycle were identified in the unsaponified leaf extracts of all transgenic lines, except the U/U; B/+ line in which zeaxanthin was not found. Neither zeaxanthin nor antheraxanthin were identified in the Az reference line. However, compared to Azygous, the U/0; B/+ and U/U; B/B lines were found to have significantly higher levels of antheraxanthin and only the U/0; B/+ line was found to have significantly higher levels of zeaxanthin. The large variances in the levels of these two compounds in the analysed lines might result from a strong signal overlap with the adjacent chlorophyll peaks. For instance, unlike in the unsaponified leaf extract, zeaxanthin was identified in the saponified leaf extract of the U/U; B/+ line (Figure 3.9). However, since accumulation of zeaxanthin and antheraxanthin is dependent on the light intensity, the distribution of plants within the glasshouse chamber may also influence their presence in the individual plants leading to a greater variability within the lines. Nonetheless, it is noteworthy that these xanthophylls were only detected in the leaves of the transgenic lines and not in the Az plants, even when the extracts were saponified (Figure 3.9).

Lutein and its precursor α -carotene are the compounds of the α -branch of the carotenoid biosynthetic pathway. The levels of α -carotene were decreased in all transgenic lines but only in the U/U; B/B line this change was not significant. Interestingly, compared with the Az line, lutein was only significantly lower in the U/0; B/+ line and it did not seem to be significantly affected in the other transgenic lines. Moreover, the first compound of the β -branch of the carotenoid biosynthetic pathway and the precursor of zeaxanthin, β -carotene was also significantly lower

in the U/0; B/+ line but not in the other F₂ lines. Therefore, although all transgenic lines accumulated the xanthophylls downstream of zeaxanthin, only the U/0; B/+ line did so at the expense of the α -branch carotenoids and β -carotene.

Phytoene, the precursor for carotenoid biosynthesis, was significantly increased compared with Azygous in all transgenic lines except U/U; B/B. However, since the absolute increases were between 1.6 and 2.9 $\mu\text{g g}^{-1}$ DW and the levels of phytoene were low overall (between 4.2 and 7.1 $\mu\text{g g}^{-1}$ DW), it was difficult to conclude whether these changes were biologically relevant. The total carotenoid content in the U/0; B/B, U/0; B/+ and U/U; B/B lines was significantly and markedly higher compared with the Az line. The U/0; B/B line accumulated on average 2.1 times more carotenoids in its leaves and the U/0; B/+ and U/U; B/B lines accumulated 1.5 times more carotenoids than Azygous. Only the U/U; B/+ line was not found to be significantly different from the reference line, although, on average, it still accumulated more carotenoids than the Az line. Therefore, it seems that any combination of *S. galapagense* CYC-B and transgenic *CrtR-b2* leads to an increased carotenoid content in the leaf tissue mainly due to the increased levels of violaxanthin and luteoxanthin.

Analysis of the chlorophylls in the five lines showed that the U/0; B/B line accumulated 1.3 times more chlorophyll A than the Az line, while non-significant differences were found between the remaining lines. Similarly, total chlorophylls were only found to be significantly increased in the U/0; B/B line due to the increased chlorophyll A content since chlorophyll B was not different in this line or, in fact, in any of the other F₂ transgenic lines. Therefore, the ratio of chlorophyll A to chlorophyll B was only significantly higher in the U/0; B/B line, whereas the other transgenic lines had similar ratios to Azygous. However, in all transgenic lines the ratio of total chlorophylls to total carotenoids was significantly lower compared with the Az line. This occurred because the increase in total leaf carotenoid levels in the transgenic lines was not accompanied by a proportionally high increase in total chlorophyll content, leading to the decreased ratio. However, it was interesting that only the U/0; B/B line had significantly increased chlorophyll A, whereas the other lines did not, despite the fact that all F₂ transgenic lines had similarly increased total carotenoids. Perhaps only a very high increase in leaf carotenoids, particularly violaxanthin, as seen in the U/0; B/B line, requires a concomitant increase in chlorophyll A in order to maintain the absorptive properties of the photosynthetic tissue.

3.2.6 Effect of saponification on leaf pigment extraction

An attempt was previously made when analysing leaf extracts of the U/U and B/B parental lines and the F₁ hybrids to assess the effect of saponification on carotenoid extraction. However, due to the limited sample size, the statistical analysis could not be performed. Therefore, the much larger F₂ population was selected to carry out this investigation. The same biological replicates

were used in each method of extraction and the same leaf material was used to obtain the unsaponified and saponified extracts. The carotenoids obtained from the five F₂ population lines using these two methods were then compared to each other (Figure 3.9).

It was found that saponification significantly reduced amounts of extracted lutein, luteoxanthin and neoxanthin in all lines. Generally, the xanthophylls (except violaxanthin) were affected the most, while the hydrocarbon carotenoids (α -carotene, β -carotene and phytoene) were affected very little or not at all. Therefore, the chemical structure of a compound most likely determines its susceptibility to oxidation and loss during saponification. In fact, the levels of zeaxanthin also appeared to be lower in the saponified extracts than the unsaponified ones in the lines where zeaxanthin was detected using both extraction methods (U/0; B/B, U/0; B/+ and U/U; B/B). Zeaxanthin was not identified in the unsaponified leaf extract of the U/U; B/+ line due to a strong overlap with the neighbouring chlorophyll A peak. This is most likely the reason why no significant differences in zeaxanthin levels were found between the extraction methods. Similarly, antheraxanthin was partially obstructed by the neighbouring chlorophyll B peak and saponification might have actually helped with the identification of this compound. However, no significant differences in the antheraxanthin content were found between the two extraction methods with the exception of the U/U; B/+ line in which significantly higher levels of this xanthophyll were obtained from the saponified extract. Therefore, although antheraxanthin and zeaxanthin might also be affected by saponification, the interference from the neighbouring chlorophyll peaks with much stronger amplitudes does not allow for a proper evaluation.

Interestingly, the extent to which the compounds are affected by saponification may also be dependent on the sample matrix. The U/0; B/B line was the only line with significantly lower levels of violaxanthin and β -carotene in the saponified leaf extracts than the non-saponified ones. This was also the line in which neoxanthin and lutein were affected the most significantly compared with the other lines. Additionally, it was also the only line in which phytoene was lower in the saponified extract although this difference was not found to be significant.

Saponification may be useful for the removal of chlorophylls which obstruct the neighbouring peaks with lower amplitudes. However, if pigment amounts from the saponified extracts are used instead of the unsaponified ones, significant differences can be lost or, in fact, new differences can be discovered. For instance, if neoxanthin obtained from the saponified leaf extract of the U/0; B/B line was compared to the Az reference line, no statistically significant difference would be found (data not shown). On the other hand, when β -carotene from the saponified extracts of the Az and U/U; B/+ lines was compared, a significant decrease was found (data not shown). Therefore, data obtained from saponified samples should be treated with caution and may require additional evaluation.

Effect of saponification on carotenoid extraction

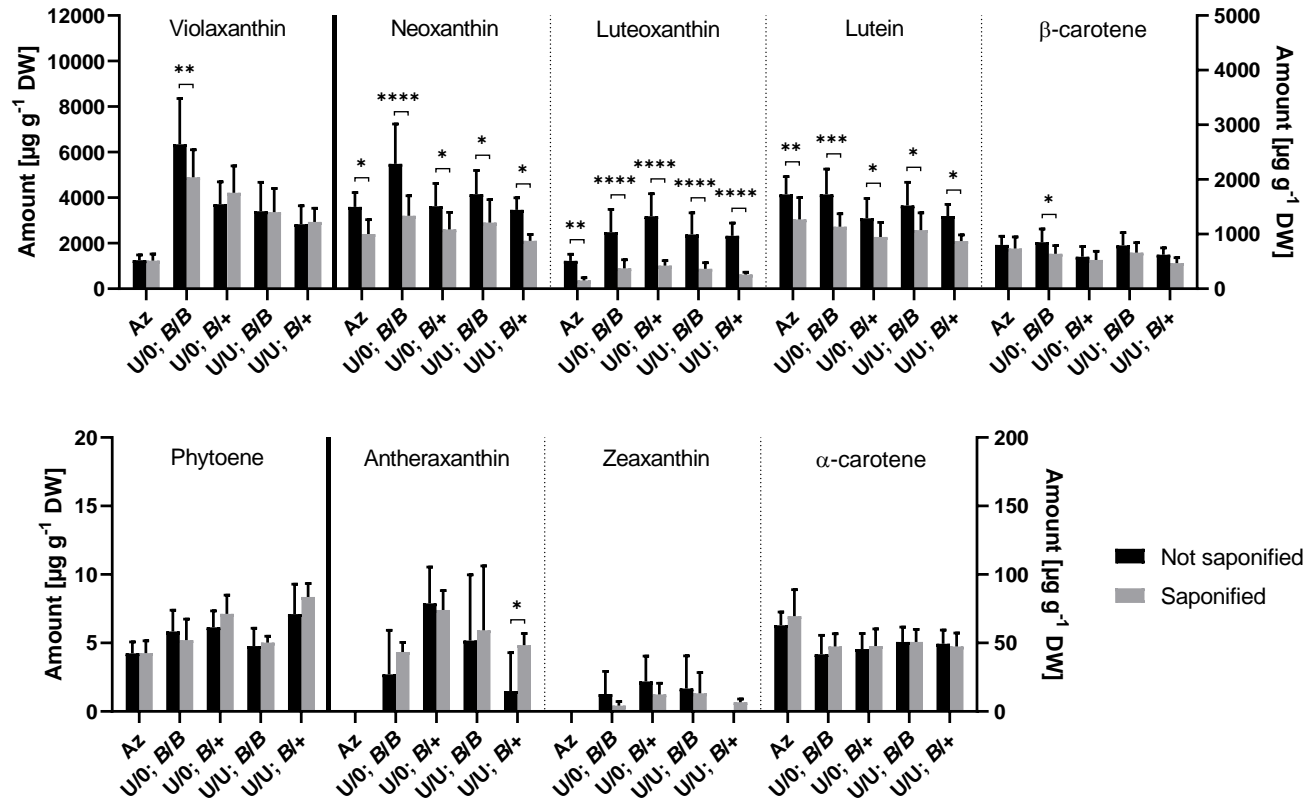


Figure 3.9. Comparison of carotenoids obtained from unsaponified (black bars) and saponified (grey bars) leaf extracts of the F₂ lines. Saponification predominantly reduced the amounts of extracted xanthophylls (neoxanthin, luteoxanthin and lutein) except violaxanthin, which seemed to be mostly unaffected. Hydrocarbon carotenoids (α -carotene, β -carotene and phytoene) were generally unaffected. The sample matrix might also have had an effect since the U/0; B/B line was affected the most. The left y-axes only apply to violaxanthin (top) and phytoene (bottom); the amounts of the remaining compounds are given on the right y-axes. Data are displayed as $\bar{x} \pm \text{SD}$. The effect of saponification on the compounds in each line was analysed using 2-way ANOVA with Sidak's multiple comparisons test. Data normality was validated with Shapiro-Wilk test. The number of biological replicates, N, for each line is provided in Figure 3.8B; * $P < 0.05$, ** $P < 0.01$, *** $P < 0.001$, **** $P < 0.0001$.

3.2.7 Fruit pigment analysis of F₂ population lines

The carotenoids extracted from mature fruit of the F₂ population lines were analysed on the HPLC system similarly to the leaf extracts. From the HPLC chromatograms (Figure 3.10A) it could be seen that the fruit of the Az line primarily accumulated lycopene (peak no. 9), which was responsible for their intensely red colouration (Figure 3.7A). In the U/U; B/B and U/U; B/+ lines the major pigment was β -carotene (peak no. 8), which caused the fruit to appear orange. The ripe fruit of the U/O; B/B and U/O; B/+ lines also contained β -carotene as their major pigment, and therefore they were orange as well. However, these two lines also accumulated some lutein (peak no. 5) and additionally, they were the only lines in which zeaxanthin (peak no. 6) was identified. The fruit of the lines hemizygous for transgenic *CrtR-b2* were lighter in colour than the fruit of the lines homozygous for the transgene because of their much lower levels of β -carotene, as indicated by the smaller absorption units on their HPLC chromatograms.

Quantification of carotenoids was carried out based on the HPLC traces (Figure 3.10B). The fruit pigment profile of the U/U parental line was more similar to the Az line than any other F₂ line. Both of these lines contained very little xanthophylls and lycopene was their major carotenoid. The B/B parental line was more similar to the F₂ lines homozygous for transgenic *CrtR-b2* due to their high levels of α - and β -carotene. On the other hand, the F₂ lines hemizygous for the transgene were the most different from their U/U and B/B parents.

The four transgenic lines were first compared to the Az line and then all F₂ lines were compared to each other to assess statistically significant changes in their pigment levels. Zeaxanthin was only identified in mature fruit of the U/O; B/B and U/O; B/+ lines at 7.3 and 9.4 $\mu\text{g g}^{-1}$ DW, respectively. Although these levels were low overall, they were, respectively, 2.4 and 3.1 times higher than the zeaxanthin levels in mature fruit of the F₁ hybrid no. 1 (3.0 $\mu\text{g g}^{-1}$ DW; Table 3.1). In terms of other xanthophylls, only the U/O; B/B line was found to contain significantly higher levels of violaxanthin, neoxanthin and antheraxanthin in its fruit than the Az line. Although, luteoxanthin was identified in mature fruit of all transgenic lines, only the U/O; B/B and U/U; B/B lines accumulated significantly higher levels compared with the Az reference line. Interestingly, even though none of the F₂ transgenic lines contained similar levels of violaxanthin to the ones found in the fruit of the F₁ hybrid no. 1 (224.2 $\mu\text{g g}^{-1}$ DW), some of the F₂ lines still accumulated substantial proportions of their total carotenoids as xanthophylls. For instance, in the U/O; B/B and U/O; B/+ lines, close to 61% and a little over 32% of the total carotenoids, respectively, were comprised of xanthophylls. In the Az reference line and the two lines homozygous for transgenic *CrtR-b2*, xanthophylls only comprised close to 2% of the total carotenoid content.

The carotenoids of the α -branch of the carotenoid biosynthetic pathway, α -carotene and lutein, were affected differently in the lines hemizygous and homozygous for transgenic *CrtR-b2*. The

levels of α -carotene were significantly lower in the U/0; B/B and U/0; B/+ lines, whereas in the U/U; B/B and U/U; B/+ lines they were significantly higher than in Azygous. Lutein however, was only significantly lower in the U/0; B/B line, whereas the other transgenic lines had similar levels to the Az line. Therefore, the α -branch carotenoids were lower in the lines hemizygous for transgenic *CrtR-b2*, whereas the lines homozygous for transgenic *CrtR-b2* accumulated more α -carotene and similar levels of lutein compared to Azygous. This was not surprising since D'Ambrosio *et al.* (2011) reported that the *CrtR-b2* transcript levels were reduced in all tissues of plants homozygous at the transgene U locus. In fruit, the functional chromoplast-specific lycopene β -cyclase converts δ -carotene to α -carotene. If levels of the hydroxylase decrease, the subsequent hydroxylation of α -carotene to lutein also decreases. The reduced *CrtR-b2* transcript levels also explain the high β -carotene content in the U/U; B/B and U/U; B/+ lines, which essentially makes them very similar to the B/B parental line. The levels of β -carotene were not different between the Az, U/0; B/B and U/0; B/+ lines, indicating that the active hydroxylase allows for the further conversion of carotenoids down the β -branch of the biosynthetic pathway. Compared with Azygous, the levels of phytoene and lycopene were significantly reduced in all transgenic lines. The largest decrease was recorded in the U/0; B/B line in which phytoene and lycopene were, respectively, 78 and 2 500 times lower than in the Az line. Additionally, the total carotenoid content in the U/0; B/B line was almost 17 times lower than in Azygous. Interestingly, in the U/U; B/B line phytoene and lycopene were, respectively, 3.6 and 50 times lower than in the Az line, yet the total carotenoid levels in these lines were not different. Therefore, the low levels of precursors do not necessarily coincide with low total carotenoid levels.

Finally, the fruit levels of α -tocopherol (vitamin E) were significantly lower in the U/0; B/B and U/0; B/+ lines than the Az line, whereas in the U/U; B/B and U/U; B/+ lines, α -tocopherol was significantly higher and not different, respectively. However, the U/0; B/B and U/0; B/+ lines contained higher levels of α -tocopherol (143.3 and 151.6 $\mu\text{g g}^{-1}$ DW, respectively) than total carotenoids (138.2 and 133.6 $\mu\text{g g}^{-1}$ DW, respectively). In comparison, in the Az, U/U; B/B and U/U; B/+ lines, the ratios of total carotenoids to α -tocopherol were 9:1, 7:1 and 4:1, respectively. This is significant as carotenoids and tocopherols are stored within specific sub-chromoplast compartments. Therefore, the chromoplast structure may change or adapt in response to the altered pigment composition. This in turn may affect the storage capacity of the chromoplasts and their mechanism of carotenoid sequestration. Alternatively, the chromoplast structure and its compartments may not be affected by the change in carotenoid composition but the xanthophylls may be adopting different orientations within the storing membranes than the hydrocarbon carotenoids, such as lycopene or β -carotene. This may allow for a greater accommodation of α -tocopherol without a concurrent increase in total carotenoid content.

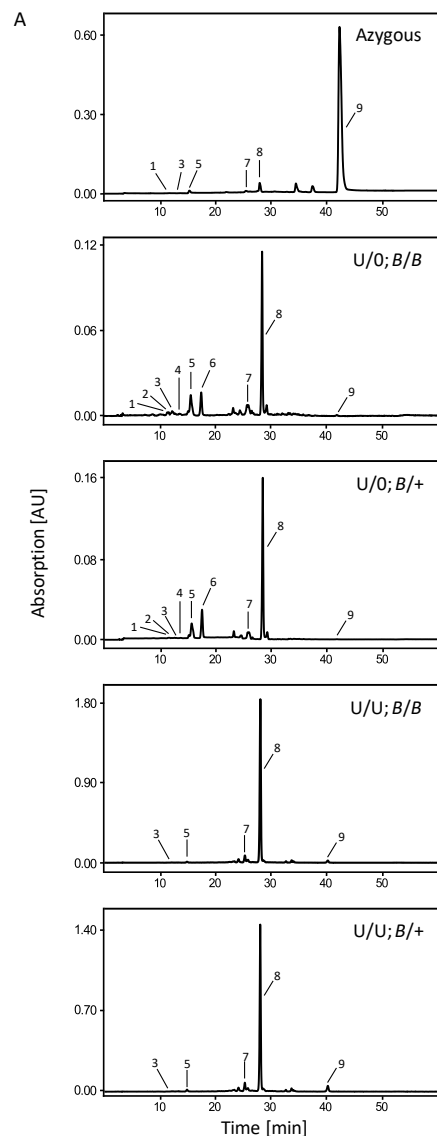


Figure 3.10. (A) HPLC chromatograms of mature fruit extracts of the indicated F₂ population lines. 1 – violaxanthin, 2 – neoxanthin, 3 – luteoxanthin, 4 – antheraxanthin, 5 – lutein, 6 – zeaxanthin, 7 – α-carotene, 8 – β-carotene, 9 – lycopene. **(B)** Quantification of isoprenoids and α-tocopherol from mature fruit of the F₂ population lines. The reported values were used to obtain total carotenoids (CAR; α-tocopherol not included) and total xanthophylls (XAN). The amounts of the compounds are reported as μg g⁻¹ DW. The data are presented as the mean of N biological replicates ± SD; nd – not detected. The pigments from the four transgenic lines (U/O; B/B, U/O; B/+, U/U; B/B and U/U; B/+) were compared to the Azygous line using one-way ANOVA with Dunnett’s multiple comparison test or Kruskal-Wallis test with Dunn’s multiple comparison test as appropriate; green shading indicates significant increases, red – significant decreases. Additionally, multiple comparisons one-way ANOVA with Tukey’s post-hoc test was carried out to compare the F₂ population lines to each other; compact letter display was used to indicate homogeneous subsets. Data normality was validated with Shapiro-Wilk test. Significant results are reported for P < 0.05. Parental lines (U/U and B/B) are included for comparison only.

3.2.8 Identification of zeaxanthin on different platforms

When attempting to generate a new source of a particular product, it is important to confirm that the accumulated compound is indeed the desired one. Therefore, in order to obtain an independent line of evidence for the compound's identity, it is important to verify the product on a different platform from the one on which it was initially analysed.

Thin-layer chromatography (TLC) was selected as an alternative method to confirm the identity of zeaxanthin. TLC is a quick and simple technique to carry out and requires less solvents than HPLC. Plants containing zeaxanthin in their ripe fruit were first identified on the HPLC system (Figure 3.11A). In fact, all plants belonging to either the U/0; B/B or U/0; B/+ line were found to contain zeaxanthin. Based on the HPLC-generated zeaxanthin standard curve, the amounts of zeaxanthin were found to lay between 2.6 and 14.1 $\mu\text{g g}^{-1}$ DW in the U/0; B/B line and 6.5 and 16.6 $\mu\text{g g}^{-1}$ DW in the U/0; B/+ line. Three plants with the highest and most consistent zeaxanthin content were analysed by TLC (Figure 3.11B). The fruit extracts of these three plants were run along a commercial zeaxanthin standard and the fruit extract of the Azygous reference line.

At the end of the analysis, two bands were visible on the line containing the zeaxanthin standard. The top, bright orange band (black triangle in Figure 3.11B) was found to correspond to the zeaxanthin standard (left, top and middle chromatograms in Figure 3.11C). Bands with the R_f values corresponding to the zeaxanthin standard, were also identified in the three transgenic plants but not in Azygous. These bands were scratched off the plate and subsequently analysed on the HPLC system. This analysis confirmed that a compound of the spectrum characteristic of zeaxanthin was not identified in the Az line (bottom left chromatogram in Figure 3.11C). On the other hand, the three transgenic plants were found to contain a compound of the same retention time (RT) and spectrum as the zeaxanthin standard, confirming the identity of this compound (right chromatograms in Figure 3.11C). Therefore, TLC can be used as an alternative and quick method for identification of zeaxanthin in tomato fruit extracts.

The second band on the line containing the zeaxanthin standard (empty triangle in Figure 3.11B) was not identified in Azygous nor in any of the transgenic plants. This band was not analysed further but it could be a degradation or oxidation product of zeaxanthin. It is also possible that this band could contain some impurities. When analysing this particular zeaxanthin standard, a small peak was visible next to the main zeaxanthin peak (top left chromatogram in Figure 3.11C). It is not uncommon for carotenoid standards to contain other compounds, depending on the source the standard is derived from. The purity of zeaxanthin analytical standards based on HPLC assay is typically reported as 95% or above; therefore, the presence of small amounts of impurities is expected. It is also possible that certain impurities may not be detected by HPLC but they can be more readily identified on other platforms such as TLC.

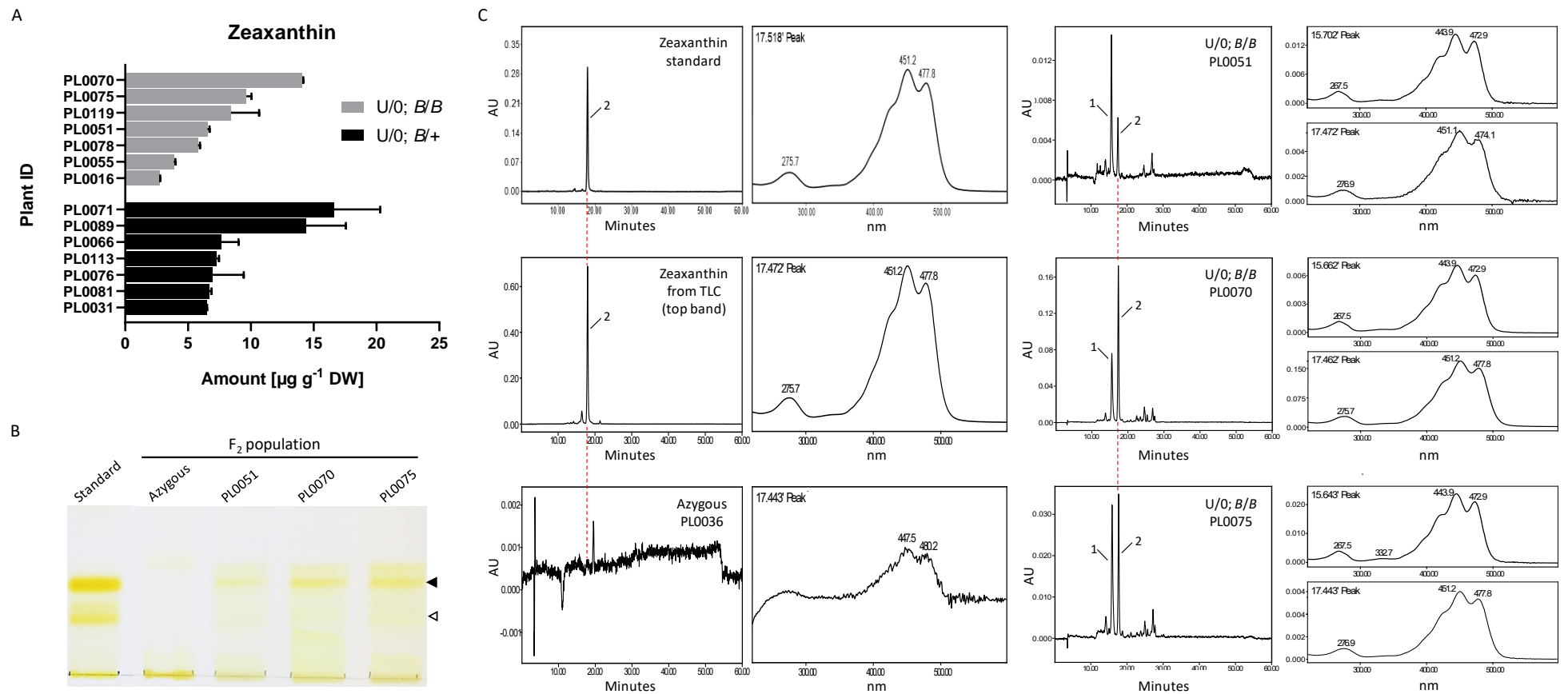


Figure 3.11. (A) Quantification of zeaxanthin from mature fruit of the *U/O; B/B* (grey bars) and *U/O; B/+* (black bars) lines on the HPLC system. The data are presented as the mean of three technical replicates \pm SD. (B) Fruit extracts from F_2 population lines (Azygous and *U/O; B/B*) were resolved on a TLC plate against the zeaxanthin standard. The mobile phase was optimised for xanthophyll separation with hydrocarbon carotenoids running with the solvent front and xanthophylls remaining closer to the origin. Only the bottom part of the plate is shown. The bands with the R_f values corresponding to the zeaxanthin standard (black arrowhead) were scratched off the plate, extracted and analysed on the HPLC system. The empty arrow indicates a possible oxidation/degradation product of zeaxanthin. (C) HPLC analysis of the extracted bands. The spectra of the identified peaks are shown next to the chromatograms. The same zeaxanthin standard as used for TLC was run on the HPLC system for comparison (top, left). Zeaxanthin was not identified in the Azygous line as no clear zeaxanthin peak was present. However, zeaxanthin was identified in the three *U/O; B/B* plants. The expected position of the zeaxanthin peak is indicated by the red dotted line. All spectra were extracted at 450 nm; 1 – lutein (15.7' Peak), 2 – zeaxanthin (17.5' Peak).

3.2.9 Analysis of gene combinations in leaves and fruit of F₂ population lines

In order to better understand how the different combinations of *S. galapagense* *CYC-B* allele and transgenic *CrtR-b2* affected the pigment profiles of the leaf and fruit tissues of the F₂ lines, the lines sharing the same zygosity of one of these genes were compared with each other. In total, four comparisons between the transgenic lines were made. In the first analysis, the U/0; B/B line was compared with the U/0; B/+ line and statistically significant increases and decreases in pigment levels in the U/0; B/B line were discovered. Since this first comparison involved two lines which were both hemizygous for transgenic *CrtR-b2*, it specifically allowed to examine the effect of *S. galapagense* *CYC-B* zygosity on pigments in plants hemizygous for the transgene. The second comparison was made between the U/U; B/B and U/U; B/+ lines. This analysis allowed to examine the effect of *S. galapagense* *CYC-B* zygosity in plants homozygous for the transgene. The third comparison was made between the U/0; B/B and U/U; B/B lines, thus allowing to examine the effect of the transgene zygosity in plants homozygous for *S. galapagense* *CYC-B* allele. The last comparison was made between the U/0; B/+ and U/U; B/+ lines, which allowed to assess the effect of the transgene zygosity in plants heterozygous for *S. galapagense* *CYC-B* allele. The pigments from the leaves (Figure 3.12A) and fruit (Figure 3.12B) of the four transgenic lines were compared in this manner. This analysis helped to establish the best combination of the genes for accumulation of zeaxanthin in mature fruit of the transgenic lines.

The most important conclusion of the above analysis was that *S. galapagense* *CYC-B* allele and transgenic *CrtR-b2* conferred different pigment profiles depending on whether their particular combination appeared in the leaf or fruit tissue. For instance, the total carotenoid levels were higher in leaves of the plants homozygous for *S. galapagense* *CYC-B* when the transgene was found in a hemizygous rather than homozygous state. In the fruit however, the same gene combination had quite a different effect. In plants homozygous for *S. galapagense* *CYC-B* allele, the total carotenoid content was higher in fruit of the plants which were homozygous for the transgene than the ones in which the transgene was in a hemizygous state. In fact, the total carotenoid levels were also higher in fruit of the plants homozygous for transgenic *CrtR-b2* than the hemizygous ones given that they were heterozygous for *S. galapagense* *CYC-B*. In the leaves however, the situation was reversed. This is, somehow, not a surprising result as the carotenoid biosynthetic pathway is regulated differently in leaves and fruit of tomato plants. Therefore, the same steps in the pathway can be catalysed by functionally similar enzymes, which are encoded by different, yet related, tissue-specific genes. However, the specific differences that occur in these two tissues are important and need to be thoroughly analysed. This is because the effect of a particular gene combination on the plant photosynthetic performance should be taken into consideration; especially when it promotes the accumulation of a desired compound in the fruit.

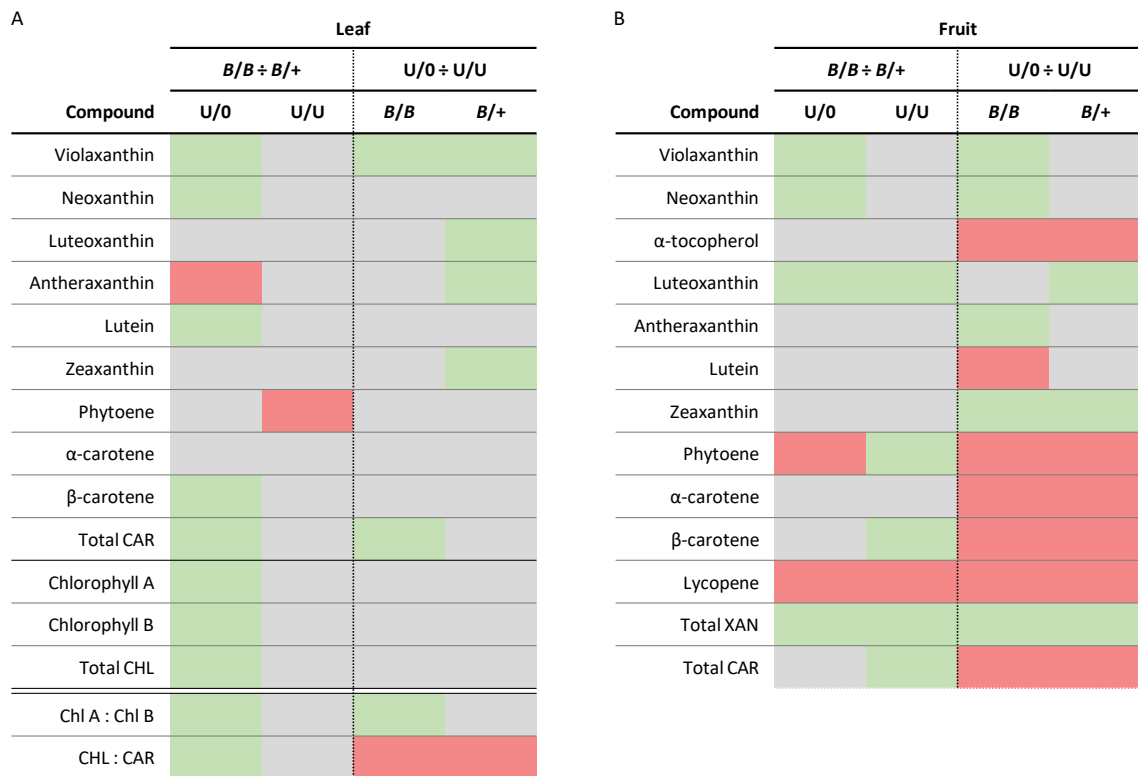


Figure 3.12. Effects of different gene combinations on leaf (A) and fruit (B) pigment profiles. The first column shows the comparison between the *U/0; B/B* and *U/0; B/+* lines; thus it specifically examines the effect of *S. galapagense CYC-B* zygosity in plants hemizygous for transgenic *CrtR-b2*. The second column compares the effect of *S. galapagense CYC-B* zygosity in plants homozygous for transgenic *CrtR-b2* (*U/U; B/B* over *U/U; B/+*). The third column compares the effect of transgene zygosity in plants homozygous for *S. galapagense CYC-B* (*U/0; B/B* over *U/U; B/B*). The last column compares the effect of transgene zygosity in plants heterozygous for *S. galapagense CYC-B* (*U/0; B/+* over *U/U; B/+*). The analysis was carried out using unpaired t-test (two-tailed) or Mann-Whitney test (two-tailed) as appropriate. Data normality was validated with Shapiro-Wilk test. Green shading indicates significant increases, red – significant decreases, grey – no significant changes between the lines. Significant results are reported for $P < 0.05$.

The first two comparisons were performed to examine if the change in *S. galapagense CYC-B* zygosity affected the accumulation of pigments in lines which shared the same transgene zygosity. In leaves of the lines hemizygous for the transgene (*U/0*), some xanthophylls (lutein, neoxanthin and violaxanthin), β -carotene and also the total carotenoid levels were higher in the plants homozygous for *S. galapagense CYC-B* (*B/B*) than the heterozygous ones (*B/+*). This is somehow a surprising result because *S. galapagense CYC-B* is a chromoplast-specific β -cyclase with highest activity in fruit and flowers of tomato plants. These data suggest, however, that this enzyme is also active in leaf chloroplasts. Moreover, the double dose of the cyclase (*B/B* against *B/+*) correlates with significant increases of some carotenoids and the chlorophylls. However, a strikingly different result was observed in leaves of the plants homozygous for the transgene (*U/U*). In these plants the change in *S. galapagense CYC-B* zygosity did not result in statistically significant differences between the lines sharing the same transgene zygosity. In other words, the *U/U; B/B* and *U/U; B/+* lines were statistically not different. This stands in contradiction to what was seen in the *U/0* lines. It is impossible to infer the reason why this happens without a detailed analysis of gene expression in the leaves of the transgenic lines. However, a possible

explanation may be linked to the reduced *CrtR-b2* transcript levels in plants homozygous for the transgene compared with the hemizygous ones (D'Ambrosio *et al.*, 2011). Firstly, the reduction in hydroxylase activity may limit the flux in the pathway beyond its point of action. Secondly, the production of xanthophylls requires a coordinated action of the cyclase and the hydroxylase. Perhaps due to the lower metabolic flux in plants homozygous for the transgene, the change in *S. galapagense* *CYC-B* zygosity only has an effect in plants hemizygous for transgenic *CrtR-b2*.

In fruit of the lines hemizygous for the transgene (U/O), the xanthophylls from the end of the pathway (luteoxanthin, neoxanthin and violaxanthin) were higher in the plants homozygous for *S. galapagense* *CYC-B* (B/B) than the heterozygous ones (B/+), whereas the carotenes from the beginning of the pathway (lycopene and phytoene), were lower. Therefore, the double dose of the cyclase (B/B against B/+) promoted the accumulation of the end of the pathway xanthophylls at the expense of phytoene and lycopene. On the other hand, in the lines homozygous for the transgene (U/U), the double dose of the cyclase (B/B against B/+) promoted the accumulation of β -carotene at the expense of lycopene. Therefore, in the fruit, the change in *S. galapagense* *CYC-B* zygosity resulted in statistically significant differences between the lines sharing the same transgene zygosity, whether U/O or U/U. This was different from what was found in the leaves in which the change in *S. galapagense* *CYC-B* zygosity did not affect pigment accumulation in the lines homozygous for the transgene. Since *S. galapagense* *CYC-B* is a fruit ripening-specific gene, its transcription is tightly regulated in the tissue it is expressed in. Therefore, its activity in the fruit may be more sensitive to changes in gene dosage, which could explain the differences between these two tissues. The high β -carotene content in fruit of the U/U lines was most likely caused by the reduced *CrtR-b1* and *CrtR-b2* transcript levels (D'Ambrosio *et al.*, 2011); however, the increased activity of the cyclase could explain why β -carotene was even higher in the plants homozygous for *S. galapagense* *CYC-B* than the heterozygous ones. Perhaps even with a reduced flux down the carotenoid biosynthetic pathway, the change in *S. galapagense* *CYC-B* zygosity has an effect due to the presence of specific regulatory mechanisms in the fruit. Interestingly, lycopene was decreased in both lines sharing the same transgene zygosity. This further supports the observation that in the fruit, a double dose of the cyclase increases its activity.

The last two comparisons were carried out to assess if the change in transgene zygosity affected pigment accumulation in plants sharing the same *S. galapagense* *CYC-B* zygosity. In leaves, the change in transgene zygosity affected carotenoid accumulation without altering the chlorophyll content in both lines sharing the same *S. galapagense* *CYC-B* zygosity, whether B/B or B/+. Generally, the presence of the transgene in a hemizygous state promoted the accumulation of xanthophylls; however the type of the stored xanthophyll depended on *S. galapagense* *CYC-B* zygosity. The plants homozygous for *S. galapagense* *CYC-B* preferentially accumulated

violaxanthin, which solely contributed to the increased carotenoid content, while the plants heterozygous for *S. galapagense* *CYC-B* accumulated more of the intermediary xanthophylls, such as zeaxanthin and antheraxanthin without a concurrent increase in total carotenoids. These results imply that the presence of the transgene in a hemizygous state with *S. galapagense* *CYC-B* in a heterozygous state is the best gene combination for the accumulation of zeaxanthin in leaves. However, if violaxanthin is preferred, the combination of the transgene in a hemizygous state with *S. galapagense* *CYC-B* in a homozygous state should be used.

In fruit of the lines sharing the same *S. galapagense* *CYC-B* zygosity, the accumulation of the β -branch xanthophylls was favoured in plants hemizygous for the transgene, albeit at the expense of other carotenoids, resulting in a lower total carotenoid content. In both lines, the carotenes from the beginning of the carotenoid biosynthetic pathway (phytoene, lycopene and β -carotene) and also all carotenoids from the α -branch of the pathway (α -carotene and lutein) were higher in plants homozygous for the transgene. Therefore, similarly to what was found in leaves, the transgene in a homozygous state would not be chosen if the accumulation of xanthophylls was desired. Instead, the lines hemizygous for the transgene and homozygous for *S. galapagense* *CYC-B* need to be selected to achieve greater levels of xanthophylls in the fruit. However, if an increased accumulation of zeaxanthin is specifically required, lines hemizygous for the transgene and heterozygous for *S. galapagense* *CYC-B* should be used instead.

3.2.10 Sub-chromoplast fractionation of F₂ population lines

In order to identify the sites of deposition of the previously unencountered xanthophylls in the plastids and to examine if their presence has affected the sequestration of other carotenoids, fractionation at a sub-chromoplast level was carried out. The chromoplasts were isolated from fruit of the five F₂ population lines and subsequently separated into fractions on a discontinuous sucrose gradient. In the first experiment, the U/O lines with different zygositys of *S. galapagense* *CYC-B* were compared to the Azygous line (Figure 3.13). In the second experiment, the U/U lines with different zygositys of *S. galapagense* *CYC-B* were compared to Azygous (Figure 3.14). Each sucrose gradient contained two distinct sectors. The first one comprised the first two fractions (F1 and F2) from the top of the gradient. These fractions contain free plastoglobuli (Nogueira *et al.*, 2013) which are plastid lipoprotein particles involved in lipid (e.g. tocopherol) synthesis and metabolism. The second sector was much wider and spanned fractions 12 to 26 (F12 – F26). These fractions contain membrane compartments of the chromoplasts (Nogueira *et al.*, 2013). In all lines, this sector also appeared to contain crystal-like structures. Following the collection of fractions from the sucrose gradients, these were extracted and analysed on the UPLC system in order to identify their contents. The distribution of each compound across the gradient was plotted on the same graph for the lines analysed during the same fractionation experiment.

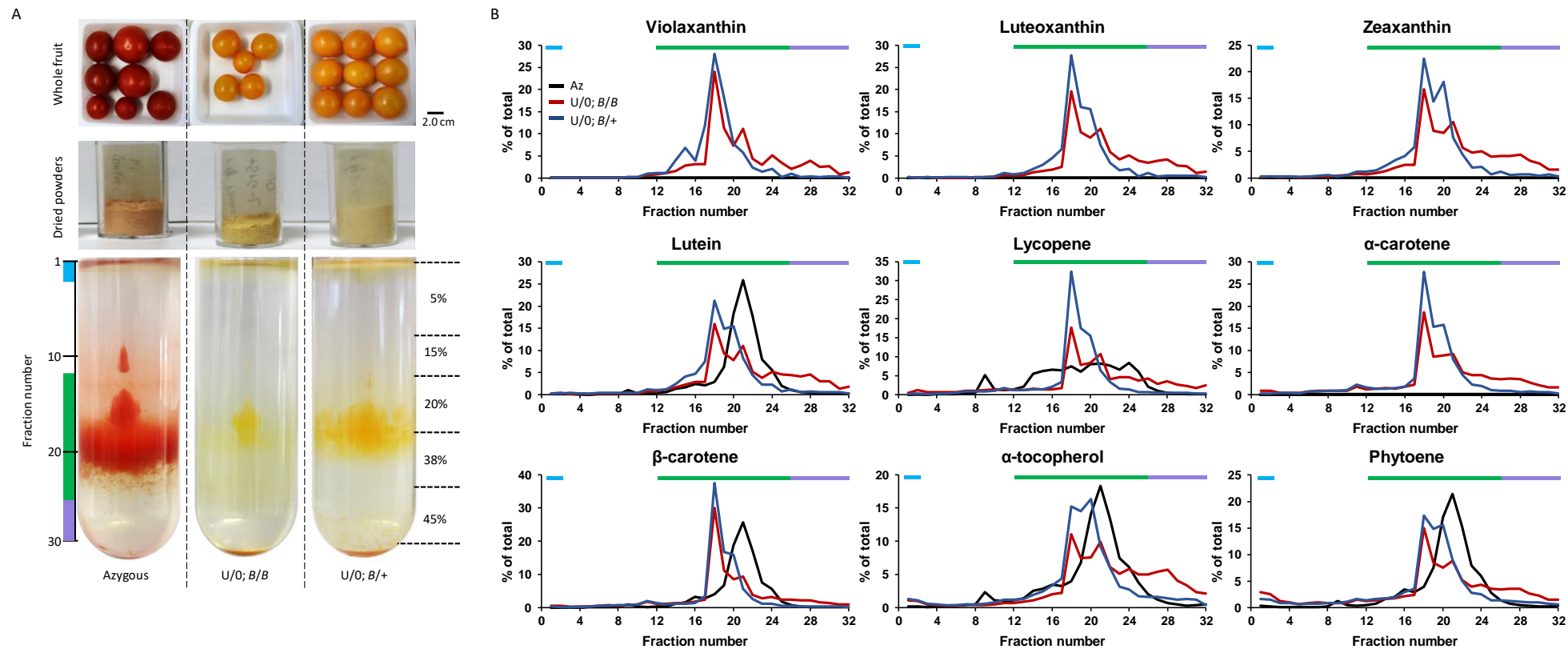


Figure 3.13. Sequestration of carotenoids and α -tocopherol in sub-plastidial compartments of the Azygous, U/O; B/B and U/O; B/+ fruit. **(A)** Separation of sub-chromoplast compartments on a discontinuous sucrose gradient. The numbering of 1 ml fractions and layering of the sucrose gradient are indicated on the left and right sides of the tubes, respectively. The blue stripe on the fraction number scale indicates the layer of free plastoglobuli, green – the layer of membranes and crystals, violet – stromal proteins. Whole fruit and freeze-dried powders of each line are shown above their corresponding sucrose gradients for comparison. Fruit sizes are indicated by the black marker. **(B)** Distribution of compounds across the sucrose gradients as analysed by UPLC. The content of compounds in each sub-chromoplast fraction is expressed as a percentage relative to the total content of a given compound in the fractionated sample. The sub-chromoplast compartments are indicated by the same colours as in **(A)**. No α -carotene was detected in the Azygous line due to a strong overlap with the lycopene peak.

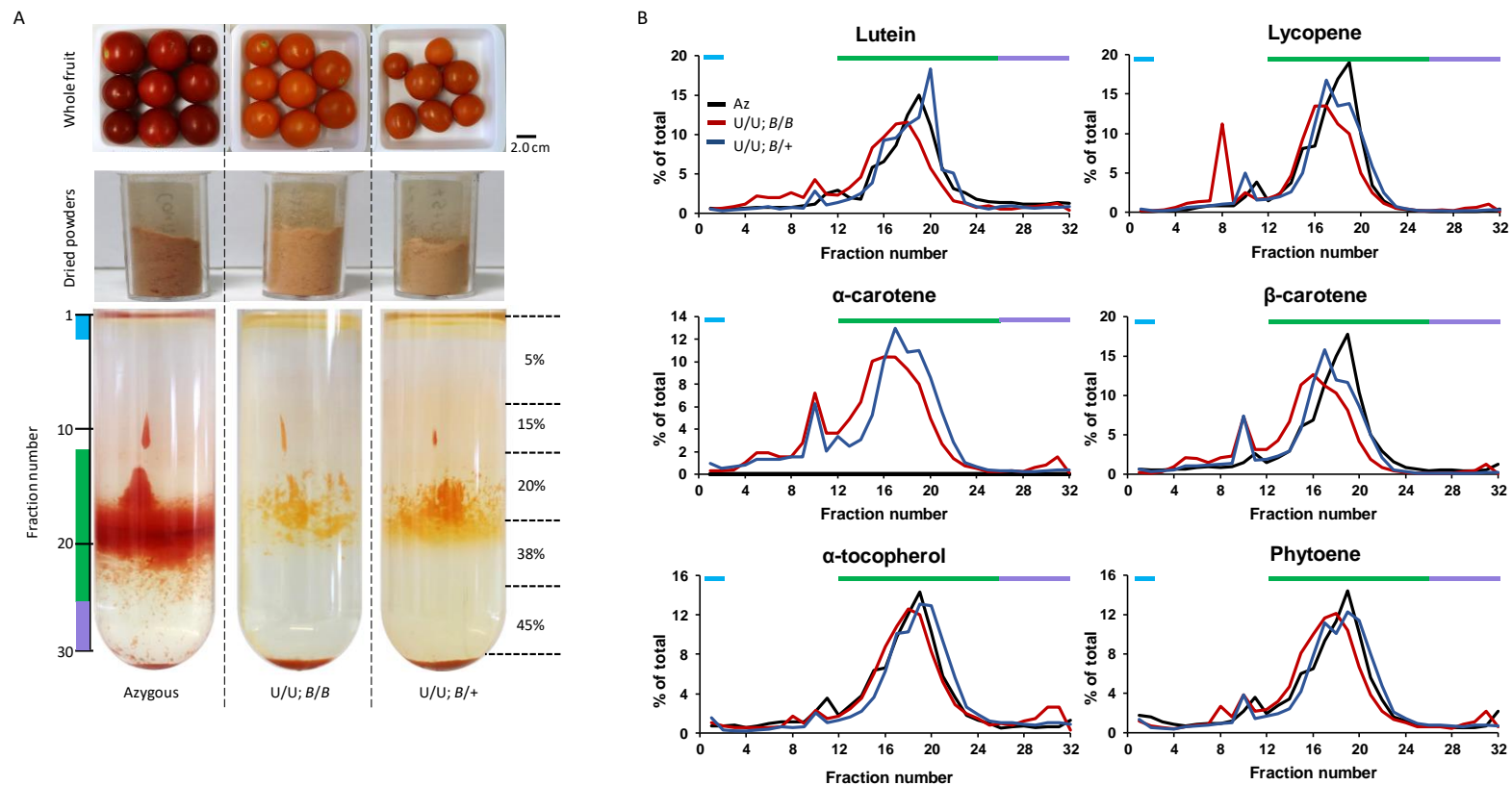


Figure 3.14. Sequestration of carotenoids and α -tocopherol in sub-plastidial compartments of the Azygous, U/U; B/B and U/U; B/+ fruit. **(A)** Separation of sub-chromoplast compartments on a discontinuous sucrose gradient. The numbering of 1 ml fractions and layering of the sucrose gradient are indicated on the left and right sides of the tubes, respectively. The blue stripe on the fraction number scale indicates the layer of free plastoglobuli, green – the layer of membranes and crystals, violet – stromal proteins. Whole fruit and freeze-dried powders of each line are shown above their corresponding sucrose gradients for comparison. Fruit sizes are indicated by the black marker. **(B)** Distribution of compounds across the sucrose gradients as analysed by UPLC. The content of compounds in each sub-chromoplast fraction is expressed as a percentage relative to the total content of a given compound in the fractionated sample. The sub-chromoplast compartments are indicated by the same colours as in **(A)**. No α -carotene was detected in the Azygous line due to a strong overlap with the lycopene peak.

The major difference between the sucrose gradients of the *Azygous*, *U/0; B/B* and *U/0; B/+* lines was the colour (Figure 3.13A). Lycopene, which was identified as the major carotenoid in fruit of the *Az* line (Figure 3.10A), was also responsible for the intense red colour of the sucrose gradient of this line. The two transgenic lines contained little lycopene in comparison with the *Az* line and the orange colouration of their sucrose gradients was caused by the presence of β -carotene and the xanthophylls. All three lines contained a visible layer of plastoglobuli of a similar depth. They also contained crystal-like structures in the sector where the membrane structures had settled. However, this sub-compartment appeared to be wider in the *Az* line than in the two transgenic lines. Following analysis of the collected fractions on the UPLC system, the distribution of compounds across the gradient was found to be very similar between the two transgenic lines (Figure 3.13B). In fact, these lines were sequestering the identified compounds mainly into the membrane sub-compartments settled between F17 and F22 with two major peaks appearing at F18 and either F20 or F21. However, in the *Az* line, the same compounds were found over a wider region. Specifically, the greatest proportions of lutein, β -carotene, α -tocopherol and phytoene were found between F18 and F26 with a single peak at F21, whereas lycopene was spread more evenly between F13 and F26. Finally, the transgenic lines contained higher proportions of α -tocopherol and phytoene in the free plastoglobuli than the *Az* line. In summary, these data suggest that the carotenoids are mainly found in the membranes, but in the *U/0; B/B* and *U/0; B/+* lines they appear to be more localised.

In the second experiment, the sectors containing free plastoglobuli at the top of the sucrose gradient and the crystal-like structures in the middle of it, were also visible (Figure 3.14A). The gradient of the *Az* line was red, whereas the gradients of the *U/U; B/B* and *U/U; B/+* lines were orange. Additionally, a small, crystal-like structure in the colour of the middle section was clearly visible around F10 in all lines. A similar aggregate was also present in the *Az* and *U/0; B/+* lines (Figure 3.13A) and possibly the *U/0; B/B* line, as indicated by a small increase in the contents of α - and β -carotene in F11 (Figure 3.13B). However, the aggregates in the *U/0; B/B* and *U/0; B/+* lines were much smaller than the ones present in the *U/U; B/B* and *U/U; B/+* lines (Figure 3.14A). Following the UPLC analysis of the fractions, these aggregates were found to mostly contain lycopene, α - and β -carotene (Figure 3.14B). Additionally, the *U/U; B/B* and *U/U; B/+* lines were found to sequester carotenoids similarly to the *Az* line. All carotenoids were deposited in the membrane sub-compartments between F14 and F24. The *Az*, *U/U; B/B* and *U/U; B/+* lines also contained similar proportions of α -tocopherol and phytoene in the plastoglobuli.

Collectively, these data suggest that the *U/U; B/B* and *U/U; B/+* lines sequester carotenoids similarly to the *Az* plants, whereas the *U/0; B/B* and the *U/0; B/+* lines deposit carotenoids in the membranes as well, but these seem to be targeted to particular compartments.

3.2.11 Analysis of primary metabolites of F₂ population lines

The changes to carotenoid deposition at the sub-cellular level imply that perturbations beyond the carotenoid biosynthetic pathway had occurred in the transgenic lines. Therefore, metabolite profiling of mature fruit of the five F₂ population lines was carried out in order to assess the global effects on metabolism. Close to 150 metabolites were identified, quantified relative to the internal standard and compared between the lines. Additionally, the metabolite profiles of

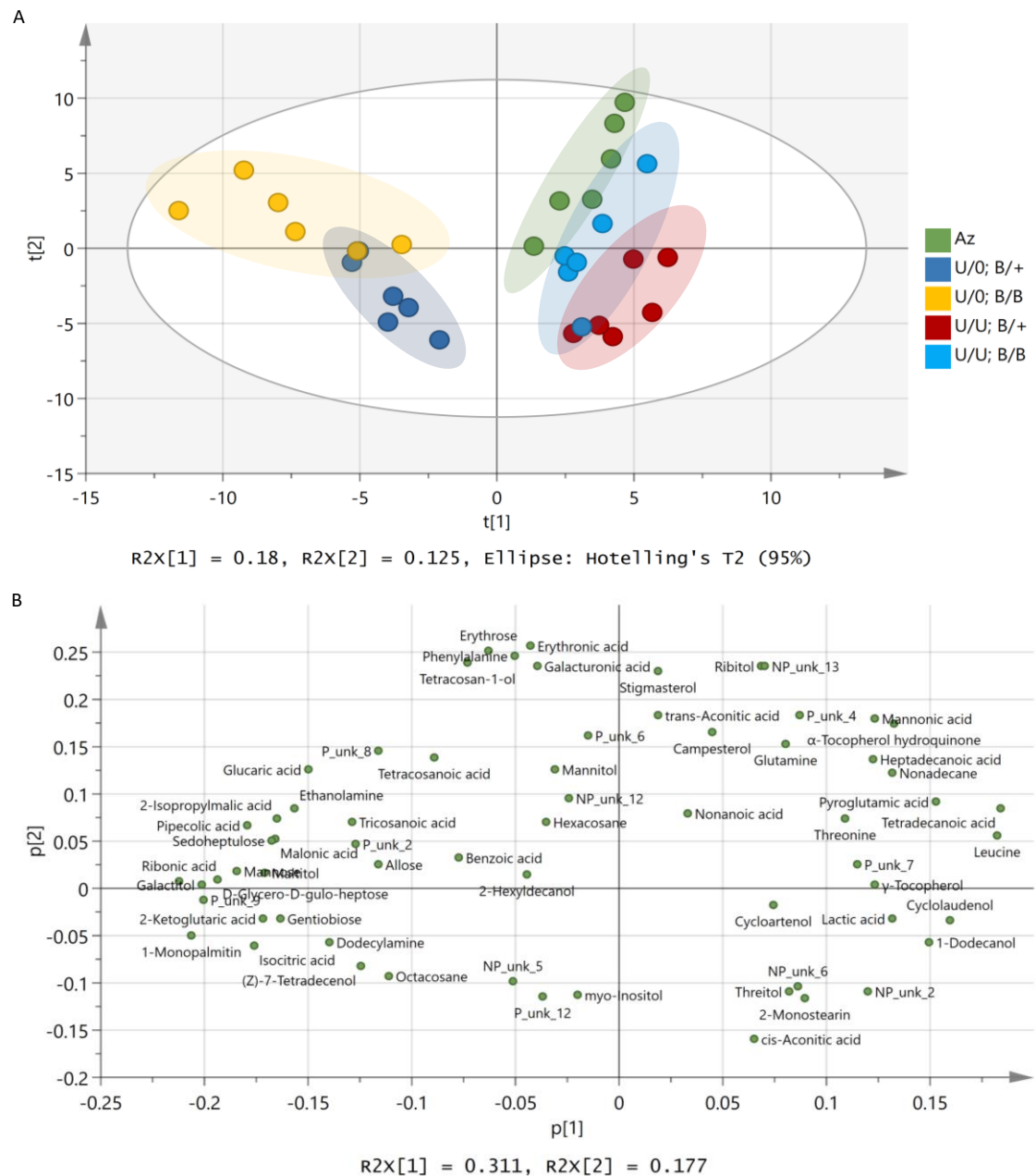


Figure 3.15. Principal component analysis (PCA) of the metabolites identified by GC-MS analysis of polar and non-polar extracts from ripe fruit of the indicated lines. **(A)** Score scatter plot illustrating clustering of the lines along the direction of maximum variance in the data (the first principal component, $t[1]$) and the second major source of variation (the second principal component, $t[2]$) orthogonal to the first. Shaded areas indicate 95% confidence regions. **(B)** Loading scatter plot of the first two principal components ($p[2]$ against $p[1]$) indicating the metabolites, which force separation of the lines. Only the compounds found to be significantly different between the five lines were included on the plot. The data were analysed using one-way ANOVA with Fisher's Least Significant Difference (LSD) post-hoc test and the significance was assessed based on False Discovery Rate (FDR) adjusted p -values ($FDR < 0.05$). Six biological replicates were used per line.

the U/0; B/B line, the line accumulating the highest absolute amounts of the xanthophylls, and the Az reference line were compared to assess the effects of increased levels of xanthophylls on other metabolites in tomato fruit.

Polar and non-polar fruit extracts of the Az line and the four transgenic lines (U/0; B/B, U/0; B/+, U/U; B/B and U/U; B/+) were analysed by gas chromatography-mass spectrometry (GC-MS). Multivariate analysis of the identified metabolites was carried out using principal component analysis (PCA) to assess the overall variance amongst the tested lines (Figure 3.15A). The analysis showed that all five lines formed distinctive clusters. However, the U/0; B/B and U/0; B/+ lines were found to group closer together, whereas the Az, U/U; B/B and U/U; B/+ lines formed a second distinctive cluster and separated away from the U/0; B/B and U/0; B/+ lines. The loading scatter plot indicated that the separation of the U/0; B/B and U/0; B/+ lines was driven

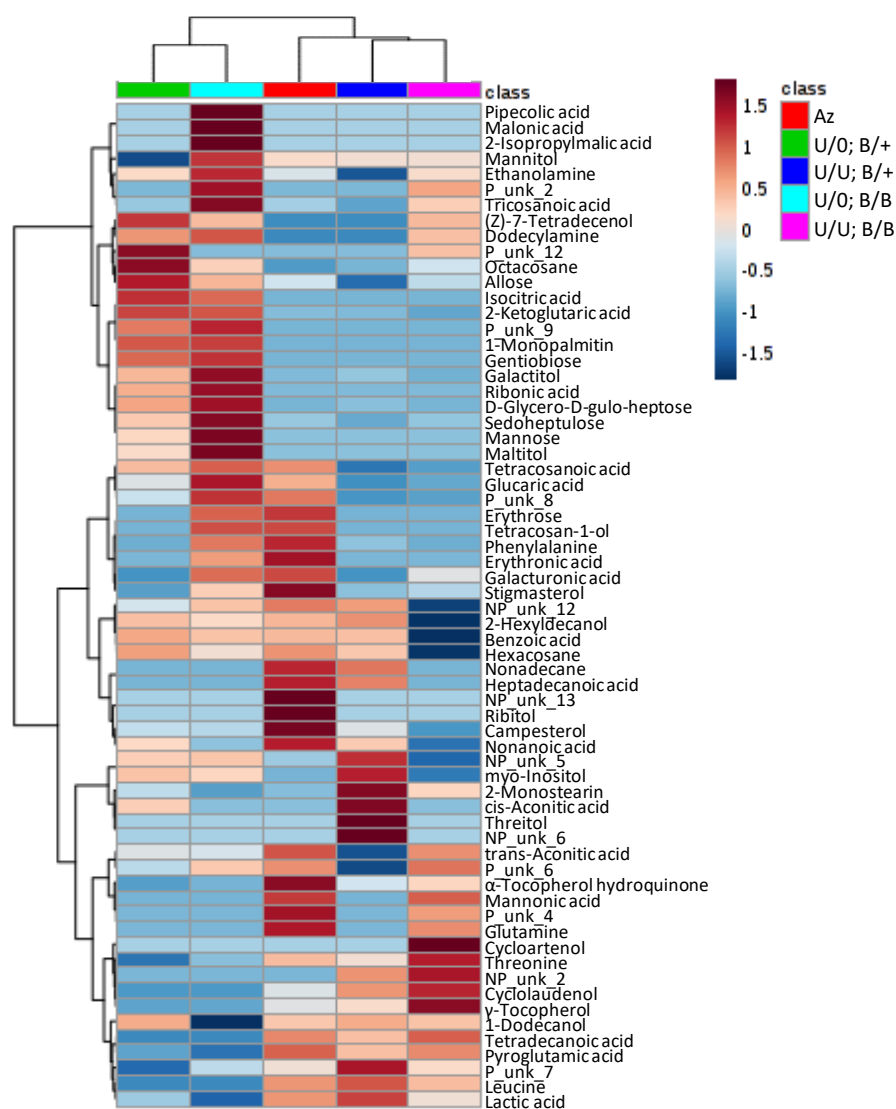


Figure 3.16. Heat map comparison of the 65 metabolites found to be significantly different between the five F₂ lines. The map identifies compounds which are unusually high (red) or low (blue) in fruit of the tested lines. Distinctive clustering of the lines based on the presence of metabolites is apparent. The lines were compared using one-way ANOVA with Fisher's Least Significant Difference (LSD) post-hoc test. The obtained *p*-values were adjusted for the False Discovery Rate (FDR) and only metabolites with FDR < 0.05 were reported as significant. Six biological replicates were used per line.

by ribonic acid, 1-monopalmitin, galactitol, an unknown polar compound (P_unk_9), D-glycero-D-gulo-heptose, mannose, pipercolic acid, isocitric acid and 2-ketoglutaric acid (Figure 3.15B). The separation of the Az, U/U; B/B and U/U; B/+ lines was driven by tetradecanoic acid, leucine, cyclolaudenol, pyroglutamic acid, 1-dodecanol, α -tocopherol hydroquinone and lactic acid.

The five lines were compared, and 65 metabolites were found to be significantly different between them. The levels of the significantly altered metabolites were compared and displayed in the form of a heat map to indicate the compounds with increased or decreased levels compared to the other lines (Figure 3.16). This comparison showed that the U/O; B/B and U/O; B/+ lines had similarly increased compounds and clustered together, whereas the U/U; B/B and U/U; B/+ lines were more similar and clustered together with the Az reference line.

In order to better understand the changes in metabolite composition that arose in the fruit of the xanthophyll-accumulating tomato, the U/O; B/B line was compared to the Az reference line and the changes were visualised onto a simplified display of the major biochemical pathways (Figure 3.17). Although the compounds driving the separation of the two lines (Figure 3.15B) were not associated with the same biochemical pathway, they could be assigned to six distinctive groups: sugars and their derivatives, phytosterols, fatty acids and their derivatives, the tricarboxylic acid (TCA) cycle compounds, amino acid derivatives and geranylgeranyl-pyrophosphate (GGPP) derivatives. Generally, levels of certain sugars (for example sucrose and mannose) and their derivatives (for example maltitol and gluconic acid) were higher in the transgenic U/O; B/B line than the Az reference line. Phytosterols (stigmaterol, campesterol and cyclolaudenol) were lower in the U/O; B/B line than Az. Next, fatty acids and their derivatives (hydrocarbons and fatty alcohols) were generally lower in the U/O; B/B line, however tricosanoic acid, octacosane and (Z)-7-tetradecenol were higher. Aconitic acid, an intermediate in the TCA cycle, was lower than in the Az line, whereas other compounds of the TCA cycle, such as isocitric acid and 2-ketoglutaric acid, were higher. The derivatives of glutamic acid were lower in the transgenic U/O; B/B line, whereas the derivatives of lysine, serine, arginine and leucine, were higher than in the Az line. Finally, some of the GGPP derivatives, such as the tocopherols and hydrocarbon carotenoids were lower in the U/O; B/B line, whereas β -xanthophylls were higher.

A number of unidentified metabolites were also found to be either higher or lower in the transgenic U/O; B/B line than the Az line. One of these metabolites, an unknown polar compound (P_unk_9), was found to drive the separation of the U/O; B/B line on the loading scatter plot (Figure 3.15B). However, many compounds were not found to be significantly different between these two lines. Additionally, a substantial number of the primary metabolites indicated on the scheme in Figure 3.17 were not identified. This was most likely due to the absence of these compounds or the inability of the analytical technique used to detect them.

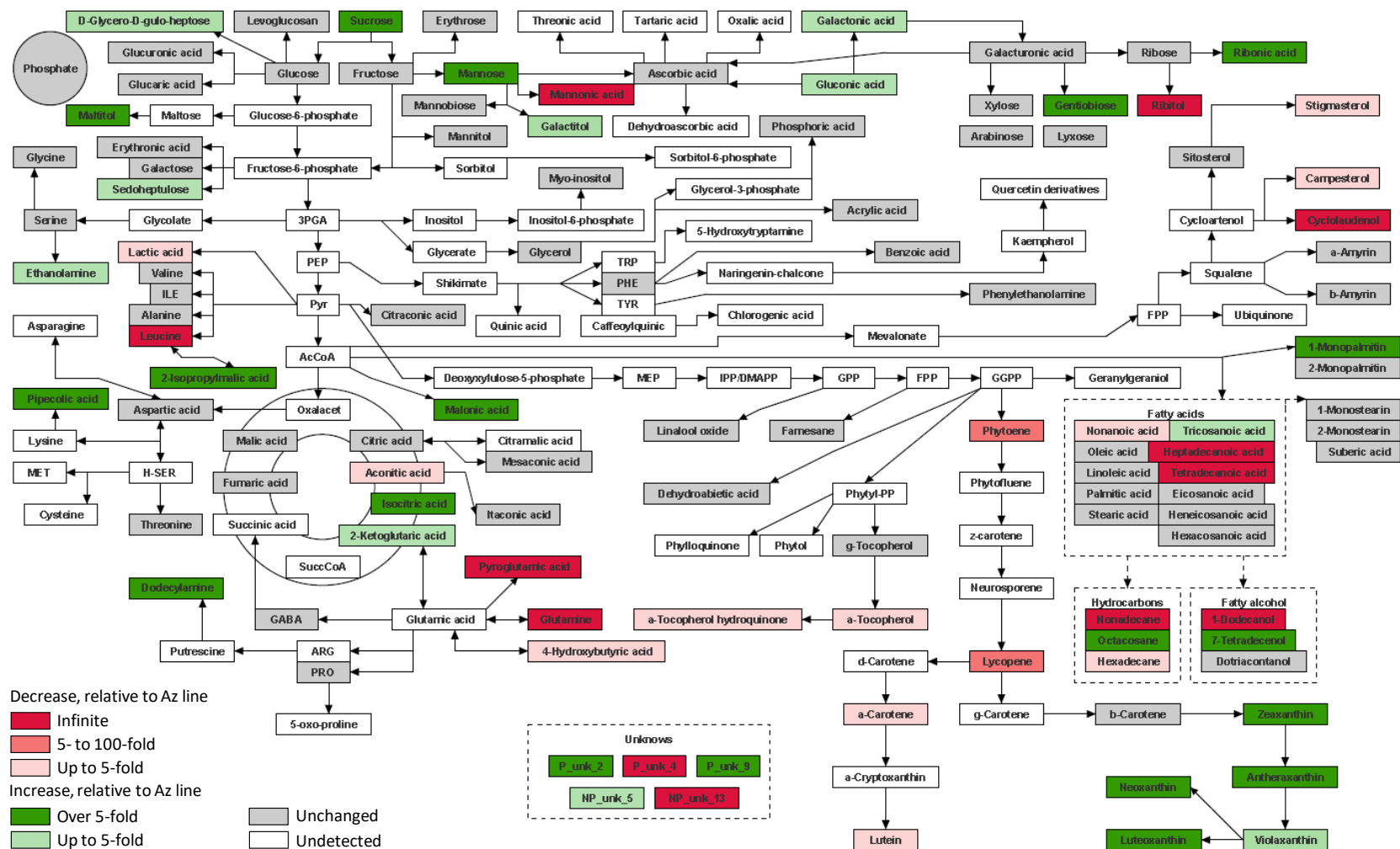


Figure 3.17. Changes in fruit metabolites of the U/0; B/B line compared to the Az reference line displayed over schematic biochemical pathways. Carotenoids, identified through HPLC, were added to the display. 3PGA, glyceraldehyde 3-phosphate; Ac-CoA, acetyl-coenzyme A; ARG, arginine; DMAPP, dimethylallyl pyrophosphate; FPP, farnesyl diphosphate; GGPP, geranylgeranyl diphosphate; GPP, geranyl diphosphate; H-SER, homoserine; ILE, isoleucine; MEP, 2-C-methyl-D-erythritol 4-phosphate; MET, methionine; PEP, phosphoenolpyruvate; PHE, phenylalanine; PRO, proline; Pyr, pyruvate; SuccCoA, succinyl-coenzyme A; TRP, tryptophan; TYR, tyrosine.

3.2.12 Volatile compounds analysis of F₂ population lines

In order to further explore changes in metabolism, volatile organic compounds (VOCs) of mature fruit of the Az line and the four transgenic lines (U/O; B/B, U/O; B/+, U/U; B/B and U/U; B/+) were analysed using solid-phase microextraction (SPME). Multivariate analysis of the 110 identified VOCs was carried out using principal component analysis (PCA) to assess the overall variance amongst the lines (Figure 3.18A). This analysis led to a discovery of three distinctive clusters. The

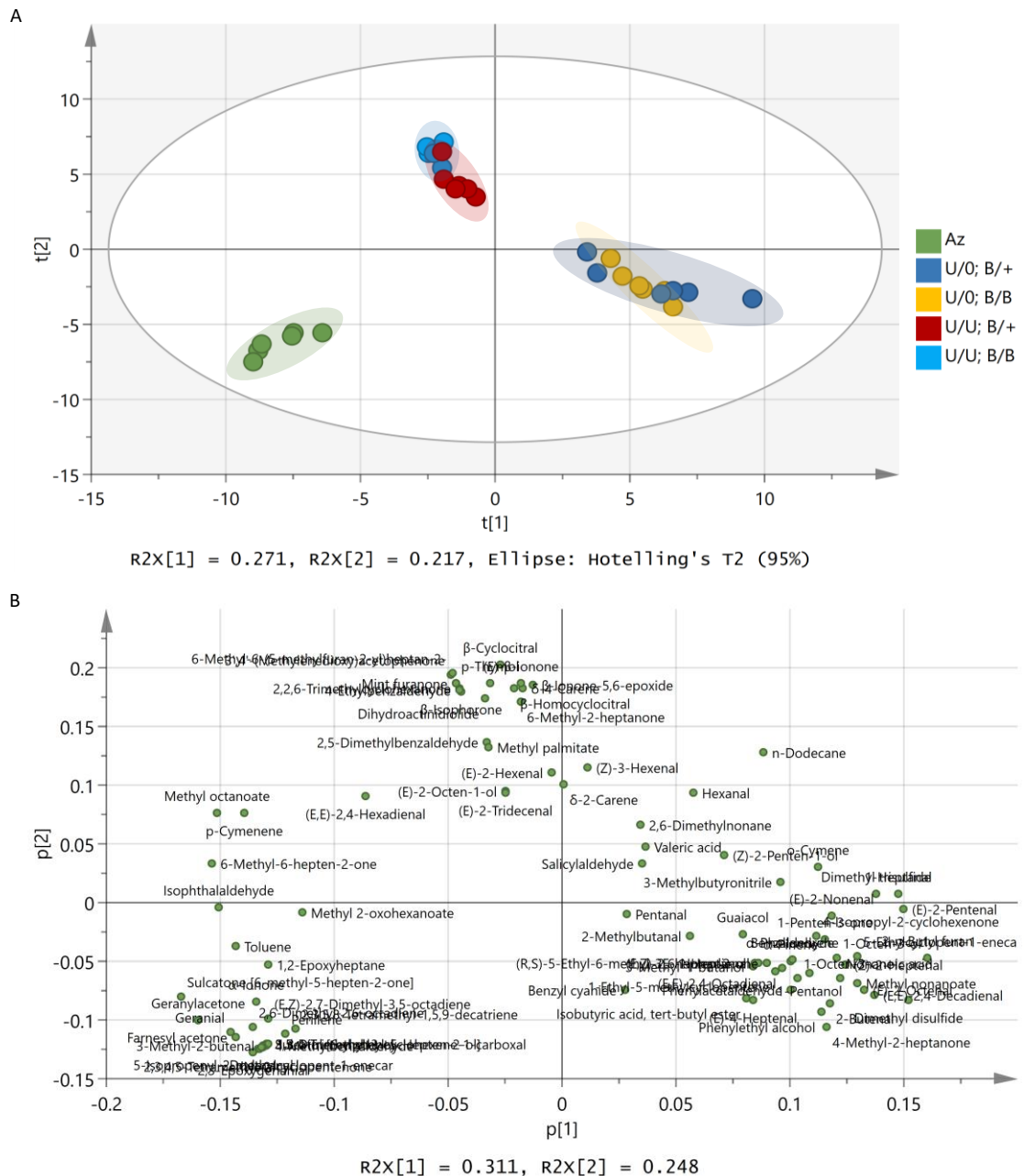


Figure 3.18. Principal component analysis (PCA) of the volatile compounds detected by SPME analysis of mature fruit of the indicated tomato lines. **(A)** Score scatter plot illustrating clustering of the lines along the direction of maximum variance in the data (the first principal component, $t[1]$) and the second major source of variation (the second principal component, $t[2]$) orthogonal to the first. Shaded areas indicate 95% confidence regions. **(B)** Loading scatter plot of the first two principal components ($p[2]$ against $p[1]$) indicating the metabolites which force separation of the lines. Only the compounds found to be significantly different between the five lines were included on the plot. The data were analysed using one-way ANOVA with Fisher's Least Significant Difference (LSD) post-hoc test and the significance was assessed based on False Discovery Rate (FDR) adjusted p -values (FDR < 0.05). Six biological replicates were used per line except for the U/U; B/+ line where $N = 5$.

(*E*)- β -ionone, 6-methyl-2-heptanone, mint furanone, 2,2,6-trimethylcyclohexanone, β -ionone-5,6-epoxide, 4-ethylbenzaldehyde, 3',4'-(methylenedioxy)acetophenone, dihydroactinidiolide, δ -4-carene and 6-methyl-6-(5-methylfuran-2-yl)heptan-2-one. The separation of the U/0; B/B and U/0; B/+ lines was driven by 2-n-butyl furan, dimethyl disulfide, (*E*)-2-pentenal, 1-heptanal, dimethyl trisulfide, methyl nonanoate, (*E,E*)-2,4-decadienal, (*E*)-2-octenal, 5-ethylcyclopent-1-enecarboxaldehyde, (*Z*)-2-heptenal, nonanoic acid, 1-octen-3-ol, 2-butenal, 1-penten-3-one, (*E*)-2-nonenal, phenylethyl alcohol and 4-methyl-2-heptanone.

The five lines were compared, and 92 VOCs were found to be significantly different between them. The levels of the significantly altered VOCs were compared and displayed in the form of a heat map to indicate the compounds with increased or decreased levels compared to the other lines (Figure 3.19). This comparison showed that similar VOCs were increased in the U/U; B/B and U/U; B/+ lines and that these two lines clustered together. The U/0; B/B and U/0; B/+ lines clustered together as they shared a number of VOCs which were higher in these two lines than in the remaining ones. However, certain differences between the VOCs profiles of the U/0; B/B and U/0; B/+ lines were apparent. Finally, the Az line contained yet a different group of VOCs which were higher in this line compared to the transgenic lines. However, the Az line clustered closer to the lines homozygous for transgenic *CrtR-b2* than the hemizygous ones.

In order to better understand the changes that took place in the VOCs profile of the xanthophyll-accumulating tomato, the U/0; B/B line was compared with the Az line and the changes were visualised onto a simplified display of biochemical pathways (Figure 3.20). The VOCs driving the separation of these two lines were also found to be significantly different between them. The compounds driving the separation of the Az line were also higher in this line and similarly, the compounds driving the separation of the U/0; B/B line were higher in this line. The major differences between these two lines were seen in the VOCs derived from some fatty acids, certain amino acids and the carotenoid biosynthetic pathway. In the U/0; B/B line, the VOCs derived from certain fatty acids, such as oleic acid, linoleic acid and linolenic acid, were higher compared to the Az line. The VOCs derived from phenylalanine were lower in the U/0; B/B line, whereas VOCs originating from leucine and methionine were higher than in the Azygous line. Interestingly, the majority of VOCs originating from the carotenoid biosynthetic pathway were lower in the U/0; B/B line except (*R,S*)-5-ethyl-6-methyl-3*E*-hepten-2-one, dihydroactinidiolide and 4-isopropyl-2-cyclohexenone, which were higher in this line than Azygous. (*R,S*)-5-ethyl-6-methyl-3*E*-hepten-2-one is derived from sulcatone, which is a breakdown product of lycopene. Dihydroactinidiolide is derived from β -ionone, which is a breakdown product of β -carotene. 4-Isopropyl-2-cyclohexenone is derived from β -cyclocitral, which is either synthesised directly from geranial or formed during the breakdown of β -carotene.

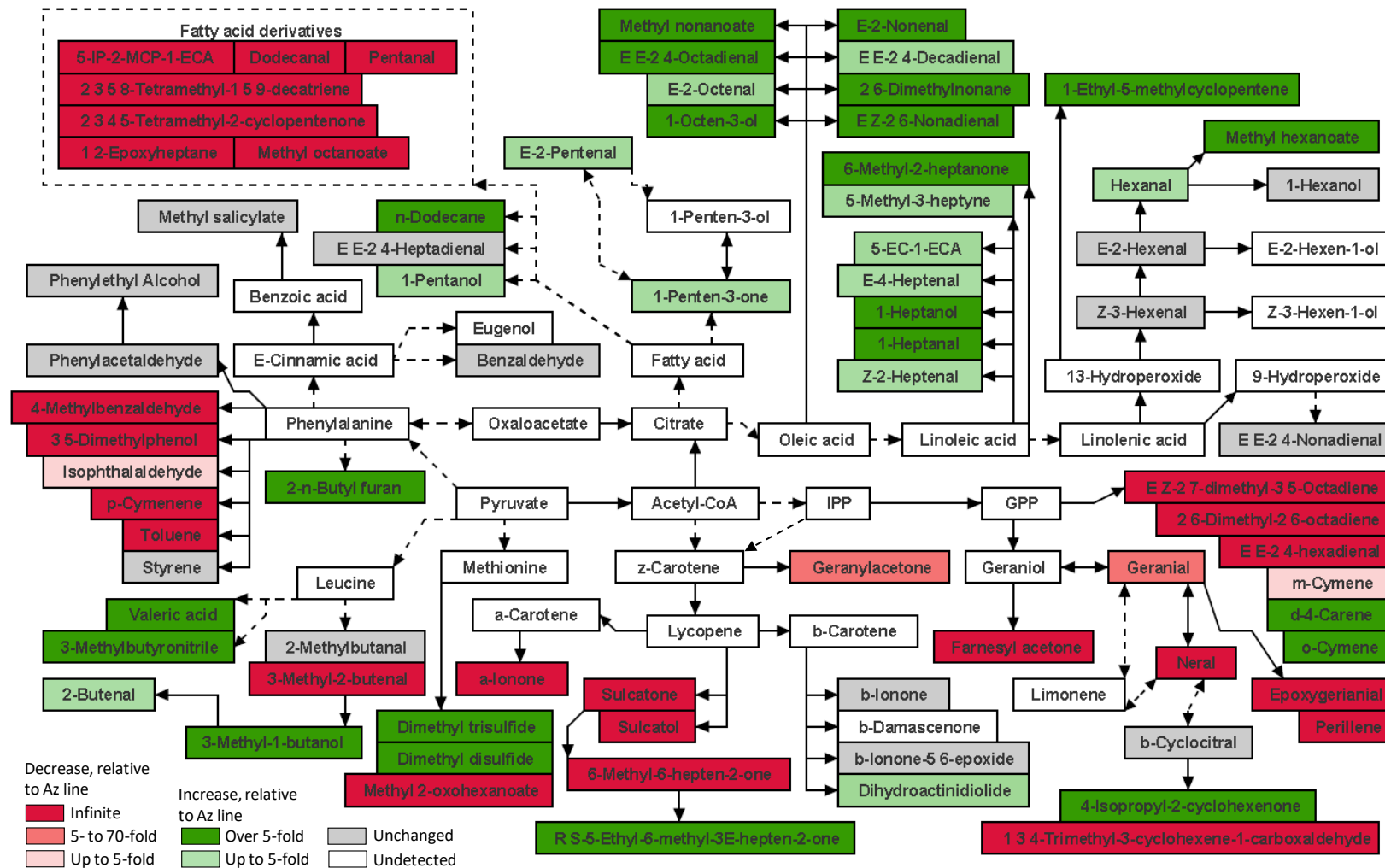


Figure 3.20. Changes in fruit VOCs of the U/0; B/B line compared to the Az line displayed over schematic biochemical pathways. The scheme was based on Zhang *et al.* (2015) and Seo *et al.* (2018). 5-EC-1-ECA, 5-ethylcyclopent-1-enecarboxaldehyde; 5-IP-2-MCP-1-ECA, 5-isopropenyl-2-methylcyclopent-1-enecarboxaldehyde; Acetyl-CoA, acetyl-coenzyme A; GPP, geranyl diphosphate; IPP, isopentenyl pyrophosphate.

3.2.13 Ripening series of the selected F₂ population lines

In order to further investigate the changes in pigment accumulation in fruit of the xanthophyll-accumulating lines and to infer possible reasons for the low total carotenoid levels in mature fruit of these lines, a ripening series experiment was conducted. In this experiment, fruit of the Az, U/O; B/B and U/O; B/+ lines at four different stages of development, namely immature green (IG), mature green (MG), turning (T) and ripe (R), were collected (Figure 3.21). The immature and mature green fruit of the transgenic lines appeared to have a yellow tinge to them in comparison to the green fruit of the Az line. At the turning stage, the green fruit of the Az line developed red sectors, whereas the transgenic lines were turning uniformly yellow throughout. At the ripe stage, only the Az fruit were red, whereas the transgenic fruit turned orange.

By analysing the carotenoid profiles of the ripe fruit, it was shown that the transgenic lines contained much lower carotenoid levels compared with the Az line. Therefore, to establish if the ripening process of the two transgenic lines has been affected, the pigments of the fruit at the different developmental stages were extracted and analysed on the HPLC system (Figure 3.22).

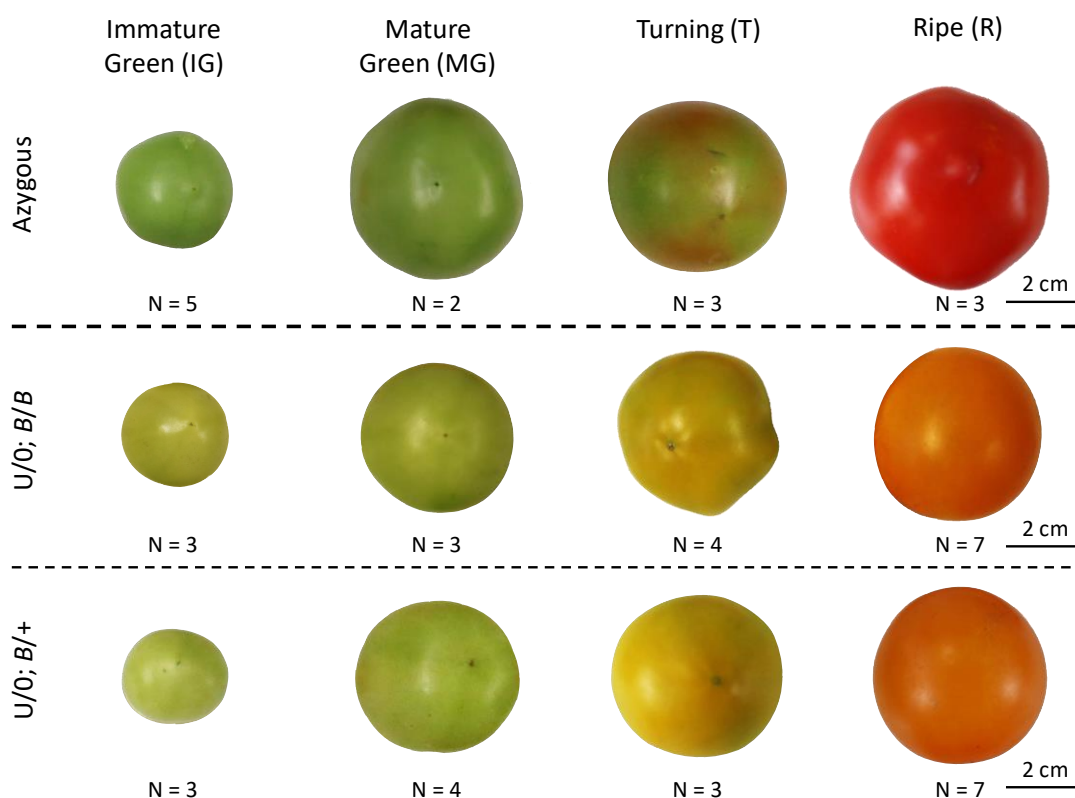


Figure 3.21. Representative phenotypes of fruit of the Azygous, U/O; B/B and U/O; B/+ lines collected at the indicated stages of development: immature green (IG), mature green (MG), turning (T) and ripe (R). The immature and mature green fruit of the two transgenic lines (U/O; B/B and U/O; B/+) appear to have a yellow hue to them, whereas the fruit of the Azygous line at the same stages of development are green. At the turning stage of development, the transgenic fruit become yellow in colour and then change to orange once ripe. The fruit of the Azygous line start to develop the characteristic red colour at the turning stage, which covers the entire surface of the fruit once ripe. The number of biological replicates, N, used for the analysis of pigments is indicated underneath each fruit.

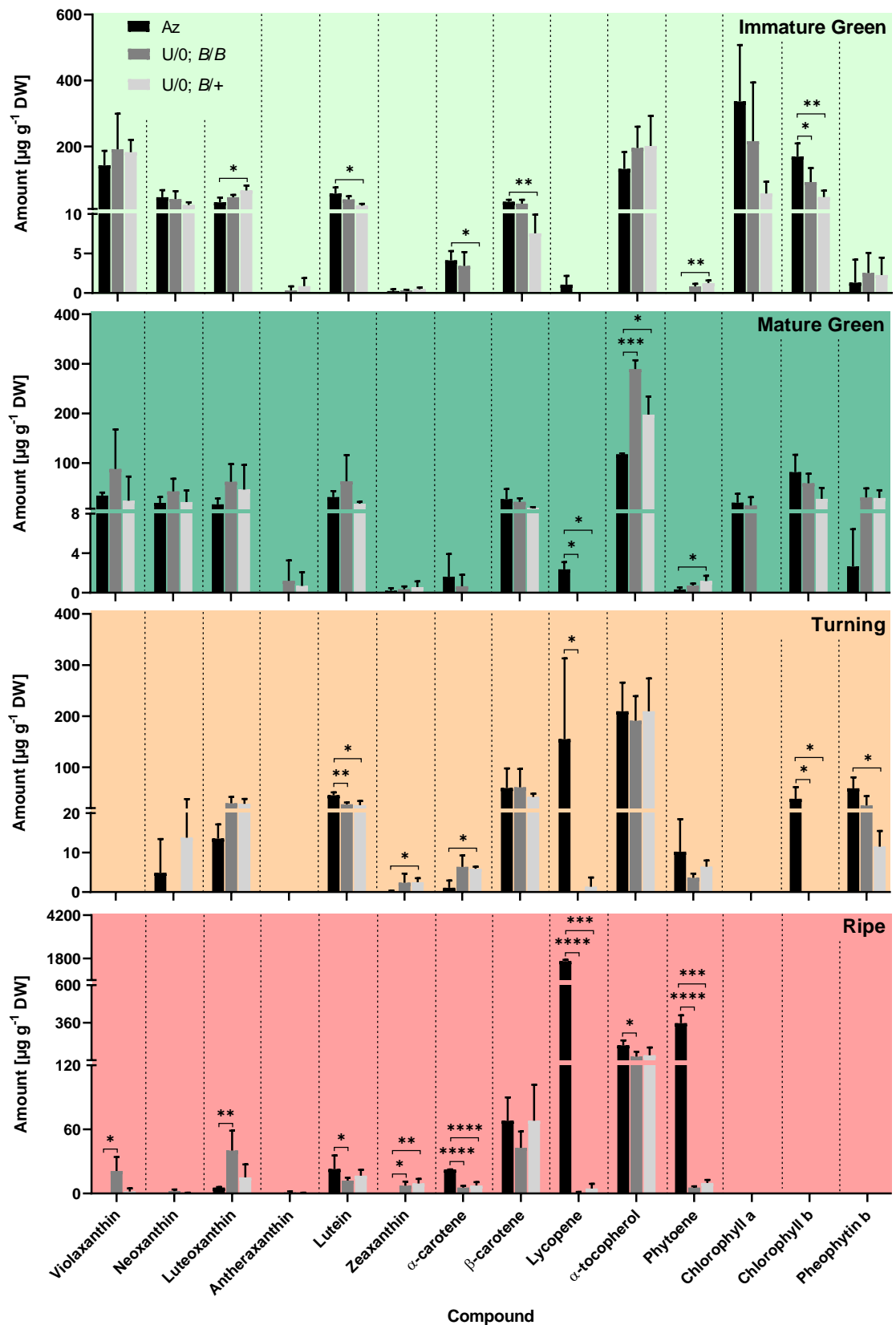


Figure 3.22. Changes in the amounts of isoprenoids and chlorophylls during fruit ripening of the Azygos (Az), U/0; B/B and U/0; B/+ lines. The compounds of the two transgenic lines (U/0; B/B and U/0; B/+) were compared to the Az line using one-way ANOVA with Dunnett's multiple comparison test or Kruskal-Wallis test with Dunn's multiple comparison test, as appropriate. Data normality was validated with Shapiro-Wilk test. The numbers of biological replicates, N, which were used at each stage of fruit development, are provided in Figure 3.21. The y-axes are split into top and bottom sections and additionally, at the mature stage of development, a middle section, in order to make the small peaks visible. The y-axes above start with the same values as indicated at the top of the y-axes underneath them. Data are displayed as $\bar{x} \pm \text{SD}$; * $P < 0.05$, ** $P < 0.01$, *** $P < 0.001$, **** $P < 0.0001$.

Based on the HPLC analysis, it was determined that in fruit of the Az line, the levels of all xanthophylls, excluding antheraxanthin, which was undetected at all stages, decreased between the IG and R stages of development. Additionally, many of these xanthophylls were undetected in fruit of this line at the later stages of development. In fact, only luteoxanthin and lutein were identified in the ripe fruit of the Az reference line. In fruit of the U/0; B/B line, the levels of violaxanthin, neoxanthin and antheraxanthin decreased sharply from the IG to the T stage of development. In fact, violaxanthin, neoxanthin and antheraxanthin were not detected in fruit of this line at the T stage. However, at the R stage of development, these three xanthophylls were present in fruit of the U/0; B/B line. The concentration of luteoxanthin in fruit of the U/0; B/B line decreased from the IG to the T stage and then increased at the R stage to almost the same level as was present at the IG stage (45.4 and 40.3 $\mu\text{g g}^{-1}$ DW at the IG and R stages, respectively). Lutein was the only xanthophyll which steadily decreased in fruit of the U/0; B/B line between the MG and R stages. On the other hand, zeaxanthin increased steadily from the IG to the R stage in this line. In fruit of the U/0; B/+ line, similarly to what was seen in the U/0; B/B line, the levels of violaxanthin and antheraxanthin decreased from the IG to the T stage. In fact, at the T stage of development, violaxanthin and antheraxanthin were undetected in fruit of the U/0; B/+ line; however at the R stage, some small amounts of these two xanthophylls were present. The levels of neoxanthin, luteoxanthin and lutein decreased from the IG to the R stage in fruit of the U/0; B/+ line, whereas the concentration of zeaxanthin, steadily increased. The largest, 8- and 4.2-fold increases in zeaxanthin levels in fruit of the U/0; B/B and U/0; B/+ lines, respectively, were recorded between the MG and T stages of development.

The levels of α - and β -carotene in fruit of the Az line increased 5.5- and 2.1-fold, respectively, from the IG to the R stage of development. On the other hand, the levels of α - and β -carotene in fruit of the U/0; B/B line, increased from the IG to the T stage 1.9- and 2.3-fold, respectively, but then decreased 1.2 and 1.4 times, respectively, from the T to the R stage. However, overall, the levels of α - and β -carotene increased 1.6-fold between the IG and R stages in fruit of the U/0; B/B line. In fruit of the U/0; B/+ line, α -carotene was only detected at the T stage, while β -carotene was already present at the IG stage. From the point of their first detection until the R stage, the levels of α - and β -carotene increased 1.3- and 9-fold, respectively, in this line.

Phytoene was first detected in fruit of the Az line at the MG stage of development at very low levels (0.3 $\mu\text{g g}^{-1}$ DW). Subsequently, a 34- and 35-fold increase in phytoene levels was recorded for the Az line from the MG to the T stage and the T to the R stage, respectively. In the U/0; B/B line, phytoene was first identified at the IG stage (0.8 $\mu\text{g g}^{-1}$ DW). The levels of phytoene in this line increased 5.0- and 1.5-fold from the MG to the T stage and the T to the R stage, respectively. In fruit of the U/0; B/+ line, phytoene was also first identified at the IG stage (1.2 $\mu\text{g g}^{-1}$ DW). The

fold increases in phytoene levels from the MG to the T stage and the T to the R stage in fruit of the U/0; B/+ line were almost the same as in the U/0; B/B line. In the Az reference line, lycopene was already detected at the IG stage ($1.1 \mu\text{g g}^{-1}$ DW) and from the MG to the T stage and from the T to the R stage it increased 65 and 11 times, respectively, reaching the highest amount of $1\ 650.3 \mu\text{g g}^{-1}$ DW in the ripe fruit. In the U/0; B/B line, lycopene was only detected in the ripe fruit at $0.7 \mu\text{g g}^{-1}$ DW. In the U/0; B/+ line, lycopene was first detected in fruit at the T stage of development and then it increased 3.4 times, reaching $4.7 \mu\text{g g}^{-1}$ DW in the ripe fruit.

Finally, the changes in chlorophyll levels across the different fruit developmental stages were analysed in the three lines. In the Az line, chlorophyll A was undetected at the T stage, whereas chlorophyll B was only undetected at the R stage. In the U/0; B/B line, both chlorophyll types were already undetected at the T stage. Noteworthy, at the MG stage, many plants belonging to the U/0; B/B line had already lost chlorophyll A completely from their fruit, whereas in all plants of the Az line, chlorophyll A was still present, even though the variance between individual plants was high. The absolute amounts of chlorophyll A in MG fruit of the Az and U/0; B/B lines were 20.1 ± 18.0 and $14.4 \pm 19.4 \mu\text{g g}^{-1}$ DW, respectively. In the U/0; B/+ line, chlorophyll A was already undetected at the MG stage, whereas chlorophyll B was undetected at the T stage.

The presented data suggest that the yellow hue to the transgenic fruit at the IG and MG stages could be partially attributed to the lower than in the Az line chlorophyll levels. Additionally, the transgenic lines lose both types of chlorophyll faster than the Az line, unmasking the yellow and orange colours of xanthophylls during the fruit development. Importantly, the presence of the yellow hue could not be attributed to an increase in any particular compound or a group of thereof, as otherwise very little difference was seen between the carotenoid contents of the three lines at the IG and MG stages. Moreover, the dramatic increase in the levels of phytoene and lycopene seen in fruit of the Az line was not present in the transgenic lines. Carotenoid accumulation is an important part of fruit ripening, which indicates that at least one aspect of the ripening process has been altered in the transgenic lines. Finally, the levels of zeaxanthin in fruit of the transgenic lines increased throughout the ripening process, suggesting a continuous synthesis. Similarly, the increase in violaxanthin levels from the T to the R stage indicates that the xanthophylls were not retained from the earlier stages, but rather synthesised *de novo* in ripe fruit. Therefore, the low carotenoid levels in fruit of the transgenic lines could be the result of a continuous conversion of the hydroxylated carotenoids into other metabolites. Additionally, some of the carotenoid-derived compounds may be acting as negative regulators of carotenoid biosynthesis and causing a shortage of substrates due to downregulation of genes earlier in the pathway. Alternatively, the inability of plants to accumulate high levels of xanthophylls can be caused by the lack of adaptation of fruit chromoplasts to store these types of compounds.

3.2.14 Analysis of fruit firmness of the selected F₂ population lines

The ripening series revealed that certain aspects of the fruit ripening process, such as chlorophyll breakdown and carotenoid accumulation, have been altered in the transgenic lines. In order to examine whether other aspects of this process have been affected as well, tissue firmness of ripe fruit of the Az line and the xanthophyll-accumulating U/0; B/B line was measured and compared. Fruit softening is a developmentally programmed ripening process associated with biochemical changes at the cell wall involving hydrolytic enzymes which break down cell wall polymers such as cellulose, hemicellulose and pectin. It was found that, on average, the fruit of the transgenic line were firmer than the fruit of the Az reference line by 9% (Figure 3.23).

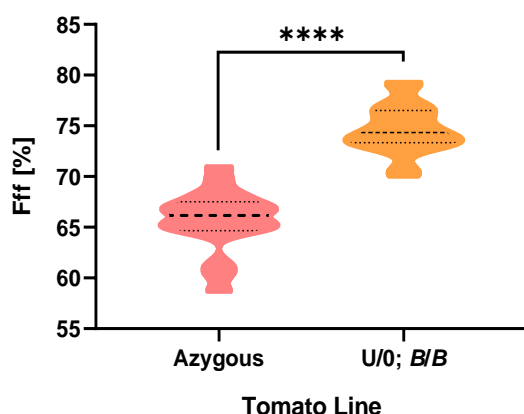


Figure 3.23. Mature fruit of the U/0; B/B line are significantly firmer than mature fruit of the Azygous line. The fruit firmness is presented as a percentage of the fruit firmness factor (Fff), which indicates the fraction of energy absorbed by the fruit. The thicker and thinner dashed lines within the violin plots indicate the median and the quartiles, respectively. The width of each plot represents the frequency of data points in a given region. Data normality was confirmed with Shapiro-Wilk test. The means of the two groups were compared using unpaired t-test; N = 6; **** P < 0.0001.

3.2.15 Transmission electron microscopy of the selected F₂ population lines

The transition of chloroplasts into chromoplasts is one of the most noticeable aspects of the fruit ripening process. In order to investigate if and how this process has been altered in the xanthophyll-accumulating tomato, chromoplasts of ripe fruit of the Az and U/0; B/B lines were imaged using transmission electron microscopy (TEM) and compared. The differences in their ultrastructure may help to explain the low carotenoid content in fruit of the transgenic lines.

The most striking difference between the two lines was the presence of large, electron dense lycopene crystals in chromoplasts of the Az line (Figure 3.24A), which were not found in chromoplasts of the U/0; B/B line (Figure 3.24B). In tomato chromoplasts, lycopene deposits as long, narrow, almost needle-like, crystalloids in association with an extended thylakoid system (Mohr, 1979; micrographs no. 1, 2, 5 and 6 in Figure 3.24A). However, these crystals may be dissolved and washed out during sample preparation for TEM imaging. When this happens, the thylakoid systems surrounding these crystals collapse and the crystal remnants are preserved as ribbon-like membranes (Oleszkiewicz *et al.*, 2018; micrographs no. 3 and 4 in Figure 3.24A). The chromoplasts of crystalline type were very rare in fruit of the U/0; B/B line and contained small crystalloid remnants within them (micrograph no. 6 in Figure 3.24B). Instead, the chromoplasts of the U/0; B/B line were mostly of globular and membranous types. Some chromoplasts of this

line contained structures made out of concentrically arranged internal membranes (tubular membranes (T) in micrographs no. 2 and 6 in Figure 3.24B). These membranous infoldings were not present in the micrographs of the Az reference line. Interestingly, in proximity of many chloroplasts in the transgenic line, dense, circular structures were seen. These structures are presumed to be lipid droplets (LD). The same droplets were very rarely found in proximity of the chloroplasts in the Azygous plants, where they also were less intensely stained. Despite these differences, the chloroplasts of the Az and U/O; B/B lines were not found to be significantly different in terms of size (3.6 ± 2.1 and 4.8 ± 1.8 μm , respectively) and number of plastoglobuli (13.6 ± 8.9 and 19.5 ± 6.8 , respectively). However, the plastoglobuli of the Az line were found to be 1.6 times larger and more intensely stained than the plastoglobuli of the transgenic line.

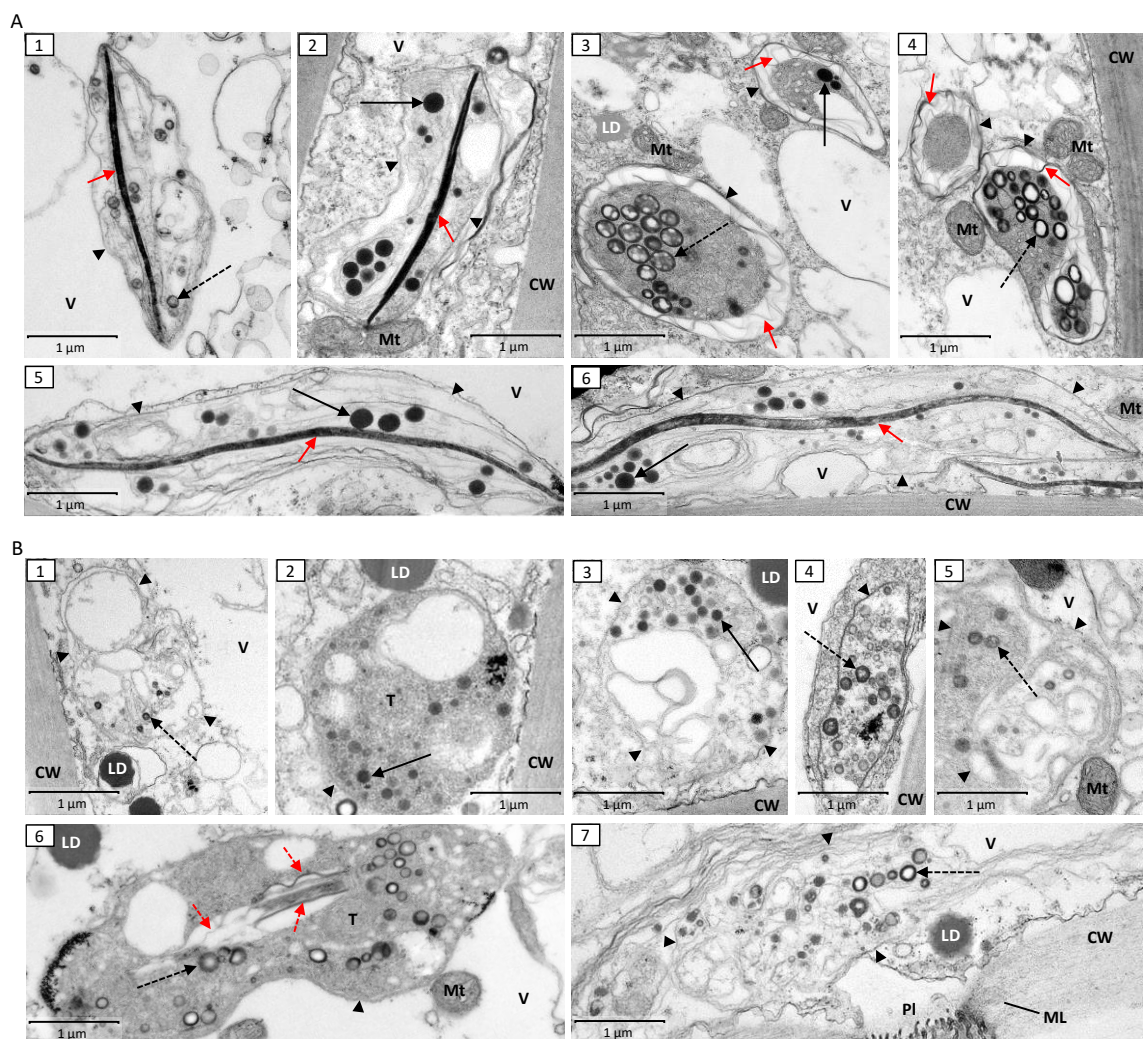


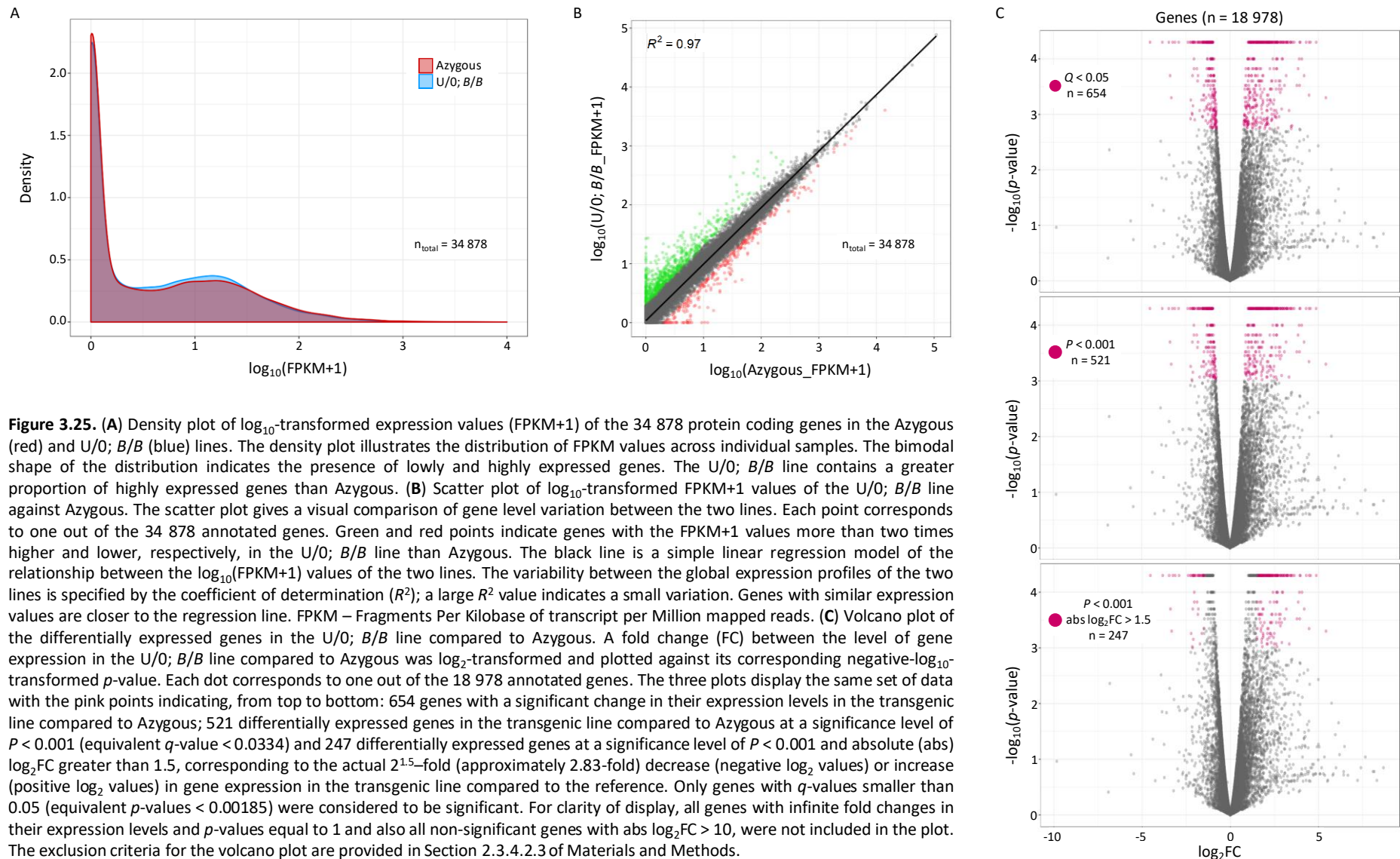
Figure 3.24. TEM micrographs of chloroplasts from ripe fruit of the Azygous (A) and U/O; B/B line (B). Chloroplasts of different types were identified in these lines: crystalline (A: 1–6; B: 6), globular (B: 2, 4) and membranous (B: 1, 3, 5, 7). Full red arrows point to lycopene crystals or their remnants within residual membrane sacs of elongated thylakoids; dashed red arrows indicate other crystalloid deposits, possibly of β -carotene. Black arrowheads indicate plastid envelopes capable of accommodating elongated crystalloids as seen in fruit of the Az line. Black arrows point to morphologically different plastoglobuli at various stages of crystalloid development: round, unchanged globules (full arrows) and globules with small crystalloids (dashed arrows). First sign of crystalloid formation within plastoglobuli is indicated by their differential staining properties. CW – cell wall; LD – lipid droplet; ML – middle lamella; Mt – mitochondrion; PI – plasmodesmata; T – tubular membranes; V – vacuole. Transparent areas within chloroplasts most likely result from swollen thylakoids. Staining artefacts are visible in A: 5 and B: 2, 4, 6 as black aggregates.

3.2.16 Transcriptome analysis of the selected F₂ population lines

In order to better understand the mechanisms responsible for the changes in certain aspects of the fruit ripening process and for the low carotenoid content in ripe fruit of the xanthophyll-accumulating line, an RNA-Seq analysis of the fruit transcriptome of the Azygous reference line and the transgenic U/0; B/B line at the turning stage of development was carried out. Three biological replicates (plants) were used per line and total RNA was extracted from a pooled sample of three fruit from each plant. The quality of extracted RNA was first assessed by electrophoresis on a non-denaturing agarose gel (Supplementary Figure 1.6A). The two bands indicating the 28S and 18S ribosomal subunits were clearly visible meaning that the RNA samples were suitable for RNA-Seq analysis. Following shipment of the samples, these were reassessed by the provider of sequencing services to determine the extent of their degradation. All samples were found to be of sufficient quality (RIN > 7; Supplementary Figure 1.6B and Supplementary Table 1.2) and were subsequently used for library construction.

Following the initial quality control analysis of the raw reads, density (Figure 3.25A) and scatter (Figure 3.25B) plots of the Az and U/0; B/B lines were generated. These plots are useful for summarising the gene expression data. The density plot showed that at the turning stage of fruit development, the Az line had more untranscribed genes ($\log_{10}(\text{FPKM}+1)$ of 0) than the U/0; B/B line. On the other hand, the U/0; B/B line had more of the highly expressed transcripts than the Az line ($\log_{10}(\text{FPKM}+1)$ between 0.5 and 2). However, both lines had a similar number of genes expressed at a very high level ($\log_{10}(\text{FPKM}+1)$ above 2). The scatter plot revealed that the transcriptomes of the two lines were very similar ($R^2 = 0.97$). However, globally, more genes were upregulated than downregulated in the U/0; B/B line relative to Azygous.

The transcript level of each gene in the U/0; B/B line was compared to its corresponding value in the Az line and the data were displayed in the form of a volcano plot (Figure 3.25C). The genes with negative \log_2 -fold changes were downregulated in the transgenic line compared to the Az line and those with positive \log_2 -fold changes, were upregulated. Genes with infinite changes in their expression levels were not included on the plot for clarity of display but were included in the discussion. The volcano plot showed that, relative to Azygous, more genes were upregulated than downregulated in the transgenic line. The total of 654 genes were found to be differentially expressed in the transgenic line (top plot in Figure 3.25C). At a more stringent significance level ($P < 0.001$), 521 differentially expressed genes were identified (middle plot in Figure 3.25C). In order to make the functional classification of the identified genes easier, only the ones with an absolute fold change greater than 2.83 were selected. This led to the discovery of 247 genes (bottom plot in Figure 3.25C). These genes and the 39 genes with an infinite change in their expression levels at the same significance level were functionally classified (Figure 3.26).



After applying the criteria described above, 286 differentially expressed genes were identified in the U/0; B/B line. 239 (84%) of these were upregulated and 47 (16%) were downregulated relative to the Azygous line (Figure 3.26A). Infinite changes were recorded in 36 (15%) of the upregulated genes and 3 (6%) of the downregulated genes. The upregulated and downregulated genes were then grouped according to their identified functions (Figure 3.26B). The majority of the downregulated genes were related to plant development (11), cell wall processes (6) and stress responses (5) and few of them were involved in flavonoid (2), lipid (2), carotenoid (1) and steroid (1) metabolism. Additionally, only this group included four genes involved in nitrogen metabolism. Amongst the upregulated genes, most of them were found to be involved in plant development (55), stress responses (35), cell wall processes (25), lipid metabolism (19) and defense responses (19). Interestingly, only in this group, 21 genes involved in various cellular events, such as cell cycle progression, protein synthesis and cellular trafficking, were identified. This strongly suggests that at the turning stage of development, fruit of the U/0; B/B line are more metabolically active than fruit of the Azygous reference line. Additionally, the group of the upregulated genes included two photoreceptors, four genes involved in volatile metabolism and 12 genes encoding cellular transporters for sugars, lipids, amino acids, peptides, nucleosides and nitrates. The full lists of the 239 upregulated and the 47 downregulated genes with their known functions are provided in Supplementary Tables 1.3 and 1.4, respectively.

Without applying the additional selection criteria described above and instead considering all significantly different genes ($Q < 0.05$), including those with infinite changes in their expression levels, 693 genes were found to be differentially expressed in the U/0; B/B line. The 286 functionally classified genes (Figure 3.26) comprised only 41% of all differentially expressed genes. Therefore, some genes involved in carotenoid biosynthesis might have been excluded due to the applied criteria. In order to circumvent this problem, a manual search of the genes known to encode enzymes of the MVA, MEP and carotenoid biosynthetic pathways was carried out in the Cuffdiff output file. The list of differentially expressed genes related to carotenoid biosynthesis is provided in Table 3.3. At the turning stage of fruit development, the expression of *CYC-B* and *CrtR-b2* was 4.2 and 19.8 times higher, respectively, in the U/0; B/B line than in the Az line. Interestingly, two lycopene ϵ -cyclases, required for cyclisation of lycopene to δ -carotene, were also found to be upregulated, although only one significantly. The Orange Ripening (*ORR*) gene was also significantly upregulated. *ORR* regulates the plastidial redox status required for the activity of carotenoid biosynthetic enzymes such as *PDS* and *ZDS*. Finally, a member of the MVA pathway belonging to the terpene cyclase/mutase family of enzymes, was also found to be significantly upregulated in the transgenic line. The two significantly downregulated genes of the carotenoid biosynthetic pathway were *GGPS2* and *LUT1*. Additionally, *PSY1* and *CRTISO* were also found to be downregulated, albeit this change was not found to be significant.

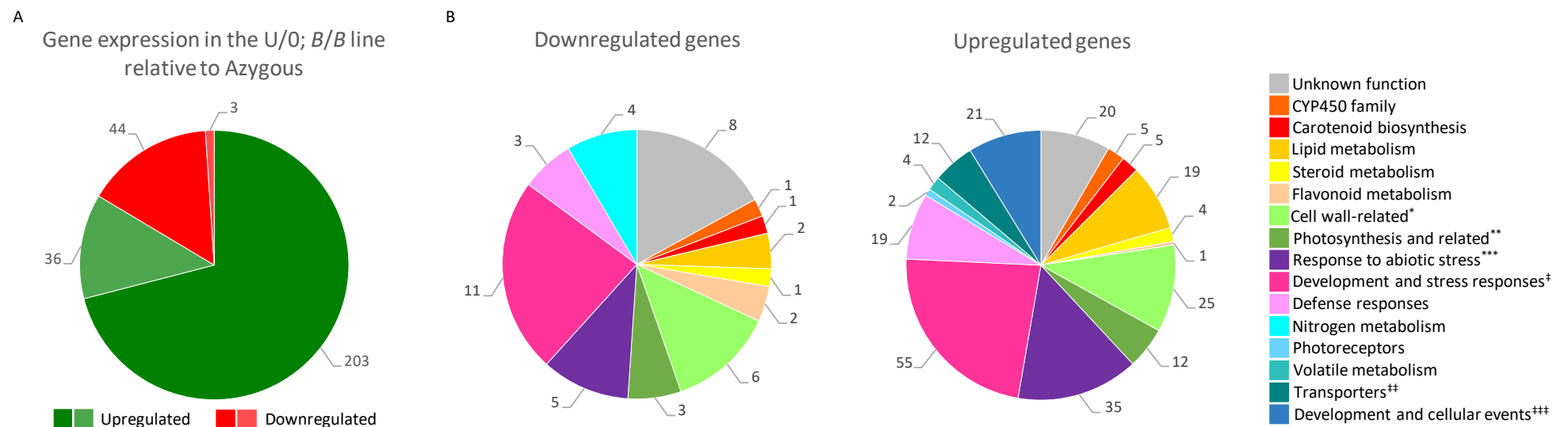


Figure 3.26. Summary of the differentially expressed genes between the U/O; B/B line and the Azygous reference line. The charts only include genes which were downregulated or upregulated more than 2.83-fold in the U/O; B/B line compared to Azygous. **(A)** Out of the 286 identified genes, 47 were found to be downregulated (red) and 239 were found to be upregulated (green) in the U/O; B/B line. Lighter shades of the respective colours indicate genes with an infinite change in their expression levels. **(B)** Classification of the genes was based on their function or the family to which they belong. The information on gene function was obtained from studies on functional knockouts, RNA interference and gene overexpression in *Arabidopsis thaliana*, *Oryza sativa*, *Solanaceae* and *Brassicaceae*. The grouping is not definitive but is a good approximation since some of the genes have multiple functions. For instance, genes involved in cell wall organisation were often found to be related to pathogen resistance and vice versa. Some of these genes could also be involved in stress responses. The upregulated and downregulated genes are listed in Supplementary Tables 1.3 and 1.4, respectively. *also includes chitinases; **also includes one respiratory gene; ***many of the genes are induced by ABA or other hormones; †includes LRR-RK/PAMPs signalling and hormonal/stress responses; **sugar, lipid, amino acid, peptide, nucleoside and nitrate transporters; ***cell cycle progression; synthesis, folding, processing and trafficking of proteins; DNA repair and maintenance; RNA processing.

Table 3.3. List of carotenoid-related genes found to be differentially expressed in the U/O; B/B line compared to the Azygous reference line as analysed by RNA-Seq. Genes highlighted in grey did not reach the specified significance level (their *p*-values are included next to their names); however, they are included for the purpose of discussion.

Gene ID	Gene Name	Identified Function	Fold Change	References
Upregulated genes				
<i>Solyc12g008980.2</i>	Lycopene ϵ -cyclase (<i>P</i> = 0.004)	- introduces ϵ -end rings; required for α -carotene and lutein biosynthesis	3.4	Fraser & Bramley, 2004
<i>Solyc12g006510.2</i>	Terpene cyclase/mutase family member	- triterpenoid biosynthetic process - terpenoids comprise the most chemically and structurally diverse family of natural products including steroids and carotenoids	3.5	Christianson, 2017
<i>Solyc01g102950.3</i>	Lycopene β/ϵ -cyclase	- catalyses the addition of β -ionone end groups to the end of lycopene molecules; catalyses the single ϵ -cyclisation reaction which converts lycopene to δ -carotene and neurosporene to α -zeacarotene - required for lutein biosynthesis	3.7	Cunningham <i>et al.</i> , 1996
<i>Solyc06g074240.2</i>	Chromoplast-specific lycopene β -cyclase (<i>CYC-B</i>)	- responsible for formation of β -carotene from lycopene; introduces β -end rings	4.2	Nogueira <i>et al.</i> , 2017
<i>Solyc04g057980.3</i>	Orange Ripening (<i>ORR</i>)	- part of the NADH dehydrogenase (NDH) complex (subunit M); supports nonphotochemical electron fluxes from stromal electron donors to plastoquinone - essential for the fruit ripening process	5.0	Nashilevitz <i>et al.</i> , 2010
<i>Solyc03g007960.3</i>	β -carotene hydroxylase 2 (<i>CrtR-b2</i>)	- non-heme diiron carotene β -hydroxylase involved in biosynthesis of β -derived xanthophylls	19.8	D'Ambrosio <i>et al.</i> , 2011
Downregulated genes				
<i>Solyc03g031860.3</i>	Phytoene synthase 1 (<i>PSY1</i>) (<i>P</i> = 0.136)	- increases during fruit ripening and decreases as the fruit ripening progresses - chromoplast-specific	1.7	Fraser & Bramley, 2004
<i>Solyc10g081650.2</i>	Prolycopene isomerase (<i>CRTISO</i>) (<i>P</i> = 0.007)	- carotene <i>cis-trans</i> -isomerase that converts 7,9,9'- <i>tri-cis</i> -neurosporene to 9'- <i>cis</i> -neurosporene and 7,9,9',7'- <i>tetra-cis</i> -lycopene (also known as prolycopene) into all- <i>trans</i> -lycopene	1.9	Isaacson <i>et al.</i> , 2004
<i>Solyc04g079960.1</i>	Geranylgeranyl pyrophosphate synthase 2 (<i>GGPS2</i>)	- catalyses the <i>trans</i> -addition of the three molecules of IPP onto DMAPP to form geranylgeranyl pyrophosphate (GGPP), an important precursor of carotenoids and geranylated proteins - chromoplast-specific	2.0	Ament <i>et al.</i> , 2006
<i>Solyc07g042480.3</i>	Carotene ϵ -monooxygenase, chloroplastic (<i>LUT1</i>)	- specific for ϵ - and β -ring hydroxylation of α -carotene; has low activity towards the β -rings of β -carotene; preferred substrate in planta is not α -carotene but the ϵ -ring of zeinoxanthin - loss-of-function mutants lack lutein and accumulate higher levels of zeinoxanthin and β -xanthophylls	4.7	Tian <i>et al.</i> , 2003; Tian <i>et al.</i> , 2004; Fiore <i>et al.</i> , 2006

3.3 Discussion

3.3.1 Selection of the reference line

The F₂ population of 185 plants is a segregating population meaning that it consists of genetically diverse progeny. The individual plants were assigned to one of the five lines (U/0; B/B, U/0; B/+, U/U; B/B, U/U; B/+ or 0/0; +/+, which is generally referred to as Azygous in this work) based on the presence or absence of the genes of interest, namely *S. galapagense* *CYC-B* allele and transgenic *CrtR-b2*. However, since this population is derived from the parental lines of different genetic backgrounds (Moneymaker, Red Setter and UC204B; Figure 3.1), all five lines have a random mixture of these backgrounds, different for each line. In other words, plants belonging to each line are different mosaics of the parental lines with different mixtures of chromosomes to the plants of other lines, even though they are derived from the same pedigree. This means that the plants of the Azygous line cannot be assumed to have an equivalent background. Therefore, the Azygous line is not the true genetic background of the F₂ population.

The true genetic background could only be achieved by the generation of near-isogenic lines (NILs) through repeated backcrossing. The process of backcrossing needs to be repeated over six generations in order to recover 99.2% of the recurrent parent genome in lines introgressed with the genes of interest (Hasan *et al.*, 2015). However, due to the relatively long generation time of tomato plants of about 3 – 4 months, it was not possible to generate NILs in the given timeframe. Therefore, even though the Azygous line was far from perfect, it was the closest to the true genetic background of the F₂ population and was selected as the reference line for the four transgenic lines. Moreover, the four transgenic lines face the same issue as the Azygous line. The presence of the different gene combinations in the four transgenic lines was associated with specific traits in these lines. However, due to their complex genetic backgrounds it cannot be ruled out that other genes are responsible for or contribute to the observed characteristics. Moreover, some traits may result from the interactions between genes from different chromosomes via *trans*-acting factors (Ranjan *et al.*, 2016) and the presence of chromosomes from different backgrounds means that these interactions can be different for each line.

It is very likely that the observed changes in the leaf (Figure 3.8) and fruit (Figure 3.10) pigment profiles of the studied lines are the direct result of the introduced genes since their role in carotenoid biosynthesis is clearly understood. Additionally, the changes to carotenoid sequestration in the studied lines (Figures 3.13 and 3.14) are almost irrefutably associated with the changes in carotenoid composition of these lines. However, this may not be true for all observed changes, especially the more complex traits, such as the changes in steady states of primary metabolites (Figure 3.16) and VOCs (Figure 3.19) or the changes in certain aspects of

the fruit ripening process (Figures 3.22 and 3.23). Interestingly, despite the concerns associated with the mixed genetic backgrounds of the individual lines, these segregated into different clusters when analysed by PCA (Figures 3.15 and 3.18). This suggests that the effects exerted by the specific gene combinations are rather strong, which justifies the classification of plants into specific lines. This in turn allows to ascertain the validity of data and to accept the obtained results, while at the same time understanding the underlying issues associated with the mixed genetic backgrounds. The ideal solution to these issues would entail the generation of NILs carrying the required combinations of *S. galapagense* *CYC-B* allele and transgenic *CrtR-b2* in order to display more definite traits and increase the strength of association. However, the most pragmatic approach would be to increase the number of biological replicates in order to better represent the genetic variability of each line.

3.3.2 RT-qPCR as a screening method for determining zygosity

Previously, it was shown that RT-qPCR was not a reliable method for determining zygosity of transgenic plants due to high variability between the replicates, and so it was recommended that other techniques, such as Southern blotting, should be used instead (Bubner *et al.*, 2004). However, other studies successfully demonstrated that qPCR-based methods can be used for establishing zygosity in tomato plants (German *et al.*, 2003). Similarly, in this work, RT-qPCR was shown to be a fast and reliable technique for determining zygosity of transgenic plants. The advancement of available technologies, including improvements in analytical platforms and chemistries, means that PCR-based assays alone can be used for this type of analysis. However, when used in conjunction, Southern blot and RT-qPCR allow for a more complete inspection of the gene or genes of interest, and therefore, should be interpreted together.

Generally, insertion of a single, intact copy of the transgene into the genome of a recipient plant is required in order to achieve a stable expression of that gene. The integration of multiple inserts often leads to the loss of expression of some or all copies of the transgene (Tark-Dame *et al.*, 2018). Therefore, the presence of multiple inserts can make the molecular and phenotypic characterisation of the transgenic plants difficult (Tissier *et al.*, 1999). The parental U/U line developed by D'Ambrosio *et al.* (2011) and used in this work, was reported by the authors to contain a single transgene insertion in a homozygous state. In the F₂ population, the transgene segregated at an approximately 3:1 ratio (132 plants positive for the CaMV 35S promoter and 53 negative), which is indicative of the presence of a dominant allele or a transgene at a single locus (Passricha *et al.*, 2016). However, if multiple inserts are found at the same locus, they can be inherited as one unit due to their close linkage and will not be detected through segregation analysis (Głowacka *et al.*, 2016). Therefore, to confirm the presence of a single copy of the insert in transgenic plants used in this work, Southern blot analysis was carried out. The U/U parental

plant and three CaMV 35S-positive plants of the F₂ population selected for this analysis produced two bands on the X-ray film. The first signal originated from the endogenous copy of *CrtR-b2* since the same band was present in the non-transgenic control plant (the E-band in Figure 3.5B). The second signal was caused by hybridisation of the probe to the transgenic copy of *CrtR-b2* and was absent from the non-transgenic control plant (the T-band in Figure 3.5B). The presence of a single transgenic band in the analysed plants indicates the presence of a single copy of the transgene at the U locus.

The next step was to determine zygosity of the transgene in the CaMV 35S-positive plants of the F₂ population. In this work, each biological sample (plant) was analysed in triplicate and little variability was seen between the technical replicates in the RT-qPCR assay (Figure 3.6B). This allowed for an unequivocal assignment of zygosity (or dosage) of transgenic *CrtR-b2* to each plant. Moreover, the method was initially validated on five different first filial generations resulting from crossing of different transgenic plants with a plant negative for the transgene (Supplementary Figure 1.4E). According to the Mendel's laws of genetic inheritance, the entire offspring of a cross would be positive for the transgene if its transgenic parent was homozygous at the U locus or roughly 50% of the offspring would be positive if the transgenic parent was hemizygous. Additionally, all plants, which have inherited the transgene, would be hemizygous at the U locus. Therefore, the CaMV 35S-positive plants originating from different transgenic parents were selected and analysed by RT-qPCR. As predicted, all of them were found to be hemizygous for transgenic *CrtR-b2* (dosage of 1), thus validating the technique (Figure 3.6B).

However, for the above method to be successful, a calibrator plant of a known transgene zygosity was required as the reference genotype. Several calibrator plants were identified through the segregation analysis (Table 3.2) and these were subsequently used in the RT-qPCR assay. Segregation analysis is the most reliable method for determining zygosity of unlinked genes but it requires a relatively long period of time to be carried out. In this case, a minimum of eight days was required for cotyledon development and additional time was necessary for the plants to develop extra leaves which could be collected for DNA extraction. Moreover, the developing plants require space and resources and the number of biological replicates needs to be sufficient in order to obtain statistically significant results.

An alternative method, which could be used to select reference plants for the RT-qPCR assay, is Southern blotting. It is less time consuming than the segregation analysis as it can be completed within two to three days but compared to PCR-based methods, it requires larger amounts of high-quality DNA which can be difficult to obtain from small plants. Moreover, Southern blotting has a low throughput compared to other screening methods. However, it is routinely used to determine the number of inserts in the founder transgenic organism due to its low false-positive

discovery rate of the transformation events. To determine zygosity of the gene of interest using Southern blotting, the intensity of the band to which the probe has hybridised is measured and compared to a plant of known zygosity or to other plants if the calibrator is not available (Passricha *et al.*, 2016). When this was done for the plants analysed in this work, the U/U parental line, contrary to what was reported by D'Ambrosio *et al.* (2011), was found to be hemizygous for the transgene, whereas two F₂ plants appeared to have three transgenic U loci (Figure 3.5B). This inconsistency could be explained by the low quality of the gel that was used in the normalisation step (Supplementary Figure 1.4D) but also by the fact that Southern blotting may not be quantitative enough to reliably detect a two-fold difference. Interestingly, when the intensity of the transgenic band in each plant was normalised to the endogenous copy of *CrtR-b2* (the E-band in Figure 3.5B) and compared between the plants, the U/U parental line was found to contain a double dosage of the transgene. However, since endogenous *CrtR-b2* is a single-copy gene (Galpaz *et al.*, 2006), the ratio of 1 between the T- and E-bands was expected for plants homozygous for the transgene and the ratio of 0.5 was expected for hemizygous plants. Therefore, it is likely that hybridisation of the probe to the endogenous copy was less efficient than hybridisation to the transgenic copy, which shared a greater sequence overlap and only a relative comparison between the plants provided the result consistent with what was reported previously. The subsequent analysis by RT-qPCR confirmed that the U/U parental line provided by D'Ambrosio *et al.* (2011) and used in PCR screening (Figures 3.3A, 3.3B and 3.5A), pigment analysis (Figure 3.4 and Table 3.1) and Southern blotting (Figure 3.5B), was homozygous for the transgene (data not shown). This, however, was inconsistent with segregation of the transgene in the F₁ population since only one hybrid was positive for the CaMV 35S promoter, indicating that the transgenic parent was hemizygous (Figure 3.3A). The most likely reason for this is that, in the initial crossing between the parental lines, unlike it was reported, the U/U line must have already been crossed once, possibly with the ZW line, segregating out one transgenic U locus before being crossed with the B/B line later (Figure 3.1). This would explain why all F₁ hybrids were positive for *S. galapagense* *CYC-B* (Figure 3.3B) but only one inherited the transgene.

In the presented work, Southern blotting was used to confirm the presence of a single copy of the insert in transgenic plants. Segregation analysis was used to select calibrator plants of known transgene zygosity. These were subsequently used in RT-qPCR to determine transgene zygosity in plants of the F₂ population. The genotypic characterisation of the lines studied in this work was critical in establishing the changes that occurred as a consequence of the specific gene combinations in these lines. Therefore, the development of a fast and efficient protocol with the use of RT-qPCR greatly aided the classification of the lines according to their genetic make-up. Additionally, contrary to previous reports (Bubner *et al.*, 2004), it was shown that RT-qPCR is sensitive enough to reliably detect a two-fold difference in template concentration.

3.3.3 Silencing of the hydroxylase in a homozygous state

Although, the presence of multiple inserts is known to enhance the efficiency of gene silencing in transgenic plants (Meyer & Saedler, 1996), this process can also occur in plants containing a single copy of the transgene due to the gene dosage (De Wilde *et al.*, 2001) or position effects (Meza *et al.*, 2002; Singh *et al.*, 2008). Transgenes under the control of the strong CaMV 35S promoter are particularly prone to post-transcriptional silencing due to their high levels of expression (Elmayan & Vaucheret, 1996) and this is the reason why the Cauliflower Mosaic Virus has evolved its 19S protein as a silencing suppressor (Love *et al.*, 2007). Moreover, if the transgene contains sequences homologous to an endogenous gene, the expression of both can be significantly impaired, resulting in a phenomenon known as co-suppression (Meyer & Saedler, 1996; Stam *et al.*, 1997).

D'Ambrosio *et al.* (2011) reported that the endogenous *CrtR-b2* gene was silenced in tissues of transgenic plants which were homozygous at the U locus. However, the supplementary gene expression data provided by the authors did not support this conclusion. On closer inspection, the evidence of silencing of the endogenous *CrtR-b2* gene was only found in petals. In other tested tissues, such as leaf and fruit at the immature green, mature green and ripe stages of development, the transcript levels of the endogenous *CrtR-b2* gene were lower in the transgenic plants homozygous at the U locus than in the transgenic plants hemizygous at the U locus but they were still higher than in the non-transgenic plants; hence, silencing did not occur in these tissues. However, there was a clear evidence of silencing of the endogenous *CrtR-b1* gene in all tissues except leaves with the strongest reduction in immature green fruit followed by petals. Nonetheless, these data are consistent with the observations presented in this work.

The presence of *CrtR-b2* transcripts was detected in petals and fruit at all stages of development of non-transgenic plants but not in their leaves. In leaves of the transgenic plants, expression of *CrtR-b2* was higher in the U/O line than the U/U line (D'Ambrosio *et al.*, 2011). Therefore, since *CrtR-b2* is normally absent from leaves of tomato plants, the presence of *CrtR-b2* transcripts in leaves of transgenic plants and absence of *CrtR-b1* silencing in the U/U line, explains why any combination of transgenic *CrtR-b2* and *S. galapagense* *CYC-B* in the four transgenic lines studied in this work leads to a higher content of violaxanthin in these lines than in Azygous (Figure 3.8B). The highest increase in violaxanthin was recorded in lines hemizygous for transgenic *CrtR-b2*, which is consistent with the highest levels of *CrtR-b1* and *CrtR-b2* transcripts in the U/O line. In fact, the dramatic increase in the levels of *CrtR-b1* transcripts in leaves of the U/O line reported by D'Ambrosio *et al.* (2011) may explain why the change in *S. galapagense* *CYC-B* zygosity affects xanthophyll accumulation only in plants hemizygous for the transgene but not in homozygous ones (Figure 3.12A). Firstly, even though *CYC-B* encodes a fruit-specific cyclase, it is expressed in

tomato leaves at low levels (Stigliani *et al.*, 2011). Secondly, since in the carotenoid biosynthetic pathway the hydroxylase acts downstream of the cyclase, the increase in *CrtR-b1* in hemizygous plants removes the metabolic bottleneck and allows the hydroxylase to work in coordination with the cyclase resulting in higher levels of violaxanthin and neoxanthin in the U/0; *B/B* line than in the U/0; *B/+* line. The same levels of *CrtR-b1* transcripts in the U/U line as in the non-transgenic line mean that the metabolic bottleneck is in place and the change in *S. galapagense* *CYC-B* zygosity does not increase accumulation of violaxanthin in the U/U; *B/B* line compared to the U/U; *B/+* line. Alternatively, expression of other carotenoid-related genes may be altered in leaves of transgenic lines hemizygous at the U locus. For instance, D'Ambrosio *et al.* (2011) found that in the U/0 line but not in the U/U line, the expression of *PSY1* was higher than in the non-transgenic plants, similarly to *CrtR-b1*. Therefore, other genes, including *LCY-B*, which encodes a chloroplast-specific cyclase, could be upregulated, and this should be verified.

The F₂ population lines homozygous for the transgene (U/U; *B/B* and U/U; *B/+*) accumulated primarily β -carotene in their ripe fruit (Figure 3.10), similarly to the *B/B* parental line (Figure 3.4 and Table 3.1). This is consistent with the silencing of *CrtR-b1* and reduction in *CrtR-b2* transcript levels in fruit of the U/U lines at all stages of development. Interestingly, lutein was not affected in the U/U; *B/B* and U/U; *B/+* lines (Figure 3.10), despite being a product of hydroxylation itself. This is consistent with the previous reports that the non-heme diiron hydroxylases, such as *CrtR-b1* and *CrtR-b2*, are primarily responsible for the formation of β -xanthophylls, whereas the enzymes primarily responsible for synthesis of lutein, namely CYP97A29 and CYP97C11, are cytochrome P450 (CYP) monooxygenases (Stigliani *et al.*, 2011). Finally, the differences in gene expression between the leaf and fruit tissues of the transgenic lines presented by D'Ambrosio *et al.* (2011) suggest that transcription of tissue-specific genes is under tight spatial regulation; however, genes which are not normally expressed in a given tissue are not subject to the same strict regulatory mechanisms.

Due to their high β -carotene content, fruit of the transgenic plants homozygous at the U locus were easily distinguishable from fruit of the plants hemizygous at the U locus (Figure 3.7A). This greatly facilitated the classification of plants according to their genotypes. Moreover, plants homozygous for transgenic *CrtR-b2* produced variegated leaves (Figure 3.6C and 3.7B). The development of differently coloured sectors in tissues of transgenic plants has been reported previously. Perhaps the most well-known case was described by Napoli *et al.* (1990), in which the attempt to overexpress chalcone synthase (CHS) in pigmented petals of petunia (*Petunia hybrida*) resulted in generation of white or patterned flowers in 42% of the transgenic plants. The introduction of the transgene resulted in co-suppression of the endogenous and transgenic copies of *CHS* creating a block in anthocyanin biosynthesis. A similar case was described by

Velten *et al.* (2012) in tobacco plants (*Nicotiana tabacum*) engineered to overexpress *AtMYB90* (*PAP2*), an R2R3 Myb gene involved in the production of anthocyanins in *Arabidopsis thaliana*. Transgenic tobacco plants hemizygous for *PAP2* were uniformly dark purple due to their high anthocyanin levels, whereas plants homozygous for *PAP2* expressed a variegated, purple-green phenotype. The reduction in anthocyanin pigmentation was correlated with the reduction in *PAP2* transcript levels in plants homozygous for the transgene. The differently coloured zones on leaves of the transgenic lines studied in this work (U/U; B/B and U/U; B/+) may also be the result of altered pigment accumulation. Perhaps excising these zones and analysing their pigment profiles could help to better understand how the presence of the transgene in a homozygous state has affected the photosynthetic tissue.

In the presented work, a link between zygosity of transgenic *CrtR-b2*, the colour of ripe fruit and the presence of leaf variegations has been established. However, the measurement of transcript levels of *CrtR-b1*, *CrtR-b2* and other carotenoid-related genes was not carried out in all of the transgenic lines. This measurement, for example with the use of reverse transcription qPCR, needs to be performed before it can be concluded that the phenotype of the U/U; B/B and U/U; B/+ lines is indeed the result of silencing of *CrtR-b1* or *CrtR-b2* or reduction in their transcript levels as previously reported by D'Ambrosio *et al.* (2011) for the U/U parent.

3.3.4 HPLC as an analytical and quantitative technique

Throughout this chapter, most of leaf and fruit extracts were analysed and quantified on the HPLC system. Although UPLC could identify the same compounds in the analysed extracts (Supplementary Figure 1.2) and was significantly faster (8 minutes for UPLC against 60 minutes for HPLC), the close overlapping of some peaks, especially in the xanthophyll region, made the quantification of these compounds difficult. Therefore, HPLC was selected as the method of choice and used for the generation of standard curves, which were subsequently used for quantification of isoprenoids and chlorophylls. As shown by the consistency between the retention times and peak areas resulting from injections of known amounts of analytical standards (Supplementary Figure 1.1), HPLC was proven to be a robust and reliable method for carotenoid quantification. Furthermore, HPLC was used extensively as an analytical technique to characterise pigment profiles of tomato leaf and fruit tissues (Figures 3.4, 3.8A and 3.10A). The HPLC analysis of fruit extracts revealed that the differences between the pigment profiles of the four transgenic lines and the Az line (Figure 3.10A) were reflected in the different colours of the fruit (Figure 3.7A). Moreover, HPLC was also used for assessment of the purity of the in-house prepared carotenoid standards (Figure 3.2A). Finally, HPLC was also employed for purification of some of these standards since the compounds of interest were resolving as separate peaks on this system, which could not be achieved with the UPLC (Figure 3.2C).

With the use of HPLC quantification it was possible to show that saponification of the leaf extracts prior to pigment extraction affected some carotenoid compounds (Figure 3.9). This is important as some studies choose to perform saponification prior to extraction. For instance, some fruit, for example goji berries or bell peppers, sequester xanthophylls as fatty acid esters. One might, therefore, choose to saponify these extracts in order to identify which xanthophylls form the esterified compounds and then quantify the amounts of given xanthophylls. However, if saponification significantly reduces the amounts of certain xanthophylls, as shown in this study, the reported values might be, in fact, lower than the real ones. This is particularly important when a compound has a recommended daily limit which should not be exceeded.

Finally, it was rather surprising to see that the analytical standard of zeaxanthin, when run on the HPLC system, appeared to be a pure compound (top left chromatogram in Figure 3.11C) and yet, when run on the TLC plate (Figure 3.11B), it appeared to contain a breakdown product or another impurity. The purity of many standards is reported based on an HPLC assay; therefore, it may be possible that the purchased analytical standards contain other compounds which had not been identified during preparation of the product on a given platform and so, the actual purity may be lower than the one reported (Betz *et al.*, 2011).

3.3.5 Accumulation of xanthophylls in ripe tomato fruit

The addition of an extra copy of the tomato β -carotene hydroxylase 2 (*CrtR-b2*) onto the high β -carotene background led to the accumulation of zeaxanthin and other xanthophylls in ripe tomato fruit (Figure 3.4 and Table 3.1). The positive identification of zeaxanthin was confirmed by resolving the fruit extracts on two different analytical platforms (HPLC in Figure 3.10 and TLC in Figure 3.11). By taking the plants to the next generation, it was shown that accumulation of zeaxanthin was a heritable trait, which was heavily dependent on the zygosity of the transgene (Figures 3.10 and 3.12). However, since the percentage content of xanthophylls in ripe fruit varied significantly between the generations (close to 77% in F_1 population and 62% and 32% in the F_2 population U/O ; B/B and U/O ; $B/+$ lines, respectively), it is thought that the accumulation of xanthophylls in tomato fruit is strongly dependent on the environmental conditions as well. Moreover, since most of the fruit pigment analyses were carried out on the population that was still segregating, high variability between the generations and the individual plants, assigned to the same line based on the presence of the genes of interest, was expected.

The most significant finding of this chapter is that accumulation of zeaxanthin in ripe fruit of the U/O ; B/B and U/O ; $B/+$ lines is occurring as the result of de novo synthesis of zeaxanthin.

This was shown in the ripening series experiment (Figure 3.22). Firstly, since zeaxanthin acts as an accessory pigment and is closely associated with the chloroplasts, it is possible that some zeaxanthin remains in the fruit after the transition of chloroplasts into chromoplasts. However,

the levels of zeaxanthin increased steadily in both transgenic lines from the IG to the R stage of fruit development. For instance, in the U/0; B/B fruit, the levels of zeaxanthin were found to be 0.32, 0.35, 2.40, 7.30 $\mu\text{g g}^{-1}$ DW at the IG, MG, T and R stages, respectively. In the U/0; B/+ line, the levels of zeaxanthin were 0.49, 0.57, 2.50 and 9.44 $\mu\text{g g}^{-1}$ DW at the IG, MG, T and R stages, respectively. In the Az line, the levels of zeaxanthin were found to decrease throughout the ripening process reaching 0.24, 0.19 and 0.13 $\mu\text{g g}^{-1}$ DW at the IG, MG and T stages and no zeaxanthin was detected in ripe fruit. Secondly, the increase in zeaxanthin from the T to R stage is not the result of enzymatic conversion of violaxanthin to zeaxanthin since violaxanthin was not detected in fruit of the transgenic lines at the T stage of development. In fact, the presence of violaxanthin in ripe fruit of the U/0; B/B and U/0; B/+ lines is also the result of de novo synthesis. At the IG stage, fruit of the U/0; B/B and U/0; B/+ lines were found to contain, respectively, 191.3 and 182.4 $\mu\text{g g}^{-1}$ DW of violaxanthin, which at the MG stage decreased to 88.1 and 24.3 $\mu\text{g g}^{-1}$ DW, respectively. At the T stage, neither of the lines was found to contain violaxanthin; however at the R stage, 21.0 and 1.76 $\mu\text{g g}^{-1}$ DW of violaxanthin were detected in the U/0; B/B and U/0; B/+ line, respectively. In the Az line, the levels of violaxanthin decreased from 142.2 at the IG stage to 34.4 $\mu\text{g g}^{-1}$ DW at the MG stage and no violaxanthin was detected at the later stages of development. Moreover, it is known that the conversion of violaxanthin to zeaxanthin requires ascorbate as a reducing agent, which is oxidised to dehydroascorbate (DHA) during this process (Jahns *et al.*, 2009). Interestingly, the RNA-Seq analysis revealed that dehydroascorbate reductase (DHAR; *Solyc09g056180*), the enzyme responsible for reducing DHA to ascorbate (Kabir *et al.*, 2011), was significantly downregulated (3-fold) in the U/0; B/B line compared to Azygous (Supplementary Table 1.3).

Although the U/0; B/B and U/0; B/+ lines were able to accumulate xanthophylls in ripe fruit, their total carotenoid content was much lower compared with the Az line (Figure 3.10B). The reasons for this are not known but the huge increases in the levels of phytoene and lycopene recorded during the fruit ripening process of the Az line were not present in either of the transgenic lines (Figure 3.22). Therefore, the low carotenoid content of transgenic fruit could be an indication of delayed ripening. However, since chlorophyll degradation in tomato fruit is rather slow (Egea *et al.*, 2011), the faster loss of chlorophyll from the green fruit of the transgenic lines (Figures 3.21 and 3.22) implies that the ripening process has been accelerated (Guyer *et al.*, 2014; Su *et al.*, 2015). The premature transition of chloroplasts into chromoplasts may be the result of increased carotenoid metabolism. Therefore, the low levels of phytoene and lycopene in fruit of the transgenic lines are more likely the result of cyclisation and metabolism of the cyclised product due to the presence of the two genes of interest. Moreover, Ethylene Response Factor (ERF) D.4 (*Solyc10g050970*) was downregulated 2.9-fold in the U/0; B/B line compared to Azygous. ERF D.4 is preferentially expressed in young unripe fruit and its expression

declines at the onset of ripening (Liu *et al.*, 2016b). Additionally, fruit ripening-related genes, such as certain glycosyltransferases (*Solyc07g043500*, *Solyc12g088710* and *Solyc12g098580*), alcohol dehydrogenase 2 (ADH2; *Solyc09g025210*) and polygalacturonase non-catalytic subunit AroGP2 (*Solyc05g005550*), were found to be upregulated in the U/0; B/B line (Supplementary Table 1.3).

It was expected that by combining the high β -carotene background with the overexpression of β -carotene hydroxylase, high levels of β -xanthophylls would be achieved. However, the levels of xanthophylls in the U/0; B/B line were much lower than what was expected from the available pool of β -carotene. Xanthophylls are generally considered as photosynthetic pigments and they are found within the thylakoid membranes of chloroplasts either in a free form or in association with proteins (Morosinotto *et al.*, 2003). The loss of these membranes following the transition of chloroplasts into chromoplast during fruit ripening may limit the capacity of chromoplasts to accumulate xanthophylls. For instance, compared to its parents, the F₁ hybrid no. 1 had lower total fruit carotenoid content but higher total leaf carotenoid content (Table 3.1), which clearly illustrated the different capacities of these two organelles to store additional xanthophylls. Interestingly, pepper fruit accumulate very high levels of xanthophylls and 95% of these are found in specific lipoprotein structures known as fibrils (Deruère *et al.*, 1994). Therefore, tomato chromoplast may be unable to accumulate high levels of xanthophylls due to the absence of internal structures adapted for this purpose.

TEM analysis of ripe fruit revealed the presence of membranous infoldings in chromoplasts of the U/0; B/B line (structures labelled T in Figure 3.24B), which were absent from the Az line (Figure 3.24A). It is known that the synthesis and accumulation of carotenoids can directly affect chromoplast differentiation and structure (Fraser *et al.*, 2007; Lado *et al.*, 2015; Lu *et al.*, 2017). Therefore, the increased biosynthesis of xanthophylls may also induce changes at the sub-chromoplast level. If this is the case, the sequestration of carotenoids may also be altered. In fact, the results of the sub-chromoplast fractionation experiment suggested that carotenoid sequestration in the U/0; B/B and U/0; B/+ lines (Figure 3.13) was more targeted and directed at specific membrane compartments, whereas in the Azygous, U/U; B/B and U/U; B/+ lines (Figure 3.13) carotenoids were spread more evenly in the membranes. At high concentrations, hydrocarbon carotenoids, such as lycopene and β -carotene, deposit in the form of crystals, which are not confined to any particular chromoplast compartment. On the other hand, endogenous xanthophylls, especially their *cis*-isomers, cannot form crystals because the bent shape of molecules interferes with their alignment and the presence of polar, hydroxyl groups favours structured position in membranes rather than crystallisation. Thus, it is likely that the oxygen-containing xanthophylls are targeted to specific membrane compartments, whereas the

accumulation of non-polar carotenoids is not subject to the same limits. Moreover, the membranous infoldings in chromoplasts of the U/0; B/B line may be a form of adaptation whose purpose is to increase the storage capacity of these organelles. In summary, the chromoplast ultrastructure can be modified to accommodate the continually synthesised xanthophylls, but the capacity to store them in membranes is limited leading to their low levels.

Alternatively, the low carotenoid content in fruit of the U/0; B/B line could be explained by the continuous conversion of β -xanthophylls into downstream metabolites such as volatile organic compounds (VOCs) or plant hormones, for example ABA. It was previously noticed that when the carotenoid biosynthetic pathway was modified with an aim to direct metabolic flux towards the formation of zeaxanthin, violaxanthin was accumulated instead (D'Ambrosio *et al.*, 2011; G Diretto 2018, personal communication, 16 May). The same observation was made in this work. The fruit (Figure 3.10) and particularly leaves (Figure 3.8) of the transgenic lines preferentially accumulated violaxanthin instead of zeaxanthin. Therefore, the increased metabolic flow upstream of zeaxanthin may lead to increased enzymatic activity downstream of zeaxanthin and formation of carotenoid-derived compounds. Furthermore, some of these compounds may act as signalling molecules regulating genes upstream in the carotenoid biosynthetic pathway. For instance, the expression of ERF C.2 was found to be 10 times greater in the U/0; B/B line than in the Azygous line (Supplementary Table 1.3). ERF C.2 is normally expressed at low levels in fruit but shows a negative correlation with lycopene levels (Abiri *et al.*, 2017; Zhuo *et al.*, 2017). Interestingly, some ERFs are known to be induced by ABA (Heyman *et al.*, 2018).

SPME analysis identified two carotenoid-derived VOCs which were significantly higher in fruit of the U/0; B/B line than the Azygous line (Figure 3.20), although it cannot be excluded that other, unidentified, carotenoid-derived VOCs had also been affected. The first VOCs was identified as 4-isopropyl-2-cyclohexenone, also known as cryptone. Up to date (September 1st, 2019), very little information is available on this metabolite. Based on the structural similarity, violaxanthin, β -carotene or metabolites of β -carotene, for example β -cyclocitral, are suggested as precursors of cryptone. The second VOC was identified as dihydroactinidiolide. This VOC is generated from β -ionone (derivative of β -carotene) through the intermediate 5,6-epoxy- β -ionone. Interestingly, none of the known zeaxanthin-derived VOCs, such as 3-hydroxy- β -cyclocitral, 4-oxoisophorone and safranal, were detected in the U/0; B/B line or the Azygous line (data not shown). This may suggest that zeaxanthin is not accessible to CCDs and may further support the observation that zeaxanthin is sequestered into specific membrane compartments making it unavailable for enzymatic cleavage.

Previously, dihydroactinidiolide was found to accumulate rapidly in *Arabidopsis* leaves exposed to high light stress and to modulate the expression of singlet oxygen-responsive genes (Shumbe

et al., 2014). Some of the genes upregulated in *Arabidopsis* due to increased dihydroactinidiolide concentration included CALEOSIN 3 (AT2G33380), an UDP-glycosyltransferase (AT2G15490) and LOW TEMPERATURE-INDUCED (AT3G50970), which is known to be involved in cold acclimation. Interestingly, a gene encoding oleosin (*Solyc06g034040*) was infinitely upregulated in fruit of the U/0; B/B line. Similarly, three different genes encoding glycosyltransferases (*Solyc07g043500*, *Solyc12g088710* and *Solyc12g098580*) were also expressed at higher levels than in the Az line. Finally, several genes responsible for freezing tolerance and low temperature acclimatisation were also upregulated in the U/0; B/B line. Some of these genes were identified as the Late Embryogenesis Abundant (LEA) proteins (*Solyc01g095140* and *Solyc02g062770*; Supplementary Table 1.3).

Since some of the carotenoid-derived VOCs were shown to regulate gene expression, it may be possible that the low total carotenoid content in fruit of the U/0; B/B line was caused by downregulation of genes in the carotenoid biosynthetic pathway. In fact, the RNA-Seq analysis revealed that some key enzymes involved in carotenoid biosynthesis were downregulated in the U/0; B/B line (Table 3.3). The expression of chromoplast-specific geranylgeranyl pyrophosphate synthase 2 (*GGPS2*; *Solyc04g079960*), which catalyses the *trans*-addition of the three molecules of IPP onto DMAPP to form geranylgeranyl pyrophosphate (GGPP), a precursor for carotenoids and geranylated proteins (Ament *et al.*, 2006), was 2 times lower compared to the Azygous line. Moreover, the expression of chromoplast-specific phytoene synthase (*PSY1*; *Solyc03g031860*) and polycopene isomerase (*CRTISO*; *Solyc10g081650*) was, respectively, 1.7 and 1.9 times lower than in the Azygous line, although these changes were not statistically significant. However, the reduction in *GGPS2* expression in the U/0; B/B line could explain the low levels of phytoene and lycopene in this line. Interestingly, carotene ϵ -monooxygenase (*LUT1*; *Solyc07g042480*), was found to be downregulated 4.7-fold in the U/0; B/B line. The loss-of-function *LUT1* mutants accumulate higher levels of β -xanthophylls (Tian *et al.*, 2003) and the downregulation of this gene could explain why the U/0; B/B line favours the accumulation of xanthophylls from the β -branch of the carotenoid biosynthetic pathway (Figure 3.12B).

The idea of a continuous synthesis of zeaxanthin is supported by the fact that chromoplast-specific lycopene β -cyclase (*CYC-B*) and β -carotene hydroxylase 2 (*CrtR-b2*) were significantly upregulated in the U/0; B/B line by design. Therefore, the idea that the continuous conversion of β -xanthophylls into further metabolites limits their accumulation is feasible. Interestingly, the Orange Ripening (*ORR*) gene was also significantly upregulated in the U/0; B/B line. *ORR* provides a redox electron chain required for the activity of carotenoid biosynthetic enzymes such as *PDS* and *ZDS* (Nashilevitz *et al.*, 2010). However, this redox chain may also be required for reactions further down the pathway. The epoxidation of zeaxanthin requires NADPH as a reductant, and

it was suggested that the sites of NADP reduction and zeaxanthin epoxidation are in close proximity to each other (Siefermann & Yamamoto, 1975). The *ORR* gene encodes a subunit of the NADH dehydrogenase (NDH) complex. Since the NDH complex promotes the electron flux from stromal electron donors to plastoquinone (Nashilevitz *et al.*, 2010) and the plastoquinone shuttles electrons from photosystem II to the cytochrome *b₆f* complex (Van Eerden *et al.*, 2017), the upregulation of *ORR* expression may lead to higher NADPH accumulation. In fact, the *ORR* mutant had significantly reduced levels of NADPH (Nashilevitz *et al.*, 2010). This supports the idea that the conversion of zeaxanthin into violaxanthin continues to take place due to the continuous demand for NADPH.

3.3.6 Identification of candidate genes

The RI line was generated by introgression of *CYC-B* from the wild tomato species *Solanum galapagense* onto the *S. lycopersicum* cultivar UC204B background (Figure 3.1). However, the actual size of the introgression is not known. Therefore, it was expected that some of the differentially expressed genes identified through the RNA-Seq analysis could be attributed to the introgressed region. In fact, *S. galapagense* is known to be resistant to a wide spectrum of insects (Vosman *et al.*, 2018; Vosman *et al.*, 2019). Therefore, it was not surprising that many of the upregulated genes in the U/0; B/B line were related to defense responses (Figure 3.26). Moreover, the genetic background is different between Azygous and the U/0; B/B line, therefore not all differentially expressed genes are equally relevant.

Another group of genes, which was found to be upregulated in the U/0; B/B line, was linked to cell wall-related events, such as cell wall remodelling. This finding is rather unsurprising since the cell wall is the first barrier between the pathogen and the plant, so specific cell wall-related events are expected to be advantageous and to promote resistance against certain pathogens. In fact, many of the differentially expressed genes, which were related to cell wall restructuring and reinforcement, were also found to participate in resistance mechanisms against pathogens (Figure 3.26 and Supplementary Table 1.3). Indeed, it was found that ripe fruit of the U/0; B/B line were significantly firmer than those of the Azygous line (Figure 3.23). The RNA-Seq analysis identified two classes of genes which could contribute to the enhanced fruit firmness. Two pectinesterases (*Solyc04g082140* and *Solyc06g009190*) were 2.9 and 11 times more expressed in the U/0; B/B line than in the Azygous line, respectively. Pectinesterases have oxidoreductase activity and are involved in modification of the cell wall via demethylesterification of pectin into pectate and methanol. Counterintuitively, it was found that the silencing of pectinesterase enhanced the rate of fruit softening during ripening (Phan *et al.*, 2007). Therefore, upregulation of these genes may increase fruit firmness. Two xyloglucan endotransglucosylases/hydrolases (XTHs; *Solyc09g008320* and *Solyc03g031800*) were also found to be upregulated. They are

responsible for catalysing xyloglucan endohydrolysis (XEH) and/or endotransglycosylation (XET) and for promoting cell expansion by breaking the xyloglucan cross-links between cellulose microfibrils before reforming them. It was reported that a decrease in the expression of XTHs and the subsequent decrease in the enzyme activity during ripening may contribute to fruit softening (Miedes & Lorences, 2009). Improvement of fruit shelf life by the enhancement of fruit firmness is a topic of ongoing research due to its agronomic and industrial relevance. Therefore, pectinesterases and XTHs are potential targets for improving fruit quality.

Analysis of primary metabolites (Figure 3.17) revealed that some sugars, such as sucrose and mannose, were higher in ripe fruit of the U/0; B/B line than Azygous. The higher levels of sucrose could be explained by the increased expression of sucrose synthase (*SuSy*; *Solyc12g009300*) and glucose-6-phosphate isomerase (*G6PI*; *Solyc12g098130*) in this line (Supplementary Table 1.3). These two genes were, respectively, 4.6 times and infinitely upregulated in the U/0; B/B line. It was previously shown that ABA treatment increased the expression of *G6PI* in maiden grass (*Miscanthus sinensis*) and gibberellins (GAs) enhanced the transcription of the *SuSy* gene in cotton fibres (Bai *et al.*, 2014). GAs form a large family of plant growth regulators and it was suggested that they could promote the deposition of the secondary cell wall by enhancing the expression of *SuSy* genes (Bai *et al.*, 2014). GAs are synthesised through the MEP pathway from GGPP through the action of three classes of enzymes, namely terpene synthases, cytochrome P450 monooxygenases and 2-oxoglutarate-dependent dioxygenase (2-ODD). Interestingly, the expression of 2-ODD (*Solyc12g006380*) in the U/0; B/B line was 5.1 times higher than in the Az line (Supplementary Table 1.3). Therefore, the higher levels of sucrose in fruit of the U/0; B/B line may result from the increased synthesis of GAs, which contribute to defense mechanisms by modifying the cell wall structure or composition. In fact, multiple studies provide evidence for the involvement of GAs in plant cell wall development and immunity to pathogens (reviewed by De Bruyne *et al.*, 2014). Although the direct measurement of GAs was not carried out, certain morphological changes in the U/0; B/B line suggest that their levels were increased. For instance, GAs are known to regulate the length of stem internodes by stimulating cell elongation, in effect increasing the height of plants (Sun *et al.*, 2019). The plants of the U/0; B/B line were much taller and had longer internodes than the plants of the Az line (Supplementary Figure 1.7). Moreover, the exogenous application of GA₃ was shown to decrease the diameter of tomato fruit by almost a half compared to the wild type (Bünger-Kibler & Bangerth, 1982) and fruit of the U/0; B/B line were also found to be smaller than fruit of the Azygous line (Figure 3.7A).

Many of the changes to the secondary metabolites could be linked to the gene expression data. For instance, squalene is a triterpene and it acts as a precursor for the synthesis of plant sterols (phytosterols) such as campesterol and stigmasterol (Sonawane *et al.*, 2016). A member of the

terpene cyclase/mutase family (*Solyc12g006510*), known to be involved in the biosynthesis of triterpenoids (Christianson, 2017), was found to be 3.5-fold upregulated in fruit of the U/0; B/B line. Yet, the derivatives of squalene were lower in this line compared to Azygous (Figure 3.17). However, the RNA-Seq analysis also revealed that several glycosyltransferases (*Solyc07g043500*, *Solyc12g088710* and *Solyc12g098580*) were upregulated between 4.9-fold and 15.1-fold in the U/0; B/B line (Supplementary Table 1.3). This is significant as these glycosyltransferases act on several phytosterols like sitosterol, campesterol and stigmasterol, leading to the biosynthesis of sterol glycosides (SGs) and acyl sterol glycosides (ASGs), which are the most abundant sterol derivatives in higher plants (Louveau *et al.*, 2011; Cárdenas *et al.*, 2016; Ramirez-Estrada *et al.*, 2017; Nakayasu *et al.*, 2018). Therefore, the increased activity of glycosyltransferases in fruit of the U/0; B/B line could explain its lower levels of phytosterols. Squalene is also a precursor for the synthesis of steroidal glycoalkaloids (SGAs) and some of the identified glycosyltransferases are also involved in the biosynthesis of SGAs. For example, CYP88B1 (GAME4: *Solyc12g006460*), a member of cytochrome P450 family involved in later steps of SGAs biosynthesis (Cárdenas *et al.*, 2016; Hameed *et al.*, 2018; Vasav & Barvkar, 2019), was found to be 22 times upregulated in the U/0; B/B line. SGAs contribute to pathogen resistance and could be another important target for future studies; however, they are toxic to humans and thus considered anti-nutritional (Cárdenas *et al.*, 2016).

The GC-MS analysis (Figure 3.17) showed that the levels of many fatty acids, such as oleic and linoleic acid, were not different between the Azygous and the U/0; B/B line. Yet, the analysis of volatiles (Figure 3.20) showed that many VOCs derived from the oleic or linoleic acid were higher in the U/0; B/B line. The increased levels of fatty acid-derived VOCs may suggest an increase in fatty acid biosynthesis and metabolism. Interestingly, TEM micrographs of ripe fruit revealed the presence of lipid droplets near chromoplasts in the U/0; B/B line, which were not as frequent in the Azygous line (Figure 3.24). The presence of multiple lipid droplets could indicate an increased metabolism of lipids. In fact, many genes related to the lipid metabolism were upregulated in the U/0; B/B line (Supplementary Table 1.3).

CYP77A19 (*Solyc05g055400*), a member of cytochrome P450, was one of the genes linked to the lipid metabolism, which was found to be highly upregulated (23.5-fold). CYP77A19 oxidises fatty acids with chain lengths ranging from 12 to 18 carbon atoms (Grausem *et al.*, 2014). Another identified gene encodes an ABC transporter-like family-protein (*Solyc12g044820*) involved in transmembrane transport and lipid metabolism (Ofori *et al.*, 2018). Two genes belonging to the acetyl-CoA carboxylase (ACC) complex (*Solyc05g005535* and *Solyc04g039820*), were also highly upregulated. The upregulation of these genes is significant as the ACC complex catalyses the irreversible carboxylation of acetyl-CoA to malonyl-CoA and malonyl-CoA is a substrate for fatty

acids biosynthesis (Ke *et al.*, 2000). Further, two genes encoding 3-ketoacyl-CoA synthases (KAS; *Solyc08g067410* and *Solyc09g083050*) were found to be upregulated in the U/O; B/B line. KAS is involved in fatty acid and wax biosynthesis and it was shown that a partial loss of KAS activity in *Arabidopsis* led to a temperature-dependent decrease in fatty acid production in plastids and hypersensitivity of PSII to low temperature (Takami *et al.*, 201). Sec14p-like phosphatidylinositol transfer family protein (*Solyc09g015080*) was also found to be highly upregulated. This protein has lipid binding and transport activities and enables a crosstalk between lipid metabolism and lipid signalling (Bankaitis *et al.*, 2010). Acyl-protein thioesterase 2 (TE2s; *Solyc12g042890*) was also highly upregulated in the U/O; B/B line. Plant TEs control the amount and composition of fatty acids entering the storage lipid pool (Mayer & Shanklin, 2005).

The increase in the expression of many genes associated with fatty acid metabolism could explain the increase in fatty acid-derived VOCs in the U/O; B/B line. In fact, the link between these two processes could be provided by another two genes, which were found to be infinitely upregulated in the U/O; B/B line. The first one encodes caleosin (*Solyc12g096930*), a Ca²⁺-binding domain protein associated with lipid bodies. Caleosins are involved in oxylipin metabolism and in the generation of oxidised fatty acids. Oxylipins are lipophilic signalling molecules derived from the oxidation of polyunsaturated fatty acids and in plants, the C18 polyenoic fatty acids, such as linoleic acid and linolenic acid, are the major precursors of oxylipins. Importantly, some volatile compounds are derived from the oxylipin pathway because the sequential action of lipoxygenase, hydroperoxide lyase and alcohol dehydrogenase on free unsaturated fatty acids leads to the production of volatile aldehydes and alcohols (Yilmaz, 2001; Weichert *et al.*, 2002; Partridge & Murphy, 2009). The second gene linking the lipid synthesis and generation of VOCs is oleosin (*Solyc06g034040*). Oleosins are involved in lipid storage and they interact with lipid and phospholipid moieties of lipid bodies. The oleosin-coated lipid bodies allow for storage of volatile sesquiterpenes. Moreover, it was found that oleosins promote the formation of oil bodies and regulate their size (Chapman *et al.*, 2012; Vanhercke *et al.*, 2017; Delatte *et al.*, 2018; Shimada *et al.*, 2018). Therefore, the increase in expression of the gene encoding oleosin could be closely linked to the increase in the number of lipid droplets and could be a response to increased fatty acid metabolism.

Finally, a number of genes involved in the generation of VOCs were upregulated in fruit of the U/O; B/B line. One of the most significant and infinitely increased was alcohol dehydrogenase 2 (ADH2; *Solyc09g025210*), which was already implicated in the oxylipin pathway. Additionally, a short-chain dehydrogenase-reductase (*Solyc12g056600*), which has alcohol dehydrogenase activity and acts on hexanal, phenylacetaldehyde, (*E*)-2-hexenal and acetaldehyde and the corresponding alcohols (Moummou *et al.*, 2012), was found to be upregulated 9.3 times.

Perhaps, since the carbon flow towards carotenoid biosynthesis has been altered in the *U/O; B/B* line, some of it is redirected towards the production of lipids (fatty acids and their derivatives as well as phytosterols and their derivatives), which could explain the presence of lipid droplets (Figure 3.24B), increase in the fatty-acid derived volatiles (Figure 3.20) and upregulation of the genes discussed above. The ripe fruit of the *U/O; B/B* line have a pleasant, fruity odour and since certain volatiles positively contribute to fruit flavour and aroma, the differentially expressed genes could be targets for future studies aiming to improve these qualities.

3.3.7 Proposal of a regulatory mechanism

The findings discussed above can be summarised into a hypothetical pathway involving certain regulatory elements (Figure 3.27).

The overexpression of *CYC-B* and *CrtR-b2* in tomato fruit increases metabolic flux through the carotenoid biosynthetic pathway and promotes synthesis of zeaxanthin. However, zeaxanthin is not retained, but rather converted into downstream xanthophylls as suggested by the increase in ORR activity and reduction in recycling of ascorbate. The continuous synthesis of violaxanthin

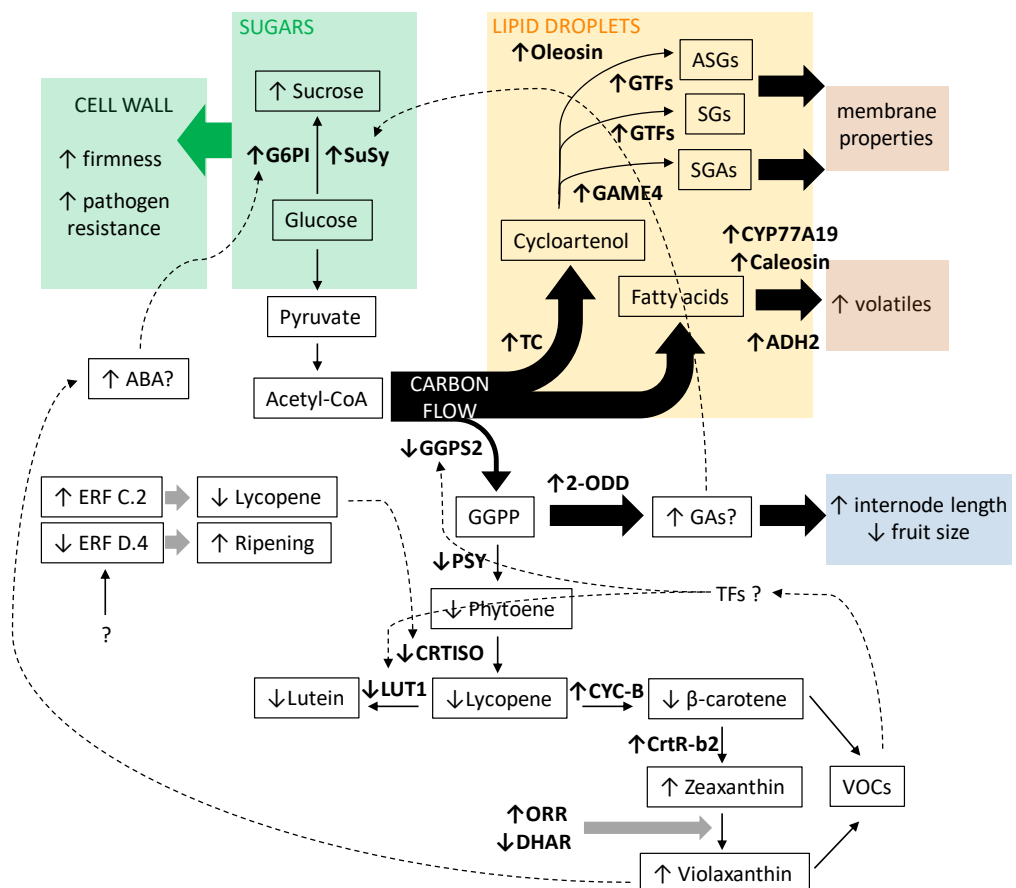


Figure 3.27. Summary of the interactions between carotenoids, VOCs and fatty acids. 2-ODD, 2-oxoglutarate-dependent dioxygenases; ABA, abscisic acid; ADH2, alcohol dehydrogenase 2; ASGs, acyl sterol glycosides; CRTISO, prolycopene isomerase; CrtR-b2, β -carotene hydroxylase; CYC-B, lycopene β -cyclase; DHAR, dehydroascorbate reductase; ERF, Ethylene Response Factor; G6PI, glucose-6-phosphate isomerase; GA, gibberellins; GGPS2, geranylgeranyl pyrophosphate synthase 2; GGPP, geranylgeranyl pyrophosphate; GTFs, glycosyltransferases; LUT1, carotene ϵ -monoxygenase; ORR, Orange Ripening; PSY, phytoene synthase; SGs, sterol glycosides; SGAs, steroidal glycoalkaloids; SuSy, sucrose synthase; TC, terpene cyclase; TFs, transcription factors.

supports the production of ABA. The increase in ABA levels upregulates G6PI, which promotes sucrose synthesis. Additionally, violaxanthin and other carotenoids are converted into VOCs, which, possibly through transcription factors, exert a negative feedback on the expression of the genes upstream in the carotenoid biosynthetic pathway such as *GGPS2*, *PSY1*, *CRTISO* and *LUT1*. This, in turn, leads to decreased levels of phytoene, lycopene and lutein in the fruit. However, since the expression of *CYC-B* and *CrtR-b2* remains high, the little carbon flux that enters the pathway at the level of phytoene is used up by the continuous conversion of the xanthophylls into VOCs, which depletes phytoene and lycopene to very low levels but, at the same time, supports limited synthesis of zeaxanthin. Therefore, the carbon flow is diverted towards the production of fatty acids, phytosterols and GAs. The higher levels of GAs increase the length of stem internodes, reduce fruit size and upregulate sucrose synthase increasing the accumulation of sucrose, which affects the cell wall properties and possibly contributes to the increased fruit firmness and pathogen resistance. The increased carbon flow towards the production of fatty acids and phytosterols and increased lipid metabolism are reflected by the increased number of oil droplets, whose formation is stimulated by the high expression of oleosin. However, the fatty acids and phytosterols are not retained, but rather converted into other metabolites. The fatty acids are converted into volatiles through the oxylipin pathway. The phytosterols are converted into SGs and ASGs, which modify membrane properties, or SGAs, which contribute to plant resistance against pathogens.

3.3.8 Calculation of fruit weight providing the recommended dose of zeaxanthin

The U/0; B/B and U/0; B/+ lines accumulated 7.3 and 9.4 $\mu\text{g g}^{-1}$ DW of zeaxanthin in their ripe fruit, respectively. This means that the daily recommended dose of zeaxanthin of 2 mg can be delivered in 274 and 213 g of dry fruit powder of these two lines, respectively. Assuming that 95% of the tomato fruit is made up by water, 5.48 kg of fresh tomato fruit of the U/0; B/B line or 4.26 kg of fresh fruit of the U/0; B/+ line would need to be consumed in order to provide the recommended daily dose of zeaxanthin. It is very unlikely that this amount of fruit could be consumed by anyone in a course of a single day, and therefore, it is quite unlikely that any of these two lines could be used as a new food source of zeaxanthin, even without taking into account the regulations applicable to genetically modified organisms.

Although the generation of a new, renewable plant source of zeaxanthin was not achieved when the presented gene combinations were introduced, this work led to two major conclusions:

- **The production and accumulation of zeaxanthin and other β -xanthophylls in tomato fruit through de novo synthesis is possible.**
- **A further increase in the level of zeaxanthin in fruit may be achieved by decreasing the conversion of zeaxanthin to violaxanthin.**

Chapter IV: Generation and characterisation of zeaxanthin-accumulating tomato lines

4.1 Introduction

The previous chapter (Chapter III) described the steps taken to develop tomato lines capable of accumulating xanthophylls in their ripe fruit, with particular focus on enhancing the content of zeaxanthin. The generated lines were characterised and two of them (U/0; B/B and U/0; B/+) were found to store free xanthophylls in their fruit. However, the levels of zeaxanthin in these lines were too low to provide the daily recommended dose of this xanthophyll in the amount of fresh fruit that one would be able to consume in the course of a single day. Nonetheless, it was shown that zeaxanthin could be produced and accumulated in ripe tomato fruit and this has encouraged the following work aiming to further increase the levels of this xanthophyll.

The analysis of fruit pigments carried out in Chapter III revealed that the U/0; B/B line contained, on average, 21.0 $\mu\text{g g}^{-1}$ DW of violaxanthin in its ripe fruit (Figure 3.10B). This pool of violaxanthin represents a potential source from which zeaxanthin can be derived. Firstly, violaxanthin could be converted back to zeaxanthin by the enzyme violaxanthin de-epoxidase (VDE). Secondly, by downregulating the activity of zeaxanthin epoxidase (ZEP), the forward conversion of zeaxanthin to violaxanthin could be reduced. In order to test whether reducing the conversion of zeaxanthin to violaxanthin would lead to a higher zeaxanthin content in tomato fruit, the mutated allele of *ZEP*, encoding an enzyme with reduced activity, was introduced into the U/0; B/B and U/0; B/+ lines. This particular allele of *ZEP* was discovered and characterised in the *high-pigment 3* (*hp3*) tomato mutant accumulating lycopene and zeaxanthin in its ripe fruit (Galpaz *et al.*, 2008).

The downregulation of ZEP activity is critical for the accumulation of zeaxanthin. This was first shown in tomato plants transformed with *ZEP* in an antisense orientation, which led to silencing of the endogenous gene. The homozygous antisense plants accumulated more zeaxanthin and less violaxanthin and neoxanthin in their leaves than the wild type plants (Thompson *et al.*, 2000). However, similar phenotypes were described in other *ZEP* mutants generated in various plants using different approaches. For instance, random mutagenesis with EMS allowed to isolate a mutant of *ZEP* (*zea1*) accumulating zeaxanthin under normal growth conditions in marine microalga, *Dunaliella tertiolecta* (Kim *et al.*, 2018). The *zea1* mutant was found to contain a single amino acid substitution (G446D) in the catalytic domain of ZEP, which led to the loss of enzyme function due to the loss of substrate-binding specificity of the mutated protein. In rice, *Oryza sativa*, the insertion of an endogenous mutagen retrotransposon *Tos17* into one of the introns of *ZEP* led to the splicing inhibition and impairment of ZEP activity, generating a strong viviparous mutant with a wilty phenotype (Agrawal *et al.*, 2001). The mutant also contained low levels of ABA and lacked neoxanthin and violaxanthin but showed increased accumulation of zeaxanthin in its leaves. The transformation of potato (*Solanum tuberosum*) with antisense and sense constructs encoding *ZEP* increased the levels of zeaxanthin between 4-fold and 130-fold

and up to 40 $\mu\text{g g}^{-1}$ DW (Römer *et al.*, 2002). The transformed lines also exhibited up to 5.7-fold increases in total carotenoid levels but violaxanthin was drastically reduced and its intermediate, antheraxanthin, was identified in some of the lines. Interestingly, the levels of ABA remained unchanged. Finally, several *Arabidopsis thaliana* mutants of *ZEP* (*aba1*) were isolated as well. The EMS-induced, ABA-deficient mutants *aba1-1*, *aba1-3*, *aba1-4* and *aba1-5* showed increased levels of zeaxanthin, decreased levels of violaxanthin and neoxanthin and a wilted phenotype (Koorneef *et al.*, 1982; Rock & Zeevaart, 1991; Léon-Kloosterziel *et al.*, 1996). Similarly, the EMS-induced *aba1-6* mutant showed enhanced accumulation of zeaxanthin but, unlike the other mutants, was not susceptible to wilting (Niyogi *et al.*, 1998). Most notably, the null T-DNA insertional mutant *aba1-7* accumulated 43 times more zeaxanthin in its seeds than the *Col-0* ecotype (Gonzalez-Jorge *et al.*, 2016). Additionally, antheraxanthin, violaxanthin and neoxanthin were not detected in this mutant but β -carotene and lutein were increased 3.2- and 2.2-fold, respectively. In tomato however, the *hp3* allele is the only, other than the wild type, allele of *ZEP* known to date, which was isolated from the EMS-induced mutant identified through its ABA-deficient phenotype (Galpaz *et al.*, 2008).

The examples outlined above provide solid evidence that higher levels of zeaxanthin in plant tissues could be achieved by the reduction of *ZEP* activity. This chapter describes the generation and screening of lines containing three genes of interest, namely the *hp3* allele of *ZEP*, transgenic *CrtR-b2* and *S. galapagense* *CYC-B*. Following the selection of the genotypes of interest, these were characterised for their carotenoid content in leaf and fruit tissues. The comparison was made with the parental lines and the lines characterised in Chapter III to establish if combining *ZEP* with impaired activity with the high β -carotene background and overexpression of *CrtR-b2* led to an improvement in zeaxanthin content and if the sequestration of carotenoids at the sub-chromoplast level was altered. Further work was carried out to verify if and how the change in leaf carotenoid composition affected the photosynthetic performance of the newly generated lines. This assessment is important if the new lines are to be grown for commercial purposes as compromising photosynthetic efficiency can negatively impact fruit quality and yield. Finally, analysis of primary metabolites and VOCs was carried out. This analysis was necessary in order to better understand if and how the combination of *S. galapagense* *CYC-B*, transgenic *CrtR-b2* and the *hp3* allele of *ZEP* affected other sectors of metabolism.

4.2 Results

4.2.1 Introduction of the *hp3* allele into the U/0; B/B and U/0; B/+ lines

The strategy used to introduce the *hp3* allele into the U/0; B/B and U/0; B/+ lines is provided in Figure 4.1A. Since the ABA-deficient phenotype is only expressed when the *hp3* allele of *ZEP* is

in a homozygous state and the three genes of interest segregate independently, only one plant out of 32 (3.1% frequency) was expected to be of the $U/0; B/B; hp3/hp3$ genotype and two plants out of 32 (6.3% frequency) were expected to be of the $U/0; B/+; hp3/hp3$ genotype. In order to increase the chance of isolating the desired genotypes, the F_2 triple cross segregating population was germinated on MS media supplemented with kanamycin. By doing so, transgenic lines could be selected, which would reduce the number of screening steps.

Some of the seeds were unable to germinate on the prepared media, whereas others produced healthy-looking cotyledons or visibly stressed cotyledons with purple stems (Figure 4.1B). Only the healthy-looking cotyledons ('Brown' in Figure 4.1B) were able to grow once transferred into the soil. These were subsequently screened similarly to the double crosses in Chapter III. The suitability of primers for screening was confirmed on parental lines (Figures 3.5A and 3.5C). The presence of the transgene was verified by PCR amplification for a fragment of the CaMV 35S promoter (data not shown). The zygosity of the transgene was established by RT-qPCR (data not shown). The zygosity of *S. galapagense* *CYC-B* was determined by amplifying fragments of the *S. galapagense* and *S. lycopersicum* *CYC-B* promoters (data not shown).

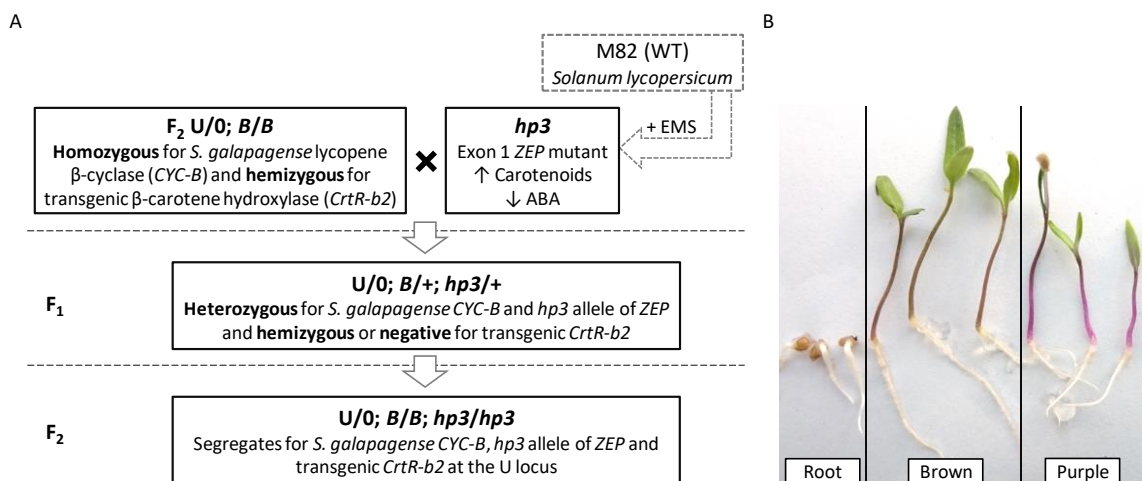


Figure 4.1. (A) Strategy used to create triple crosses. All steps were performed during the presented study except the generation of the *hp3* line (dashed box and arrow). The F_1 $U/0; B/+; hp3/+$ hybrid was produced by crossing the F_2 $U/0; B/B$ line homozygous for *S. galapagense* chromoplast-specific lycopene β-cyclase (*CYC-B*) and hemizygous for transgenic copy of the tomato chromoplast-specific β-carotene hydroxylase (*CrtR-b2*). The F_1 hybrid was advanced to the F_2 generation by self-fertilisation. The segregation pattern of transgenic *CrtR-b2* in F_1 populations, originating from different transgenic parents, was used to determine the transgene zygosity of these parents in Chapter III. Hence, the segregation of three genes in the F_2 population produces 27 unique allele combinations and only a single genotype is listed. Names of the tomato lines are in bold; the *hp3* line background is given in the grey box; the black cross indicates a crossing event. Genotypes: '+' – wild type allele at any locus; *B* – *S. galapagense* *CYC-B* allele (dominant); *hp3* – *high-pigment 3* allele of ZEP (recessive); *U* – *CrtR-b2* transgene insertion; *0* – lack of transgene insertion. Hence, if written alone, *hp3* refers to the original line described by Galpaz *et al.* (2008). ABA – abscisic acid; EMS – ethyl methanesulfonate; ZEP – zeaxanthin epoxidase. (B) 8-day-old seedlings of the F_2 triple crosses germinated on MS media supplemented with kanamycin. The germination on kanamycin was carried out to select for plants positive for transgenic *CrtR-b2*. Some of the seeds only developed radicles (Root) and were unable to grow further. However, the majority of seeds developed normal cotyledons with typically coloured hypocotyls (Brown), which were able to grow normally once transferred to the soil. Interestingly, some seeds developed stunted cotyledons with purple hypocotyls indicating the presence of a stressor (Purple), but these did not grow following their transfer to the soil.

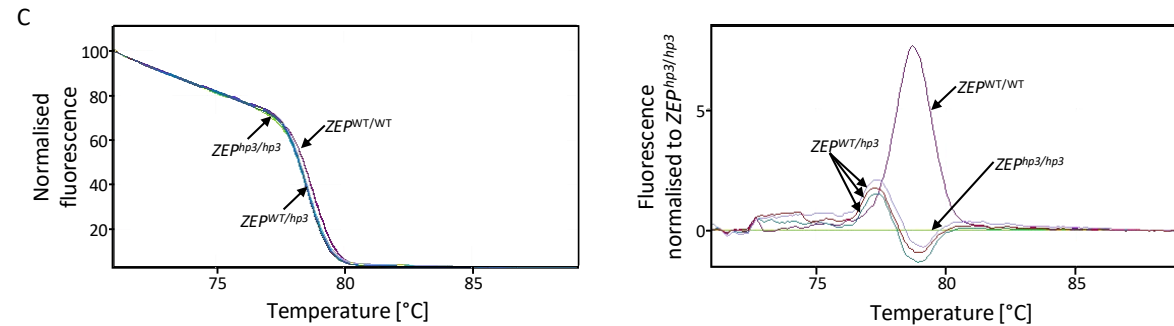
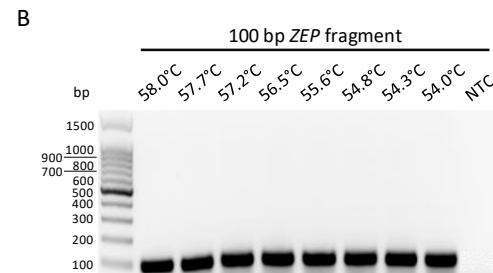
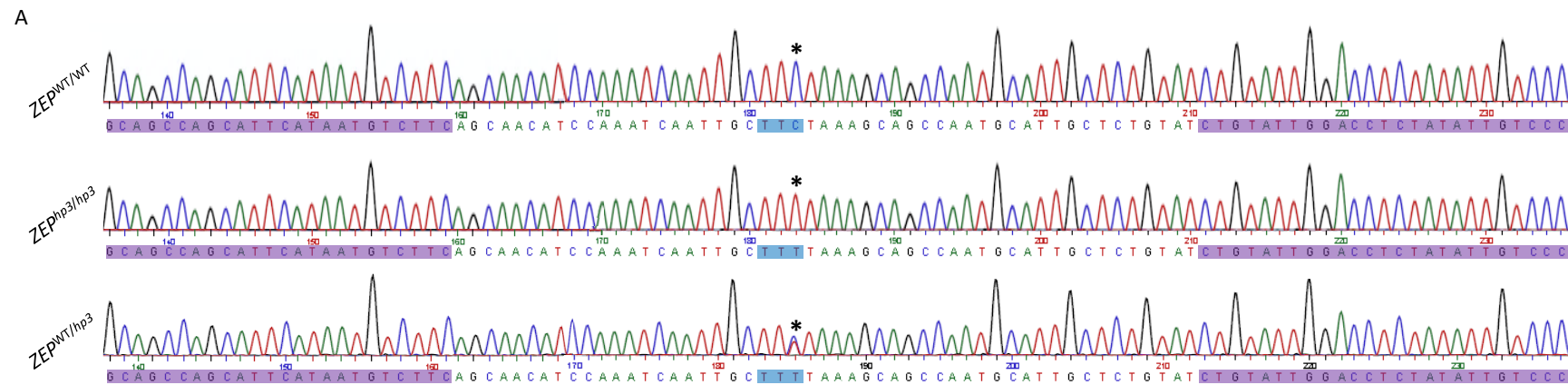
Importantly, the germination of the F₂ triple cross segregating population on the selective media led to the elimination of the line which had segregated out the three genes of interest. However, even without the selection, only one plant out of 64 would have this genotype and would be difficult to isolate regardless. Additionally, this line would not be the true genetic background of this population due to its mixed genetic background as discussed in the previous chapter for the Azygous line. Therefore, due to the lack of true control, most of the comparisons were done against the *hp3* line. However, since the objective was to verify if the combination of the high β -carotene background and overexpression of *CrtR-b2* with reduced activity of ZEP could further increase the accumulation of zeaxanthin, this line was considered to be a better reference since the *hp3* line already accumulated zeaxanthin in its ripe fruit. Additionally, when relevant, comparisons were made against the Az and U/0; B/B lines described in Chapter III, which were grown together with the F₂ triple cross segregating population. This analysis was done in order to verify whether an improvement in zeaxanthin content was achieved in the new line in comparison to the zeaxanthin-accumulating line generated in Chapter III and how this new line was different from Azygous.

However, in order to select appropriate lines for these analyses, the plants carrying two mutated alleles of ZEP had to be distinguished from the plants carrying a single mutated allele. In order to identify these plants, High Resolution Melt (HRM) analysis was carried out.

4.2.2 High Resolution Melt analysis to identify the *hp3* allele

The *hp3* phenotype is only expressed when the mutated allele is present in a homozygous state. Conventional PCR with sequencing could be used to identify plants carrying the mutated allele. However, this is not an efficient method if a large population, such as the one used in this study (200 plants), needs to be screened. In order to select the plants carrying both mutated alleles of ZEP, such as in the *hp3* tomato line, HRM analysis was carried out. HRM is much simpler, faster and cheaper than conventional genotyping methods. Moreover, it allows for the identification of a single base pair difference between the analysed fragments of DNA.

In this screening method, three fragments of DNA, spanning the region where the mutation in the *hp3* allele had occurred, were selected as reference genotypes. The first fragment is the wild type (WT) allele of ZEP, which produces a fully functional protein and is denoted as WT/WT for the purpose of this experiment. The second fragment is the heterozygote containing one WT allele of ZEP and one mutated allele from the *hp3* line, which is denoted as WT/*hp3*. The third fragment is the homozygote consisting of two mutated alleles of ZEP and is denoted as *hp3*/*hp3*. The three fragments, namely WT/WT, *hp3*/*hp3* and WT/*hp3*, were amplified from the U/0; B/B line, *hp3* line and F₁ U/0; B/+; *hp3*/+ hybrid, respectively (Supplementary Figure 2.1) and then sequenced.



D

ID	Line	Genotype	Score [%]
1	<i>hp3</i>	<i>ZEP^{hp3/hp3}</i>	99.6
2	F ₂ U/O; B/B	<i>ZEP^{WT/WT}</i>	99.4
3	F ₁ U/O; B/+; <i>hp3</i> /+	<i>ZEP^{WT/hp3}</i>	97.2
4		<i>ZEP^{WT/hp3}</i>	96.6
5	F ₂ triple crosses	<i>ZEP^{hp3/hp3}</i>	96.8
6		<i>ZEP^{WT/WT}</i>	94.6

Figure 4.2. (A) Sequenced *ZEP^{WT/WT}*, *ZEP^{hp3/hp3}* and *ZEP^{WT/hp3}* allele fragments amplified from the F₂ U/O; B/B line, *hp3* line and F₁ U/O; B/+; *hp3*/+ hybrid, respectively. The codon with the mutated nucleotide (*) is highlighted in blue. The double peak at the third position of the *ZEP^{WT/hp3}* chromatogram indicates the presence of both alleles. The attachment sites of the primers used for HRM are highlighted in violet. (B) Specificity of the HRM primers was confirmed across a range of temperatures. (C) Normalised melt curves (left) of the three fragments allowed to identify the C to T transition between the two homoduplexes (green and violet) and heteroduplex (blue). Difference plot (right) of the melt curves normalised against the *ZEP^{hp3/hp3}* allele. (D) Auto-calling of unknown genotypes of the F₂ triple cross population based on the reference genotypes (shaded). Confidence scores are provided as an integrity check; each plant was analysed in triplicate. Only representative genotypes are shown.

The sequencing confirmed that the selected reference genotypes contained the expected DNA fragments (Figure 4.2A). The WT allele of *ZEP* produced a single peak identified as cytosine (C) in the concerned codon (asterisk in Figure 4.2A). In the *hp3* line, thymine (T) was detected in place of cytosine. The replacement of C by T agreed with what was reported previously for the *hp3-1* allele of *ZEP* (Galpaz *et al.*, 2008). Therefore, through sequencing, it was established that the mutated allele of *ZEP* in the *hp3* line was the one responsible for generating a strong, wilted phenotype as opposed to the *hp3-2* allele, which does not produce such a strong effect. Finally, in the line containing one WT and one *hp3* allele of *ZEP*, two overlapping peaks of cytosine and thymine of the same amplitudes were identified, indicating that this line was heterozygous.

It is important for the DNA fragments used in HRM analysis to be relatively short in order to identify single base changes. A pair of primers, spanning a 100 bp fragment across the region of interest, was designed (bases highlighted in violet in Figure 4.2A). The specificity of the primers was then confirmed across a wide range of temperatures (Figure 4.2B) and subsequently, these were used in the HRM experiment. The experiment showed that the three fragments produced melt curves of distinctive shapes (left graph in Figure 4.2C). By generating a difference plot (right graph in Figure 4.2C) normalised to one of the genotypes (here, the *hp3/hp3* fragment), the characteristic curves produced by the WT and heterozygous plants were clearly distinguishable. The entire F₂ triple cross segregating population was screened in this manner using the three DNA fragments as reference genotypes. The software automatically assigned the genotypes and confidence scores to the analysed plants (Figure 4.2D).

4.2.3 Phenotypic characterisation of the selected lines

PCR, RT-qPCR and HRM were used to screen the entire F₂ triple cross segregating population of 200 plants. Based on the results of these screens, four *hp3* lines with different combinations of *S. galapagense* *CYC-B* and transgenic *CrtR-b2* were identified. The fruit and flower phenotypes of these lines were characterised and compared to the Azygous reference line and the U/0; *B/B* line (Figure 4.3).

Only the fruit of the Az and *hp3* lines were red (Figure 4.3A). The fruit of the U/0; *B/B* line and the four triple crosses were orange. However, the fruit of the U/0; *B/B* line appeared lighter than the fruit of the U/0; *B/B*; *hp3/hp3* and U/0; *B/+*; *hp3/hp3* lines, which, in turn, were lighter than the fruit of the U/U; *B/B*; *hp3/hp3* and U/U; *B/+*; *hp3/hp3* lines. Interestingly, the flowers of the *hp3* line and the U/0; *B/B*; *hp3/hp3* and U/0; *B/B*; *hp3/hp3* lines had a similar, beige colour (Figure 4.3B). On the other hand, the flowers of the U/U; *B/B*; *hp3/hp3* and U/U; *B/+*; *hp3/hp3* lines appeared yellow with a green discolouration at the tip of the stamen and were more similar to the flowers of the Az line. The flowers of the U/0; *B/B* line were also yellow, but their stamen was uniformly coloured and lacked a pronounced discolouration at its tip.

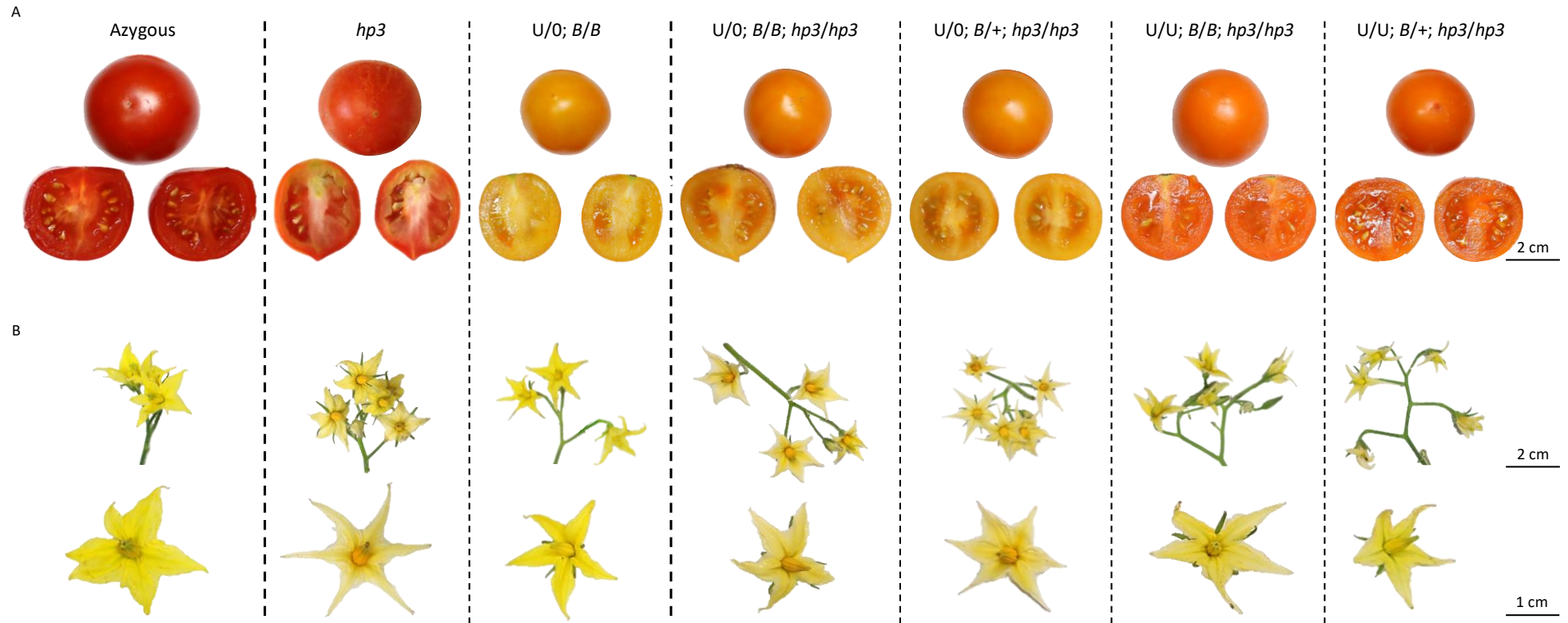


Figure 4.3. Side-by-side comparison of the fruit (A) and flower (B) phenotypes of the indicated tomato lines. (A) Only the *Azygous* and *hp3* lines share the characteristic red colour of a typical tomato. All crosses hemizygous for transgenic copy of *CrtR-b2* (U/0) appear amber-orange. However, the triple crosses (U/0; B/B; *hp3/hp3* and U/0; B/+; *hp3/hp3*) appear to have a slightly darker pericarp and jelly than the double cross (U/0; B/B). The triple crosses homozygous for transgenic copy of *CrtR-b2* (U/U; B/B; *hp3/hp3* and U/U; B/+; *hp3/hp3*) appear darker compared to the other crosses. The change in *S. galapagense* *CYC-B* zygosity does not seem to influence the colour of the triple cross. The fruit of the *hp3* line do not appear uniform in colour and this trait is absent in the triple crosses. The fruit of the crosses are smaller than fruit of the reference lines. (B) The flowers of the *Azygous* and U/0; B/B lines appear the most intense yellow compared to the other lines. However, the green discolouration at the tip of the stamen in the *Azygous* line is absent from the U/0; B/B line in which the stamen is uniformly yellow. The petals of the *hp3* line are paler than the petals of the *Azygous* line but appear similar to the triple crosses hemizygous for transgenic copy of *CrtR-b2* (U/0; B/B; *hp3/hp3* and U/0; B/+; *hp3/hp3*), which also share similarly coloured, dark-orange stamens with discoloured tips. The flowers of the U/U; B/B; *hp3/hp3* and U/U; B/+; *hp3/hp3* lines are yellow but are not as intense as in the U/0; B/B line and have discoloured stamens, similarly to the *Azygous* line.

4.2.4 Leaf pigment analysis of the selected lines

Leaf pigments of the *Azygous*, *hp3* and *U/0; B/B* lines and the four triple crosses were extracted and analysed on the HPLC system. From the chromatograms of saponified leaf extracts, it could be seen that in the *Az* line, the two major peaks were lutein (peak no. 5) followed by β -carotene (peak no. 8; Figure 4.4A). In the *U/0; B/B* line, the major peaks were violaxanthin (peak no. 1), followed by lutein and β -carotene. In the *hp3* line, the major peak was lutein, followed by the equally tall β -carotene and zeaxanthin (peak no. 6) peaks. In all of the triple crosses, zeaxanthin appeared as the major peak, followed by lutein, β -carotene and antheraxanthin (peak no. 4).

Since zeaxanthin was found to be the major pigment in leaves of the triple crosses, their non-saponified leaf extracts were analysed by HPLC, quantified and compared to reference lines and to each other. The leaf pigment profiles of the four triple crosses were very different from the parental *U/U* and *B/B* lines (Figure 4.4B). In fact, the triples crosses hemizygous at the *U* locus only shared a similar total chlorophyll to total carotenoid ratio with their *U/U* parent, whereas in the triple crosses homozygous at the *U* locus, this ratio was more similar to the *B/B* parent. The four triple crosses were next compared to the *hp3* line in order to assess if the introduction of specific gene combinations led to a greater accumulation of zeaxanthin or any major pigment changes. In fact, zeaxanthin was found to be significantly higher in all triple crosses compared to the *hp3* line. The largest, 3.0-fold increase was recorded in the *U/0; B/+; hp3/hp3* line and the smallest, 2.3-fold increase in the *U/U; B/B; hp3/hp3* line. Neoxanthin and luteoxanthin were also significantly higher in all triple crosses than in the *hp3* line. The largest, 8.3-fold increase in neoxanthin was found in the *U/U; B/+; hp3/hp3* line and the smallest, 5.1-fold increase was found in the *U/0; B/B; hp3/hp3* line. Luteoxanthin was not detected in the *hp3* line whereas the crosses stored between 224.1 (*U/0; B/B; hp3/hp3*) and 427.4 (*U/U; B/+; hp3/hp3*) $\mu\text{g g}^{-1}$ DW of this compound. The levels of violaxanthin were higher in all triple crosses than in the *hp3* line, however, significant changes were only found in the *U/0; B/+; hp3/hp3* and *U/U; B/+; hp3/hp3* lines. In these lines, the levels of violaxanthin were found to be, respectively, 13.1 and 14.9 times higher than in the *hp3* line. Similarly, the levels of antheraxanthin were higher in all triple crosses and only in the *U/0; B/B; hp3/hp3* line this change was not significant. The greatest, 3.1-fold change in antheraxanthin levels was found in the *U/0; B/+; hp3/hp3* line and the smallest, 2.7-fold change in *U/U; B/B; hp3/hp3* line. Overall, the introduction of *S. galapagense* *CYC-B* and transgenic *CrtR-b2* in any combination into the *hp3* background led to significant increases in the levels of leaf xanthophylls. Moreover, as a consequence of increases in the levels of many xanthophylls, the total leaf carotenoid content was also significantly higher in the triple crosses compared to the *hp3* line. The highest, 2.2-fold increase was recorded in the *U/U; B/+; hp3/hp3* line and the smallest, 1.5-fold increase was found in the *U/0; B/B; hp3/hp3* line.

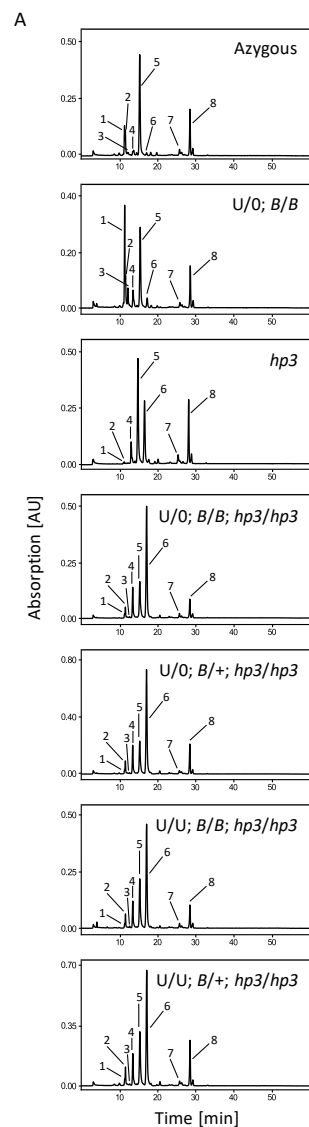


Figure 4.4. (A) HPLC chromatograms of saponified leaf extracts of the indicated lines. 1 – violaxanthin, 2 – neoxanthin, 3 – luteoxanthin, 4 – antheraxanthin, 5 – lutein, 6 – zeaxanthin, 7 – α-carotene, 8 – β-carotene. (B) Quantification of isoprenoids and chlorophylls from the non-saponified leaf extracts of the *hp3* line and the indicated triple crosses. The reported values were used to obtain total carotenoids (CAR) and total chlorophylls (CHL). The ratios of chlorophyll A to chlorophyll B (Chl A : Chl B) and total chlorophylls to total carotenoids (CHL : CAR) were also calculated. The amounts of the compounds are reported as $\mu\text{g g}^{-1}$ DW. The data are presented as the mean of N biological replicates \pm SD; nd – not detected. The pigments from the triple crosses (U/O; B/B; *hp3/hp3*, U/O; B/+; *hp3/hp3*, U/U; B/B; *hp3/hp3* and U/U; B/+; *hp3/hp3*) were compared to the *hp3* line using one-way ANOVA with Dunnett's multiple comparison test; green shading indicates significant increases, red – significant decreases. Additionally, multiple comparisons one-way ANOVA with Tukey's post-hoc test was carried out to compare the lines to each other; compact letter display was used to indicate homogeneous subsets. Data normality was validated with Shapiro-Wilk test. Significant results are reported for $P < 0.05$. Parental lines (U/U and B/B) are included for comparison only. Phytoene was not detected due to larger sample dilution.

Further analysis of leaf pigments revealed that carotenoids of the α -branch of the pathway were affected differently. The levels of α -carotene in the triple crosses were not found to be different from the *hp3* line. However, the levels of lutein were affected and only in the U/U; *B/+*; *hp3/hp3* line this change was not significant. The lutein levels were between 1.3 (U/U; *B/+*; *hp3/hp3*) and 1.6 times (U/U; *B/B*; *hp3/hp3*) lower than in the *hp3* line. Interestingly, the first carotenoid of the β -branch of the carotenoid biosynthetic pathway, β -carotene, was found to be significantly lower (1.6-fold) in the U/U; *B/B*; *hp3/hp3* line compared to the *hp3* line but significantly higher (1.4-fold) in the U/U; *B/+*; *hp3/hp3* line. The levels of β -carotene in the remaining triple crosses did not differ significantly from the *hp3* line. Overall, these data suggest that the introduction of *S. galapagense* *CYC-B* allele and transgenic *CrtR-b2* in any combination into the *hp3* background favours the products of the β -branch of the carotenoid biosynthetic pathway.

The levels of chlorophylls in leaves of the *hp3* line and the triple crosses were compared as well. Chlorophyll A was found to be significantly lower (2.2-fold) only in the U/U; *B/B*; *hp3/hp3* line. Similarly, this line also had a slightly (1.3-fold) but significantly reduced chlorophyll B content. As a consequence, this was also the only line with significantly reduced total chlorophyll levels (1.8-fold) compared to the *hp3* line. The U/U; *B/+*; *hp3/hp3* and U/U; *B/+*; *hp3/hp3* lines had significantly increased (1.2- and 1.3-fold, respectively) levels of chlorophyll B; however, their total chlorophyll content was not different from the *hp3* line. Interestingly, all triple crosses had a significantly lower ratio of chlorophyll A to chlorophyll B than the *hp3* line. Similarly, the ratios of total chlorophyll to total carotenoids of the triple crosses were also significantly lower. This could potentially affect the photosynthetic performance of these plants. Therefore, this issue was addressed later in this chapter.

In the previous chapter, the U/U; *B/B* line was identified as the line with the highest xanthophyll content. To assess if the introduction of the *hp3* allele into this line would improve zeaxanthin content due to decreased activity of ZEP, a direct comparison was made between the Azygous, U/U; *B/B*, *hp3* and U/U; *B/B*; *hp3/hp3* lines. Additionally, this comparison would also provide the relative contributions of each gene to zeaxanthin accumulation. In fact, the levels of zeaxanthin found in leaves of the U/U; *B/B*; *hp3/hp3* line were 38, 12 and 2.6 times higher than in the Az, U/U; *B/B* and *hp3* lines, respectively (Figure 4.5). All increases were found to be statistically significant, whereas the difference in zeaxanthin content between the Azygous and U/U; *B/B* lines was not. Therefore, the presence of the three genes resulted in a significant and profound improvement in the levels of zeaxanthin in the leaf tissue. Moreover, the *hp3* allele was found to contribute the most to this process.

The differences between the content of other pigments in leaves of the Az, U/U; *B/B*, *hp3* and U/U; *B/B*; *hp3/hp3* lines were also analysed. This was done in order to better understand the

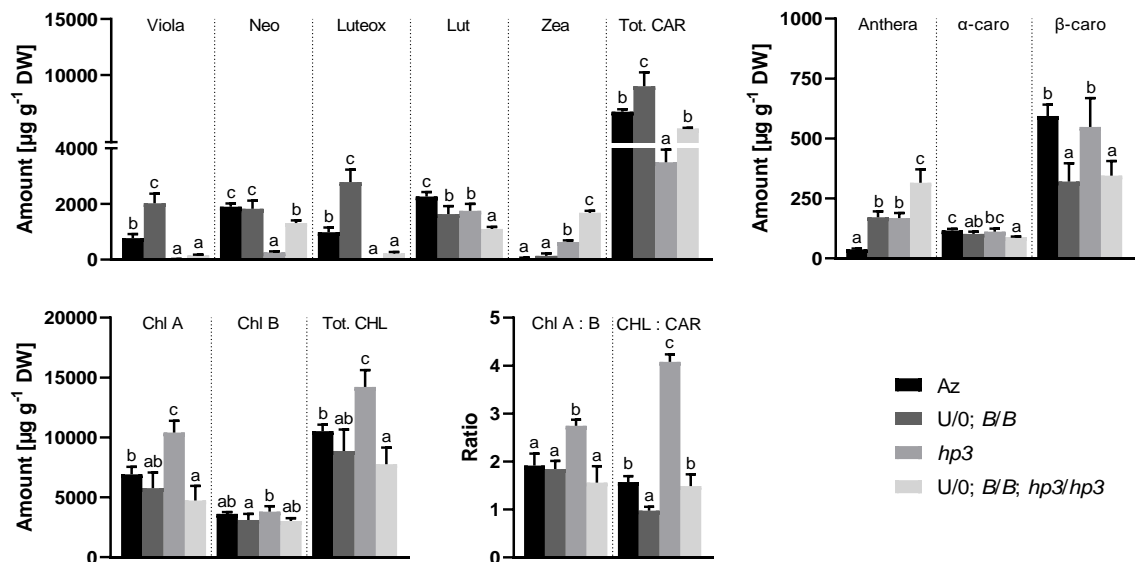


Figure 4.5. Comparison of non-saponified leaf extracts of the F_3 population Azygous ($N = 7$) and $U/0; B/B$ ($N = 10$) lines against the $hp3$ ($N = 6$) and $F_2 U/0; B/B; hp3/hp3$ lines ($N = 3$). The lines were compared to each other using one-way ANOVA with Tukey's multiple comparison test or Kruskal-Wallis test with Dunn's multiple comparison test as appropriate; compact letter display was used to indicate homogeneous subsets. Data normality was validated with Shapiro-Wilk test. Significant results are reported for $P < 0.05$.

changes that had occurred within the pathway that led to the increased content of zeaxanthin. For instance, the levels of antheraxanthin were significantly higher in the $U/0; B/B; hp3/hp3$ line (1.8-fold) than in the $U/0; B/B$ and $hp3$ lines but also in the $U/0; B/B$ and $hp3$ lines (4.5-fold) than in the Az line. However, no difference was found between the $U/0; B/B$ and $hp3$ lines. Therefore, the increased activity of the cyclase and hydroxylase, in combination, drove the accumulation of antheraxanthin to the same extent as ZEP with compromised activity alone. Additionally, the triple cross accumulated as much antheraxanthin as the $U/0; B/B$ and $hp3$ lines together but the effect of combining these two lines on the accumulation of zeaxanthin was synergistic. The accumulation of violaxanthin and luteoxanthin was affected in the same way in the four lines. Both xanthophylls were found to be significantly higher in the $U/0; B/B$ line than in Azygous but much lower in the $hp3$ and $U/0; B/B; hp3/hp3$ lines than in the Az and $U/0; B/B$ lines. Neoxanthin, a derivative of violaxanthin and the precursor of ABA, was also found to be significantly lower in the $U/0; B/B; hp3/hp3$ line than in the Az and $U/0; B/B$ lines but higher than in the $hp3$ line. This suggest that the fully functional ZEP in the Az and $U/0; B/B$ lines drives a continuous conversion of antheraxanthin into violaxanthin, which is then converted to luteoxanthin or neoxanthin by different enzymes. However, in the $hp3$ and $U/0; B/B; hp3/hp3$ lines, this process is reduced due to compromised ZEP activity, which results in lower levels of luteoxanthin and neoxanthin.

The levels of α -carotene were significantly lower in the $U/0; B/B; hp3/hp3$ line compared to the Az and $hp3$ lines but were not different from the $U/0; B/B$ line. However, lutein was significantly lower in the $U/0; B/B; hp3/hp3$ line than in the other three lines. Moreover, the levels of lutein in the $U/0; B/B$ and $hp3$ lines were also found to be significantly lower than in the Az line. The

levels of β -carotene were significantly lower in the U/0; B/B; *hp3/hp3* and U/0; B/B lines than in the Az and *hp3* lines, but no difference was found between the transgenic and non-transgenic lines. Interestingly, despite all these changes in individual carotenoid levels, the total carotenoid content of the U/0; B/B; *hp3/hp3* line was not different from the Az line and only the U/0; B/B line had a significantly higher total carotenoid content. Overall, these data suggest that, in the leaf, the combinations of the genes in the U/0; B/B; *hp3/hp3* and U/0; B/B lines favour the accumulation of β -xanthophylls but in presence of the *hp3* allele this process is impeded at the level of antheraxanthin, which limits a further increase in the total carotenoid content.

Finally, the chlorophyll levels between the Az, *hp3*, U/0; B/B and U/0; B/B; *hp3/hp3* lines were compared. Chlorophyll A and total chlorophyll levels were lower in the U/0; B/B; *hp3/hp3* line and higher in the *hp3* line than in the Az line and very little difference was seen in chlorophyll B content between the lines. However, the ratio of chlorophyll A to chlorophyll B was only higher in the *hp3* line compared to the other lines. The ratio of total chlorophyll to total carotenoids was significantly lower in the U/0; B/B line and significantly higher in the *hp3* line than in the Az and U/0; B/B; *hp3/hp3* lines and these last two lines were not different from each other in this aspect. Therefore, the photosynthetic performance of the Azygous and U/0; B/B; *hp3/hp3* lines should theoretically be similar as the balance between the photosynthetic pigments has been maintained, whereas the photosynthetic performance of the other two lines should be different.

4.2.5 Fruit pigment analysis of the selected lines

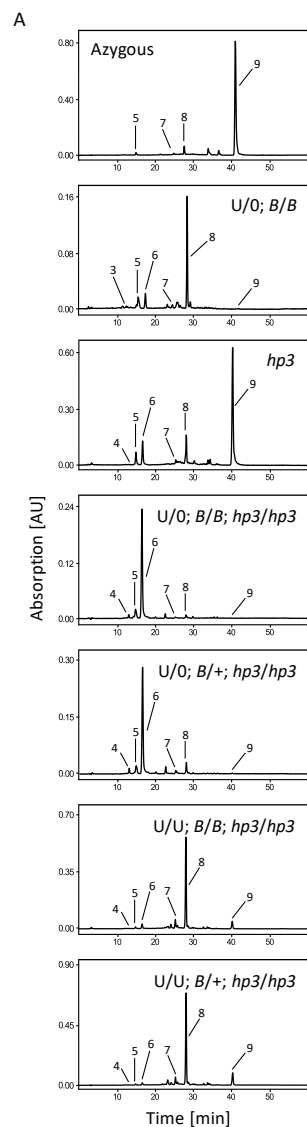
The fruit pigments of the Az, *hp3* and U/0; B/B lines and the triple crosses (U/0; B/B; *hp3/hp3*, U/0; B/+; *hp3/hp3*, U/U; B/B; *hp3/hp3* and U/U; B/+; *hp3/hp3*) were extracted and analysed as well. Although the assessment of changes in leaf pigment content is important in the context of photosynthetic performance and it helps to better understand the flow through the carotenoid biosynthetic pathway, the target organ for an increased accumulation of zeaxanthin is the fruit. The fruit analysis showed that lycopene (peak no. 9) was the major pigment of the Az as well as the *hp3* line (Figure 4.6A). However, zeaxanthin (peak no. 6) was also identified in the *hp3* line at the intensity similar to β -carotene (peak no. 8). Zeaxanthin was also present in the U/0; B/B line next to lutein (peak no. 5) but β -carotene was the major pigment in fruit of this line. Only in the U/0; B/B; *hp3/hp3* and U/0; B/+; *hp3/hp3* lines, zeaxanthin was the major and almost the only pigment present. Finally, in the U/U; B/B; *hp3/hp3* and U/U; B/+; *hp3/hp3* lines, β -carotene was found to be the major carotenoid.

The compounds identified in ripe fruit of the four triple crosses were quantified and compared to the parental lines, the *hp3* line and to each other (Figure 4.6B). The triple crosses homozygous at the U locus were found to be the most similar to their B/B parent due to their high β -carotene content, whereas the triples crosses hemizygous at the U locus were very different from the

parental U/U and B/B lines. Compared to the *hp3* line, the zeaxanthin levels were significantly higher in fruit of the U/0; B/B; *hp3/hp3* and U/0; B/+; *hp3/hp3* lines. Interestingly, in both these lines the same, 1.3-fold change was recorded. On the other hand, in the U/U; B/B; *hp3/hp3* and U/U; B/+; *hp3/hp3* lines, the zeaxanthin levels were significantly lower by 4.5- and 5.5-fold, respectively, compared to the *hp3* line. Antheraxanthin was only significantly increased in fruit of the U/0; B/+; *hp3/hp3* line although, on average, it was also higher in the U/0; B/B; *hp3/hp3* line but this change was not significant. Although the *hp3* line accumulated zeaxanthin in its ripe fruit, only 8% of its total carotenoid content was comprised by this xanthophyll. In fruit of the U/0; B/B; *hp3/hp3* and U/0; B/+; *hp3/hp3* lines, zeaxanthin comprised 82% and 80% of the total carotenoids, respectively. In the U/U; B/B; *hp3/hp3* and U/U; B/+; *hp3/hp3* lines, zeaxanthin made up only 2% of the total carotenoids. Therefore, although the accumulation of zeaxanthin occurred at the expense of other carotenoids, only the combination of the genes of interest in the U/0; B/B; *hp3/hp3* and U/0; B/+; *hp3/hp3* lines led to a significant increase in zeaxanthin levels and greatly increased its contribution to the total carotenoid content.

Compared to the *hp3* line, α -carotene was significantly lower in fruit of the U/0; B/B; *hp3/hp3* and U/0; B/+; *hp3/hp3* lines and higher in the U/U; B/B; *hp3/hp3* and U/U; B/+; *hp3/hp3* lines but only in the U/U; B/+; *hp3/hp3* line the increase was significant. The levels of β -carotene were also significantly lower in the U/0; B/B; *hp3/hp3* and U/0; B/+; *hp3/hp3* lines and higher in the U/U; B/B; *hp3/hp3* and U/U; B/+; *hp3/hp3* lines but this time only in the U/U; B/B; *hp3/hp3* line significantly. However, lutein was significantly lower in all triple crosses than in the *hp3* line. This is consistent with the observation that the U/U; B/B; *hp3/hp3* and U/U; B/+; *hp3/hp3* lines have a functional cyclase that catalyses the conversion of δ -carotene to α -carotene and γ -carotene to β -carotene, but, similarly to the U/U line, their *CrtR-b1* and *CrtR-b2* transcripts are lower, which leads to lower levels of zeaxanthin. In the U/0; B/B; *hp3/hp3* and U/0; B/+; *hp3/hp3* lines, the cyclase and hydroxylase are fully functional; however, since zeaxanthin is the most accumulated product, this combination seems to favour the β -branch of the carotenoid biosynthetic pathway downstream of β -carotene but not beyond the point of antheraxanthin.

Compared to the *hp3* line, phytoene was only significantly lower in the U/0; B/B; *hp3/hp3* and U/0; B/+; *hp3/hp3* lines by, respectively, 116 and 96 times. The levels of phytoene in the other crosses were not affected. However, lycopene was significantly lower in all triple crosses than in the *hp3* line. The largest, almost 730-fold decrease was recorded in the U/0; B/B; *hp3/hp3* line and the smallest, 4.8-fold decrease in the U/U; B/+; *hp3/hp3* line. These data indicate that the fully functional cyclase and hydroxylase in the triple crosses lead to significant decreases in the levels of phytoene and lycopene, whereas the fully functional cyclase alone lowers the levels of lycopene without affecting the levels of phytoene.



B

Compound	Fruit							
	U/U	B/B	hp3	U/U; B/B; hp3/hp3	U/U; B/+; hp3/hp3	U/U; B/B; hp3/hp3	U/U; B/+; hp3/hp3	
α -tocopherol	132.2 \pm 2.7	107.8 \pm 1.8	255.2 \pm 44.4 ^b	160.2 \pm 31.7 ^a	137.8 \pm 6.4 ^a	197.2 \pm 2.0 ^{ab}	226.6 \pm 23.2 ^b	
Antheraxanthin	0.3 \pm 0.1	3.2 \pm 1.0	0.6 \pm 0.3 ^a	2.9 \pm 2.1 ^a	3.4 \pm 1.7 ^a	0.4 \pm 0.4 ^a	0.8 \pm 0.4 ^a	
Lutein	25.4 \pm 1.4	17.7 \pm 0.6	86.7 \pm 15.0 ^b	23.1 \pm 3.3 ^a	25.0 \pm 2.6 ^a	14.7 \pm 1.0 ^a	13.8 \pm 2.1 ^a	
Zeaxanthin	nd	1.4 \pm 0.2	145.2 \pm 22.4 ^b	187.0 \pm 12.4 ^c	183.7 \pm 14.7 ^c	32.0 \pm 5.0 ^a	26.5 \pm 10.2 ^a	
Phytoene	193.4 \pm 3.0	69.6 \pm 1.6	220.3 \pm 100.5 ^b	1.9 \pm 1.1 ^a	2.3 \pm 1.0 ^a	181.9 \pm 84.4 ^b	181.4 \pm 54.1 ^b	
α -carotene	11.9 \pm 0.2	121.2 \pm 16.8	31.3 \pm 3.9 ^b	3.3 \pm 0.4 ^a	3.4 \pm 1.4 ^a	86.2 \pm 26.2 ^c	64.5 \pm 9.9 ^c	
β -carotene	45.6 \pm 6.0	1567.8 \pm 23.4	166.0 \pm 43.9 ^{ab}	8.8 \pm 2.1 ^{ab}	8.4 \pm 5.7 ^a	1426.1 \pm 864.9 ^c	589.8 \pm 279.6 ^b	
Lycopene	699.2 \pm 44.0	55.3 \pm 1.0	1163.9 \pm 80.9 ^c	1.6 \pm 0.5 ^a	2.0 \pm 0.6 ^a	61.6 \pm 43.4 ^a	241.7 \pm 91.7 ^b	
Total XAN	25.7 \pm 1.4	22.3 \pm 1.2	232.4 \pm 21.3 ^b	213.0 \pm 16.8 ^b	212.1 \pm 16.8 ^b	47.0 \pm 6.4 ^a	40.8 \pm 11.8 ^a	
Total CAR	975.8 \pm 44.5	1836.2 \pm 28.9	1813.9 \pm 245.1 ^b	228.6 \pm 18.4 ^a	228.2 \pm 21.0 ^a	1802.8 \pm 925.7 ^b	1118.2 \pm 334.6 ^b	
	N	1	1	3	3	6	2	4

Figure 4.6. (A) HPLC chromatograms of ripe fruit extracts of the indicated tomato lines. 1 – violaxanthin, 2 – neoxanthin, 3 – luteoxanthin, 4 – antheraxanthin, 5 – lutein, 6 – zeaxanthin, 7 – α -carotene, 8 – β -carotene, 9 – lycopene. **(B)** Quantification of isoprenoids and α -tocopherol from ripe fruit of the *hp3* line and the indicated triple crosses. The reported values were used to obtain total carotenoids (CAR; α -tocopherol not included) and total xanthophylls (XAN). The amounts of the compounds are reported as $\mu\text{g g}^{-1}$ DW. The data are presented as the mean of N biological replicates \pm SD; nd – not detected. The pigments from the triple crosses (U/U; B/B; *hp3/hp3*, U/U; B/+; *hp3/hp3*, U/U; B/B; *hp3/hp3* and U/U; B/+; *hp3/hp3*) were compared to the *hp3* line using one-way ANOVA with Dunnett's multiple comparison test or Welch ANOVA test with Dunnett's T3 multiple comparisons test for the groups with unequal variances; green shading indicates significant increases, red – significant decreases. Additionally, multiple comparisons one-way ANOVA with Tukey's post-hoc test was carried out to compare the lines to each other; compact letter display was used to indicate homogeneous subsets. Data normality was validated with Shapiro-Wilk test. Significant results are reported for $P < 0.05$. Parental lines (U/U and B/B) are included for comparison only.

Finally, the levels of α -tocopherol were only significantly lower in the U/0; B/B; *hp3/hp3* and U/0; B/+; *hp3/hp3* lines compared to the *hp3* line. In these lines the ratios of total carotenoids to α -tocopherol were 1.4:1 and 1.7:1. In the *hp3*, U/U; B/B; *hp3/hp3* and U/U; B/+; *hp3/hp3* lines these ratios were 7:1, 9:1 and 5:1, respectively. Therefore, it seems that the U/0; B/B; *hp3/hp3* and U/0; B/+; *hp3/hp3* lines can accumulate proportionally greater levels of α -tocopherol than the remaining lines despite their low total carotenoid content.

The comparison between fruit pigments of the Az, *hp3*, U/0; B/B and U/0; B/B; *hp3/hp3* lines was carried out similarly to what was done in the leaf. Zeaxanthin was not detected in fruit of the Az line; however, in comparison to the U/0; B/B and *hp3* lines, a 50- and 1.3-fold increase in the zeaxanthin content, respectively, was achieved in the U/0; B/B; *hp3/hp3* line (Figure 4.7). As reported for leaves, the *hp3* allele was also found to contribute the most to the accumulation of zeaxanthin in fruit. Antheraxanthin was identified only in the *hp3* and U/0; B/B; *hp3/hp3* lines; however, due to a high variability between the individual plants, these two lines were not found to be significantly different from each other. Moreover, the absolute amounts of antheraxanthin in these lines were very low and hardly significant. Luteoxanthin was only identified in fruit of the U/0; B/B line most likely due to the increased activity of the cyclase and hydroxylase but it was absent from the Azygous, *hp3* and U/0; B/B; *hp3/hp3* lines. Perhaps the combination of the endogenous cyclase and endogenous hydroxylase in fruit of the Az line is not strong enough to drive the accumulation of β -xanthophylls, whereas in the *hp3* and U/0; B/B; *hp3/hp3* lines, the presence of ZEP with compromised activity reduces the conversion of zeaxanthin into other xanthophylls, limiting their accumulation. Interestingly, the total xanthophyll content was not significantly different between the *hp3* and U/0; B/B; *hp3/hp3* lines, suggesting that there is a maximum capacity for their storage in tomato fruit, irrespective of the genetic background.

The levels of α -carotene were significantly lower in fruit of the U/0; B/B and U/0; B/B; *hp3/hp3* lines compared to the Az and *hp3* lines, but they were not significantly different from each other. Interestingly, the lutein levels in fruit of the Az and U/0; B/B; *hp3/hp3* lines were not found to

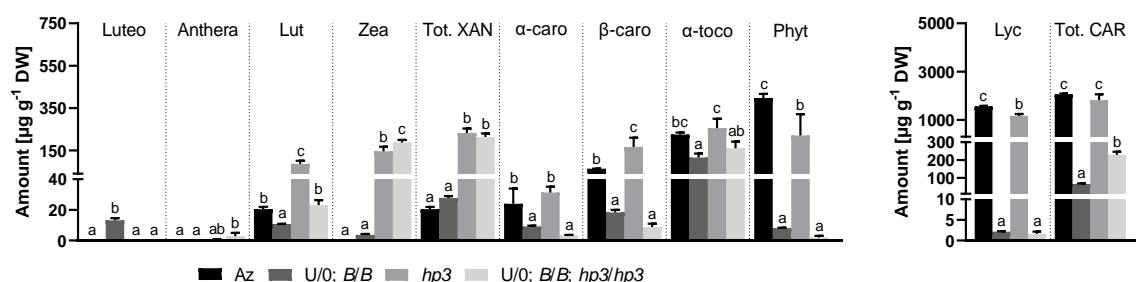


Figure 4.7. Comparison of ripe fruit extracts of the F₃ population Azygous (N = 3) and U/0; B/B (N = 3) lines against the *hp3* (N = 3) and F₂ U/0; B/B; *hp3/hp3* lines (N = 3). The lines were compared using one-way ANOVA with Tukey's multiple comparison test; compact letter display was used to indicate homogeneous subsets. Data normality was validated with Shapiro-Wilk test. Significant results are reported for $P < 0.05$.

be significantly different. Additionally, they were significantly lower and higher than the lutein levels in the *hp3* and *U/0; B/B* lines, respectively. This shows that the combination of the cyclase and hydroxylase favours the β -branch of the carotenoid biosynthetic pathway, but the presence of ZEP with compromised activity allows for a greater accumulation of lutein. This observation was consistent with the reported levels of β -carotene, which were significantly lower in fruit of the *U/0; B/B* and *U/0; B/B; hp3/hp3* lines compared to the *Az* and *hp3* lines, suggesting that the flow down the β -branch was continuous. However, due to the metabolic block at the level of ZEP in the *U/0; B/B; hp3/hp3* line, some of this flow was diverted towards the α -branch of the pathway, allowing for a greater accumulation of lutein in these plants.

The phytoene and lycopene levels were significantly lower in the *U/0; B/B* and *U/0; B/B; hp3/hp3* lines compared to the *Az* and *hp3* lines and no difference was found between the two transgenic lines. It is likely that phytoene and lycopene are being used for the synthesis of the downstream xanthophylls due to the presence of the two genes of interest. However, the total carotenoid levels in the *U/0; B/B* and *U/0; B/B; hp3/hp3* lines were also significantly lower compared to the *Az* and *hp3* lines. Therefore, not all of the available lycopene was converted into xanthophylls. It seems that the capacity of fruit chromoplast to store oxygenated carotenoids is lower than for hydrocarbon carotenoids. However, equally likely, the xanthophylls in fruit of the *U/0; B/B* and *U/0; B/B; hp3/hp3* lines may be used in other biochemical pathways to form other products, such as VOCs or hormones, thus participating in the depression of phytoene and lycopene. Alternatively, the enhanced activity of the cyclase and hydroxylase in fruit of the *U/0; B/B* and *U/0; B/B; hp3/hp3* lines, possibly through the action of transcription factors or due to the increased accumulation of catabolites, exerts a negative feedback regulation, which suppresses the expression of genes very early in the carotenoid biosynthetic pathway, resulting in lower levels of the precursors.

Finally, the levels of α -tocopherol were found to be 1.9 and 1.4 times lower in the *U/0; B/B* and *U/0; B/B; hp3/hp3* lines, respectively, compared to the *Azygous* line. However, despite a quite dramatic change in the total carotenoid contents of the *U/0; B/B* and *U/0; B/B; hp3/hp3* lines (32- and 9.0-fold decreases, respectively) compared to the *Az* line, the change in α -tocopherol was not proportional. This may be connected with the way these compounds are stored within the compartments of the chromoplast allowing for a greater accommodation of α -tocopherol in the transgenic lines despite the massive reduction in the total carotenoid content.

4.2.6 Analysis of gene combinations in leaves and fruit

In order to assess what combinations of the cyclase (*S. galapagensis* *CYC-B*) and the hydroxylase (transgenic *CrtR-b2*) supported the accumulation of the compounds of interest, the comparison between the lines sharing the same zygosity of one of these genes was carried out for the leaf

(Figure 4.8A) and fruit (Figure 4.8B) pigments of the triple crosses. This comparison is equivalent to the one done for the double crosses in Chapter III, Section 3.2.9, with the exception that here the presence of two *hp3* alleles is a common factor for all triple crosses.

The most striking difference between the leaf and fruit tissues of the triple crosses was that in the leaf, the change in cyclase zygosity had the strongest effect, while the fruit was only affected by the change in hydroxylase zygosity. The observation that the leaf pigments were generally lower when the cyclase was in a homozygous state in plants sharing the zygosity of the other genes, was quite surprising. Firstly, because *S. galapagense* *CYC-B* is a fruit specific cyclase, but more importantly, the double dosage of this dominant allele led to a global decrease in pigments rather than an increase. Out of the two lines, the triple crosses hemizygous for the transgene were more affected than the homozygous ones. Another surprising finding was that in the fruit, the change in cyclase zygosity in plants sharing the zygosity of the other genes, did not affect the accumulation of pigments at all. Collectively, these data show that the change in zygosity of the cyclase in the triple crosses only affects their leaf but not fruit pigments.

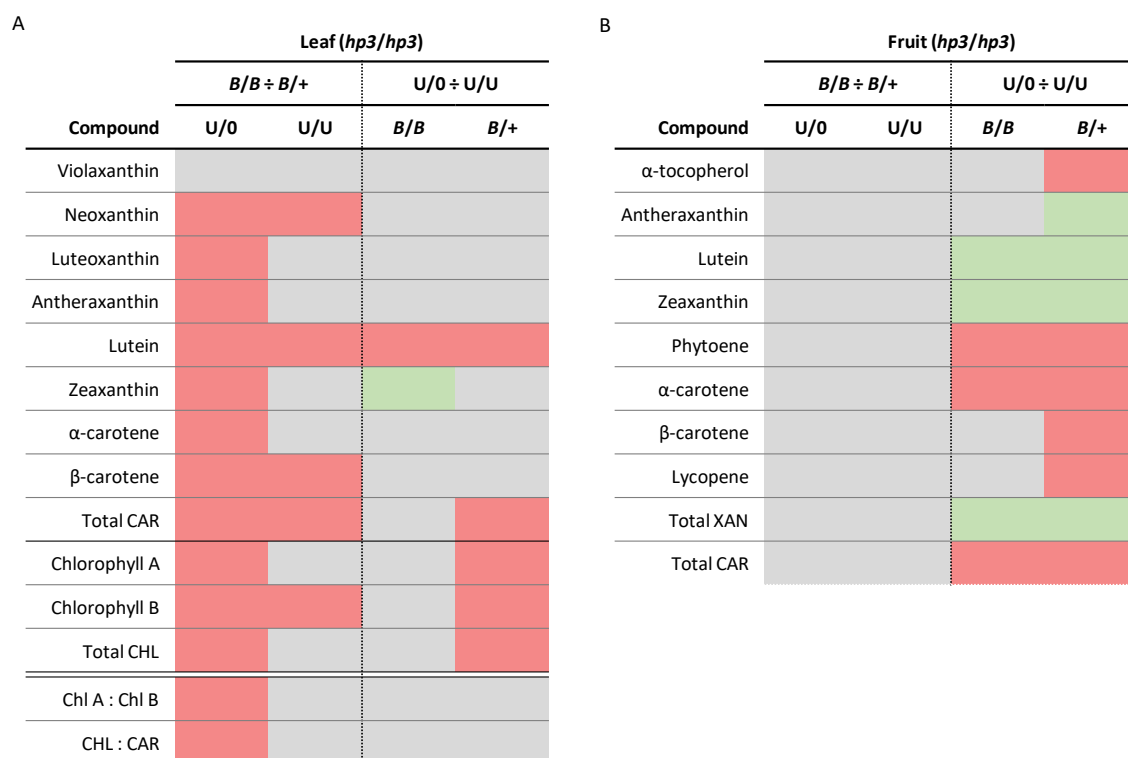


Figure 4.8. Effects of different gene combinations on leaf (A) and fruit (B) pigment profiles. The first column shows the comparison between the *U/0; B/B; hp3/hp3* and *U/0; B/+; hp3/hp3* lines; thus it specifically examines the effect of *S. galapagense* *CYC-B* zygosity in the *hp3* background hemizygous for transgenic *CrtR-b2*. The second column compares the effect of *S. galapagense* *CYC-B* zygosity in the *hp3* background homozygous for transgenic *CrtR-b2* (*U/U; B/B; hp3/hp3* over *U/U; B/+; hp3/hp3*). The third column compares the effect of transgene zygosity in the *hp3* background homozygous for *S. galapagense* *CYC-B* (*U/0; B/B; hp3/hp3* over *U/U; B/B; hp3/hp3*). The last column compares the effect of transgene zygosity in the *hp3* background heterozygous for *S. galapagense* *CYC-B* (*U/0; B/+; hp3/hp3* over *U/U; B/+; hp3/hp3*). The analysis was carried out using unpaired t-test (two-tailed) or Mann-Whitney test (two-tailed) as appropriate. Data normality was validated with Shapiro-Wilk test. Green shading indicates significant increases, red – significant decreases, grey – no significant changes between the lines. Significant results are reported for $P < 0.05$.

In the leaf, zeaxanthin was only higher in lines homozygous for the cyclase when the transgene was found in a hemizygous state. This, however, was accompanied by lower lutein levels. In the lines heterozygous for the cyclase, the presence of the transgene in a hemizygous state also led to lower lutein levels and also negatively affected the total carotenoid and chlorophyll contents. However, overall, very little change in the pigment content was found between the two lines when the hydroxylase zygosity was changed. On the other hand, in the fruit, many carotenoids were lower in lines sharing the same zygosity of the cyclase when the transgene was present in a hemizygous rather than homozygous state. However, this was accompanied by a concurrent increase in the total xanthophyll content and individual xanthophylls, including antheraxanthin, lutein and zeaxanthin. In the fruit, the lines heterozygous for the cyclase were affected more by the change in zygosity of the transgene. Collectively, these data suggest that the accumulation of xanthophylls in the fruit occurs at the expense of other carotenoids in lines hemizygous for the transgene irrespective of the cyclase zygosity, whereas in the leaf, this effect is much weaker.

The major conclusion of this analysis is that, since there is little difference between the fruit pigment profiles of the *U/0; B/B; hp3/hp3* and *U/0; B/+; hp3/hp3* lines and, at the same time, the *U/0; B/+; hp3/hp3* line is higher in leaf pigments, the *U/0; B/+; hp3/hp3* line is potentially a better source of xanthophylls and other carotenoids. However, it cannot be ruled out that the leaf pigments are controlled by other loci that are segregating in the genetic background.

4.2.7 Flower pigment analysis of the selected lines

The phenotypic characterisation of the studied lines revealed certain similarities and differences in the colouration of their flowers (Figure 4.3B). Flowers can store high levels of carotenoids and this is achieved by esterification of hydroxylated carotenoids with fatty acids. In order to assess if a particular combination of the genes of interest led to a change in the carotenoid composition or to different esterification patterns, the pigments of the flowers were extracted and analysed on the HPLC system (Figure 4.9A). The differences in colours of the flowers were reflected in their different pigment profiles. Only the intense yellow flowers of the *Az* and *U/0; B/B* lines were found to contain large amounts of xanthophyll diesters (blue shaded region in Figure 4.9A). Some amounts of the diesters were also found in the yellow flowers of the *U/U; B/B; hp3/hp3* and *U/U; B/+; hp3/hp3* lines; however, these appeared to be much less abundant. On the other hand, in the beige flowers of the *hp3*, *U/0; B/B; hp3/hp3* and *U/0; B/+; hp3/hp3* lines, only small amounts of the diesters were found. Xanthophyll monoesters were only present in flowers of the *Az* and *U/0; B/B* lines (green shaded region in Figure 4.9A) and, at the same time, only small amounts of free xanthophylls were detected in these lines (yellow shaded region in Figure 4.9A). The *hp3* line and the four triple crosses contained mostly free xanthophylls. In fact, the major xanthophyll identified in these lines was zeaxanthin.

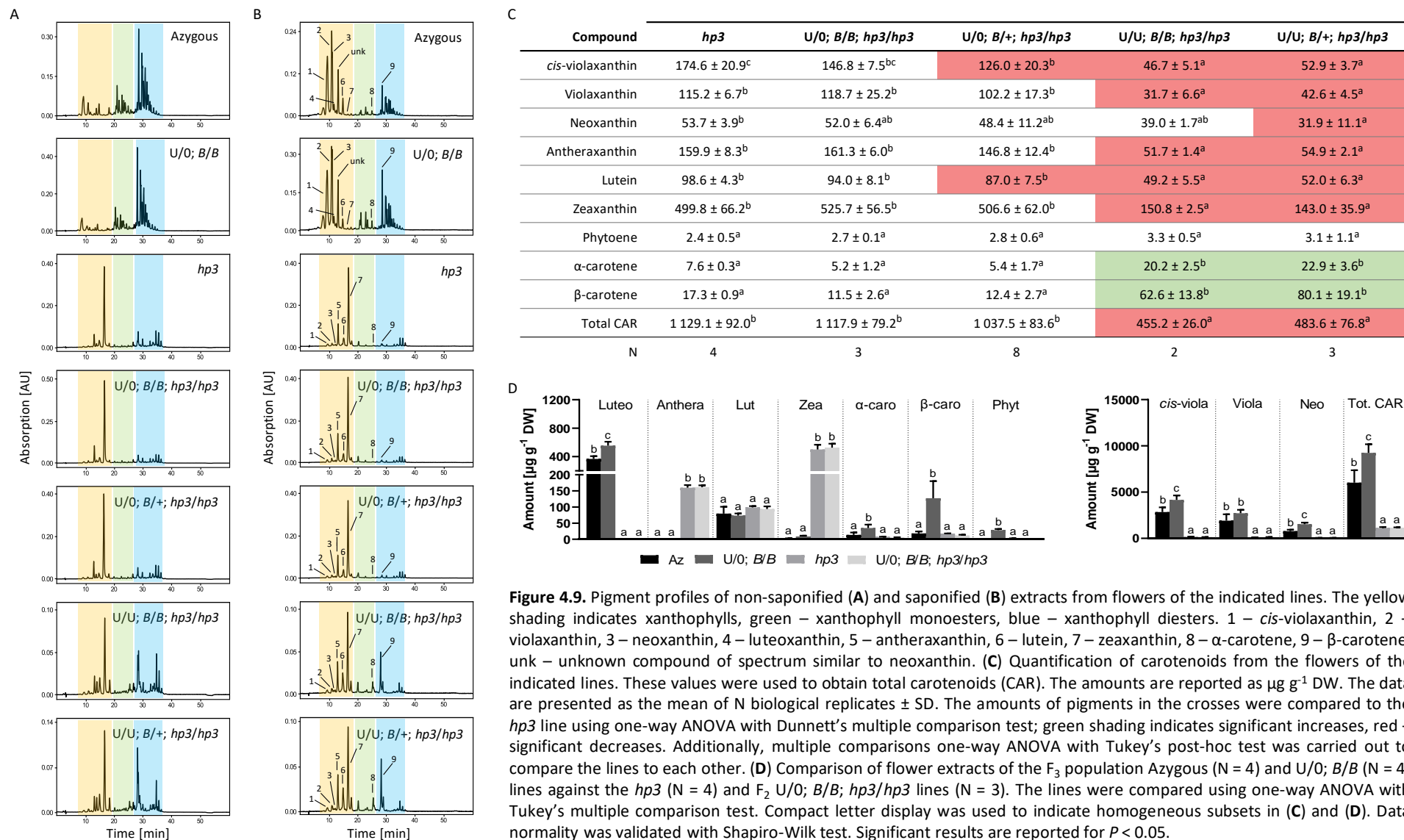


Figure 4.9. Pigment profiles of non-saponified (A) and saponified (B) extracts from flowers of the indicated lines. The yellow shading indicates xanthophylls, green – xanthophyll monoesters, blue – xanthophyll diesters. 1 – *cis*-violaxanthin, 2 – violaxanthin, 3 – neoxanthin, 4 – luteoxanthin, 5 – antheraxanthin, 6 – lutein, 7 – zeaxanthin, 8 – α-carotene, 9 – β-carotene, unk – unknown compound of spectrum similar to neoxanthin. (C) Quantification of carotenoids from the flowers of the indicated lines. These values were used to obtain total carotenoids (CAR). The amounts are reported as $\mu\text{g g}^{-1}$ DW. The data are presented as the mean of N biological replicates ± SD. The amounts of pigments in the crosses were compared to the *hp3* line using one-way ANOVA with Dunnett’s multiple comparison test; green shading indicates significant increases, red – significant decreases. Additionally, multiple comparisons one-way ANOVA with Tukey’s post-hoc test was carried out to compare the lines to each other. (D) Comparison of flower extracts of the F₃ population Azygous (N = 4) and U/O; B/B (N = 4) lines against the *hp3* (N = 4) and F₂ U/O; B/B; *hp3/hp3* lines (N = 3). The lines were compared using one-way ANOVA with Tukey’s multiple comparison test. Compact letter display was used to indicate homogeneous subsets in (C) and (D). Data normality was validated with Shapiro-Wilk test. Significant results are reported for $P < 0.05$.

In order to identify which xanthophylls were esterified in the flowers, the flower samples were saponified prior to the extraction and subsequently analysed on the HPLC system (Figure 4.9B). The most important observation was that the pigment profiles of the *hp3* line and the four triple crosses remained almost unchanged following the saponification and only small decreases in the peak intensities in the diester region were seen. On the other hand, the saponified flower extracts of the *Az* and *U/0; B/B* lines contained a much greater proportion of free xanthophylls than the non-saponified extracts. In both of these lines, the largest reduction was recorded in the content of diesters, albeit they were still present, meaning that the xanthophylls were not fully hydrolysed. The largest increases in the contents of free xanthophylls in saponified flower extracts of the *Azygous* and *U/0; B/B* lines were recorded for *cis*-violaxanthin, violaxanthin and neoxanthin and a small increase was recorded for lutein. In saponified flower extracts of the *hp3* line and the four triple crosses, small increases in free antheraxanthin and lutein were found as compared to the non-saponified extracts, meaning that these were also present in the esterified form, albeit at very low levels. Since saponification was shown to reduce the amounts of certain carotenoids and, in particular, xanthophylls obtained during the extraction process (Figure 3.9), the increase in the peak intensities of all xanthophyll compounds, except zeaxanthin, strongly implies that these must have been freed up. These data additionally show that none of the plants containing the *hp3* allele of *ZEP* were able to esterify zeaxanthin, whereas antheraxanthin and lutein were esterified to a low extent. The *Azygous* and *U/0; B/B* lines were unable to accumulate zeaxanthin, but they accumulated violaxanthin, neoxanthin and lutein instead, which they were also able to esterify to a large extent.

Since the pigment profiles of the *hp3* line and the triple crosses were very similar, quantification of the saponified flower extracts was carried out to assess changes in the levels of carotenoids (Figure 4.9C). In fact, no statistically significant differences were found between the *hp3* and *U/0; B/B; hp3/hp3* lines. The saponified flower extracts of the *hp3* and *U/0; B/+; hp3/hp3* lines were also very similar with only *cis*-violaxanthin and lutein found to be significantly lower in the *U/0; B/+; hp3/hp3* line. The *U/0; B/B; hp3/hp3* line accumulated the highest levels of zeaxanthin in its flowers reaching over 0.5 mg g⁻¹ DW, which was 2.8 times higher than in the fruit of this line. In flowers of the *U/U; B/B; hp3/hp3* and *U/U; B/+; hp3/hp3* lines, the carotenoid levels were generally lower in comparison to the *hp3* line, with the exception of α - and β -carotene, which were significantly higher and phytoene, which was unchanged. The levels of zeaxanthin in the crosses homozygous for the transgene were between 3.3 and 3.5 times lower than in the *hp3* line. The lower xanthophyll levels and the higher levels of α - and β -carotene in these two lines are most likely due to silencing of *CrtR-b1* and *CrtR-b2* in the petals, similarly to what was reported for the *U/U* parental line. This implies that, in the flower, the functional β -hydroxylase is necessary to obtain higher levels of xanthophylls and higher total carotenoid levels as well.

Finally, the comparison between the Az, *hp3*, U/0; *B/B* and U/0; *B/B*; *hp3/hp3* lines was carried out to assess changes that occurred when the given combinations of the genes of interest were introduced. The U/0; *B/B*; *hp3/hp3* line accumulated 210 and 60 times more zeaxanthin in its flowers than the Az and U/0; *B/B* lines, respectively, but no difference was found between the triple cross and the *hp3* line. Therefore, the *hp3* allele was solely responsible for the increased accumulation of this xanthophyll. Antheraxanthin was identified in the U/0; *B/B*; *hp3/hp3* and *hp3* lines but no difference was found between these two lines. Luteoxanthin was identified in the Az and U/0; *B/B* lines and the U/0; *B/B* line accumulated 1.5 times more of this xanthophyll than the Az line. The levels of lutein were not found to be significantly different between the lines, although, on average, they were the highest in the *hp3* line. The levels of *cis*-violaxanthin, violaxanthin and neoxanthin were significantly lower in the *hp3* and U/0; *B/B*; *hp3/hp3* lines than in the Az and U/0; *B/B* lines. The levels of *cis*-violaxanthin were 1.5- and 28-fold higher in the U/0; *B/B* line than in the Az and U/0; *B/B*; *hp3/hp3* lines, respectively. The difference between the levels of violaxanthin in the Az and U/0; *B/B* lines was not found to be significant; however, both lines accumulated significantly higher levels of this compound than the U/0; *B/B*; *hp3/hp3* line (16 and 23 times more, respectively). The neoxanthin levels were found to be the highest in the U/0; *B/B* line and were 2.0- and 30-fold higher than in the Az and U/0; *B/B*; *hp3/hp3* lines, respectively. The α -carotene, β -carotene and phytoene levels were also found to be the highest in the U/0; *B/B* line and they were not different between the Az, *hp3* and U/0; *B/B*; *hp3/hp3* lines. The total carotenoid levels in flowers of the *hp3* and U/0; *B/B*; *hp3/hp3* lines were not significantly different from each other but those of the U/0; *B/B*; *hp3/hp3* line were found to be 5.4 and 8.3 times lower than in the Az and U/0; *B/B* lines, respectively.

The above data lead to five important observations. Firstly, the colour differences between the analysed flowers are reflected by the differences in their pigment profiles. Secondly, zeaxanthin cannot be esterified in the flower. Thirdly, the lack of esterification leads to lower carotenoid levels in the triple crosses. Next, the presence of *S. galapagense* *CYC-B* and transgenic *CrtR-b2* increases the levels of all carotenoids except lutein, antheraxanthin and zeaxanthin. Finally, the accumulation of zeaxanthin is only achieved when the allele of *ZEP* with compromised activity is introduced and a further increase in zeaxanthin content cannot be attained by increasing the activity of the cyclase and hydroxylase. However, a functional β -carotene hydroxylase is required for zeaxanthin accumulation. Therefore, the deposition of zeaxanthin may be limited because this xanthophyll is being stored away in particular chromoplast compartments. This zeaxanthin could be inaccessible to esterification, or the enzyme responsible for this reaction is not present in tomato flowers. Moreover, the deposition of zeaxanthin may be restricted by the availability of the structures within which it can be stored, limiting the amounts of this xanthophyll that the plant can accumulate in the flower chromoplasts.

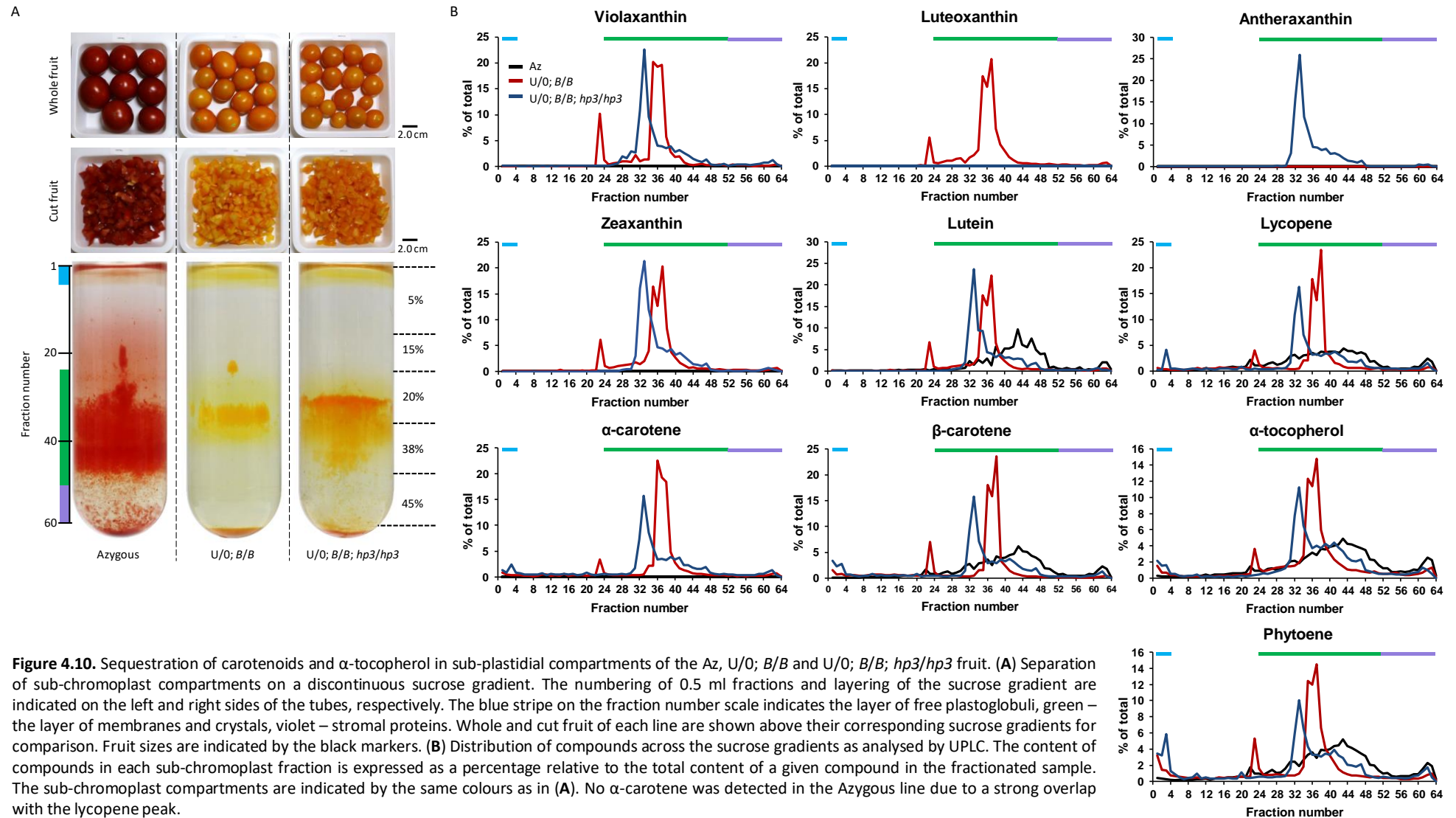
4.2.8 Sub-chromoplast fractionation of the selected lines

In order to better understand how the xanthophylls are sequestered within the chromoplast, sub-chromoplast fractionation of the *Az*, *U/0; B/B* and *U/0; B/B; hp3/hp3* lines was carried out (Figure 4.10). The fruit of the *Az* line were red and so was its sucrose gradient, whereas the two transgenic lines were orange (Figure 4.10A). However, the fruit of the *U/0; B/B; hp3/hp3* line, especially when cut, were visibly darker throughout their pericarp. The sucrose gradients were also very different between the three lines. The middle membrane sub-compartment of the *Az* line was the widest. In the *U/0; B/B* line this sub-compartment contained crystal-like deposits, similarly to the *U/0; B/B; hp3/hp3* line; however, in the triple cross, these crystalloid structures were darker in colour and were layered higher in the gradient than in the *U/0; B/B* line. All three lines had a visible layer of free plastoglobuli of the same width at the top of their gradients.

Analysis of the individual fractions on the UPLC system reflected the visual appearance of the sucrose gradient of each line (Figure 4.10B). In the transgenic lines, the identified compounds were found predominantly in the membrane sub-compartment and were confined to a narrow region spanning four fractions. However, there was a shift between the layers in the *U/0; B/B* and *U/0; B/B; hp3/hp3* lines because in the latter, the same compounds were identified in the earlier fractions. In the *Az* line, the identified compounds were also found in the membranes but they were spread over a much wider region spanning close to 20 fractions. Proportionally, more α -carotene, β -carotene, α -tocopherol and phytoene were found in the plastoglobule fractions of the transgenic lines with the triple cross containing the highest percentage content. Lycopene was only found in the plastoglobuli of the triple cross. These data suggest that in the transgenic lines, carotenoids are targeted to specific compartments within the chromoplasts, whereas in the *Azygous* line, carotenoids are spread more evenly throughout the plastids.

4.2.9 Photosynthetic performance

The analysis of the leaf carotenoid profiles of the selected lines has shown significant changes in their composition. Since carotenoids are associated with the antenna complexes and function as accessory pigments in photosynthesis, the assessment of photosynthetic performance was carried out to verify if this process was affected. The assessment of photosynthetic activity was done indirectly by measuring the quantum efficiency of photosystem II (PSII). This measurement is expressed as the ratio of the F_v value to the F_m value (F_v/F_m). The ratio of 0.85 is considered to be optimal. Calibration of the instrument was required prior to the analysis. First, the time for dark adaptation, which is the length of time needed for all PSII centres to open, was determined (Supplementary Figure 2.2A). Next, a saturating pulse was applied to the dark-adapted leaves to induce a maximum level of fluorescence by closing the reactions centres. The intensity of the saturating pulse was established experimentally as well (Supplementary Figure 2.2B).



The F_v/F_m ratios of all transgenic lines as well as the *hp3* line were significantly lower compared to the Az line (Figure 4.11). However, no significant differences were found between the triple crosses and the *hp3* line. Additionally, the U/0; B/B line was found to have a significantly higher ratio of F_v/F_m than the U/0; B/B; *hp3/hp3* line, which suggested that the presence of the *hp3* allele of *ZEP* had the limiting effect on photosynthetic performance.

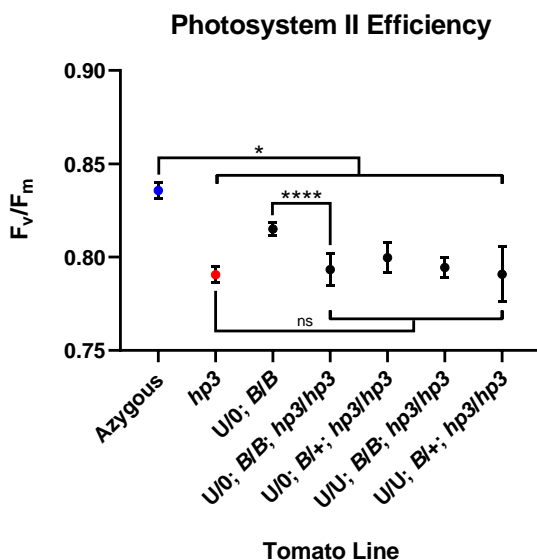


Figure 4.11. Comparison of photosystem II (PSII) efficiency between the indicated lines. PSII efficiency was found to be significantly lower in all lines compared to the Azygous line. None of the triple crosses were found to be different from the *hp3* line. However, compared to the U/0; B/B line, the U/0; B/B; *hp3/hp3* line was found to have a lower PSII efficiency. Collectively, these data show that, although the *S. galapagense* *CYC-B* and transgenic *CrtR-b2* lower the PSII efficiency, it is the *hp3* allele that ultimately limits the F_v/F_m ratio. Data normality and equality of variances were tested with Shapiro-Wilk and Brown-Forsythe tests, respectively. One-way ANOVA with Dunnett's multiple comparisons test was used to analyse the groups with equal variances (*hp3* vs U/0; B/B vs U/0; B/B; *hp3/hp3*). Welch ANOVA with Dunnett's T3 multiple comparisons test was used in the analysis of the groups with unequal variances (Az vs the other lines and *hp3* vs triple crosses). At least three plants were analysed per line. All measurements were performed in triplicates. Data are displayed as $\bar{x} \pm SD$; * $P < 0.05$, ** $P < 0.01$, *** $P < 0.001$, **** $P < 0.0001$.

The presence of the three genes of interest (*S. galapagense* *CYC-B*, transgenic *CrtR-b2* and the *hp3* allele of *ZEP*) in different combinations has led to different carotenoid profiles. To further explore how the carotenoid composition in leaves of the studied lines was related to the PSII efficiency, the ratios of the total chlorophyll content to the total carotenoid content (CHL:CAR) of the leaf tissues were plotted against their corresponding F_v/F_m ratios (Figure 4.12A). However, no significant correlation between the F_v/F_m values and the ratios of the total chlorophyll to the total carotenoids was discovered. Interestingly, the Azygous, *hp3* and U/0; B/B lines appeared to follow a parabolic relationship in which the optimal ratio of the total chlorophyll to the total carotenoids was required to achieve the maximum quantum performance of PSII (black dotted curve in Figure 4.12A). However, none of the triple crosses were found to follow this trend. In fact, the CHL:CAR ratios of the triple crosses were very close to the CHL:CAR ratio of the Azygous line, yet their F_v/F_m ratios were much closer to the F_v/F_m ratio of the *hp3* line. Therefore, other factors, for example the relative contents of individual carotenoids, could be contributing to the results seen. In order to explore this further, the F_v/F_m value of each line was plotted against its corresponding ratio of the total chlorophyll to the zeaxanthin content (CHL:ZEA). This resulted in the discovery of a strong linear correlation (Figure 4.12B). Although the involvement of other compounds in determining the F_v/F_m ratio cannot be ruled out, the presented data strongly suggest that the efficiency of PSII is not only influenced by the ratio of the total chlorophyll to the total carotenoids but also by the relative contents of individual carotenoids in the leaf tissue.

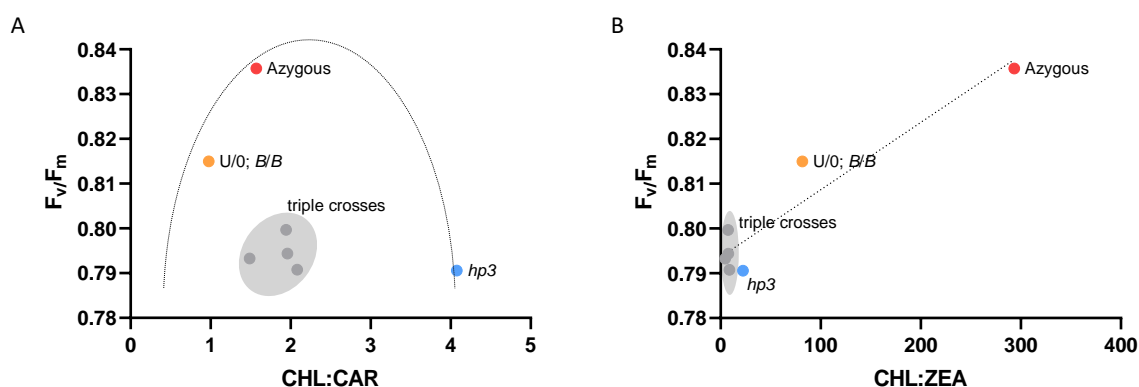


Figure 4.12. Plots of the F_v/F_m ratios of the indicated tomato lines against their corresponding ratios of total chlorophyll to total carotenoids (CHL:CAR) (A) and total chlorophyll to zeaxanthin (CHL:ZEA) (B). Although no significant correlation was found in (A), it may seem that the optimum F_v/F_m value (0.84) depends on the CHL:CAR ratio. However, the triple crosses do not follow this trend. The dotted black curve indicates a theoretical relationship. On the other hand, when the F_v/F_m values of the indicated lines are plotted against their CHL:ZEA ratios, a significant linear trend (dotted black line) is discovered (Pearson's correlation coefficient, $R = 0.9483$, $P < 0.01$; $R^2 = 0.8993$).

4.2.10 Analysis of primary metabolites of the selected lines

The polar and non-polar extracts from ripe fruit of the four triple crosses (U/0; B/B; *hp3/hp3*, U/0; B/+; *hp3/hp3*, U/U; B/B; *hp3/hp3* and U/U; B/+; *hp3/hp3*) and the *hp3* line were analysed by gas chromatography-mass spectrometry (GC-MS). Multivariate analysis of the 150 identified metabolites was carried out using principal component analysis (PCA) to determine the overall variance between the tested lines (Figure 4.13A). The analysis revealed that all five lines formed distinctive clusters. However, the *hp3* line clustered away from the triple crosses, which formed separate clusters much closer to each other and at almost the same position along the first principal component. The loading scatter plot indicated that the separation of the *hp3* line was driven by leucine, squalene, tetradecanoic acid, γ -tocopherol, tetracosan-1-ol, galacturonic acid, an unknown non-polar compound (NP_unk_13), oleyl alcohol (*cis*-9-octadecen-1-ol), oxalic acid, cycloartenol, cyclolaudenol, stigmasterol, α -tocopherol hydroquinone, isocitric acid, mannose, xylose, threonine, pipercolic acid, β -sitosterol and α -tocopherol (Figure 4.13B). The separation of the triple crosses was driven by *myo*-inositol, ribonic acid, D-glycerol-D-gulo-heptose, undecane, benzoic acid, 1-monostearin, 9-octadecenoic acid, an unknown polar compound (P_unk_9), sucrose, *myo*-inositol phosphate and sedoheptulose.

The five lines were compared to each other and 93 metabolites were found to be significantly different between them. The levels of the significantly altered metabolites were compared to each other and displayed in the form of a heat map to indicate the compounds with increased or decreased levels compared to the other lines (Figure 4.14). This analysis revealed that the *hp3* line was the most different from the four transgenic lines and contained two relatively large groups of metabolites, which were only found to be higher and lower in this line but not in any of the triple crosses. The four transgenic lines clustered closer together but within this cluster,

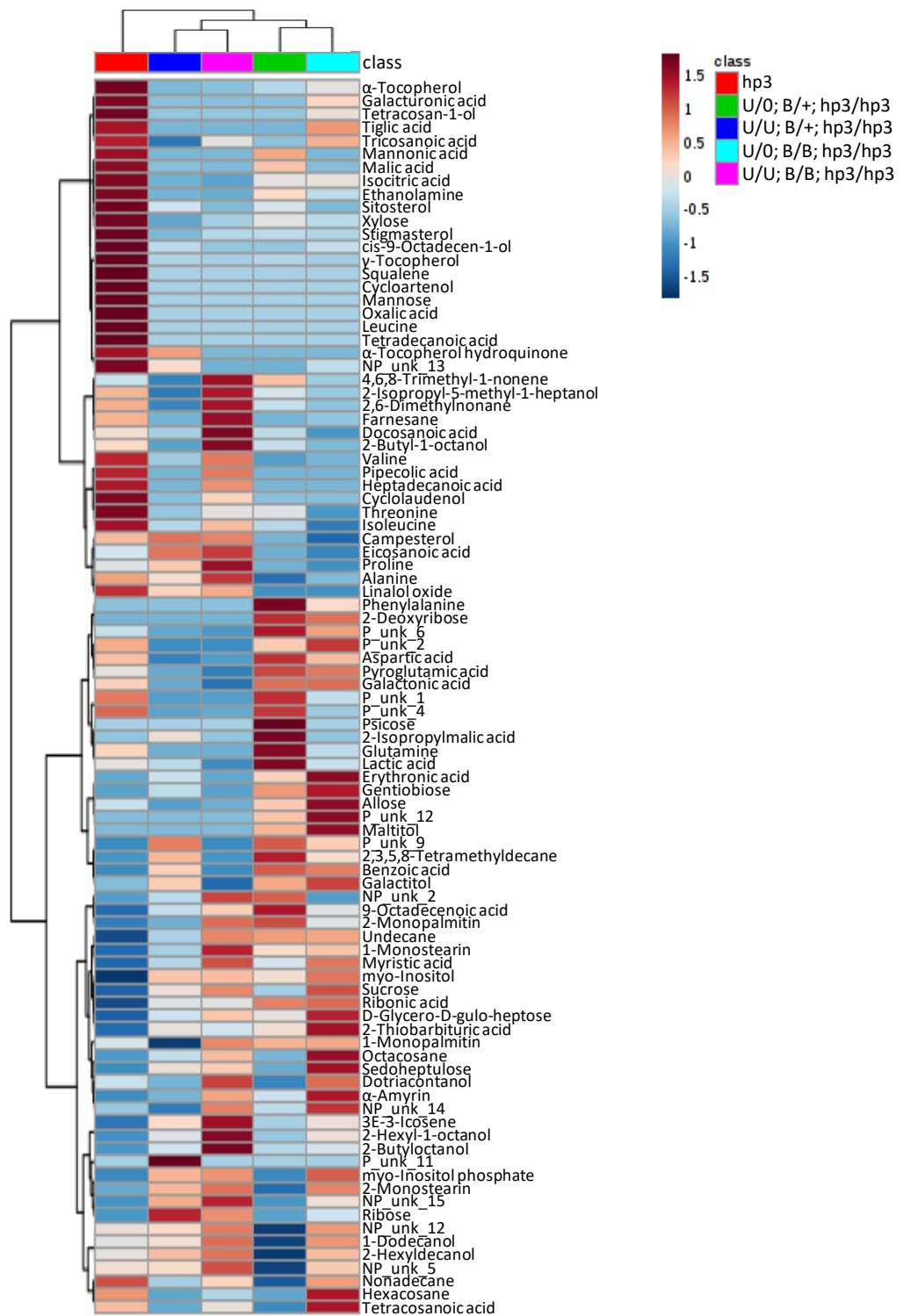


Figure 4.14. Heat map comparison of the 93 metabolites found to be significantly different between the five lines. The map identifies compounds which are unusually high (red) or low (blue) in fruit of the tested lines. Distinctive clustering of the lines based on the presence of metabolites is apparent. The lines were compared using one-way ANOVA with Fisher's Least Significant Difference (LSD) post-hoc test. The obtained p -values were adjusted for the False Discovery Rate (FDR) and only metabolites with $FDR < 0.05$ were reported as significant. For the number of biological replicates, refer to Figure 4.6B.

on technical replicates instead. However, despite the low number of biological replicates for one of the crosses, the lines hemizygous for transgenic *CrtR-b2* shared a large group of metabolites, which were lower in these two lines compared to the others. Additionally, these two crosses shared a smaller group of metabolites, which were only found to be higher in this sub-group.

Interestingly, the lines homozygous for *S. galapagense* *CYC-B* shared a relatively large group of metabolites, which were only found to be higher in these two crosses compared to the other lines. However, these were also the lines with the lowest numbers of biological replicates, so definite conclusions may be difficult to draw.

In order to better understand the changes in metabolite composition that occurred in ripe fruit of the zeaxanthin-accumulating triple cross, the U/0; *B/B*; *hp3/hp3* line was compared to the *hp3* line and the changes were visualised onto a simplified display of the major biochemical pathways (Figure 4.15). The compounds driving the separation of these lines on the loading plot (Figure 4.13B) were also found to be significantly different between them. In fact, all metabolites found to be significantly different between these two lines could be assigned to six different biochemical pathways: lactic acid and amino acids derived from pyruvate, sugars and their derivatives, phytosterols, fatty acids and their derivatives, derivatives of geranylgeranyl-pyrophosphate (GGPP) and finally, compounds of the tricarboxylic acid (TCA) cycle, including derivatives of amino acids from the TCA cycle. Lactic acid and the amino acids derived from pyruvate were found to be lower in the U/0; *B/B*; *hp3/hp3* line than in the *hp3* line. Generally, sugars were higher in the triple cross than in the *hp3* line. The levels of all identified phytosterols were lower in the U/0; *B/B*; *hp3/hp3* line than in the *hp3* line except α -amyrin, which was higher. The great majority of the identified TCA cycle compounds, such as fumaric acid, isocitric acid, citric acid, aconitic acid and malic acid, were lower in the U/0; *B/B*; *hp3/hp3* line. Further, some derivatives of the amino acids originating from the TCA cycle were also lower. The identified GGPP derivatives were generally lower in the triple cross than in the *hp3* line except zeaxanthin, which was higher. Some of fatty acid derivatives, such as hydrocarbons, fatty acid alcohols and monostearins, were higher in the triple cross although, most of the identified fatty acids were either not different or lower compared to the *hp3* line. The only fatty acid found to be higher in the U/0; *B/B*; *hp3/hp3* line was 9-octadecenoic acid (*trans*-oleic acid).

Finally, a number of unidentified compounds was found to be higher in the U/0; *B/B*; *hp3/hp3* line than in the *hp3* line. These compounds could be of interest since some of them were driving the separation of these lines on the loading scatter plot (Figure 4.13B). In comparison to the metabolites which were found to be altered, relatively few compounds were not found to be different between the two lines. This implies that global changes in the primary and secondary metabolism occurred as the result of introducing *S. galapagense* *CYC-B* and transgenic *CrtR-b2* into the lines carrying the *hp3* alleles of *ZEP*. However, since the individual plants assigned to specific lines originated from a population of a mixed genetic background, other genes, which are segregating in the genetic background, may be responsible for or contribute to the observed changes.

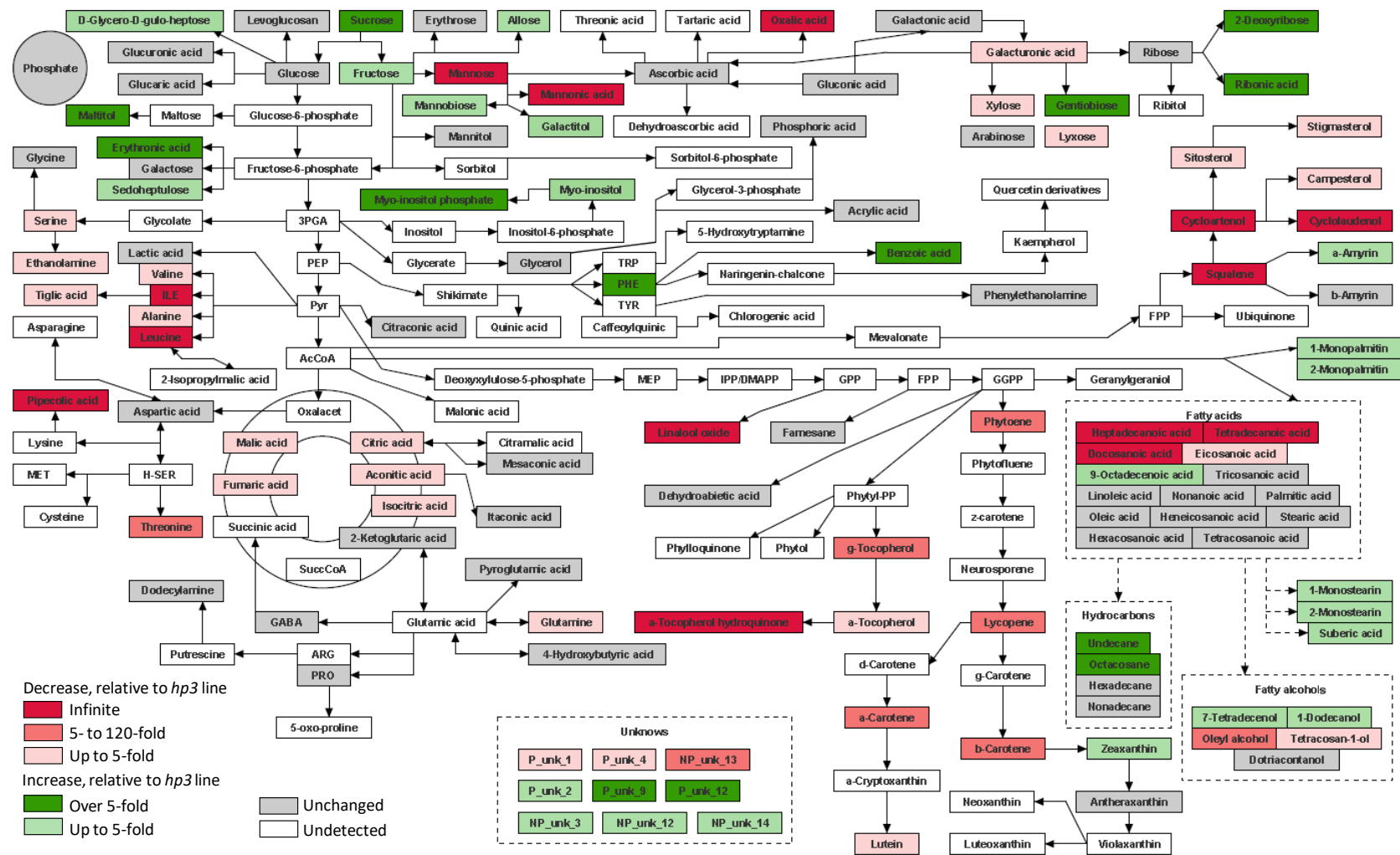


Figure 4.15. Changes in fruit metabolites of the U/O; B/B; *hp3/hp3* line compared to the *hp3* control displayed over schematic biochemical pathways. Carotenoids, identified through HPLC, were added to the display. 3PGA, glyceraldehyde 3-phosphate; Ac-CoA, acetyl-coenzyme A; ARG, arginine; DMAPP, dimethylallyl pyrophosphate; FPP, farnesyl diphosphate; GGPP, geranylgeranyl diphosphate; GPP, geranyl diphosphate; H-SER, homoserine; ILE, isoleucine; MEP, 2-C-methyl-D-erythritol 4-phosphate; MET, methionine; PEP, phosphoenolpyruvate; PHE, phenylalanine; PRO, proline; Pyr, pyruvate; SuccCoA, succinyl-coenzyme A; TRP, tryptophan; TYR, tyrosine.

4.2.11 Volatile compounds analysis of the selected lines

Volatile organic compounds (VOCs) from ripe fruit of the four triple crosses (*U/0; B/B; hp3/hp3*, *U/0; B/+; hp3/hp3*, *U/U; B/B; hp3/hp3* and *U/U; B/+; hp3/hp3*) and the *hp3* line were analysed using solid-phase microextraction (SPME). Multivariate analysis of the 108 identified VOCs was carried out using principal component analysis (PCA) to assess the overall variance between the lines (Figure 4.16A). This led to the discovery of three distinctive clusters. The *hp3* line clustered

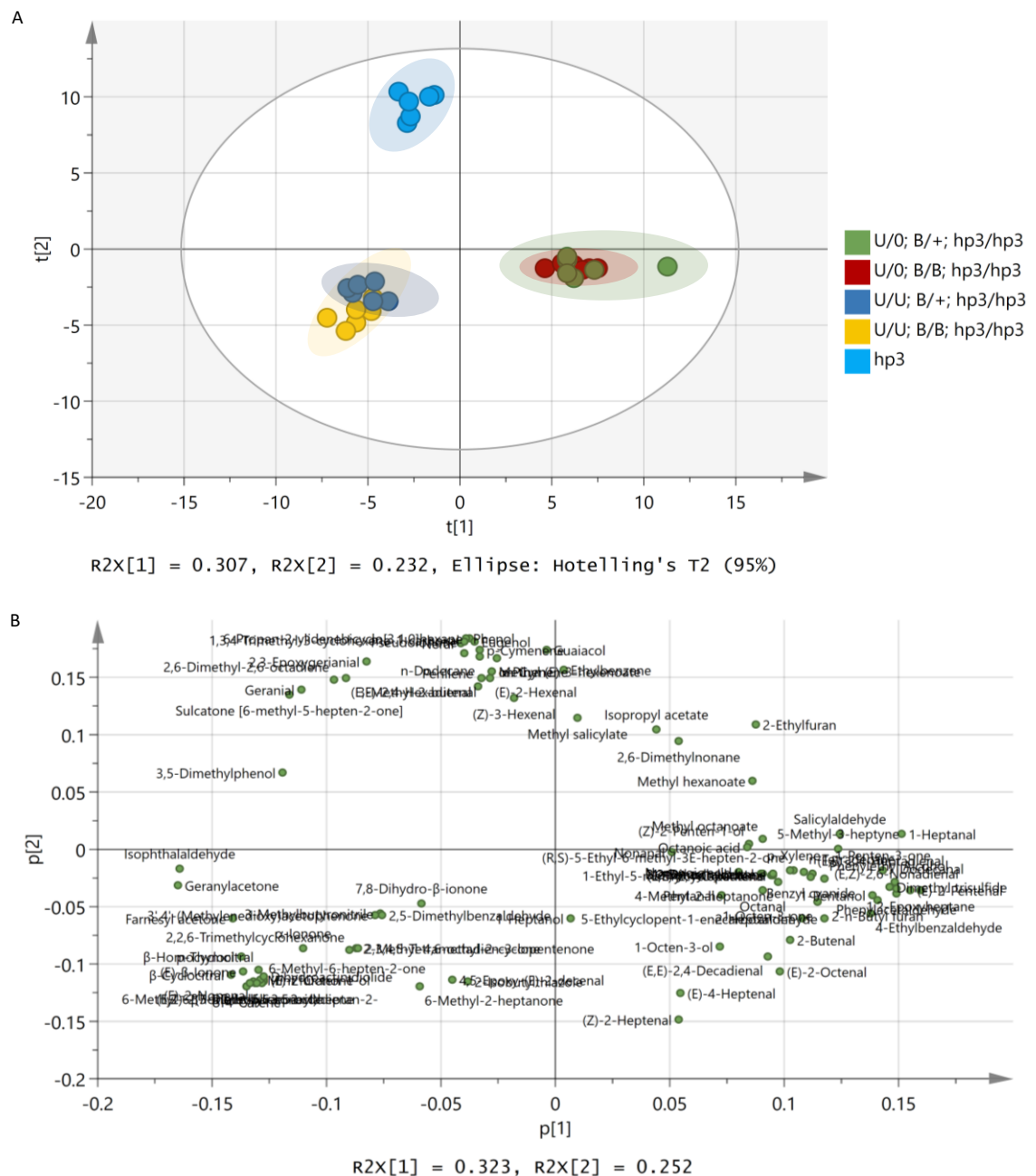


Figure 4.16. Principal component analysis (PCA) of the volatile compounds detected by SPME analysis of ripe fruit of the indicated tomato lines. **(A)** Score scatter plot illustrating clustering of the lines along the direction of maximum variance in the data (the first principal component, $t[1]$) and the second major source of variation (the second principal component, $t[2]$) orthogonal to the first. Shaded areas indicate 95% confidence regions. **(B)** Loading scatter plot of the first two principal components ($p[2]$ against $p[1]$) indicating the metabolites which force separation of the lines. Only the compounds found to be significantly different between the five lines were included on the plot. The data were analysed using one-way ANOVA with Fisher's Least Significant Difference (LSD) post-hoc test and the significance was assessed based on False Discovery Rate (FDR) adjusted p -values (FDR < 0.05). For the number of biological replicates, refer to Figure 4.6B.

away from the transgenic lines. The U/U; B/B; *hp3/hp3* and U/U; B/+; *hp3/hp3* lines formed a second cluster. The third cluster was formed by the U/O; B/B; *hp3/hp3* and U/O; B/+; *hp3/hp3* lines. The loading scatter plot (Figure 4.16B) indicated that the separation of the *hp3* line was driven by phenol, pseudoionone, neral, 6-propan-2-ylidenebicyclo[3.1.0]hexane, n-dodecane, eugenol, *m*-cymene, *p*-cymenene, α -pinene, 1,3,4-trimethyl-3-cyclohexene-1-carboxaldehyde,

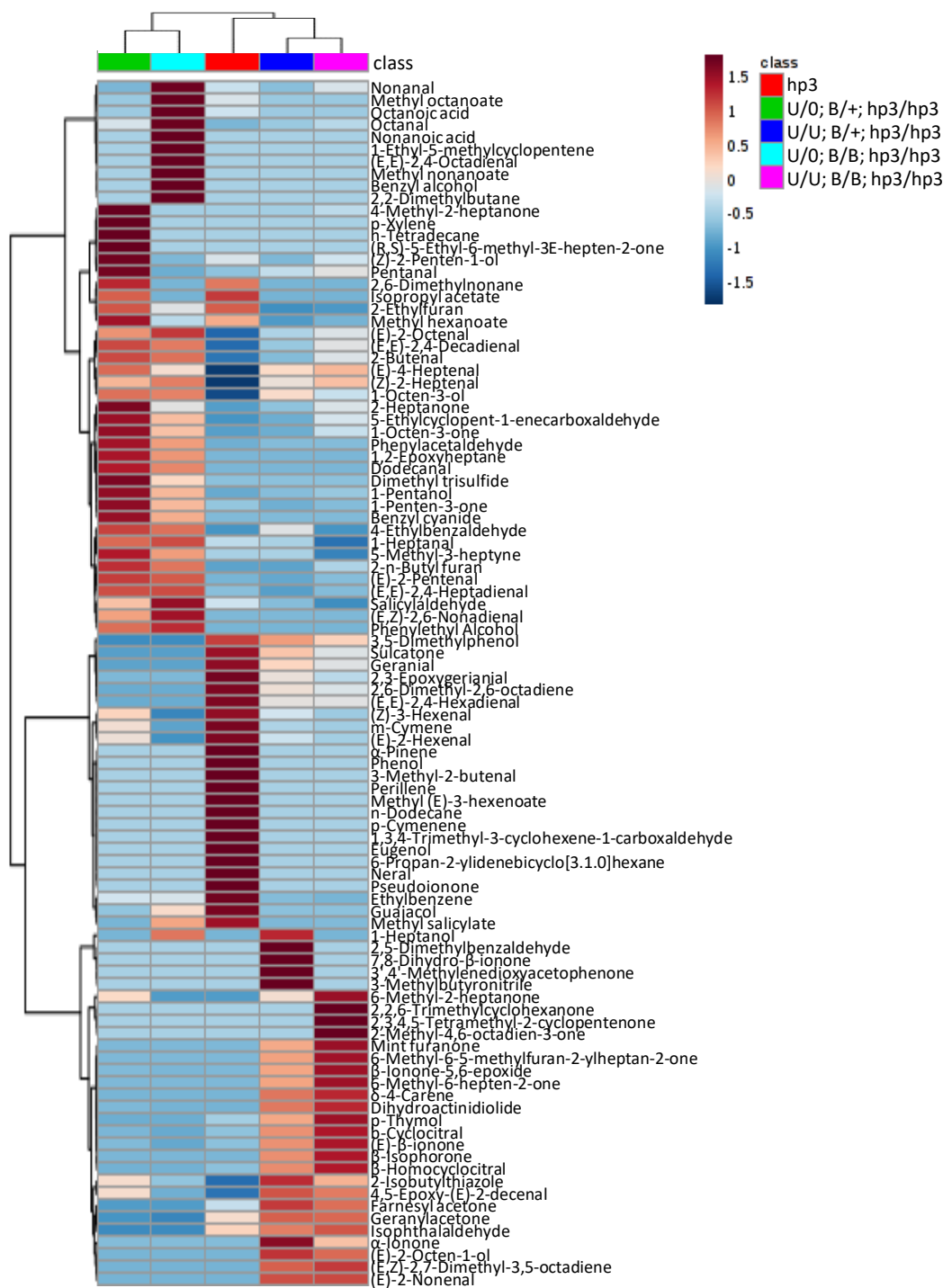


Figure 4.17. Heat map comparison of the 98 volatile compounds found to be significantly different between the five lines. The map identifies compounds that are unusually high (red) or low (blue) in fruit of the tested lines. Distinctive clustering of the lines based on the presence of metabolites is apparent. The lines were compared using one-way ANOVA with Fisher's Least Significant Difference (LSD) post-hoc test. The obtained *p*-values were adjusted for the False Discovery Rate (FDR) and only metabolites with FDR < 0.05 were reported as significant. For the number of biological replicates, refer to Figure 4.6B.

3-methylbutenal, methyl (*E*)-3-hexenoate, (*E*)-2-hexenal, perillene, (*Z*)-3-hexenal and guaiacol. The separation of the U/U; B/B; *hp3/hp3* and U/U; B/+; *hp3/hp3* lines was forced by farnesyl acetone, geranylacetone, isophthalaldehyde, *p*-thymol, β -cyclocitral, (*E*)- β -ionone, δ -4-carene, β -homocyclocitral, 6-methyl-6-(5-methylfuran-2-yl)heptan-2-one, mint furanone, β -isophorone, dihydroactinidiolide, (*E*)-2-octen-1-ol, (*E,Z*)-2,7-dimethyl-3,5-octadiene, β -ionone-5,6-epoxide, 6-methyl-6-hepten-2-one and (*E*)-2-nonenal. Finally, the separation of the U/O; B/B; *hp3/hp3* and U/O; B/+; *hp3/hp3* lines was driven by (*E,Z*)-2,6-nonadienal, 1,2-epoxyheptane, dimethyl trisulfide, (*E*)-2-pentenal, 1-heptanal, phenylacetaldehyde, 1-penten-3-one, 2-n-butyl furan, dodecanal, 1-pentanol and 4-ethylbenzaldehyde.

The five lines were compared and 98 VOCs were found to be significantly different between them. The levels of the significantly altered VOCs were compared to each other and displayed as a heat map to indicate the compounds with increased or decreased levels compared to the other lines (Figure 4.17). This comparison showed that a large group of VOCs was only found to be higher in the *hp3* line but not in the triple crosses. The two lines homozygous for transgenic *CrtR-b2* were very similar to each other and therefore, clustered together. Interestingly, these two lines were found to cluster closer to the *hp3* line than to the other two triple crosses. The two lines hemizygous for transgenic *CrtR-b2* clustered together, and although there was a lot of overlap between the compounds that were similarly higher or lower in these two lines, certain differences between these crosses were apparent.

In order to better understand the changes that took place in the VOCs profiles of the zeaxanthin-accumulating fruit, the U/O; B/B; *hp3/hp3* line was compared to the *hp3* control and the changes were visualised onto a simplified display of biochemical pathways (Figure 4.18). The VOCs driving the separation of the two lines were also found to be significantly different between them. The largest difference between the analysed lines was seen in the VOCs originating from the MVA pathway. Most of these VOCs, which were either derived from the breakdown of carotenoids or synthesised from geranyl diphosphate (GPP), were lower in the triple cross. Interestingly, many VOCs derived from fatty acids were higher in the U/O; B/B; *hp3/hp3* line than in the *hp3* control except for the derivatives of linolenic acid, which were generally lower or unchanged. Many derivatives of phenylalanine were lower in the triple cross than in the *hp3* line except for benzyl cyanide, (2-methylphenyl)methyl formate and the derivatives of benzaldehyde (benzyl alcohol and 4-ethylbenzaldehyde). Finally, the derivatives of (*E*)-cinnamic acid, eugenol and guaiacol, were lower in the U/O; B/B; *hp3/hp3* line compared to the *hp3* line. This analysis revealed that a global change occurred between the two analysed lines at the level of VOCs. It appears that there was a shift towards an increased generation of fatty acid-derived volatiles and a decrease in the formation of GPP-derived volatiles in the U/O; B/B; *hp3/hp3* line.

4.2.12 Comparison with existing food sources of zeaxanthin

Certain green leafy vegetables, such as spinach and kale, are widely advertised as good sources of lutein and zeaxanthin and therefore, their consumption is encouraged to support healthy eyesight. The leaf extracts of spinach and kale were analysed and compared to the leaf extract of the *U/0; B/B; hp3/hp3* line to verify this claim. The HPLC chromatograms of the saponified leaf extracts revealed that violaxanthin and lutein were the major pigments in leaves of the two vegetables. However, in neither one of them, unlike in the *U/0; B/B; hp3/hp3* line, zeaxanthin was identified (Figure 4.19A).

The quantification of pigments from unsaponified leaf extracts of these plants indeed showed that only the *U/0; B/B; hp3/hp3* line accumulated zeaxanthin at $1.7 \text{ mg g}^{-1} \text{ DW}$ (Figure 4.19B). However, the claim that spinach and kale help to maintain a healthy eyesight is supported by their high contents of lutein, since these two accumulated 1.1 and $0.7 \text{ mg g}^{-1} \text{ DW}$ of this pigment, respectively. However, the *U/0; B/B; hp3/hp3* line accumulated lutein at almost the same level as spinach. Therefore, the leaves of the triple cross are a richer source of macular xanthophylls than spinach and kale. The green tissues of the triple cross could be used as an additional source of xanthophylls, which could be obtained through extraction, thus reducing biological waste. On the other hand, spinach and kale accumulated, respectively, 17 and 10 times more violaxanthin than the *U/0; B/B; hp3/hp3* line. Therefore, these leafy vegetables could potentially become rich sources of zeaxanthin due to their high violaxanthin contents. The levels of zeaxanthin of these plants could be improved by downregulating the activity of ZEP or through physiological means, thus increasing the number of food sources rich in both macular pigments.

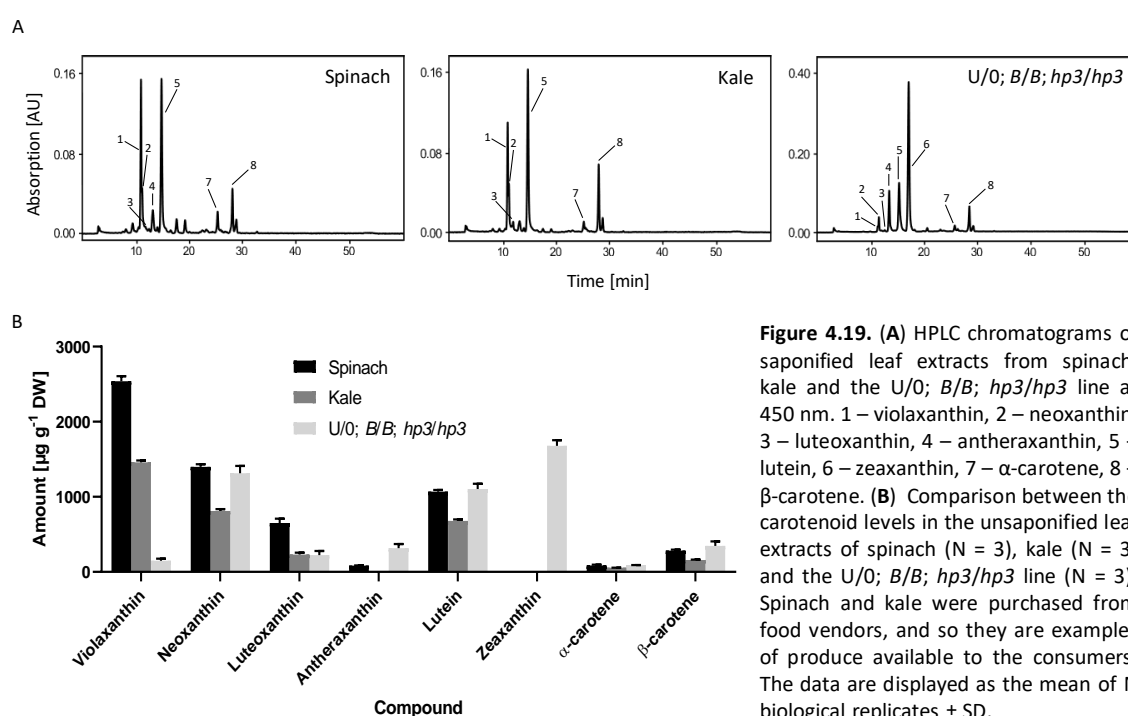


Figure 4.19. (A) HPLC chromatograms of saponified leaf extracts from spinach, kale and the *U/0; B/B; hp3/hp3* line at 450 nm. 1 – violaxanthin, 2 – neoxanthin, 3 – luteoxanthin, 4 – antheraxanthin, 5 – lutein, 6 – zeaxanthin, 7 – α -carotene, 8 – β -carotene. (B) Comparison between the carotenoid levels in the unsaponified leaf extracts of spinach (N = 3), kale (N = 3) and the *U/0; B/B; hp3/hp3* line (N = 3). Spinach and kale were purchased from food vendors, and so they are examples of produce available to the consumers. The data are displayed as the mean of N biological replicates \pm SD.

4.3 Discussion

4.3.1 Generation of a new, renewable source of zeaxanthin

Combining the high β -carotene background with the overexpression of β -carotene hydroxylase (*CrtR-b2*) and the *hp3* alleles of *ZEP* led to an almost exclusive accumulation of zeaxanthin in the ripe tomato fruit. For instance, the U/0; B/B; *hp3/hp3* line accumulated $187.0 \mu\text{g g}^{-1}$ DW of this xanthophyll, which was almost 82% of the total fruit carotenoid content. Comparing these levels to the ones presented in Chapter III, the U/0; B/B; *hp3/hp3* line was found to accumulate 26 and 20 times more zeaxanthin in its fruit than the U/0; B/B and U/0; B/+ lines, respectively. However, when the U/0; B/B; *hp3/hp3* line was compared to the U/0; B/B line grown together in the same season (the F₃ population grown from autumn 2017 to spring 2018), close to a 51-fold increase in the content of zeaxanthin was recorded. The possible effects of different growth seasons on the studied lines are discussed later in this chapter.

The recommended daily dose of zeaxanthin (2 mg) could be provided in 11 g of the dry tomato powder of the U/0; B/B; *hp3/hp3* line. Assuming that the water content of tomato fruit is close to 95%, this weight of powder corresponds to 219 g of raw fruit, which is equivalent to 17 cherry tomatoes. This amount of tomato fruit can be consumed in the course of a single day. Therefore, by designing the tomato line, which almost exclusively accumulated zeaxanthin in its ripe fruit, a potential new plant source of this xanthophylls was generated.

4.3.2 HRM as a screening method

Selection of tomato lines carrying two copies of the *hp3* allele of *ZEP* was carried out using the HRM analysis (Figure 4.2). These lines could also be identified by conventional sequencing as it was initially done to establish the type of mutation in the *hp3* parental line and also to select the reference genotypes (Figure 4.2A). However, genotyping of large populations is an expensive and timely process, even with the overall cost of sequencing dropping dramatically in recent years. The use of HRM addresses these issues. HRM is a high-throughput method, which can be automated, but more importantly, it allows to detect a single base-pair change and to classify the analysed samples according to the alleles they contain (Figures 4.2C and D). Moreover, HRM provides results faster and is more cost effective than conventional sequencing methods.

An alternative method, which could be used to identify single nucleotide polymorphisms (SNPs), is Kompetitive Allele Specific PCR (KASP). KASP is even easier to perform since it does not require the DNA melting step and it assigns genotypes based on the different colours of fluorescence emitted by the fragments containing the different SNPs. In this sense, KASP is considered to be even better than HRM since it can provide the results during the PCR amplification step in real time once the fluorescent signal is strong enough to exceed background emissions. However,

since KASP genotyping depends purely on the reaction chemistry, whereas HRM distinguishes the alleles based on a physical process, KASP is more prone to PCR inhibition than HRM, resulting in a greater number of miscalled alleles and a decreased accuracy of results (Seed World, 2018). Therefore, HRM is a far more robust method and is perhaps better for polymorphism screening of large populations.

4.3.3 Accumulation of zeaxanthin in ripe tomato fruit

In this chapter, it was shown that the introduction of the *hp3* alleles of *ZEP* into the U/0; B/B tomato line resulted in a substantial and significant increase in the contents of zeaxanthin and antheraxanthin in the leaf (Figure 4.5) and fruit (Figure 4.7) and in a significant decrease in the downstream xanthophylls such as violaxanthin, neoxanthin and luteoxanthin. Additionally, the metabolic block at the level of *ZEP* allowed for a greater accumulation of lutein in the fruit of the U/0; B/B; *hp3/hp3* line compared to the U/0; B/B line. In fact, the lutein levels in this triple cross were similar to the lutein levels of the Azygous line (Figure 4.7). This is significant, since lutein, similarly to zeaxanthin, is implicated in reducing the risk of age-related degenerative eye conditions (Sujak *et al.*, 1999; Delcourt *et al.*, 2006; Age-Related Eye Disease Study 2 Research Group, 2013; Dawczynski *et al.*, 2013). Therefore, it can be concluded that an **increase in the accumulation of zeaxanthin in tomato fruit can only be achieved by introducing a metabolic block at the level of *ZEP* in the carotenoid biosynthetic pathway**. Interestingly, zeaxanthin was not accumulated at comparably high levels in the U/U; B/B; *hp3/hp3* and U/U; B/+; *hp3/hp3* lines despite the presence of the block at the level of *ZEP*. The explanation for this can be found in the supplementary gene expression data provided by D'Ambrosio *et al.* (2011). The synthesis of zeaxanthin requires a functional β -carotene hydroxylase and in the parental U/U line, both of the hydroxylases involved in this process, namely *CrtR-b1* and *CrtR-b2*, were affected. In fruit of the U/U plants, the transcript levels of *CrtR-b2* were lower at all stages of development than in the U/0 plants but silencing of the endogenous copy of *CrtR-b2* did not occur since its transcript levels were higher than in the non-transgenic plants. However, the presence of the transgene in a homozygous state in the U/U lines resulted in co-suppression of endogenous *CrtR-b1* in fruit at all stages of development. Therefore, the triple crosses homozygous at the transgenic U locus accumulated primarily β -carotene in their ripe fruit (Figure 4.6B) and this was reflected in the appearance of their pericarps, which were darker in colour than those of the lines hemizygous at the transgenic U locus (Figure 4.3A).

Although the highest levels of zeaxanthin were identified in fruit of the U/0; B/B; *hp3/hp3* line (187.0 $\mu\text{g g}^{-1}$ DW), the parental *hp3* line also contained substantial amounts of this xanthophyll (145.2 $\mu\text{g g}^{-1}$ DW; Figure 4.6B). However, in comparison to the *hp3* parent, the accumulation of zeaxanthin in the fruit of the triple cross was accompanied by an almost complete depletion of

phytoene, lycopene, α -carotene and β -carotene (Figure 4.6B). Therefore, it can be concluded that the overexpression of *CYC-B* and *CrtR-b2* drives the conversion of lycopene and β -carotene to zeaxanthin in the U/0; B/B; *hp3/hp3* line. However, the increase in zeaxanthin levels in fruit of the U/0; B/B; *hp3/hp3* line was lower than expected, given the pool of lycopene available in the *hp3* line (1 163.9 $\mu\text{g g}^{-1}$ DW). This strongly suggests that the capacity to store zeaxanthin in ripe tomato fruit is limited. In fact, this limited capacity may be reflected by the global changes in primary and secondary metabolites that occurred in the ripe fruit of the U/0; B/B; *hp3/hp3* line (Figures 4.15 and 4.18).

Many amino acids (alanine, isoleucine, leucine, serine, threonine and valine), the intermediates of the TCA cycle (aconitic acid, citric acid, fumaric acid, isocitric acid and malic acid), isoprenoids (carotenoids and tocopherols), some fatty acids (docosanoic, eicosanoic, heptadecanoic and tetradecanoic) and phytosterols (campesterol, cycloartenol, cyclolaudenol, sitosterol, squalene and stigmasterol) were lower in fruit of the U/0; B/B; *hp3/hp3* line than in the *hp3* line. On the other hand, some sugars, such as sucrose and fructose, were higher in the cross, despite finding no significant change in photosynthetic performance between these two lines (Figure 4.11). The precursors of terpenoids and fatty acids (glyceraldehyde 3-phosphate, pyruvate and acetyl-CoA), are derived from fructose and glucose (Decourcelle *et al.*, 2015). Therefore, a lower flux through the glycolytic pathway in fruit of U/0; B/B; *hp3/hp3* line may allow for a greater accumulation of carbohydrates. Interestingly, it was reported that the exogenous application of glucose through the transpiration stream to leaves of tomato plants (*S. lycopersicum* variety *cerasiforme*, cultivar West Virginia 106), resulted in lower carotenoid and chlorophyll levels compared to the control plants (Mortain-Bertrand *et al.*, 2008). Moreover, the lower carotenoid content in the leaves of these plants correlated with the downregulation of some of the genes of the MEP pathway (*DXS*, *PSY2*, *PDS* and *LCY-B*). The U/0; B/B; *hp3/hp3* line also had a reduced chlorophyll content in its leaves compared with the *hp3* line (Figure 4.4B). Therefore, the changes at the level of primary metabolites in fruit of the U/0; B/B; *hp3/hp3* line may be components of a response mechanism, which reflects the limited capacity of tomato fruit chromoplasts to store zeaxanthin and exerts its effect by limiting the flux through the glycolytic pathway.

The aroma of ripe fruit of the *hp3* tomato is described in terms of green notes and is reminiscent of freshly cut grass. On the other hand, ripe fruit of the U/0; B/B; *hp3/hp3* line have a pleasant smell characteristic of fresh strawberries. The VOCs responsible for the green notes, such as (*E*)-2-hexenal and (*Z*)-3-hexenal, were lower in fruit of the U/0; B/B; *hp3/hp3* line (Figure 4.18). The aroma of strawberries is attributed to benzyl acetate. In fact, many derivatives of benzyl alcohol, which is a precursor of benzyl acetate, were higher in fruit of the U/0; B/B; *hp3/hp3* line. Moreover, phenylalanine, the precursor of many benzene-containing VOCs, was the only amino

acid found to be significantly higher in fruit of the *U/0; B/B; hp3/hp3* line compared to the *hp3* line (Figure 4.15). Additionally, many derivatives of fatty acids were also found to be significantly higher in the triple cross. Therefore, the changes in levels of individual VOCs were responsible for the strawberry aroma of the ripe fruit of the *U/0; B/B; hp3/hp3* line and loss of green notes characteristic of the *hp3* tomato line.

The VOCs derived from carotenoids were found to be lower in ripe fruit of the *U/0; B/B; hp3/hp3* line compared to the *hp3* line (Figure 4.18), which could be attributed to the low levels of their precursors (phytoene, lycopene and β -carotene) in the triple cross. In fact, some VOCs known to originate from the degradation of β -carotene, such as β -ionone and β -cyclocitral, were found to be significantly lower, whereas sulcatone, a derivative of lycopene, was not detected in ripe fruit of the *U/0; B/B; hp3/hp3* line. Interestingly, none of the known zeaxanthin-derived VOCs, such as 3-hydroxy- β -cyclocitral, 4-oxoisophorone and safranal, were identified in any of the lines carrying the *hp3* alleles of *ZEP* (data not shown). Perhaps zeaxanthin is not accessible to the cleaving enzymes or the enzymes required for this cleavage are not present in tomato fruit. Finally, none of the other IPP-derived VOCs, including dihydroactinidiolide, pseudoionone and neral, were found to be higher in fruit of the *U/0; B/B; hp3/hp3* line. As discussed in the previous chapter, some of these VOCs may exert a feedback regulation on the expression of carotenoid-related genes and thus control the accumulation of isoprenoids at different levels within the MEP pathway or perhaps even beyond it.

As described in the previous chapter, the overexpression of genes directly involved in zeaxanthin synthesis in tomato fruit did not lead to an increased accumulation of this xanthophyll. Instead, an increase in the levels of downstream xanthophylls, such as violaxanthin and neoxanthin, was achieved. This most likely occurred due to uninterrupted metabolism of zeaxanthin, which also prevented this xanthophyll from being retained. Therefore, the violaxanthin levels in leaves and fruit of tomato plants are normally always higher than those of zeaxanthin. However, unlike in the previous chapter, neither violaxanthin nor neoxanthin were identified in the fruit extracts of the *U/0; B/B* line (Figure 4.7). However, the *U/0; B/B* line was the only one in which luteoxanthin was found. Luteoxanthin was not detected in the *Az* line nor in any of the lines carrying the *hp3* alleles of *ZEP*. Since luteoxanthin is derived from violaxanthin, its presence strongly implies that only the *U/0; B/B* line accumulated violaxanthin in its fruit, which was then readily converted to luteoxanthin.

The differences in xanthophyll levels between the consecutive generations can be explained by several factors. The parent of the F_3 *U/0; B/B* population was selected from the F_2 segregating population based on its high content of zeaxanthin. Therefore, certain differences between the two consecutive populations were expected. However, even though the selected lines contained

the same combination of the genes of interest, they were not isogenic and other genes, which were segregating in the background, could contribute to the presented results. Therefore, the use of non-isogenic lines was perhaps the most important reason for the observed differences. Furthermore, the growth conditions, such as temperature and light intensity, are other factors that could be partially responsible for changes between xanthophyll profiles of the consecutive generations. The F₃ U/0; B/B population was grown in the winter season together with the *hp3* line and the triple crosses, whereas the F₂ U/0; B/B population was grown during the summer. Although the seasonal variability in carotenoid composition of tomato plants has not been the subject of extensive research, several studies reported that the carotenoid profiles of ripe fruit were different depending on the time of harvest (Slimestad & Verheul, 2005; Raffo *et al.*, 2006; Zanfini *et al.*, 2007). Moreover, the analysis of seasonal effects on the levels of xanthophylls in pumpkin (*Cucurbita moschata*) revealed that the accumulation of lutein and zeaxanthin was variable throughout the year (Jaswir *et al.*, 2014). Therefore, it is likely that the accumulation of xanthophylls in tomato fruit is also seasonal, especially since the synthesis of zeaxanthin and violaxanthin is highly dependent on light intensity (Jahns *et al.*, 2009; Jahns & Holzwarth, 2012).

In summary, since only a limited improvement in the concentration of zeaxanthin was achieved in the triple cross as compared to the *hp3* line, it appears that from the health benefit point of view, the *hp3* line is the best for providing the necessary food supplements. In other words, the *hp3* line is a good all-rounder, whose ripe fruit are high in lycopene, zeaxanthin, β-carotene and lutein. The major downside of the *hp3* line is perhaps its low fruit yield due to ABA deficiency; however, this issue may be addressed through external application of the deficient hormone. The major advantage of the U/0; B/B; *hp3/hp3* line is that its fruit require minimal bioprocessing due to the almost exclusive accumulation of zeaxanthin. Therefore, the whole fruit or dried fruit powder of this line can be added directly to chicken feed or to other animal formulations.

4.3.4 Possible limits to zeaxanthin accumulation

The limited capacity of tomato chromoplasts to store zeaxanthin can be illustrated by comparing the accumulation of this and other pigments between the leaves (Figure 4.5), fruit (Figure 4.7) and flowers (Figure 4.9D) of the different tomato lines. For instance, the U/0; B/B; *hp3/hp3* line accumulated much higher levels of zeaxanthin in its leaves, flowers and fruit than the Az line. The total leaf carotenoid contents of these two lines were not found to be significantly different but the total fruit and flower carotenoid levels of the triple cross were much lower than those of the Az line. Therefore, the chloroplasts of tomato plants can accumulate much higher levels of zeaxanthin than their chromoplasts without a simultaneous reduction of the total carotenoid content. In fact, the levels of zeaxanthin in the leaves of the U/0; B/B; *hp3/hp3* line were almost 9 times higher than in the fruit and 3 times higher than in the flower.

All triple crosses accumulated significantly higher levels of zeaxanthin and total carotenoids in their leaves than the *hp3* line (Figure 4.4B). Perhaps, the increased capacity of the triple crosses to store zeaxanthin, and carotenoids in general, were facilitated by a higher number of plastids or by their enlargement, as was found to be the case for the *hp3* line in comparison to its control, the WT cultivar M82 (Galpaz *et al.*, 2008). However, the increase in zeaxanthin was not followed by a proportional increase in the total chlorophyll content in any of the triple crosses as it was the case for the *hp3* line in relation to the WT cultivar M82. This suggests that an improvement in the storage capacity for carotenoids in chloroplasts was achieved at the structural level. Some changes to chloroplast ultrastructure, such as the increased availability of thylakoid membranes or alterations to thylakoid membrane composition, could allow for the accumulation of greater amounts of zeaxanthin. However, without a thorough examination of chloroplast ultrastructure, a combination of different mechanisms cannot be excluded at this stage.

The esterification of xanthophylls with fatty acids allows for their overaccumulation in pepper fruit (Hornero-Méndez & Mínguez-Mosquera, 2000) and flowers of tomato plants (Ariizumi *et al.*, 2014), although this is certainly true for other flowers as well. Previously, it was reported that violaxanthin and neoxanthin were the major carotenoid pigments of tomato flower petals and were predominantly stored in esterified form (Ariizumi *et al.*, 2014). In this work, it was also found that flowers of the *Az* and *U/O; B/B* lines accumulated mainly carotenoid esters and most of these were identified as derivatives of violaxanthin and neoxanthin (Figures 4.9A and B). In fact, the total carotenoid levels in flowers of the *U/O; B/B* line were found to be 1.5 times higher than in the *Azygous* line and most of this change was attributed to the increase in the levels of violaxanthin and neoxanthin (Figure 4.9D). Therefore, the chromoplasts of tomato flowers use esterification to accommodate additional xanthophylls, which allows for an increase in the total carotenoid content.

The absence of the biochemical machinery required for the esterification of carotenoids would at least partially explain the limited capacity of tomato fruit chromoplasts to store zeaxanthin, and xanthophylls in general. In this work, only free xanthophylls were identified in ripe fruit of the analysed lines (Figure 4.6), including the *F₁* hybrid no. 1 described in Chapter III, which mostly accumulated violaxanthin in its fruit (Figure 3.5). However, it was shown that tomato fruit were capable of accumulating high levels of ketocarotenoids as fatty acid esters (Enfissi *et al.*, 2019). What was also significant was that the esterified ketocarotenoids were predominantly found in plastoglobuli, whereas free ketocarotenoids were mostly associated with the membrane sub-compartments of chromoplasts (Enfissi *et al.*, 2019). The ripe fruit of the *U/O; B/B; hp3/hp3* line were shown to primarily accumulate zeaxanthin, therefore the orange band in the discontinuous sucrose gradient indicated the layer at which zeaxanthin settled (Figure 4.10). This band was

narrow, well defined and did not overlap with the membrane sub-compartments of the Az and U/O; B/B lines. The sequestration of carotenoids in the Az line was spread more widely across the membrane sub-compartments. The U/O; B/B line deposited carotenoids in the membranes as well, but within a much narrower sector than the Azygous line. However, since the levels of zeaxanthin in fruit of the U/O; B/B line were over 50 times lower than in the triple cross, the layer at which it settled was not visible. The characteristic way in which zeaxanthin separates on the sucrose gradient implies that this xanthophyll is stored in specific sub-compartments. This most likely limits its deposition in tomato chromoplasts but also makes it not accessible to esterification. Interestingly, the accumulation of zeaxanthin in tomato fruit is very different from that of pepper in which zeaxanthin is almost exclusively found in esterified form (Hornero-Méndez & Mínguez-Mosquera, 2000). However, the mechanism of carotenoid sequestration in tomato fruit is also very different from that of peeper in which carotenoids are accumulated in specific lipoprotein fibrils that are not found in tomato chromoplasts (Deruère *et al.*, 1994).

One of the most important findings of this work was that zeaxanthin was not esterified in flowers of tomato plants despite their ability to do so, which was illustrated by the presence of fatty acid esters of violaxanthin and neoxanthin (Figure 4.9). Previous studies failed to identify zeaxanthin in flower petals of wild-type tomato plants (Galpaz *et al.*, 2008; Ariizumi *et al.*, 2014) and in this work, only low levels of zeaxanthin were found in the Az and U/O; B/B lines, which otherwise accumulated high levels of the xanthophyll esters. Therefore, it appears that zeaxanthin is not normally present at high levels in tomato flowers unless a metabolic block at the level of ZEP is introduced, which was shown in the lines carrying the *hp3* alleles of *ZEP* (Figures 4.9A and B). The *PALE YELLOW PETAL (PYP)* mutant of tomato was unable to accumulate xanthophyll esters and was found to contain significantly lower carotenoid levels in its flowers than the wild type plants (Ariizumi *et al.*, 2014). *PYP* is a loss-of-function mutant in the gene encoding an enzyme belonging to the acyltransferase-related family of proteins. Since the expression of genes of the carotenoid biosynthetic pathway was not found to be altered in the *PYP* mutant, the low levels of carotenoids in its flowers were attributed to the increased catabolism of free violaxanthin and neoxanthin by carotenoid cleavage dioxygenases (CCDs). It was also suggested that the flowers of tomato plants could be using esterification to prevent the xanthophylls from being cleaved by CCDs. Therefore, there may be a functional reason as to why zeaxanthin is not esterified. The conversion of zeaxanthin into the downstream xanthophylls is required for the synthesis of ABA. Moreover, as a photosynthetic pigment, zeaxanthin participates in the xanthophyll cycle. If the esterification of xanthophylls prevents them from being cleaved by CCDs as suggested by Ariizumi *et al.* (2014), it can also prevent ZEP from converting zeaxanthin to violaxanthin. The xanthophylls in the leaves are not esterified and since zeaxanthin is not normally accumulated in tomato fruit or flowers, it can be perceived by tomato plants as a photosynthetic pigment in

all of its tissues. Therefore, zeaxanthin would not be esterified in order to allow the xanthophyll cycle to function as necessary and to ensure that the production of ABA continues. Finally, with the esterification of violaxanthin and neoxanthin in tomato flowers, the pathway to ABA would still be blocked. However, in this work it was found that the flowers of the *Azygous* and *U/0; B/B* lines kept some amounts of the *cis*-isomer of violaxanthin in a non-esterified form (Figure 4.9A). Therefore, by maintaining a small pool of free violaxanthin, the pathway to ABA remains open in flowers of tomato plants.

However, it must be appreciated that the chromoplasts of tomato flowers and fruit are very different in terms of their capacity to produce and store xanthophyll esters. For instance, the *U/0; B/B* line, which was found to accumulate the highest levels of carotenoids in its flowers (Figure 4.9D), had the lowest total fruit carotenoid content (Figure 4.7). Therefore, the lack of zeaxanthin esterification in the flowers of tomato plants may not arise from the need to keep it non-esterified for physiological reasons, but because specific acyltransferases are not present. Moreover, since none of the known zeaxanthin-derived VOCs were identified in ripe fruit of the *U/0; B/B; hp3/hp3* line (Figure 4.18) or in any of the other zeaxanthin-accumulating lines, the esterification of zeaxanthin in tomato plants may not be at all necessary to prevent it from being cleaved. In fact, the fruit of tomato plants may not contain the necessary CCDs for this reaction. Alternatively, the sequestration of zeaxanthin into specific compartments of chromoplasts can make it unavailable to these enzymes.

Little is known about the mechanisms controlling the accumulation of xanthophylls in tomato fruit since these are generally considered as sources of hydrocarbon carotenoids. Based on the findings of this chapter, several possibilities were discussed, which could at least partially explain the limits to zeaxanthin accumulation in fruit of tomato plants. A brief summary of these points is given here. Zeaxanthin may be perceived as a photosynthetic pigment in all tissues of tomato plants, and therefore, be sequestered into specific membrane compartments where it normally functions. The availability of these membranes limits its concentration. Additionally, the site of zeaxanthin deposition may not be accessible to some enzymes, including acyltransferases and CCDs, meaning that zeaxanthin-derived VOCs and fatty acid esters of this xanthophyll are not produced. The absence of these metabolites can be also caused by lack of enzymes specific for this purpose. Finally, the role of zeaxanthin in the xanthophyll cycle stops it from being retained at higher levels due to its constant metabolism in response to the light intensity.

The capacity of tomato fruit chromoplasts for hydrocarbon carotenoids and xanthophylls is very different. For instance, the ripe fruit of the *hp3* line were found to accumulate very high levels of lycopene in the presence of high levels of zeaxanthin but their total xanthophyll content was not found to be different from the *U/0; B/B; hp3/hp3* line (Figure 4.7). Therefore, tomato fruit

can easily accommodate hydrocarbon carotenoids on top of xanthophylls but the increase in the level of one xanthophyll happens at the expense of another. This shows that the mechanism of sequestration of hydrocarbon carotenoids is different from that of xanthophylls and there is no overlap between their sites of deposition. Hydrocarbon carotenoids (lycopene and β -carotene) form crystals due to their hydrophobic nature, whereas the structure of xanthophylls favours their structured position in lipid bilayers rather than crystallisation. The presence of numerous membranes in chloroplasts allows for the accommodation of extra zeaxanthin without the need to reduce the levels of other xanthophylls (Figure 4.4A). Therefore, it is not surprising that the loss of these membranes during the chloroplast to chromoplast transition greatly restricts the amounts of accumulated xanthophylls.

The above examples illustrate that the mechanism of pigment sequestration in tomato plants is not only different between chloroplasts and chromoplasts but also between xanthophylls and hydrocarbon carotenoids. Therefore, instead of trying to enhance zeaxanthin levels in tomato fruit, which do not have the necessary structural adaptations for its storage, it makes a better sense to manipulate its levels in leaves, since chloroplasts have much greater storage capacity for xanthophylls. Unlike humans, who are unable to convert violaxanthin to zeaxanthin at the macula or anywhere else in the body, plants can do so easily as a part of the xanthophyll cycle. Therefore, in order to provide the necessary macular pigments, which can be later deposited at the fovea, zeaxanthin and lutein or esters of thereof, need to be directly ingested. However, in plants, the levels of zeaxanthin can be manipulated physiologically with stressors (temperature or high light) during growth or by post-harvest treatments. Plants rich in violaxanthin, especially green leafy vegetables, such as spinach and kale, would benefit most from such treatments. For instance, the 2-hour incubation of spinach leaves in 0.5 M acetate buffer at pH 5.0 and 37°C was shown to convert 70% of its violaxanthin pool to zeaxanthin (Clausén *et al.*, 2010). The excess of acetic acid was shown to be easily removed by incubation in distilled water for further 2 hours. Additionally, this treatment was not found to affect the appearance of the leaves. In another study, a two-step protocol involving the application of environmental stressors (chilling, high light and drought) and a post-harvest treatment (boiling and vinegar dressing) was developed (Esteban *et al.*, 2014). The first step was used to increase the total pool of xanthophylls, whereas the second step was used to specifically increase the content of zeaxanthin. The application of these two consecutive treatments allowed to enhance the content of zeaxanthin up to 15-fold in spinach and 28-fold in rocket. Finally, the application of stressors was also used to enhance the carotenoid content in plant tissues other than the leaf. For example, the levels of zeaxanthin in the germinated corn were increased 1.5-fold following irradiation with UV-B (He *et al.*, 2019). The presented examples illustrate that the increase in the content of zeaxanthin in certain plants can be achieved without genetic manipulation.

4.3.5 Photosynthetic performance

The measurement of photosynthetic performance of edible plant crops grown in open fields for commercial purposes is important for establishing potential impacts on the biomass and fruit production. Similarly, when new crops are generated, any factors affecting photosynthesis, such as changes in photosystem II (PSII) photochemistry and chlorophyll content, must be evaluated as these may determine the commercial value of that crop and influence the decision whether or not to market it.

The measurement of the quantum efficiency of PSII (F_v/F_m) is commonly used for the assessment of plant photosynthetic performance. However, some studies claimed that the reduction in total leaf chlorophyll content or changes to the ratio of chlorophyll A to chlorophyll B were also good indicators of impaired photosynthesis (Viljevac *et al.*, 2013). Based on the finding that high F_v/F_m ratios were associated with high chlorophyll levels in leaves, other studies even suggested that the measurement of chlorophyll content alone could be used to assess photosynthetic activity (Sharma *et al.*, 2015). However, in this work, it was found that changes in the F_v/F_m ratio were not always accompanied by related changes in the chlorophyll levels.

The total leaf chlorophyll content (Figure 4.5) and the F_v/F_m ratio (Figure 4.11) were significantly higher in the Azygous line than in the U/0; B/B; *hp3/hp3* line. This relationship was consistent with previous reports (Viljevac *et al.*, 2013). However, the Azygous and U/0; B/B lines were not found to be different in terms of their total leaf chlorophyll contents (Figure 4.5), yet the F_v/F_m ratio of the U/0; B/B line was significantly lower than that of Azygous (Figure 4.11). The reverse was observed between the *hp3* and U/0; B/B; *hp3/hp3* lines. The chlorophyll levels in the leaves of the triple cross were lower than in the *hp3* line (Figure 4.4B) but their F_v/F_m ratios were not found to be significantly different (Figure 4.11). Therefore, a decrease in total leaf chlorophyll content is not always accompanied by a reduction in the F_v/F_m ratio. Moreover, high F_v/F_m ratios are not always associated with high levels of chlorophyll. Among the analysed lines, the Az line had the highest F_v/F_m ratio (0.84) and its total leaf chlorophyll content was 10 530.0 $\mu\text{g g}^{-1}$ DW. The *hp3* line accumulated even higher chlorophyll levels in its leaves (14 217.7 $\mu\text{g g}^{-1}$ DW) than the Az line but had a significantly lower F_v/F_m ratio (0.79; 6% reduction compared to Azygous).

Furthermore, this work did not establish a clear relationship between the ratio of chlorophyll A to chlorophyll B and the corresponding F_v/F_m values. The ratios of chlorophyll A to chlorophyll B of the Az, U/0; B/B, and U/0; B/B; *hp3/hp3* lines were not found to be different (Figure 4.5), yet a significant difference was discovered between their F_v/F_m values (Figure 4.11). For the *hp3* line and the four triple crosses, this relationship was reversed (Figure 4.4B). In all triple crosses, the ratio of chlorophyll A to chlorophyll B was found to be significantly lower than in the *hp3* line, yet no difference was seen between their F_v/F_m values.

The absence of a clear relationship between the chlorophyll levels, the ratios of chlorophyll A to chlorophyll B and the corresponding F_v/F_m values in the analysed lines suggests that other factors must be involved. Carotenoids participate in photosynthesis by acting as accessory pigments to chlorophyll A, so any changes to their composition may affect the F_v/F_m measurement. The ratios between the total chlorophyll content and the total carotenoid content in leaves of all lines were plotted against their corresponding F_v/F_m values (Figure 4.12A). The Az, U/0; B/B and *hp3* lines followed a parabolic trend in which the optimal F_v/F_m ratio was achieved when the chlorophyll levels were about twice as high as the carotenoid levels. However, the four triple crosses did not fit this trend. Therefore, a different relationship was explored based on the idea that zeaxanthin is known to be directly involved in quenching of chlorophyll fluorescence. The ratio between the total chlorophyll content and the concentration of zeaxanthin (CHL:ZEA) in leaves of each line was plotted against its corresponding F_v/F_m value and a strong linear correlation was discovered (Figure 4.12B). In fact, the high levels of zeaxanthin in the leaves of the *hp3* line and the triple crosses could at least partially explain their lower F_v/F_m ratios since this xanthophyll has a much greater capacity to dissipate excess light energy compared to the other carotenoid pigments.

The *hp3* line is an ABA-deficient mutant characterised by poor water retention due to its inability to control stomatal closure in response to drought. Although ABA levels were not measured in the triple crosses, they are also likely to be ABA-deficient due to the type of the mutation these lines carry. Therefore, the F_v/F_m ratio may also be affected by stomatal closure. In fact, a negative linear correlation was found between the F_v/F_m ratios and stomatal conductance (g_s) in tomato plants under regular irrigation ($R = -0.592$, $P < 0.05$; Nemeskéri *et al.*, 2019) and in sugarcane varieties undergoing waterlogging treatment ($R = -0.606$, $P < 0.05$; Soleh *et al.*, 2018). However, the regulation of stomatal closure by ABA may not be straightforward. In fact, the exogenous application of ABA caused a reduction in the g_s value in spring wheat (*Triticum aestivum*), which was proportional to the concentration of the hormone but as the leaves aged, they were found to be less responsive to the ABA treatment (Atkinson *et al.*, 1989). It was subsequently found that the stomatal sensitivity of the spring wheat to ABA decreased as the plants aged and their sensitivity to ethylene increased while the synthesis of the latter remained fairly constant (Chen *et al.*, 2013). Therefore, analysis of ABA and ethylene levels in relation to stomatal closure and the F_v/F_m ratio is necessary in order to draw definite conclusions.

To summarise, when selecting methods for evaluation of photosynthetic performance in plants of interest, a measurement of the chlorophyll content alone may not be sufficient in order to establish if the photosynthetic activity has been affected. Moreover, the evidence presented here imply that the F_v/F_m ratio does not only depend on the leaf chlorophyll content but on other compounds, such as hormones or carotenoids and the specific ratios between them.

Chapter V: CRISPR/Cas9-targeted editing of zeaxanthin epoxidase

5.1 Introduction

CRISPR/Cas9-mediated genome editing is a novel, targeted and rapidly developing molecular tool, which, if employed wisely, can revolutionise plant biotechnology and breeding. Moreover, this technique has an enormous potential to expand the field of functional genomics because it allows for the development of previously unavailable single-gene knockouts, which otherwise would be difficult to characterise. CRISPR/Cas9 has been successfully used in tomato to target several genes of the carotenoid biosynthetic pathway, namely β -carotene hydroxylase 2, *CrtR-b2* (D'Ambrosio *et al.*, 2018), prolycopene isomerase, *CRTISO* (Dahan-Meir *et al.*, 2018), lycopene β -cyclase 1 and 2, *LCY-B1* and *LCY-B2* (Li *et al.*, 2018b), lycopene ϵ -cyclase, *LCY-E* (Li *et al.*, 2018b), phytoene synthase 1, *PSY1* (D'Ambrosio *et al.*, 2018; Dahan-Meir *et al.*, 2018) and stay-green 1, *SGR1* (Li *et al.*, 2018b). For example, the targeting of *SGR1* led to the generation of a new tomato line with a 5.1-fold increase in the lycopene levels compared to the control plants.

Thus far, no successful editing of zeaxanthin epoxidase, *ZEP* in tomato or, in fact, in any member of the Streptophyta clade, with the use of the CRISPR/Cas9 system has been reported. The only known case of CRISPR/Cas9-mediated editing of *ZEP* was described in a single-celled green alga *Chlamydomonas reihardtii* strain CC-4349 (Baek *et al.*, 2016; Baek *et al.*, 2018). This knockout of *ZEP* was induced by preassembled DNA-free CRISPR/Cas9 ribonucleoproteins and resulted in a 56-fold increase in the accumulation of zeaxanthin compared to the unedited microalgae.

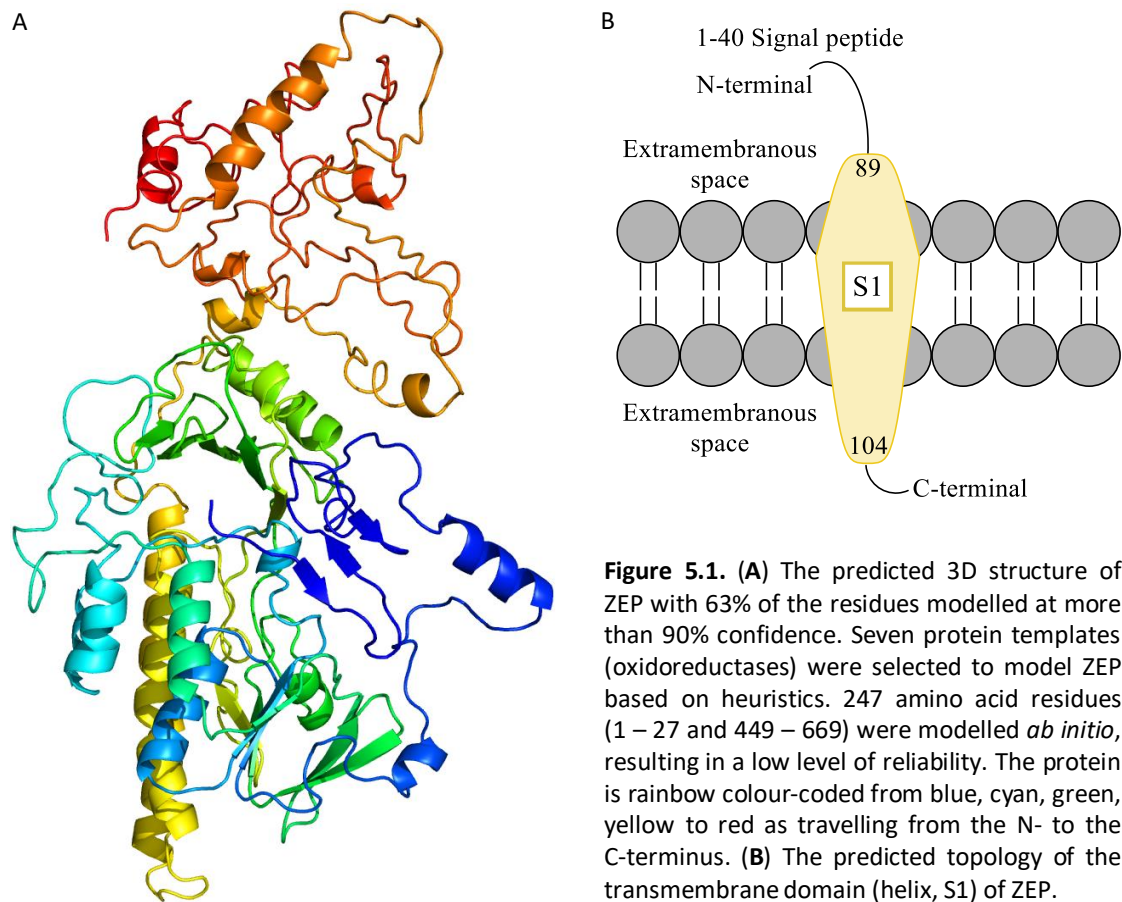
Increasing levels of zeaxanthin in plants is of particular interest due to its nutraceutical value. As a food supplement, zeaxanthin is taken to support eye health by protecting against age-related macular degeneration. Therefore, an approach involving the use of CRISPR/Cas9 was employed to reduce the activity of *ZEP* in tomato plants in order to increase the accumulation of zeaxanthin in fruit. Additionally, it was believed that this procedure would lead to the generation of novel alleles of *ZEP* and contribute to a better understanding of the role of this enzyme in carotenoid and ABA biosynthesis. In comparison to other gene targeting techniques, there is a chance that CRISPR/Cas9 will generate a weaker allele or a range of different alleles, whereas methods such as RNAi will block the enzyme activity without introducing genetic variety.

5.2 Results

5.2.1 Selection of target sequences within *ZEP*

The 3D structure of *ZEP* has not yet been determined. In order to select target sites for editing in this enzyme, the wild type (WT) amino acid sequence of *ZEP* (UniProtKB Accession P93236) was modelled *in silico* using Phyre2 server (Kelley *et al.*, 2015). This led to the generation of a 3D model of the protein structure (Figure 5.1A). The presence of a transmembrane domain at the

N-terminus (S1) was predicted in this model (Figure 5.1B), which was consistent with previous studies reporting that ZEP was membrane-associated (Schwarz *et al.*, 2015).



Further modelling was carried out in order to predict the presence of pockets. The pockets are concavities on the protein surface thought to interact with other molecules such as substrates (Yu *et al.*, 2010). Several pockets were identified (Figure 5.2A), which appeared to closely overlap with the regions of the protein that had the highest mutational sensitivity (Figure 5.2B). A more detailed analysis revealed that the largest pockets were localised at the following amino acid positions: 91 – 97, 114 – 127, 129 – 134, 161 – 165, 189 – 204, 247 – 254, 287 – 313, 355 – 360, 376 – 395, 439 – 449. One of these, a large GPIQIQ pocket, was detected upstream of the site of the missense mutation of glutamic acid at the position 142 in the *hp3* tomato line (Figure 5.2C). Interestingly, this residue was not predicted to have a high mutational sensitivity, yet it is known that the *hp3* allele leads to a strong mutant phenotype. Based on this modelling, two distinct amino acid targets within the sequence of ZEP were selected. First target, alanine at the position 137 (Figure 5.2D), found just upstream of the *hp3* mutation site, was predicted to have a high mutational sensitivity. Second target, threonine at the position 365 (Figure 5.2E) was localised upstream of a large LGDS-HAMQPN pocket and predicted to have a low mutational sensitivity. Alanine 137 and threonine 365 appear in the exons 1 and 6 of ZEP, respectively (Figure 5.3).

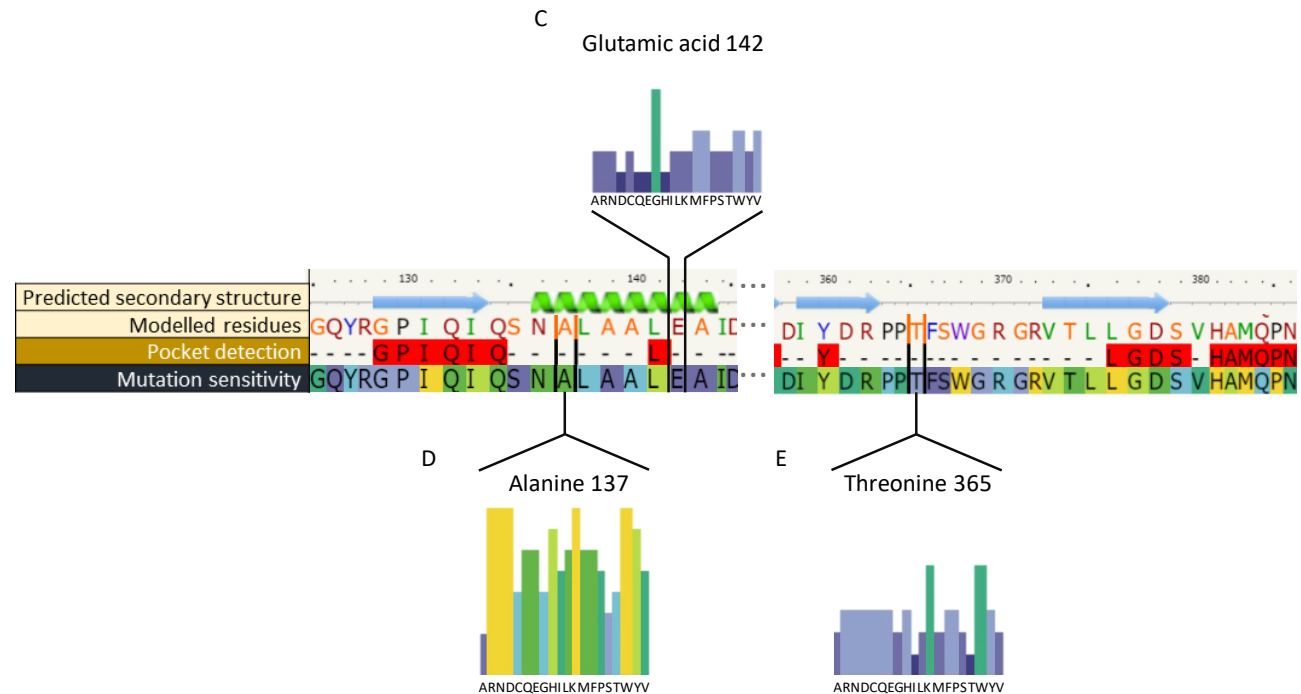
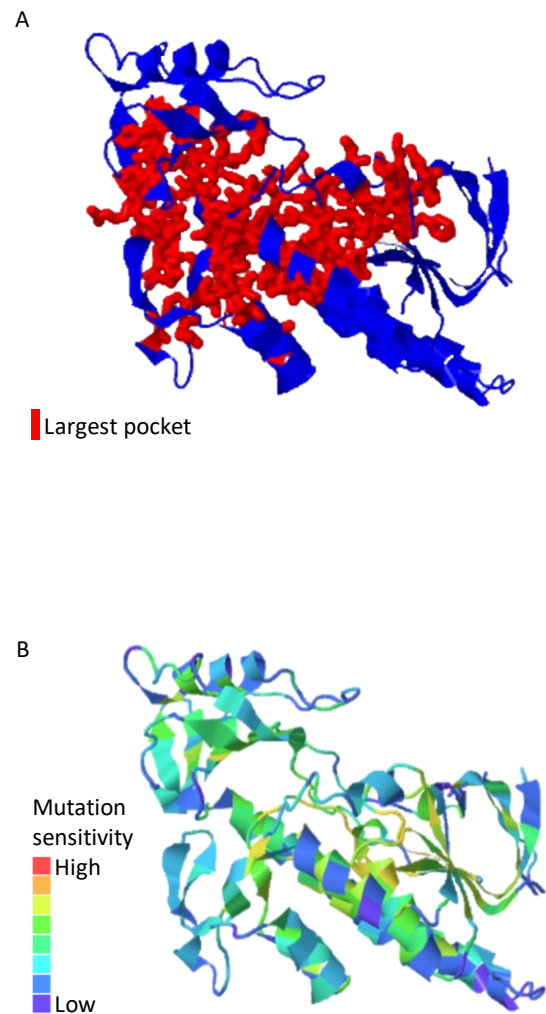


Figure 5.2. (A) Pocket detection (red) in ZEP indicating possible locations of the active sites. (B) Prediction of functional and/or phenotypic effects of missense mutations occurring at the given amino acid residues. The positions are coloured according to the averaged effects of the 20 possible mutations at that position with red and blue indicating highest and lowest sensitivities, respectively. (C) Predicted effects of mutations at the residue 142 (glutamic acid); this residue is found downstream of a large pocket (position 129 – 134) and is replaced with lysine in the *hp3* tomato line. Mutational sensitivity of alanine at the position 137 (D) and threonine at the position 365 (E) displayed against predicted pockets (highlighted in red). The colours and heights of the bars indicate expected effects of missense mutations of the indicated residues into the listed underneath amino acids from mild (short and blue) to severe (tall and red). The predictions are based on the crystal structure of CabE, an aromatic hydroxylase from angucyline biosynthesis.

The gene encoding zeaxanthin epoxidase, *ZEP* is located on chromosome 2 (Figure 5.3A) and contains 16 exons and 15 introns (Figure 5.3B). Typically, the Cas9 protein cuts the DNA strand three nucleotides upstream of the PAM sequence (Liang *et al.* 2016). Using the WT sequence of *ZEP* (GCA_000188115.2), the specific target sites were selected, which would place the site of the Cas9 cut directly after threonine 365 in the exon 6 (Figure 5.3C) and exactly at alanine 137 in the exon 1 (Figure 5.3D).

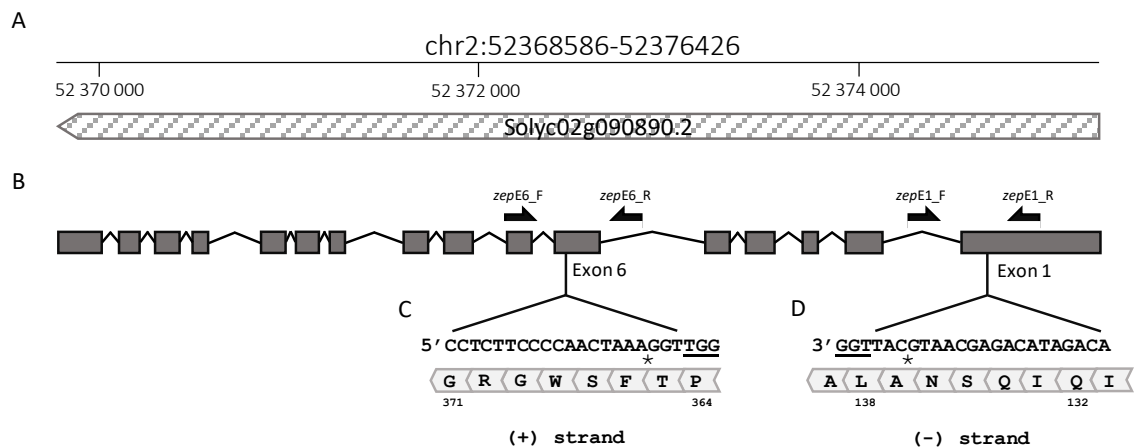


Figure 5.3. (A) Position of *ZEP* within the tomato genome. (B) Position of exons (grey rectangles) within *ZEP* (exon 1 – rightmost, 16 – leftmost). Black half-arrows indicate the attachment sites of the primers used in screening for edits in *ZEP*. Sequences of the 20 nucleotide-long Cas9 target sites in exon 6 (C) and exon 1 (D) with the corresponding amino acid sequences; the DNA strand with the targeted site is indicated underneath. The protospacer adjacent motif (PAM) sequence (TGG) is underlined in both targets. Asterisks (*) indicate the predicted cut sites of Cas9 localised three base pairs upstream of PAM.

The selected DNA targets were fitted to the single-guide RNAs (sgRNAs) scaffold and modelled *in silico* to predict the presence of the essential secondary structures. The sgRNAs are required for the RNA-guided site-specific DNA cleavage. It has been determined that the intact stem loop RAR as well as the stem loops 2 and 3 of the sgRNAs were essential for genome editing, whereas the stem loop 1 was not (Liang *et al.* 2016). The sgRNA targeting exon 6 was speculated to lack the non-essential stem loop 1 in CONTRAfold modelling (Figure 5.4A). However, when modelled against the characteristic constraint of the sgRNA, the stem loop 1 was predicted to hold stably in that conformation (Figure 5.4B). Although the essential stem loop 2 was not presumed to be present in the guide targeting exon 6, there was still a high probability that it could form a stable structure within the constraint. The other essential loops (RAR and loop 3) were both predicted to form and hold in a stable conformation (Figures 5.4A and B). The sgRNA targeting exon 1 was anticipated to contain all the essential loops in CONTRAfold modelling with the stem loop 1 only partially formed (Figure 5.4C). However, when fitted to the constraint, all the loops in the sgRNA targeting exon 1 were predicted to hold the structural position with a high level of probability (Figure 5.4D). Based on the structure, the sgRNA targeting exon 1 was expected to be a more efficient guide.

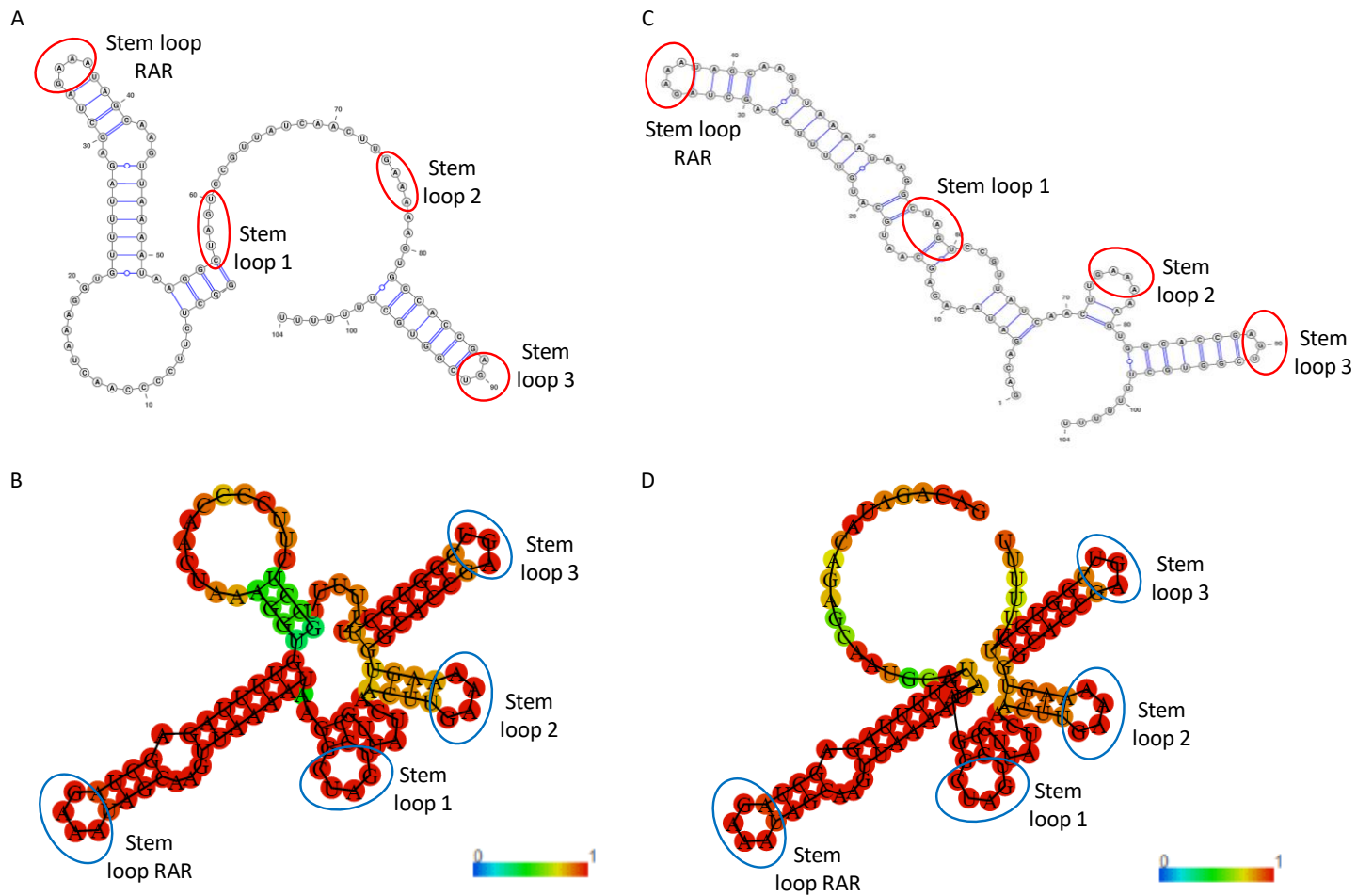


Figure 5.4. *In silico* prediction of secondary structures of sgRNAs targeting exon 6 (A) and exon 1 (C) using CONTRAfold inference engine based on calculating base-pairing probabilities. *In silico* prediction of minimum free energy (MFE) secondary structures of sgRNAs targeting exon 6 (B) and exon 1 (D) based on the provided constraint. The probability for each nucleotide to hold the structural position is represented by the colour from blue to red, corresponding to the lowest and highest probabilities, respectively. Loops 1, 2, 3 and repeat and anti-repeat region (RAR) are circled.

5.2.2 Assembly and verification of CRISPR/Cas9 expression cassettes

The CRISPR/Cas9 expression cassettes, holding the sgRNAs targeting either the exon 1 or 6, were assembled using the Golden-Gate cloning. This technique was selected as it allows for a seamless joining of multiple DNA parts in a predefined linear order in a single reaction vessel (Weber *et al.*, 2011; Belhja *et al.*, 2013). The parts necessary for this assembly were obtained from Addgene and verified through restriction digestion (Supplementary Figure 3.1 and Table 2.11).

The sgRNAs targeting the exon 6 (sgRNA_zepe6) and exon 1 (sgRNA_zepe1) were prepared by amplifying the scaffolds with the primer pairs that incorporated the specific 20 nucleotide-long DNA target sequences selected previously (Figure 5.5A). The sgRNA_zepe6 and sgRNA_zepe1 scaffolds were purified and used to assemble level 1 pICH47751::zepe6 and pICH47751::zepe1 constructs, respectively. Predicted digestion patterns (Table 5.1) of the level 1 constructs were compared against the actual fragments resulting from the digestion of the plasmids with *BpiI* alone or double digestion with *NotI* and *SfiI* (Figure 5.5B). All pICH47751::zepe6 digested with *BpiI* produced bands of the expected sizes except plasmid VII, where an additional faint band at 3 000 bp was seen (Figure 5.5B). Following the digestion of pICH47751::zepe6 with *NotI/SfiI*, the bands of the expected sizes were produced in all plasmids except construct III, where the larger 3 026 bp band was not present and additionally, the super-coiled plasmid appeared at a greater molecular weight compared to the other vectors. The majority of pICH47751::zepe1 constructs digested with *BpiI* generated the predicted fragment patterns except constructs I and II where an additional 3 000 bp band and a much fainter 2 000 bp band were seen (Figure 5.5B). Digestion

Table 5.1. Predicted sizes of fragments generated through *in silico* restriction enzyme digests of the assembled constructs with the specified enzymes.

		Construct	Fragments (bp)
+BbsI		pICH47751	4 352 + 616
		pICH47751:: zepe6 zepe1	4 352 + 237
+NotI/SfiI	CpG methylated	pICH47751	4 968
		pICH47751:: zepe6 zepe1	4 589
	CpG unmethylated	pICH47751	3 033 + 1 935
		pICH47751:: zepe6 zepe1	3 026 + 1 563
+EcoRV		pICSL4723	7 477 + 3 822 + 1 649
		pICSL4723:: zepe6 zepe1	8 410 + 3 870

of all pICH47751::*zepE1* constructs (I – VII) with *NotI/SfiI* produced bands of the expected sizes. Plasmids pICH47751::*zepE6* constructs I, IV and V were then selected for forward and reverse sequencing across the assembled region. All of the sequenced plasmids matched the *in silico* assembled template (Figure 5.6A). Plasmids pICH47751::*zepE1* constructs I, IV and V were also sequenced and all, including construct I with an incorrect digestion pattern, matched the *in silico* assembled template (Figure 5.6B). The sequenced level 1 plasmids with the correct digestion patterns were selected for the preparation of the level 2 binary vectors pICSL4723::*zepE6* and pICSL4723::*zepE1*. The assembled level 2 plasmids were digested with *EcoRV* (Figure 5.5C) and then compared against the predicted fragment sizes (Table 5.1). Five of the six pICSL4723::*zepE6* vectors (constructs II – VI), showed the correct digestion patterns. Plasmid pICSL4723::*zepE6* construct I appeared not to be digested properly as it run at the same size as the undigested empty level 2 plasmid. Alternatively, this plasmid might have re-ligated without the insert. Four of the six pICSL4723::*zepE1* plasmids had the correct digestion patterns, while vectors I and V, appeared to be empty. Alternatively, these constructs could contain multiple inserts ligated together. Plasmids pICSL4723::*zepE6* and pICSL4723::*zepE1* with the correct digestion patterns were sequenced at the right (Figure 5.7A) and left (Figure 5.7B) borders across the assembled DNA segments. The sequenced regions matched exactly the *in silico* assembled level 2 templates confirming the correct joining of the modules. The linear maps of the fully constructed level 1 sgRNAs and level 2 CRISPR/Cas9 expression cassettes, showing the attachment sites for the sequencing primers, are provided in Figure 5.8. More detailed, full plasmid maps of the level 1 and level 2 constructs are given in Supplementary Figure 3.3.

The efficiency of Golden-Gate assembly of level 1 and 2 vectors was calculated by comparing the total number of colonies on the plate with the number of colonies carrying the empty level 1 (blue) or empty level 2 (red) vectors (Supplementary Figure 3.2). Overall, the efficiency of the Golden-Gate assembly was high, reaching nearly 90% for the level 1 constructs and close to 70% for the level 2 constructs (Table 5.2). Moreover, most of the plasmids, once tested by restriction digestion, appeared to contain fragments of the correct sizes. In summary, Golden-Gate cloning is a fast and efficient method for the assembly of multi-modular constructs.

Table 5.2. Efficiency of the Golden-Gate assembly of the level 1 and level 2 vectors calculated as a ratio of the number of white clones to the total number of all clones for each of the designed guides.

	Level 1			Level 2		
	Blue clones	Total	Efficiency	Red clones	Total	Efficiency
Exon 6	288	3148	91%	216	776	72%
Exon 1	408	3592	87%	224	644	65%

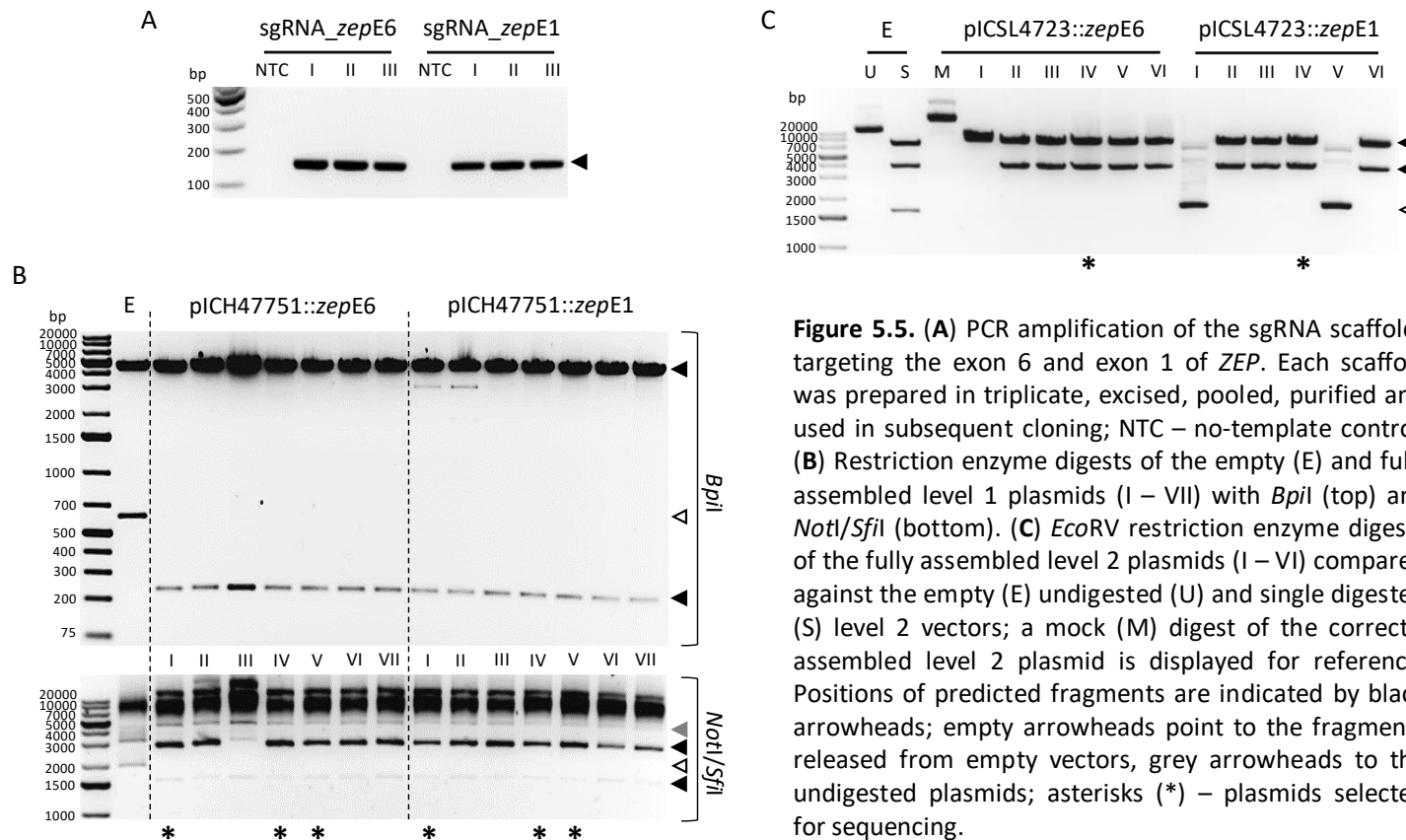


Figure 5.5. (A) PCR amplification of the sgRNA scaffolds targeting the exon 6 and exon 1 of *ZEP*. Each scaffold was prepared in triplicate, excised, pooled, purified and used in subsequent cloning; NTC – no-template control. (B) Restriction enzyme digests of the empty (E) and fully assembled level 1 plasmids (I – VII) with *Bpil* (top) and *NotI/SfiI* (bottom). (C) *EcoRV* restriction enzyme digests of the fully assembled level 2 plasmids (I – VI) compared against the empty (E) undigested (U) and single digested (S) level 2 vectors; a mock (M) digest of the correctly assembled level 2 plasmid is displayed for reference. Positions of predicted fragments are indicated by black arrowheads; empty arrowheads point to the fragments released from empty vectors, grey arrowheads to the undigested plasmids; asterisks (*) – plasmids selected for sequencing.

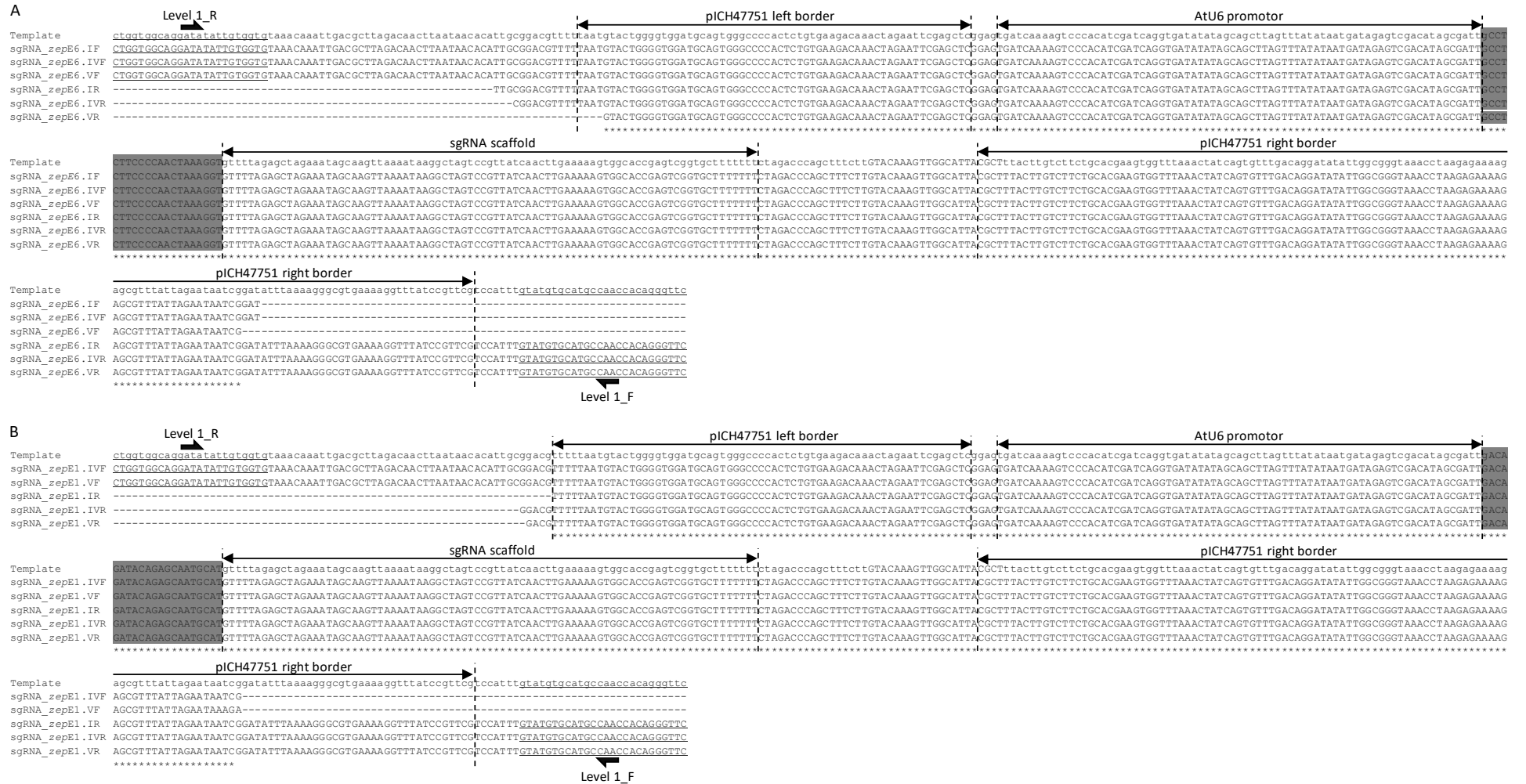


Figure 5.6. Alignment of the sequenced level 1 constructs harbouring guides targeting the exon 6 (A) and exon 1 (B) against their respective templates. Each construct was sequenced with the forward (F) and reverse (R) primers to the region of interest. The plasmids selected for analysis are indicated in Figure 5.5B. Multiple alignment was performed using fast Fourier transform (MAFFT) algorithm. Sequences of the 20 bp-long targets within *ZEP* are highlighted in grey; underlined sequences indicate primer attachment sites; asterisks (*) indicate the matching sequences.

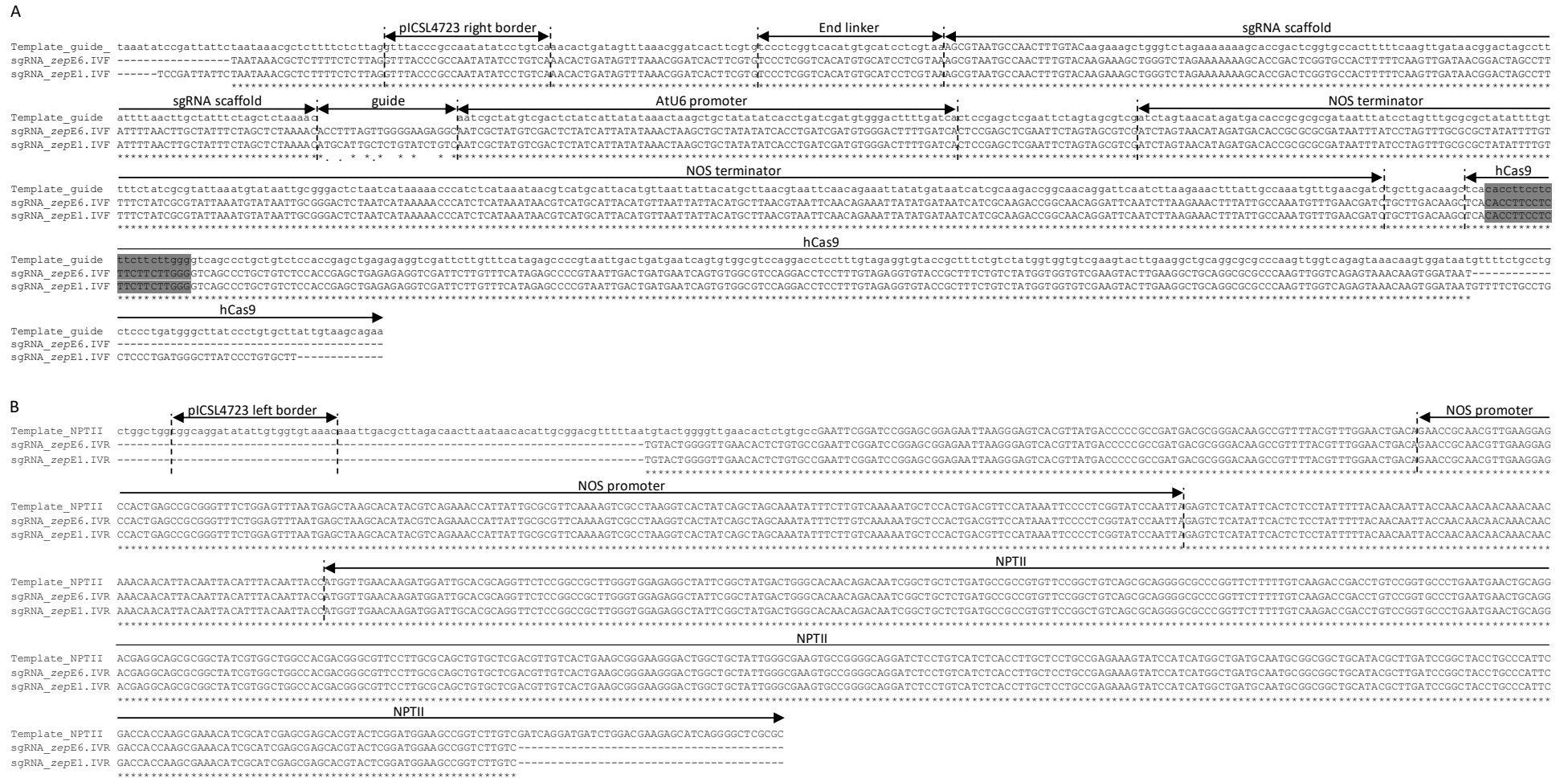


Figure 5.7. MAFFT alignment of the forward and reverse sequenced level 2 constructs at their right (A) and left (B) borders, respectively. The variable guide region was omitted from the template to aid the alignment of shared modules at the right border. The plasmids selected for sequencing are indicated in Figure 5.5C. The nuclear localisation signal (NLS) of hCas9 is highlighted in grey; asterisks (*) indicate the matching sequences.

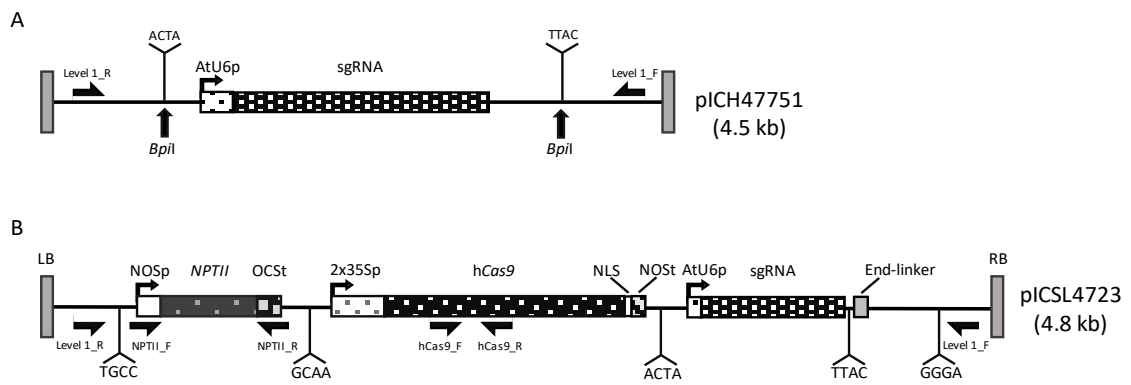


Figure 5.8. Plasmid maps of the level 1 (A) and level 2 (B) constructs assembled using the Golden-Gate cloning strategy; fragments are not to scale. Positions of *Bpil* restriction sites are indicated in the level 1 plasmid; the sites are eliminated following ligation into higher levels. Plasmid backbones, primer attachment sites (black half-arrows) and 4 bp adapter sequences between the assembled parts (Y-crosses) are indicated. The constructs are named by their target regions: exon 1 (*zepE1*) and exon 6 (*zepE6*) in level 1 (pICH47751::*zepE1* and pICH47751::*zepE6*) and level 2 (pICSL4723::*zepE1* and pICSL4723::*zepE6*).

The level 2 binary vectors were used to transform *Agrobacterium tumefaciens* strain LBA4404. *A. tumefaciens* was verified to contain the correct constructs with restriction enzyme digestion and PCR (Supplementary Figure 3.4A) and then used in the stable transformation of tomato. The leaf explants of Ailsa Craig (AC) variety were split into three groups: AC controls not exposed to the *A. tumefaciens* suspension but taken through the tissue culture, exposed to *A. tumefaciens* transformed with pICSL4723::*sgRNA_zepE6* and exposed to *A. tumefaciens* transformed with pICSL4723::*sgRNA_zepE1* (Supplementary Figure 3.4B).

5.2.3 Screening of AC primary transformants (T_0)

In order to establish an efficient screening strategy of the primary transformants (T_0 plants), the level 2 binary plasmids (pICSL4723::*sgRNA_zepE6* and pICSL4723::*sgRNA_zepE1*) were used as templates to amplify the hCas9 and NPTII fragments (Figure 5.9A). The same fragments were also screened for in the T_0 plants and the level 2 plasmids, either pICSL4723::*sgRNA_zepE6* or pICSL4723::*sgRNA_zepE1*, were used as positive controls for their respective transformation experiments. The detection of these fragments in the analysed transformants would indicate a successful integration of the CRISPR/Cas9 cassette into the plant's genome and potentially, the presence of DNA edits. The primer attachment sites for the hCas9 and NPTII fragments in the level 2 plasmids are indicated in Figure 5.8B. The specificity of the primers was tested on the AC control plants, which, as expected, were found to be negative for both of these fragments (Figure 5.9B). Additionally, the targeted regions within exon 1 and exon 6 were amplified from the AC control plants (Figure 5.9B) and forward and reverse sequenced (Figure 5.9C) to obtain the native fragments necessary for the comparison against the edited plants. The sequenced fragments aligned exactly against the WT gene sequence of *ZEP* (GCA_000188115.2). The primer attachment sites for the exon 6 and exon 1 regions are indicated in Figure 5.3B.

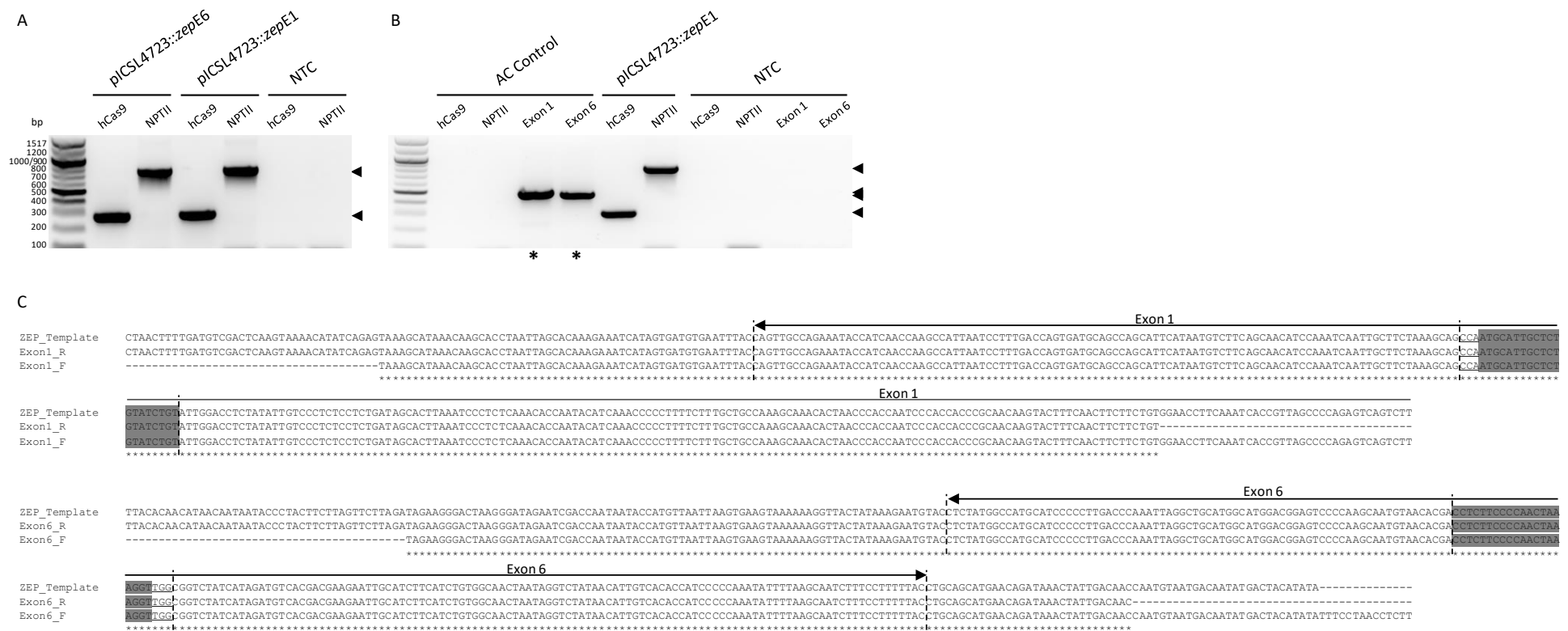


Figure 5.9. (A) Amplification of the hCas9 and NPTII fragments from the assembled level 2 constructs. **(B)** Amplification of the hCas9, NPTII, exon 1 and exon 6 fragments from an untransformed AC control plant. NTC – no-template control. Black arrowheads indicate positions of predicted fragments; asterisks (*) – fragments selected for sequencing. The molecular marker used is the same in both cases. **(C)** MAFFT alignment of the exon 1 (top) and exon 6 (bottom) fragments from an untransformed AC control plant. The positions of the exons are annotated with the PAM sequences underlined and the target regions highlighted in grey; asterisks (*) indicate the matching sequences. Both fragments were sequenced with the forward (F) and reverse (R) primers.

T₀ plants transformed with pICSL4723::sgRNA_zepe6 were first screened for the presence of the hCas9 and NPTII fragments (Figure 5.10A). The DNA of the plants found to be positive for both of these was used as a template to amplify across the region of the exon 6 where edits were expected. The PCR amplicons of the exon 6 from any of the tested plants did not run as separate bands, so it was expected that if a mutation had been introduced, it must have involved a few nucleotides only (Figure 5.10B). The same PCR fragments were also sequenced (Figure 5.10C). Some of the sequenced products generated chromatograms with overlapping peaks but were still able to be processed successfully (T₀ ID 9.6.1). This suggests that at least some cells of these plants were edited, and the overlap was the consequence of a small amount of different DNA templates in the mix. However, in other PCR products, the peak overlap was so extreme that it led to a collapsed sequencing (T₀ ID 9.6.2). This suggests that a high proportion of cells of these plants was edited and the sequencing could not be completed due to the presence of multiple templates. Interestingly, the overlapping peaks on the chromatograms usually started exactly three nucleotides upstream of the PAM sequence (T₀ ID 9.6.2) or very close to it (T₀ ID 9.6.1). Finally, some plants positive for hCas9 and NPTII (T₀ ID 9.6.3), were found to have completely clear chromatograms of the sequenced PCR products of the WT exon 6. This implies that despite the successful integration of the CRISPR/Cas9 expression cassette, the editing did not take place and only the WT alleles of *ZEP* were amplified during the PCR reaction.

Only T₀ plants positive for hCas9/NPTII and returning an overlapping chromatogram following sequencing of the exon 6 PCR product, were considered to be successfully edited. In order to assess the types and frequencies of the mutations in the edited plants as well as to verify some unedited plants positive for hCas9/NPTII, the PCR fragments spanning the exon 6 (Figure 5.10B) were cloned into TOPO vectors and between 10 and 20 clones were sequenced. This allowed to obtain a snapshot of different PCR products present in the population and hence, identify the types and frequencies of the edits that had taken place in each plant. The results of this screen, listing the modified DNA sequences, types and frequencies of the identified mutations as well as the types of novel alleles of *ZEP*, are provided in Table 5.3. The T₀ plants transformed with pICSL4723::sgRNA_zepe1 were screened in exactly the same way as described above. However, compared to the exon 6 targeting, transformation with pICSL4723::sgRNA_zepe1 yielded very few T₀ plants. Some T₀ plants targeted at the exon 1 only contained a very faint band for the hCas9 fragment but were negative for NPTII (Supplementary Figure 3.5). This ambiguity was also sometimes present in the T₀ plants targeted at the exon 6 but could be easily eliminated through sequencing of the PCR products of the targeted regions. Finally, only a single T₀ plant (ID 12.7.24) was found to be positive for hCas9 and NPTII, although the NPTII band appeared to be very faint (Supplementary Figure 3.5). The types of alleles discovered in the three plants targeted at the exon 1 and found to be positive for at least hCas9 are presented in Table 5.4.

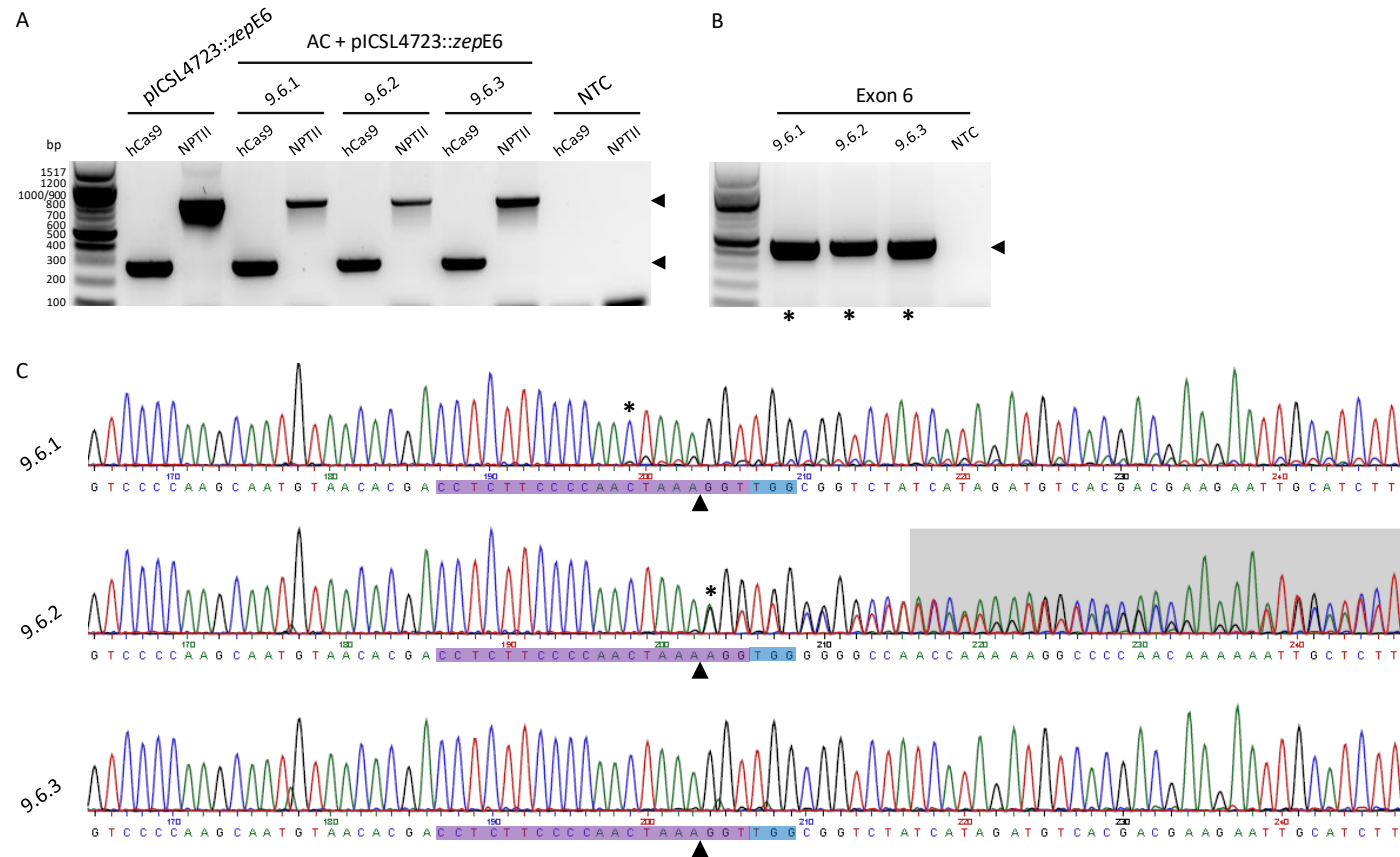


Figure 5.10. (A) Screening for the presence of the hCas9 and NPTII fragment from AC tomato plants transformed with pICSL4723::zepE6 targeting the exon 6. (B) Amplification of the exon 6 fragments from the plants positive for hCas9 and NPTII screened in (A). NTC – no-template control. Black arrowheads indicate positions of predicted fragments; asterisks (*) – fragments selected for sequencing. The molecular markers used are the same in both cases. (C) Sequencing of the exon 6 fragments from (B); target sequences are highlighted in violet, PAM – in blue; black arrowheads indicate the expected position of the Cas9 cut. The asterisk (*) in two of the sequences (identifier 9.6.1 and 9.6.2) indicate the beginning of the overlapping chromatogram. Only fragments sequenced with the forward primers are presented.

Table 5.3. Types and frequencies of mutations in hCas9/NPTII-positive transformants targeted at the exon 6 (target – highlighted in grey; PAM sequence – underlined). DNA (5'→3') and protein sequences are displayed against unedited templates (top rows). Positions of amino acids and missense mutations (bold) are indicated; WT – wild type; Δ – deletion; IS – insertion; bp – base pair; X – premature stop codon.

Identifier	DNA sequence	Mutation	Altered protein sequence	Frequency
AC control	ACCTCTTCCCCAACTAAAGGT <u>TGGC</u>	WT	n/a	100%
9.6.1	ACCTCTTCCCCAACTAAAGGT <u>TGGC</u>	WT	n/a	63%
	ACCTCTTCCCCAACTAAAGGT <u>TGGC</u> ACCTCTTCCCCAA-----GGT <u>TGGC</u>	Δ5 bp	³⁶⁵ FSWGRGRVTL ³⁶⁶ LGDSVHAMQPNLGGGCM ³⁶⁷ AI ³⁶⁸ E ³⁶⁹ ³⁶⁵ LGKRS CVYIAWGLR PC HAA X ³⁸³	32%
	A+21nt CCTCTTCCCCAACTAAAGGT <u>TGG</u> +92nt T AΔ21nt-----Δ92nt T	Δ137 bp	³³² LKIFGGWCDNVI ³³³ DL ³³⁴ LVA ³³⁵ DE ³³⁶ DAIL ³³⁷ RR ³³⁸ DI ³³⁹ Y ³⁴⁰ ³³² LIRP CHAA X ³³⁹	5%
	ACCTCTTCCCCAACTAAAGGT <u>TGGC</u>	WT	n/a	37%
9.6.2	ACCTCTTCCCCAACTAAA-GGT <u>TGGC</u> ACCTCTTCCCCAACTAAAAGGT <u>TGGC</u>	IS1 bp	³⁶⁶ FSWGRGRVTL ³⁶⁷ LGDSVHAMQPNLGGGCM ³⁶⁸ AI ³⁶⁹ E ³⁷⁰ ³⁶⁶ FX ³⁶⁶	48%
	ACCTCTTCCCCAACTAAA-GGT <u>TGGC</u> ACCTCTTCCCCAACTAAATGGT <u>TGGC</u>	IS1 bp	³⁶⁵ FSWGRGRVTL ³⁶⁶ LGDSVHAMQPNLGGGCM ³⁶⁷ AI ³⁶⁸ E ³⁶⁹ ³⁶⁵ TX ³⁶⁶	5%
	ACCTCTTCCCCAACTAAAGGT <u>TGGC</u> ACCTCTTCCCCAAC-----GGT <u>TGGC</u>	Δ4 bp	³⁶⁵ FSWGRGRVTL ³⁶⁶ LGDSVHAMQPNLGGGCM ³⁶⁷ AI ³⁶⁸ E ³⁶⁹ ³⁶⁵ VGEEV LHCLG TF SM PC SLI WV KG DAW P X ³⁹³	5%
	CCTCTTCCCCAACTAAAGGT <u>TGGC</u> +9nt T CCTCT-----Δ9nt T	Δ28 bp	³⁵⁹ IYDRPPTFSWGRGRVTL ³⁶⁰ LGDSVHAM ³⁶¹ ³⁵⁹ TX ³⁵⁹	5%
9.6.3	ACCTCTTCCCCAACTAAAGGT <u>TGGC</u>	WT	n/a	100%
12.6.2	ACCTCTTCCCCAACTAAAGGT <u>TGGC</u>	WT	n/a	90%
	C+39nt CCTCTTCCCCAACTAAAGGT <u>TGG</u> +30nt T CΔ39nt-----Δ30nt T	Δ92 bp	³⁵² DAILRRDIY ³⁶⁰ ³⁵² DA X ³⁵⁴	10%
12.6.3	ACCTCTTCCCCAACTAAAGGT <u>TGGC</u>	WT	n/a	50%
	ACCTCTTCCCCAACTAAAGGT <u>TGGC</u> ACCTCTTCCCCAACT-----GT <u>TGGC</u>	Δ4 bp	³⁶⁵ FSWGRGRVTL ³⁶⁶ LGDSVHAMQPNLGGGCM ³⁶⁷ AI ³⁶⁸ E ³⁶⁹ ³⁶⁵ VGEEV LHCLG TF SM PC SLI WV KG DAW P X ³⁹³	20%
	ACCTCTTCCCCAACTAAAGGT <u>TGGC</u> ACCTC-----GGT <u>TGGC</u>	Δ13 bp	³⁶⁵ FSWGRGRVTL ³⁶⁶ LGDSVHAMQPNLGGGCM ³⁶⁷ AI ³⁶⁸ E ³⁶⁹ ³⁶⁵ TEV LHCLG TF SM PC SLI WV KG DAW P X ³⁹⁰	10%
	ACCTCTTCCCCAACTAAAGGT <u>TGGC</u> ACCTCTTCCCCA-----GGT <u>TGGC</u>	Δ6 bp	³⁶⁵ FSWGRGRVTL ³⁶⁶ LGDSVHAMQPNLGGGCM ³⁶⁷ AI ³⁶⁸ E ³⁶⁹ ³⁶⁵ T --WGRGRVTL ³⁶⁶ LGDSVHAMQPNLGGGCM ³⁶⁷ AI ³⁶⁸ E ³⁶⁹	10%
	ACCTCTTCCCCAACTAAA-GGT <u>TGGC</u> ACCTCTTCCCCAACTAAAAGGT <u>TGGC</u>	IS1 bp	³⁶⁵ FSWGRGRVTL ³⁶⁶ LGDSVHAMQPNLGGGCM ³⁶⁷ AI ³⁶⁸ E ³⁶⁹ ³⁶⁵ FX ³⁶⁶	10%
	ACCTCTTCCCCAACTAAAGGT <u>TGGC</u> ACCTCTTCCCCAACTA--GGT <u>TGGC</u>	Δ2 bp	³⁶⁵ FSWGRGRVTL ³⁶⁶ LGDSVHAMQPNLGGGCM ³⁶⁷ AI ³⁶⁸ E ³⁶⁹ ³⁶⁵ TX ³⁶⁵	75%
12.6.8	ACCTCTTCCCCAACTAAAGGT <u>TGGC</u> ACCTCTC-----C	Δ16 bp	³⁶³ PPTFSWGRGRVTL ³⁶⁴ LGDSVHAMQPNLGGGCM ³⁶⁵ AI ³⁶⁶ E ³⁶⁷ ³⁶³ EEV LHCLG TF SM PC SLI WV KG DAW P X ³⁸⁹	25%
	ACCTCTTCCCCAACTAAAGGT <u>TGGC</u>	WT	n/a	30%
12.6.18	ACCTCTTCCCCAACTAAAGGT <u>TGGC</u> ACCTCTTCCCCAACTA--GGT <u>TGGC</u>	Δ2 bp	³⁶⁵ FSWGRGRVTL ³⁶⁶ LGDSVHAMQPNLGGGCM ³⁶⁷ AI ³⁶⁸ E ³⁶⁹ ³⁶⁵ TX ³⁶⁵	50%
	ACCTCTTCCCCAACTAAAGGT <u>TGGC</u> ACCTCTTCCCCAACTA-AGGT <u>TGGC</u>	Δ1 bp	³⁶⁵ FSWGRGRVTL ³⁶⁶ LGDSVHAMQPNLGGGCM ³⁶⁷ AI ³⁶⁸ E ³⁶⁹ ³⁶⁵ TLV GEEV LHCL G TF SM PC SLI WV KG DAW P X ³⁹⁴	20%
12.6.23	ACCTCTTCCCCAACTAAAGGT <u>TGGC</u>	WT	n/a	100%
12.6.26	ACCTCTTCCCCAACTAAAGGT <u>TGGC</u>	WT	n/a	100%
12.6.32	ACCTCTTCCCCAACTAAAGGT <u>TGGC</u>	WT	n/a	70%
	ACCTCTTCCCCAACTAAAGGT <u>TGGC</u> ACCTCTTCCCCAA-----GGT <u>TGGC</u>	Δ5 bp	³⁶⁵ FSWGRGRVTL ³⁶⁶ LGDSVHAMQPNLGGGCM ³⁶⁷ AI ³⁶⁸ E ³⁶⁹ ³⁶⁵ LGKRS CVYIAWGLR PC HAA X ³⁸³	30%

Table 5.4. Types and frequencies of mutations in hCas9-positive transformants targeted at the exon 1 (target – highlighted in grey; PAM sequence – underlined). DNA (5'→3') and protein sequences are displayed against unedited templates (top rows). Positions of amino acids and missense mutations (bold) are indicated; WT – wild type; Δ – deletion; bp – base pair; X – premature stop codon.

Identifier	DNA sequence	Mutation	Altered protein sequence	Frequency
AC control	GCCAATGCATTGCTCTGTATCTGTA	WT	n/a	100%
12.7.1	GCCAATGCATTGCTCTGTATCTGTA	WT	n/a	100%
12.7.10	GCCAATGCATTGCTCTGTATCTGTA	WT	n/a	60%
12.7.24	GCCAATGCATTGCTCTGTATCTGTA GCCAATG-----TGTATCTGTA	Δ8 bp	¹³¹ IQIQSNALAAL ¹³² EAILDLVAEDIMN ¹³³ ¹³¹ I QI H IG CFRSN X ¹⁴¹	20%
	GCCAATGCATTGCTCTGTATCTGTA GCCAATG-ATTGCTCTGTATCTGTA	Δ1 bp	¹³¹ IQIQSNALAAL ¹³² EAILDLVAEDIMN ¹³³ ¹³¹ IQIQSN HWLL X ¹⁴⁰	20%

Out of the 34 plantlets that came out of the tissue culture, 10 T₀ plants targeted at the exon 6 were found to be positive for hCas9 and NPTII (Table 5.3). Seven of these were found to have some changes in the exon 6. The mutation frequency varied from 10% (T₀ ID 12.6.2) up to 100% (ID 12.6.8). Four of the edited plants, T₀ ID 9.6.1, 9.6.2, 12.6.3 and 12.6.18, had at least two different and novel alleles of *ZEP* in addition to the WT. The maximum of four novel alleles were identified in the same T₀ plant (ID 9.6.2 and 12.6.3). Two T₀ plants, ID 12.6.2 and 12.6.32 had one novel allele of *ZEP* in addition to the WT. Three plants, ID 9.6.3, 12.6.23 and 12.6.26, even though positive for hCas9 and NPTII, were found to only contain the WT alleles of *ZEP*.

Most of the identified DNA modifications included insertions of a single base or small, 1 – 5 bp deletions. The majority of the new *ZEP* alleles had a premature STOP codon introduced as the result of the edits except for T₀ ID 12.6.3, where the in-frame deletion of 6 bp produced an allele of *ZEP* with two amino acids deleted. However, this allele was only present at a 10% frequency. Some plants were found to have exceptionally large deletions. For example, 5% of the alleles in T₀ ID 9.6.1 had a deletion of 137 bp, the same number of alleles in T₀ ID 9.6.2 had a deletion of 28 bp and a deletion of 92 bp at a 10% frequency occurred in T₀ ID 12.6.2. Although, these large deletions were identified after sequencing the TOPO plasmids, the PCR products themselves did not resolve as separate bands during gel electrophoresis, which means that these edits must have been very rare and they were picked up in the screen by chance.

Finally, a single plant edited at the exon 6, T₀ ID 12.6.8 (Supplementary Figure 3.6), was found to be of particular interest and was studied in more detail (further sections). This plant did not contain any WT alleles of *ZEP* but only genes encoding truncated versions of the protein. This shows that this plant carried a ballistic edit affecting both chromosomes. Interestingly, however, the most frequent edit in this plant was a small, 2 bp deletion present in 75% of the sequenced TOPO vectors. The remaining 25% of the exon 6 PCR fragments carried a larger, 16 bp deletion in the same area. Therefore, the mutation that took place was not symmetric and it was most likely a result of a second edition occurring later in development.

Editing of the exon 1 of *ZEP* was overall unsuccessful as no modified plants, which could be used beyond the initial screen, survived once transferred into the glasshouse. The total of 14 plantlets came out of the tissue culture experiment for this group. However, most of these plants were found to be escapes. Only three plants were found to be positive for hCas9 and, out of these three, only one plant was found to be also positive for NPTII (Supplementary Figure 3.5). This single plant (ID 12.7.24) was found to be edited at the exon 1, while the other two (ID 12.7.1 and 12.7.10), only contained the WT alleles of *ZEP* (Table 5.4). The edited plant was determined to contain two novel alleles of *ZEP*, both at the same frequency of 20%. The novel alleles contained either a single-nucleotide or a 8 bp deletion, both starting 3 bp upstream of the PAM sequence.

Both of these edits introduced a premature STOP codon that led to the production of a truncated version of the protein. It was not possible to carry out any further analyses of this T₀ plant as, following its transfer into the glasshouse, the plant dried out. However, *in silico* modelling of the novel alleles identified in this plant was carried out (5.2.6) in an attempt to explain the lack of adaptation of this transformant and its extreme vulnerability to water loss.

5.2.4 General characterisation of T₀ plants

Phenotypic characterisation of T₀ transformants edited at the exon 1 was not possible as none of the plants survived beyond the initial plantlet stage. However, some of the plants, which were exposed to *A. tumefaciens* transformed with pICSL4723::sgRNA_zepe1, but which were found to be unedited (ID 12.7.1 and 12.7.22), were still characterised and used for comparison as these experienced exactly the same conditions (bacterial suspension, tissue culture and glasshouse acclimatisation) as the other edited plants.

Several T₀ transformants targeted at the exon 6 grew to a full size and these were characterised further. The fruit and flowers of some of these plants, depending on the availability of the material at the time of analysis, were compared in Figure 5.11. The three plants, ID 9.6.2, 12.6.3 and 12.6.8, which were edited at the frequency of 50% or more, had consistently smaller fruit compared to the AC control and the plants with no (ID 9.6.3) or low (ID 12.6.2) editing frequency (Figure 5.11A). Plant ID 12.6.2, edited at only 10% frequency, had fruit of a very similar size to the AC control. On the other hand, the unedited plant ID 9.6.3 appeared to have smaller fruit than the AC control or plant ID 12.6.2, but its fruit were still larger than the fruit of the other edited plants. Interestingly, the plant carrying the biallelic mutation, ID 12.6.8 had the smallest fruit out of all T₀ plants, while the fruit of the two other edited plants (ID 9.6.2 and 12.6.3) were very similar to each other but larger than the fruit of ID 12.6.8. Moreover, fruit of the two most edited plants, ID 9.6.2 and 12.6.8, appeared to be slightly lighter than other fruit.

The flowers of some of the edited and unedited T₀ plants were compared as well (Figure 5.11B). The flowers of the AC control plant appeared yellow and had yellow-coloured stamens. Similarly looking flowers were found on the unedited plants ID 9.6.3 and 12.7.1. The flowers of the plant edited at the exon 6 at a 10% frequency, ID 12.6.2, were also yellow and very similar to the AC control. The flowers collected from the two most edited plants, ID 9.6.2 and 12.6.8, were very different from the AC control – they were paler, almost beige-coloured and had characteristically orange-coloured stamens. Interestingly, flowers of the same colour were found in the *hp3* line (Figure 4.3). Only flowers of a single colour were found on the plants with the highest editing frequency, ID 9.6.2 and 12.6.8, but on the plant edited at a 37% frequency, ID 9.6.1, two different types of flowers were identified. The first type had the same colour as the AC control plant and the second was very similar to the flowers of the *hp3* line and the 100% edited plant, ID 12.6.8.

This difference between these two types of flowers collected from plant ID 9.6.1 could be clearly visible when the whole flower trusses of the two different colours (yellow and pale/beige) were placed next to each other (Supplementary Figure 3.7).

The presence of two different types of flowers on the same plant strongly suggests that parts of this chimeric plant must have originated from the cells, which had been edited to a different extent. It seems that some parts of this plant were very strongly edited, so much so that they looked exactly like the 100% edited plant ID 12.6.8. Other parts of the same plant might not have been edited at all or could have been edited at a much lower frequency since the flowers looked similar to the AC control. Finally, none of the plants edited at the exon 6 were susceptible to water loss, except the plant carrying the biallelic mutation, ID 12.6.8, which was much more demanding in terms of watering regime. Noteworthy, the phenotype of this plant could not be recovered and once some of the leaves wilted, they dried out completely and fell off.

Some of the plants edited at the exon 6 and some unedited plants were further characterised by measuring their F_v/F_m ratios (Figure 5.12). The F_v/F_m ratio represents the intrinsic (maximum) efficiency of Photosystem II, PSII (Genty *et al.*, 1989). This maximum efficiency is equivalent to the quantum efficiency of PSII when all reaction centres are open (Maxwell & Johnson, 2000). In dark-adapted plants, the F_v/F_m ratio is used to indicate plant photosynthetic performance. The optimal F_v/F_m ratio is around 0.84, so any deviation from this value could provide information about processes that have affected the efficiency of non-photochemical quenching (Maxwell & Johnson, 2000). Certain stresses that the plant is exposed to could lower its F_v/F_m ratio as well. The F_v/F_m values of the *Azygous* (Az) and *hp3* lines, described in the previous chapters, were used here for comparison and displayed in Figure 5.12. As it was not possible to carry out any statistical analyses on the T_0 transformants, the averaged values of three measurements from each plant were displayed in the figure and compared with each other. The F_v/F_m ratio of the *hp3* line was significantly lower than that of the Az line. The averaged F_v/F_m ratios of all T_0 plants, except plants ID 12.6.18 and 12.6.8, were closer to the Az line than to the *hp3* line. All unedited T_0 plants (0% editing frequency) were very close to the AC control in terms of their F_v/F_m values. Also, the F_v/F_m ratios of the primary transformants edited at anywhere between 10% and 63% (ID 12.6.2, 12.6.32, 9.6.1, 12.6.3 and 9.6.2) were more similar to the AC control.

It was found that only the plants edited at a 70% (ID 12.6.18) and a 100% (ID 12.6.8) frequency, were more similar to the *hp3* line in terms of their F_v/F_m ratios but were not as low. Interestingly, plant ID 12.6.18 was found to have a highly variable F_v/F_m ratio depending on which part of the plant the measurement was taken from. This further supports the observation that CRISPR/Cas9 editing can lead to the generation of chimeric plants with different parts of the plant carrying different types and frequencies of the edits.

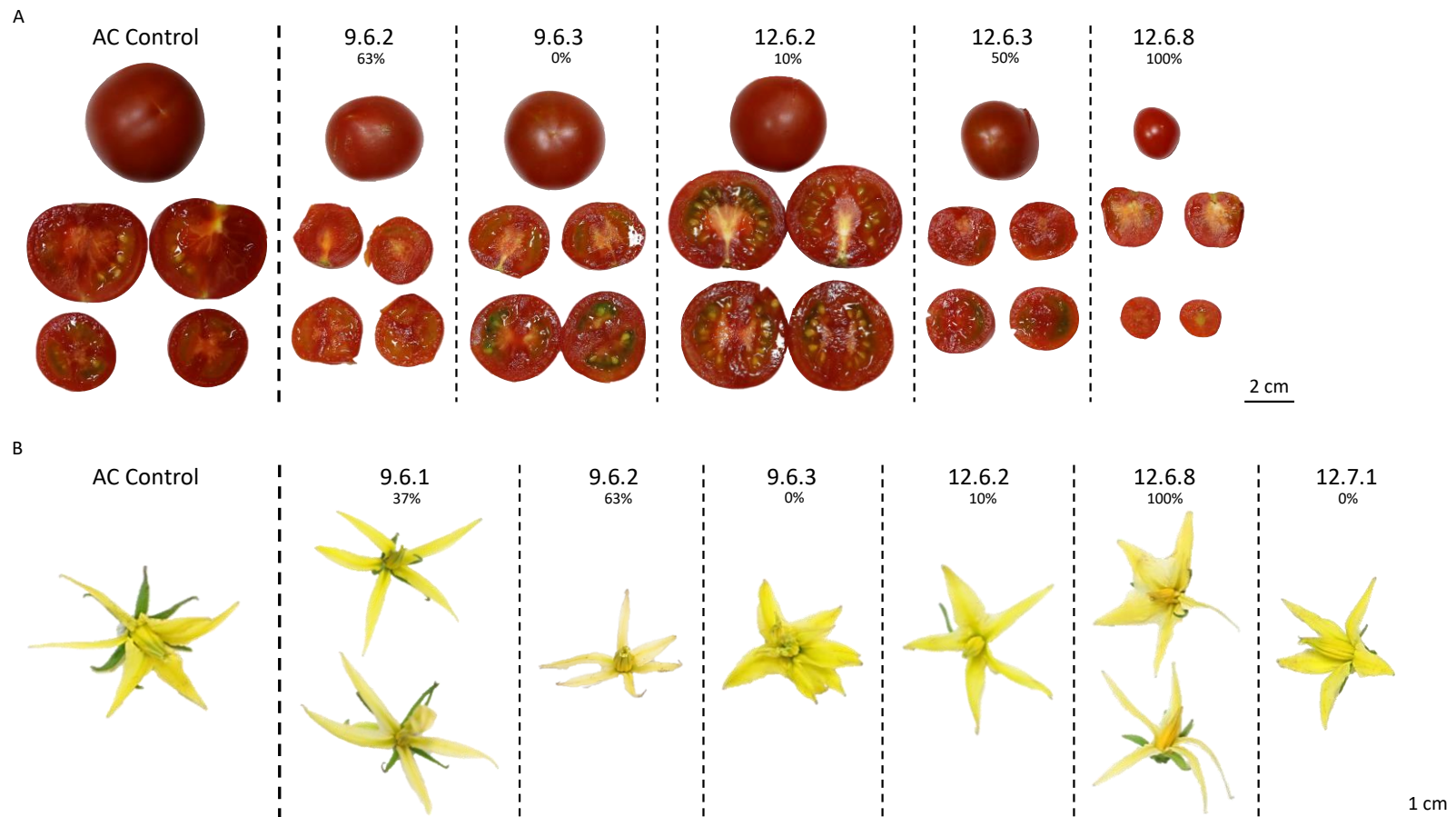


Figure 5.11. Comparison of fruit (A) and flower (B) phenotypes of CRISPR/Cas9 edited plants targeted at the exon 1 (ID 12.7.1) and the exon 6 (all except ID 12.7.1). (A) Compared to the AC control and the plants with low frequencies of edits (ID 9.6.3 and 12.6.2), the plants with high frequencies of edits (ID 9.6.2, 12.6.3 and 12.6.8) have visibly smaller fruit. The fruit of the plant harbouring the biallelic edit (ID 12.6.8) are the smallest and appear to be lighter than other fruit. The next most edited plant (ID 9.6.2) also has lighter fruit compared to the control and other transformants. (B) The flowers of the unedited plants (ID 9.6.3 and 12.7.1) and the plant with lowest editing frequency (ID 12.6.2) appear bright yellow and similar to the AC control. The petals of the plants with high frequencies of edits (ID 9.6.2 and 12.6.8) are paler than the control and have orange stamens, similarly to the *hp3* line. Interestingly, two distinct types of flowers were collected from ID 9.6.1; some of the flowers shared the unedited phenotype while the others, appeared paler and more similar to the edited lines, indicating that this plant is chimeric. The percentage number underneath the plant ID indicates the editing frequency.

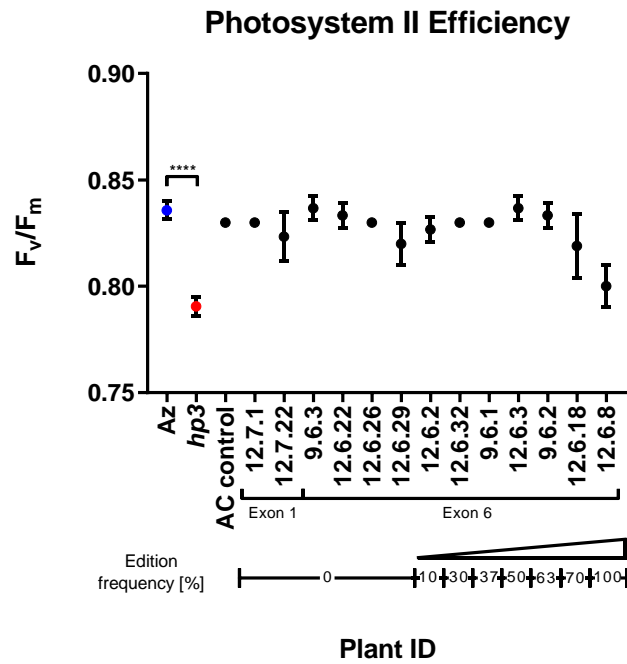
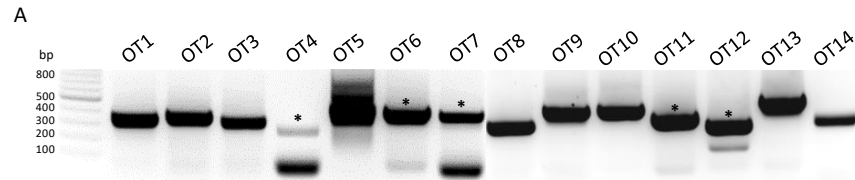


Figure 5.12. Photosystem II efficiency of the screened AC transformants (black, N = 1) against control lines: Az (blue; N = 7) and *hp3* (red; N = 6). Two-tailed T-test was carried out to assess the difference between the control lines; data normality and equality of variances were tested with Shapiro – Wilk and the F-test, respectively. A direct comparison between the transformants and the controls was not possible due to insufficient sample size; however a reduction in the F_v/F_m ratio can be seen in the plant harbouring a truncated version of the protein due to the biallelic mutation in *ZEP* (Plant ID 12.6.8). Mutation frequencies are indicated for the plants edited at the target gene. Measurements were performed in triplicates except ID 12.6.18 (repeated on three different occasions due to high inconsistency between the readings). Data are displayed as $\bar{x} \pm SD$; * $P < 0.05$, ** $P < 0.01$, *** $P < 0.001$, **** $P < 0.0001$.

Because of its phenotype, which closely mimicked that of the *hp3* line, T_0 plant ID 12.6.8 was analysed in more detail. The top off-target (OT) score of sgRNA_zepe6 (0.477) was similar to its on-target score (0.480). Therefore, the main off-targets of this guide were screened in ID 12.6.8 to confirm that the phenotype could indeed be attributed to the biallelic edit at the exon 6 of *ZEP* and not to some other region. The OTs identified for sgRNA_zepe6 are listed in Table 2.13. The top 12 OTs (off-scores 0.477 – 0.090) and also two lower-ranked targets, which were found within gene introns, were selected for this analysis. The OTs were first amplified from the DNA of ID 12.6.8 (Figure 5.13A). All OTs fragments could be isolated successfully, except for the OT5, which was difficult to purify from the gel due to the presence of multiple bands. However, even though it was not possible to obtain its sequence, the OT5 had the off-score of 0.197 and was positioned in an intergenic region, thus it was considered to be of a low importance and most likely did not influence the phenotype of this plant. The sequencing of the isolated OTs revealed that none of the off-targets were modified. Therefore, it could be concluded that sgRNA_zepe6 specifically targeted the exon 6 of *ZEP*. Interestingly, some SNPs were identified in the intergenic region where the OT9 was located (Figure 5.13B).



B

OT1_Template GTTCACCCCTAAAATGGCAGTGAACCTGCATACAAGGAGGAAGTCCAACCTACGGTTGGCAGTCGACAGACCGCTTATCCAAAATAGACTGTCCCGTCTACCTTTAGTTGGATAAGATATTGACAATGGTTCTCCTCCCTCCTAGTCTAAGTCCCTACCGACGACACACATCGATGGGGCGTCGATAGGCCACAGGCATTGATGCTCCAT
 OT1_R GTTCACCCCTAAAATGGCAGTGAACCTGCATACAAGGAGGAAGTCCAACCTACGGTTGGCAGTCGACAGACCGCTTATCCAAAATAGACTGTCCCGTCTACCTTTAGTTGGATAAGATATTGACAATGGTTCTCCTCCCTCCTAGTCTAAGTCCCTACCGACGACACACATCGATGGGGCGTCGATAGGCCACAGGCATTGATGCTCCAT
 OT1_F -----CTAAAATGGCAGTGAACCTGCATACAAGGAGGAAGTCCAACCTACGGTTGGCAGTCGACAGACCGCTTATCCAAAATAGACTGTCCCGTCTACCTTTAGTTGGATAAGATATTGACAATGGTTCTCCTCCCTCCTAGTCTAAGTCCCTACCGACGACACACATCGATGGGGCGTCGATAGGCCACAGGCATTGATGCTCCAT
 * * * * *

OT2_Template CGATCAGGCGCCGAGAGTATGATATTAGTATCACAGATATGCACTTAAAATGATCCCTTGCTGTGTCAACAACAGTTCAGTGTGTATGAATGCAAAAATCTACCTGAAGTGTCAATCCATAAGCTGAATCTATCTTTAGTTTGGGAGAGCAATTATACTTCCATGACTTACAGAAGGAGTAGCAGATGTCAAATTAGCGCTGGG
 OT2_R CGATCAGGCGCCGAGAGTATGATATTAGTATCACAGATATGCACTTAAAATGATCCCTTGCTGTGTCAACAACAGTTCAGTGTGTATGAATGCAAAAATCTACCTGAAGTGTCAATCCATAAGCTGAATCTATCTTTAGTTTGGGAGAGCAATTATACTTCCATGACTTACAGAAGGAGTAGCAGATGTCAAATTAGCGCTGGG
 OT2_F -----TGATATTAGTATCACAGATATGCACTTAAAATGATCCCTTGCTGTGTCAACAACAGTTCAGTGTGTATGAATGCAAAAATCTACCTGAAGTGTCAATCCATAAGCTGAATCTATCTTTAGTTTGGGAGAGCAATTATACTTCCATGACTTACAGAAGGAGTAGCAGATGTCAAATTAGCGCTGGG
 * * * * *

OT3_Template tgtttgatgtaattacttctgtcttactATCATATTGCTTGTGGTGTGTGCTTCTCTTGGTTCAAATCGAAAAGGAAAAGTATAGACTTGGGTACTCTTCAGCTGTATCCCTGTCAGACATCTTTGTTAGTGCCTTGTCTTCCCAACAAAAGGTAGGAAAATCAACGACCTTTTTGATTTGTCAAACGTGTTGTCATCTTTTATTTA
 OT3_R TGTTTGATGTAATTACTTGTCTTACTATCATATTGCTTGTGGTGTGTGCTTCTCTTGGTTCAAATCGAAAAGGAAAAGTATAGACTTGGGTACTCTTCAGCTGTATCCCTGTCAGACATCTTTGTTAGTGCCTTGTCTTCCCAACAAAAGGTAGGAAAATCAACGACCTTTTTGATTTGTCAAACGTGTTGTCATCTTTTATTTA
 OT3_F -----GTTTGTCTTCTCTTCAAATCGAAAAGGAAAAGTATAGACTTGGGTACTCTTCAGCTGTATCCCTGTCAGACATCTTTGTTAGTGCCTTGTCTTCCCAACAAAAGGTAGGAAAATCAACGACCTTTTTGATTTGTCAAACGTGTTGTCATCTTTTATTTA
 * * * * *

OT4_Template TCCTTCTTCTGTGGGAAAGTATGTCGTTCTCCCTTTGGTGAATGAAATCGTAGGCTTTCCATGCACATATGAAATGATTTCACTGGATTTTTGCAAAATTTTAACTCTTCAATTTATGGTAAATCGAGTAGAGCATAGGATGTTTGTGATTAGGATTAGGATTAACGTTTCTCTCCCAACAAAAGGTGGGAGGAGGAATGCA
 OT4_R TCCTTCTTCTGTGGGAAAGTATGTCGTTCTCCCTTTGGTGAATGAAATCGTAGGCTTTCCATGCACATATGAAATGATTTCACTGGATTTTTGCAAAATTTTAACTCTTCAATTTATGGTAAATCGAGTAGAGCATAGGATGTTTGTGATTAGGATTAGGATTAACGTTTCTCTCCCAACAAAAGGTGGGAGGAGGAATGCA
 OT4_F -----AGGCTTTCCATGCACATATGAAATGATTTCACTGGATTTTTGCAAAATTTTAACTCTTCAATTTATGGTAAATCGAGTAGAGCATAGGATGTTTGTGATTAGGATTAGGATTAACGTTTCTCTCCCAACAAAAGGTGGGAGGAGGAATGCA
 * * * * *

OT6_Template TTTAGATATCATCGAACGATTAGGATCACATTTGGATGTAGCAAAAGATCAAATGTTGAAAAGAATTTCAAGTCTTCTCTGCTGGGGTGTGGCCCTTGGTCGCGCGGATGGTCAATATCTTACCATCGCAATTTGGGGTCCACATAATGTCCATGTGCTTCCACTTTTGTAGTTCAGGAAAAGGATCAGTCTTAAGTTCCATACAAGC
 OT6_R -----TCGAACGATTAGGATCACATTTGGATGTAGCAAAAGATCAAATGTTGAAAAGAATTTCAAGTCTTCTCTGCTGGGGTGTGGCCCTTGGTCGCGCGGATGGTCAATATCTTACCATCGCAATTTGGGGTCCACATAATGTCCATGTGCTTCCACTTTTGTAGTTCAGGAAAAGGATCAGTCTTAAGTTCCATACAAGC
 OT6_F --TAGATGATCATCGAACGATTAGGATCACATTTGGATGTAGCAAAAGATCAAATGTTGAAAAGAATTTCAAGTCTTCTCTGCTGGGGTGTGGCCCTTGGTCGCGCGGATGGTCAATATCTTACCATCGCAATTTGGGGTCCACATAATGTCCATGTGCTTCCACTTTTGTAGTTCAGGAAAAGGATCAGTCTTAAGTTCCATACAAGC
 * * * * *

OT7_Template TTACCATATACTGTATATCTATAATAGTACTTTGGTGTGTAAAAGGATAGTATGAGATATTACATTAATAATAGTTTTCTTCTGATTAATTTGTTGGATTTCTTAAATGAAAATATATATTTGTTAGATCTGGCTCCACTTTTGTAGTGGGAAGAGTTGTTGAATCTTGATGGGATACACCTTCATTCTCGAAATATACTTAAGGA
 OT7_R TTACCATATACTGTATATCTATAATAGTACTTTGGTGTGTAAAAGGATAGTATGAGATATTACATTAATAATAGTTTTCTTCTGATTAATTTGTTGGATTTCTTAAATGAAAATATATATTTGTTAGATCTGGCTCCACTTTTGTAGTGGGAAGAGTTGTTGAATCTTGATGGGATACACCTTCATTCTCGAAATATACTTAAGGA
 OT7_F -----TATAGTACTTTGGTGTGTAAAAGGATAGTATGAGATATTACATTAATAATAGTTTTCTTCTGATTAATTTGTTGGATTTCTTAAATGAAAATATATATTTGTTAGATCTGGCTCCACTTTTGTAGTGGGAAGAGTTGTTGAATCTTGATGGGATACACCTTCATTCTCGAAATATACTTAAGGA
 * * * * *

OT8_Template TAAACTCAAGTCTCATATCTCCA TAAGAGATAAGTCCATCCCTATTTGGTTATTGAACACACCTCCAGTGGGCTGTGCACGTAAGGGTGTAGAGTGTGTTAAAGTCCACATTTGGTGGGGAATAGATAGTGGTCTATTATGTGGACTTGAGCAATCCACCTCTGAAAGTGTAGGTTGAGTTAAACCAAGTATTTATA
 OT8_R TAAACTCAAGTCTCATATCTCCA TAAGAGATAAGTCCATCCCTATTTGGTTATTGAACACACCTCCAGTGGGCTGTGCACGTAAGGGTGTAGAGTGTGTTAAAGTCCACATTTGGTGGGGAATAGATAGTGGTCTATTATGTGGACTTGAGCAATCCACCTCTGAAAGTGTAGGTTGAGTTAAACCAAGTATTTATA
 OT8_F -----CCATCCCTATTTGGTTATTGAACACACCTCCAGTGGGCTGTGCACGTAAGGGTGTAGAGTGTGTTAAAGTCCACATTTGGTGGGGAATAGATAGTGGTCTATTATGTGGACTTGAGCAATCCACCTCTGAAAGTGTAGGTTGAGTTAAACCAAGTATTTATA
 * * * * *

OT9_Template AAAACCCCTCTTTATGCTAGTAGACATTGTACTTTGCACCTCATGAGAATATTTGGTAAACCTACCCCTCTTTTGGGAAGAGACACCATATATTGAACTTACCTTTATTTGGGAAGGGAACCTCTCATTTGTCAAGTTCACCTGAGTGTCAAGTAACTTTCCCTTTTGGAAAAGCCTTAAAGTTTTTATTAACATTACTACATAAGACATGA
 OT9_R AAAACCCCTCTTTATGCTAGTAGACATTGTACTTTGCACCTCATGAGAATATTTGGTAAACCTACCCCTCTTTTGGGAAGAGACACCATATATTGAACTTACCTTTATTTGGGAAGGGAACCTCTCATTTGTCAAGTTCACCTGAGTGTCAAGTAACTTTCCCTTTTGGAAAAGCCTTAAAGTTTTTATTAACATTACTACATAAGACATGA
 OT9_F -----GCATTTGACTTTGCACCTCATGAGAATATTTGGTAAACCTACCCCTCTTTTGGGAAGAGACACCATATATTGAACTTACCTTTATTTGGGAAGGGAACCTCTCATTTGTCAAGTTCACCTGAGTGTCAAGTAACTTTCCCTTTTGGAAAAGCCTTAAAGTTTTTATTAACATTACTACATAAGACATGA
 * * * * *

OT10_Template ttttttGTGTTGGCCAAATCATGTATCACATTTCAAACCTTGCAACCTAATTTTGTGTTGAATAAAACCATATAAACCTCTCcttttttGATTGAATCTCTTTTCATTACAACTACTCTTCATTTCCCAACTAAATGTAGTATACTTTATCCATTATCATGATATCCTTTAACATGGAGCTTAAACGTTTGTGTTTGTGTTT
 OT10_R TTTTGTGTTGGCCAAATCATGTATCACATTTCAAACCTTGCAACCTAATTTTGTGTTGAATAAAACCATATAAACCTCTCcttttttGATTGAATCTCTTTTCATTACAACTACTCTTCATTTCCCAACTAAATGTAGTATACTTTATCCATTATCATGATATCCTTTAACATGGAGCTTAAACGTTTGTGTTTGTGTTT
 OT10_F TTTTGTGTTGGCCAAATCATGTATCACATTTCAAACCTTGCAACCTAATTTTGTGTTGAATAAAACCATATAAACCTCTCcttttttGATTGAATCTCTTTTCATTACAACTACTCTTCATTTCCCAACTAAATGTAGTATACTTTATCCATTATCATGATATCCTTTAACATGGAGCTTAAACGTTTGTGTTTGTGTTT
 * * * * *

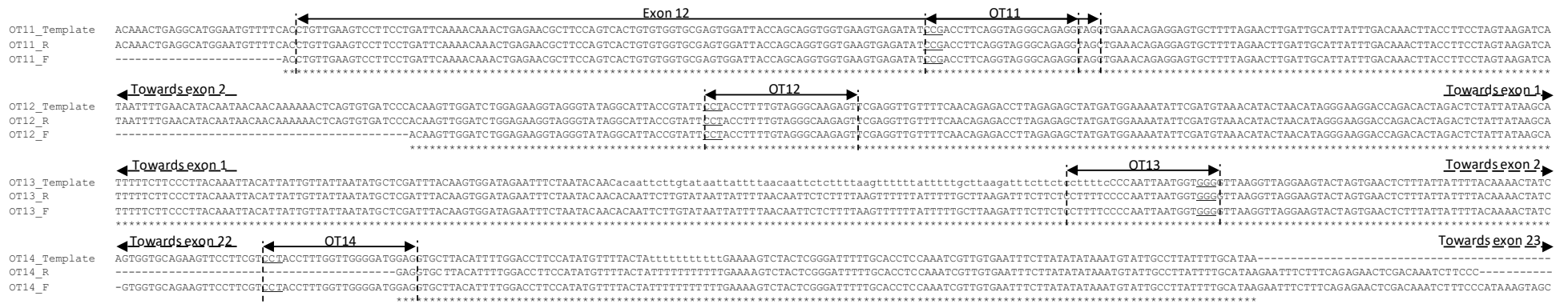


Figure 5.13. (A) Amplification of CRISPR/Cas9 off-target sites from the plant (ID 12.6.8) harbouring a biallelic mutation in the exon 6 of *ZEP*; asterisks (*) indicate fragments of the expected sizes further selected for sequencing. **(B)** MAFFT alignment of sequenced off-target sites against their respective templates. Positions of the off-target sites with underlined PAM sequences and exons are annotated; asterisks (*) indicate the matching sequences. The amplicons were sequenced with the forward (F) and reverse (R) primers.

5.2.5 Pigment analysis of leaf and fruit tissues

The pigment profiles of some of the T₀ transformants, the AC control and the *hp3* line (used here for comparison as it is known to accumulate zeaxanthin), were obtained through HPLC analysis (Figure 5.14). Out of all edited at the exon 6 T₀ plants, only plant ID 12.6.8, carrying a biallelic mutation, accumulated the amounts of zeaxanthin comparable to the *hp3* fruit (Figure 5.14A). In fact, plant ID 12.6.8 accumulated 1.2 times more zeaxanthin in its fruit than the *hp3* tomato line (169.4 ± 2.5 against $145.5 \pm 22.4 \mu\text{g g}^{-1}$ DW). Additionally, both mutants of *ZEP* and the AC control had similar total carotenoids levels (Figure 5.14B). Interestingly, all T₀ transformants accumulated higher levels of zeaxanthin in its fruit than the AC control, although these were still very low in comparison to the *hp3* line or plant ID 12.6.8.

Trace amounts of antheraxanthin ($0.6 \pm 0.3 \mu\text{g g}^{-1}$ DW) were detected in fruit of the *hp3* line. Luteoxanthin was not identified in plant ID 12.6.8 nor the *hp3* line but some small amounts of this xanthophyll were found in the plants which retained some WT activity of *ZEP*. The highest levels of luteoxanthin ($20.9 \pm 2.9 \mu\text{g g}^{-1}$ DW) were detected in the AC control plant. The highest lutein levels were found in the *hp3* line and plant ID 12.6.8 (86.7 ± 15.0 and $84.6 \pm 0.9 \mu\text{g g}^{-1}$ DW, respectively). The other plants were found to accumulate between $35.6 \pm 1.7 \mu\text{g g}^{-1}$ DW (ID 9.6.2) and $51.2 \pm 4.0 \mu\text{g g}^{-1}$ DW (AC control) of lutein.

The *hp3* line and plant ID 12.6.8 accumulated the highest levels of α -tocopherol (255.2 ± 44.4 and $235.7 \pm 23.6 \mu\text{g g}^{-1}$ DW, respectively) followed by plant ID 12.6.2 ($195.7 \pm 1.3 \mu\text{g g}^{-1}$ DW). The other plants contained from 134.7 ± 22.3 (ID 9.6.2) to 148.9 ± 5.4 (AC control) $\mu\text{g g}^{-1}$ DW of this compound. The highest levels of phytoene were found in the *hp3* line but there was a large variance between the individual plants ($220.3 \pm 100.5 \mu\text{g g}^{-1}$ DW). The AC control, plants ID 12.6.8 and ID 12.6.3 had comparable phytoene levels (from 138.3 ± 3.4 to $105.5 \pm 6.2 \mu\text{g g}^{-1}$ DW). The lowest levels of phytoene (from 70.2 ± 5.2 to $79.6 \pm 1.9 \mu\text{g g}^{-1}$ DW) were found in plants ID 9.6.2, 9.6.3 and 12.6.2. The levels of α -carotene were similar in the analysed plants and laid between 29.3 ± 1.4 (ID 9.6.2) and $45.0 \pm 5.8 \mu\text{g g}^{-1}$ DW (ID 12.6.2). The highest content of β -carotene was found in ID 12.6.2 ($253.4 \pm 13.0 \mu\text{g g}^{-1}$ DW), followed by the AC control ($200.4 \pm 8.2 \mu\text{g g}^{-1}$ DW). The other plants contained between 136.0 ± 17.2 (ID 9.6.2) and $187.7 \pm 2.8 \mu\text{g g}^{-1}$ DW (ID 12.6.8) of this compound. Plant ID 9.6.3 stored the highest levels of lycopene ($1\ 739.6 \pm 69.9 \mu\text{g g}^{-1}$ DW), followed by ID 12.6.2 ($1\ 638.0 \pm 49.6 \mu\text{g g}^{-1}$ DW). The AC control, plants ID 12.6.8 and ID 12.6.3 contained similar lycopene levels ($1\ 367.0 \pm 215.2$, $1\ 328.2 \pm 37.1$ and $1\ 253.9 \pm 24.8 \mu\text{g g}^{-1}$ DW, respectively). Plant ID 9.6.2 stored the lowest amounts of lycopene ($870.5 \pm 54.9 \mu\text{g g}^{-1}$ DW). Plants ID 9.6.3 and ID 12.6.2 had the highest total carotenoid contents, which were related to their high lycopene levels, whereas plant ID 9.6.2 had the lowest total carotenoid content, which was reflected by its lowest lycopene levels (Figure 5.14B).

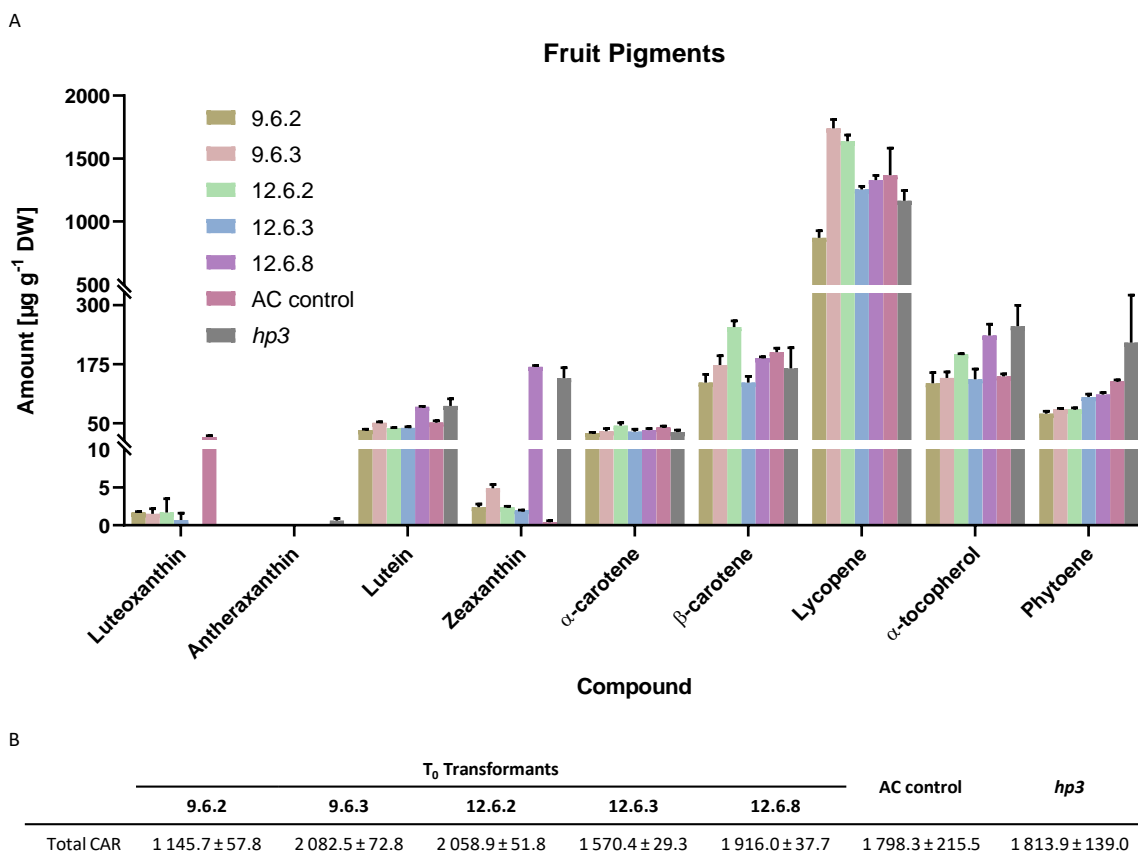


Figure 5.14. (A) Comparison of fruit pigments and α -tocopherol of the selected T₀ plants against the *hp3* line. The levels of zeaxanthin detected in the plant harbouring a biallelic mutation, T₀ plant ID 12.6.8, were 420-fold higher than in the AC control plant, 14.5-fold higher than the averaged amounts of zeaxanthin accumulated in the remaining T₀ transformants (ID 9.6.2, 9.6.3, 12.6.2 and 12.6.3) and 1.2-fold higher than in the *hp3* line. At the time of analysis, ripe fruit were only available from the listed T₀ plants. Traces of antheraxanthin were found in the *hp3* line. Neither violaxanthin nor neoxanthin were detected in any of the analysed fruit. Data are displayed as $\bar{x} \pm \text{SD}$. The means were calculated from three technical repeats for each of the T₀ transformants and three biological replicates for the *hp3* line. (B) Total fruit carotenoid levels (CAR, α -tocopherol not included) of the tomato plants from (A).

The fruit carotenoid profiles of plant ID 12.6.8 and the *hp3* line were similar. The leaf carotenoid profiles of these two plants and the AC control were also compared and quantified (Figure 5.15). To make this comparison easier, the extracts were saponified prior to the extraction to remove chlorophyll. The major pigments found in the leaf extract of the AC control were violaxanthin, neoxanthin, lutein, zeaxanthin, α -carotene and β -carotene (Figure 5.15A). The same compounds were identified in the *hp3* line but the violaxanthin and neoxanthin peaks were much smaller than in the AC control, whereas the zeaxanthin peak was much taller. Moreover, antheraxanthin was identified in the *hp3* line but not in the AC control. Interestingly, violaxanthin, neoxanthin and antheraxanthin were not found in plant ID 12.6.8; however, similarly to the *hp3* line, a very tall zeaxanthin peak was recorded in this plant. The identified pigments were then quantified (Figure 5.15B). High levels of zeaxanthin were only detected in the *hp3* line and plant ID 12.6.8 (822.2 ± 106.7 and $858.8 \pm 10.7 \mu\text{g g}^{-1}$ DW, respectively) and much smaller levels of zeaxanthin were found in the AC control ($58.3 \pm 4.0 \mu\text{g g}^{-1}$ DW). Additionally, the *hp3* line also accumulated antheraxanthin at $247.8 \pm 40.3 \mu\text{g g}^{-1}$ DW. The AC control plant contained the highest levels of

lutein ($1\,914.0 \pm 49.3 \mu\text{g g}^{-1}$ DW), whereas the *hp3* line and plant ID 12.6.8 accumulated lutein at similar levels ($1\,443.9 \pm 232.9$ and $1\,369.9 \pm 33.1 \mu\text{g g}^{-1}$ DW, respectively). Only the AC control accumulated substantial amounts of violaxanthin ($1\,508.6 \pm 54.9 \mu\text{g g}^{-1}$ DW) and neoxanthin ($1\,464.2 \pm 26.6 \mu\text{g g}^{-1}$ DW). All three plants contained very similar levels of α -carotene, but the AC control contained higher amounts of β -carotene ($565.7 \pm 12.1 \mu\text{g g}^{-1}$ DW) than the *hp3* line or the plant ID 12.6.8 (493.8 ± 156.7 and $415.3 \pm 11.1 \mu\text{g g}^{-1}$ DW, respectively).

Saponification of a sample prior to extraction affects the levels of some carotenoids; therefore, non-saponified leaf extracts of some of the T_0 transformants, AC control plant and *hp3* line were analysed on the HPLC system as well. This also allowed for the quantification of chlorophyll in these plants. Table 5.5 lists the amounts of the identified compounds. The frequency of edits did not influence the total carotenoid content of the analysed plants. For example, the 100% edited plant ID 12.6.8 had comparable total leaf carotenoid levels to plant ID 9.6.3, which had not been edited. Similarly, plant ID 12.6.18, edited at a 70% frequency, and the unedited plant ID 12.7.1 also had very similar total leaf carotenoid levels. Plant ID 12.6.8 and the *hp3* line stored similar amounts of carotenoid in their leaves. The T_0 transformants with a 70% editing frequency or more (ID 12.6.8 and 12.6.18) and the *hp3* line had higher zeaxanthin levels compared to the other plants. Out of these three, the exon 6 edited plant ID 12.6.8 accumulated the highest amounts of zeaxanthin ($912.2 \pm 34.2 \mu\text{g g}^{-1}$ DW). Except plant ID 12.7.1, the levels of zeaxanthin positively correlated with an increasing frequency of the *ZEP* edits. Violaxanthin and neoxanthin were not detected in plant ID 12.6.8. The *hp3* line accumulated only small amounts of these two xanthophylls compared to the other T_0 plants. Luteoxanthin was detected in all plants except for ID 12.6.8 and the *hp3* line and in these plants, the levels of this xanthophyll were very similar to violaxanthin. Antheraxanthin was identified in all plants except for ID 12.6.8 and ID 12.8.18. The highest antheraxanthin levels were found in the *hp3* line ($167.3 \pm 22.3 \mu\text{g g}^{-1}$ DW). The levels of lutein, α -carotene and β -carotene in plant ID 12.6.8 and the *hp3* line were similar. Phytoene was detected at low levels in all plants except for ID 12.6.8 and the *hp3* line. Although, the chlorophyll content was different between the analysed plants, the ratio of chlorophyll A to chlorophyll B was close to 2:1 in all of them except for ID 9.6.1, where this ratio was slightly lower (1.4:1).

Interestingly, even though the levels of total carotenoids and total chlorophyll were different between the individual plants, the ratios of total chlorophyll to total carotenoids were between 1.3:1 and 2:1 except for plant ID 12.6.8 and the *hp3* line where these ratios were 3.6:1 and 3.9:1, respectively. Finally, the ratios of total chlorophyll to zeaxanthin were calculated as well. The *hp3* line and plant ID 12.6.8 had the lowest ratios of total chlorophyll to zeaxanthin (21.4:1 and 12.8:1, respectively). The second lowest ratio was found in plant ID 12.6.18 (36.1:1) with the rest of the plants having their ratios above 40:1.

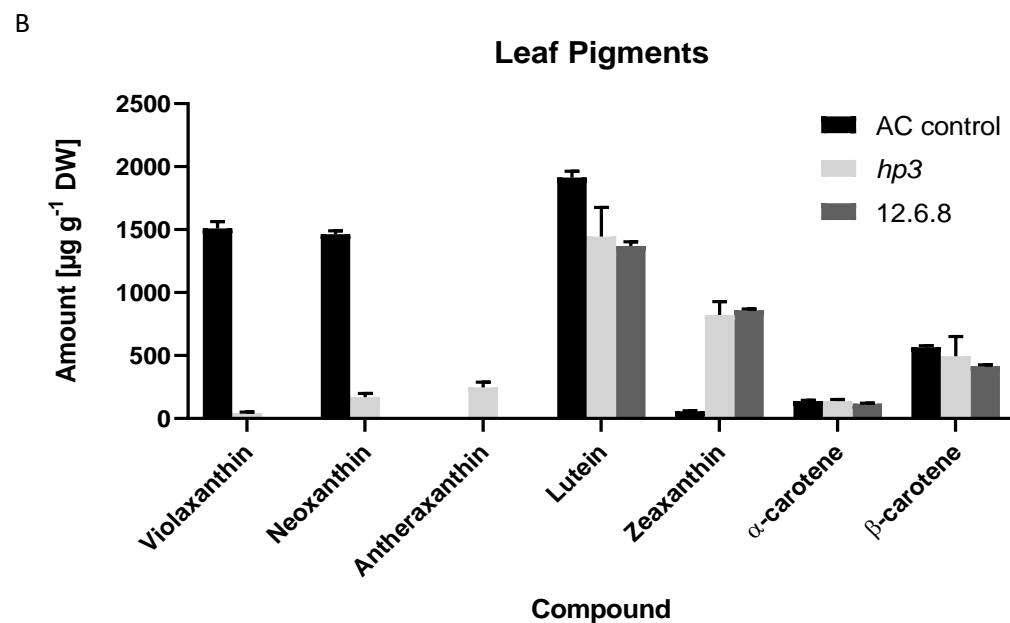
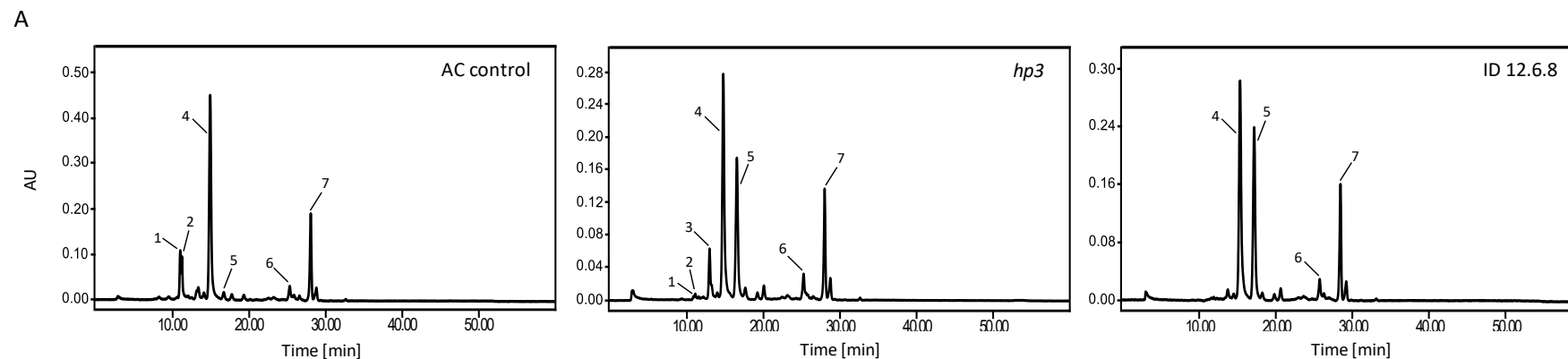


Figure 5.15. (A) HPLC chromatograms of saponified leaf extract of the AC control, the *hp3* tomato line and the T_0 plant ID 12.6.8 harbouring a biallelic mutation of *ZEP*. The spectra were extracted at 450 nm. The peaks of the compounds of interest are labelled. 1 – violaxanthin, 2 – neoxanthin, 3 – antheraxanthin, 4 – lutein, 5 – zeaxanthin, 6 – α -carotene, 7 – β -carotene. (B) Quantification of the major pigments from saponified leaf extracts of the three plants analysed above. Only the AC control accumulated high levels of violaxanthin and neoxanthin in its leaves. Antheraxanthin was only found in leaves of the *hp3* line. The *hp3* line and T_0 plant ID 12.6.8 accumulated 14 and 15 times more zeaxanthin than the AC control, respectively. Data are displayed as $\bar{x} \pm \text{SD}$. The means were calculated from three technical repeats for the T_0 transformants and six biological replicates for the *hp3* line.

Table 5.5. Quantification of isoprenoids and chlorophylls from the non-saponified leaf extracts of the indicated T₀ transformants, the AC control and the *hp3* line. The reported values were used to obtain total carotenoids (CAR) and total chlorophylls (CHL). The ratios of chlorophyll A to chlorophyll B (Chl A : Chl B), total chlorophylls to total carotenoids (CHL : CAR) and total chlorophylls to zeaxanthin (CHL : Zeaxanthin) were calculated as well. The amounts of the compounds are reported as $\mu\text{g g}^{-1}$ DW. The data are presented as the mean of three technical repeats \pm SD for T₀ plants and AC control and six biological replicates for the *hp3* line; nd – not detected.

Compound	T ₀ Transformants								AC control	<i>hp3</i>
	9.6.1	9.6.2	9.6.3	12.6.2	12.6.3	12.6.8	12.6.18	12.7.1		
Violaxanthin	399.1 \pm 44.9	305.1 \pm 24.8	400.3 \pm 33.8	502.0 \pm 18.6	454.4 \pm 20.5	nd	528.0 \pm 20.7	603.8 \pm 130.4	1 279.5 \pm 36.6	35.6 \pm 7.9
Neoxanthin	1 719.9 \pm 35.1	932.3 \pm 48.1	931.3 \pm 41.2	1 143.7 \pm 23.0	1 274.9 \pm 49.5	nd	1 041.9 \pm 33.8	1 342.6 \pm 70.0	2 175.5 \pm 25.4	255.8 \pm 37.4
Luteoxanthin	397.8 \pm 87.8	262.2 \pm 20.7	342.5 \pm 42.5	498.0 \pm 33.1	493.5 \pm 14.4	nd	433.0 \pm 46.7	416.6 \pm 68.2	769.9 \pm 14.5	nd
Antheraxanthin	36.9 \pm 5.5	29.4 \pm 2.4	23.1 \pm 4.3	37.3 \pm 3.5	39.0 \pm 2.3	nd	nd	36.4 \pm 11.7	84.8 \pm 1.5	167.3 \pm 22.3
Lutein	2 595.6 \pm 78.3	1 122.0 \pm 78.5	1 094.2 \pm 39.8	1 349.4 \pm 29.0	1 485.1 \pm 80.1	1 681.0 \pm 41.5	1 754.2 \pm 9.8	1 705.4 \pm 33.6	2 578.8 \pm 47.0	1 751.5 \pm 255.6
Zeaxanthin	96.4 \pm 2.0	109.1 \pm 6.5	57.3 \pm 5.6	48.1 \pm 5.4	105.7 \pm 10.1	912.2 \pm 34.2	236.8 \pm 5.8	105.1 \pm 26.8	67.7 \pm 6.9	632.9 \pm 56.5
Phytoene	7.4 \pm 0.3	4.7 \pm 0.6	5.2 \pm 1.3	3.8 \pm 1.1	3.9 \pm 0.4	nd	2.9 \pm 0.5	3.9 \pm 0.7	3.0 \pm 0.2	nd
α -carotene	125.5 \pm 2.3	83.3 \pm 2.2	78.9 \pm 2.4	89.0 \pm 1.1	102.3 \pm 3.4	93.8 \pm 1.7	96.7 \pm 3.9	92.4 \pm 2.5	123.3 \pm 2.8	111.7 \pm 12.6
β -carotene	467.3 \pm 19.9	228.2 \pm 16.9	236.0 \pm 10.2	271.7 \pm 4.7	231.9 \pm 42.6	515.5 \pm 29.9	477.3 \pm 21.9	356.9 \pm 15.4	639.0 \pm 14.0	548.3 \pm 119.9
Total CAR	5 845.8 \pm 132.4	3 076.2 \pm 99.3	3 168.9 \pm 79.9	3 943.0 \pm 53.6	4 190.7 \pm 106.9	3 202.5 \pm 61.6	4 597.6 \pm 66.2	4 663.1 \pm 169.7	7 721.5 \pm 68.2	3 503.0 \pm 291.6
Chlorophyll A	4 289.9 \pm 436.9	3 604.1 \pm 312.8	3 680.2 \pm 178.8	4 602.7 \pm 100.0	5 217.8 \pm 123.7	8 398.2 \pm 170.6	5 516.2 \pm 448.1	6 627.1 \pm 476.2	9 138.8 \pm 307.0	9 726.9 \pm 860.1
Chlorophyll B	2 994.6 \pm 103.2	1 757.5 \pm 81.7	1 716.4 \pm 71.8	2 136.9 \pm 36.8	2 431.2 \pm 46.9	3 266.7 \pm 63.9	3 168.6 \pm 44.6	2 602.3 \pm 122.9	4 254.1 \pm 44.2	3 800.5 \pm 452.5
Total CHL	7 284.6 \pm 448.9	5 361.5 \pm 323.3	5 396.7 \pm 192.6	6 739.6 \pm 106.5	7 649.0 \pm 132.2	11 664.9 \pm 182.2	8 684.9 \pm 450.3	9 229.5 \pm 491.8	13 393.0 \pm 310.2	13 527.4 \pm 971.8
Chl A : Chl B	1.4 \pm 0.2	2.1 \pm 0.2	2.1 \pm 0.1	2.2 \pm 0.1	2.1 \pm 0.1	2.6 \pm 0.1	1.7 \pm 0.1	2.5 \pm 0.2	2.1 \pm 0.1	2.6 \pm 0.4
CHL : CAR	1.3 \pm 0.1	1.7 \pm 0.1	1.7 \pm 0.1	1.7 \pm 0.0	1.8 \pm 0.1	3.6 \pm 0.1	1.8 \pm 0.1	2.0 \pm 0.1	1.7 \pm 0.0	3.9 \pm 0.4
CHL : Zeaxanthin	75.6 \pm 5.0	49.1 \pm 4.2	94.2 \pm 9.8	140.2 \pm 15.9	72.4 \pm 7.0	12.8 \pm 0.5	36.7 \pm 2.1	87.8 \pm 22.9	197.8 \pm 20.7	21.4 \pm 2.5

5.2.6 *In silico* modelling of novel alleles of *ZEP*

To better understand how the premature truncation of *ZEP* at the exon 6 in plant T₀ ID 12.6.8 could lead to its severe wilted phenotype, *in silico* modelling of the protein structure (Figure 5.16) and ligand binding predictions (Figures 5.18B and C) of the novel alleles discovered in this plant were carried out. The modelling could help to understand why this plant accumulated high levels of zeaxanthin similarly to the *hp3* line, but lacked antheraxanthin in its tissues. Although it was not possible to analyse the plant T₀ ID 12.7.24 edited at the exon 1, 3D modelling (Figure 5.17) and ligand binding predictions (Figures 5.18D and E) of its novel alleles of *ZEP* were carried out. This could help to explain why this plant was so vulnerable to water loss. Finally, the *hp3* allele of *ZEP* was modelled as well (Figure 5.19) and compared to the other structures.

The truncated at the exon 6 alleles of *ZEP* retained a defined 3D shape (Figures 5.16B and C). The arrangement of α -helices and β -pleated sheets in the models closely resembled the shape of the N-terminus of the WT allele of *ZEP*. In the truncated alleles of *ZEP*, the transmembrane domain was preserved (Figures 5.16B and C). Interestingly, the ligand binding domains of the WT and the truncated alleles of *ZEP* appeared to be in proximity to the transmembrane domain (Figures 5.18B and C). In fact, some parts of this domain were predicted to interact directly with the ligand itself. Although the two new and truncated at the exon 1 alleles of *ZEP* retained the amino acids that in the WT formed the transmembrane domain, the domain itself was no longer present as a structural feature (Figures 5.17B and C). Interestingly, ligands were still expected to interact with that part of the α -helix, which in the WT allele formed the transmembrane domain. The *hp3* allele of *ZEP* carries a missense mutation in its N-terminus. The *in silico* modelling of this allele predicted the presence of a transmembrane domain at the N-terminus. Moreover, in this model, the α -helices and β -pleated sheets were preserved (Figure 5.19A). However, the 3D structure at the C-terminus was distorted with a long chain of amino acids extending away from the N-terminus (Figure 5.19A). The ligand binding site was predicted to be in the same place as in the WT allele of *ZEP* in close proximity to the transmembrane domain and, as before, some parts of the domain itself were predicted to interact with the ligand (Figure 5.19B).

It is understood that a loss of a large part of the protein can elicit the nonsense-mediated decay (NMD) pathway in tomato plants, which is responsible for degrading transcripts with premature termination codons, and thus it prevents the accumulation of potentially harmful, C-terminally truncated proteins (Christie *et al.*, 2011). Hence, the introduced edits would most certainly produce null alleles. Nonetheless, before it could be confirmed that indeed NMD had occurred in the edited plants, the described above modelling was carried out to illustrate where within the protein the mutations have occurred and what their potential effects could be, if the genes encoding these truncated proteins were to be expressed.

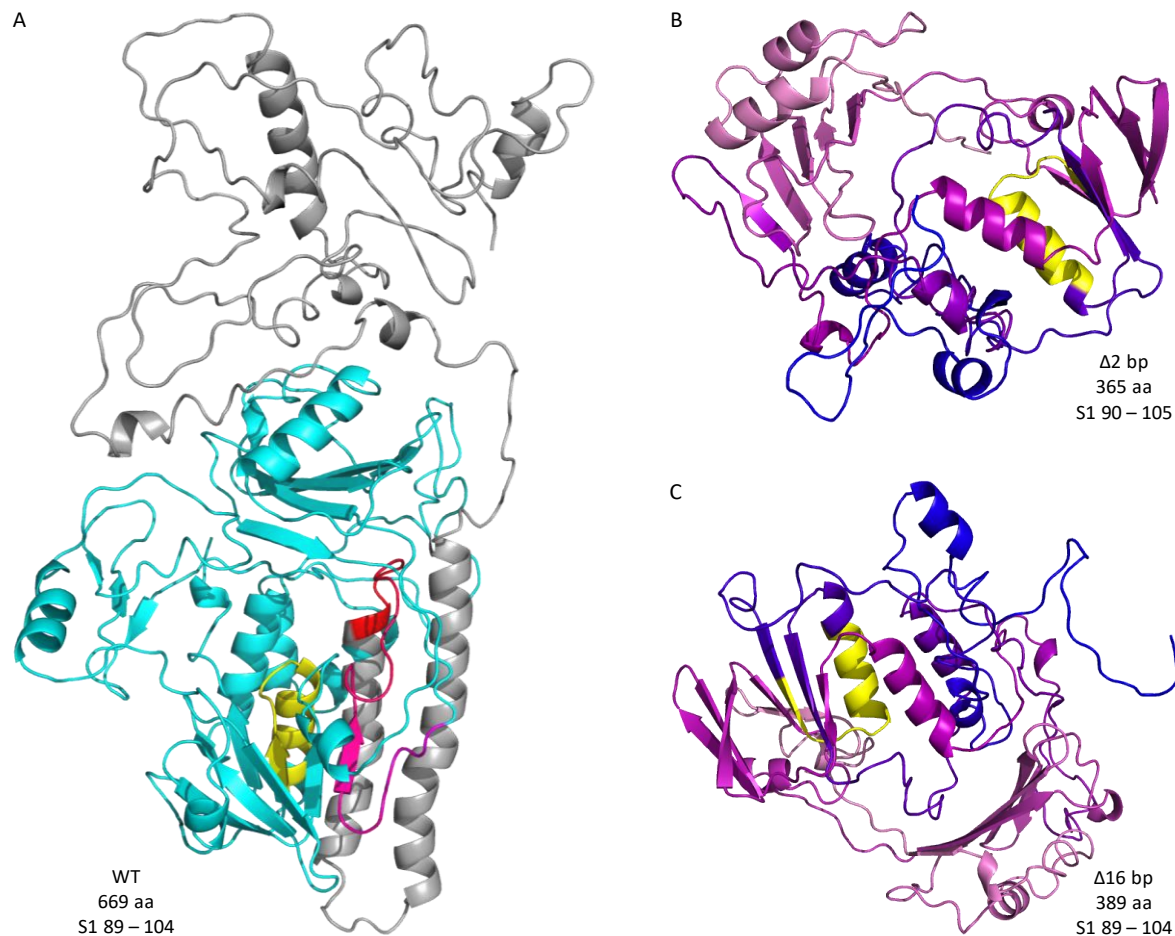


Figure 5.16. (A) Predicted 3D structure of the wild type (WT) allele of ZEP (the model as in Figure 5.1 rotated clockwise about the y -axis by 230°). Following *Agrobacterium* mediated stable transformation, a single plant (identifier 12.6.8; Table 5.3) was found to harbour a biallelic, CRISPR/Cas9-mediated edit at the exon 6, which led to the production of a truncated version of the protein. Two distinctive modifications of the exon 6 were identified: a 2 bp deletion and 16 bp deletion, leading to the production of a truncated protein with 365 and 389 amino acids, respectively. The results of the above modifications at the amino acid sequence level, originating from the underlying changes at the DNA level, are overlaid on the WT model of ZEP and indicated with the following colours: grey – part of the WT allele of ZEP lost following the introduction of a premature STOP codon, leading to the truncation of the amino acid chain after the exon 6; cyan-magenta joint – position of the truncation of the protein chain after amino acid threonine 365 as a result of the 2 bp deletion; red-grey joint – position of the truncation of the protein chain after amino acid 389 (glutamine replaced by proline) as a result of the 16 bp deletion; magenta-red strip – difference in the amino acid length between the two truncated versions of the protein: this region is only present in the allele harbouring the 16 bp deletion and has altered amino acid sequence compared to the WT (missense mutations in the last 26 amino acids; refer to Table 5.3 for the sequence); cyan – part of ZEP between the exons 1 and 6 remaining in the new, truncated alleles. The predicted 3D models of the two novel alleles of ZEP resulting from the 2 bp (B) and 16 bp (C) deletions of the DNA. In both novel alleles, 97% of residues were modelled at more than 90% confidence with 10 and 12 residues being modelled *ab initio* in (B) and (C), respectively. Models (B) and (C) were based on 10 and 7 protein templates (oxidoreductases), respectively. The protein chains of the novel alleles are colour coded from blue through purple to pink as travelling from the N- to the C-terminus. The predicted transmembrane domains (S1, single helix) were detected in all of the three protein models and are indicated in yellow. Modifications at the DNA level, lengths of each protein chain and positions of the S1 domains are indicated next to each allele.

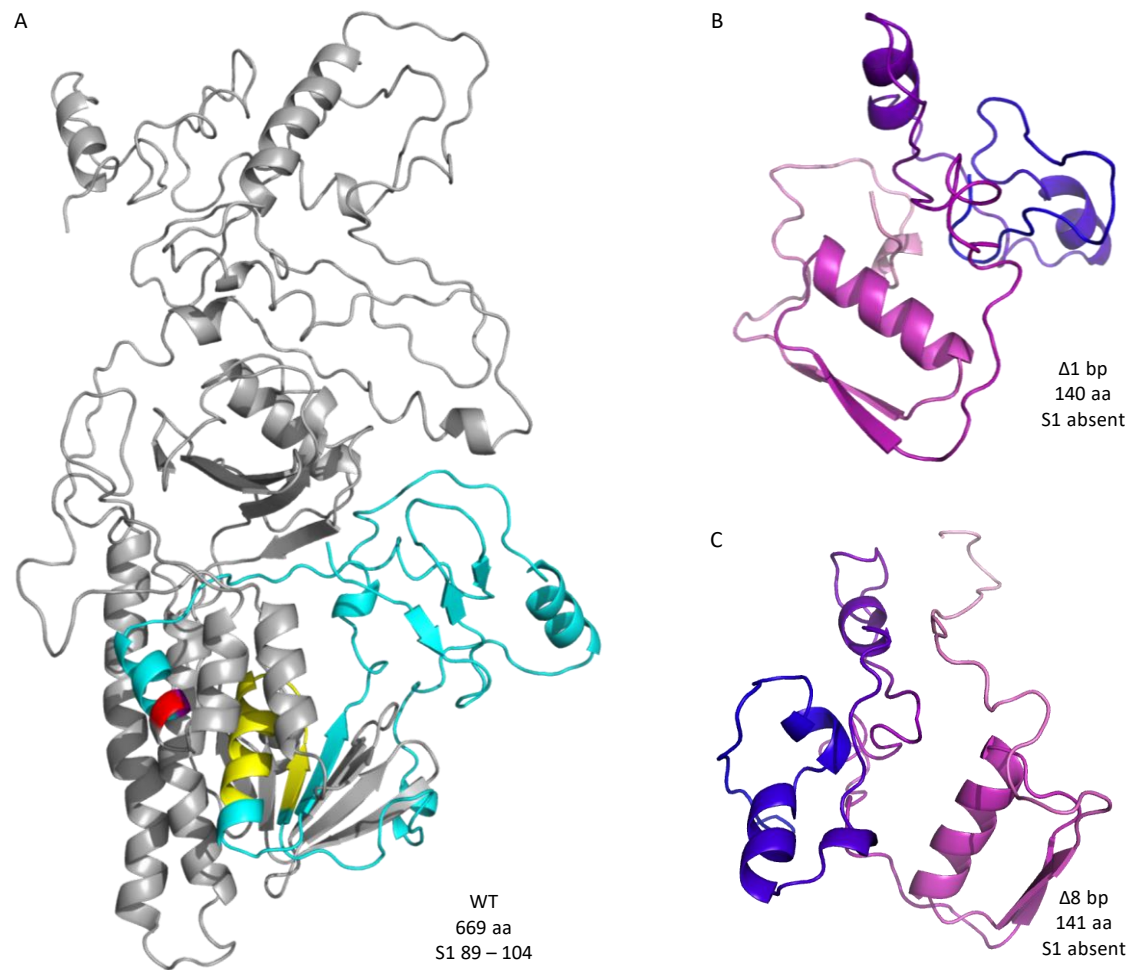


Figure 5.17. (A) Predicted 3D structure of the wild type (WT) allele of ZEP (the model as in Figure 5.1 rotated 25° clockwise about the y-axis). Following *Agrobacterium* mediated stable transformation, a single plant (identifier 12.7.24; Table 5.4) was identified as a chimera harbouring the WT and the edited alleles of ZEP. The CRISPR/Cas9-mediated edit at the exon 1 led to the production of a truncated version of the protein. Two distinctive modifications of the exon 1 were identified: a 1 bp and 8 bp deletion, which led to the production of a truncated protein with 140 and 141 amino acids, respectively. The results of the above editing at the amino acid sequence level, originating from the underlying changes at the DNA level, are overlaid on the WT model of ZEP and indicated with the following colours: grey – part of the WT allele of ZEP lost following the introduction of a premature STOP codon, leading to the truncation of the amino acid chain beyond the exon 1; cyan-magenta joint – position of the truncation of the protein chain after amino acid 140 (alanine replaced by leucine; 4 last amino acids altered) as the result of the 1 bp deletion; magenta-red joint – position of the truncation of the protein chain after amino acid 141 (leucine replaced by asparagine; 8 last amino acids altered) as the result of the 8 bp deletion; cyan – part of the exon 1 remaining in the new, truncated alleles. The predicted 3D models of the two novel alleles of ZEP resulting from the 1 bp (B) and the 8 bp (C) deletions in the DNA. 92% (11 residues modelled *ab initio*) and 87% (18 residues modelled *ab initio*) of amino acid residues were modelled at more than 90% confidence in (B) and (C), respectively. However, 59% and 60% of the sequence was predicted to be disordered in (B) and (C), respectively (disordered regions cannot be meaningfully predicted). Models (B) and (C) were based on 6 and 4 protein templates (oxidoreductases), respectively. The protein chains of the novel alleles are colour coded from blue through purple to pink as travelling from the N- to the C-terminus. The predicted transmembrane domain (S1, single helix) was detected only in the WT allele and is indicated in yellow. Modifications at the DNA level, lengths of each protein chain and the position of the S1 domain are indicated next to each allele.

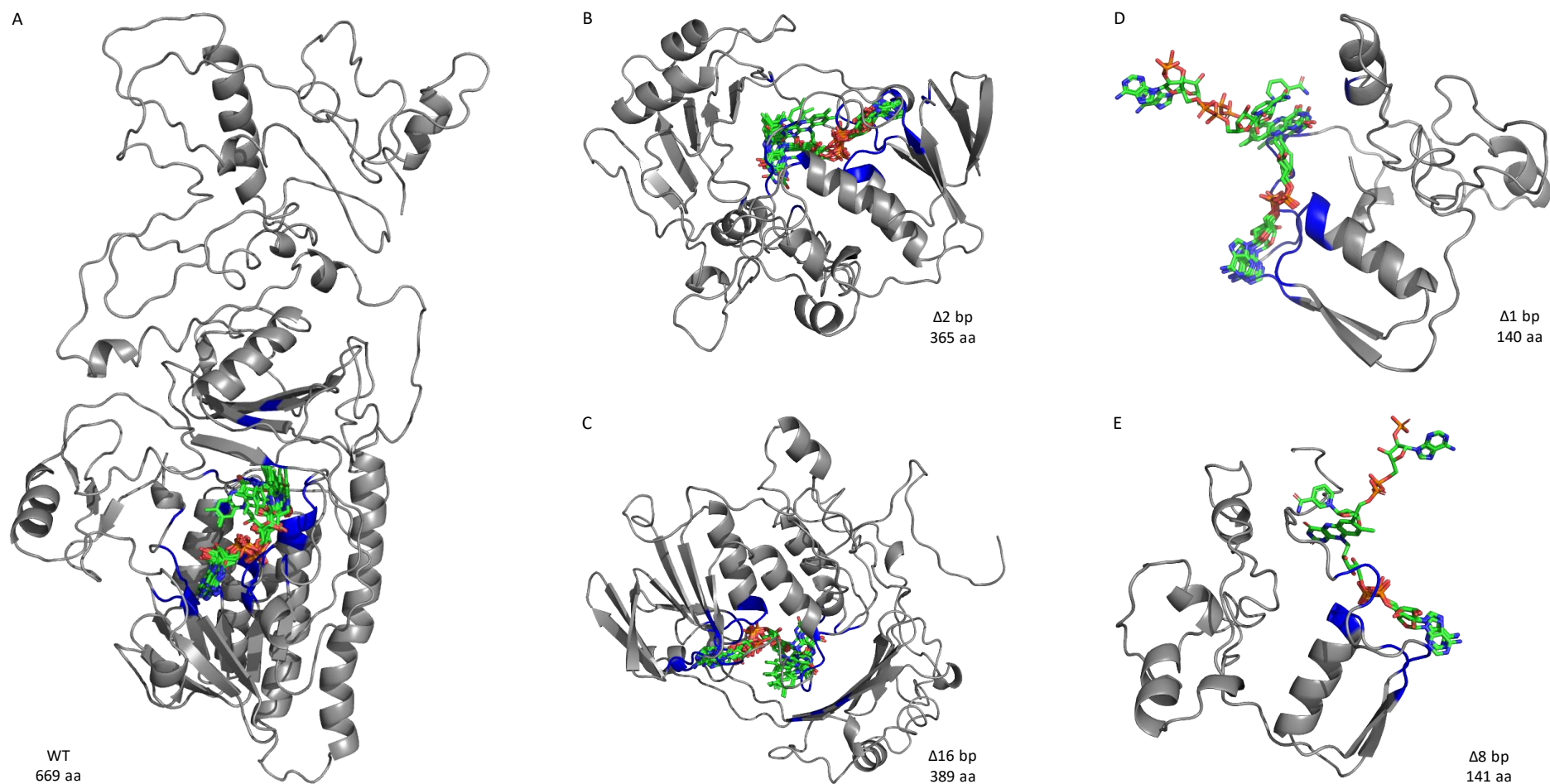


Figure 5.18. (A) Two ligand clusters were identified within the structure of WT ZEP. The major ligand cluster binding FAD with the 25 possible arrangements of the ligand within the cluster are displayed. The arrangement of WT ZEP as displayed in Figure 5.16. (B) and (C) A single, FAD-binding ligand cluster was identified in both truncated at the exon 6 alleles of ZEP. FAD is displayed in its 25 possible arrangements within the cluster. The models are displayed in the same orientation as in Figure 5.16. (D) and (E) Three ligand clusters were identified within the structure of the truncated at the exon 1 alleles of ZEP. The ligands predicted to bind in both clusters are ADP, FAD and NAP and NDP additionally in (D). The possible arrangements of the ligands – 10 for (D) and 7 for (E), are displayed as well. The models are displayed in the same orientation as in Figure 5.17. Amino acid residues predicted to bind with the ligands are coloured blue in all structures. Hence, the proximity of the ligand clusters to the predicted transmembrane domains in Figure 5.16.

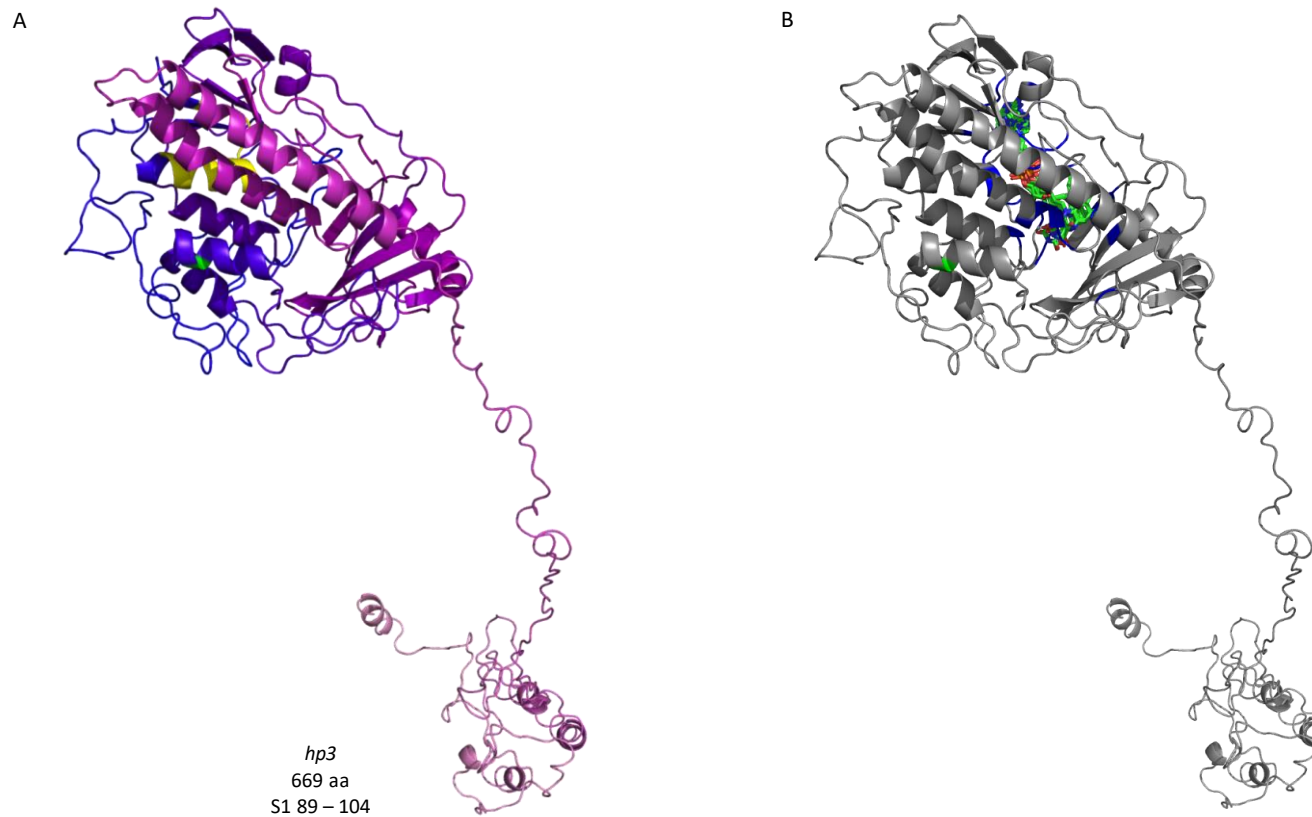


Figure 5.19. (A) Predicted 3D structure of the *hp3* allele of ZEP with 58% of the residues modelled at more than 90% confidence; six protein templates (oxidoreductases) were selected to model the allele based on heuristics. 282 amino acid residues (1 – 62 and 449 – 669) were modelled *ab initio* resulting in a low level of reliability. The predicted transmembrane domain (S1, single helix) is indicated in yellow. The protein model is colour-coded from blue through purple to pink as travelling from the N- to the C-terminus. (B) Two ligand clusters were identified within the structure of the *hp3* allele of ZEP. The major ligand cluster binding FAD with the 25 possible arrangements of the ligand within the cluster is displayed. Amino acid residues predicted to bind with the ligand are coloured blue. The missense mutation leading to the substitution of the negatively charged glutamic acid into the positively charged lysine at the position 142 is indicated in green in both models.

5.3 Discussion

5.3.1 CRISPR/Cas9 editing generates chimeric plants

Although, CRISPR/Cas9-mediated editing offers a great opportunity to study genes of previously unknown functions, the newly generated phenotypes and gene modifications are not always straightforward. If CRISPR/Cas9-mediated editing takes place during later stages of the plant's growth and development and not in the cells of the callus that the plant regenerates from, genetically chimeric plants, with different types of edits affecting different regions of the same plant, will develop (Volpi e Silva & Patron, 2017).

Pan *et al.* (2016) demonstrated this clearly by targeting the gene encoding phytoene desaturase, *PDS* in tomato plants. *PDS* catalyses the conversion of phytoene to phytofluene, which is a rate limiting step of the carotenoid biosynthetic pathway. The disruption of *PDS* results in an albino phenotype (Qin *et al.*, 2007a). Compared to the unedited control plants (Figure 5.20A), the T_0 transformant displayed phenotypes of varying degrees and localisations within the same plant. Some plants, although not majorly edited, could be seen to have some parts fully coloured white (Figure 5.20B), while the others were very extensively edited and displayed the complete albino phenotype (Figure 5.20D). One particularly interesting phenotype was also identified in which the plant was clearly edited but the phenotype was somehow diffused throughout the tissues (Figure 5.20C). The distribution of tissues with dysfunctional *PDS* was easy to spot due to the expressive phenotype.

Similarly, it is quite likely that some of the T_0 plants generated in this study were also chimeric, which could explain some of the interesting results obtained. Compared to the *PDS* mutation, editing of *ZEP* is not as easily recognisable as it does not lead to a profound colour change of the green tissues. However, as reported by Galpaz *et al.* (2008), compromising the function of *ZEP* led to the colour change of the flowers from yellow to beige. The presence of beige flowers was identified in plants ID 9.6.1, 9.6.2 and 12.6.8 (Figure 5.11B). Since plant ID 9.6.1 also had yellow flowers (Supplementary Figure 3.7), clearly some parts of the plant must have been fully edited, similarly to what was seen in Figure 5.20B, with other parts of the same plant either being edited



Figure 5.20. Targeting phytoene desaturase, *PDS* in tomato may generate T_0 plants of varying levels and sites of editing here clearly expressed by the albino phenotype. (A) WT. (B) Chimeric mutant displaying the phenotype only in one part of the plant. (C) Chimeric mutant with a more diffused phenotype. (D) Biallelic mutant (Pan *et al.*, 2016).

at a low frequency or not edited at all. Out of the three T_0 plants producing beige flowers, only plant ID 12.6.8 displayed the ABA-deficient phenotype characteristic of the *hp3* line. Neither ID 9.6.1 nor ID 9.6.2 showed any wilting, which further confirmed the chimeric nature of these plants. Both of these accumulated similar levels of zeaxanthin in their leaves, which were much lower than in either ID 12.6.8 or the *hp3* line, but at the same time, slightly higher than in the less frequently edited plants (Table 5.5). Therefore, at the time of collection, plant ID 9.6.2 most likely produced flowers only from the edited trusses as other observations indicated that this plant was not ABA-deficient.

Another interesting phenotype was observed in plant ID 12.6.18. This plant was found to be highly edited at a 70% frequency (Table 5.3), had a bushy appearance but was not susceptible to wilting. This plant was also found to contain higher levels of zeaxanthin in the leaf tissue than the less frequently edited transformants but comparable levels of violaxanthin and neoxanthin (Table 5.5). Interestingly, the F_v/F_m ratio of this plant was very inconsistent, sometimes being closer to the *hp3* line, and sometimes to the less edited plants (Figure 5.12). This strongly implies that this plant was also a chimera with more of a diffused phenotype as seen in Figure 5.20C. This could also explain the lack of antheraxanthin in its leaves (Table 5.5) as discussed further below. One of the alleles discovered in plant ID 12.6.18 was the same as the one found in plant ID 12.6.8. The other allele was different, but it was similarly truncated at the exon 6 (Table 5.3). As plant ID 12.6.8 was ABA-deficient, which was manifested by its strong susceptibility to wilting, the function of ZEP in plant ID 12.6.18 must have been compromised as well. However, plant ID 12.6.18 did not wilt, which suggested that the WT activity of ZEP remaining in the diffused tissues of this plant was sufficient to provide high enough levels of violaxanthin to maintain the production of ABA. Antheraxanthin, therefore, was not detected because in the edited cells it was not produced at all, hence the higher levels of zeaxanthin, but in the unedited cells, it was immediately converted to violaxanthin, hence violaxanthin and neoxanthin levels were similar to other plants. Since ABA is mobile in the chimeric plants, these did not present with a wilted phenotype because their unedited tissues were able to support the sufficient production of this hormone.

Another challenging aspect of CRISPR/Cas9 editing is phenotyping of the primary transformants. This is primarily based on the identification of the CRISPR/Cas9 expression cassette in the plant's genome and subsequent amplification and sequencing of the targeted regions (Figures 5.9 and 5.10; Tables 5.3 and 5.4). Although this seems to be straightforward, if a plant is edited similarly to the one shown in Figure 5.20B, the presence of Cas9/NPTII or mutations may not be detected depending on which part of the plant is analysed. This seemed to be the case for plant ID 9.6.3 (Figure 5.11), which was found to be positive for Cas9/NPTII but essentially unedited (Table 5.3).

Interestingly, this plant was found to have slightly higher zeaxanthin levels in its fruit compared to plants ID 9.6.2 (63% edited), ID 12.6.2 (10% edited) and ID 12.6.3 (50% edited). At the same time, this plant was found to have the second lowest levels of zeaxanthin in its leaves, which were only slightly higher than these of plant ID 12.6.2. Interestingly, the levels of zeaxanthin in the leaf tissues of the exon 6 targeted plants strongly correlated with the increasing frequencies of the edits (Spearman correlation coefficient, $R = 0.9643$, $P = 0.0028$). This, however, was only true for the leaf tissues but did not hold for the fruit pigments (Spearman correlation coefficient, $R = 0.2052$, $P = 0.7406$). This may be significant since the DNA obtained for genotyping of the primary transformants was extracted from their leaves. Therefore, the screening results of the CRISPR/Cas9 edited plants may be highly dependent on the time of the tissue collection as well as the part of the plant the tissue is collected from. The identification of edits may be simply missed because they have not happened yet or happened in other parts of the plant.

Similarly, the identification of the types of edits may be more challenging. In this study, typically between 10 and 20 bacterial clones with the PCR fragments amplified from the target sites were analysed. Taking the chimeric nature of the plants, this number may not be sufficient to obtain a good representation of the edited sequences. Some fragments, especially large deletions, may be selected by chance and be over-represented in the final count. For example, a large, 137 bp deletion was estimated to be present at a 5% frequency in plant ID 9.6.1. As the amplified region of the exon 6 was 441 bp-long, clearly a deletion of this size would appear as a separate band on the gel, yet it was not detected (Figure 5.10B). On the other hand, if very large deletions are present, larger than the amplified sequence, these will be missed completely. Large deletions, however, are quite rare, especially when a single guide is used; therefore, increasing the size of the screened region quite certainly will not provide more information (Allen *et al.*, 2019). The problems associated with screening of the CRISPR/Cas9 edited plants could be overcome by collecting leaf material for DNA extraction from various parts of the plant, preferably slightly later in development than at the plantlet stage and by analysing them separately. The number of sequenced bacterial clones could also be increased. However, both of these modifications will increase the cost and duration of the screening. The generation of chimeric plants poses certain challenges and makes some results difficult to interpret. However, once the new alleles are generated, the plants can be taken to subsequent generations where the CRISPR/Cas9 cassette can be lost and the alleles segregated to obtain clean phenotypes, which can be studied further.

A successful editing of plants is highly dependent on the structure of sgRNAs (Liang *et al.*, 2016), therefore selection of the target sequences is very important. Protein modelling could help to identify regions where pockets are found (Figure 5.2) and based on this information, the targets can be selected. This study aimed to modify ZEP close to the mutation site in the *hp3* allele.

Coincidentally, the selected target sequence, once incorporated into the guide, was expected to form a stable structure and to contain all essential stem-loops of a sgRNA (Figures 5.4C and D). However, based on the results of this study, it was not possible to evaluate whether the designed sgRNA was too efficient or not efficient at all at its target site. Compared to the exon 6 targeting, only one plant truncated at the exon 1 was identified. The sgRNA targeting the exon 1 could be too efficient and this plant happened to survive because, somehow, it carried a less frequent edit. Alternatively, the sgRNA against the exon 1 could not be efficient at all and the generation of this single plant happened by chance. The latter possibility seems to be less likely because if it was true, at least some unedited plants containing the CRISPR/Cas9 expression cassette would be expected to come through the tissue culture experiment. Either way, the truncation of ZEP at the exon 1 may be lethal. The single plant identified to carry the allele of ZEP truncated at the exon 1 could be a chimera and, if the first explanation is more likely, this plant could be quite extensively edited, indeed. It is also possible that the leaf collected for DNA extraction was the only one with a lower frequency of edits and since it was removed, the plant lost its only source of ABA and dried out.

The explanation given above is highly hypothetical, but apart from the target sequence, the two binary plasmids used in the stable transformation of tomato were identical (Figures 5.7 and 5.8B, Supplementary Figure 3.3) and yet, plants edited at the exon 6 of ZEP were successfully isolated. The exon 6 was selected as another target because it was the second closest to the mutation site in the *hp3* allele that had a sgRNA of a relatively good but not excellent quality. In fact, this guide was selected to lack certain features that would make it less efficient (Figures 5.4A and B). This approach was taken because if the knockout of ZEP was lethal, a less efficient sgRNA could generate a 'leaky' mutant, similarly to the *hp3* line, without fully abolishing the function of ZEP. Most edits identified at the exon 6 were small, generally less than 10 bp, deletions (Table 5.3). Small nucleotide deletions were the most frequent type of edit identified in other studies as well (Allen *et al.*, 2019). Small, especially 1 bp insertions in the exon 6 were also found but these were not as frequent as the deletions, which was consistent with previously published literature (Allen *et al.*, 2019). Because of its particularly high editing frequency, plant ID 12.6.8 was selected for the off-target analysis. None of the OTs were found to be edited in this plant, including the one with its off-score closest to the on-score of the target (Figure 5.13) and the sub-optimal design of the sgRNA could have contributed to this. However, it remains unknown whether the still present sgRNA_*zepE6* and Cas9, once they 'run out' of the on-target, they will start editing the off-targets.

Finally, the Golden-Gate assembly of plasmid constructs was found to be easier to design, much faster to perform and more efficient than traditional cloning methods. This technique seemed

to be particularly efficient at the assembly of smaller construct as in the case of level 1 plasmids (Table 5.2). Moreover, most of the constructs displayed the correct patterns upon restriction digestion (Figures 5.5B and C) and were found to be properly joined at least across the modular region (Figures 5.6 and 5.7). The modular cloning greatly reduces the risk of introducing single base mutations that are a common feature of PCR-based methods.

5.3.2 A novel, exon 6-truncated allele of *ZEP* mimics the *hp3* phenotype

The CRISPR/Cas9-mediated editing of the gene encoding zeaxanthin epoxidase was successful at introducing mutations at the exon 6. The phenotype of one plant, ID 12.6.8 was found to be very similar to the phenotype of the *hp3* line (wilting and pigment profiles of fruit (Figure 5.14) and leaf (Figure 5.15) tissues). Since only two, truncated at the exon 6 alleles of *ZEP* and no edits at the off-targets were identified in this plant, its phenotype was attributed to these novel alleles (Figure 5.16). However, this truncation of *ZEP* at the exon 6 could be described as a ‘stronger’ mutation than the misfolded *hp3* allele (Figure 5.19). The *hp3* tomato line accumulated high levels of antheraxanthin and low levels of violaxanthin and neoxanthin in its leaves (Figure 5.15 and Table 5.5), so the function of *ZEP* was not fully abolished but heavily compromised in this line. The plants with fully functional *ZEP* contained lower levels of antheraxanthin in their leaves as they could efficiently convert this xanthophyll to violaxanthin, which was present in higher amounts than in the *hp3* line. Since plant ID 12.6.8 did not accumulate any of these pigments, its version of *ZEP* appeared to lose its function completely.

Perhaps the *hp3* allele, despite the loss of its structure at the C-terminus, was still able to interact with zeaxanthin, whereas plant ID 12.6.8 lost its zeaxanthin-binding domain completely, hence the lack of zeaxanthin-derived products (Figure 5.17 and 5.19). The plants of the *hp3* line were not susceptible to wilting under glasshouse conditions, unlike plant ID 12.6.8. Moreover, it was not possible to obtain cuttings of plant ID 12.6.8 as these dried out very quickly following their transfer to the soil, although propagating the *hp3* line through cuttings did not pose a challenge. Luteoxanthin, a violaxanthin derivative (Whittle & Casselton, 1975), was not detected in leaves of the *hp3* line. Perhaps violaxanthin was channelled towards the production of neoxanthin and ABA as more essential products for plant homeostasis. In its fruit, plant ID 12.6.8 accumulated slightly higher levels of zeaxanthin than the *hp3* line, but at the same time lacked antheraxanthin (Figure 5.14), which further suggested that the functionality of the exon 6-truncated alleles was more compromised than that of the *hp3* allele. In the *hp3* line and ID 12.6.8 the levels of lutein in fruit were similarly higher compared to the other plants. Possibly, certain regulatory feedback mechanisms were involved at the gene level, which diverted the metabolic flux towards the α -branch of the carotenoid biosynthetic pathway to counteract the increase in zeaxanthin levels. The increase in zeaxanthin in fruit of the *hp3* line and plant ID 12.6.8 was also accompanied by

the increase in the levels of α -tocopherol (Figure 5.14). It was not possible to conclude the same from the leaf extracts as α -tocopherol could not be unambiguously detected and quantified due to a strong overlap with the violaxanthin peak. However, since violaxanthin was absent from the fruit extracts, α -tocopherol was not obstructed and it could be quantified. Galpaz *et al.* (2008) reported that the *hp3* tomato line had a greater number of plastids in its fruit compared to the WT control. Since the thylakoid membranes have a limited capacity to store zeaxanthin (Hieber *et al.*, 2004), the greater number of plastids could help to accommodate extra amounts of this xanthophyll. The increase in the availability of membrane compartments can also improve the storage capacity for α -tocopherol leading to the elevated levels of this compound.

Ripe fruit of plant ID 12.6.8 were lighter in colour compared to fruit of the other T₀ transformants (Figure 5.11A). This was most likely due to their increased zeaxanthin content but also perhaps their slightly higher lutein and α -tocopherol levels (Figure 5.14A). Ripe fruit of plant ID 9.6.2 also appeared to be lighter in colour compared to fruit of the other transformants (Figure 5.11A), but this was most likely caused by their reduced lycopene levels and the generally lower total fruit carotenoid content (Figure 5.14). Interestingly, this was also the plant that had the lowest total leaf carotenoid content (Table 5.5). However, overall, the total carotenoid levels in fruit of the analysed plants (Figure 5.14) did not correlate with the total leaf carotenoid content (Table 5.5; Pearson correlation coefficient, $R = 0.072$), indicating that different regulatory mechanisms were operating at the level of carotenoid biosynthesis in both of these tissues.

The photosynthetic performance, expressed as the F_v/F_m ratio, was found to be lower only in the two ABA-deficient plants (the *hp3* line and plant ID 12.6.8), whereas plant ID 12.6.18 provided inconsistent readings (Figure 5.12). The lower F_v/F_m values seemed to correlate with the higher ratios of the total chlorophyll to total carotenoid content in leaves of these plants (Table 5.5). In the plants whose F_v/F_m readings were close to optimal, the ratio of the total chlorophyll to total carotenoid content was 2:1 or lower. Therefore, the photosynthetic performance of these plants was not dependent on the chlorophyll levels or the carotenoid content, but rather on the ratio between the two. A specific ratio of the macular pigments in the human retina was described previously and determined to provide the greatest quenching effects in order to protect the delicate structures of the eye (Li *et al.*, 2010a). It appeared that in the analysed plants an increase in the accumulation of chlorophyll was followed by a simultaneous increase in the carotenoid content or vice versa. However, in the *hp3* line and ID 12.6.8 the increase in the total chlorophyll content was not accompanied by a related increase in the total carotenoid levels, most likely because these plants reached the maximum membrane capacity for storage of carotenoids and particularly zeaxanthin (Hieber *et al.*, 2004). As the result, the ratio between the chlorophyll and the carotenoid content at which the optimal non-photochemical quenching was achieved, was

disrupted, leading to the lower F_v/F_m reading. It remains debatable whether the small decrease in the F_v/F_m ratio of plants with compromised activity of ZEP is directly related to a change in the rate of carbon fixation, and thus biologically relevant. According to previously published work (Murchie & Lawson, 2013; Sharma *et al.*, 2015), a decline in the F_v/F_m ratio was not necessarily reflected by compromised photosynthetic performance. However, this measurement could be used as a fast phenotyping method for the identification of plants with compromised ZEP activity as higher F_v/F_m ratios showed a strong negative correlation with increasing levels of zeaxanthin in the leaf tissues (Pearson correlation coefficient, $R = -0.9294$, $P = 0.0001$).

Although it is generally believed that the introduced edits at the exon 6 of ZEP would produce null alleles, it would be interesting to know whether there was a functional difference between the two truncated alleles identified in plant ID 12.6.8 once they segregate in later generations. Modelling of these alleles (Figure 5.16) did not indicate any major differences, but nonetheless, a functional assessment remains to be done. The measurement of ABA levels in plant ID 12.6.8 was not carried out either. Given the chimeric nature of the CRISPR/Cas9-edited plants, it is quite likely that some rudimentary WT activity of ZEP remained in this plant if some of its cells were unedited. This could be the reason why this plant was able to grow but it was not possible to propagate it through cuttings. Once the novel alleles of ZEP segregate in the next generations and clean edits are recovered, the levels of ABA can be severely reduced and it may be very difficult, or even impossible, to grow these plants without an extra level of attendance. The usual method adopted for the ABA-deficient plants is to spray them with the hormone. Finally, the size of tomato fruit is an important agronomic trait. The fruit of plant ID 12.6.8 were very small (Figure 5.11A). It remains to be seen if in the next generations the fruit size of this ZEP mutant remains similarly affected.

5.3.3 Summary of ZEP activity

Previously, it was shown that ZEP was predominantly localised in the stroma of the chloroplasts, mostly in association with the thylakoid membranes and, at much lower levels, also bound to the chloroplast envelope (Schwarz *et al.*, 2015). However, others have suggested that ZEP was a peripheral, membrane associated protein, rather than a transmembrane one, that was weakly bound to the lipid bilayer (Schaller *et al.*, 2012), and thus able to transit from the thylakoid to envelope side (Ruiz-Sola & Rodríguez-Concepción, 2012). The enzyme violaxanthin de-epoxidase (VDE), responsible for catalysing the reaction opposite to ZEP, has only been identified inside the thylakoid lumen and is activated at acidic pH under elevated light levels (Schwarz *et al.*, 2015). Therefore, the thylakoids are the site of the xanthophyll cycle in the chloroplasts, but the forward and reverse steps of this cycle are separated on the opposite sides of the membranes (Ruiz-Sola & Rodríguez-Concepción, 2012).

Within the thylakoid and envelope membranes of chloroplasts, zeaxanthin adopts a particular transmembrane orientation with the average tilt angle of 42.7° relatively to the plane of the lipid bilayer (Grudzinski *et al.*, 2017). This arrangement places the hydroxylated β -rings close to the hydrophilic phosphate groups at the opposite sides of the membrane. However, the question remains, how ZEP is able to convert zeaxanthin to violaxanthin if it only has access to the end of the molecule on the stromal but not on the thylakoid lumen side, given that the orientation of zeaxanthin within the thylakoid membranes is as described above. Previous research has shown that the conversion of zeaxanthin to antheraxanthin is faster than the subsequent conversion of antheraxanthin to violaxanthin (Schaller *et al.*, 2012). This is consistent with the topological arrangement of zeaxanthin in the membrane and the availability of one of the terminal groups for epoxidation. However, it is unclear how the second terminal group is made accessible to ZEP since it is located on the other side of the phospholipid bilayer. The generation of violaxanthin from antheraxanthin would require this molecule to be flipped, which would expose the another hydroxylated β -ring to ZEP. In fact, a mechanism involving the rotation of antheraxanthin at the thylakoid membrane was previously proposed for the conversion of violaxanthin to zeaxanthin (Havaux, 1998).

The 'flipping' of antheraxanthin within the thylakoid membrane could be facilitated by specific complexes present inside the phospholipid bilayer. In fact, Jahns *et al.* (2009) proposed that the inverted hexagonal structures (H_{II}), assembled from monogalactosyldiacylglycerol molecules, participated in the conversion of violaxanthin to zeaxanthin. However, the presence of these accessory molecules did not agree with the pigment profile of the *hp3* line. If the accessory molecules were present, the *hp3* allele of ZEP would still be able to convert antheraxanthin to violaxanthin since it already could convert zeaxanthin to antheraxanthin. However, if ZEP itself needs to interact with other molecules to facilitate this process, this could be impaired due to the loss of its structure at the C-terminus (Figure 5.19A). However, it is much more likely that the *hp3* allele encodes the version of ZEP that is just less stable, less or partially active or poorly localised. Hence, the presence of specific complexes within the thylakoid membranes cannot be ruled out. Since plant ID 12.6.8 most likely carried a null allele of ZEP, it was unable to convert zeaxanthin to its further metabolites, and therefore, it did not accumulate any antheraxanthin in its leaves (Table 5.5).

However, the conversion of antheraxanthin to violaxanthin could also be facilitated by simple physical factors, such as pH and light intensity, and may not require the involvement of other molecules. For example, the molecules of antheraxanthin can undergo isomerisation from the *trans*- to the *cis*-configuration due to the change in the light intensity or the pH levels inside the thylakoid lumen. This would bring the second hydroxylated β -ring closer to the catalytic domain

Chapter VI: General discussion

6.1 Summary and key points

In summary, this work led to the generation of a new tomato variety high in zeaxanthin, which has a potential to become a new food source of this xanthophyll. Moreover, a number of new *ZEP* alleles have been generated with a potential to express a stronger phenotype than the *hp3* tomato line. These alleles can be used for crossing with the *U/0; B/B* line in an attempt to further increase the accumulation of zeaxanthin in ripe tomato fruit.

The three major points of this work are:

- Chapter III: **Overexpression of the genes responsible for zeaxanthin synthesis, namely lycopene β -cyclase (*CYC-B*) and β -carotene hydroxylase (*CrtR-b2*), in tomato fruit, does not lead to a direct increase in zeaxanthin content but rather its further conversion into the downstream xanthophylls, mainly violaxanthin and luteoxanthin and possibly volatile compounds and hormones, such as ABA.**
- Chapter IV: **Accumulation of zeaxanthin at higher levels in fruit of tomato plants can only be achieved when a block at the level of ZEP is introduced. However, most likely due to structural limitations of the chromoplasts, there is a maximum capacity of the fruit to store zeaxanthin.**
- Chapter V: **The new, strong knockout alleles of *ZEP* mimicking the *hp3* phenotype were generated with the use of the CRISPR/Cas9 system.**

The summary of these key points is provided in Figure 6.1.

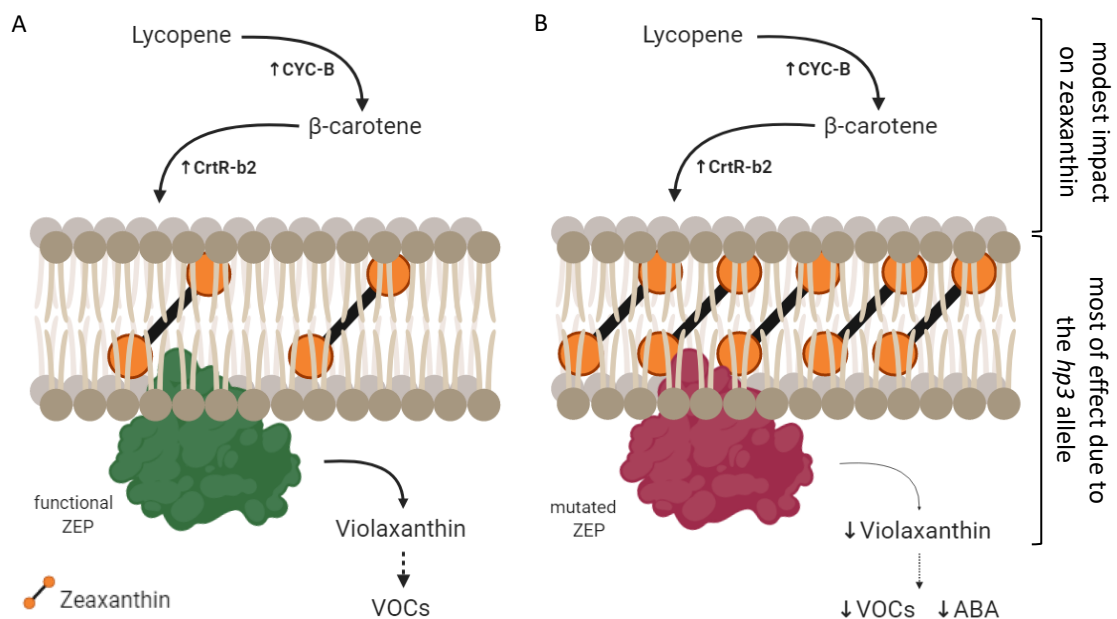


Figure 6.1. Summary of the conclusions of Chapters III – V. (A) With functional ZEP, little zeaxanthin is accumulated since it is converted into further metabolites. (B) Only when ZEP is mutated, accumulation of zeaxanthin at higher levels is possible. However, the availability of membrane compartments can limit its concentration. The close association of ZEP with the membranes can explain the need to sequester zeaxanthin into specific membrane compartments.

It has to be reiterated that the manipulation of complex biosynthetic pathways often disturbs the metabolic homeostasis. A clear knowledge of the biochemistry and regulatory mechanisms within the manipulated pathways is necessary in order to understand the changes that take place at the global level. Finally, the manipulations used to increase the metabolic flux through a biosynthetic pathway, may not necessarily be accompanied by higher levels of compounds of interest due to the presence of other limiting factors, either at a structural or a regulatory level. These limits need to be identified and addressed in order to find possible solutions to these constraints and to achieve a desirable increase in the metabolite accumulation.

6.2 Industrial relevance

From a commercial perspective, it is much easier to market something that the customers are already familiar with and tomato is one of the most widely cultivated plants. The ripe fruit of the zeaxanthin-accumulating line are almost a pure source of this xanthophyll (82% of the total carotenoid content). This is relevant economically if the fruit is to be used for the generation of food supplements or in animal feed, since very little downstream processing may be necessary. Moreover, this line contains high levels of vitamin E (tocopherols), which adds to its nutritional value. However, the ripe fruit of the *hp3* tomato line, while also rich in zeaxanthin and vitamin E, remain a much better source of other carotenoids, such as lycopene and β -carotene, and these are known to benefit the human health as well.

By introducing a block at the level of *ZEP* in the *U/0; B/B* line, a 12.4-fold increase in the content of zeaxanthin was achieved in leaves of the *U/0; B/B; hp3/hp3* line. This is commercially relevant as zeaxanthin available in the green tissues of plants can also be extracted. Purified zeaxanthin can be used in supplements but also in animal feed. This in turn can reduce the amount of green waste and minimise the use of land to increase the profit. The amount of zeaxanthin, which can be obtained from the green parts of the *U/0; B/B; hp3/hp3* tomato line, is much greater than what can be delivered from the currently recommended food sources, such as spinach and kale (Figure 4.19). However, the current extraction methods employ the use of non-polar solvents such as hexane, which are harmful to humans and the environment.

Importantly, it was shown that an improvement in the content of zeaxanthin could be achieved by introducing a block at the level of *ZEP*. It was also shown that spinach and kale, although poor sources of zeaxanthin, contained high levels of violaxanthin (Figure 4.19). Therefore, methods, such as EMS/TILLING, or novel genome editing technologies employing the CRISPR/Cas9 system, could be used to improve the content of zeaxanthin in these crops as well. Since it was shown that the leaf tissue has a greater capacity to store xanthophylls (Figure 4.4), the generation of other potential, and perhaps even better sources, is possible.

The triple crosses, similarly to the *hp3* line, had reduced F_v/F_m ratios compared to the wild type tomato plants (Figure 4.11). It was previously shown that, when grown in the field, the *hp3* line had reduced biomass, fruit yield and fruit size compared to the control. However, no difference between the wild type and the *hp3* line was seen when the two were grown in the glasshouse (Galpaz *et al.*, 2008). Thus, growing the lines carrying the *hp3* alleles of *ZEP* under the glasshouse conditions can ensure that no adverse effects on plant biomass and fruit quality are seen in the triple cross. However, this form of cultivation is more expensive than the growth in open fields and generally perceived as less 'eco-friendly'.

From the commercial perspective and the point of view of the supplier, plant varieties that do not breed true are more valuable since their seeds are required to be purchased on a regular basis by the grower. The triple cross accumulating zeaxanthin in its fruit does not breed true due to the reduction of *CrtR-b2* transcripts and the silencing of *CrtR-b1* in plants homozygous at the transgenic U locus. Therefore, retaining seeds of this line for the next harvest would only allow to recover 50% of the plants with the required zygoty of the hydroxylase. However, from the point of view of the grower, this is of course problematic and may discourage the cultivation of this crop whatsoever. Moreover, if certain crops, which do not breed true, are marketed as good sources of important food supplements and made available globally, poorer countries may not be able to afford to purchase new batches of seeds a year on. This makes the generation of such food crops ethically questionable.

Finally, the use of GM plants needs to be addressed since specific regulations are in place when handling such organisms. In fact, many countries ban their cultivation and import. However, GM plants may be used for different purposes than for human consumption. For example, GM plants can be used for the extraction of high value compounds or can be incorporated into the animal feed and different regulations are applicable for such cases. The fruit of the U/0; B/B; *hp3/hp3* tomato line could be used to enhance the colour of poultry meat, egg yolks and fish. Moreover, other methods of compound delivery are available instead of ingestion. For example, curcumin-coated nanocarriers were administered as eye drops and found to have a neuroprotective effect in degenerative eye conditions (Davis *et al.*, 2018). Thus, other delivery methods for zeaxanthin may also be available in the future.

6.3 Future directions and recommendations

In the presented work, particular steps were taken in order to generate tomato lines capable of accumulating zeaxanthin in their ripe fruit. The almost exclusive accumulation of zeaxanthin in fruit of tomato plants was attributed to the specific combination of the three genes of interest, namely transgenic copy of *CrtR-b2* in a hemizygous state, *S. galapagense* *CYC-B* allele either in

a homozygous or heterozygous state and the *hp3* allele of *ZEP* in a homozygous state. However, certain issues are found within this methodology and these should be addressed in the future.

The two key points for further work are:

- **Can the observed effects on zeaxanthin accumulation be verified in NILs? All current data are based on mixed genetic backgrounds, except for the CRISPR/Cas9-edited plants against the AC control.**
- **Is *CrtR-b1* or *CrtR-b2* silenced in the crosses homozygous at the transgenic U locus? Some of the conclusions are based on the gene expression data available on the U/U parental line provided by D'Ambrosio *et al.* (2011), but whether the same changes occurred in the lines analysed in this work has not been verified.**

Further points that should be addressed include:

- Stability of zeaxanthin-accumulating lines (U/0; B/B; *hp3/hp3* and U/0; B/+; *hp3/hp3*). This requires growth over many generations in order to establish if the accumulation of zeaxanthin remains equally high.
- Production of ABA in the zeaxanthin-accumulating lines. The increased production of ABA by the U/0; B/B line could explain its low total fruit carotenoid content. Moreover, ethylene measurement should be carried out in this line in order to address the changes in certain aspects of the fruit ripening process (Figure 3.22).
- A number of candidate genes related to fruit firmness and flavour have been identified (Section 3.3.6). These represent potential targets for the improvement of fruit quality and other important agronomic traits, such as taste and aroma.
- It remains to be seen if by crossing the U/0; B/B line with the stronger *ZEP* mutant (plant ID 12.6.8), generated using the CRISPR/Cas9 system, a further increase in the levels of zeaxanthin in tomato fruit can be achieved.
- The high content of α -tocopherol in the U/0; B/B (Figure 3.10B) and U/0; B/B; *hp3/hp3* (Figure 4.6B) lines, coupled to the increase in the fatty acid metabolism (Figures 3.20 and 4.18), points to structural changes at the membrane compartments. Tocopherols deposit inside membranes and any changes in the availability or composition of these structures can allow for a greater storage of pigments. The chromoplasts of the U/0; B/B line were analysed by TEM and membranous infoldings were found inside these plastids, which were absent from the Az control plants (Figure 3.24). However, the chromoplast ultrastructure of the U/0; B/B; *hp3/hp3* line has not been examined. Additionally, the analysis of the flower chromoplasts of the zeaxanthin-accumulating lines would allow to establish if and how they respond to the increased biosynthesis of zeaxanthin, which, in turn, could help to better understand the limits to its deposition.

- It may be possible to increase the accumulation of xanthophylls in ripe tomato fruit by the overexpression of acyltransferases. Berry *et al.* (2019) identified an ortholog of *PYP*, a ripening-specific acyltransferase (*rsAcT*), in chilli pepper. It was also found that in the fruit of chilli pepper, the increased accumulation of carotenoids was associated with the increased expression of *rsAcT*. In tomato flowers, *PYP* is involved in the esterification of violaxanthin and neoxanthin (Ariizumi *et al.*, 2014); thus, the overexpression of *PYP* in the U/0; B/B line under a fruit-specific promoter could lead to an increased xanthophyll accumulation by promoting their esterification. Enfissi *et al.* (2019) showed that tomato fruit were able to esterify ketocarotenoids, the derivatives of xanthophylls. Therefore, an active acyltransferase must be present in tomato fruit. However, the esterification of zeaxanthin in the flowers and fruit of tomato plants does not occur. The overexpression of *PYP* under a tissue-specific promoter could help to answer the following questions. Firstly, if the esterification of xanthophylls in tomato fruit is possible at all, and if so, whether this can improve their accumulation. Secondly, if zeaxanthin can be esterified, how this affects its levels, the levels of other xanthophylls and the structure of the fruit and flower chromoplasts. Several tomato fruit-specific promoters that are active in the green fruit and throughout the ripening process were identified (Hiwasa-Tanase *et al.*, 2012) and could be used to express *PYP* in the target tissues. Additionally, *Arabidopsis* flower-specific promoters, showing the same patterns of expression in tomato flowers are known and could be used as well (Fernandez *et al.*, 2009).

6.4 Issues and alternative approaches

It seems that tomato fruit lack the structural adaptations that would allow them to accumulate high levels of zeaxanthin. Therefore, it may not be at all worthwhile to try to manipulate their levels of xanthophylls through metabolic engineering and different approaches should be taken. For instance, given that the lack of internal membranes inside the chromoplasts does not allow for a high accumulation of zeaxanthin, the focus should be to improve the storage capacity of these organelles. The *hp3* line already accumulates fairly high amounts of zeaxanthin in its fruit and the further increase in the content of this xanthophyll may simply be achieved through crossing with other lines, for example the *green flesh (gf)* mutant, which maintains chloroplast compartments during the chromoplast differentiation (Cheung *et al.*, 1993) or the lines known to contain a higher number of plastids in their ripe fruit, such as the *hp1* or *hp2* mutants (Yen *et al.*, 1997; Bino *et al.*, 2005; Kolotilin *et al.*, 2007).

Alternatively, the focus on improving the content of zeaxanthin should be shifted towards plants that are already good accumulators of xanthophylls, such as spinach and kale, or other green leafy vegetables in general. The improvement in the levels of zeaxanthin can again be achieved

through means other than genetic manipulation as discussed in Chapter IV, Section 4.3.4. These methods include the application of stressors, for example, high light intensity or temperature, during the cultivation period or post-harvest treatments, such as addition of vinegar prior to the consumption. The foods prepared in this manner are not particularly regulated and do not carry the stigma of GM crops.

The modelling of the novel alleles of *ZEP* generated with the use of CRISPR/Cas9 was carried out. However, in the presented work, the generated alleles were most likely null and such modelling would not be informative. It would be better to use the modified CRISPR/Cas9 systems known as the base editors, such as the cytosine base editor (CBE; Komor *et al.*, 2016) or the adenine base editor (ABE; Gaudelli *et al.*, 2017), which can specifically target a nucleotide and exchange it for another, thus conserving the frame. Therefore, although modelling can be informative, the gene editing system employed in this work cannot make the use of it.

There are many issues associated with the development and release of GM crops. Although the GM plants can provide important insights into many biological processes, they are generally not considered as natural and some question their safety to people and the environment. Moreover, many countries ban their cultivation or import. The CRISPR/Cas9 genome editing technology can address some of the concerns associated with the GM crops. For example, in *Agrobacterium* mediated transformation of rice, suicide genes were added to the CRISPR/Cas9 constructs. This allowed to isolate transgene-free plants in a single generation accelerating the selection process (He *et al.*, 2018), but also prevented the release of the pollen and seeds with the selection marker to the environment. However, these plants are still considered to be transgenic due to the presence of the edits they contain, which, in fact, will be released to the environment. Therefore, perhaps it would be better to consider the use of natural variants, for example, identified by TILLING, to avoid the issues associated with the GM crops. For instance, the high β -carotene levels in the RI parental line were achieved due to the presence of a natural variation in the gene promoter. Similarly, an increase in the activity of β -carotene hydroxylase could be achieved through the identification of lines naturally overexpressing this gene. This would allow to avoid issues associated with the use of the CaMV 35S promoter for the expression of genes, such as silencing and co-suppression.

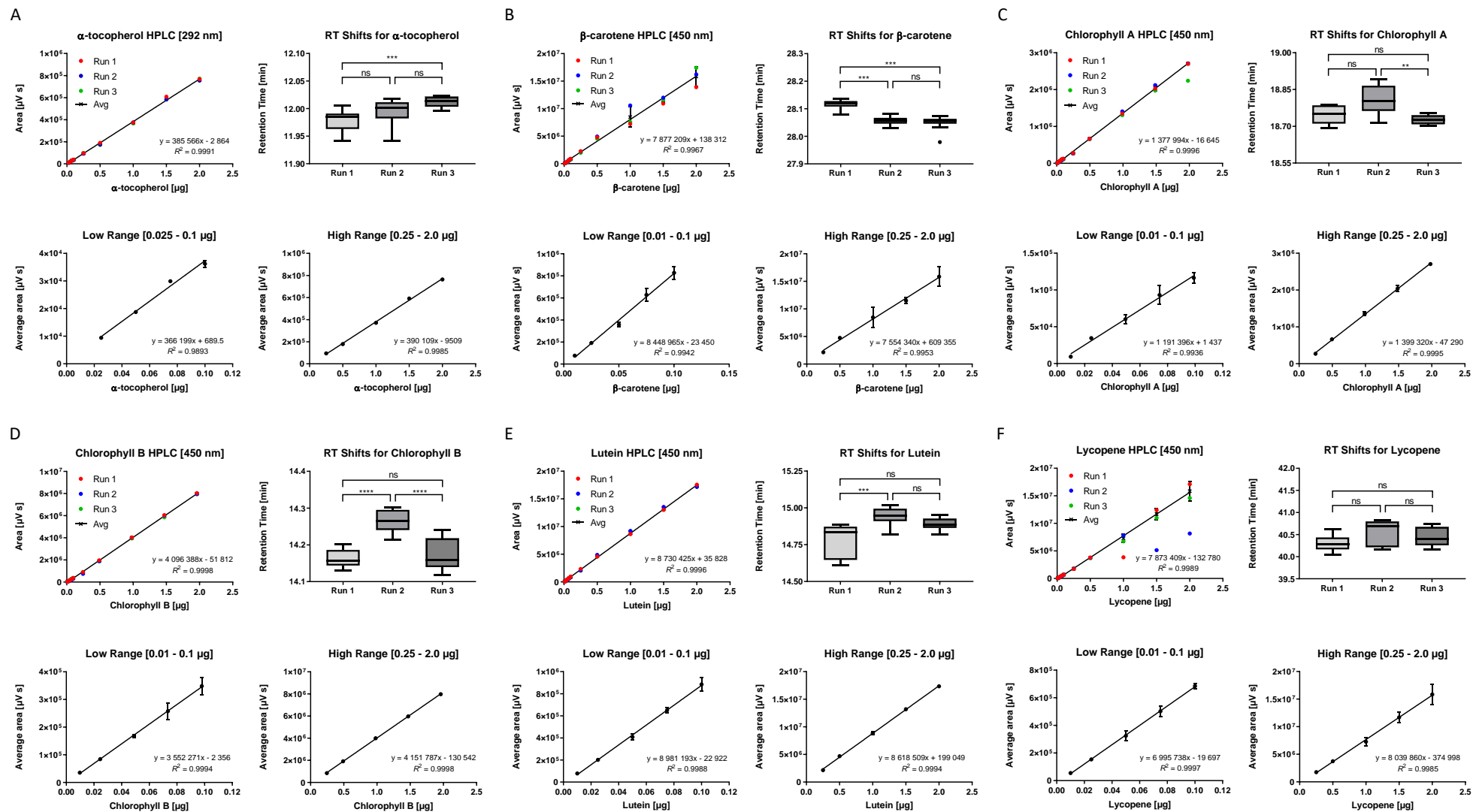
Finally, the lines used throughout this work were not NILs. Therefore, it has to be reiterated that the observed phenotypes could be a result of other genes that were segregating together with the genes of interest. The presence of such a complex background is problematic since it cannot be unequivocally concluded that the observed phenotypes are caused by the actions carried out. This will have particular implications for publication and even make some of the presented data questionable.

Appendices

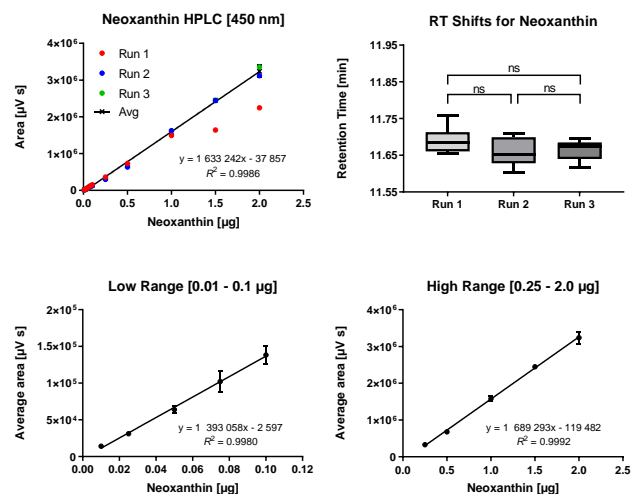
The following appendices contain additional figures and tables not included in the main body of the text. The figures and tables present supplementary information which could be referred to as necessary in order to enhance the understanding of certain aspects of the used methodology or to support the statements made in the main body of the thesis.

7.1 Appendix 1

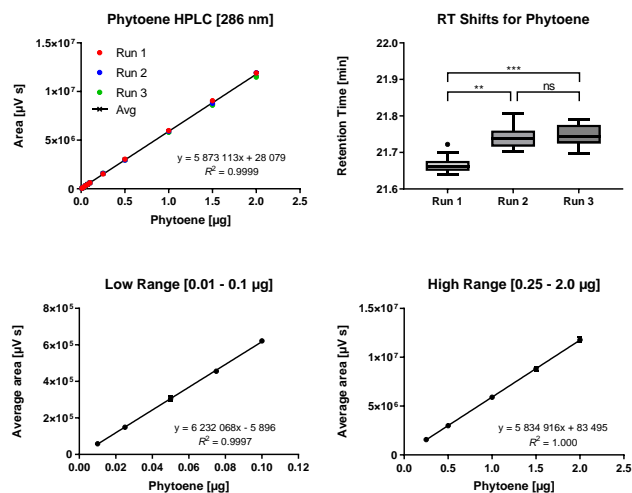
The following appendix contains supplementary figures and tables, which complement the results of Chapter III: Characterisation of tomato lines overexpressing *CYC-B* and *CrtR-b2*.



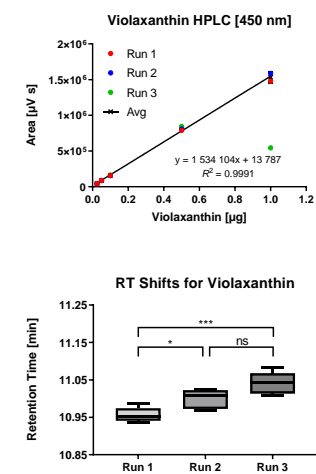
G



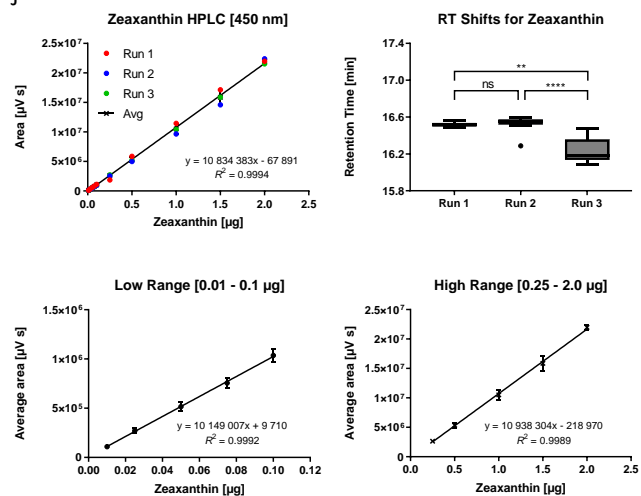
H



I



J



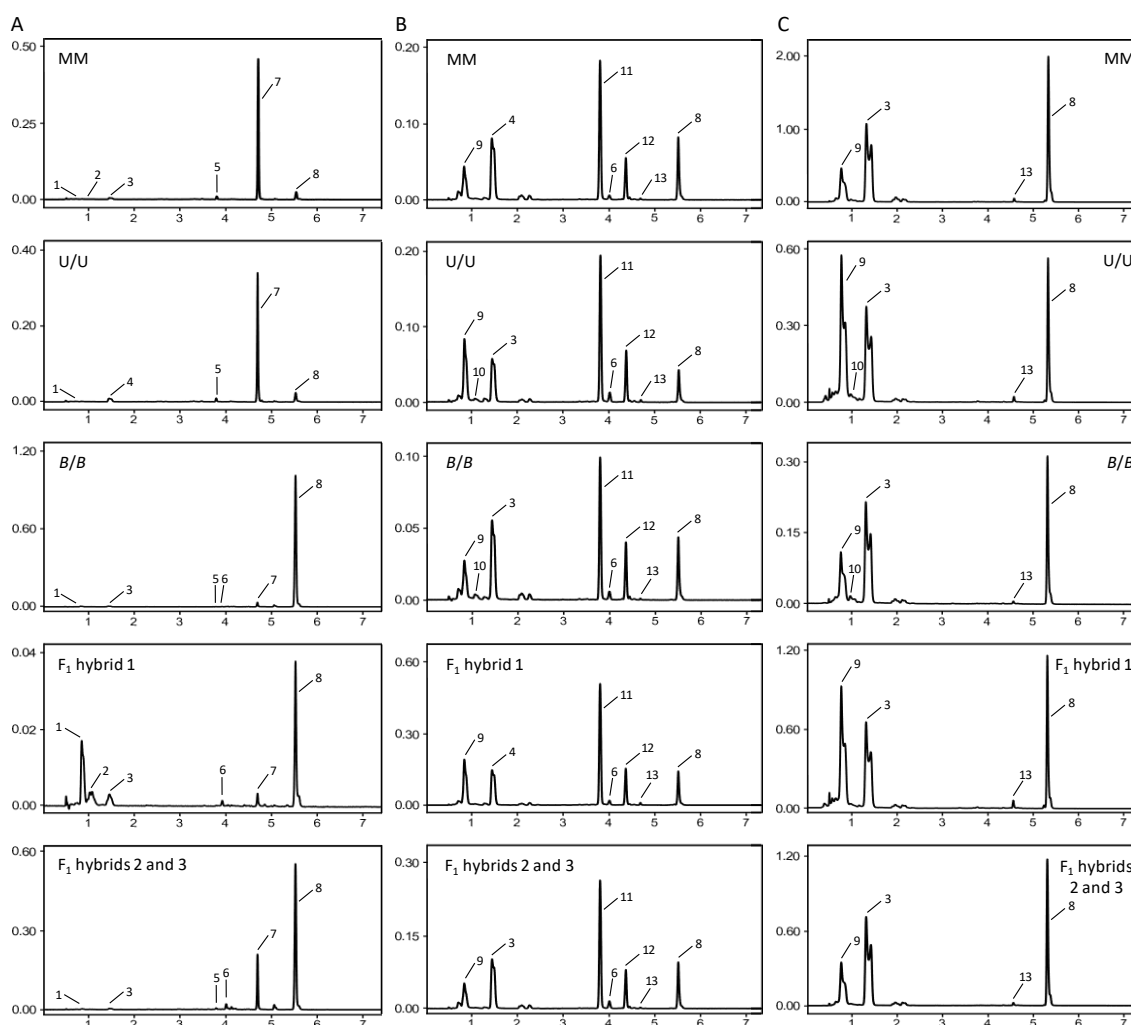
Supplementary Figure 1.1. Standard curves of the selected isoprenoid compounds generated on the HPLC system (A – J) at the indicated light wavelengths [nm]. For each of the compounds, three separate curves were prepared and the individual runs (Run 1 – 3) were overlaid on top of the averaged peak areas ($\bar{x} \pm \text{SD}$) across the full range of the amounts of the standard tested (top left graphs). The calibration curves were modelled based on the averaged peak areas using linear regression which provided the equation in form of $y = ax + b$, where a is the slope of the line and b – the y-axis intercept. The coefficient of determination, R^2 was calculated to provide a measure of the accuracy of the model. Data points resulting from incorrect sample injections were not included in the analysis. Shifts in the retention times (RT) were evaluated for each compound and displayed as box-and-whisker plots (Tukey's method) with the outliers indicated as individual black points (top right). The normality of RT shift data was verified with Shapiro-Wilk test and analysed either with one-way ANOVA and Tukey *post hoc* test (parametric) or Kruskal-Wallis and Dunn's *post hoc* test (non-parametric) to assess the RT variation between the individual runs. Each dose-response relationship, except violaxanthin, was additionally analysed in the low (bottom left) and high (bottom right) standard ranges. For some data points, the error bars are shorter than the height of the symbol and are therefore, not displayed. * $P < 0.5$, ** $P < 0.01$, *** $P < 0.001$, **** $P < 0.0001$, ns – not significant.

Supplementary Table 1.1. Summary of the coefficients (*a* and *b*) used in quantification of isoprenoids and chlorophylls at the specified light wavelengths (nm). The border value is the average area of the peaks resulting from the injections of 0.10 and 0.25 µg of the standard. Low and high range coefficients are applied to peaks with areas below and above the border value, respectively.

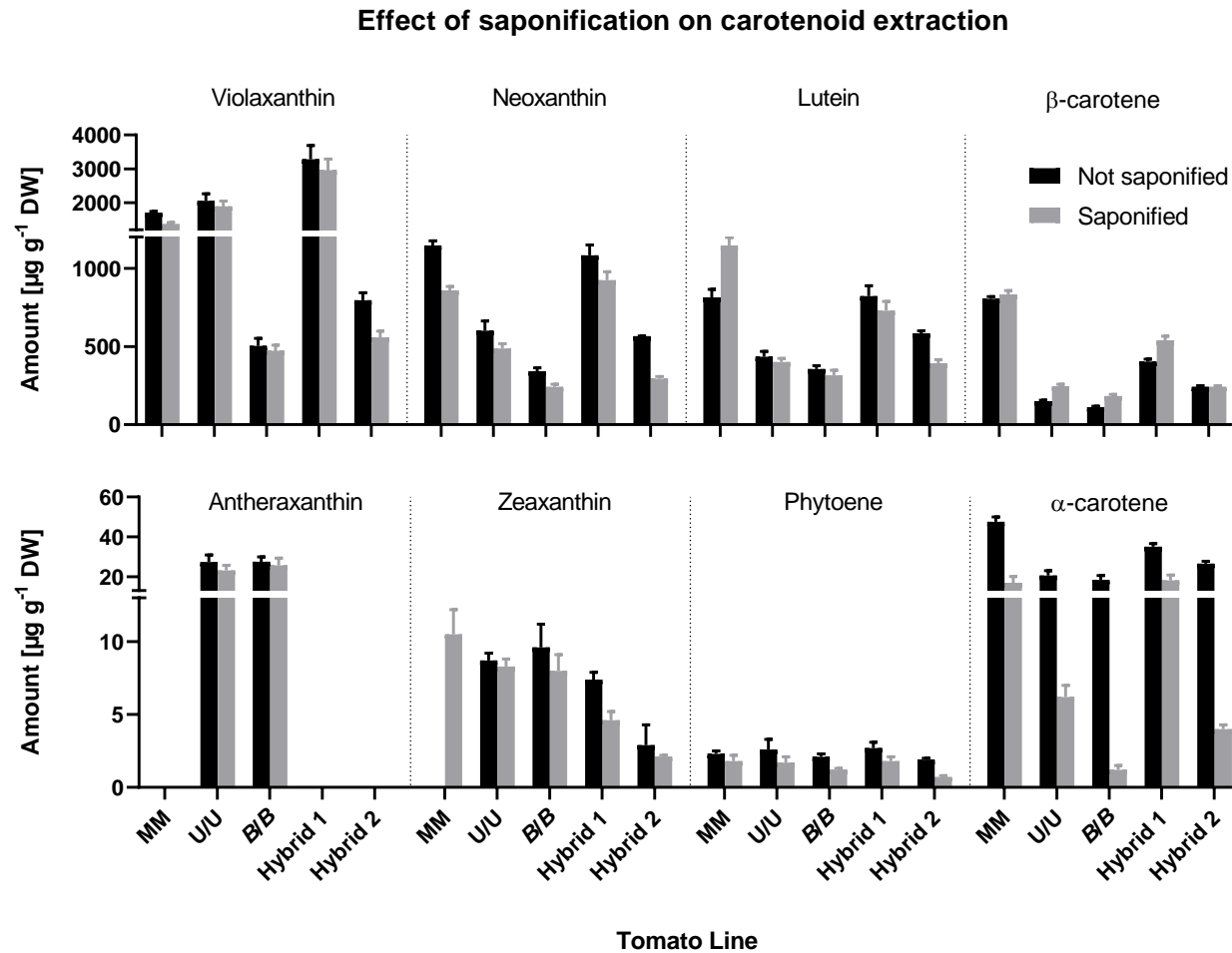
	Low Range		High Range		Border	nm
	<i>a</i>	<i>b</i>	<i>a</i>	<i>b</i>		
HPLC α-tocopherol	366 199	689.5	390 109	-9 509	65 000	292
Antheraxanthin*	10 149 007	9 710	10 938 304	-218 970	1 800 000	450
β-carotene [†]	8 448 965	-23 450	7 554 340	609 355	1 400 000	450
β-cryptoxanthin**	8 448 965	-23 450	7 554 340	609 355	1 400 000	450
Chlorophyll A	1 191 396	1 437	1 399 320	-47 290	190 000	450
Chlorophyll B [‡]	3 552 271	-2 356	4 151 787	-130 542	550 000	450
Lutein	8 981 193	-22 922	8 618 509	199 049	1 500 000	450
Luteoxanthin***	1 534 104	13 787	1 534 104	13 787	400 000	450
Lycopene	6 995 738	-19 697	8 039 860	-374 998	1 200 000	450
Neoxanthin	1 393 058	-2 597	1 689 293	-119 482	230 000	450
Phytoene	6 232 068	-5 896	5 834 916	83 495	1 000 000	286
Violaxanthin	1 534 104	13 787	1 534 104	13 787	400 000	450
Zeaxanthin	10 149 007	9 710	10 938 304	-218 970	1 800 000	450

* calibration curve for zeaxanthin ** calibration curve for β-carotene *** calibration curve for violaxanthin

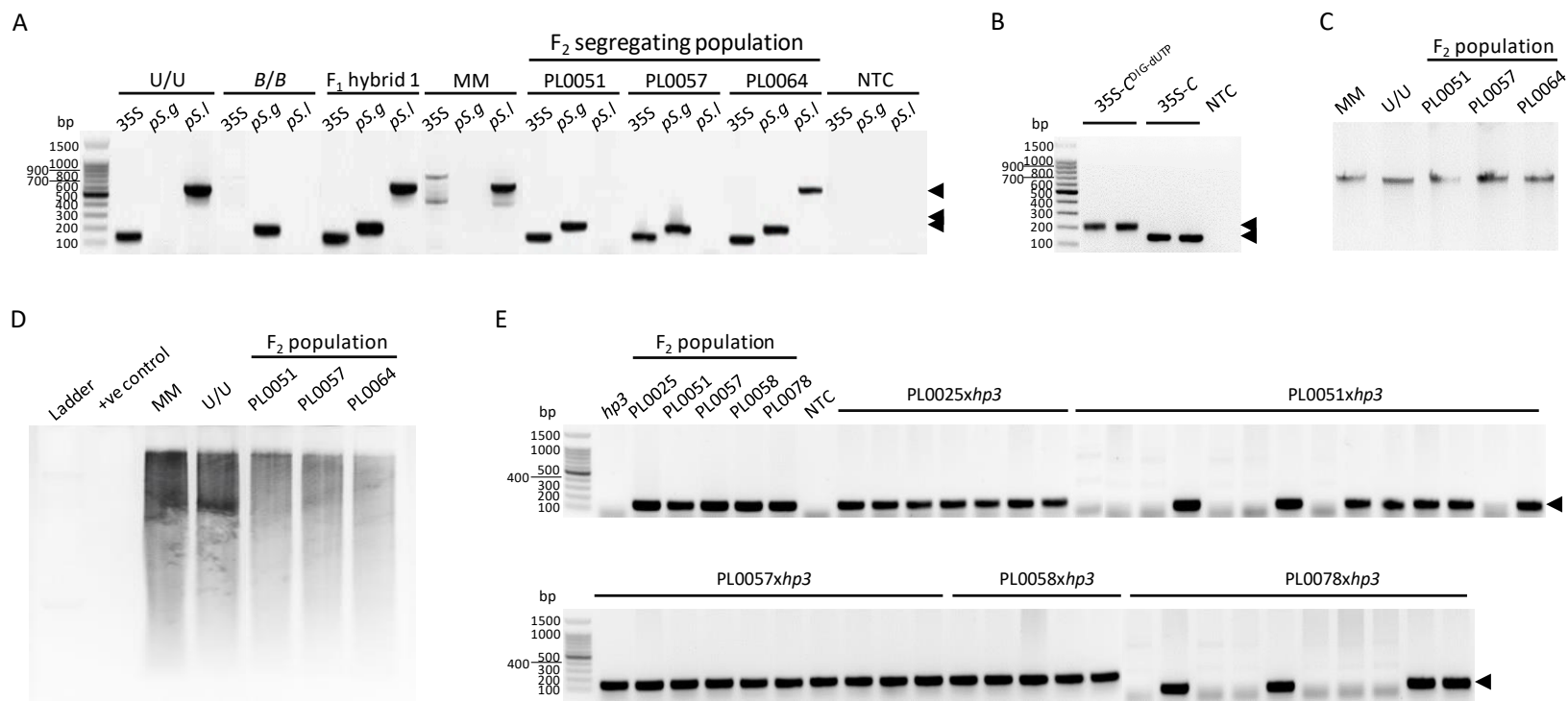
[†] used for quantification of α-carotene [‡] used for quantification of pheophytin B



Supplementary Figure 1.2. UPLC was used to confirm the presence of compounds in the fruit (A), leaf (B) and saponified leaf (C) extracts of the indicated lines at 450 nm. Nearly all compounds found on the HPLC system were identified. 1 – violaxanthin, 2 – luteoxanthin/antheraxanthin co-eluting, 3 – zeaxanthin/lutein co-eluting, 4 – lutein, 5 – γ-carotene, 6 – β-carotene 5,6-epoxide, 7 – lycopene/α-carotene co-eluting, 8 – β-carotene, 9 – neoxanthin/violaxanthin co-eluting, 10 – antheraxanthin, 11 – chlorophyll B, 12 – chlorophyll A, 13 – α-carotene.



Supplementary Figure 1.3. Comparison of leaf carotenoid extracts of the indicated tomato lines without (black bars) and following (grey bars) saponification. Generally, saponification reduced the amounts of extracted carotenoids, except in case of β -carotene, which seemed to be increased following saponification. Zeaxanthin was detected in all lines tested except MM due to a strong overlap with the chlorophyll A peak. Since the pigment profiles of the F_1 hybrids 2 and 3 were very similar, only hybrid no. 2 is shown. The data are presented as the mean of three technical replicates \pm SD; biological replicates, $N = 1$.



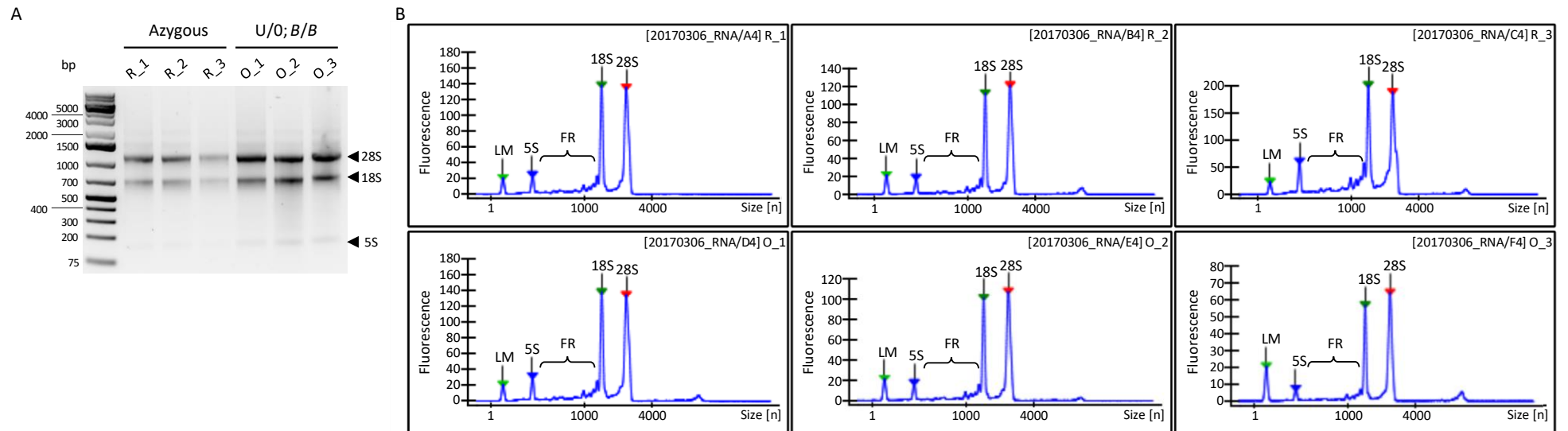
Supplementary Figure 1.4. (A) PCR screen of the F₂ plants used in Southern blotting for the presence of CaMV 35S (35S), *S. galapagense* *CYC-B* (pS.g) and *S. lycopersicum* *CYC-B* (pS.l) against the reference genotypes. U/U – line homozygous for *CrtR-b2* (chromoplast-specific β -carotene hydroxylase) under the control of the CaMV 35S promoter; B/B – line homozygous for *S. galapagense* *CYC-B* (chromoplast-specific lycopene β -cyclase); F₁ hybrid 1 – parent of the F₂ population; MM – Moneymaker; NTC – no-template control. Black arrowheads indicate positions of predicted fragments. (B) Comparison of the 35S-*CrtR-b2* DIG-dUTP labelled probe (35S-C^{DIG-dUTP}) against the unlabelled 35S-*CrtR-b2* fragment (35S-C). (C) Verification of the quality of genomic DNA of the plants selected from the F₂ population and used in Southern blot. (D) Separation of genomic DNA used in Southern blot analysis following its digestion with *Hind*III. The ladder and the positive control (35S-*CrtR-b2*-TOPO vector) are not clearly visible on the gel. (E) Full screen of the F₁ progeny of the selected F₂ plants crossed with the *hp3* line for the 35S-*CrtR-b2* fragment indicating the presence of transgenic *CrtR-b2*. Each gel line corresponds to an individual plant.

```

PDS_Template  TTTTATTAGCTATCTAGGTTCTTGCTGCCTTGGGGGTGGAGGGGTAAGAGAGAACTTAATTTCAGTGTACCTGCAGTTTTGGAAAAGAGTCTACAGATCTACTTCTCAGTTTTATTGGTTGTGGAAATCTGTACAAATATAAGCATTGCCAAAAGTTGGAGAAGTTAAAC
PDS_TOPO      -----TCTAGGTTCTTGCTGCCTTGGGGGTGGAGGGGTAAGAGAGAACTTAATTTCAGTGTACCTGCAGTTTTGGAAAAGAGTCTACAGATCTACTTCTCAGTTTTATTGGTTGTGGAAATCTGTACAAATATAAGCATTGCCAAAAGTTGG-----
                *****
CaMv_Template  AGATCAGAAGTACTATTCCAGTATGGACGATTCAAGGCTTGCTTCACAAACCAAGGCAAGTAATAGAGATTGGAGTCTCTAAAAAGGTAGTCCCACTGAATCAAAGCCATGGAGTCAAAGATTCAAATAGAGGACCTAACAGAACTCGCCGTAAGAGCTGGCGAACAGTT
35S_TOPO      -----TATGGACGATTCAAGGCTTGCTTCACAAACCAAGGCAAGTAATAGAGATTGGAGTCTCTAAAAAGGTAGTCCCACTGAATCAAAGCCATGGAGTCAAAGATTCAAATAGAGGACCTAACAGAACTCGCCGTAAGAGAC-----
                *****

```

Supplementary Figure 1.5. MAFFT alignment of the *PDS* (top) and CaMV 35S (bottom) fragments cloned into their respective TOPO vectors. Both fragments were sequenced with the T7 forward primer. Primers used for the amplification of the *PDS* and CaMV 35S fragments in RT-qPCR are underlined; asterisks (*) indicate the matching sequences; mismatched nucleotides are highlighted in grey. For RT-qPCR, occasional mismatches outside the primer annealing sites are acceptable.



Supplementary Figure 1.6. (A) Assessment of the integrity of total RNA on agarose gel. The positions of the ribosomal subunits are indicated with black arrowheads. The DNA ladder is used for resolution and does not indicate the sizes of the RNA bands. (B) Electropherograms of the samples provide information on the level of RNA degradation. RIN numbers, indicating highly degraded (RIN of 1) and the most intact (RIN of 10) samples, are computed based on the entire electrophoretic trace. Top row – F₂ plants of the Azygous line (PL0131, PL0133 and PL0136; O/O; +/+ genotype); bottom row – F₂ plants of the U/O; B/B line (PL0070, PL0078, PL0083). 5S, 18S and 28S – ribosomal subunits; FR – Fast Region; LM – Lower Marker.

Supplementary Table 1.2. Summary of the quality of RNA samples used in preparation of the cDNA library for sequencing. Fast Area corresponds to the area of the Fast Region between the 5S and 18S ribosomal peaks (Supplementary Figure 1.6B); anomalies in the Fast Region are considered critical. R – red; O – orange; RIN – RNA Integrity Number.

Plant ID	Tomato line	Total Conc. [ng ul ⁻¹]	Quality Score (RIN)	rRNA Fast Area Ratio*	rRNA Height Ratio [28S/18S]	18S % Total*	28S % Total*	5S % Total*
R_1	Azygous	367.11	8.7	0.19	0.99	22.1	41.7	3.7
R_2		292.19	8.7	0.15	1.09	20.0	36.9	3.6
R_3		625.42	7.9	0.25	0.95	16.2	33.6	5.0
O_1	U/O; B/B	399.00	8.3	0.18	0.99	20.3	32.1	4.5
O_2		241.58	8.8	0.16	1.08	22.0	38.0	3.9
O_3		142.74	9.2	0.13	1.15	20.1	44.4	2.9

* Percent of total area

Supplementary Table 1.3. List of significantly upregulated genes in the U/0; B/B line with over a 2.83-fold increase compared to the Azygous reference line; inf – infinite increase.

Gene ID	Gene Name	Identified Function	Fold Increase	References
CYP450 family				
<i>Solyc04g050620.3</i>	CYP736A1	- TCP transcription factor involved in growth, development and defense mechanism; induces biosynthesis of brassinosteroids, jasmonic acid and flavonoids - may be involved in regulation of floral tissues developing genes and leaf blade development in tomato plants	7.8	Li, 2015; Vasav & Barvkar, 2019
<i>Solyc04g071800.3</i>	CYP92B7	- contains motifs present in bean phenylalanine ammonia-lyase (PAL); co-ordinates regulation of phenylpropanoid metabolism - PAL catalyses the first step of the general phenylpropanoid pathway, a step that is common to the production of many metabolites including flavonoids, coumarins, phytoalexins, phenolic volatiles, hydrolysable tannins and lignin	9.3	Bate <i>et al.</i> , 1998; Halpin, 2004; Vasav & Barvkar, 2019
<i>Solyc12g006460.2</i>	CYP88B1 (GAME4)	- involved in a later step of the steroidal glycoalkaloids (SGAs) biosynthetic pathway	22.2	Cárdenas <i>et al.</i> , 2016; Hameed <i>et al.</i> , 2018; Vasav & Barvkar, 2019
<i>Solyc05g055400.3</i>	CYP77A19	- hydroxylates lauric acid (C12:0) on position ω -1 to ω -5; oxidises fatty acids with chain length ranging from C12 to C18; catalyses hydroxylation of 16-hydroxypalmitic acid leading to dihydroxypalmitic (DHP) acids, the major C16 cutin and suberin monomers; produces epoxides from linoleic acid (C18:2) - induced by methyl jasmonate	23.5	Grausem <i>et al.</i> , 2014
<i>Solyc04g051730.1</i>	CYP96A15	- midchain alkane hydroxylase (MAH); responsible for formation of secondary alcohols and ketones in stem cuticular wax	inf	Greer <i>et al.</i> , 2007
Carotenoid biosynthesis				
<i>Solyc12g006510.2</i>	Terpene cyclase/mutase family member	- triterpenoid biosynthetic process - terpenoids comprise the most chemically and structurally diverse family of natural products including steroids and carotenoids	3.5	Christianson, 2017
<i>Solyc01g102950.3</i>	Lycopene β/ϵ -cyclase	- catalyses the addition of β -ionone end groups to the end of lycopene molecules; catalyses the single ϵ -cyclisation reaction which converts lycopene to δ -carotene and neurosporene to α -zeaxanthin - required for lutein biosynthesis	3.7	Cunningham <i>et al.</i> , 1996
<i>Solyc06g074240.2</i>	Chromoplast-specific lycopene β -cyclase	- responsible for formation of β -carotene from lycopene; introduces β -end rings	4.2	
<i>Solyc04g057980.3</i>	Orange Ripening	- part of the NADH dehydrogenase (NDH) complex; supports nonphotochemical electron fluxes from stromal electron donors to plastoquinone - essential for the fruit ripening process	5.0	Nashilevitz <i>et al.</i> , 2010
<i>Solyc03g007960.3</i>	β -carotene hydroxylase 2	- non-heme diiron carotene β -hydroxylase involved in biosynthesis of β -derived xanthophylls	19.8	D'Ambrosio <i>et al.</i> , 2011

Supplementary Table 1.3. Continued (2/18).

Gene ID	Gene Name	Identified Function	Fold Increase	References
Lipid metabolism				
<i>Solyc01g094010.3</i> <i>Solyc12g010910.2</i> <i>Solyc04g010250.3</i>	α/β -hydrolases superfamily protein	- lipid metabolic processes	3.2 – 5.6	Lo <i>et al.</i> , 2004
<i>Solyc07g056320.3</i>	Glycerol-3-phosphate acyltransferase	- involved in fruit cutin biosynthesis - overexpression improves chilling tolerance in tomato	4.5	Sui <i>et al.</i> , 2007; Petit <i>et al.</i> , 2016
<i>Solyc12g044820.2</i>	ABC transporter-like family protein	- protein involved in transmembrane transport and lipid metabolism	4.8	Ofori <i>et al.</i> , 2018
<i>Solyc09g090510.3</i>	Cyclopropane-fatty-acyl-phospholipid synthase	- involved in lipid biosynthesis	4.9	Bao <i>et al.</i> , 2002
<i>Solyc05g005535.1</i> <i>Solyc04g039820.2</i>	Acetyl-coenzyme A carboxylase carboxyl transferase subunit β , chloroplastic	- component of the acetyl coenzyme A carboxylase (ACC) complex - involved in fatty acid biosynthesis, long-chain fatty acid biosynthesis, malonyl-CoA biosynthesis	6.1 – inf	Ke <i>et al.</i> , 2000
<i>Solyc08g067410.2</i> <i>Solyc09g083050.3</i>	3-ketoacyl-CoA synthase (KAS)	- involved in fatty acid (very long chain fatty acids between 20 and 26 carbons in length) and wax biosynthesis - downregulated by darkness and low temperature; upregulated by salt, drought and osmotic stress - mutants have thinner stems with altered wax composition and are more sensitive to dehydration - partial loss of KAS activity in <i>Arabidopsis</i> results in a temperature-dependent decrease in fatty acid production in plastids and hypersensitivity of PSII to low temperature (KAS mutation accelerates PSII photodamage); de novo biosynthesis of fatty acids plays a critical role in the response of the photosynthetic machinery to low temperatures - the full activity of KAS is required for the biogenesis of the intact electron transport machinery in thylakoid membranes and is especially important for the process of responding to low temperatures	6.2 – 8.3	Todd <i>et al.</i> , 1999; Blacklock & Jaworski, 2006; Trenkamp <i>et al.</i> , 2004; Takami <i>et al.</i> , 2010
<i>Solyc09g015080.3</i>	Sec14p-like phosphatidylinositol transfer family protein	- has lipid binding and transport activity - provides mechanisms for crosstalk between lipid metabolism and lipid signalling	7.6	Bankaitis <i>et al.</i> , 2010
<i>Solyc12g042890.2</i>	Acyl-protein thioesterase 2 (TE2s)	- plant TEs terminate the acyl-acyl carrier protein track of fatty acid biosynthesis and play an essential role in determining the amount and composition of fatty acids entering the storage lipid pool	8.3	Mayer & Shanklin, 2005
<i>Solyc02g079510.3</i>	Peroxidase	- involved in lipid homeostasis; controls metabolic flux and availability of fatty acids	9.6	Kohlwein <i>et al.</i> , 2013
<i>Solyc12g096930.2</i>	Caleosin	- has peroxygenase activity and Ca ²⁺ -binding domains; associated with lipid bodies; involved in generation of oxidised fatty acids (FAs) in stress related signalling pathways involving ABA and salicylic acid - involved in oxylipin metabolism during biotic and abiotic stress responses - oxylipins are lipophilic signalling molecules derived from the oxidation of polyunsaturated FAs; in plants the C18 polyenoic FAs are the major precursors of oxylipins - oxylipin pathway is involved in volatiles biosynthesis – the pathway uses free unsaturated FAs with the sequential action of lipoxygenase, hydroperoxide lyase and alcohol dehydrogenase to produce volatile aldehydes and alcohols	inf	Yilmaz, 2001; Weichert <i>et al.</i> , 2002; Partridge & Murphy, 2009

Supplementary Table 1.3. Continued (3/18).

Gene ID	Gene Name	Identified Function	Fold Increase	References
Lipid metabolism				
<i>Solyc06g034040.1</i>	Oleosin	<ul style="list-style-type: none"> - involved in lipid storage, response to freezing, seed oil biogenesis, transmembrane transport - promotes formation of oil bodies and regulates their size; interacts with lipid and phospholipid moieties of lipid bodies; oleosin-coated lipid bodies allow for storage of volatile sesquiterpenes - overexpression of oleosins increases oil content, decreases size of oil bodies and increases seed freezing tolerance - lack of oleosins promotes fusion of oil bodies in the cells during seed maturation 	inf	Chapman <i>et al.</i> , 2012; Vanhercke <i>et al.</i> , 2017; Delatte <i>et al.</i> , 2018; Shimada <i>et al.</i> , 2018
<i>Solyc12g010590.2</i>	O-acyltransferase WSD1	<ul style="list-style-type: none"> - bifunctional wax ester synthase/diacylglycerol acyltransferase - involved in cuticular wax biosynthesis; upregulated in the stem epidermis during active wax synthesis 	inf	Xu <i>et al.</i> , 2017
Steroid metabolism				
<i>Solyc07g043500.1</i> <i>Solyc12g088710.2</i> <i>Solyc12g098580.1</i>	Glycosyltransferases	<ul style="list-style-type: none"> - involved in biosynthesis of sterol glycosides (SGs) and acyl sterol glycosides (ASGs) which are the most abundant sterol derivatives in higher plants; act on several sterols like sitosterol, campesterol and stigmasterol; involved in biosynthesis of steroidal alkaloids and upstream isoprenoids in the plant mevalonate pathway - glycosylated sterols and free sterols are primarily located in cell membranes where in combination with other membrane-bound lipids play a key role in modulating their properties and functioning - steroidal glycoalkaloids (SGAs) are cholesterol-derived molecules produced by solanaceous species; they contribute to pathogen defence but are toxic to humans and considered anti-nutritional - act on abscisic acid (ABA) but not on auxin (IAA); differentially regulated in response to biotic and abiotic stress conditions as well as upon treatment with abscisic acid and methyl jasmonate - highly expressed during fruit ripening and flower development - volatile compounds that constitute the fruit aroma of ripe tomato are often sequestered in glycosylated form 	4.9 – 15.1	Louveau <i>et al.</i> , 2011; Cárdenas <i>et al.</i> , 2016; Ramirez-Estrada <i>et al.</i> , 2017; Nakayasu <i>et al.</i> , 2018
<i>Solyc00g009120.3</i>	Short-chain dehydrogenase/reductase family protein	<ul style="list-style-type: none"> - responsible for structural diversity and toxicity of steroidal specialised metabolites 	6.1	Sonawane <i>et al.</i> , 2018
Flavonoid metabolism				
<i>Solyc12g006380.2</i>	2-oxoglutarate-dependent dioxygenase (2-ODD)	<ul style="list-style-type: none"> - involved in glucosinolate, flavonoid, alkaloid, gibberellin (GA) and amino acid metabolism - tricarboxylic acid (TCA) cycle intermediate 2-oxoglutarate (2-OG) is used as an obligatory substrate in a range of oxidative reactions catalysed by 2-OG-dependent dioxygenases; TCA cycle plays an important role in modulating the rate of flux from 2-OG to amino acid metabolism 	5.1	Farrow & Facchini, 2014
Cell wall related				
<i>Solyc11g066720.2</i>	UDP-apiiose/xylose synthase	<ul style="list-style-type: none"> - synthesises an essential cell wall precursor; enhances protection against oxidative stress as UV irradiation of plant cell suspension cultures causes a large increase in UDP-apiiose/UDP-xylose synthase (AUX) mRNA activity - D-apiiose the only plant cell wall monosaccharide with a branched carbon skeleton and is found in rhamnogalacturonan II (RG-II), apiogalacturonan, and several apioglycosides - nearly 1 200 glycosides contain apiiose (phenolics, terpenes and terpenoids, saponines, cyanogenic glucosides, aliphatic and aromatic alcohols, lactones and at least one alkaloid) 	2.9	Mølhøj <i>et al.</i> , 2003; Pičmanová & Møller, 2016

Supplementary Table 1.3. Continued (4/18).

Gene ID	Gene Name	Identified Function	Fold Increase	References
Cell wall related				
<i>Solyc04g082140.3</i> <i>Solyc06g009190.3</i>	Pectinesterase	- has oxidoreductase activity; modifies cell walls by demethylesterification of the cell wall pectin into pectate and methanol - silencing of the gene in fruit results in an enhancement to the rate of softening during ripening	2.9 – 11.0	Phan <i>et al.</i> , 2007
<i>Solyc02g082920.3</i> <i>Solyc10g055820.2</i> <i>Solyc07g009500.2</i>	Chitinase	- hydrolyses chitin, chitosan, lipochitooligosaccharides, peptidoglycan, arabinogalactan and glycoproteins containing N-acetylglucosamine; also involved in plant abiotic stress responses (osmotic, salt, cold, wounding and heavy metal stresses) - involved in defense response to fungus; plants overexpressing a chitinase and/or a β -1,3-glucanase are less susceptible to fungal attacks - differentially regulated by wounding, pathogen challenge, methyl jasmonate, ethylene, salicylic acid and gibberellin; jasmonic acid induced class I and class IV but not class II chitinase, whereas salicylic acid induced all three classes of chitinase	3.0 – 7.2	Grover, 2012; Cao & Tan, 2019
<i>Solyc08g005800.3</i>	Pectinacetylsterase family protein	- hydrolyses acetyl esters in homogalacturonan regions of pectin; involved in cell wall organisation	3.2	de Souza <i>et al.</i> , 2014
<i>Solyc05g005560.4</i>	Polygalacturonase isoenzyme 1 β -subunit	- non-catalytic subunit of the polygalacturonase isozyme 1 (PG1); necessary and sufficient to convert the polygalacturonase from its monomeric form PG2 to its heterodimeric form PG1; seems to limit the depolymerisation and solubilisation of cell wall polyuronides during ripening - overexpression of the β -subunit of polygalacturonase 1 decreases pectin content and cell adhesion and increases abiotic stress sensitivity in rice	3.4	Liu <i>et al.</i> , 2014
<i>Solyc04g071650.3</i> <i>Solyc10g083670.2</i>	Cellulose synthase	- involved in plant cellulose biosynthesis and polymerisation of the backbones of noncellulosic polysaccharides (hemicelluloses) of plant cell wall	3.4 – 29.4	Wightman & Turner, 2010
<i>Solyc09g008320.3</i> <i>Solyc03g031800.3</i>	Xyloglucan endotransglucosylase/hydrolase (XTH)	- catalyses xyloglucan endohydrolysis (XEH) and/or endotransglycosylation (XET); cleaves and re-ligates xyloglucan polymers, an essential constituent of the primary cell wall, and thereby participates in cell wall construction of growing tissues; XET is thought to promote cell expansion by breaking the xyloglucan cross-links between cellulose microfibrils before reforming them - involved in maintenance of the structural integrity of the cell wall during fruit development - decrease in XTHs expression, and the subsequent decrease in activity during ripening may contribute to fruit softening	3.5 – 5.5	Miedes & Lorences, 2009
<i>Solyc04g072850.3</i>	β -D-xylosidase	- involved in modifications of the cell wall of developing and ripening tomato fruit; participates in the breakdown of xylans and/or arabinoxylans - its activity is highest during early fruit growth, before decreasing during later development and ripening	3.6	Itai <i>et al.</i> , 2003
<i>Solyc08g060970.3</i>	Polygalacturonase AF118567	- involved in cell wall organisation and in the local and systemic activation of defense responses against herbivores and pathogens	3.6	Bergey <i>et al.</i> , 1999

Supplementary Table 1.3. Continued (5/18).

Gene ID	Gene Name	Identified Function	Fold Increase	References
Cell wall related				
<i>Solyc02g092215.1</i>	Galactosyl transferase GMA12/MNN10 family protein	- involved in biosynthesis of xyloglucan	4.1	Faik <i>et al.</i> , 2002
<i>Solyc12g009300.2</i>	Sucrose synthase (SuSy)	- affects carbon partitioning to increase cellulose production and altered cell wall ultrastructure - overexpression of SuSy alters secondary cell wall cellulose content without influencing plant growth; elevated concentration of cellulose is associated with an increase in cell wall crystallinity without affecting the secondary wall microfibril angle	4.6	Coleman <i>et al.</i> , 2009; Barrero-Sicilia <i>et al.</i> , 2011
<i>Solyc02g087790.2</i>	Aldose 1-epimerase	- converts α -aldose to the β -anomer - upregulated by water stress; participates in plant defence mechanisms	5.6	Alvarez <i>et al.</i> , 2008
<i>Solyc05g005550.3</i>	Polygalacturonase non-catalytic subunit AroGP2	- involved in cell wall organisation, cell wall biogenesis/degradation, fruit ripening - overexpression accelerates stomatal opening and changes in molecular mass and abundance, which affect the wall mechanics	6.2	Atkinson <i>et al.</i> , 2002; Rui <i>et al.</i> , 2017
<i>Solyc12g014620.2</i>	14 kDa proline-rich protein DC2.15	- involved in cell wall modification; cross-links each other or links to other components (i.e., saccharides and lignin) to form effective protection layer after pathogen infection or wounding - upregulation contributes to stress-tolerance by reinforcing cell walls	6.3	Fan <i>et al.</i> , 2014; Lu <i>et al.</i> , 2015
<i>Solyc05g005080.3</i>	Endo-1,4- β -glucanase (EG)	- has cellulase activity; affects secondary cell wall development by contributing to the cell wall crystallisation process - expressed as a response to drought in drought-tolerant genotypes - constitutive overexpression in transgenic tomato fruit does not increase xyloglucan depolymerisation or fruit softening - degradation of a proportion of matrix glycans other than xyloglucan does not result in fruit softening; fruit softening is not limited by the amount of EGase activity present during ripening	6.5	Harpster <i>et al.</i> , 2002; Glass <i>et al.</i> , 2015
<i>Solyc04g063210.3</i>	Caffeoyl-CoA O-methyltransferase (CCoAOMT)	- participates in lignin biosynthesis - involved in the reinforcement of the plant cell wall in response to wounding or pathogen challenge by the increased formation of cell wall-bound ferulic acid polymers	7.5	Zhong <i>et al.</i> , 2000
<i>Solyc01g059965.1</i>	β -1,3-glucanase	- breaks down β -1,3-glucans such as callose or curdlan; callose is produced in response to wounding, infection by pathogens, aluminium and abscisic acid - plays a key role in cell division, trafficking of materials through plasmodesmata, withstanding abiotic stresses and flower formation through to seed maturation; defends plants against fungal pathogens either alone or in association with chitinases and other antifungal proteins - differentially regulated by wounding, methyl jasmonate, ethylene, and gibberellin in tomato seeds and leaves	7.7	Balasubramanian <i>et al.</i> , 2012; Gupta <i>et al.</i> , 2013; Cao & Tan, 2019
<i>Solyc05g014000.3</i>	Pectatelyase	- involved in the maceration and soft rotting of plant tissue	22.2	Marín-Rodríguez <i>et al.</i> , 2002

Supplementary Table 1.3. Continued (6/18).

Gene ID	Gene Name	Identified Function	Fold Increase	References
Cell wall related				
<i>Solyc03g083770.1</i>	Plant invertase/pectin methyltransferase inhibitor superfamily protein	- involved in pectin catabolic process and cell wall modification - could be part of a plant defense machinery against necrotrophs activated by both jasmonic acid and ethylene aimed to maintain cell wall integrity, preventing excessive damage to host tissues	inf	Lionetti <i>et al.</i> , 2017
Photosynthesis and related				
<i>Solyc10g007290.3</i>	Phosphoenolpyruvate carboxylase	- involved in carbon fixation - related to rapid growth of tomato fruit	2.9	Guillet <i>et al.</i> , 2012
<i>Solyc09g083190.3</i>	NAD(P)H dehydrogenase 18	- photosynthetic NDH subcomplex B5 - catalyses the transfer of electrons from NADH and NADPH to several quinones in vitro; may act as detoxification enzyme and protect against auxin-induced oxidative stress	3.0	Peng <i>et al.</i> , 2009; Ifuku <i>et al.</i> , 2011
<i>Solyc06g060340.3</i>	Photosystem II subunit S (PsbS)	- involved in non-photochemical quenching – maintains the balance between dissipation and utilisation of light energy to minimise generation of oxidising molecules, thereby protecting the plant against photo-oxidative damage - plants with increased PsbS expression show less stomatal opening in response to light, resulting in a 25% reduction in water loss per CO ₂ assimilated under field conditions	3.1	Głowacka <i>et al.</i> , 2018
<i>Solyc01g079470.3</i>	CP12	- acts as a linker essential in the assembly of a core complex of PRK/GAPDH; coordinates the reversible inactivation of chloroplast enzymes GAPDH and PRK during darkness in photosynthetic tissues - overexpression increases chilling tolerance and promotes growth with increased plant height and fresh weight	3.1	Li <i>et al.</i> , 2018a
<i>Solyc07g063600.3</i>	Chlorophyll a-b binding protein, chloroplastic	- the light-harvesting chlorophyll a/b-binding (LHCB) proteins are the apoproteins of the light-harvesting complex of photosystem II - enables more efficient absorption of light energy; involved in cellular response to ABA stimulus, cold and desiccation; required for stomatal response to ABA - the light-harvesting complex (LHC) functions as a light receptor – it captures and delivers excitation energy to photosystems with which it is closely associated; binds at least 14 chlorophylls (8 Chl-a and 6 Chl-b) and carotenoids such as lutein and neoxanthin - plays a positive role in guard cell signalling in response to ABA and suggests that they may be involved in ABA signalling partly by modulating ROS homeostasis	3.3	Liu <i>et al.</i> , 2013; Pietrzykowska <i>et al.</i> , 2018
<i>Solyc12g036170.2</i>	Photosynthetic NDH subcomplex B4	- part of the chloroplast NDH complex, composed of a mixture of chloroplast and nucleus encoded subunits; component of the NDH subcomplex B - couples the redox reaction to proton translocation, and thus conserves the redox energy in a proton gradient	3.7	Ifuku <i>et al.</i> , 2011
<i>Solyc01g110360.3</i>	Fructose-bisphosphate aldolase	- involved in step 4 of the sub-pathway that synthesises D-glyceraldehyde 3-phosphate and glyceraldehyde phosphate from D-glucose - overexpression of fructose 1,6-bisphosphate aldolase in plastids enhances growth and photosynthesis	4.0	Uematsu <i>et al.</i> , 2012

Supplementary Table 1.3. Continued (7/18).

Gene ID	Gene Name	Identified Function	Fold Increase	References
Photosynthesis and related				
<i>Solyc02g063150.3</i>	RuBP carboxylase small subunit	- increases the catalytic turnover rate and K_m for CO_2 of the enzyme and slightly decreases the specificity for CO_2	4.7	Morita <i>et al.</i> , 2014
<i>Solyc10g050990.1</i>	Pyruvate kinase	- involved in step 5 of the sub-pathway that synthesises pyruvate from D-glyceraldehyde 3-phosphate - overexpression of pyruvate kinase does not influence the activities of other enzymes in the pathway nor it changes intermediary metabolite levels	6.3	Ruijter <i>et al.</i> , 1997
Response to abiotic stress				
<i>Solyc07g048040.1</i>	Calcium-dependent lipid-binding domain-containing protein	- may act as a repressor of abiotic stress response - abiotic stress unbalances cell ion homeostasis and plants tend to readjust it, regulating membrane transporters and channels; abscisic acid (ABA) and the second messenger Ca^{2+} are central in such processes, as they are involved in the regulation of protein kinases and phosphatases that control ion transport activity in response to environmental stimuli	3.2	de Silva <i>et al.</i> , 2011; Diaz <i>et al.</i> , 2016
<i>Solyc01g095140.3</i> <i>Solyc02g062770.2</i>	Late embryogenesis abundant protein (LEA)	- accumulates in response to cellular dehydration - protects other proteins from aggregation due to desiccation or osmotic stresses associated with low temperature	3.2 – inf	Goyal <i>et al.</i> , 2005
<i>Solyc03g019670.3</i>	Non-hemolytic phospholipase C	- differentially expressed under abiotic stresses (salt, cold and drought) and during various developmental stages - promotes responses to ABA and tolerance to hyperosmotic stress	3.3	Peters <i>et al.</i> , 2010
<i>Solyc05g051460.3</i>	Homeobox associated leucine zipper protein	- linked with hormone signalling pathways, especially with ABA sensing and transduction - overexpression confers a hypersensitive response to ABA in roots, a delay in inflorescence stem elongation, rounder rosette leaves, shorter petioles, enhanced branching in the inflorescence stem, tolerance to freezing temperatures, severe drought and salinity; tolerant behaviour is achieved by stabilising cell membranes through the induction of glucanase (GLU) and the genes encoding the pathogenesis related proteins PR2 and PR4 - positively regulates protein phosphatases type 2C (PP2C) and represses PYL5 and PYL8, two ABA receptors, in response to ABA stimulus	3.4	Perotti <i>et al.</i> , 2017
<i>Solyc04g054740.3</i>	Inositol-1-phosphate synthase	- catalyses the first step of <i>myo</i> -inositol biosynthesis, a product that plays crucial roles in plants as an osmoprotectant, transduction molecule, cell wall constituent and production of stress related molecule - overexpression of inositol 1-phosphate synthase enhances level of tolerance to salt stress	3.4	Joshi <i>et al.</i> , 2013; Nisa <i>et al.</i> , 2016
<i>Solyc06g072700.3</i> <i>Solyc01g080070.3</i> <i>Solyc06g036310.3</i>	Heavy metal transport/detoxification superfamily protein	- involved in transport of metallic ions inside the cell, detoxification mechanisms, especially those involved in cadmium tolerance, transcriptional responses to cold and drought and plant-pathogen interactions - has a functional link with SWEET1	3.4 – 4.3	de Abreu-Neto <i>et al.</i> , 2013
<i>Solyc04g054730.3</i>	Sulfate transporter	- involved in response to drought and salinity	3.6	Gallardo <i>et al.</i> , 2014
<i>Solyc09g097760.3</i>	Glycine-rich protein	- overexpression of glycine-rich RNA-binding protein in tomato renders fruits with higher protein content after cold storage	3.7	Ruggieri <i>et al.</i> , 2018

Supplementary Table 1.3. Continued (8/18).

Gene ID	Gene Name	Identified Function	Fold Increase	References
Response to abiotic stress				
<i>Solyc01g010180.3</i>	DEA(D/H)-box RNA helicase family protein	- an RNA helicase found to be required in cellular processes such as pre-mRNA processing and rearranging of ribonucleoproteins (RNP) complexes - regulates salt and drought tolerance and stress-related genes in tomato	4.1	Zhu <i>et al.</i> , 2015
<i>Solyc03g123630.3</i>	Pectin methylesterase	- contributes to a change in cell-wall composition/structure particularly in guard cell walls for regulating cell wall plasticity as well as stromal aperture size, which comprise critical determinants of plant adaptation to heat stress	4.2	Wu <i>et al.</i> , 2018
<i>Solyc10g005960.1</i> <i>Solyc07g045440.1</i>	Fasciclin-like arabinogalactan protein (FLA)	- belongs to a subclass of arabinogalactan proteins (AGPs) that have, in addition to predicted AGP-like glycosylated regions, putative cell adhesion domains known as fasciclin domains - may function in fiber initiation and elongation by affecting AGP composition and the integrity of the primary cell wall matrix; may affect pollen intine formation, possibly by participating in cellulose deposition - can respond to various biotic and abiotic stresses, such as salt stress, cold stress, drought stress, heat stress, and exogenous hormone ABA, pyrabactin and fluridone - application of ABA suppresses the non-redundant role of FLA in the salt response; positively regulates the response to low ABA concentration in roots and is required for the normal expression of ABA- and abiotic stress-induced genes - mutants show a drastic reduction of root elongation growth combined with radial swelling of the elongation zone under salt stress; FLA might act on ABA signal transduction upstream of cell wall deposition	4.2 – 4.3	MacMillan <i>et al.</i> , 2010; Geng-Qing <i>et al.</i> , 2013; Seifert <i>et al.</i> , 2014; Zang <i>et al.</i> , 2015
<i>Solyc10g005690.3</i>	Chloride channel protein	- contributes to a number of plant-specific functions, such as regulation of turgor, stomatal movement, nutrient transport and metal tolerance	4.3	Um <i>et al.</i> , 2018
<i>Solyc04g071615.1</i>	ASR4	- upregulated in plant vegetative organs following exposure to salt stress, osmotic stress or the plant abiotic stress hormone abscisic acid (ABA) - provides adaptation in <i>S. chilense</i> populations that live in extremely dry environments	4.5	Fischer <i>et al.</i> , 2011; Golan <i>et al.</i> , 2014
<i>Solyc03g096290.3</i>	Plasma membrane intrinsic protein 1.7	- ectopic expression increases fruit size and enhances drought tolerance of transgenic tomatoes	4.7	Wang <i>et al.</i> , 2017b
<i>Solyc05g007180.3</i>	Jasmonic acid 1	- involved in methyl jasmonate-induced tomato fruit chilling tolerance possibly by ameliorating the antioxidant enzyme system of fruit and increasing proline and lycopene levels	5.1	Min <i>et al.</i> , 2018
<i>Solyc11g039980.2</i>	ATP synthase subunit α	- F-type ATPases have 2 components, CF ₁ – the catalytic core and CF ₀ – the membrane proton channel; CF ₁ has five subunits: α_3 , β_3 , γ_1 , δ_1 , ϵ_1 ; CF ₀ has three main subunits: a, b and c - produces ATP from ADP in the presence of a proton gradient across the membrane - involved in cold response and acclimation	6.4	Goulas <i>et al.</i> , 2006
<i>Solyc09g007020.2</i>	Pathogenesis-related protein	- accumulation of this protein in post-warmed chilled tomato fruit is a pre-emptive cold stress response and possibly a defense response mechanism related to Cold Stress-Induced Disease Resistance (SIDR) phenomenon	6.8	Goyal <i>et al.</i> , 2016

Supplementary Table 1.3. Continued (9/18).

Gene ID	Gene Name	Identified Function	Fold Increase	References
Response to abiotic stress				
<i>Solyc04g014530.1</i>	Ethylene Response Factor C.2	- enhances freezing tolerance of plants through ethylene biosynthesis and the ethylene signalling pathway; acts possibly by upregulation of polyamine turnover, antioxidant protection and proline accumulation - displays low expression in fruit but shows a negative correlation with <i>trans</i> -lycopene accumulation, suggesting its putative role in fruit ripening	10.1	Abiri <i>et al.</i> , 2017; Zhuo <i>et al.</i> , 2017
<i>Solyc02g084850.3</i>	Abscisic acid and environmental stress-inducible protein TAS14	- involved in cold acclimation, response to ABA, response to water deprivation	43.0	Xiong <i>et al.</i> , 2006
<i>Solyc01g009660.2</i>	Low-temperature-induced 65 kDa-like protein	- involved in responses to abiotic stresses; induced by cold, drought, salt and by ABA	inf	Yamaguchi-Shinozaki & Shinozaki, 1993
<i>Solyc03g096540.3</i>	PLAT domain-containing protein 1	- positive regulator of abiotic stress tolerance (cold, salt stress, water deprivation), involved in the regulation of plant growth; may be a downstream target of ABA signalling pathway	inf	Hyun <i>et al.</i> , 2014
<i>Solyc05g053160.3</i>	AWPM-19-like membrane family protein	- increases dramatically when there is an increase in the level of ABA - upregulation leads to greater tolerance of freezing	inf	Koike <i>et al.</i> , 1997
<i>Solyc04g007790.3</i>	MLP-like protein	- functions as a positive regulator during abscisic acid responses and confers drought tolerance	inf	Wang <i>et al.</i> , 2016
<i>Solyc08g080480.3</i>	Monomeric α -amylase inhibitor	- protein localised mainly in the plasma membranes of nutrient reservoir activity - induced by abscisic acid, salt and drought - transgenic plants overexpressing the gene were more tolerant to salt and drought stresses and showed significantly lower amylase activity and glucose and malic acid levels than non-transgenic wild type (WT) plants (inhibition of amylase activity leads to a closure of stomatal apertures and thus improves plant tolerance to salt and drought); under salt stress, the root cells of the transgenic plants secreted more Na ⁺ and guard cells took up more Ca ²⁺ ions	inf	Xiao <i>et al.</i> , 2013
<i>Solyc12g098130.1</i>	Glucose-6-phosphate isomerase, cytosolic 1	- synthesises D-glyceraldehyde 3-phosphate and glycerone phosphate from D-glucose - downregulated by drought stress; upregulated by ABA - overexpression plays a significant role in glucose metabolism, starch hydrolysis and sucrose synthesis - drought stress leads to a reduction in carbon fixation, which is ascribed physiologically to the closing of stomata in the leaves and attributed biochemically to a decrease in photosynthesis altering the carbohydrate metabolic equilibrium	inf	Seong <i>et al.</i> , 2013
Development and stress responses				
<i>Solyc01g097510.3</i>	Annexin 3	- Ca ²⁺ -dependent phospholipid binding; pollen development, germination, tube growth; response to cold, heat, salt stress, water deprivation - may be involved in secretion and fruit ripening; interacts with enzyme callose (1,3- β -glucan) synthase	2.8	Mortimer <i>et al.</i> , 2008
<i>Solyc11g013130.2</i>	Cysteine-rich/transmembrane domain protein A	- modulates resistance against pathogens including oomycetes and fungi; controls ABA-mediated signalling pathways; regulates flowering time in response to stress (e.g. UV-C), polar lipid content; promotes phosphatidylinositol (PI) and 18:0 but prevents 18:2 and 18:3 polar lipids accumulation	2.9	Venancio & Aravind, 2010

Supplementary Table 1.3. Continued (10/18).

Gene ID	Gene Name	Identified Function	Fold Increase	References
Development and stress responses				
<i>Solyc11g072480.2</i>	Tetraspanin	- may serve as molecular facilitators, collecting proteins together to improve the stability and activity of signalling complexes; also implicated in membrane fusion, cell motility, and cell aggregation - tetraspanins interact with each other or with other membrane proteins to form tetraspanin-enriched microdomains that play important roles in development, pathogenesis and immune responses via facilitating cell-cell adhesion and fusion, integration of biotic and abiotic stress signalling, ligand binding and intracellular trafficking	2.9	Mani <i>et al.</i> , 2015; Reimann <i>et al.</i> , 2017
<i>Solyc02g080530.3</i> <i>Solyc02g079500.4</i> <i>Solyc04g071900.3</i> <i>Solyc01g006290.3</i> <i>Solyc04g064690.3</i>	Peroxidase	- involved in removal of H ₂ O ₂ , oxidation of toxic reductants, biosynthesis and degradation of lignin, suberisation, auxin catabolism, ethylene biosynthesis, response to environmental stresses such as wounding, pathogen attack and oxidative stress - overexpression of peroxidase increases tolerance to the abiotic stresses such as heat and cold stress, high salinity and metal ions in high concentrations and accelerates the growth rate and number of xylem vessels - allows to overcome the growth arrest of cell walls in stress tolerant plants by using ROS-mediated cleavage of cell wall polymers	2.9–10.7	Vicuna, 2005; Tenhaken, 2015
<i>Solyc02g082440.2</i>	NSP-interacting kinase 2	- involved in plant development and defence against geminivirus	3.0	Santos <i>et al.</i> , 2010
<i>Solyc12g008660.1</i>	Zinc finger transcription factor 73	- mostly involved in the response to mannitol, heat, salicylic acid, ethylene or methyl jasmonate treatments	3.0	Xu, 2014
<i>Solyc04g057940.3</i> <i>Solyc01g066740.3</i> <i>Solyc02g069290.3</i>	Transducin/WD40 repeat-like superfamily protein	- WD40 domains act as scaffolding molecules assisting proper activity of other proteins, and are involved in multi-cellular processes; they act as a site of protein-protein interactions or multi-interacting platforms, driving the assembly of protein complexes or as mediators of transient interplay among other proteins - in <i>Arabidopsis</i> , members of WD40 protein superfamily are known as key regulators of plant-specific events, biologically playing important roles in development and also during stress signalling	3.0–3.4	Gachomo <i>et al.</i> , 2014
<i>Solyc04g048900.3</i>	Calreticulin	- high affinity Ca ²⁺ -binding protein in the sarcoplasmic reticulum and endoplasmic reticulum (ER) - involved in providing stress tolerance against different abiotic and biotic stresses, plants growth and development - facilitates the folding of newly synthesised glycoproteins, regulates the Ca ²⁺ homeostasis in the ER lumen and regulates plant defense against biotrophic pathogens	3.2	Jia <i>et al.</i> , 2009
<i>Solyc02g071820.3</i> <i>Solyc02g071880.3</i> <i>Solyc06g074070.3</i>	Receptor-like protein kinase (RPK)	- likely to respond to the external challenges presented by an ever-changing environment - involved in hormonal response pathways, cell differentiation, plant growth and development, self-incompatibility, and symbiont and pathogen recognition - overproduction of RPK enhances abiotic stress tolerance through increased transcription of water stress- and ROS-responsive genes	3.2–4.8	Morris & Walker, 2003; Osakabe <i>et al.</i> , 2010
<i>Solyc11g011920.2</i>	Glutamate decarboxylase	- catalyses the production of GABA; GABA accumulates rapidly when plants are exposed to stress and GABA accumulation functions in defense against drought and insect herbivory - GABA is also involved in regulating metabolic pathways like the Krebs cycle; it additionally acts as a signalling molecule in plant growth and development	3.3	Takayama <i>et al.</i> , 2015; Bown & Shelp, 2016; Scholz <i>et al.</i> , 2017

Supplementary Table 1.3. Continued (11/18).

Gene ID	Gene Name	Identified Function	Fold Increase	References
Development and stress responses				
<i>Solyc12g049400.2</i>	Jasmonate-zim-domain protein	- differentially regulated by methyl jasmonate, gibberellins, auxins and ABA - has important effects on regulating the adaptability to biotic and abiotic stresses and maintaining the normal development in plants; involved in resistance to pathogens, regulates the progression of cell death during host and non-host interactions	3.6	Ishiga <i>et al.</i> , 2013; Wang <i>et al.</i> , 2017c
<i>Solyc04g014400.3</i> <i>Solyc05g026240.2</i> <i>Solyc03g006030.3</i> <i>Solyc10g050110.1</i>	LRR receptor-like kinase (LRR-RLKs)	- has a function in defense against pathogens and development such as cell proliferation, stem cell maintenance, hormone perception, host-specific as well as non-host specific defense response, wounding response, and symbiosis	3.6 – 15.3	Torii, 2004; Wang <i>et al.</i> , 2017a
<i>Solyc07g026650.3</i>	1-aminocyclopropane-1-carboxylate (ACC) oxidase 5	- enzyme involved in the biosynthesis of ethylene; may promote stem elongation by maximising the extensibility cells, possibly by activating ethylene biosynthesis, in response to very-long-chain fatty acids (VLCFAs C20:0 to C30:0)	3.7	Qin <i>et al.</i> , 2007b
<i>Solyc02g070430.3</i>	Gibberellin 2 oxidase	- overexpression of a novel class of gibberellin 2-oxidases decreases gibberellin levels and creates dwarf plants	3.7	Schomburg <i>et al.</i> , 2003
<i>Solyc03g080190.3</i> <i>Solyc04g009860.3</i> <i>Solyc09g008560.3</i>	2-oxoglutarate (2OG) and Fe(II)-dependent oxygenase superfamily protein	- involved in DNA repair, histone demethylation, post-translational modification and iron sensing, gibberellin biosynthesis and catabolism, ethylene biosynthesis, auxin catabolism, salicylic acid catabolism, flavonoid biosynthesis and metabolism	3.8 – 7.1	Farrow & Facchini, 2014
<i>Solyc01g110365.1</i>	Serine/threonine-protein kinase WNK (With No Lysine)-like protein	- regulates flowering time by modulating the photoperiod pathway	4.3	Wang <i>et al.</i> , 2008
<i>Solyc03g025670.3</i>	PAR1 protein	- acts as negative regulator of a variety of shade avoidance syndrome (SAS) responses, including seedling elongation and photosynthetic pigment accumulation; may function in integrating shade and hormone transcriptional networks in response to light and auxin changes - plants overexpressing PAR1 are dwarf with compact rosettes and inflorescences, epinastic leaves, shorter flowering stems and siliques, have a general dark-green phenotype and are insensitive to gibberellin (GA) or high temperature in hypocotyl elongation - PAR1 promotes photomorphogenesis by inhibiting PIF4, which is a key negative regulator of photomorphogenesis – PAR1 directly interacts with PIF4 and blocks PIF4 binding to DNA	4.5	Hao <i>et al.</i> , 2012
<i>Solyc06g035720.3</i>	BAG family molecular chaperone regulator 2	- co-chaperone that regulates diverse cellular pathways, such as programmed cell death and stress response - required for basal immunity against fungal phytopathogens; involved in response to heat and light intensity; induced by heat shock, salicylic acid (SA), ABA, calcium, hydrogen peroxide and pathogen attack - cleavage of BAG6 is necessary for autophagy and fungal resistance in plants; overexpression of BAG6 results in a lesion mimic phenotype; BAG6 cleavage is triggered by pathogen infection or PAMPs	4.5	Doukhanina <i>et al.</i> , 2006; Li <i>et al.</i> , 2016
<i>Solyc01g087540.3</i>	Imidazolonepropionase	- involved in histidine metabolism/GABA biosynthesis - histidine functions in plants as a chelator and transporter of metal ions	4.6	Stepansky & Leustek, 2006

Supplementary Table 1.3. Continued (12/18).

Gene ID	Gene Name	Identified Function	Fold Increase	References
Development and stress responses				
<i>Solyc12g087950.1</i>	AT hook motif DNA-binding family protein	- transcription factor that specifically binds AT-rich DNA sequences related to the nuclear matrix attachment regions (MARs) - regulates flowering, increases seedling establishment, enhances plant biomass and improves plant immunity	5.0	Yun <i>et al.</i> , 2012; Zhao <i>et al.</i> , 2014
<i>Solyc03g112060.3</i>	Quinolate synthase A	- involved in NAD biosynthesis; NAD-consuming events play a part in biotic and abiotic stress responses and development; levels of poly(ADP-ribose) (PAR) that is synthesised from NAD is proportional to stress severity but downregulation of PARP enhances stress tolerance, possibly owing to a decrease in NAD consumption in the plant - ABA synthesis is very sensitive to NADP(H)-dependent processes such as zeaxanthin epoxidase and xanthoxin dehydrogenase; chloroplast NAD kinase is essential for the proper photosynthetic machinery of PSII and the xanthophyll cycle; disturbance of NAD homeostasis shows pleiotropic effects in the response to stresses - since zeaxanthin epoxidase is involved in ABA biosynthesis, ABA-related physiological processes such as stomatal movement may be influenced by chloroplastic NADP biosynthesis	5.2	Hashida <i>et al.</i> , 2009
<i>Solyc10g076710.2</i>	Phosphoinositide phospholipase C	- regulates stress tolerance (cold, water deprivation) and development in plants; involved in lipid catabolic processes - production of the second messenger molecules diacylglycerol (DAG) and inositol 1,4,5-trisphosphate (IP3) is mediated by activated phosphatidylinositol-specific phospholipase C enzymes required for secondary responses to ABA signals	5.2	Singh & Pandey, 2016; Abd-El-Halim & Joosten, 2017
<i>Solyc04g078195.1</i>	Gibberellin regulated protein	- gibberellin-regulated protein that may function in hormonal controlled steps of development such as seed germination, flowering and seed maturation; involved in response to ABA	5.4	Raventos <i>et al.</i> , 2000
<i>Solyc02g068877.1</i>	Phosphate-responsive 1 family protein	- essential for expansion in leaves; involved in response to brassinosteroids; provides protection to plants during chilling and drought stress	5.9	Schröder <i>et al.</i> , 2009
<i>Solyc10g018780.2</i>	Squamosa promoter binding protein (SPB) 8a	- has a role in leaf development, vegetative phase change, flower and fruit development, plant architecture, sporogenesis, gibberellic acid signalling, thermotolerance and toxin response	7.2	Chao <i>et al.</i> , 2017
<i>Solyc11g072600.2</i>	APETALA2d	- developmental regulator that modulates the involvement of ethylene in tomato fruit ripening – negative regulator of fruit ripening; expressed as a drought responsive protein in drought-tolerant genotype; induced by low or high temperature, dehydration or high salinity - overexpression enhances tolerance to salt stress and enhances resistance against pathogen attack	8.5	Park <i>et al.</i> , 2001; Chung <i>et al.</i> , 2010; Müller & Munné-Bosch, 2015
<i>Solyc01g090790.3</i>	bHLH transcription factor	- plays important role in physiological, developmental and metabolic processes; expressed as a drought responsive protein in drought-tolerant plants	9.0	Castilhos <i>et al.</i> , 2004
<i>Solyc02g089250.3</i> <i>Solyc06g074260.3</i>	Pollen Ole e 1 allergen and extensin family protein	- pollen allergen putatively involved in stress responses and metabolic processes such as cell wall metabolism during pollen development	10.7 – 13.8	Chen <i>et al.</i> , 2016

Supplementary Table 1.3. Continued (13/18).

Gene ID	Gene Name	Identified Function	Fold Increase	References
Development and stress responses				
<i>Solyc02g082740.1</i>	Dirigent protein	- imparts stereoselectivity on the phenoxy radical-coupling reaction, yielding optically active lignans from two molecules of coniferyl alcohol in the biosynthesis of lignans, flavonolignans, and alkaloids and thus plays a central role in plant secondary metabolism - involved in modulating cell wall metabolism during abiotic and biotic stress exposure hormonal regulations and developmental processes	12.4	Paniagua <i>et al.</i> , 2017
<i>Solyc01g111145.1</i>	Proline-rich protein (RRP)	- structural protein of cell wall; involved in plant development and environmental stress; significantly downregulated under drought stress; may regulate free cellular proline levels during drought stress by regulating their own gene expression - transcription of PRP in plants is synchronised with the cellular proline concentration under environmental stress in order to provide drought tolerance to plants; downregulation of PRP gene is coupled with simultaneous increase in cellular proline concentration in all tissues under drought stress, except the roots to preserve the available cellular proline to function as osmoprotectant during stress	14.5	Gujjar <i>et al.</i> , 2018
<i>Solyc04g072470.3</i>	Defensin	- has a dual function in defense and development	inf	Stotz <i>et al.</i> , 2009
<i>Solyc03g005940.3</i>	Histone acetyltransferase	- plays vital roles in plant resistance to the bacterial pathogens; regulates plant responses to ABA	inf	Liao <i>et al.</i> , 2016
<i>Solyc03g116975.1</i>	SNARE-interacting KEULE-like protein	- drives membrane fusion and contributes to membrane and protein targeting and delivery; essential to the mechanics of cell growth and development, facilitates a number of homeostatic and evoked responses in plants, from hormone signalling to pathogen defence	inf	Grefen & Blatt, 2008
<i>Solyc08g082790.3</i>	Mechanosensitive channel of small conductance-like 10	- opens in response to stretch forces in the membrane lipid bilayer; provides protection against hypo-osmotic shock, responding both to stretching of the cell membrane and to membrane depolarisation - involved in the wound-triggered early signal transduction pathway and possibly in regulating the positive feedback synthesis of jasmonate	inf	Zou <i>et al.</i> , 2016
<i>Solyc12g036415.1</i>	SAUR-like auxin-responsive protein family	- primary auxin response gene involved in auxin signalling pathway; may affect ethylene receptor signalling and promote plant growth - differentially expressed during abiotic (cold, salt and drought) stresses	inf	Wu <i>et al.</i> , 2012
Defense response				
<i>Solyc07g053720.3</i>	S-alkyl-thiohydroximate lyase-like	- involved in glucosinolate biosynthesis; functions in auxin homeostasis; required for glucosinolate activation in response to pathogens - glucosinolates and their products have a negative effect on many insects, resulting from a combination of deterrence and toxicity	2.9	Tsao <i>et al.</i> , 2002
<i>Solyc02g022850.1</i>	FAD-binding Berberine family protein	- involved in cell wall metabolism; part of the pathogen defense system of plants by forming an inhibitory protein complex with xylan-specific endoglucanase (XEG), which is released by the pathogen to digest the xyloglucan	3.0	Daniel <i>et al.</i> , 2015; Daniel <i>et al.</i> , 2017

Supplementary Table 1.3. Continued (14/18).

Gene ID	Gene Name	Identified Function	Fold Increase	References
Defense response				
<i>Solyc03g058950.3</i>	Inositol hexakisphosphate and diphosphoinositol-pentakisphosphate kinase	- acts in concert with the IP6K kinases to synthesise the diphosphate group-containing inositol pyrophosphates diphosphoinositol pentakisphosphate, PP-InsP5 and bis-diphosphoinositol tetrakisphosphate, (PP)2-InsP4; PP-InsP5 and (PP)2-InsP4 regulate a variety of cellular processes, including apoptosis, vesicle trafficking, cytoskeletal dynamics, and exocytosis - involved in jasmonic acid and ethylene-dependent systemic resistance, involved in vitamin E homeostasis via the regulation of γ -tocopherol biosynthesis; positive regulator of innate immune response against fungi and insects by triggering the production of jasmonate-induced pools of (PP)2-InsP4 and subsequent activation of SCF(CO1) E3 ubiquitin ligase complexes with JAZ proteins	3.1	Desai <i>et al.</i> , 2014; Laha <i>et al.</i> , 2015
<i>Solyc07g007750.3</i>	Defensin protein	- has peptidase inhibitor activity and dual function in defense and development	3.5	Stots <i>et al.</i> , 2009
<i>Solyc07g049670.3</i>	Benzyl alcohol O-benzoyltransferase	- involved in formation of volatile ester benzylbenzoate, a minor constituent of the floral aroma - upregulated in the leaf during the hypersensitive reaction provoked by a pathogen infection	3.8	Czernic <i>et al.</i> , 1996
<i>Solyc01g087850.2</i>	Serine protease SBT3	- contributes to insect resistance in tomato	3.9	Meyer <i>et al.</i> , 2016
<i>Solyc08g077060.3</i>	Zinc finger, LSD1-type	- negative regulation of plant-type hypersensitive response; regulates transcription, via either repression of a pro-death pathway or activation of an anti-death pathway, in response to signals emanating from cells undergoing pathogen-induced hypersensitive cell death	4.1	Dietrich <i>et al.</i> , 1997; He <i>et al.</i> , 2011
<i>Solyc04g007070.3</i>	Disease resistance protein (NBS-LRR class) family	- belongs to the plant resistance (R) genes; interacts with pathogen effectors to induce defense responses - R proteins play roles in detecting and recognising pathogen effectors and initiating multiple signal transductions inside the plant cells to initiate different responses that will aid in pathogen destruction and prevention of further infections	4.6	Lee & Yeom, 2015
<i>Solyc08g079870.3</i>	Subtilisin	- contributes to insect resistance in tomato; induced in response to wounding and insect attack in injured leaves but not in healthy systemic tissues - regulates pectin methylesterases (PMEs)	4.8	Meyer <i>et al.</i> , 2016
<i>Solyc09g082330.2</i>	SM80.1 Vicilin	- has antibacterial and antifungal activity against a range of species	5.4	Marcus <i>et al.</i> , 1999
<i>Solyc06g061230.3</i>	Metalloprotease inhibitor	- involved in defensive role against insect attacks	5.6	Villanueva <i>et al.</i> , 1998
<i>Solyc03g116225.1</i>	42kDa chitin-binding protein	- involved in plant-pathogen interactions - located at the plasmalemma-wall interface, intercellular spaces and binds to the pathogen <i>Colletotrichum lindemuthianum</i> in vitro and in planta	6.0	Bindschedler <i>et al.</i> , 2006
<i>Solyc01g097270.3</i>	Pathogen-induced protein	- controls the resistance to pathogen infections	6.4	Cao & Tan, 2019

Supplementary Table 1.3. Continued (15/18).

Gene ID	Gene Name	Identified Function	Fold Increase	References
Defense response				
<i>Solyc01g091170.3</i>	Arginase 2 ARG2	<ul style="list-style-type: none"> - one of the two arginases in tomato; catalyses the catabolism of arginine into ornithine and urea; arginine and ornithine are precursors for polyamine biosynthetic pathways - induced in leaves by wounding, mediated by the jasmonic acid signalling pathway and infections by pathogens - overexpression of arginase lowers susceptibility to infections by pathogens 	6.7	Bracus <i>et al.</i> , 2012
<i>Solyc11g022590.1</i>	Trypsin inhibitor-like protein precursor	<ul style="list-style-type: none"> - exhibits Kunitz trypsin protease inhibitor activity; involved in modulating programmed cell death (PCD) in plant-pathogen interactions, response to hydrogen peroxide, insects, salt stress and wounding - overexpression results in reduced lesion development after infection 	7.2	Li <i>et al.</i> , 2008
<i>Solyc07g052790.2</i> <i>Solyc07g052780.3</i>	Disease resistance protein (TIR-NBS-LRR class)	<ul style="list-style-type: none"> - monitors the status of plant proteins that are targeted by pathogen effectors 	inf	McHale <i>et al.</i> , 2006
Photoreceptors				
<i>Solyc02g071260.3</i>	Phytochrome	<ul style="list-style-type: none"> - modulates flowering time - overexpression causes early flowering 	3.2	Hajdu <i>et al.</i> , 2015
<i>Solyc01g097770.3</i>	Phototropin 2	<ul style="list-style-type: none"> - acts as a blue light photoreceptor in a signal-transduction pathway for photo-induced movements; phosphorylates BLUS1, a kinase involved in stomatal opening; mediates calcium spiking of extra- and intracellular origins in response to blue light; involved in hypocotyl phototropism - contributes to the chloroplast accumulation in low blue light and mediates their translocation (avoidance response) at high fluence 	7.4	Sakai <i>et al.</i> , 2001; Takemiya <i>et al.</i> , 2013
Volatiles metabolism				
<i>Solyc12g056600.3</i>	Short-chain dehydrogenase-reductase	<ul style="list-style-type: none"> - has alcohol dehydrogenase (NAD) activity; involved in carbohydrate mediated signalling, carboxylic acid biosynthetic process and terpenoid biosynthetic process - preferentially expressed in fruit with a maximum expression at the breaker stage; acts on hexanal, phenylacetaldehyde, (E)-2-hexenal and acetaldehyde and the corresponding alcohols - involved in formation of aroma volatiles by interconverting alcohols and aldehydes 	9.3	Moummou <i>et al.</i> , 2012
<i>Solyc11g010990.2</i>	Alcohol dehydrogenase, C-terminal (ADH)	<ul style="list-style-type: none"> - catalyses the reversible oxidation of alcohols to their corresponding acetaldehyde or ketone with the concomitant reduction of NAD - involved in ester volatile biosynthesis and seed development; helps protect plants from the effects of hypoxic stress 	15.4	Yilmaz, 2001; Qin <i>et al.</i> , 2017
<i>Solyc06g059840.3</i>	Branched chain α -keto acid dehydrogenase E1- α subunit	<ul style="list-style-type: none"> - has α-ketoacid dehydrogenase activity; catalyses an irreversible step in the catabolism of the branched-chain amino acids L-isoleucine, L-valine, and L-leucine, acting on their deaminated derivatives L-α-keto-β-methylvalerate, α-ketoisovalerate, and α-ketoisocaproate, respectively - branched chain amino acids are important in fruit respiration, but also reveal that keto acids, rather than amino acids, are the likely precursors for the branched chain flavour volatiles 	18.3	Kochevenko <i>et al.</i> , 2012

Supplementary Table 1.3. Continued (16/18).

Gene ID	Gene Name	Identified Function	Fold Increase	References
Volatiles metabolism				
<i>Solyc09g025210.3</i>	Alcohol dehydrogenase-2 (ADH2)	- accumulates late in ripening together with flavour volatiles suggesting its role in interconversion of the volatile aldehydes and alcohols; important in flavour development - plants overexpressing ADH2 have higher levels of hexanol and Z-3- hexenol	inf	Speirs <i>et al.</i> , 1998; Yilmaz, 2001
Transporters				
<i>Solyc02g079220.3</i>	Sugar transporter protein 1	- involved in transport of glucose; expressed predominantly in sink tissue, with the highest expression in young fruits - acts as a factor for the regulation of shoot branching depending on extracellular sugar contents; plays an important role in the plant defence against fungal attacks	2.8	Otori <i>et al.</i> , 2019
<i>Solyc10g075110.2</i> <i>Solyc01g090360.3</i>	Non-specific lipid-transfer protein	- transfers phospholipids as well as galactolipids across membranes; may play a role in wax or cutin deposition in the cell walls of expanding epidermal cells; bind lipids to disrupt microbial penetration into cell membranes - play important roles in resistance to biotic and abiotic stress and in plant growth and development, such as sexual reproduction, seed development and germination	3.3 – inf	Liu <i>et al.</i> , 2015; Tam <i>et al.</i> , 2015
<i>Solyc02g079350.3</i>	Equilibrative nucleoside transporter family protein	- mediates transport of nucleosides, vitamins and phytohormones; functions in nucleotide metabolism	3.4	Girke <i>et al.</i> , 2014
<i>Solyc02g093870.3</i> <i>Solyc04g079560.3</i>	Amino acid transporter, transmembrane	- lysine/histidine transporter	3.4 – 15.7	Nühse <i>et al.</i> , 2004
<i>Solyc04g076780.3</i>	Oligopeptide transporter	- involved in the intake of small peptides and in histidine transport	4.8	Tsay <i>et al.</i> , 2007
<i>Solyc03g034375.1</i>	Lipid transfer protein	- overexpression of lipid transfer protein (LTP) enhances resistance to plant pathogens and LTP functions in long-distance systemic signalling - enhances salt and drought stresses tolerance	5.2	Sarowar <i>et al.</i> , 2009
<i>Solyc06g060620.3</i>	Nitrate transporter	- nitrate transport; mediates calcium tolerance	5.4	Li <i>et al.</i> , 2010b
<i>Solyc03g097580.3</i>	Bidirectional sugar transporter SWEET	- mediates low-affinity uptake and efflux of glucose across the membrane; expression of a SWEET transporter among wild species of tomato determines the hexose composition of ripening tomato fruit - plants overexpressing SWEET have improved germination, increased freezing tolerance and under cold stress are unable to accumulate fructose, while under nitrogen starvation, both glucose and fructose, but not sucrose, are less abundant; overexpressing plants also exhibit increased growth efficiency and show improved nitrogen use efficiency when nitrate is sufficiently available, while under conditions of limiting nitrogen, wild-type biomasses are higher	9.9	Klemens <i>et al.</i> , 2013; Shammai <i>et al.</i> , 2018
<i>Solyc07g043000.3</i> <i>Solyc01g109390.3</i>	Bifunctional inhibitor/lipid-transfer protein/seed storage 2S albumin superfamily protein	- encodes an apoplastic lipid transfer protein that is involved in systemic acquired resistance	16.7 – inf	Mandal <i>et al.</i> , 2011; Champigny <i>et al.</i> , 2013

Supplementary Table 1.3. Continued (17/18).

Gene ID	Gene Name	Identified Function	Fold Increase	References
Development and cellular events				
<i>Solyc04g051490.3</i>	Essential meiotic endonuclease 1B	- forms a complex with MUS81 that functions as endonuclease in DNA recombination and repair processes - may be required in mitosis for the processing of stalled or collapsed replication fork intermediates; plays a role in DNA repair and in genotoxic stress-induced homologous recombination (HR) in somatic cells	3.2	Geuting <i>et al.</i> , 2009
<i>Solyc10g078265.1</i> <i>Solyc03g007170.3</i>	Peptidyl-prolyl <i>cis-trans</i> isomerase (PPI)	- accelerates folding of proteins; catalyses the <i>cis-trans</i> isomerisation of proline imidic peptide bonds in oligopeptides; histone remodelling factor involved in chromatin-based gene silencing; reinforces H3K27 methylation - required for the formation and development of leaves, for normal phyllotaxy and for the formation, maintenance and activity of root and shoot apical meristems; enhanced expression increases resistance to pathogens	3.2 – 3.6	Li <i>et al.</i> , 2007; Mokryakova <i>et al.</i> , 2014
<i>Solyc07g017530.3</i>	Conserved oligomeric Golgi complex subunit 3	- component of a putative conserved oligomeric Golgi (COG) complex that is thought to be involved in tethering of retrograde intra-Golgi vesicles - required for proper deposition of cell wall materials in pollen tube growth	3.3	Tan <i>et al.</i> , 2016
<i>Solyc02g087980.3</i>	Structural maintenance of chromosomes protein	- central component of cohesin, a complex required for chromosome cohesion during the cell cycle; cohesion is coupled to DNA replication and is involved in DNA repair	3.4	Schubert <i>et al.</i> , 2009
<i>Solyc10g086150.2</i>	RNA-binding (RRM/RBD/RNP motifs) family protein	- chloroplast rRNA processing	3.6	Reichel <i>et al.</i> , 2016
<i>Solyc09g090400.3</i>	Translation initiation factor eIF-2B protein	- regulates various aspects of plant development and their interaction with environment; associated with interaction of plants with different abiotic stresses, such as high temperature, salinity and oxidative stress	3.6	Dutt <i>et al.</i> , 2015
<i>Solyc04g011390.1</i>	Histone H4	- core component of nucleosome; histones play a central role in transcription regulation, DNA repair, DNA replication and chromosomal stability - functional H3/H4 histone is a chaperone mediating abiotic stress adaptation by transcriptional regulation of diverse stress-related genes	3.7	Tripathi <i>et al.</i> , 2016
<i>Solyc12g088530.2</i>	Cyclin A3.1	- positive regulation of cell cycle	4.2	Takahashi <i>et al.</i> , 2010
<i>Solyc11g069700.2</i>	Elongation factor 1- α	- promotes the GTP-dependent binding of aminoacyl-tRNA to the A-site of ribosomes during protein biosynthesis - correlates with higher levels of protein synthesis in developing tissues	4.3	Pokalsky <i>et al.</i> , 1989
<i>Solyc11g011980.3</i>	Transducin/WD40 repeat-like superfamily protein	- acts as a scaffolding molecule assisting proper activity of other proteins - functions in several cellular, metabolic and molecular pathways, biologically playing important roles in plant development and also during stress signalling	4.3	Mishra <i>et al.</i> , 2012
<i>Solyc01g104850.3</i> <i>Solyc01g108460.2</i>	Carboxypeptidase	- related to tomato fruit ripening	4.3 – 4.6	Mehta & Mattoo, 1996

Supplementary Table 1.3. Continued (18/18).

Gene ID	Gene Name	Identified Function	Fold Increase	References
Development and cellular events				
<i>Solyc01g100030.4</i>	Deoxyuridine triphosphatase	- encodes an essential enzyme of nucleotide metabolism; hydrolyses dUTP to dUMP and pyrophosphate providing a precursor (dUMP) for the synthesis of thymine nucleotides needed for DNA replication, and limiting intracellular pools of dUTP - UDP-glucose (UDP-Glc) is produced from uridine triphosphate (UTP) and glucose-1-phosphate by the unique stroma-localised UDP-Glc pyrophosphorylase; UDP-glucose is used in sulfoquinovosyl diacylglycerol biosynthesis	4.8	Inoguchi <i>et al.</i> , 2015; Kobayashi, 2016
<i>Solyc03g115050.3</i>	Replication A 70 kDa DNA-binding subunit	- required for DNA recombination, repair and replication - involved in repair of double-strand DNA breaks (DSBs) induced by genotoxic stresses	6.3	Ishibashi <i>et al.</i> , 2006
<i>Solyc01g107730.3</i>	D-type cyclin-2	- transduces the signals leading to fruit growth by cell divisions	6.8	Kvarnheden <i>et al.</i> , 2000
<i>Solyc10g054080.2</i>	Kinesin-related protein	- kinesin-like motor enzyme that plays a critical role in the organisation of phragmoplast microtubules during cytokinesis - supports phragmoplast expansion and cell-plate growth in plant cells; binds microtubules in an ATP-sensitive manner	7.2	Lee <i>et al.</i> , 2017
<i>Solyc09g065470.3</i>	7S globulin	- part of the flavour quality of tomato fruit and a good source of dietary protein for producing leucine, tyrosine, glutamic acid and aspartic acid	inf	Liu <i>et al.</i> , 2016a

Supplementary Table 1.4. List of significantly downregulated genes in the U/O; B/B line with over a 2.83-fold decrease compared to the Azygous reference line; inf – infinite decrease.

Gene ID	Gene Name	Identified Function	Fold Decrease	References
CYP450 family				
<i>Solyc05g015350.3</i>	CYP450 78A5 monooxygenase	- regulates domestication trait in cultivated tomato; involved in stigma colour formation; promotes organ growth without affecting the size of the early primordium - loss-of-function mutants form smaller organs	11.1	Anastasiou <i>et al.</i> , 2007; Stransfeld <i>et al.</i> , 2010
Carotenoid biosynthesis				
<i>Solyc07g042480.3</i>	Carotene ϵ -monooxygenase, chloroplastic (<i>LUT1</i>)	- specific for ϵ - and β -ring hydroxylation of α -carotene; has low activity towards the β -rings of β -carotene; preferred substrate in planta is not α -carotene but the ϵ -ring of zeinoxanthin - loss-of-function mutants lack lutein and accumulate higher levels of zeinoxanthin and β -xanthophylls	4.7	Tian <i>et al.</i> , 2003; Tian <i>et al.</i> , 2004; Fiore <i>et al.</i> , 2006
Lipid metabolism				
<i>Solyc08g005630.3</i>	Long-chain-alcohol oxidase	- involved in the ω -oxidation pathway of lipid degradation	3.5	Matsuba <i>et al.</i> , 2013
<i>Solyc04g080250.3</i>	Deoxyuridine 5'-triphosphate nucleotidohydrolase (<i>DUT</i>)	- involved in nucleotide metabolism; produces dUMP, the immediate precursor of thymidine nucleotides and decreases the intracellular concentration of dUTP - downregulation increases pool of UTP to produce sfoquinosyl diacylglycerol (SQDG) - SQDGs protect the catalytic component of chloroplast proton-linked ATP synthase (CF_1) against cold inactivation	4.0	Kleppinger-Sparace <i>et al.</i> , 1985; Okankenko <i>et al.</i> , 2008
Steroid metabolism				
<i>Solyc01g106820.3</i>	Sterol regulatory element-binding protein (SREBP) site 2 protease, putative	- SREBPs are membrane-bound transcription factors that activate genes involved in cholesterol synthesis - provides the means by which cellular cholesterol exerts negative feedback on cholesterol synthesis	2.9	Shao & Espenshade, 2014
Flavonoid metabolism				
<i>Solyc10g018140.2</i>	Dihydroflavonol 4-reductase-like (<i>DFR</i>)	- bifunctional enzyme involved in flavonoid metabolism - downregulation of <i>DFR</i> expression using RNAi reduces anthocyanin accumulation and increases flavonols quercetin-3-O-hexose-hexoside and quercetin-3-O-glucoside - quercetin-3-O-glucoside increases fruit bitterness	4.0	Wang <i>et al.</i> , 2013; Ferrer-Gallego <i>et al.</i> , 2016
<i>Solyc12g098620.2</i>	bHLH transcription factor 072	- putatively involved in the regulation of genes of the flavonoid pathway	4.3	Rigano <i>et al.</i> , 2016
Cell wall related				
<i>Solyc03g093080.3</i>	Xyloglucan endotransglucosylase/hydrolase	- catalyses xyloglucan endohydrolysis (XEH) and/or endotransglycosylation (XET) - involved in the modification of cell wall structure by cleaving and, often, also re-joining xyloglucan molecules in primary plant cell walls	2.8	Rose <i>et al.</i> , 2002

Supplementary Table 1.4. Continued (2/4).

Gene ID	Gene Name	Identified Function	Fold Decrease	References
Cell wall related				
<i>Solyc12g006260.1</i>	L-fucokinase/GDP-L-fucose pyrophosphorylase	<ul style="list-style-type: none"> - bifunctional enzyme involved in the salvage pathway which converts free L-fucose to GDP-L-fucose - loss-of-function mutant has no visible phenotype and no alteration of the sugar composition of cell wall polysaccharides but accumulates free L-fucose - monosaccharide L-fucose is a constituent of cell wall polysaccharides and sugar moieties of glycoproteins; L-fucosyl residues occur as nonreducing terminal residues in xyloglucan and arabinogalactan protein - L-fucosylated trisaccharide side chains of xyloglucan modulate the interaction of xyloglucan with cellulose microfibrils affecting the mechanical properties of plant cell walls - GDP-L-fucose has an essential role in leaf shape acquisition by sustaining differential growth at the leaf margins 	3.3	Kotake <i>et al.</i> , 2008; Gonçalves <i>et al.</i> , 2017
<i>Solyc03g097050.3</i>	Cellulose synthase-like protein	<ul style="list-style-type: none"> - putative, Golgi-localised β-glycan synthase that polymerises the backbones of noncellulosic polysaccharides (hemicelluloses) of plant cell wall - essential for root hair elongation but not initiation 	4.1	Wang <i>et al.</i> , 2001
<i>Solyc12g098810.2</i>	Chitinase family protein	<ul style="list-style-type: none"> - involved in lignin accumulation and root system architecture 	8.7	Cao & Tan, 2019
<i>Solyc06g075100.3</i>	Glycosyl transferase, family 2	<ul style="list-style-type: none"> - responsible for transfer of nucleotide-diphosphate sugars to substrates such as polysaccharides and lipids 	9.5	Campbell <i>et al.</i> , 1997
Photosynthesis and related				
<i>Solyc09g056180.3</i>	Dehydroascorbate reductase (DHAR)	<ul style="list-style-type: none"> - involved in cold and wound stress response of tomato; recycles ascorbic acid (Asc) - suppression of DHAR expression results in preferential loss of chlorophyll a, lower steady state of Rubisco and lower rate of CO₂ assimilation - through its Asc recycling function, DHAR affects levels of foliar ROS and photosynthetic activity during leaf development 	3.0	Chen & Gallie, 2006; Kabir <i>et al.</i> , 2011
<i>Solyc02g067750.3</i>	Carbonic anhydrase (CA)	<ul style="list-style-type: none"> - catalyses reversible hydration of CO₂ - downregulation of CA reduces lipid biosynthesis 	4.1	Hoang & Chapman, 2002
<i>Solyc08g059710.3</i>	EEIG1/EHBP1 N-terminal domain-containing protein	<ul style="list-style-type: none"> - responsible for movement of chloroplasts in response to blue light - links actin/microfilament-binding adaptors to the membrane 	4.7	Zhang & Aravind, 2010
Response to abiotic stress				
<i>Solyc10g050970.1</i>	Ethylene Response Factor (ERF) D.4	<ul style="list-style-type: none"> - ERFs are downstream components of ethylene signalling; regulates expression of ethylene-responsive genes - preferentially expressed in young unripe fruits; expression declines at the onset of ripening 	2.9	Liu <i>et al.</i> , 2016b
<i>Solyc03g124110.2</i> <i>Solyc08g007820.1</i> <i>Solyc08g007830.1</i>	C-repeat binding factor (CBF)	<ul style="list-style-type: none"> - low temperature-induced transcription factor - constitutive overexpression of CBF does not increase freezing tolerance 	2.9–4.1	Zhang <i>et al.</i> , 2004

Supplementary Table 1.4. Continued (3/4).

Gene ID	Gene Name	Identified Function	Fold Decrease	References
Development and stress responses				
<i>Solyc05g046340.2</i>	Phosphomannomutase (PMM)	- involved in ascorbic acid biosynthesis and synthesis of GDP-mannose and dolichol-phosphate-mannose required for critical mannosyl transfer reactions	3.1	Qian <i>et al.</i> , 2007
<i>Solyc01g087590.3</i>	Polyamine oxidase (PAO)	- PAO, a flavin adenine dinucleotide-dependent enzyme, functions in PA catabolism; PAO is a key element for the oxidative burst, which is essential for induction of programmed cell death - polyamines (PAs) are implicated in developmental processes and stress responses of plants; PAs stimulate DNA replication, transcription and translation, contribute to plant morphogenesis, growth, embryogenesis, organ development, leaf senescence, abiotic and biotic stress response and infection by fungi and viruses	3.5	Yoda <i>et al.</i> , 2006; Hao <i>et al.</i> , 2018
<i>Solyc01g007020.3</i> <i>Solyc01g007010.3</i> <i>Solyc01g007040.3</i> <i>Solyc01g007030.3</i>	U-box domain-containing family protein	- involved in hormone regulation, biotic and abiotic response, self-incompatibility and development - functions as an E3 ubiquitin ligase; may be involved in ABA-mediated signalling pathway and response to water stress; a negative regulator of PAMP-triggered immunity	3.6 – 7.5	González-Lamothe <i>et al.</i> , 2006; Libault <i>et al.</i> , 2007
<i>Solyc06g082080.3</i>	Protein phosphatase 2C	- major negative regulator of ABA responses during seed germination and cold acclimation; confers insensitivity to ABA; prevents stomata closure - repressed by PYR/PYL/RCAR ABA receptors in ABA-dependent manner - induced by low temperature, drought, high salt and ABA - silenced mutants have accelerated development of freezing tolerance and enhanced expression of cold- and ABA-induced genes	3.7	Tähtiharju & Palva, 2001; Santiago <i>et al.</i> , 2012
<i>Solyc01g109120.3</i>	Transducin/WD40 repeat-like superfamily protein	- adaptor proteins that provide specificity to the E3 ubiquitin ligase complexes that mark target proteins with ubiquitin for degradation; involved in plant development and reproduction - silencing produces pleiotropic phenotypes and impairs secondary cell wall modification	4.4	Wang <i>et al.</i> , 2015
<i>Solyc01g005770.3</i>	Pentatricopeptide repeat-containing (PPR) family protein	- PPR proteins are modular RNA-binding proteins which mediate several aspects of gene expression in organelles and the nucleus; facilitate processing, splicing, editing, stability and translation of RNAs - may play a role in defense against necrotrophic fungi and abiotic stress tolerance; may be involved in ABA signalling	4.8	Laluk <i>et al.</i> , 2011; Mei <i>et al.</i> , 2014; Manna, 2015
<i>Solyc01g108240.3</i>	Ethylene Response Factor (ERF) D.3	- responsible for modulating transcription of ethylene-regulated genes - expressed as a drought responsive protein in drought-tolerant genotypes	5.3	Gong <i>et al.</i> , 2010
<i>Solyc01g005730.3</i>	Leucine-rich repeat receptor-like protein kinase family protein (LRR-RKs)	- membrane localised proteins that regulate developmental and defense-related processes including cell proliferation, stem cell maintenance, hormone perception, host-specific as well as non-host-specific defense - sense PAMPs (e.g. chitin from fungal cell walls) and DAMPs (e.g. cell wall fragments, cytoplasmic proteins)	10.5	Torii, 2004
<i>Solyc07g023995.1</i>	Ankyrin repeat-containing protein	- involved in salt stress tolerance; may act through abscisic acid (ABA) signalling pathways; promotes production of reactive oxygen species (ROS) - loss-of-function mutants do not display a visible phenotype under normal growth conditions, but have increased salt-stress tolerance and reduced ROS accumulation under salt-stress conditions	inf	Sakamoto <i>et al.</i> , 2008

Supplementary Table 1.4. Continued (4/4).

Gene ID	Gene Name	Identified Function	Fold Decrease	References
Defense response				
<i>Solyc00g060810.3</i>	Sn-1 protein (SN1)	- cell wall and extracellular region secreted protein of antimicrobial activity; involved in defense response - SN1 silencing affects cell division, leaf primary metabolism, and cell wall composition suggesting that SN1 has additional roles in growth and development beyond its previously assigned role in plant defense	3.4	Nahirňak <i>et al.</i> , 2012
<i>Solyc11g071760.3</i>	Regulator of gene silencing AY642285	- induced in response to tobacco mosaic virus; highly upregulated in early stages of powdery mildew infection in the compatible interaction compared to the incompatible interactions - in incompatible interactions, when resistance genes are present, this gene is significantly decreased, proportionally to the strength of the corresponding resistance genes	3.7	Nakahara <i>et al.</i> , 2012; Seifi <i>et al.</i> , 2014
<i>Solyc07g040663.1</i>	Enhanced Downy Mildew 2 (EDM2)	- negative regulator of the defense response and cell death - loss-of-function mutants display enhanced resistance to powdery mildew and do not show powdery-mildew-induced lesions	inf	Nie <i>et al.</i> , 2011
Nitrogen metabolism				
<i>Solyc10g083940.1</i>	Nodulin-like/Major Facilitator Superfamily protein	- homologs of nodulin genes are found in genomes of plants that are unable to nodulate - involved in transport of various solutes and interaction of plants with pathogenic microbes, highlighting the implication of solute transport in plant innate immunity	2.8	Denancé <i>et al.</i> , 2014
<i>Solyc07g041280.3</i>	Nitrilase/cyanide hydratase and apolipoprotein N-acyltransferase family protein	- involved in metabolic processes of nitrogen compounds; converts indoleacetoneitrile to the plant growth factor indole-3-acetic acid (auxin) - mutations in nitrilase result in reduced sensitivity to auxin-like effects of indoleacetoneitrile	4.5	Pace & Brenner, 2001
<i>Solyc03g034320.3</i>	Class I glutamine amidotransferase-like superfamily protein (GAT1)	- involved in glutamine metabolic process; glutamine amidotransferases (GATases) catalyse removal of ammonia groups from glutamine and their transfer to a substrate to form a new carbon-nitrogen group - GAT1-like proteins are involved in plant development and regulation of cell death in response to pathogens - highly repressed by long-term nitrogen stress; mutations of this gene cause enhanced branching phenotype	10.0	Zhu & Kranz, 2012; Bae <i>et al.</i> , 2013
<i>Solyc01g108630.3</i>	Nii1 nitrite reductase	- involved in the secondary step of nitrate assimilation; induced by nitrate; reduces nitrite to ammonium in the chloroplasts - downregulated by abiotic, especially prolonged, stresses	23.1	Davenport <i>et al.</i> , 2015; Goel & Singh, 2015

A



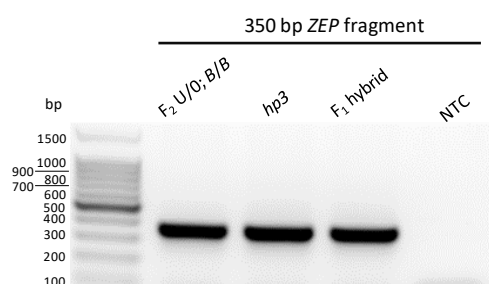
B



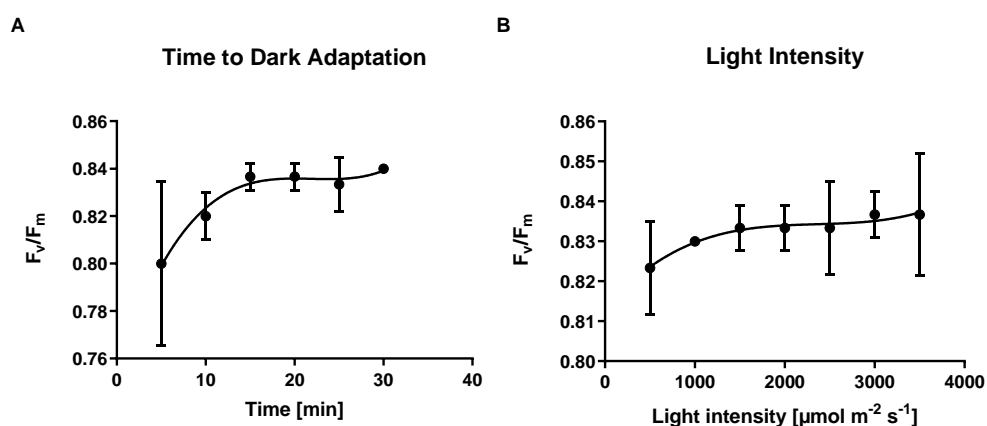
Supplementary Figure 1.7. Comparison of the height of the F_2 population plants assigned to the Azygous (A) and the U/O; B/B line (B). Both lines were grown in the same glasshouse and at the same time. The arrows indicate the same metal beam in both photos.

7.2 Appendix 2

The following appendix contains supplementary figures and tables, which complement the results of Chapter IV: Generation and characterisation of zeaxanthin-accumulating tomato lines.



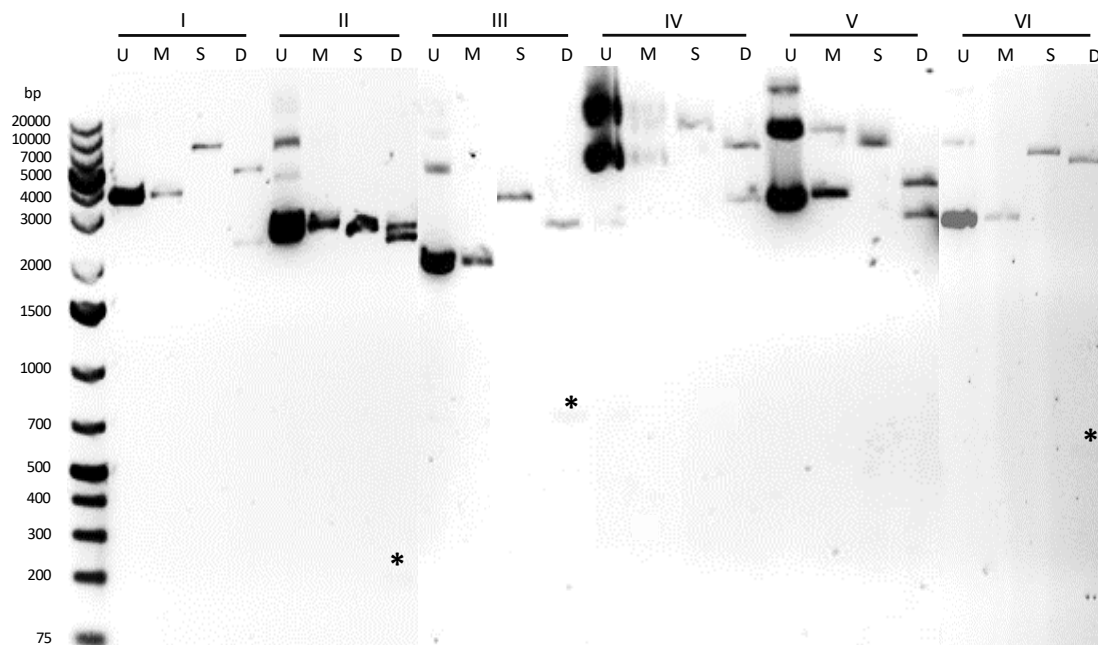
Supplementary Figure 2.1. The *F*₂ U/O; B/B line, *hp3* line and *F*₁ U/O; B/+; *hp3*/+ hybrid were used to amplify the 350 bp-long fragment of the exon 1 of *ZEP*, spanning the region where the missense mutation in the *hp3* line occurred. The fragments were then sequenced to confirm the presence of only the wild type allele of *ZEP* (*ZEP*^{WT/WT}) in the U/O; B/B line, only the *hp3* allele (*ZEP*^{*hp3*/*hp3*}) in the *hp3* line and both alleles of *ZEP* (*ZEP*^{WT/*hp3*}) in the *F*₁ U/O; B/+; *hp3*/+ hybrid. NTC – no-template control.



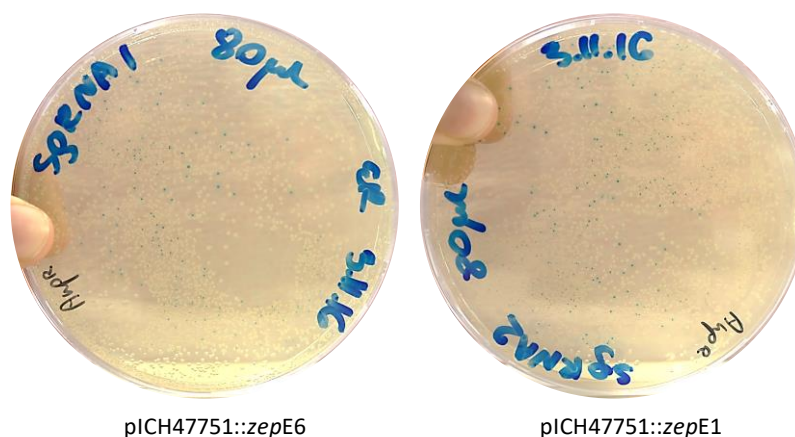
Supplementary Figure 2.2. Preparation of the instrument for the use in the measurement of Photosystem II efficiency. The efficiency is reported as the ratio of the F_v to F_m values, which is considered to be a sensitive indicator of plant photosynthetic performance. In healthy samples, the maximum F_v/F_m value of about 0.85 is typically recorded. Initial measurements were performed on Azygous plants to establish the time needed to dark adaptation (**A**) and the intensity of the light beam used (**B**). The values, beyond which no significant changes were observed, were selected: 20 minutes for dark adaptation and 2 500 $\mu\text{mol m}^{-2} \text{s}^{-1}$ beam intensity. Each measurement was performed on three biological replicates. Data are displayed as $\bar{x} \pm \text{SD}$.

7.3 Appendix 3

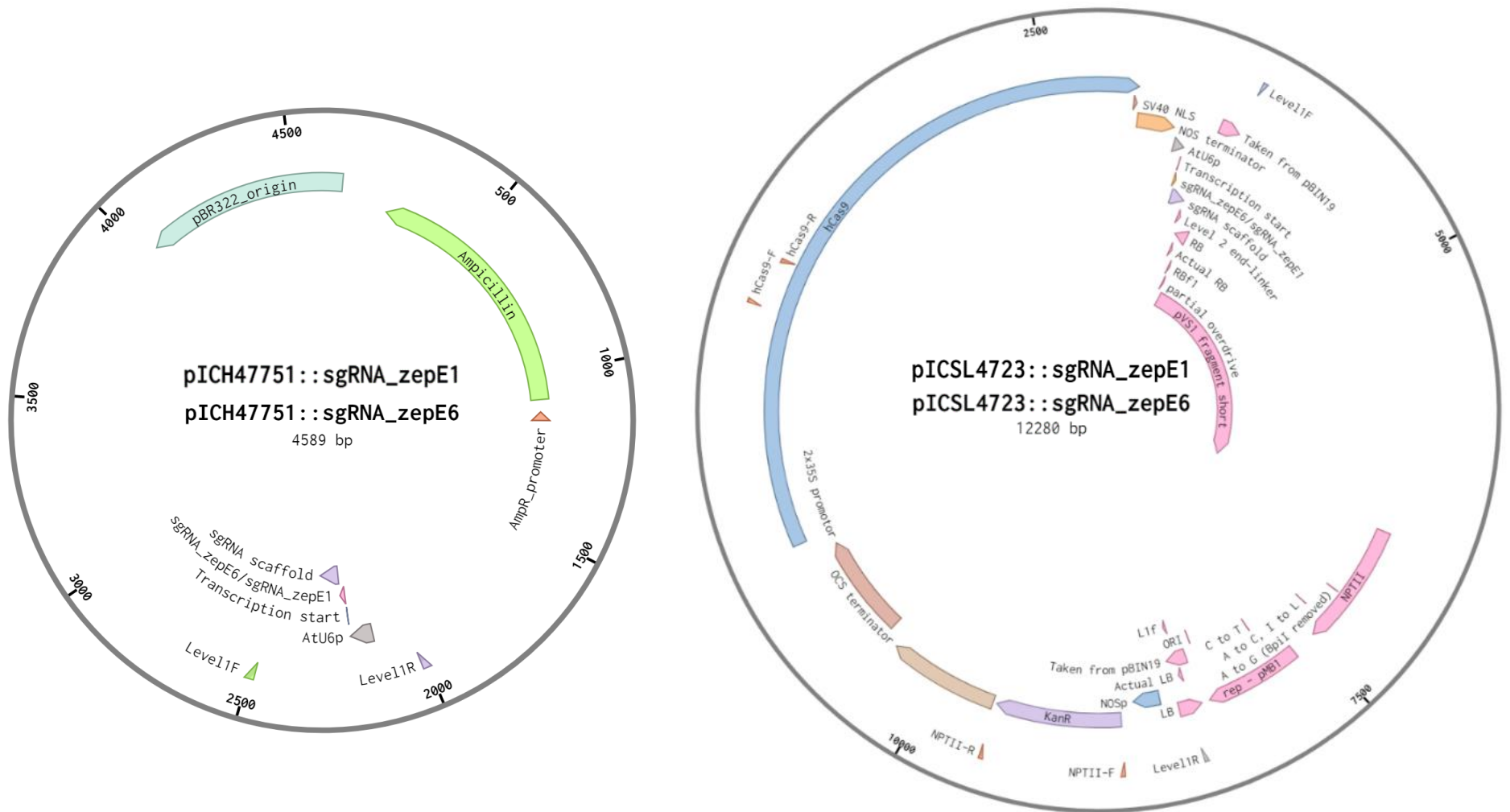
The following appendix contains supplementary figures and tables, which complement the results of Chapter V: CRISPR/Cas9-targeted editing of zeaxanthin epoxidase.



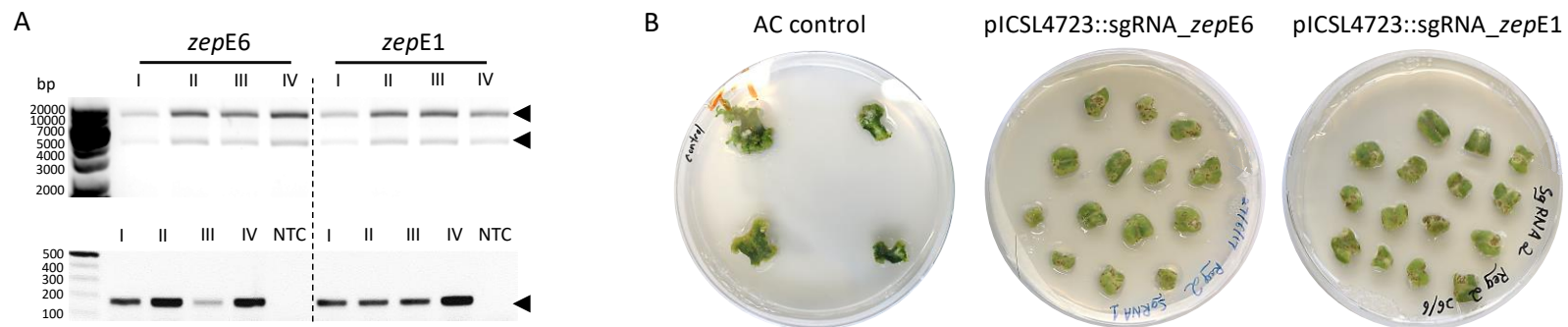
Supplementary Figure 3.1. Restriction digest of plasmids used to construct level 1 and 2 vectors. The lines contain undigested (U), mock-digested (M), single (S) and double (D) digested plasmids. The enzymes used in the reactions and sizes of the predicted fragments are provided in Table 2.11. Asterisks (*) indicate bands only visible at longer exposure times. I – pICH86966::AtU6p::sgRNA_PDS (sgRNA scaffold); II – pICSL01009::AtU6p (AtU6 promoter); III – pICH41766 (level 2 end-linker); IV – pICH47742::2x35S-5'UTR-hCas9(STOP)-NOST (human codon optimised Cas9); V – pICSL11024 (pICH47732::NOSp-NPTII-OCST; confers kanamycin resistance); VI – pICH47751 (level 1 vector).



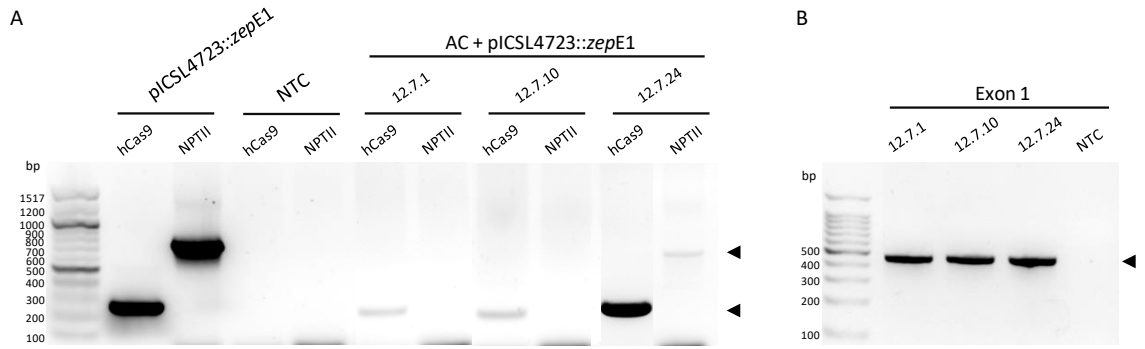
Supplementary Figure 3.2. *E. coli* transformed with pICH47751::zepE6 (left) and pICH47751::zepE1 (right) constructs; 80 μ l of the bacterial suspension was plated out in each case. Blue colonies most likely contained re-ligated empty level 1 plasmids (pICH47751). Efficiency of the digestion-ligation reaction was estimated at $89 \pm 2.8\%$ (ratio of the number of white clones to the total number of clones). Transformation efficiency of the in-house prepared chemically competent *E. coli* DH5 α , as tested by transformation with pUC19 plasmid, reached 5.25×10^7 CFU μ g $^{-1}$ (data not shown), a value considered to indicate a good efficiency in these types of cells.



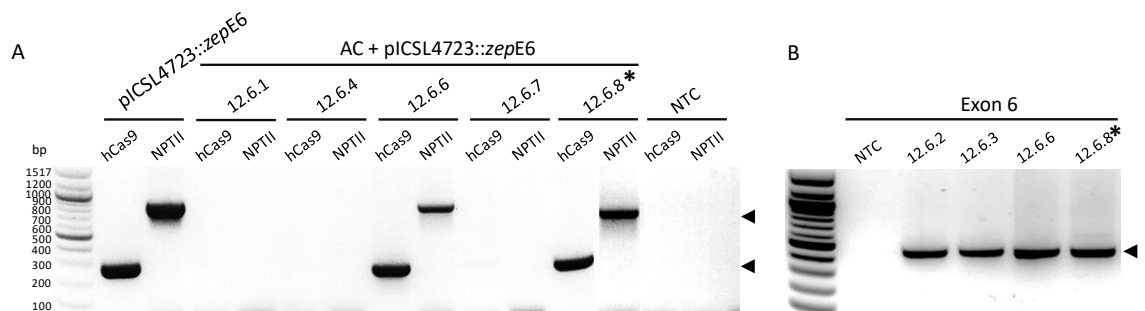
Supplementary Figure 3.3. Plasmid maps of the fully assembled level 1 (left) and level 2 (right) constructs. The modules and primer attachment sites are annotated. The modular composition of each construct of the same level is the same except for the 20 bp-long sequence targeting *ZEP* at the specified locations (exon 6 or exon 1).



Supplementary Figure 3.4. (A) Verification of *Agrobacterium tumefaciens* LBA4404 cultures transformed with the level 2 binary plasmids harbouring the CRISPR/Cas9 expression cassettes targeting either exon 6 or exon 1 of *ZEP* and intended for the use in tomato stable transformation: level 2 plasmids were extracted from the bacteria and analysed through restriction enzyme digestion (top) and used as templates to amplify the guide regions (bottom). Each reaction was performed in quadruplet. Black arrowheads indicate positions of predicted fragments; NTC – no-template control. (B) Early stage tissue culture transformation plates of the tomato leaf explants unexposed to bacterial suspension (AC control) and exposed to the suspension of bacteria transformed with the level 2 binary constructs (either pICSL4723::sgRNA_zepe6 or pICSL4723::sgRNA_zepe1).



Supplementary Figure 3.5. (A) Screening for the presence of the hCas9 and NPTII fragments from AC tomato plants transformed with pICSL4723::zepE1 targeting exon 1. (B) Amplification of the exon 1 fragments from the plants screened in (A). NTC – no-template control. Black arrowheads indicate positions of predicted fragments.



Supplementary Figure 3.6. Screening of a group of AC plants transformed with pICSL4723::zepE6 targeting exon 6 amongst which the plant harbouring a biallelic edit of *ZEP* (plant identifier 12.6.8, indicated with an asterisk (*)) was first identified. Amplification of the NPTII and hCas9 fragments (A) and amplification of the part of the exon 6 covering the site of a possible mutation (B). The molecular markers used are the same in both cases. NTC – no-template control. Black arrowheads indicate positions of predicted fragments.



Supplementary Figure 3.7. The flower trusses collected from the same CRISPR/Cas9 edited tomato plant (ID 9.6.1). The colour difference between the two types of flowers found on the chimera are clearly visible. Bright yellow (left) and pale (right) flowers most likely originate from unedited and edited cells, respectively.

Reference List

- Abd-El-Haliem, A.M. & Joosten, M.H.** (2017) Plant phosphatidylinositol-specific phospholipase C at the center of plant innate immunity. *J Integr Plant Biol.* **59** (3): 164-79.
- Abiri, R., Shaharuddin, N.A., Maziah, M., Yusof, Z.N.B., Atabaki, N., Sahebi, M., Valdiani, A., Kalhori, N., Azizi, P. & Hanafi, M.M.** (2017) Role of ethylene and the APETALA2/ethylene response factor superfamily in rice under various abiotic and biotic stress conditions. *Environ Exper Bot.* **134**: 33-44.
- Access Economics.** (2010) *The Global Economic Cost of Visual Impairment*. [Online] Available from: http://www.icoph.org/dynamic/attachments/resources/globalcostofvi_finalreport.pdf.
- Addgene.** Non-profit plasmid repository. <http://www.addgene.org/>.
- Age-Related Eye Disease Study Research Group.** (2007) The relationship of dietary carotenoid and vitamin A, E, and C intake with age-related macular degeneration in a case-control study: AREDS Report No. 22. *Arch Ophthalmol.* **125** (9): 1225-32.
- Age-Related Eye Disease Study 2 Research Group.** (2013) Lutein + zeaxanthin and omega-3 fatty acids for age-related macular degeneration: the Age-Related Eye Disease Study 2 (AREDS2) randomized clinical trial. *JAMA.* **309** (19): 2005-15.
- Agrawal, G.K., Yamazaki, M., Kobayashi, M., Hirochika, R., Miyao, A. & Hirochika, H.** (2001) Screening of the rice viviparous mutants generated by endogenous retrotransposon *Tos17* insertion. Tagging of a zeaxanthin epoxidase gene and a novel *OsTATC* gene. *Plant Physiol.* **125** (3): 1248-57.
- Akhtar, T.A., Surowiecki, P., Siekierska, H., Kania, M., Van Gelder, K., Rea, K.A., Virta, L.K.A., Vatta, M., Gawarecka, K., Wojcik, J., Danikiewicz, W., Buszewicz, D., Swiezewska, E. & Surmacz, L.** (2017) Polyprenols Are Synthesized by a Plastidial *cis*-Prenyltransferase and Influence Photosynthetic Performance. *Plant Cell.* **29** (7): 1709-25.
- Alcalde, E. & Fraser, P.D.** (2016) Metabolite profiling of *Phycomyces blakesleeanus* carotene mutants reveals global changes across intermediary metabolism. *Microbiology.* **162** (11): 1963-71.
- Alcantara, S. & Sanchez, S.** (1999) Influence of carbon and nitrogen sources on *Flavobacterium* growth and zeaxanthin biosynthesis. *J Ind Microbiol Biotechnol.* **23** (1): 697-700.
- Allen, F., Crepaldi, L., Alsinet, C., Strong, A.J., Kleshchevnikov, V., De Angeli, P., Páleniková, P., Khodak, A., Kiselev, V., Kosicki, M., Bassett, A.R., Harding, H., Galanty, Y., Muñoz-Martínez, F., Metzakopian, E., Jackson, S.P. & Parts, L.** (2019) Predicting the mutations generated by repair of Cas9-induced double-strand breaks. *Nat Biotechnol.* **37** (1): 64-72.
- Altincicek, B., Kovacs, J.L. & Gerardo, N.M.** (2012) Horizontally transferred fungal carotenoid genes in the two-spotted spider mite *Tetranychus urticae*. *Biol Lett.* **8** (2): 253-7.
- Alvarez, S., Marsh, E.L., Schroeder, S.G. & Schachtman, D.P.** (2008) Metabolomic and proteomic changes in the xylem sap of maize under drought. *Plant Cell Environ.* **31** (3): 325-40.
- Aman, R., Schieber, A. & Carle, R.** (2005) Effects of Heating and Illumination on *Trans-Cis* Isomerization and Degradation of β -Carotene and Lutein in Isolated Spinach Chloroplasts. *J Agric Food Chem.* **53** (24): 9512-8.
- Amat, J.A., Rendón, M.A., Garrido-Fernández, J., Garrido, A., Rendón-Martos, M. & Pérez-Gálvez, A.** (2010) Greater flamingos *Phoenicopterus roseus* use uropygial secretions as make-up. *Behav. Ecol. Sociobiol.* **65** (4): 665-73.
- Ament, K., Van Schie, C.C., Bouwmeester, H.J., Haring, M.A. & Schuurink RC.** (2006) Induction of a leaf specific geranylgeranyl pyrophosphate synthase and emission of (*E,E*)-4,8,12-trimethyltrideca-1,3,7,11-tetraene in tomato are dependent on both jasmonic acid and salicylic acid signaling pathways. *Planta.* **224** (5): 1197-208.
- Anastasiou, E., Kenz, S., Gerstung, M., MacLean, D., Timmer, J., Fleck, C. & Lenhard, M.** (2007) Control of plant organ size by KLUH/CYP78A5-dependent intercellular signaling. *Dev Cell.* **13** (6): 843-56.
- Aphalo, P. J.** (2016) Learn R ...as you learnt your mother tongue. Leanpub, Helsinki.

- Apweiler, R., Bairoch, A., Wu, C.H., Barker, W.C., Boeckmann, B., Ferro, S., Gasteiger, E., Huang, H., Lopez, R., Magrane, M., Martin, M.J., Natale, D.A., O'Donovan, C., Redaschi, N. & Yeh, L.S.** (2017) UniProt: the universal protein knowledgebase. *Nucleic Acids Res.* **32** (Database issue): D115-9.
- Ariizumi, T., Kishimoto, S., Kakami, R., Maoka, T., Hirakawa, H., Suzuki, Y., Ozeki, Y., Shirasawa, K., Bernillon, S., Okabe, Y., Moing, A., Asamizu, E., Rothan, C., Ohmiya, A. & Ezura, H.** (2014) Identification of the carotenoid modifying gene PALE YELLOW PETAL 1 as an essential factor in xanthophyll esterification and yellow flower pigmentation in tomato (*Solanum lycopersicum*). *Plant J.* **79** (3): 453-65.
- Arnold, J.B.** (2019) ggthemes: Extra Themes, Scales and Geoms for 'ggplot2'. R package version 4.1.0. Available from: <https://CRAN.R-project.org/package=ggthemes>.
- Asai, A., Yonekura, L. & Nagao, A.** (2008) Low bioavailability of dietary epoxyxanthophylls in humans. *Br J Nutr.* **100** (2): 273-7.
- Asker, D., Awad, T.S., Beppu, T. & Ueda, K.** (2018) Screening, Isolation, and Identification of Zeaxanthin-Producing Bacteria. *Methods Mol Biol.* **1852**: 193-209.
- Asker, D., Beppu, T. & Ueda, K.** (2007) *Mesoflavibacter zeaxanthinifaciens* gen. nov., sp. nov., a novel zeaxanthin-producing marine bacterium of the family Flavobacteriaceae. *Syst Appl Microbiol.* **30** (4): 291-6.
- Atkinson, C.J., Davies, W.J. & Mansfield, T.A.** (1989) Changes in Stomatal Conductance in Intact Ageing Wheat Leaves in Response to Abscisic Acid. *J. Exp. Bot.* **40** (9): 1021-8.
- Atkinson, R.G., Schröder, R., Hallett, I.C., Cohen, D. & MacRae, E.A.** (2002) Overexpression of polygalacturonase in transgenic apple trees leads to a range of novel phenotypes involving changes in cell adhesion. *Plant Physiol.* **129** (1): 122-33.
- Attokaran, M.** (2017) Marigold. In: Attokaran, M. (eds.) *Natural Food Flavors and Colorants*. 2nd ed. Chicago, IL: John Wiley & Sons Ltd and the Institute of Food Technologists, pp. 277-81.
- Avital, S., Brumfeld, V. & Malkin, S.** (2006) A micellar model system for the role of zeaxanthin in the non-photochemical quenching process of photosynthesis--chlorophyll fluorescence quenching by the xanthophylls. *Biochim Biophys Acta.* **1757** (7): 798-810.
- Bae, C., Kim, S.M., Lee, D.J. & Choi, D.** (2013) Multiple classes of immune-related proteases associated with the cell death response in pepper plants. *PLoS One.* **8** (5): e63533.
- Baek, K., Kim, D.H., Jeong, J., Sim, S.J., Melis, A., Kim, J.S., Jin, E. & Bae, S.** (2016) DNA-free two-gene knockout in *Chlamydomonas reinhardtii* via CRISPR-Cas9 ribonucleoproteins. *Sci Rep.* **6**: 30620.
- Baek, K., Yu, J., Jeong, J., Sim, S.J., Bae, S. & Jin, E.** (2018) Photoautotrophic production of macular pigment in a *Chlamydomonas reinhardtii* strain generated by using DNA-free CRISPR-Cas9 RNP-mediated mutagenesis. *Biotechnol Bioeng.* **115** (3): 719-28.
- Bai, W.Q., Xiao, Y.H., Zhao, J., Song, S.Q., Hu, L., Zeng, J.Y., Li, X.B., Hou, L., Luo, M., Li, D.M. & Pei, Y.** (2014) Gibberellin overproduction promotes sucrose synthase expression and secondary cell wall deposition in cotton fibers. *PLoS One.* **9** (5): e96537.
- Balasubramanian, V., Vashisht, D., Cletus, J. & Sakthivel, N.** (2012) Plant β -1,3-glucanases: their biological functions and transgenic expression against phytopathogenic fungi. *Biotechnol Lett.* **34** (11): 1983-90.
- Ballottari, M., Mozzo, M., Girardon, J., Hienerwadel, R. & Bassi, R.** (2013). Chlorophyll Triplet Quenching and Photoprotection in the Higher Plant Monomeric Antenna Protein Lhcb5. *J. Phys. Chem. B.* **117** (38): 11337-48.
- Bankaitis, V.A., Mousley, C.J. & Schaaf, G.** (2010) The Sec14 superfamily and mechanisms for crosstalk between lipid metabolism and lipid signaling. *Trends Biochem Sci.* **35** (3): 150-60.
- Bao, X., Katz, S., Pollard, M. & Ohlrogge, J.** (2002) Carbocyclic fatty acids in plants: biochemical and molecular genetic characterization of cyclopropane fatty acid synthesis of *Sterculia foetida*. *Proc Natl Acad Sci U S A.* **99** (10): 7172-7.

- Barrero-Sicilia, C., Hernando-Amado, S., González-Melendi, P. & Carbonero P.** (2011) Structure, expression profile and subcellular localisation of four different sucrose synthase genes from barley. *Planta*. **234** (2): 391-403.
- Barsan, C., Zouine, M., Maza, E., Bian, W., Egea, I., Rossignol, M., Bouyssie, D., Pichereaux, C., Purgatto, E., Bouzayen, M., Latché, A. & Pech, J.C.** (2012) Proteomic analysis of chloroplast-to-chromoplast transition in tomato reveals metabolic shifts coupled with disrupted thylakoid biogenesis machinery and elevated energy-production components. *Plant Physiol*. **160** (2): 708-25.
- Bartalucci, G., Coppin, J., Fisher, S., Hall, G., Helliwell, J.R., Helliwell, M. & Liaaen-Jensen, S.** (2007) Unravelling the chemical basis of the bathochromic shift in the lobster carapace; new crystal structures of unbound astaxanthin, canthaxanthin and zeaxanthin. *Acta Crystallogr B*. **63** (Pt 2): 328-37.
- Barua, A.B. & Olson, J.A.** (2001) Xanthophyll epoxides, unlike beta-carotene monoepoxides, are not detectably absorbed by humans. *J Nutr*. **131** (12): 3212-5.
- Bate, N.J., Sivasankar, S., Moxon, C., Riley, J.M., Thompson, J.E. & Rothstein, S.J.** (1998) Molecular characterization of an *Arabidopsis* gene encoding hydroperoxide lyase, a cytochrome P-450 that is wound inducible. *Plant Physiol*. **117** (4): 1393-400.
- Batesky, D.C., Goldfogel, M.J. & Weix, D.J.** (2017) Removal of Triphenylphosphine Oxide by Precipitation with Zinc Chloride in Polar Solvents. *J Org Chem*. **82** (19): 9931-6.
- Beddard, G.S., Davidson, R.S. & Trethewey, K.R.** (1977) Quenching of chlorophyll fluorescence by β -carotene. *Nature*. **267** (5609): 373-4.
- Belhaj, K., Chaparro-Garcia, A., Kamoun, S. & Nekrasov, V.** (2013) Plant genome editing made easy: targeted mutagenesis in model and crop plants using the CRISPR/Cas system. *Plant Methods*. **9** (1): 39.
- Benchling.** [Biology Software]. (2017) Retrieved from <https://benchling.com>.
- Bergey, D.R., Orozco-Cardenas, M., de Moura, D.S. & Ryan, C.A.** (1999) A wound- and systemin-inducible polygalacturonase in tomato leaves. *Proc Natl Acad Sci U S A*. **96** (4): 1756-60.
- Bernstein, P.S., Khachik, F., Carvalho, L.S., Muir, G.J., Zhao, D.Y. & Katz, N.B.** (2001) Identification and quantitation of carotenoids and their metabolites in the tissues of the human eye. *Exp Eye Res*. **72** (3): 215-23.
- Berry, A., Janssens, D., Hümbelin, M., Jore, J.P., Hoste, B., Cleenwerck, I., Vancanneyt, M., Bretzel, W., Mayer, A.F., Lopez-Ulibarri, R., Shanmugam, B., Swings, J. & Pasamontes, L.** (2003) *Paracoccus zeaxanthinifaciens* sp. nov., a zeaxanthin-producing bacterium. *Int J Syst Evol Microbiol*. **53** (Pt 1): 231-8.
- Berry, H.M., Rickett, D.V., Baxter, C.J., Enfissi, E.M.A. & Fraser, P.D.** (2019) Carotenoid biosynthesis and sequestration in red chilli pepper fruit and its impact on colour intensity traits. *J Exp Bot*. **70** (10): 2637-50.
- Betz, J.M., Brown, P.N. & Roman, M.C.** (2011) Accuracy, precision, and reliability of chemical measurements in natural products research. *Fitoterapia*. **82** (1): 44-52.
- Bhosale, P. & Bernstein, P.S.** (2005) Synergistic effects of zeaxanthin and its binding protein in the prevention of lipid membrane oxidation. *Biochim Biophys Acta*. **1740** (2): 116-21.
- Bhosale, P., Larson, A.J. & Bernstein, P.S.** (2004) Factorial analysis of tricarboxylic acid cycle intermediates for optimization of zeaxanthin production from *Flavobacterium multivorum*. *J Appl Microbiol*. **96** (3): 623-9.
- Bian, W., Barsan, C., Egea, I., Purgatto, E., Chervin, C., Zouine, M., Latché, A., Bouzayen, M. & Pech, J-C.** (2011) Metabolic and Molecular Events Occurring during Chromoplast Biogenesis. *J Bot*. **2011**: Article ID 289859.
- Billsten, H.H., Bhosale, P., Yemelyanov, A., Bernstein, P.S. & Polivka, T.** (2003) Photophysical properties of xanthophylls in carotenoproteins from human retinas. *Photochem Photobiol*. **78** (2): 138-45.

- Bindschedler, L.V., Whitelegge, J.P., Millar, D.J. & Bolwell, G.P.** (2006) A two component chitin-binding protein from French bean – association of a proline-rich protein with a cysteine-rich polypeptide. *FEBS Lett.* **580** (6): 1541-6.
- Bino, R.J., Ric de Vos, C.H., Lieberman, M., Hall, R.D., Bovy, A., Jonker, H.H., Tikunov, Y., Lommen, A., Moco, S. & Levin, I.** (2005) The light-hyperresponsive high pigment-2dg mutation of tomato: alterations in the fruit metabolome. *New Phytol.* **166** (2): 427-438.
- Blacklock, B.J. & Jaworski, J.G.** (2006) Substrate specificity of *Arabidopsis* 3-ketoacyl-CoA synthases. *Biochem Biophys Res Commun.* **346** (2): 583-90.
- Bonastre, J., Le Pen, C., Anderson, P., Ganz, A., Berto, P. & Berdeaux, G.** (2002) The epidemiology, economics and quality of life burden of age-related macular degeneration in France, Germany, Italy and the United Kingdom. *Eur J Health Econ.* **3** (2): 94-102.
- Bone, R.A., Landrum, J.T., Cao, Y., Howard, A.N. & Alvarez-Calderon, F.** (2007) Macular pigment response to a supplement containing meso-zeaxanthin, lutein and zeaxanthin. *Nut Met (Lond).* **4**: 12.
- Bone, R.A., Landrum, J.T., Fernandez, L. & Tarsis, S.L.** (1988) Analysis of the macular pigment by HPLC: retinal distribution and age study. *Invest Ophthalmol Vis Sci.* **29** (6): 843-9.
- Bone, R.A., Landrum, J.T., Friedes, L.M., Gomez, C.M., Kilburn, M.D., Menendez, E., Vidal, I. & Wang, W.** (1997) Distribution of lutein and zeaxanthin stereoisomers in the human retina. *Exp Eye Res.* **64**: 211-8.
- Bone, R.A., Landrum, J.T., Guerra, L.H. & Ruiz, C.A.** (2003) Lutein and zeaxanthin dietary supplements raise macular pigment density and serum concentrations of these carotenoids in humans. *J Nutr.* **133** (4): 992-8.
- Bone, R.A., Landrum, J.T., Hime, G.W., Cains, A. & Zamor, J.** (1993) Stereochemistry of the human macular carotenoids. *Invest Ophthalmol Vis Sci.* **34** (6): 2033-40.
- Bone, R.A., Landrum, J.T., Mayne, S.T., Gomez, C.M., Tibor, S.E. & Twaroska, E.E.** (2001) Macular pigment in donor eyes with and without AMD: a case-control study. *Invest Ophthalmol Vis Sci.* **42** (1): 235-40.
- Bovier, E.R., Renzi, L.M. & Hammond, B.R.** (2014) A Double-Blind, Placebo-Controlled Study on the Effects of Lutein and Zeaxanthin on Neural Processing Speed and Efficiency. *PLoS One.* **9** (9): e108178.
- Bown, A.W. & Shelp, B.J.** (2016) Plant GABA: Not Just a Metabolite. *Trends Plant Sci.* **21** (10): 811-3.
- Brauc, S., De Vooght, E., Claeys, M., Geuns, J.M., Höfte, M. & Angenon, G.** (2012) Overexpression of arginase in *Arabidopsis thaliana* influences defence responses against *Botrytis cinerea*. *Plant Biol (Stuttg).* **14** (Suppl 1): 39-45.
- Breithaupt, D. E.** (2007) Modern application of xanthophylls in animal feeding – a review. *Trends Food Sci Technol.* **18** (10): 501-6.
- Breithaupt, D.E., Weller, P., Wolters, M. & Hahn, A.** (2004) Comparison of plasma responses in human subjects after the ingestion of 3R,3R'-zeaxanthin dipalmitate from wolfberry (*Lycium barbarum*) and non-esterified 3R,3R'-zeaxanthin using chiral high-performance liquid chromatography. *Br J Nutr.* **91** (5): 707-13.
- Bressler, N.M., Silva, J.C., Bressler, S.B., Fine, S.L. & Green, W.R.** (1994) Clinicopathologic correlation of drusen and retinal pigment epithelial abnormalities in age-related macular degeneration. *Retina.* **14** (2): 130-42.
- Brewer, P.B., Yoneyama, K., Filardo, F., Meyers, E., Scaffidi, A., Frickey, T., Akiyama, K., Seto, Y., Dun, E.A., Cremer, J.E., Kerr, S.C., Waters, M.T., Flematti, G.R., Mason, M.G., Weiller, G., Yamaguchi, S., Nomura, T., Smith, S.M., Yoneyama, K. & Beveridge, C.A.** (2016) LATERAL BRANCHING OXIDOREDUCTASE acts in the final stages of strigolactone biosynthesis in *Arabidopsis*. *Proc Natl Acad Sci U S A.* **113** (22): 6301-6.
- Britton, G.** (1995a) Structure and properties of carotenoids in relation to function. *FASEB J.* **9** (15): 1551-8.
- Britton, G.** (1995b) UV/Visible Spectroscopy. In: Britton, G., Liaaen-Jensen, S. & Pfander, H. (eds.) *Carotenoids. Volume 1B: Spectroscopy*. Basel: Birkhäuser Verlag AG, pp. 13-62.

- Britton, G.** (1996) Carotenoids. In: Hendry, G.A.F. & Houghton, J.D. (eds.) *Natural Food Colorants*. 2nd ed. New York, NY: Chapman & Hall, pp. 197-243.
- Britton, G., Brown, D.J., Goodwin, T.W., Leuenberger, F.J. & Schocher, A.J.** (1977) The carotenoids of *Flavobacterium* strain R1560. *Arch Microbiol.* **113** (1-2): 33-7.
- Broadhead, G.K., Grigg, J.R., Chang, A.A. & McCluskey, P.** (2015) Dietary modification and supplementation for the treatment of age-related macular degeneration. *Nutr Rev.* **73** (7): 448-62.
- Brown, G.C., Brown, M.M., Sharma, S., Stein, J.D., Roth, Z., Campanella, J. & Beauchamp, G.R.** (2005) The burden of age-related macular degeneration: a value-based medicine analysis. *Trans Am Ophthalmol Soc.* **103**: 173-84.
- Bubner, B., Gase, K. & Baldwin, I.T.** (2004) Two-fold differences are the detection limit for determining transgene copy numbers in plants by real-time PCR. *BMC Biotechnol.* **4**: 14.
- Bünger-Kibler, S. & Bangerth, F.** (1982) Relationship between cell number, cell size and fruit size of seeded fruits of tomato (*Lycopersicon esculentum* Mill.), and those induced parthenocarpically by the application of plant growth regulators. *Plant Growth Regul.* **1**: 143-54.
- Campbell, J.A., Davies, G.J., Bulone, V. & Henrissat, B.** (1997) A classification of nucleotide-diphospho-sugar glycosyltransferases based on amino acid sequence similarities. *Biochem J.* **326** (Pt 3): 929-39.
- Cantrell, A., McGarvey, D.J., Truscott, T.G., Rancan, F. & Bohm, F.** (2003) Singlet oxygen quenching by dietary carotenoids in a model membrane environment. *Arch Biochem Biophys.* **412** (1): 47-54.
- Cao, J. & Tan, X.** (2019) Comprehensive Analysis of the Chitinase Family Genes in Tomato (*Solanum lycopersicum*). *Plants.* **8**: 52.
- Cardenas-Toro, F.P., Alcázar-Alay, S.C., Coutinho, J.P., Godoy, H.T., Forster-Carneiro, T. & Meireles, M.A.A.** (2015) Pressurized liquid extraction and low-pressure solvent extraction of carotenoids from pressed palm fiber: Experimental and economical evaluation. *Food Bioprod Process.* **94**: 90-100.
- Cardoso, L.A.C., Karp, S.G., Vendruscolo, F., Kanno, K.Y.F., Zoz, L.I.C. & Carvalho, J.C.** (2017) Biotechnological Production of Carotenoids and Their Applications in Food and Pharmaceutical Products. In: Cvetkovic, D.J. & Nikolic, G.S. (eds.) *Carotenoids*. Rijeka: IntechOpen, pp. 125-41.
- Carretero-Paulet, L., Cairó, A., Botella-Pavía, P., Besumbes, O., Campos, N., Boronat, A. & Rodríguez-Concepción, M.** (2006) Enhanced flux through the methylerythritol 4-phosphate pathway in *Arabidopsis* plants overexpressing deoxyxylulose 5-phosphate reductoisomerase. *Plant Mol Biol.* **62** (4-5): 683-95.
- Castilhos, G., Lazzarotto, F., Spagnolo-Fonini, L., Bodanese-Zanettini, M.H. & Margis-Pinheiro, M.** (2014) Possible roles of basic helix-loop-helix transcription factors in adaptation to drought. *Plant Sci.* **223**: 1-7.
- Cazzonelli, C.I.** (2011) Carotenoids in nature: insights from plants and beyond. *Funct. Plant Biol.* **38** (11): 833-47.
- Cárdenas, P.D., Sonawane, P.D., Pollier, J., Vanden Bossche, R., Dewangan, V., Weithorn, E., Tal, L., Meir, S., Rogachev, I., Malitsky, S., Giri, A.P., Goossens, A., Burdman, S. & Aharoni, A.** (2016) GAME9 regulates the biosynthesis of steroidal alkaloids and upstream isoprenoids in the plant mevalonate pathway. *Nat Commun.* **7**: 10654.
- Cerda-Olmedo, E.** (1987) Standard growth conditions and variations. In: Cerda-Olmedo, E. & Lipson, E.D. (eds.) *Phycomyces*. Cold Spring Harbor, NY: Cold Spring Harbor Laboratory, pp. 337-9.
- Cha, K.H., Koo, S.Y. & Lee, D.U.** (2008) Antiproliferative effects of carotenoids extracted from *Chlorella ellipsoidea* and *Chlorella vulgaris* on human colon cancer cells. *J Agric Food Chem.* **56** (22): 10521-6.
- Champigny, M.J., Isaacs, M., Carella, P., Faubert, J., Fobert, P.R. & Cameron R.K.** (2013) Long distance movement of DIR1 and investigation of the role of DIR1-like during systemic acquired resistance in *Arabidopsis*. *Front Plant Sci.* **4**: 230.

- Chao, L.M., Liu, Y.Q., Chen, D.Y., Xue, X.Y., Mao, Y.B. & Chen, X.Y.** (2017) *Arabidopsis* Transcription Factors SPL1 and SPL12 Confer Plant Thermotolerance at Reproductive Stage. *Mol Plant.* **10** (5): 735-48.
- Chapman, K.D., Dyer, J.M. & Mullen, R.T.** (2012) Biogenesis and functions of lipid droplets in plants: Thematic Review Series: Lipid Droplet Synthesis and Metabolism: from Yeast to Man. *Lipid Res.* **53** (2): 215-26.
- Chávez-Parga, M.D.C., Munguía-Franco, A., Aguilar-Torres, M. & Escamilla-Silva, E.M.** (2012) Optimization of zeaxanthin production by immobilized *Flavobacterium* sp. cells in fluidized bed bioreactor. *Adv Microbiol.* **2** (4): 598-604.
- ChemUCSD.** (2011) Flash Chromatography 101. [online video] Retrieved from: <https://www.youtube.com/watch?v=fF1gXUvyGb4> (Accessed: 20.03.2018).
- Chen, C., Gong, N., Li, Z., Sun, C. & Men, Z.** (2017) Concentration Effect on Quenching of Chlorophyll a Fluorescence by All-Trans- β -Carotene in Photosynthesis. *Molecules.* **22** (10): 1585.
- Chen, F., Li, H.B., Wong, R.N., Ji, B. & Jiang, Y.** (2005) Isolation and purification of the bioactive carotenoid zeaxanthin from the microalga *Microcystis aeruginosa* by high-speed counter-current chromatography. *J Chromatogr A.* **1064** (2): 183-6.
- Chen, L., Dodd, I.C., Davies, W.J. & Wilkinson, S.** (2013). Ethylene limits abscisic acid- or soil drying-induced stomatal closure in aged wheat leaves. *Plant Cell Environ.* **36** (10): 1850-9.
- Chen, M., Xu, J., Devis, D., Shi, J., Ren, K., Searle, I. & Zhang, D.** (2016) Origin and Functional Prediction of Pollen Allergens in Plants. *Plant Physiol.* **172** (1): 341-57.
- Chen, Z. & Gallie, D.R.** (2006) Dehydroascorbate reductase affects leaf growth, development, and function. *Plant Physiol.* **142** (2): 775-87.
- Cheung, A.Y., McNellis, T. & Piekos, B.** (1993) Maintenance of Chloroplast Components during Chromoplast Differentiation in the Tomato Mutant Green Flesh. *Plant Physiol.* **101** (4): 1223-9.
- Chitchumroonchokchai, C. & Failla, M.L.** (2006) Hydrolysis of zeaxanthin esters by carboxyl ester lipase during digestion facilitates micellarization and uptake of the xanthophyll by Caco-2 human intestinal cells. *J Nutr.* **136** (3): 588-94.
- Chong, J., Soufan, O., Li, C., Caraus, I., Li, S., Bourque, G., Wishart, D.S. & Xia, J.** (2018) MetaboAnalyst 4.0: towards more transparent and integrative metabolomics analysis. *Nucleic Acids Res.* **46** (W1): W486-94.
- Christianson, D.W.** (2017) Structural and Chemical Biology of Terpenoid Cyclases. *Chem Rev.* **117** (17): 11570-648.
- Christie, M., Brosnan, C.A, Rothnagel, J.A. & Carroll, B.J.** (2011) RNA decay and RNA silencing in plants: competition or collaboration? *Front Plant Sci.* **2**: 99.
- Chung, M.Y., Vrebalov, J., Alba, R., Lee, J., McQuinn, R., Chung, J.D., Klein, P. & Giovannoni, J.** (2010) A tomato (*Solanum lycopersicum*) APETALA2/ERF gene, SIAP2a, is a negative regulator of fruit ripening. *Plant J.* **64** (6): 936-47.
- Cicchetti, E., Durore, L., Le Borgne, E. & Laville, R.** (2018) Upregulation of Skin-Aging Biomarkers in Aged NHDF Cells by a Sucrose Ester Extract from the Agroindustrial Waste of *Physalis peruviana* Calyces. *J Nat Prod.* **81** (9): 1946-55.
- Clark K., Karsch-Mizrachi, I., Lipman, D.J., Ostell, J. & Sayers, E.W.** (2016) GenBank. *Nucleic Acids Res.* **44** (Database issue): D67-72.
- Clausén, M., Huang, S., Emek, S.C., Sjöholm, I. & Åkerlund, H.-E.** (2010) Post harvest improvement of zeaxanthin content of vegetables. *J. Food Eng.* **98** (2): 192-7.
- Coleman, H.D., Yan, J. & Mansfield, S.D.** (2009) Sucrose synthase affects carbon partitioning to increase cellulose production and altered cell wall ultrastructure. *Proc Natl Acad Sci U S A.* **106** (31): 13118-23.

- Cook, H.L., Patel, P.J. & Tufail, A.** (2008) Age-related macular degeneration: diagnosis and management. *Br Med Bull.* **85** (1): 127-49.
- Corona, V., Aracri, B., Kosturkova, G., Bartley, G.E., Pitto, L., Giorgetti, L., Scolnik, P.A. & Giuliano, G.** (1996) Regulation of a carotenoid biosynthesis gene promoter during plant development. *Plant J.* **9** (4): 505-12.
- Craft, N.E. & Soares, J.H.** (1992) Relative solubility, stability, and absorptivity of lutein and β -carotene in organic solvents. *J Agric Food Chem.* **40** (3): 431-4.
- Cuéllar-Cepeda, F.A., Parra-Galindo, M.A., Urquijo, J., Restrepo-Sánchez, L.P., Mosquera-Vásquez, T. & Narváez-Cuenca, C.E.** (2019) Influence of genotype, agro-climatic conditions, cooking method, and their interactions on individual carotenoids and hydroxycinnamic acids contents in tubers of diploid potatoes. *Food Chem.* **288**: 127-38.
- Cunningham, F.X. Jr. & Gantt, E.** (2001) One ring or two? Determination of ring number in carotenoids by lycopene ϵ -cyclases. *Proc Natl Acad Sci U S A.* **98** (5): 2905-10.
- Cunningham, F.X. Jr., Pogson, B., Sun, Z., McDonald, K.A., DellaPenna, D. & Gantt, E.** (1996) Functional analysis of the beta and epsilon lycopene cyclase enzymes of *Arabidopsis* reveals a mechanism for control of cyclic carotenoid formation. *Plant Cell.* **8** (9): 1613-26.
- Czajka, J.J., Nathenson, J.A., Benites, V.T., Baidoo, E.E.K., Cheng, Q., Wang, Y. & Tang, Y.J.** (2018) Engineering the oleaginous yeast *Yarrowia lipolytica* to produce the aroma compound β -ionone. *Microb Cell Fact.* **17** (1): 136.
- Czernic, P., Huang, H.C. & Marco, Y.** (1996) Characterization of hsr201 and hsr515, two tobacco genes preferentially expressed during the hypersensitive reaction provoked by phytopathogenic bacteria. *Plant Mol Biol.* **31** (2): 255-65.
- D'Ambrosio, C., Stigliani, A.L. & Giorio, G.** (2011) Overexpression of *CrtR-b2* (carotene beta hydroxylase 2) from *S. lycopersicum* L. differentially affects xanthophyll synthesis and accumulation in transgenic tomato plants. *Transgenic Res.* **20** (1): 47-60.
- D'Ambrosio, C., Stigliani, A.L. & Giorio, G.** (2018) CRISPR/Cas9 editing of carotenoid genes in tomato. *Transgenic Res.* **27** (4): 367-78.
- Dahan-Meir, T., Filler-Hayut, S., Melamed-Bessudo, C., Bocobza, S., Czosnek, H., Aharoni, A. & Levy, A.A.** (2018) Efficient in planta gene targeting in tomato using geminiviral replicons and the CRISPR/Cas9 system. *Plant J.* **95** (1): 5-16.
- Dall'Osto, L., Piques, M., Ronzani, M., Molesini, B., Alboresi, A., Cazzaniga, S. & Bassi, R.** (2013) The *Arabidopsis nox* mutant lacking carotene hydroxylase activity reveals a critical role for xanthophylls in photosystem I biogenesis. *Plant Cell.* **25** (2): 591-608.
- Daniel, B., Konrad, B., Toplak, M., Lahham, M., Messenlehner, J., Winkler, A. & Macheroux, P.** (2017) The family of berberine bridge enzyme-like enzymes: A treasure-trove of oxidative reactions. *Arch Biochem Biophys.* **632**: 88-103.
- Daniel, B., Pavkov-Keller, T., Steiner, B., Dordic, A., Gutmann, A., Nidetzky, B., Sensen, C.W., van der Graaff, E., Wallner, S., Gruber, K. & Macheroux, P.** (2015) Oxidation of Monolignols by Members of the Berberine Bridge Enzyme Family Suggests a Role in Plant Cell Wall Metabolism. *J Biol Chem.* **290** (30): 18770-81.
- Davenport, S., Le Lay, P. & Sanchez-Tamburrino, J.P.** (2015) Nitrate metabolism in tobacco leaves overexpressing *Arabidopsis* nitrite reductase. *Plant Physiol Biochem.* **97**: 96-107.
- Davies, T.** (1998) The new automated mass spectrometry deconvolution and identification system (AMDIS). *Spectrosc Eur.* **10** (3): 24-7.
- Davis, B.M., Pahlitzsch, M., Guo, L., Balendra, S., Shah, P., Ravindran, N., Malaguarnera, G., Sisa, C., Shamsher, E., Hamze, H., Noor, A., Sornsute, A., Somavarapu, S. & Cordeiro, M.F.** (2018) Topical Curcumin Nanocarriers are Neuroprotective in Eye Disease. *Sci Rep.* **8** (1): 11066.

- Dawczynski, J., Jentsch, S., Schweitzer, D., Hammer, M., Lang, G.E. & Strobel, J.** (2013) Long term effects of lutein, zeaxanthin and omega-3-LCPUFAs supplementation on optical density of macular pigment in AMD patients: the LUTEGA study. *Graefes Arch Clin Exp Ophthalmol.* **251** (12): 2711-23.
- de Abreu-Neto, J.B., Turchetto-Zolet, A.C., de Oliveira, L.F., Zanettini, M.H. & Margis-Pinheiro, M.** (2013) Heavy metal-associated isoprenylated plant protein (HIPPI): characterization of a family of proteins exclusive to plants. *FEBS J.* **280** (7): 1604-16.
- De Bruyne, L., Höfte, M. & De Vleeschauwer, D.** (2014) Connecting growth and defense: the emerging roles of brassinosteroids and gibberellins in plant innate immunity. *Mol Plant.* **7** (6): 943-59.
- de Campo, C., Dick, M., Pereira dos Santos, P., Haas Costa, T., Paese, K., Stanisçuaski Guterres, S., de Oliveira Rios, A. & Hickmann Flôres, S.** (2019) Zeaxanthin nanoencapsulation with *Opuntia monacantha* mucilage as structuring material: Characterization and stability evaluation under different temperatures. *Colloids Surf A Physicochem Eng Asp.* **558**: 410-21.
- de Silva, K., Laska, B., Brown, C., Sederoff, H.W. & Khodakovskaya, M.** (2011) *Arabidopsis thaliana* calcium-dependent lipid-binding protein (AtCLB): a novel repressor of abiotic stress response. *J Exp Bot.* **62** (8): 2679-89.
- de Souza, A., Hull, P.A., Gille, S. & Pauly, M.** (2014) Identification and functional characterization of the distinct plant pectin esterases PAE8 and PAE9 and their deletion mutants. *Planta.* **240** (5): 1123-38.
- De Wilde, C., Podevin, N., Windels, P. & Depicker, A.** (2001) Silencing of antibody genes in plants with single-copy transgene inserts as a result of gene dosage effects. *Mol Genet Genomics.* **265** (4): 647-53.
- Decourcelle, M., Perez-Fons, L., Baulande, S., Steiger, S., Couvelard, L., Hem, S., Zhu, C., Capell, T., Christou, P., Fraser, P. & Sandmann, G.** (2015) Combined transcript, proteome, and metabolite analysis of transgenic maize seeds engineered for enhanced carotenoid synthesis reveals pleiotropic effects in core metabolism. *J Exp Bot.* **66** (11): 3141-50.
- Delatte, T.L., Scaiola, G., Molenaar, J., de Sousa Farias, K., Alves Gomes Albertti, L., Busscher, J., Verstappen, F., Carollo, C., Bouwmeester, H. & Beekwilder, J.** (2018) Engineering storage capacity for volatile sesquiterpenes in *Nicotiana benthamiana* leaves. *Plant Biotechnol J.* **16** (12): 1997-2006.
- Delcourt, C., Carrière, I., Delage, M., Barberger-Gateau, P., Schalch, W. & POLA Study Group.** (2006) Plasma lutein and zeaxanthin and other carotenoids as modifiable risk factors for age-related maculopathy and cataract: the POLA Study. *Invest Ophthalmol Vis Sci.* **47** (6): 2329-35.
- Delgado-Vargas, F. & Paredes-López, O.** (1997) Enzymatic treatment to enhance carotenoid content in dehydrated marigold flower meal. *Plant Foods Hum Nutr.* **50** (2): 163-9.
- Demmig-Adams, B., Gilmore, A.M. & Adams, W.W.** (1996) Carotenoids 3: in vivo function of carotenoids in higher plants. *FASEB J.* **10** (4): 403-12.
- Denancé, N., Szurek, B. & Noël, L.D.** (2014) Emerging functions of nodulin-like proteins in non-nodulating plant species. *Plant Cell Physiol.* **55** (3): 469-74.
- Deruère, J., Römer, S., d'Harlingue, A., Backhaus, R.A., Kuntz, M. & Camara, B.** (1994) Fibril assembly and carotenoid overaccumulation in chromoplasts: a model for supramolecular lipoprotein structures. *Plant Cell.* **6** (1): 119-33.
- Desai, M., Rangarajan, P., Donahue, J.L., Williams, S.P., Land, E.S., Mandal, M.K., Phillippy, B.Q., Perera, I.Y., Raboy, V. & Gillaspay, G.E.** (2014) Two inositol hexakisphosphate kinases drive inositol pyrophosphate synthesis in plants. *Plant J.* **80** (4): 642-53.
- Dherani, M., Murthy, G.V., Gupta, S.K., Young, I.S., Maraini, G., Camparini, M., Price, G.M., John, N., Chakravarthy, U. & Fletcher, A.E.** (2008) Blood levels of vitamin C, carotenoids and retinol are inversely associated with cataract in a North Indian population. *Invest Ophthalmol Vis Sci.* **49**: 3328-35.
- Diaz, M., Sanchez-Barrena, M.J., Gonzalez-Rubio, J.M., Rodriguez, L., Fernandez, D., Antoni, R., Yunta, C., Belda-Palazon, B., Gonzalez-Guzman, M., Peirats-Llobet, M., Menendez, M., Boskovic, J., Marquez, J.A., Rodriguez, P.L. & Albert, A.** (2016) Calcium-dependent oligomerization of CAR proteins at cell membrane modulates ABA signaling. *Proc Natl Acad Sci U S A.* **113** (3): E396-405.

- Dickinson, A.J., Lehner, K., Mi, J., Jia, K.P., Mijar, M., Dinneny, J., Al-Babili, S. & Benfey, P.N. (2019) β -Cyclocitral is a conserved root growth regulator. *Proc Natl Acad Sci U S A.* **116** (21): 10563-7.
- Dietrich, R.A., Richberg, M.H., Schmidt, R., Dean, C. & Dangl, J.L. (1997) A novel zinc finger protein is encoded by the *Arabidopsis* LSD1 gene and functions as a negative regulator of plant cell death. *Cell.* **88** (5): 685-94.
- Ding, Y., Li, H., Chen, L.L. & Xie, K. (2016) Recent Advances in Genome Editing Using CRISPR/Cas9. *Front Plant Sci.* **7**: 703.
- Doukhanina, E.V., Chen, S., van der Zalm, E., Godzik, A., Reed, J. & Dickman, M.B. (2006) Identification and functional characterization of the BAG protein family in *Arabidopsis thaliana*. *J Biol Chem.* **281** (27): 18793-801.
- Dutt, S., Parkash, J., Mehra, R., Sharma, N., Singh, B., Raigond, P., Joshi, A., Chopra, S. & Singh, B.P. (2015) Translation initiation in plants: roles and implications beyond protein synthesis. *Biol Plantarum.* **59** (3): 401-12.
- Edwards, J.A. (2016) Zeaxanthin: Review of Toxicological Data and Acceptable Daily Intake. *J Ophthalmol.* **4** (1): 11-5.
- EFSA. (2008) Opinion of the safety of 'synthetic Zeaxanthin as an ingredient in food supplements'. Scientific Opinion of the Panel on Dietetic Products, Nutrition and Allergies (Question No EFSA-Q-2007-078). *EFSA J.* **728**: 1-27.
- EFSA. (2012) Scientific Opinion: Statement on the safety of synthetic zeaxanthin as an ingredient in food supplements. *EFSA J.* **10** (10): 2891.
- EFSA FEEDAP Panel (EFSA Panel on Additives and Products or Substances used in Animal Feed). (2015) Safety and efficacy of ethoxyquin (6-ethoxy-1,2-dihydro-2,2,4-trimethylquinoline) for all animal species. *EFSA J.* **13** (11): 4272.
- Egea, I., Bian, W., Barsan, C., Jauneau, A., Pech, J.C., Latché, A., Li, Z. & Chervin, C. (2011) Chloroplast to chromoplast transition in tomato fruit: spectral confocal microscopy analyses of carotenoids and chlorophylls in isolated plastids and time-lapse recording on intact live tissue. *Ann Bot.* **108** (2): 291-7.
- Eisenhauer, B., Natoli, S., Liew, G. & Flood, V.M. (2017) Lutein and Zeaxanthin-Food Sources, Bioavailability and Dietary Variety in Age-Related Macular Degeneration Protection. *Nutrients.* **9** (2): E120.
- El Shimi, H. & Moustafa, S. (2016) Waste Vitalization of Algae Processing. *JAEMS.* **2** (5): 360-2.
- Elmayan, T. & Vaucheret, H. (1996) Expression of single copies of a strongly expressed 35S transgene can be silenced post-transcriptionally. *Plant J.* **9** (6): 78-97.
- EMA. (2018) ICH guideline Q3C (R7) on impurities: guideline for residual solvents. EMA/CHMP/ICH/82260/2006.
- Enfissi, E.M., Barneche, F., Ahmed, I., Lichtlé, C., Gerrish, C., McQuinn, R.P., Giovannoni, J.J., Lopez-Juez, E., Bowler, C., Bramley, P.M. & Fraser, P.D. (2010) Integrative transcript and metabolite analysis of nutritionally enhanced DE-ETIOLATED1 downregulated tomato fruit. *Plant Cell.* **22** (4): 1190-215.
- Enfissi, E.M., Fraser, P.D., Lois, L.M., Boronat, A., Schuch, W. & Bramley, P.M. (2005) Metabolic engineering of the mevalonate and non-mevalonate isopentenyl diphosphate-forming pathways for the production of health-promoting isoprenoids in tomato. *Plant Biotechnol J.* **3** (1): 17-27.
- Enfissi, E.M.A., Nogueira, M., D'Ambrosio, C., Stigliani, A.L., Giorio, G., Misawa, N. & Fraser, P.D. (2019) The road to astaxanthin production in tomato fruit reveals plastid and metabolic adaptation resulting in an unintended high lycopene genotype with delayed over-ripening properties. *Plant Biotechnol J.* **17** (8): 1501-13.
- Ernst, H. (2002) Recent advances in industrial carotenoid synthesis. *Pure Appl Chem.* **74** (8): 1369-82.

- Esteban, R., Fleta-Soriano, E., Buezo, J., Míguez, F., Becerril, J.M. & García-Plazaola, J.I.** (2014) Enhancement of zeaxanthin in two-steps by environmental stress induction in rocket and spinach. *Food Res Int.* **65**: 207-14.
- Estévez, J.M., Cantero, A., Reindl, A., Reichler, S. & León, P.** (2001) 1-Deoxy-D-xylulose-5-phosphate synthase, a limiting enzyme for plastidic isoprenoid biosynthesis in plants. *J Biol Chem.* **276** (25): 22901-9.
- Evans, J. & Wormald, R.** (1996) Is the incidence of registrable age-related macular degeneration increasing? *Br J Ophthalmol.* **80** (1): 9-14.
- Evans, J.R. & Lawrenson, J.G.** (2012) Antioxidant vitamin and mineral supplements for slowing the progression of age-related macular degeneration. *Cochrane Database Syst Rev.* **11**: CD000254.
- Eye Disease Case-Control Study Group.** (1993) Antioxidant Status and Neovascular Age-Related Macular Degeneration. *Arch Ophthalmol.* **111** (1): 104-9.
- Faik, A., Price, N.J., Raikhel, N.V. & Keegstra, K.** (2002) An *Arabidopsis* gene encoding an alpha-xylosyltransferase involved in xyloglucan biosynthesis. *Proc Natl Acad Sci U S A.* **99** (11): 7797-802.
- Fan, W., Lou, H.Q., Gong, Y.L., Liu, M.Y., Wang, Z.Q., Yang, J.L. & Zheng, S.J.** (2014) Identification of early Al-responsive genes in rice bean (*Vigna umbellata*) roots provides new clues to molecular mechanisms of Al toxicity and tolerance. *Plant Cell Environ.* **37** (7): 1586-97.
- Farrow, S.C. & Facchini, P.J.** (2014) Functional diversity of 2-oxoglutarate/Fe(II)-dependent dioxygenases in plant metabolism. *Front Plant Sci.* **5**: 524.
- Fernandes, A.S., Nascimento, T.C., Jacob-Lopes, E., De Rosso, V.V. & Zepka, L.Q.** (2018) Introductory chapter: carotenoids - a brief overview on its structure, biosynthesis, synthesis, and applications. In: Zepka, L.Q., Jacob-Lopes, E. & De Rosso, V.V. (eds.). *Progress in carotenoid research*. Rijeka: IntechOpen, pp. 1-16.
- Fernandez, A.I., Viron, N., Alhagdow, M., Karimi, M., Jones, M., Amsellem, Z., Sicard, A., Czerednik, A., Angenent, G., Grierson, D., May, S., Seymour, G., Eshed, Y., Lemaire-Chamley, M., Rothan, C. & Hilson, P.** (2009) Flexible tools for gene expression and silencing in tomato. *Plant Physiol.* **151** (4): 1729-40.
- Ferrer-Gallego, R., Brás, N.F., García-Estévez, I., Mateus, N., Rivas-Gonzalo, J.C., de Freitas, V. & Escribano-Bailón, M.T.** (2016) Effect of flavonols on wine astringency and their interaction with human saliva. *Food Chem.* **209**: 358-64.
- Fieser, L.F.** (1950) Absorption spectra of carotenoids; structure of vitamin A₂. *J Org Chem.* **15** (5): 930-43.
- Finazzi, G., Johnson, G.N., Dall'Osto, L., Joliot, P., Wollman, F.A. & Bassi, R.** (2004) A zeaxanthin-independent nonphotochemical quenching mechanism localized in the photosystem II core complex. *Proc Natl Acad Sci U S A.* **101** (33): 12375-80.
- Fine, S.L., Berger, J.W., Maguire, M.G. & Ho, A.C.** (2000) Age-Related Macular Degeneration. *N Engl J Med.* **342** (7): 483-92.
- Fiore, A., Dall'osto, L., Fraser, P.D., Bassi, R. & Giuliano, G.** (2006) Elucidation of the beta-carotene hydroxylation pathway in *Arabidopsis thaliana*. *FEBS Lett.* **580** (19): 4718-22.
- Fischer, I., Camus-Kulandaivelu, L., Allal, F. & Stephan, W.** (2011) Adaptation to drought in two wild tomato species: the evolution of the Asr gene family. *New Phytol.* **190** (4): 1032-44.
- Floss, D.S., Schliemann, W., Schmidt, J., Strack, D. & Walter, M.H.** (2008) RNA interference-mediated repression of *MtCCD1* in mycorrhizal roots of *Medicago truncatula* causes accumulation of C27 apocarotenoids, shedding light on the functional role of CCD1. *Plant Physiol.* **148** (3): 1267-82.
- Flügge, U.I. & Gao, W.** (2005) Transport of isoprenoid intermediates across chloroplast envelope membranes. *Plant Biol (Stuttg).* **7** (1): 91-7.
- Food and Agriculture Organization of the United Nations.** (2008) GM food safety assessment. FAO: Rome.

- Frank, H.A., Bautista, J.A., Josue, J.S. & Young, A.J.** (2000) Mechanism of Nonphotochemical Quenching in Green Plants: Energies of the Lowest Excited Singlet States of Violaxanthin and Zeaxanthin. *Biochemistry*. **39** (11): 2831-7.
- Fraser, P.D. & Bramley, P.M.** (2004) The biosynthesis and nutritional uses of carotenoids. *Prog Lipid Res.* **43** (3): 228-65.
- Fraser, P.D., Enfissi, E.M.A., Halket, J.H., Truesdale, M.R., Yu, D.M., Gerrish, C. & Bramley, P.M.** (2007) Manipulation of phytoene levels in tomato fruit: Effects on isoprenoids, plastids and intermediary metabolism. *Plant Cell*. **19** (10): 3194-211.
- Fraser, P.D., Pinto, M.E.S., Holloway, D.E. & Bramley, P.M.** (2000) Application of high-performance liquid chromatography with photodiode array detection to the metabolite profiling of plant isoprenoids. *Plant J*. **24**: 551-8.
- Fraser, P.D., Truesdale, M.R., Bird, C.R., Schuch, W. & Bramley, P.M.** (1994) Carotenoid Biosynthesis during Tomato Fruit Development (Evidence for Tissue-Specific Gene Expression). *Plant Physiol*. **105** (1): 405-13.
- Friedman, D.S., O'Colmain, B.J., Muñoz, B., Tomany, S.C., McCarty, C., de Jong, P.T., Nemesure, B., Mitchell, P. & Kempen, J.** (2004) Prevalence of age-related macular degeneration in the United States. *Arch Ophthalmol*. **122** (4): 564-72.
- Gachomo, E.W., Jimenez-Lopez, J.C., Baptiste, L.J. & Kotchoni, S.O.** (2014) GIGANTUS1 (GTS1), a member of Transducin/WD40 protein superfamily, controls seed germination, growth and biomass accumulation through ribosome-biogenesis protein interactions in *Arabidopsis thaliana*. *BMC Plant Biol*. **14**: 37.
- Gady, A.L.F., Vriezen, W.H., Van de Wal, M.H.B.J., Huang, P., Bovy, A.G., Visser, R.G.F. & Bachem, C.W.B.** (2012) Induced point mutations in the phytoene synthase 1 gene cause differences in carotenoid content during tomato fruit ripening. *Mol Breeding*, **29** (3): 801-12.
- Gale, C.R., Hall, N.F., Phillips, D.I. & Martyn, C.N.** (2003) Lutein and zeaxanthin status and risk of age-related macular degeneration. *Invest Ophthalmol Vis Sci*. **44** (6): 2461-5.
- Gallardo, K., Courty, P.E., Le Signor, C., Wipf, D. & Vernoud, V.** (2014) Sulfate transporters in the plant's response to drought and salinity: regulation and possible functions. *Front Plant Sci*. **5**: 580.
- Galpaz, N., Ronen, G., Khalfa, Z., Zamir, D. & Hirschberg J.** (2006) A chromoplast-specific carotenoid biosynthesis pathway is revealed by cloning of the tomato white-flower locus. *Plant Cell*. **18** (8): 1947-60.
- Galpaz, N., Wang, Q., Menda, N., Zamir, D. & Hirschberg, J.** (2008) Abscisic acid deficiency in the tomato mutant *high-pigment 3* leading to increased plastid number and higher fruit lycopene content. *Plant J*. **53** (5): 717-30.
- Garnett, K.M., Gierhart, D.L. & Guerra-Santos, L.H.** (1997) *3R-3'R stereoisomer of zeaxanthin for treating macular degeneration in humans*. European patent EP0774251A2.
- Garnett, K.M., Gierhart, D.L. & Guerra-Santos, L.H.** (1998) *Method of making pure 3R-3'R stereoisomer of zeaxanthin for human ingestion*. U.S. patent 5,854,015.
- Gaudelli, N.M., Komor, A.C., Rees, H.A., Packer, M.S., Badran, A.H., Bryson, D.I. & Liu, D.R.** (2017) Programmable base editing of A•T to G•C in genomic DNA without DNA cleavage. *Nature*. **551** (7681): 464-71.
- Gemmecker, S., Schaub, P., Koschmieder, J., Brausemann, A., Drepper, F., Rodriguez-Franco, M., Ghisla, S., Warscheid, B., Einsle, O. & Beyer, P.** (2015) Phytoene Desaturase from *Oryza sativa*: Oligomeric Assembly, Membrane Association and Preliminary 3D-Analysis. *PLoS One*. **10** (7): e0131717.
- Geng-Qing, H., Si-Ying, G., Wen-Liang, X., Wen, L., Peng, L., Chao-Jun, Z., Deng-Di, L., Yong, Z., Fu-Guang, L. & Xue-Bao, L.** (2013) A Fasciclin-Like Arabinogalactan Protein, GhFLA1, Is Involved in Fiber Initiation and Elongation of Cotton. *Plant Physiol*. **161** (3): 1278-90.

- Genty, B., Briantais, J.M. & Baker, N.R.** (1989) The relationship between quantum yield of photosynthetic electron transport and quenching of chlorophyll fluorescence. *Biochim Biophys Acta*. **990** (1): 87-92.
- German, M.A., Kandel-Kfir, M., Swarzberg, D., Matsevitz, T. & Granot, D.** (2003) A rapid method for the analysis of zygosity in transgenic plants. *Plant Science*. **164** (2): 183-7.
- Geuting, V., Kobbe, D., Hartung, F., Dürr, J., Focke, M. & Puchta, H.** (2009) Two distinct MUS81-EME1 complexes from *Arabidopsis* process Holliday junctions. *Plant Physiol*. **150** (2): 1062-71.
- Gierhart, D.L.** (1994) *Production of zeaxanthin and zeaxanthin-containing compositions*. Applied Food Biotechnology, Inc. U.S. patent 5,308,759.
- Girke, C., Daumann, M., Niopek-Witz, S. & Möhlmann, T.** (2014) Nucleobase and nucleoside transport and integration into plant metabolism. *Front Plant Sci*. **5**: 443.
- Glass, M., Barkwill, S., Unda, F. & Mansfield, S.D.** (2015) Endo- β -1,4-glucanases impact plant cell wall development by influencing cellulose crystallization. *J Integr Plant Biol*. **57** (4): 396-410.
- Glickman, R.D.** (2011) Ultraviolet phototoxicity to the retina. *Eye Contact Lens*. **37** (4): 196-205.
- Global Burden of Disease Study 2013 Collaborators.** (2015) Global, regional, and national incidence, prevalence, and years lived with disability for 301 acute and chronic diseases and injuries in 188 countries, 1990-2013: a systematic analysis for the Global Burden of Disease Study 2013. *Lancet*. **386** (9995): 743-800.
- Głowacka, K., Kromdijk, J., Kucera, K., Xie, J., Cavanagh, A.P., Leonelli, L., Leakey, A.D.B., Ort, D.R., Niyogi, K.K. & Long, S.P.** (2018) Photosystem II Subunit S overexpression increases the efficiency of water use in a field-grown crop. *Nat Commun*. **9** (1): 868.
- Głowacka, K., Kromdijk, J., Leonelli, L., Niyogi, K.K., Clemente, T.E. & Long, S.P.** (2016) An evaluation of new and established methods to determine T-DNA copy number and homozygosity in transgenic plants. *Plant Cell Environ*. **39** (4): 908-17.
- Goel, P. & Singh, A.K.** (2015) Abiotic Stresses Downregulate Key Genes Involved in Nitrogen Uptake and Assimilation in *Brassica juncea* L. *PLoS One*. **10** (11): e0143645.
- Golan, I., Dominguez, P.G., Konrad, Z., Shkolnik-Inbar, D., Carrari, F. & Bar-Zvi, D.** (2014) Tomato ABCISIC ACID STRESS RIPENING (ASR) gene family revisited. *PLoS One*. **9** (10): e107117.
- Gomez-Roldan, V., Fermas, S., Brewer, P.B., Puech-Pagès, V., Dun, E.A., Pillot, J.P., Letisse, F., Matusova, R., Danoun, S., Portais, J.C., Bouwmeester, H., Bécard, G., Beveridge, C.A., Rameau, C. & Rochange, S.F.** (2008) Strigolactone inhibition of shoot branching. *Nature*. **455** (7210): 189-94.
- Gonçalves, B., Maugarny-Calès, A., Adroher, B., Cortizo, M., Borrega, N., Blein, T., Hasson, A., Gineau, E., Mouille, G., Laufs, P. & Arnaud, N.** (2017) GDP-L-fucose is required for boundary definition in plants. *J Exp Bot*. **68** (21-22): 5801-11.
- Gong, P., Zhang, J., Li, H., Yang, C., Zhang, C., Zhang, X., Khurram, Z., Zhang, Y., Wang, T., Fei, Z. & Ye, Z.** (2010) Transcriptional profiles of drought-responsive genes in modulating transcription signal transduction, and biochemical pathways in tomato. *J Exp Bot*. **61** (13): 3563-75.
- Gonzalez-Jorge, S., Mehrshahi, P., Magallanes-Lundback, M., Lipka, A.E., Angelovici, R., Gore, M.A. & DellaPenna, D.** (2016) ZEAXANTHIN EPOXIDASE Activity Potentiates Carotenoid Degradation in Maturing Seed. *Plant Physiol*. **171** (3): 1837-51.
- González-Lamothe, R., Tsitsigiannis, D.I., Ludwig, A.A., Panicot, M., Shirasu, K. & Jones, J.D.** (2006) The U-box protein CMPG1 is required for efficient activation of defense mechanisms triggered by multiple resistance genes in tobacco and tomato. *Plant Cell*. **18** (4): 1067-83.
- Goulas, E., Schubert, M., Kieselbach, T., Kleczkowski, L.A., Gardeström, P., Schröder, W. & Hurry, V.** (2006) The chloroplast lumen and stromal proteomes of *Arabidopsis thaliana* show differential sensitivity to short- and long-term exposure to low temperature. *Plant J*. **47**: 720-34.
- Goyal, K., Walton, L.J. & Tunnacliffe, A.** (2005) LEA proteins prevent protein aggregation due to water stress. *Biochem J*. **388** (Pt 1): 151-7.

- Goyal, R.K., Fatima, T., Topuz, M., Bernadec, A., Sicher, R., Handa, A.K. & Mattoo, A.K.** (2016) Pathogenesis-Related Protein 1b1 (PR1b1) Is a Major Tomato Fruit Protein Responsive to Chilling Temperature and Upregulated in High Polyamine Transgenic Genotypes. *Front Plant Sci.* **7**: 901.
- Gradinaru, C.C., van Stokkum, I.H.M., Pascal, A.A., van Grondelle, R. & van Amerongen, H.** (2000) Identifying the Pathways of Energy Transfer between Carotenoids and Chlorophylls in LHCII and CP29. A Multicolor, Femtosecond Pump–Probe Study. *J Phys Chem B.* **104** (39): 9330-42.
- Grausem, B., Widemann, E., Verdier, G., Nosbüsch, D., Aubert, Y., Beisson, F., Schreiber, L., Franke, R. & Pinot, F.** (2014) CYP77A19 and CYP77A20 characterized from *Solanum tuberosum* oxidize fatty acids in vitro and partially restore the wild phenotype in an *Arabidopsis thaliana* cutin mutant. *Plant Cell Environ.* **37** (9): 2102-15.
- Greer, S., Wen, M., Bird, D., Wu, X., Samuels, L., Kunst, L. & Jetter, R.** (2007) The cytochrome P450 enzyme CYP96A15 is the midchain alkane hydroxylase responsible for formation of secondary alcohols and ketones in stem cuticular wax of *Arabidopsis*. *Plant Physiol.* **145** (3): 653-67.
- Grefen, C. & Blatt, M.R.** (2008) SNAREs – molecular governors in signalling and development. *Curr Opin Plant Biol.* **11** (6): 600-9.
- Gross, J.** (1991) *Pigments in Vegetables. Chlorophylls and Carotenoids.* 1st Edition. New York: Van Nostrand Reinhold.
- Grover, A.** (2012) Plant Chitinases: Genetic Diversity and Physiological Roles. *Cri Rev Plant Sci.* **31** (1): 57-73.
- Grudzinski, W., Matula, M., Sielewiesiuk, J., Kernen, P., Krupa, Z. & Gruszecki, W.I.** (2001) Effect of 13-*cis* violaxanthin on organization of light harvesting complex II in monomolecular layers. *Biochim Biophys Acta.* **1503** (3): 291-302.
- Grudzinski, W., Nierzwicki, L., Welc, R., Reszczynska, E., Luchowski, R., Czub, J. & Gruszecki, W.I.** (2017) Localization and Orientation of Xanthophylls in a Lipid Bilayer. *Sci Rep.* **7** (1): 9619.
- Guillet, C., Aboul-Soud, M.A., Le Menn, A., Viron, N., Pribat, A., Germain, V., Just, D., Baldet, P., Rousselle, P., Lemaire-Chamley, M. & Rothan, C.** (2012) Regulation of the fruit-specific PEP carboxylase *SPPC2* promoter at early stages of tomato fruit development. *PLoS One.* **7** (5): e36795.
- Gujjar, R.S., Karkute, S.G., Rai, A., Singh, M. & Singh, B.** (2018) Proline-rich proteins may regulate free cellular proline levels during drought stress in tomato. *Curr Sci.* **114** (4): 915-20.
- Gupta, O.P., Brown, G.C., Brown, M.M.** (2007) Age-related macular degeneration: the costs to society and the patient. *Curr Opin Ophthalmol.* **18** (3): 201-5.
- Gupta, P., Ravi, I. & Sharma, V.** (2013) Induction of β -1,3-glucanase and chitinase activity in the defense response of *Eruca sativa* plants against the fungal pathogen *Alternaria brassicicola*. *J Plant Interact.* **8** (2): 155-61.
- Gupta, S. & Van Eck, J.** (2016) Modification of plant regeneration medium decreases the time for recovery of *Solanum lycopersicum* cultivar M82 stable transgenic lines. *Plant Cell Tiss Organ Cult.* **127**: 417-23.
- Guyer, L., Hofstetter, S.S., Christ, B., Lira, B.S., Rossi, M. & Hörtensteiner, S.** (2014) Different mechanisms are responsible for chlorophyll dephytylation during fruit ripening and leaf senescence in tomato. *Plant Physiol.* **166** (1): 44-56.
- Hadden, W.L., Watkins, R.H., Levy, L.W., Regalado, E., Rivadeneira, D.M., van Breemen, R.B. & Schwartz, S.J.** (1999) Carotenoid Composition of Marigold (*Tagetes erecta*) Flower Extract Used as Nutritional Supplement. *J Agric Food Chem.* **47** (10): 4189-94.
- Hajdu, A., Ádám, É., Sheerin, D.J., Dobos, O., Bernula, P., Hiltbrunner, A., Kozma-Bognár, L. & Nagy, F.** (2015) High-level expression and phosphorylation of phytochrome B modulates flowering time in *Arabidopsis*. *Plant J.* **83** (5): 794-805.
- Halpin, C.** (2004) Investigating and Manipulating Lignin Biosynthesis in the Postgenomic Era. *Adv Bot Res.* **41**: 63-106.

- Hamada, M., Ono, Y., Kiryu, H., Sato, K., Kato, Y., Fukunaga, T., Mori, R. & Asai, K.** (2016) Rtools: a web server for various secondary structural analyses on single RNA sequences. *Nucleic Acids Res.* **44** (W1): W302-7.
- Hameed, A., Arun, A.B., Ho, H.P., Chang, C.M., Rekha, P.D., Lee, M.R., Singh, S. & Young, C.C.** (2011) Supercritical carbon dioxide micronization of zeaxanthin from moderately thermophilic bacteria *Muricauda lutaonensis* CC-HSB-11^T. *J Agric Food Chem.* **59** (8): 4119-24.
- Hameed, A., Shahina, M., Lin, S.Y., Sridhar, K.R., Young, L.S., Lee, M.R., Chen, W.M., Chou, J.H. & Young, C.C.** (2012) *Siansivirga zeaxanthinifaciens* gen. nov., sp. nov., a novel zeaxanthin-producing member of the family Flavobacteriaceae isolated from coastal seawater of Taiwan. *FEMS Microbiol Lett.* **333** (1): 37-45.
- Hameed, A., Zaidi, S.S., Shakir, S. & Mansoor, S.** (2018) Applications of New Breeding Technologies for Potato Improvement. *Front Plant Sci.* **9**: 925.
- Hammershøj, M., Kidmose, U. & Steinfeldt, S.** (2010) Deposition of carotenoids in egg yolk by short-term supplement of coloured carrot (*Daucus carota*) varieties as forage material for egg-laying hens. *J Sci Food Agric.* **90** (7): 1163-71.
- Han, O. & Mudgett, R.E.** (1992) Effects of oxygen and carbon dioxide partial pressures on *Monascus* growth and pigment production in solid-state fermentations. *Biotechnol Prog.* **8** (1): 5-10.
- Handelman, G.J., Snodderly, D.M., Adler, A.J., Russett, M.D. & Dratz, E.A.** (1992) Measurement of carotenoids in human and monkey retinas. *Methods Enzymol.* **213**: 220-30.
- Hao, Y., Huang, B., Jia, D., Mann, T., Jiang, X., Qiu, Y., Niitsu, M., Berberich, T., Kusano, T. & Liu, T.** (2018) Identification of seven polyamine oxidase genes in tomato (*Solanum lycopersicum* L.) and their expression profiles under physiological and various stress conditions. *J Plant Physiol.* **228**: 1-11.
- Hao, Y., Oh, E., Choi, G., Liang, Z. & Wang, Z.Y.** (2012) Interactions between HLH and bHLH factors modulate light-regulated plant development. *Mol Plant.* **5** (3): 688-97.
- Harpster, M.H., Dawson, D.M., Nevins, D.J., Dunsmuir, P. & Brummell, D.A.** (2002) Constitutive overexpression of a ripening-related pepper endo-1,4- β -glucanase in transgenic tomato fruit does not increase xyloglucan depolymerization or fruit softening. *Plant Mol Biol.* **50** (3): 357-69.
- Hasan, M.M., Rafii, M.Y., Ismail, M.R., Mahmood, M., Rahim, H.A., Alam, M.A., Ashkani, S., Malek, M.A. & Latif, M.A.** (2015) Marker-assisted backcrossing: a useful method for rice improvement. *Biotechnol Biotechnol Equip.* **29** (2): 237-54.
- Hashida, S.N., Takahashi, H. & Uchimiya, H.** (2009) The role of NAD biosynthesis in plant development and stress responses. *Ann Bot.* **103** (6): 819-24.
- Hashimoto, H., Uragami, C., Yukihiro, N., Gardiner, A.T. & Cogdell, R.J.** (2018) Understanding/unravelling carotenoid excited singlet states. *J R Soc Interface.* **15** (141): 20180026.
- Havaux, M.** (1998) Carotenoids as membrane stabilizers in chloroplasts. *Trends Plant Sci.* **3** (4): 147-51.
- He, S., Huang, K., Zhang, X., Yu, X., Huang, P. & An, C.** (2011) The LSD1-type zinc finger motifs of *Pisum sativa* LSD1 are a novel nuclear localization signal and interact with importin alpha. *PLoS One.* **6** (7): e22131.
- He, W., Wang, Y., Dai, Z., Liu, C., Xiao, Y., Wei, Q. & Li, D.** (2019) Effect of UV-B radiation and a supplement of CaCl₂ on carotenoid biosynthesis in germinated corn kernels. *Food Chem.* **278**: 509-14.
- He, Y., Zhu, M., Wang, L., Wu, J., Wang, Q., Wang, R. & Zhao, Y.** (2018) Programmed Self-Elimination of the CRISPR/Cas9 Construct Greatly Accelerates the Isolation of Edited and Transgene-Free Rice Plants. *Mol Plant.* **11** (9): 1210-13.
- Hencken, H.** (1992) Chemical and Physiological Behavior of Feed Carotenoids and Their Effects on Pigmentation. *Poult Sci.* **71** (4): 711-7.
- Heyman, J., Canher, B., Bisht, A., Christiaens, F. & De Veylder, L.** (2018) Emerging role of the plant ERF transcription factors in coordinating wound defense responses and repair. *J Cell Sci.* **131** (2): jcs208215.

- Hieber, A.D., Kawabata, O. & Yamamoto, H.Y.** (2004) Significance of the lipid phase in the dynamics and functions of the xanthophyll cycle as revealed by PsbS overexpression in tobacco and in-vitro de-epoxidation in monogalactosyldiacylglycerol micelles. *Plant Cell Physiol.* **45** (1): 92-102.
- Hiwasa-Tanase, K., Kuroda, H., Hirai, T., Aoki, K., Takane, K. & Ezura, H.** (2012) Novel promoters that induce specific transgene expression during the green to ripening stages of tomato fruit development. *Plant Cell Rep.* **31** (8): 1415-24.
- Hoang, C.V. & Chapman, K.D.** (2002) Biochemical and molecular inhibition of plastidial carbonic anhydrase reduces the incorporation of acetate into lipids in cotton embryos and tobacco cell suspensions and leaves. *Plant Physiol.* **128** (4): 1417-27.
- Holden, J., Eldridge, A.L., Beecher, G.R., Buzzard, M.I., Bhagwat, S., Davis, C.S., Douglass, L.W., Gebhardt, S., Haytowitz, D. & Schakel, S.** (1999) Carotenoid content of U.S. Foods: an update of the database. *J Food Compos Anal.* **12** (3): 169-96.
- Holt, N.E., Kennis, J.T.M., Dall'Osto, L., Bassi, R. & Fleming, G.R.** (2003). Carotenoid to chlorophyll energy transfer in light harvesting complex II from *Arabidopsis thaliana* probed by femtosecond fluorescence upconversion. *Chem Phys Lett.* **379** (3-4): 305-13.
- Holz, F.G., Strauss, E.C., Schmitz-Valckenberg, S. & van Lookeren Campagne, M.** (2014) Geographic atrophy: clinical features and potential therapeutic approaches. *Ophthalmology.* **121** (5): 1079-91.
- Hornero-Méndez, D. & Mínguez-Mosquera, M.I.** (2000) Xanthophyll esterification accompanying carotenoid overaccumulation in chromoplast of *Capsicum annuum* ripening fruits is a constitutive process and useful for ripeness index. *J Agric Food Chem.* **48** (5): 1617-22.
- Horton, J.C. & Hoyt, W.F.** (1991a) Quadrantic visual field defects. A hallmark of lesions in extrastriate (V2/V3) cortex. *Brain.* **114** (Pt 4): 1703-18.
- Horton, J.C. & Hoyt, W.F.** (1991b) The representation of the visual field in human striate cortex. A revision of the classic Holmes map. *Arch Ophthalmol.* **109** (6): 816-24.
- Huang, F.C., Horváth, G., Molnár, P., Turcsi, E., Deli, J., Schrader, J., Sandmann, G., Schmidt, H. & Schwab, W.** (2009) Substrate promiscuity of RdCCD1, a carotenoid cleavage oxygenase from *Rosa damascena*. *Phytochemistry.* **70** (4): 457-64.
- Huang, L.L., Coleman, H.R., Kim, J., de Monasterio, F., Wong, W.T., Schleicher, R.L., Ferris, F.L. & Chew, E.Y.** (2008) Oral Supplementation of Lutein/Zeaxanthin and Omega-3 Long Chain Polyunsaturated Fatty Acids in Persons Aged 60 Years or Older, with or without AMD. *Invest Ophthalmol Vis Sci.* **49** (9): 3864-9.
- Humphries, J.M. & Khachik, F.** (2003) Distribution of lutein, zeaxanthin, and related geometrical isomers in fruit, vegetables, wheat, and pasta products. *J Agric Food Chem.* **51** (5): 1322-7.
- Hyun, T.K., van der Graaff, E., Albacete, A., Eom, S.H., Großkinsky, D.K., Böhm, H., Janschek, U., Rim, Y., Ali, W.W., Kim, S.Y. & Roitsch, T.** (2014) The *Arabidopsis* PLAT domain protein1 is critically involved in abiotic stress tolerance. *PLoS One.* **9** (11): e112946.
- Ifuku, K., Endo, T., Shikanai, T. & Aro, E.M.** (2011) Structure of the chloroplast NADH dehydrogenase-like complex: nomenclature for nuclear-encoded subunits. *Plant Cell Physiol.* **52** (9): 1560-8.
- Inbaraj, B.S., Chien, J.T. & Chen, B.H.** (2006) Improved high performance liquid chromatographic method for determination of carotenoids in the microalga *Chlorella pyrenoidosa*. *J Chromatogr A.* **1102**: 193-9.
- IndiaMART InterMESH.** (2019) [Zeaxanthin] Available from: <https://www.indiamart.com/>.
- Inoguchi, N., Chaiseeda, K., Yamanishi, M., Kim, M.K., Jang, Y., Bajaj, M., Chia, C.P., Becker, D.F. & Moriyama, H.** (2015) Structural insights into the mechanism defining substrate affinity in *Arabidopsis thaliana* dUTPase: the role of tryptophan 93 in ligand orientation. *BMC Res Notes.* **8**: 784.
- Institute for Theoretical Chemistry, University of Vienna.** (nd.) *RNAfold* WebServer. Retrieved from: <http://rna.tbi.univie.ac.at/cgi-bin/RNAWebSuite/RNAfold.cgi>.

- Isaacson, T., Ohad, I., Beyer, P. & Hirschberg, J. (2004) Analysis in vitro of the enzyme CRTISO establishes a poly-*cis*-carotenoid biosynthesis pathway in plants. *Plant Physiol.* **136** (4): 4246-55.
- Ishibashi, T., Kimura, S. & Sakaguchi, K. (2006) A higher plant has three different types of RPA heterotrimeric complex. *J Biochem.* **139** (1): 99-104.
- Ishiga, Y., Ishiga, T., Uppalapati, S.R. & Mysore, K.S. (2013) Jasmonate ZIM-domain (JAZ) protein regulates host and non-host pathogen-induced cell death in tomato and *Nicotiana benthamiana*. *PLoS One.* **8** (9): e75728.
- Isler, O., Lindlar, H., Montavon, M., Rüegg, R. & Zeller, P. (1956) Synthesen in der Carotinoid-Reihe. 3. Mitteilung. Die Synthese von 3,4; 3',4'-Bisdehydro- β -carotin und 3,4-Monodehydro- β -carotin. *Helv. Chim. Acta.* **39** (1): 274-82.
- Issouf, M., Mearns, S.A., Fraser, K. & Hodgson, R. (2012) *Biological production of zeaxanthin*. European patent 1893769. B1.
- Itai, A., Ishihara, K. & Bewley, J.D. (2003) Characterization of expression, and cloning, of beta-D-xylosidase and alpha-L-arabinofuranosidase in developing and ripening tomato (*Lycopersicon esculentum* Mill.) fruit. *J Exp Bot.* **54** (393): 2615-22.
- Ito, M., Yamano, Y., Tode, C. & Wada, A. (2009) Carotenoid synthesis: Retrospect and recent progress. *Arch Biochem Biophys.* **483** (2): 224-8.
- IUPAC Commission on the Nomenclature of Organic Chemistry, IUPAC-IUB Commission on Biochemical Nomenclature.** (1975) Nomenclature of carotenoids (Rules approved 1974). *Pure Appl Chem.* **41** (3): 405-31.
- Jahns, P. & Holzwarth, A.R. (2012) The role of the xanthophyll cycle and of lutein in photoprotection of photosystem II. *Biochim Biophys Acta.* **1817** (1): 182-93.
- Jahns, P., Latowski, D. & Strzalka, K. (2009) Mechanism and regulation of the violaxanthin cycle: the role of antenna proteins and membrane lipids. *Biochim Biophys Acta.* **1787** (1): 3-14.
- Jaswir, J., Shahidan, N., Othman, R., Has-Yun Hashim, Y.Z. & bin Salleh, M.N. (2014) Effects of season and storage period on accumulation of individual carotenoids in pumpkin flesh (*Cucurbita moschata*). *J Oleo Sci.* **63** (8): 761-7.
- Javitt, J.C., Zhou, Z., Maguire, M.G., Fine, S.L. & Willke, R.J. (2003) Incidence of exudative age-related macular degeneration among elderly Americans. *Ophthalmology.* **110** (8): 1534-9.
- Jeffery, J., Holzenburg, A. & King, S. (2012) Physical barriers to carotenoid bioaccessibility. Ultrastructure survey of chromoplast and cell wall morphology in nine carotenoid-containing fruits and vegetables. *J Sci Food Agric.* **92** (13): 2594-602.
- Jia, X.Y., He, L.H., Jing, R.L. & Li, R.Z. (2009) Calreticulin: conserved protein and diverse functions in plants. *Physiol Plant.* **136** (2): 127-38.
- Johnson, E.J., Neuringer, M., Russell, R.M., Schalch, W. & Snodderly, D.M. (2005) Nutritional manipulation of primate retinas, III: Effects of lutein or zeaxanthin supplementation on adipose tissue and retina of xanthophyll-free monkeys. *Invest Ophthalmol Vis Sci.* **46** (2): 692-702.
- Johnson, M.P., Havaux, M., Triantaphylidès, C., Ksas, B., Pascal, A.A., Robert, B., Davison, P.A., Ruban, A.V. & Horton, P. (2007) Elevated zeaxanthin bound to oligomeric LHCII enhances the resistance of *Arabidopsis* to photooxidative stress by a lipid-protective, antioxidant mechanism. *J Biol Chem.* **282** (31): 22605-18.
- Jones, M.O., Piron-Prunier, F., Marcel, F., Piednoir-Barbeau, E., Alsadon, A.A., Wahb-Allah, M.A., Al-Doss, A.A., Bowler, C., Bramley, P.M., Fraser, P.D. & Bendahmane, A. (2012) Characterisation of alleles of tomato light signalling genes generated by TILLING. *Phytochemistry.* **79**: 78-86.
- Joshi, C. & Singhal, R.S. (2016) Modelling and optimization of zeaxanthin production by *Paracoccus zeaxanthinifaciens* ATCC 21588 using hybrid genetic algorithm techniques. *Biocatal Agric Biotechnol.* **8**: 228-35.

- Joshi, R., Ramanarao, M.V. & Baisakh, N.** (2013) *Arabidopsis* plants constitutively overexpressing a myo-inositol 1-phosphate synthase gene (SalNO1) from the halophyte smooth cordgrass exhibits enhanced level of tolerance to salt stress. *Plant Physiol Biochem.* **65**: 61-6.
- Junghans, A., Sies, H. & Stahl, W.** (2001) Macular pigments lutein and zeaxanthin as blue light filters studied in liposomes. *Arch Biochem Biophys.* **391** (2): 160-4.
- Kabir, M.H., Han, W. & Wang, M.H.** (2011) Environmental stress response of a dehydroascorbate reductase gene from tomato, and its protective role in *Escherichia coli*. *Hortic Environ Biotechnol.* **52** (6): 621.
- Kadam, S.U., Tiwari, B.K. & O'Donnell, C.P.** (2013) Application of Novel Extraction Technologies for Bioactives from Marine Algae. *J Agric Food Chem.* **61** (20): 4667-75.
- Karppi, J., Laukkanen, J.A. & Kurl, S.** (2012) Plasma lutein and zeaxanthin and the risk of age-related nuclear cataract among the elderly Finnish population. *Br J Nutr.* **108** (1): 148-54.
- Katoh, K. & Standley, D.M.** (2013) MAFFT Multiple Sequence Alignment Software Version 7: Improvements in Performance and Usability. *Mol Biol Evol.* **30** (4): 772-80.
- Ke, J., Wen, T.N., Nikolau, B. & Wurtele, E.S.** (2000) Coordinate regulation of the nuclear and plastidic genes coding for the subunits of the heteromeric acetyl-coenzyme A carboxylase. *Plant Physiol.* **122** (4): 1057-71.
- Keller, H., Reinhardt, G., Gärtner, S., Rettenmaier, N., Goacher, P., Mitchell, R., Peñaloza, D., Stahl, S. & Harvey, P.** (2017) Integrated sustainability assessment of *Dunaliella*-based algae biorefinery concepts. In: *D-Factory Project Reports, supported by the EU's FP7 under GA No. 613870*. IFEU – Institute for Energy and Environmental Research Heidelberg: Heidelberg, Germany.
- Kelley, L. A., Mezulis, S., Yates, C. M., Wass, M. N. & Sternberg, J. E.** (2015) The Phyre2 web portal for protein modeling, prediction and analysis. *Nat Protoc.* **10** (6): 845-58.
- Kersey, P.J., Allen, J.E., Allot A., Barba, M., Boddu, S., Bolt, B.J., Carvalho-Silva, D., Christensen, M., Davis, P., Grabmueller, C., Kumar, N., Liu, Z., Maurel, T., Moore, B., McDowall, M.D., Maheswari, U., Naamati, G., Newman, V., Ong, C.K., Bolser, D.M., De Silva, N., Howe, K.L., Langridge, N., Maslen, G., Staines, D.M. & Yates, A.** (2018) Ensembl Genomes 2018: an integrated omics infrastructure for non-vertebrate species. *Nucleic Acids Res.* **46** (D1): D802-8.
- Khachik, F.** (2003) An Efficient Conversion of (3R,3'R,6'R)-Lutein to (3R,3'S,6'R)-Lutein (3'-Epilutein) and (3R,3'R)-Zeaxanthin. *J Nat Prod.* **66** (1): 67-72.
- Khachik, F., Beecher, G.R., Goli, M.B. & Lusby, W.R.** (1991) Separation, identification, and quantification of carotenoids in fruits, vegetables and human plasma by high performance liquid chromatography. *Pure Appl. Chem.* **63** (1): 71-80.
- Khachik, F., Bernstein, P.S. & Garland, D.L.** (1997a) Identification of lutein and zeaxanthin oxidation products in human and monkey retinas. *Invest Ophthalmol Vis Sci.* **38** (9): 1802-11.
- Khachik, F., de Moura, F.F., Chew, E.Y., Douglass, L.W., Ferris, F.L., Kim, J. & Thompson, D.J.** (2006) The effect of lutein and zeaxanthin supplementation on metabolites of these carotenoids in the serum of persons aged 60 or older. *Invest Ophthalmol Vis Sci.* **47** (12): 5234-42.
- Khachik, F., de Moura, F.F., Zhao, D.Y., Aebischer, C.P. & Bernstein, P.S.** (2002) Transformations of selected carotenoids in plasma, liver, and ocular tissues of humans and in non-primate animal models. *Invest Ophthalmol Vis Sci.* **43** (11): 3383-92.
- Khachik, F., Spangler, C.J., Smith, J.C., Canfield, L.M., Pfander, H. & Steck, A.** (1997b) Identification, quantification, and relative concentrations of carotenoids and their metabolites in human milk and serum. *Anal Chem.* **69** (10): 1873-81.
- Kim, M., Kang, J., Kang, Y., Kang, B.S. & Jin, E.** (2018) Loss of Function in Zeaxanthin Epoxidase of *Dunaliella tertiolecta* Caused by a Single Amino Acid Mutation within the Substrate-Binding Site. *Mar Drugs.* **16** (11): E418.

- Kim, S., Park, J. & Hwang, I.K.** (2004) Composition of Main Carotenoids in Korean Red Pepper (*Capsicum annuum*, L) and Changes of Pigment Stability During the Drying and Storage Process. *J Food Sci.* **69** (1): FCT39-44.
- Kim, T., Kim, T-K. & Zoh, K-D.** (2019) Degradation kinetics and pathways of β -cyclocitral and β -ionone during UV photolysis and UV/chlorination reactions. *J Environ Manage.* **239**: 8-16.
- Kinkade, M.P. & Foolad, M.R.** (2013) Validation and fine mapping of *lyc12.1*, a QTL for increased tomato fruit lycopene content. *Theor Appl Genet.* **126** (8): 2163-75.
- Kitajima, M. & Butler, W.L.** (1975) Quenching of chlorophyll fluorescence and primary photochemistry in chloroplasts by dibromothymoquinone. *Biochim Biophys Acta.* **376** (1): 105-15.
- Klein, R., Klein, B.E., Jensen, S.C., Mares-Perlman, J.A., Cruickshanks, K.J. & Palta, M.** (1999) Age-related maculopathy in a multiracial United States population: The National Health and Nutrition Examination Survey III. *Ophthalmology.* **106** (6): 1056-65.
- Klein, R., Klein, B.E., Jensen, S.C. & Meuer, S.M.** (1997) The five-year incidence and progression of age-related maculopathy: The Beaver Dam Eye Study. *Ophthalmology.* **104** (1): 7-21.
- Klein, R., Klein, B.E., Tomany, S.C., Meuer, S.M. & Huang, G.H.** (2002) Ten-year incidence and progression of age-related maculopathy: The Beaver Dam eye study. *Ophthalmology.* **109** (10): 1767-79.
- Klein, R., Rowland, M.L. & Harris, M.I.** (1995) Racial/ethnic differences in age-related maculopathy. Third National Health and Nutrition Examination Survey. *Ophthalmology.* **102** (3): 371-81.
- Klemens, P.A., Patzke, K., Deitmer, J., Spinner, L., Le Hir, R., Bellini, C., Bedu, M., Chardon, F., Krapp, A. & Neuhaus, H.E.** (2013) Overexpression of the vacuolar sugar carrier *AtSWEET16* modifies germination, growth, and stress tolerance in *Arabidopsis*. *Plant Physiol.* **163** (3): 1338-52.
- Kleppinger-Sparace, K.F., Mudd, J.B. & Bishop, D.G.** (1985) Biosynthesis of sulfoquinovosyldiacylglycerol in higher plants: the incorporation of ^{35}S by intact chloroplasts. *Arch Biochem Biophys.* **240** (2): 859-65.
- Kobayashi, K.** (2016) Role of membrane glycerolipids in photosynthesis, thylakoid biogenesis and chloroplast development. *J Plant Res.* **129** (4): 565-80.
- Kochevenko, A., Araújo, W.L., Maloney, G.S., Tieman, D.M., Do, P.T., Taylor, M.G., Klee, H.J. & Fernie, A.R.** (2012) Catabolism of branched chain amino acids supports respiration but not volatile synthesis in tomato fruits. *Mol Plant.* **5** (2): 366-75.
- Kohlwein, S.D., Veenhuis, M. & van der Klei, I.J.** (2013) Lipid droplets and peroxisomes: key players in cellular lipid homeostasis or a matter of fat store 'em up or burn 'em down. *Genetics.* **193** (1): 1-50.
- Koike, M., Takezawa, D., Arakawa, K. & Yoshida, S.** (1997) Accumulation of 19-kDa plasma membrane polypeptide during induction of freezing tolerance in wheat suspension-cultured cells by abscisic acid. *Plant Cell Physiol.* **38** (6): 707-16.
- Kolotilin, I., Koltai, H., Tadmor, Y., Bar-Or, C., Reuveni, M., Meir, A., Nahon, S., Shlomo, H., Chen, L. & Levin, I.** (2007) Transcriptional profiling of high pigment-2dg tomato mutant links early fruit plastid biogenesis with its overproduction of phytonutrients. *Plant Physiol.* **145** (2): 389-401.
- Komor, A.C., Kim, Y.B., Packer, M.S., Zuris, J.A. & Liu, D.R.** (2016) Programmable editing of a target base in genomic DNA without double-stranded DNA cleavage. *Nature.* **533** (7603): 420-4.
- Koo, S.Y., Cha, K.H., Song, D.G., Chung, D. & Pan, C.H.** (2011) Optimization of pressurized liquid extraction of zeaxanthin from *Chlorella ellipsoidea*. *J Agric Food Chem.* **58** (2): 793-7.
- Koornneef, M., Jorna, M.L., Brinkhorst-van der Swan, D.L. & Karssen, C.M.** (1982) The isolation of abscisic acid (ABA) deficient mutants by selection of induced revertants in non-germinating gibberellin sensitive lines of *Arabidopsis thaliana* (L.) Heynh. *Theor Appl Genet.* **61** (4): 385-93.
- Kotake, T., Hojo, S., Tajima, N., Matsuoka, K., Koyama, T. & Tsumuraya, Y.** (2008) A bifunctional enzyme with L-fucokinase and GDP-L-fucose pyrophosphorylase activities salvages free L-fucose in *Arabidopsis*. *J Biol Chem.* **283** (13): 8125-35.

- Kvarnheden, A., Yao, J.L., Zhan, X., O'Brien, I. & Morris, B.A.** (2000) Isolation of three distinct CycD3 genes expressed during fruit development in tomato. *J Exp Bot.* **51** (352): 1789-97.
- Kvíčalová, Z., Alster, J., Hofmann, E., Khoroshyy, P., Litvín, R., Bína, D., Polívka, T. & Pšenčík, J.** (2016) Triplet-triplet energy transfer from chlorophylls to carotenoids in two antenna complexes from dinoflagellate *Amphidinium carterae*. *Biochim Biophys Acta.* **1857** (4): 341-9.
- Lado, J., Zacarías, L., Gurrea, A., Page, A., Stead, A. & Rodrigo, M.J.** (2015) Exploring the diversity in Citrus fruit colouration to decipher the relationship between plastid ultrastructure and carotenoid composition. *Planta.* **242** (3): 645-61.
- Laha, D., Johnen, P., Azevedo, C., Dynowski, M., Weiß, M., Capolicchio, S., Mao, H., Iven, T., Steenbergen, M., Freyer, M., Gaugler, P., de Campos, M.K., Zheng, N., Feussner, I., Jessen, H.J., Van Wees, S.C., Saiardi, A. & Schaaf, G.** (2015) VIH2 Regulates the Synthesis of Inositol Pyrophosphate InsP8 and Jasmonate-Dependent Defenses in *Arabidopsis*. *Plant Cell.* **27** (4): 1082-97.
- Laluk, K., Abuqamar, S. & Mengiste, T.** (2011) The *Arabidopsis* mitochondria-localized pentatricopeptide repeat protein PGN functions in defense against necrotrophic fungi and abiotic stress tolerance. *Plant Physiol.* **156** (4): 2053-68.
- Landrum, J.T., Bone, R.A., Moore, L.L. & Gomez, C.M.** (1999) Analysis of zeaxanthin distribution within individual human retinas. *Methods Enzymol.* **299**: 457-67.
- Landrum, J.T., Bone, R.A., Neuringer, M. & Cao, Y.** (2010) Macular Pigment: From Discovery to Function. In: Landrum, J.T. & Nolan, J.M. (eds.) *Carotenoids and Retinal Disease*. Boca Raton: CRC Press, p. 10.
- Latowski, D., Kuczyńska, P. & Strzałka, K.** (2011) Xanthophyll cycle - a mechanism protecting plants against oxidative stress. *Redox Rep.* **16** (2): 78-90.
- Lee, B.K., Piao, H.Y. & Chung, W.J.** (2002) Production of red pigments by *Monascus purpureus* in solid-state culture. *Biotechnol Bioprocess Eng.* **7** (1): 21-5.
- Lee, H.A. & Yeom, S.I.** (2015) Plant NB-LRR proteins: tightly regulated sensors in a complex manner. *Brief Funct Genomics.* **14** (4): 233-42.
- Lee, Y.R., Li, Y. & Liu, B.** (2007) Two *Arabidopsis* phragmoplast-associated kinesins play a critical role in cytokinesis during male gametogenesis. *Plant Cell.* **19** (8): 2595-605.
- Lei, Y., Lu, L., Liu, H-Y., Li, S., Xing, F. & Chen, L-L.** (2014) CRISPR-P: A web tool for synthetic single-guide RNA design of CRISPR-system in plants. *Mol Plant.* **7** (9): 1494-6.
- Lepro PharmaCompass.** (2019) [Price Tab] Available from: <https://www.pharmacompass.com>.
- Leuenberger, H.G.W., Boguth, W., Widmer, E. & Zell, R.** (1976) Synthesis of optically active natural carotenoids and structurally related compounds. I. Synthesis of the chiral key compound (4R,6R)-4-hydroxy-2,2,6-trimethylcyclohexanone. *Helv Chim Acta.* **59** (5): 1832-49.
- Leung, I.Y., Sandstrom, M.M., Zucker, C.L., Neuringer, M. & Snodderly, D.M.** (2004) Nutritional manipulation of primate retinas, II: effects of age, n-3 fatty acids, lutein, and zeaxanthin on retinal pigment epithelium. *Invest Ophthalmol Vis Sci.* **45** (9): 3244-56.
- Léon-Kloosterziel, K.M., Gil, M.A., Ruijs, G.J., Jacobsen, S.E., Olszewski, N.E., Schwartz, S.H., Zeevaart, J.A. & Koornneef, M.** (1996) Isolation and characterization of abscisic acid-deficient *Arabidopsis* mutants at two new loci. *Plant J.* **10** (4): 655-61.
- Li, B., Ahmed, F. & Bernstein, P.S.** (2010a) Studies on the singlet oxygen scavenging mechanism of human macular pigment. *Arch Biochem Biophys.* **504** (1): 56-60.
- Li, B., Vachali, P. & Bernstein, P.S.** (2010b) Human ocular carotenoid-binding proteins. *Photochem Photobiol Sci.* **9** (11): 1418-25.
- Li, H., He, Z., Lu, G., Lee, S.C., Alonso, J., Ecker, J.R. & Luan, S.** (2007) A WD40 domain cyclophilin interacts with histone H3 and functions in gene repression and organogenesis in *Arabidopsis*. *Plant Cell.* **19** (8): 2403-16.

- Li, J. & Engelberth, A.S. (2018) Quantification and purification of lutein and zeaxanthin recovered from distillers dried grains with solubles (DDGS). *Bioresour. Bioprocess.* **5**: 32.
- Li, J., Brader, G. & Palva, E.T. (2008) Kunitz trypsin inhibitor: an antagonist of cell death triggered by phytopathogens and fumonisin b1 in *Arabidopsis*. *Mol Plant.* **1** (3): 482-95.
- Li, J.Y., Fu, Y.L., Pike, S.M., Bao, J., Tian, W., Zhang, Y., Chen, C.Z., Zhang, Y., Li, H.M., Huang, J., Li, L.G., Schroeder, J.I., Gassmann, W. & Gong, J.M. (2010b) The *Arabidopsis* nitrate transporter NRT1.8 functions in nitrate removal from the xylem sap and mediates cadmium tolerance. *Plant Cell.* **22** (5): 1633-46.
- Li, K., Qiu, H., Zhou, M., Lin, Y., Guo, Z. & Lu, S. (2018a) Chloroplast Protein 12 Expression Alters Growth and Chilling Tolerance in Tropical Forage *Stylosanthes guianensis* (Aublet) Sw. *Front Plant Sci.* **9**: 1319.
- Li, S. (2015) The *Arabidopsis thaliana* TCP transcription factors: A broadening horizon beyond development. *Plant Signal Behav.* **10** (7): e1044192.
- Li, Y., Kabbage, M., Liu, W. & Dickman, M.B. (2016) Aspartyl Protease-Mediated Cleavage of BAG6 Is Necessary for Autophagy and Fungal Resistance in Plants. *Plant Cell.* **28** (1): 233-47.
- Li, X., Wang, Y., Chen, S., Tian, H., Fu, D., Zhu, B., Luo, Y. & Zhu H. (2018b) Lycopene Is Enriched in Tomato Fruit by CRISPR/Cas9-Mediated Multiplex Genome Editing. *Front Plant Sci.* **9**: 559.
- Liang, G., Zhang, H., Lou, D. & Yu, D. (2016) Selection of highly efficient sgRNAs for CRISPR/Cas9-based plant genome editing. *Sci Rep.* **6**: 21451.
- Liao, C.J., Lai, Z., Lee, S., Yun, D.J. & Mengiste, T. (2016) *Arabidopsis* HOOKLESS1 Regulates Responses to Pathogens and Abscisic Acid through Interaction with MED18 and Acetylation of WRKY33 and ABI5 Chromatin. *Plant Cell.* **28** (7): 1662-81.
- Liao, H.H., Medwid, R.D., Heefner, D.L., Sniff, K.S., Hassler, R.A., Yarus, M.J., inventors. (1995) Carotenoid producing culture using *Nesporiopsis excentricum*. U.S. patent 5,437,997.
- Liao, W.L., Nur-E-Borhan, S.A., Okada, S., Matsui, T. & Yamaguchi, K. (1993) Pigmentation of Cultured Black Tiger Prawn by Feeding with a *Spirulina*-Supplemented Diet. *NIPPON SUISAN GAKK.* **59** (1): 165-9.
- Libault, M., Wan, J., Czechowski, T., Udvardi, M. & Stacey, G. (2007) Identification of 118 *Arabidopsis* transcription factor and 30 ubiquitin-ligase genes responding to chitin, a plant-defense elicitor. *Mol Plant Microbe Interact.* **20** (8): 900-11.
- Lin, J.H., Lee, D.J. & Chang, J.S. (2015) Lutein production from biomass: Marigold flowers versus microalgae. *Bioresour Technol.* **184**: 421-8.
- Lionetti, V., Fabri, E., De Caroli, M., Hansen, A.R., Willats, W.G., Piro, G. & Bellincampi, D. (2017) Three Pectin Methyltransferase Inhibitors Protect Cell Wall Integrity for *Arabidopsis* Immunity to *Botrytis*. *Plant Physiol.* **173** (3): 1844-63.
- Liu, F., Zhang, X., Lu, C., Zeng, X., Li, Y., Fu, D. & Wu, G. (2015) Non-specific lipid transfer proteins in plants: presenting new advances and an integrated functional analysis. *J Exp Bot.* **66** (19): 5663-81.
- Liu, G.Y., Essex, A., Buchanan, J.T., Datta, V., Hoffman, H.M., Bastian, J.F., Fierer, J. & Nizet, V. (2005) *Staphylococcus aureus* golden pigment impairs neutrophil killing and promotes virulence through its antioxidant activity. *J Exp Med.* **202** (2): 209-15.
- Liu, H., Ding, Y., Zhou, Y., Jin, W., Xie, K. & Chen L.L. (2017) CRISPR-P 2.0: An Improved CRISPR-Cas9 Tool for Genome Editing in Plants. *Mol Plant.* **10** (3): 530-2.
- Liu, H., Ma, Y., Chen, N., Guo, S., Liu, H., Guo, X., Chong, K. & Xu, Y. (2014) Overexpression of stress-inducible OsBURP16, the β subunit of polygalacturonase 1, decreases pectin content and cell adhesion and increases abiotic stress sensitivity in rice. *Plant Cell Environ.* **37** (5): 1144-58.
- Liu, L., Liu, H., Li, S., Zhang, X., Zhang, M., Zhu, N., Dufresne, C.P., Chen, S. & Wang, Q. (2016a) Regulation of BZR1 in fruit ripening revealed by iTRAQ proteomics analysis. *Sci Rep.* **6**: 33635.

- Liu, M., Gomes, B.L., Mila, I., Purgatto, E., Peres, L.E., Frasse, P., Maza, E., Zouine, M., Roustan, J.P., Bouzayen, M. & Pirrello, J.** (2016b) Comprehensive Profiling of Ethylene Response Factor Expression Identifies Ripening-Associated ERF Genes and Their Link to Key Regulators of Fruit Ripening in Tomato. *Plant Physiol.* **170** (3): 1732-44.
- Liu, R., Xu, Y.H., Jiang, S.C., Lu, K., Lu, Y.F., Feng, X.J., Wu, Z., Liang, S., Yu, Y.T., Wang, X.F. & Zhang, D.P.** (2013) Light-harvesting chlorophyll a/b-binding proteins, positively involved in abscisic acid signalling, require a transcription repressor, WRKY40, to balance their function. *J Exp Bot.* **64** (18): 5443-56.
- Lo, M., Taylor, C., Wang, L., Nowack, L., Wang, T.W. & Thompson, J.** (2004) Characterization of an ultraviolet B-induced lipase in *Arabidopsis*. *Plant Physiol.* **135** (2): 947-58.
- Loane, E., Nolan, J.M., O'Donovan, O., Bhosale, P., Bernstein, P.S. & Beatty, S.** (2008) Transport and retinal capture of lutein and zeaxanthin with reference to age-related macular degeneration. *Surv Ophthalmol.* **53** (1): 68-81.
- Loeber, D.E., Russell, S.W., Toubé, T.P., Weedon, B.C.L. & Diment, J.** (1971) Carotenoids and related compounds. Part XXVIII. Synthesis of zeaxanthin, β -cryptoxanthin, and zeinoxanthin (α -cryptoxanthin). *J Chem Soc C.* **0** (0): 404-8.
- Lohr, M., Schwender, J. & Polle, J.E.** (2012) Isoprenoid biosynthesis in eukaryotic phototrophs: a spotlight on algae. *Plant Sci.* **185-186**: 9-22.
- Losey, J.E., Harmon, J., Ballantyne, F. & Brown, C.** (1997) A polymorphism maintained by opposite patterns of parasitism and predation. *Nature.* **388** (6639): 269-72.
- Louveau, T., Leitao, C., Green, S., Hamiaux, C., van der Rest, B., Dechy-Cabaret, O., Atkinson, R.G. & Chervin, C.** (2011) Predicting the substrate specificity of a glycosyltransferase implicated in the production of phenolic volatiles in tomato fruit. *FEBS J.* **278** (2): 390-400.
- Love, A.J., Laird, J., Holt, J., Hamilton, A.J., Sadanandom, A. & Milner, J.J.** (2007) Cauliflower Mosaic Virus Protein P6 Is a Suppressor of RNA Silencing. *J Gen Virol.* **88** (Pt 12): 3439-44.
- Lu, P.J., Wang, C.Y., Yin, T.T., Zhong, S.L., Grierson, D., Chen, K.S. & Xu, C.J.** (2017) Cytological and molecular characterization of carotenoid accumulation in normal and high-lycopene mutant oranges. *Sci Rep.* **7** (1): 761.
- Lu, S., Zhang, Y., Zhu, K., Yang, W., Ye, J., Chai, L., Xu, Q. & Deng, X.** (2018). The Citrus Transcription Factor CsMADS6 Modulates Carotenoid Metabolism by Directly Regulating Carotenogenic Genes. *Plant Physiol.* **176** (4): 2657-76.
- Lu, Y-B., Qi, Y-P., Yang, L-T., Lee, J., Guo, P., Ye, X., Jia, M-Y., Li, M-L. & Chen, L-S.** (2015) Long-term boron-deficiency-responsive genes revealed by cDNA-AFLP differ between *Citrus sinensis* roots and leaves. *Front Plant Sci.* **6**: 585.
- Ma, L., Dou, H.L., Wu, Y.Q., Huang, Y.M., Huang, Y.B., Xu, X.R., Zou, Z.Y. & Lin, X.M.** (2012) Lutein and zeaxanthin intake and the risk of age-related macular degeneration: a systematic review and meta-analysis. *Br J Nutr.* **107** (3): 350-9.
- Machado, F.R.S., Trevisol, T.C., Boschetto, D.L., Burkert, J.F.M., Ferreira, S.R.S., Oliveira, J.V. & Burkert, C.A.V.** (2016) Technological process for cell disruption, extraction and encapsulation of astaxanthin from *Haematococcus pluvialis*. *J Biotechnol.* **218**: 108-14.
- MacMillan, C.P., Mansfield, S.D., Stachurski, Z.H., Evans, R. & Southerton, S.G.** (2010) Fasciclin-like arabinogalactan proteins: specialization for stem biomechanics and cell wall architecture in *Arabidopsis* and *Eucalyptus*. *Plant J.* **62** (4): 689-703.
- Maggioni, L. & Spellman, O. (eds.).** (2001) *Report of a Network Coordinating Group on Vegetables*. International Plant Genetic Resources Institute, Rome, Italy. Ad hoc meeting, 26-27 May 2000, Vila Real, Portugal.
- Malinow, M.R., Feeney-Burns, L., Peterson, L.H., Klein, M.L. & Neuringer, M.** (1980) Diet-related macular anomalies in monkeys. *Invest Ophthalmol Vis Sci.* **19** (8): 857-63.

- Mandal, M.K., Chanda, B., Xia, Y., Yu, K., Sekine, K.T., Gao, Q.M., Selote, D., Kachroo, A. & Kachroo, P.** (2011) Glycerol-3-phosphate and systemic immunity. *Plant Signal Behav.* **6** (11): 1871-74.
- Mani, B., Agarwal, M. & Katiyar-Agarwal, S.** (2015) Comprehensive Expression Profiling of Rice Tetraspanin Genes Reveals Diverse Roles During Development and Abiotic Stress. *Front Plant Sci.* **6**: 1088.
- Manna, S.** (2015) An overview of pentatricopeptide repeat proteins and their applications. *Biochimie.* **113**: 93-9.
- Maoka, T.** (2011) Carotenoids in Marine Animals. *Mar Drugs.* **9** (2): 278-93.
- Marcus, J.P., Green, J.L., Goulter, K.C. & Manners, J.M.** (1999) A family of antimicrobial peptides is produced by processing of a 7S globulin protein in *Macadamia integrifolia* kernels. *Plant J.* **19**: 699-710.
- Mares-Perlman, J.A., Fisher, A.I., Klein, R., Palta, M., Block, G., Millen, A.E. & Wright, J.D.** (2001) Lutein and zeaxanthin in the diet and serum and their relation to age-related maculopathy in the third national health and nutrition examination survey. *Am J Epidemiol.* **153** (5): 424-32.
- Marín-Rodríguez, M.C., Orchard, J. & Seymour, G.B.** (2002) Pectate lyases, cell wall degradation and fruit softening. *J Exp Bot.* **53** (377): 2115-9.
- Marmor, D. & Marmor, M.F.** (2010) Simulating vision with and without macular disease. *Arch Ophthalmol.* **128** (1): 117-25.
- Masetto, A., Flores-Cotera, L.B., Díaz, C., Langley, E. & Sanchez, S.** (2001) Application of a complete factorial design for the production of zeaxanthin by *Flavobacterium* sp. *J Biosci Bioeng.* **92** (1): 55-8.
- Matsuba, Y., Nguyen, T.T., Wiegert, K., Falara, V., Gonzales-Vigil, E., Leong, B., Schäfer, P., Kudrna, D., Wing, R.A., Bolger, A.M., Usadel, B., Tissier, A., Fernie, A.R., Barry, C.S. & Pichersky, E.** (2013) Evolution of a complex locus for terpene biosynthesis in *Solanum*. *Plant Cell.* **25** (6): 2022-36.
- Maxwell, K. & Johnson, G.N.** (2000) Chlorophyll fluorescence - a practical guide. *J Exp Bot.* **51** (345): 659-68.
- Mayer, H. & Isler, O.** (1971) Total Syntheses. In: Isler, O., Gutmann, H. & Solms, U. (eds,) *Carotenoids. Chemische Reihe (Lehrbücher und Monographien aus dem Gebiete der Exakten Wissenschaften)*. Volume 23. Basel: Birkhäuser, pp. 328-464.
- Mayer, K.M. & Shanklin, J.** (2005) A structural model of the plant acyl-acyl carrier protein thioesterase FatB comprises two helix/4-stranded sheet domains, the N-terminal domain containing residues that affect specificity and the C-terminal domain containing catalytic residues. *J Biol Chem.* **280** (5): 3621-7.
- McGraw, K.J., Hill, G.E., Navara, K.J. & Parker, R.S.** (2004) Differential accumulation and pigmentation ability of dietary carotenoids in colorful finches. *Physiol Biochem Zool.* **77** (3): 484-91.
- McHale, L., Tan, X., Koehl, P. & Michelmore, R.W.** (2006) Plant NBS-LRR proteins: adaptable guards. *Genome Biol.* **7** (4): 212.
- McWilliams, A.** (2018) *The Global Market for Carotenoids FOD025F*. BCC Research LLC.
- Mehta, R.A. & Mattoo, A.K.** (1996) Isolation and Identification of Ripening-Related Tomato Fruit Carboxypeptidase. *Plant physiol.* **110** (3): 875-82.
- Mehta, S.** (2015) Age-Related Macular Degeneration. *Prim Care.* **42** (3): 377-91.
- Mei, C., Jiang, S.C., Lu, Y.F., Wu, F.Q., Yu, Y.T., Liang, S., Feng, X.J., Portoles Comeras, S., Lu, K., Wu, Z., Wang, X.F. & Zhang, D.P.** (2014) *Arabidopsis* pentatricopeptide repeat protein SOAR1 plays a critical role in abscisic acid signalling. *J Exp Bot.* **65** (18): 5317-30.
- Meissner, G. & Delbruck, M.** (1968) Carotenes and Retinal in *Phycomyces* Mutants. *Plant Physiology.* **43** (8): 1279-83.
- Meyer, M., Huttenlocher, F., Cedzich, A., Procopio, S., Stroeder, J., Pau-Roblot, C., Lequart-Pillon, M., Pelloux, J., Stintzi, A. & Schaller, A.** (2016) The subtilisin-like protease SBT3 contributes to insect resistance in tomato. *J Exp Bot.* **67** (14): 4325-38.

- Meyer, P. & Saedler, H.** (1996). Homology-dependent gene silencing in plants. *Annu. Rev. Plant Physiol.* **47** (1): 23-48.
- Meza, T.J., Stangeland, B., Mercy, I.S., Skårn, M., Nymoen, D.A., Berg, A., Butenko, M.A., Håkelién, A-M., Haslekås, C., Meza-Zepeda, L.A. & Aalen, R.B.** (2002) Analyses of single-copy *Arabidopsis* T-DNA-transformed lines show that the presence of vector backbone sequences, short inverted repeats and DNA methylation is not sufficient or necessary for the induction of transgene silencing. *Nucleic Acids Res.* **30** (20): 4556-66.
- Miedes, E. & Lorences, E.P.** (2009) Xyloglucan endotransglucosylase/hydrolases (XTHs) during tomato fruit growth and ripening. *J Plant Physiol.* **166** (5): 489-98.
- Milanowska, J. & Gruszecki, W. I.** (2005) Heat-induced and light-induced isomerization of the xanthophyll pigment zeaxanthin. *Journal of Photochemistry and Photobiology B: Biology.* **80** (3): 178-86.
- Min, D., Li, F., Zhang, X., Cui, X., Shu, P., Dong, L. & Ren, C.** (2018) SIMYC2 Involved in Methyl Jasmonate-Induced Tomato Fruit Chilling Tolerance. *J Agric Food Chem.* **66** (12): 3110-7.
- Mishra, A.K., Puranik, S. & Prasad, M.** (2012) Structure and regulatory networks of WD40 protein in plants. *J. Plant Biochem. Biotechnol.* **21** (Suppl 1): S32-9.
- Moeller, S.M., Parekh, N., Tinker, L., Ritenbaugh, C., Blodi, B., Wallace, R.B., Mares, J.A. & CAREDS Research Study Group.** (2006) Associations between intermediate age-related macular degeneration and lutein and zeaxanthin in the Carotenoids in Age-related Eye Disease Study (CAREDS): ancillary study of the Women's Health Initiative. *Arch Ophthalmol.* **124** (8): 1151-62.
- Mohr, W.P.** (1979). Pigment Bodies in Fruits of Crimson and High Pigment Lines of Tomatoes. *Annals of Botany.* **44** (4): 427-34.
- Mokriakova, M.V., Pogorelko, G.V., Bruskin, S.A., Piruzian, E.S. & Abdeeva, I.A.** (2014) The role of peptidyl-prolyl-Cis/trans-isomerase Genes of *Arabidopsis thaliana* in plant defense during the course of *Xanthomonas campestris* infection. *Genetika.* **50** (2): 157-66.
- Monforte, A.J., Friedman, E., Zamir, D. & Tanksley, S.D.** (2001) Comparison of a set of allelic QTL-NILs for chromosome 4 of tomato: Deductions about natural variation and implications for germplasm utilization. *Theor Appl Genet.* **102** (4): 572-90.
- Moran, N.A. & Jarvik, T.** (2010) Lateral transfer of genes from fungi underlies carotenoid production in aphids. *Science.* **328** (5978): 624-7.
- Morita, K., Hatanaka, T., Misoo, S. & Fukayama, H.** (2014) Unusual small subunit that is not expressed in photosynthetic cells alters the catalytic properties of rubisco in rice. *Plant Physiol.* **164** (1): 69-79.
- Morosinotto, T., Caffarri, S., Dall'Osto, L. & Bassi, R.** (2003). Mechanistic aspects of the xanthophyll dynamics in higher plant thylakoids. *Physiol Plant.* **119** (3): 347-54.
- Morris, E.R. & Walker, J.C.** (2003) Receptor-like protein kinases: the keys to response. *Curr Opin Plant Biol.* **6** (4): 339-42.
- Mortain-Bertrand, A., Stammitti, L., Telef, N., Colardelle, P., Brouquisse, R., Rolin, D. & Gallusci, P.** (2008) Effects of exogenous glucose on carotenoid accumulation in tomato leaves. *Physiol Plant.* **134** (2): 246-56.
- Mortimer, J.C., Laohavisit, A., Macpherson, N., Webb, A., Brownlee, C., Battey, N.H. & Davies, J.M.** (2008) Annexins: multifunctional components of growth and adaptation. *J Exp Bot.* **59** (3): 533-44.
- Moummou, H1., Tonfack, L.B., Chervin, C., Benichou, M., Youmbi, E., Ginies, C., Latché, A., Pech, J.C. & van der Rest, B.** (2012) Functional characterization of *SfscADH1*, a fruit-ripening-associated short-chain alcohol dehydrogenase of tomato. *J Plant Physiol.* **169** (15): 1435-44.
- Mølhøj, M., Verma, R. & Reiter, W.D.** (2003) The biosynthesis of the branched-chain sugar *d*-apiose in plants: functional cloning and characterization of a UDP-*d*-apiose/UDP-*d*-xylose synthase from *Arabidopsis*. *Plant J.* **35** (6): 693-703.

- Muniz, I.J., Kretzschmar, A.A., Rufato, L., Pelizza, T.R., Rufato, A.R. & Macedo, T.A.** (2014) General aspects of *Physalis* cultivation. *Ciência Rural*. **44** (6): 964-70.
- Murchie, E.H. & Lawson, T.** (2013) Chlorophyll fluorescence analysis: a guide to good practice and understanding some new applications. *J Exp Bot*. **64** (13): 3983-98.
- Muthusamy, V., Hossain, F., Thirunavukkarasu, N., Choudhary, M., Saha, S., Bhat, J.S., Prasanna, B.M. & Gupta, H.S.** (2014) Development of β -Carotene Rich Maize Hybrids through Marker-Assisted Introgression of β -carotene hydroxylase Allele. *PLoS ONE*. **9** (12): e113583.
- Müller, M. & Munné-Bosch, S.** (2015) Ethylene Response Factors: A Key Regulatory Hub in Hormone and Stress Signaling. *Plant Physiol*. **169** (1): 32-41.
- Müller, P., Li, X.P. & Niyogi, K.K.** (2001) Non-Photochemical Quenching. A Response to Excess Light Energy. *Plant Physiol*. **125** (4): 1558-66.
- Nahirňak, V., Almasia, N.I., Fernandez, P.V., Hopp, H.E., Estevez, J.M., Carrari, F. & Vazquez-Rovere, C.** (2012) Potato snakin-1 gene silencing affects cell division, primary metabolism, and cell wall composition. *Plant Physiol*. **158** (1): 252-63.
- Nakahara, K.S., Masuta, C., Yamada, S., Shimura, H., Kashihara, Y., Wada, T.S., Meguro, A., Goto, K., Tadamura, K., Sueda, K., Sekiguchi, T., Shao, J., Itchoda, N., Matsumura, T., Igarashi, M., Ito, K., Carthew, R.W. & Uyeda, I.** (2012) Tobacco calmodulin-like protein provides secondary defense by binding to and directing degradation of virus RNA silencing suppressors. *Proc Natl Acad Sci U S A*. **109** (25): 10113-8.
- Nakayasu, M., Shioya, N., Shikata, M., Thagun, C., Abdelkareem, A., Okabe, Y., Ariizumi, T., Arimura, G.I., Mizutani, M., Ezura, H., Hashimoto, T. & Shoji, T.** (2018) JRE4 is a master transcriptional regulator of defense-related steroidal glycoalkaloids in tomato. *Plant J*. **94** (6): 975-90.
- Nambara, E. & Marion-Poll, A.** (2005) Abscisic acid biosynthesis and catabolism. *Annu Rev Plant Biol*. **56** (1): 165-85.
- Napoli, C., Lemieux, C. & Jorgensen, R.** (1990) Introduction of a Chimeric Chalcone Synthase Gene into *Petunia* Results in Reversible Co-Suppression of Homologous Genes in trans. *Plant Cell*. **2** (4): 279-89.
- Naqvi, K.R., Melø, T., Raju, B.B., Jávorfí, T., Simidjiev, I. & Garab, G.** (1997) Quenching of chlorophyll a singlets and triplets by carotenoids in light-harvesting complex of photosystem II: comparison of aggregates with trimers. *Spectrochim. Acta A*. **53** (14): 2659-67.
- Nashilevitz, S., Melamed-Bessudo, C., Izkovich, Y., Rogachev, I., Osorio, S., Itkin, M., Adato, A., Pankratov, I., Hirschberg, J., Fernie, A.R., Wolf, S., Usadel, B., Levy, A.A., Rumeau, D. & Aharoni, A.** (2010) An orange ripening mutant links plastid NAD(P)H dehydrogenase complex activity to central and specialized metabolism during tomato fruit maturation. *Plant Cell*. **22** (6): 1977-97.
- Navarrete-Bolaños, J.L., Jiménez-Islas, H., Botello-Alvarez, E. & Rico-Martínez, R.** (2003) Mixed Culture Optimization for Marigold Flower Ensilage via Experimental Design and Response Surface Methodology. *J Agric Food Chem*. **51** (8): 2206-11.
- Navarrete-Bolaños, J.L., Jiménez-Islas, H., Botello-Alvarez, E., Rico-Martínez, R. & Paredes-López, O.** (2004) Improving Xanthophyll Extraction from Marigold Flower Using Cellulolytic Enzymes. *J Agric Food Chem*. **52** (11): 3394-8.
- Navarrete-Bolaños, J.L., Rangel-Cruz, C.L., Jiménez-Islas, H., Botello-Alvarez, E. & Rico-Martínez, R.** (2005) Pre-treatment effects on the extraction efficiency of xanthophylls from marigold flower (*Tagetes erecta*) using hexane. *Food Res Int*. **38** (2): 159-65.
- NCBI Resource Coordinators.** (2015) Database resources of the National Center for Biotechnology Information. *Nucleic Acids Res*. **43** (Database issue): D6-17.
- Nemeskéri, E., Neményi, A., Bócs, A., Pék, Z. & Helyes, J.** (2019) Physiological Factors and their Relationship with the Productivity of Processing Tomato under Different Water Supplies. *Water*. **11** (3): 586.

- Nie, H., Wu, Y., Yao, C. & Tang, D.** (2011) Suppression of *edr2*-mediated powdery mildew resistance, cell death and ethylene-induced senescence by mutations in *ALD1* in *Arabidopsis*. *J Genet Genomics*. **38** (4): 137-48.
- Ninet, L. & Renaut, J.** (1979) Carotenoids. In: Pepler, H.J. & Perlman, D. (eds.) *Microbial technology*. vol. 1, 2nd ed. New York: Academic Press, pp. 529-44.
- Niro, S., Fratianni, A., Panfili, G., Falasca, L., Cinquanta, L. & Alam, R.** (2017) Nutritional evaluation of fresh and dried goji berries cultivated in Italy. *Ital J Food Sci*. **29** (3): 398-408.
- Nisa, Z., Chen, C., Yu, Y., Chen, C., Mallano, A.I., Xiang-bo, D., Xiao-li, S. & Yan-ming, Z.** (2016) Constitutive Overexpression of Myo-inositol-1-Phosphate Synthase Gene (*GsMIPS2*) from Glycine soja Confers Enhanced Salt Tolerance at Various Growth Stages in *Arabidopsis*. *J Northeast Agric Univ*. **23** (2): 28-44.
- Niyogi, K.K., Grossman, A.R. & Björkman, O.** (1998) *Arabidopsis* mutants define a central role for the xanthophyll cycle in the regulation of photosynthetic energy conversion. *Plant Cell*. **10** (7): 1121-34.
- Nogueira, M., Berry, H., Nohl, R., Klompmaker, M., Holden, A. & Fraser, P.D.** (2016) Subchromoplast Fractionation Protocol for Different *Solanaceae* Fruit Species. *Bio-protocol* **6** (13): e1861.
- Nogueira, M., Enfissi, E.M.A., Martínez Valenzuela, M.E., Menard, G.N., Driller, R.L., Eastmond, P.J., Schuch, W., Sandmann, G. & Fraser, P.D.** (2017) Engineering of tomato for the sustainable production of ketocarotenoids and its evaluation in aquaculture feed. *Proc Natl Acad Sci U S A*. **114** (41): 10876-81.
- Nogueira, M., Mora, L., Enfissi, E.M.A., Bramley, P.M. & Fraser, P.D.** (2013) Subchromoplast Sequestration of Carotenoids Affects Regulatory Mechanisms in Tomato Lines Expressing Different Carotenoid Gene Combinations. *Plant Cell*. **25** (11): 4560-79.
- Nolan, J.M., Meagher, K., Kashani, S. & Beatty, S.** (2013) What is *meso*-zeaxanthin, and where does it come from? *Eye*. **27** (8): 899-905.
- Nuraini, M. & Djulardi, A.** (2017) Marigold Flower Extract as a Feed Additive in the Poultry Diet: Effects on Laying Quail Performance and Egg Quality. *Int J Poult Sci*. **16**: 11-5.
- Nühse, T.S., Stensballe, A., Jensen, O.N. & Peck, S.C.** (2004) Phosphoproteomics of the *Arabidopsis* plasma membrane and a new phosphorylation site database. *Plant Cell*. **16** (9): 2394-405.
- Ofori, P.A., Mizuno, A., Suzuki, M., Martinoia, E., Reuscher, S., Aoki, K., Shibata, D., Otagaki, S., Matsumoto, S. & Shiratake, K.** (2018) Genome-wide analysis of ATP binding cassette (ABC) transporters in tomato. *PLoS One*. **13** (7): e0200854.
- Okanenko, A.A., Taran, N. & Kosyk, O.I.** (2008) Plant sulfolipid. 1. Functions. *Biopolym Cell*. **24** (6): 431-40.
- Oleszkiewicz, T., Klimek-Chodacka, M., Milewska-Hendel, A., Zubko, M., Stróż, D., Kurczyńska, E., Boba, A., Szopa, J. & Baranski, R.** (2018) Unique chromoplast organisation and carotenoid gene expression in carotenoid-rich carrot callus. *Planta*. **248** (6): 1455-71.
- Orndorff, S.A., Campbell, E.A. & Medwid, R.D.** (1994) *Zeaxanthin producing strains of Neosporangiococcum excentricum*. U.S. patent 5,360,730.
- Osakabe, Y., Mizuno, S., Tanaka, H., Maruyama, K., Osakabe, K., Todaka, D., Fujita, Y., Kobayashi, M., Shinozaki, K. & Yamaguchi-Shinozaki, K.** (2010) Overproduction of the membrane-bound receptor-like protein kinase 1, RPK1, enhances abiotic stress tolerance in *Arabidopsis*. *J Biol Chem*. **285** (12): 9190-201.
- Otori, K., Tanabe, N., Tamoi, M. & Shigeoka, S.** (2019) Sugar Transporter Protein 1 (STP1) contributes to regulation of the genes involved in shoot branching via carbon partitioning in *Arabidopsis*. *Biosci Biotechnol Biochem*. **83** (3): 472-81.
- Pace, H.C. & Brenner, C.** (2001) The nitrilase superfamily: classification, structure and function. *Genome Biol*. **2** (1): REVIEWS0001.

- Paine, J.A., Shipton, C.A., Chaggar, S., Howells, R.M., Kennedy, M.J., Vernon, G., Wright, S.Y., Hinchliffe, E., Adams, J.L., Silverstone, A.L. & Drake, R.** (2005) Improving the nutritional value of Golden Rice through increased pro-vitamin A content. *Nat Biotechnol.* **23** (4): 482-7.
- Pan, C., Ye, L., Qin, L., Liu, X., He, Y., Wang, J., Chen, L. & Lua, G.** (2016) CRISPR/Cas9-mediated efficient and heritable targeted mutagenesis in tomato plants in the first and later generations. *Sci Rep.* **6**: 24765.
- Paniagua, C., Bilkova, A., Jackson, P., Dabravolski S., Riber, W., Didi, V., Houser, J., Gigli-Bisceglia, N., Wimmerova, M., Budínská, E., Hamann, T. & Hejatko, J.** (2017) Dirigent proteins in plants: modulating cell wall metabolism during abiotic and biotic stress exposure. *J Exp Bot.* **68** (13): 3287-301.
- Parisi, V., Tedeschi, M., Gallinaro, G., Varano, M., Saviano, S., Piermarocchi, S. & CARMIS Study Group.** (2008) Carotenoids and antioxidants in age-related maculopathy Italian study: multifocal electroretinogram modifications after 1 year. *Ophthalmology.* **115** (2): 324-33.
- Park, J.M., Park, C.J., Lee, S.B., Ham, B.K., Shin, R. & Paek, K.H.** (2001) Overexpression of the tobacco Tsi1 gene encoding an EREBP/AP2-type transcription factor enhances resistance against pathogen attack and osmotic stress in tobacco. *Plant Cell.* **13** (5): 1035-46.
- Partridge, M. & Murphy, D.J.** (2009) Roles of a membrane-bound caleosin and putative peroxygenase in biotic and abiotic stress responses in *Arabidopsis*. *Plant Physiol Biochem.* **47** (9): 796-806.
- Pasarin, D. & Rovinaru, C.** (2018) Sources of Carotenoids and Their Uses as Animal Feed Additives – a Review. *Scientific Papers: Series D, Animal Science* **61** (2): 74-85.
- Passricha, N., Saifi, S., Khatodia, S. & Tuteja, N.** (2016) Assessing zygosity in progeny of transgenic plants: current methods and perspectives. *J Biol Methods.* **3** (3): e46.
- Paterson, A.H., Damon, S., Hewitt, J.D., Zamir, D., Rabinowitch, H.D., Lincoln, S.E., Lander, E.S. & Tanksley, S.D.** (1991) Mendelian factors underlying quantitative traits in tomato: comparison across species, generations, and environments. *Genetics.* **127** (1): 181-97.
- Peng, L., Fukao, Y., Fujiwara, M., Takami, T. & Shikanai, T.** (2009) Efficient operation of NAD(P)H dehydrogenase requires supercomplex formation with photosystem I via minor LHCl in *Arabidopsis*. *Plant Cell.* **21** (11): 3623-40.
- Perez-Fons, L., Wells, T., Corol, D.I., Ward, J.L., Gerrish, C., Beale, M.H., Seymour, G.B., Bramley, P.M. & Fraser, P.D.** (2014) A genome-wide metabolomic resource for tomato fruit from *Solanum pennellii*. *Sci Rep.* **4**: 3859.
- Perotti, M.F., Ribone, P.A. & Chan, R.L.** (2017) Plant transcription factors from the homeodomain-leucine zipper family I. Role in development and stress responses. *IUBMB Life.* **69** (5): 280-9.
- Perry A., Rasmussen H. & Johnson E.** (2009) Xanthophyll (lutein, zeaxanthin) content in fruits, vegetables and corn and egg products. *J Food Comp Anal.* **22** (1): 9-15.
- Peters, C., Li, M., Narasimhan, R., Roth, M., Welti, R. & Wang, X.** (2010) Nonspecific phospholipase C NPC4 promotes responses to abscisic acid and tolerance to hyperosmotic stress in *Arabidopsis*. *Plant Cell.* **22** (8): 2642-59.
- Petit, J., Bres, C., Mauxion, J.P., Tai, F.W., Martin, L.B., Fich, E.A., Joubès, J., Rose, J.K., Domergue, F. & Rothan, C.** (2016) The Glycerol-3-Phosphate Acyltransferase GPAT6 from Tomato Plays a Central Role in Fruit Cutin Biosynthesis. *Plant Physiol.* **171** (2): 894-913.
- Pérez-Gálvez, A., Hornero-Méndez, D. & Mínguez-Mosquera, M.I.** (2004) Changes in the Carotenoid Metabolism of Capsicum Fruits during Application of Modelized Slow Drying Process for Paprika Production. *J Agric Food Chem.* **52** (3): 518-22.
- Pérez-Gálvez, A., Martin, H.D., Sies, H. & Stahl, W.** (2003) Incorporation of carotenoids from paprika oleoresin into human chylomicrons. *Br J Nutr.* **89** (6): 787-93.
- Pérez-Gil, J. & Rodríguez-Concepción, M.** (2013) Metabolic plasticity for isoprenoid biosynthesis in bacteria. *Biochem J.* **452** (1): 19-25.

- Phan, T.D., Bo, W., West, G., Lycett, G.W. & Tucker, G.A.** (2007) Silencing of the major salt-dependent isoform of pectinesterase in tomato alters fruit softening. *Plant Physiol.* **144** (4): 1960-7.
- Pičmanová, M. & Møller, B.L.** (2016) Apiose: one of nature's witty games. *Glycobiology.* **26** (5): 430-42.
- Pietrzykowska, M., Suorsa, M., Semchonok, D.A., Tikkanen, M., Boekema, E.J., Aro, E.M. & Jansson, S.** (2014) The light-harvesting chlorophyll a/b binding proteins Lhcb1 and Lhcb2 play complementary roles during state transitions in *Arabidopsis*. *Plant Cell.* **26** (9): 3646-60.
- Pinnola, A., Staleva-Musto, H., Capaldi, S., Ballottari, M., Bassi, R. & Polívka, T.** (2016). Electron transfer between carotenoid and chlorophyll contributes to quenching in the LHCSR1 protein from *Physcomitrella patens*. *Biochim Biophys Acta Bioenerg.* **1857** (12): 1870-8.
- Pintea, A., Rugina, D., Pop, R., Bunea, A. & Socaciu, C.** (2011) Xanthophylls protect against induced oxidation in cultured human retinal pigment epithelial cells. *J Food Composition Anal.* **24** (6): 830-6.
- Pokalsky, A.R., Hiatt, W.R., Ridge, N., Rasmussen, R., Houck, C.M. & Shewmaker, C.K.** (1989) Structure and expression of elongation factor 1 alpha in tomato. *Nucleic Acids Res.* **17** (12): 4661-73.
- Polívka, T., Herek, J.L., Zigmantas, D., Akerlund, H.E. & Sundström, V.** (1999) Direct observation of the (forbidden) S1 state in carotenoids. *Proc Natl Acad Sci U S A.* **96** (9): 4914-7.
- Prabhu, S., Rekha, P.D. & Arun, A.B.** (2014) Zeaxanthin biosynthesis by members of the genus *Muricauda*. *Pol J Microbiol.* **63** (1): 115-9.
- Prabhu, S., Rekha, P.D., Young, C.C., Hameed, A., Lin, S.Y. & Arun, A.B.** (2013) Zeaxanthin Production by Novel Marine Isolates from Coastal sand of India and its Antioxidant Properties. *Appl Biochem Biotechnol.* **171** (4): 817-31.
- Prado-Cabrero, A., Beatty, S., Stack, J., Howard, A. & Nolan, J.M.** (2016) Quantification of zeaxanthin stereoisomers and lutein in trout flesh using chiral high-performance liquid chromatography-diode array detection. *J Food Compos Anal.* **50**: 19-22.
- Provis, J.M., Diaz, C.M. & Dreher, B.** (1998) Ontogeny of the primate fovea: a central issue in retinal development. *Prog Neurobiol.* **54** (5): 549-80.
- Provis, J.M., Dubis, A.M., Maddess, T. & Carroll, J.** (2013) Adaptation of the central retina for high acuity vision: cones, the fovea and the avascular zone. *Prog Retin Eye Res.* **35**: 63-81.
- Qian, W., Yu, C., Qin, H., Liu, X., Zhang, A., Johansen, I.E. & Wang, D.** (2007) Molecular and functional analysis of phosphomannomutase (PMM) from higher plants and genetic evidence for the involvement of PMM in ascorbic acid biosynthesis in *Arabidopsis* and *Nicotiana benthamiana*. *Plant J.* **49** (3): 399-413.
- Qidwai, T., Jamal, F., Khan, M.Y. & Sharma, B.** (2014) Exploring Drug Targets in Isoprenoid Biosynthetic Pathway for *Plasmodium falciparum*. *Biochem Res Int.* **2014**: 657189.
- Qin, G., Gu, H., Ma, L., Peng, Y., Deng, X.W., Chen, Z. & Qu, L.J.** (2007a) Disruption of phytoene desaturase gene results in albino and dwarf phenotypes in *Arabidopsis* by impairing chlorophyll, carotenoid, and gibberellin biosynthesis. *Cell Res.* **17** (5): 471-82.
- Qin, G.H., Qi, X.X., Qi, Y.J., Gao, Z.H., Yi, X.K., Pan, H.F. & Xu, Y.L.** (2017) Identification and expression patterns of alcohol dehydrogenase genes involving in ester volatile biosynthesis in pear fruit. *J Integr Agric.* **16** (8): 1742-50.
- Qin, Y.M., Hu, C.Y., Pang, Y., Kastaniotis, A.J., Hiltunen, J.K. & Zhu, Y.X.** (2007b) Saturated very-long-chain fatty acids promote cotton fiber and *Arabidopsis* cell elongation by activating ethylene biosynthesis. *Plant Cell.* **19** (11): 3692-704.
- R Core Team.** (2018) R: A language and environment for statistical computing. R Foundation for Statistical Computing, Vienna, Austria. Available from: <https://www.R-project.org/>.
- Racsko, J. & Schrader, L.E.** (2012) Sunburn of Apple Fruit: Historical Background, Recent Advances and Future Perspectives. *Crit Rev Plant Sci.* **31** (6): 455-504.

- Radulović, N.S., Miljković, V.M., Mladenović, M.Z. & Nikolić, G.S.** (2017) Essential Oils of *Morus alba* and *M. nigra* Leaves: Effect of Drying on the Chemical Composition. *Nat Prod Commun.* **12** (1): 115-8.
- Raffo, A., La Malfa, G., Fogliano, V., Maiani, G. & Quaglia, G.** (2006) Seasonal variations in antioxidant components of cherry tomatoes (*Lycopersicon esculentum* cv. Naomi F1). *J Food Compos Anal.* **19** (1): 11-19.
- Rambla, J.L., Tikunov, Y.M., Monforte, A.J., Bovy, A.G. & Granell, A.** (2014) The expanded tomato fruit volatile landscape. *J Exp Bot.* **65** (16): 4613-23.
- Ramirez-Estrada, K., Castillo, N., Lara, J.A., Arró, M., Boronat, A., Ferrer, A. & Altabella, T.** (2017) Tomato UDP-Glucose Sterol Glycosyltransferases: A Family of Developmental and Stress Regulated Genes that Encode Cytosolic and Membrane-Associated Forms of the Enzyme. *Front Plant Sci.* **8**: 984.
- Ranjan, A., Budke, J.M., Rowland, S.D., Chitwood, D.H., Kumar, R., Carriedo, L., Ichihashi, Y., Zumstein, K., Maloof, J.N. & Sinha, N.R.** (2016) eQTL Regulating Transcript Levels Associated with Diverse Biological Processes in Tomato. *Plant Physiol.* **172** (1): 328-40.
- Raventos, D., Meier, C., Mattsson, O., Jensen, A.B. & Mundy, J.** (2000) Fusion genetic analysis of gibberellin signaling mutants. *Plant J.* **22** (5): 427-38.
- Reichel, M., Liao, Y., Rettel, M., Ragan, C., Evers, M., Alleaume, A.M., Horos, R., Hentze, M.W., Preiss, T. & Millar, A.A.** (2016) In Planta Determination of the mRNA-Binding Proteome of *Arabidopsis* Etiolated Seedlings. *Plant Cell.* **28** (10): 2435-52.
- Reimann, R., Kost, B. & Dettmer, J.** (2017) TETRASPANINs in Plants. *Front Plant Sci.* **8**: 545.
- Resnikoff, S., Pascolini, D., Etya'ale, D., Kocur, I., Pararajasegaram, R., Pokharel, G.P. & Mariotti, S.P.** (2004) Global data on visual impairment in the year 2002. *Bull World Health Organ.* **82** (11): 844-51.
- Richaud, D., Stange, C., Gadaleta, A., Colasuonno, P., Parada, R. & Schwember, A.R.** (2018) Identification of Lycopene epsilon cyclase (LCYE) gene mutants to potentially increase β -carotene content in durum wheat (*Triticum turgidum* L.ssp. durum) through TILLING. *PLoS One* **13** (12): e0208948.
- Rigano, M.M., Raiola, A., Docimo, T., Ruggieri, V., Calafiore, R., Vitaglione, P., Ferracane, R., Frusciante, L. & Barone, A.** (2016) Metabolic and Molecular Changes of the Phenylpropanoid Pathway in Tomato (*Solanum lycopersicum*) Lines Carrying Different *Solanum pennellii* Wild Chromosomal Regions. *Front Plant Sci.* **7**: 1484.
- Robinson, G.W.** (1963) Dynamic role of triplet states in photosynthesis. *Proc Natl Acad Sci U S A.* **49**: 521-9.
- Rock, C.D. & Zeevaart, J.A.** (1991) The *aba* mutant of *Arabidopsis thaliana* is impaired in epoxy-carotenoid biosynthesis. *Proc Natl Acad Sci U S A.* **88** (17): 7496-9.
- Ronen, G., Carmel-Goren, L., Zamir, D. & Hirschberg, J.** (2000) An alternative pathway to β -carotene formation in plant chromoplasts discovered by map-based cloning of *Beta* and *old-gold* color mutations in tomato. *Proc Natl Acad Sci U S A.* **97** (20): 11102-7.
- Rosales, J.A.S. & Torres-Cardona, M.C.M.D.** (2006) *Process for the purification of marigold xanthophylls.* U.S. patent 7,150,890.
- Rose, J.K., Braam, J., Fry, S.C. & Nishitani, K.** (2002) The XTH family of enzymes involved in xyloglucan endotransglucosylation and endohydrolysis: current perspectives and a new unifying nomenclature. *Plant Cell Physiol.* **43** (12): 1421-35.
- Rowe, T.S.** (2014) Handheld reflectometer for measuring macular pigment, CA 2814213 C.
- Römer, S., Lübeck, J., Kauder, F., Steiger, S., Adomat, C. & Sandmann, G.** (2002) Genetic engineering of a zeaxanthin-rich potato by antisense inactivation and co-suppression of carotenoid epoxidation. *Metab Eng.* **4** (4): 263-72.
- Rudnicka, A.R., Kapetanakis, V.V., Jarrar, Z., Wathern, A.K., Wormald, R., Fletcher, A.E., Cook, D.G. & Owen, C.G.** (2015) Incidence of Late-Stage Age-Related Macular Degeneration in American Whites: Systematic Review and Meta-analysis. *Am J Ophthalmol.* **160** (1): 85-93.

- Ruggieri, G. M., Triassi, A., Alvarez, C. E., Gola, A., Wiggerhauser, J., Budde, C. O., Lara, M. V., Drincovich, M. F. & Müller, G. L.** (2018) Overexpression of glycine-rich RNA-binding protein in tomato renders fruits with higher protein content after cold storage. *Biol Plantarum*. **62** (3): 501-10.
- Rui, Y., Xiao, C., Yi, H., Kandemir, B., Wang, J.Z., Puri, V.M. & Anderson, C.T.** (2017) POLYGALACTURONASE INVOLVED IN EXPANSION3 Functions in Seedling Development, Rosette Growth, and Stomatal Dynamics in *Arabidopsis thaliana*. *Plant Cell*. **29** (10): 2413-32.
- Ruijter, G.J., Panneman, H. & Visser, J.** (1997) Overexpression of phosphofructokinase and pyruvate kinase in citric acid-producing *Aspergillus niger*. *Biochim Biophys Acta*. **1334** (2-3): 317-26.
- Ruiz-Sola, M.Á. & Rodríguez-Concepción, M.** (2012) Carotenoid biosynthesis in *Arabidopsis*: a colorful pathway. *Arabidopsis Book*. **10**: e0158.
- Ruttimann, A. & Mayer, H.** (1980) Synthesis of optically active, natural carotenoids and structurally related natural products. V. Synthesis of (3*R*, 3'*R*) -, (3*S*, 3'*S*) - and (3*R*, 3'*S*; *meso*) -Zeaxanthin by Asymmetric Hydroboration. A new approach to optically active carotenoid building blocks. *Helv Chim Acta*. **63** (6): 1456-62.
- Saini, R.K. & Keum, Y.S.** (2017) Progress in Microbial Carotenoids Production. *Indian J Microbiol*. **57** (1): 129-30.
- Saini, R.K. & Keum, Y.S.** (2018) Carotenoid extraction methods: A review of recent developments. *Food Chem*. **240**: 90-103.
- Sajilata, M.G., Singhal, R.S. & Kamat, M.Y.** (2008) The Carotenoid Pigment Zeaxanthin - A Review. *Compr Rev Food Sci Food Saf*. **7** (1): 29-49.
- Sakai, T., Kagawa, T., Kasahara, M., Swartz, T.E., Christie, J.M., Briggs, W.R., Wada, M. & Okada, K.** (2001) *Arabidopsis* *nph1* and *npl1*: blue light receptors that mediate both phototropism and chloroplast relocation. *Proc Natl Acad Sci U S A*. **98** (12): 6969-74.
- Sakamoto, H., Matsuda, O. & Iba, K.** (2008) ITN1, a novel gene encoding an ankyrin-repeat protein that affects the ABA-mediated production of reactive oxygen species and is involved in salt-stress tolerance in *Arabidopsis thaliana*. *Plant J*. **56** (3): 411-22.
- Sanchez, S., Ruiz, B., Rodríguez-Sanoja, R. & Flores-Cotera, L.B.** (2013) Microbial production of carotenoids. In: McNeil, B., Archer, D., Giavasis, I. & Harvey, L. (eds.) *Microbial production of food ingredients, enzymes and nutraceuticals*. USA: Woodhead Publishing, pp. 194-233.
- Santiago, J., Dupeux, F., Betz, K., Antoni, R., Gonzalez-Guzman, M., Rodriguez, L., Márquez, J.A. & Rodriguez, P.L.** (2012) Structural insights into PYR/PYL/RCAR ABA receptors and PP2Cs. *Plant Sci*. **182**: 3-11.
- Santos, A.A., Lopes, K.V., Apfata, J.A. & Fontes, E.P.** (2010) NSP-interacting kinase, NIK: a transducer of plant defence signalling. *J Exp Bot*. **61** (14): 3839-45.
- Sarowar, S., Kim, Y.J., Kim, K.D., Hwang, B.K., Ok, S.H. & Shin, J.S.** (2009) Overexpression of lipid transfer protein (LTP) genes enhances resistance to plant pathogens and LTP functions in long-distance systemic signaling in tobacco. *Plant Cell Rep*. **28** (3): 419-27.
- Schaller, S., Wilhelm, C., Strzałka, K. & Goss, R.** (2012) Investigating the interaction between the violaxanthin cycle enzyme zeaxanthin epoxidase and the thylakoid membrane. *J Photochem Photobiol B*. **114**: 119-25.
- Schaub, P., Yu, Q., Gemmecker, S., Poussin-Courmontagne, P., Mailliot, J., McEwen, A.G., Ghisla, S., Al-Babili, S., Cavarelli, J. & Beyer, P.** (2012) On the structure and function of the phytoene desaturase CRTI from *Pantoea ananatis*, a membrane-peripheral and FAD-dependent oxidase/isomerase. *PLoS One*. **7** (6): e39550.
- Schäfer, L., Sandmann, M., Woitsch, S. & Sandmann, G.** (2006) Coordinate up-regulation of carotenoid biosynthesis as a response to light stress in *Synechococcus* PCC7942. *Plant Cell Environ*. **29** (7): 1349-56.

- Schieber, A. & Carle, R.** (2005) Occurrence of carotenoid *cis*-isomers in food: Technological, analytical, and nutritional implications. *Trends Food Sci Tech.* **16** (9): 416-22.
- Schiedt, K. & Liaaen-Jensen, S.** (1995) Isolation and Analysis. In: Britton, G., Liaaen-Jensen, S. & Pfander, H. (eds.) *Carotenoids. Volume 1A: Isolation and Analysis*. Basel: Birkhäuser Verlag AG, pp. 81-108.
- Schmidtke, P., Le Guilloux, V., Maupetit, J. & Tufféry, P.** (2010) fpocket: online tools for protein ensemble pocket detection and tracking. *Nucleic Acids Res.* **38** (Web Server issue): W582-9.
- Schmier, J.K., Jones, M.L. & Halpern, M.T.** (2006) The burden of age-related macular degeneration. *Pharmacoeconomics.* **24** (4): 319-34.
- Schneider, C.A., Rasband, W.S. & Eliceiri, K.W.** (2012) NIH Image to ImageJ: 25 years of image analysis. *Nat Methods.* **9** (7): 671-5.
- Scholz, S.S., Malabarba, J., Reichelt, M., Heyer, M., Ludewig, F. & Mithöfer, A.** (2017) Evidence for GABA-Induced Systemic GABA Accumulation in *Arabidopsis* upon Wounding. *Front Plant Sci.* **8**: 388.
- Schomburg, F.M., Bizzell, C.M., Lee, D.J., Zeevaart, J.A. & Amasino, R.M.** (2003) Overexpression of a novel class of gibberellin 2-oxidases decreases gibberellin levels and creates dwarf plants. *Plant Cell.* **15** (1): 151-63.
- Schröder, F., Lisso, J., Lange, P. & Müssig, C.** (2009) The extracellular EXO protein mediates cell expansion in *Arabidopsis* leaves. *BMC Plant Biol.* **9**: 20.
- Schubert, V., Weissleder, A., Ali, H., Fuchs, J., Lermontova, I., Meister, A. & Schubert, I.** (2009) Cohesin gene defects may impair sister chromatid alignment and genome stability in *Arabidopsis thaliana*. *Chromosoma.* **118** (5): 591-605.
- Schwarz, N., Armbruster, U., Iven, T., Brückle, L., Melzer, M., Feussner, I. & Jahns, P.** (2015) Tissue-specific accumulation and regulation of zeaxanthin epoxidase in *Arabidopsis* reflect the multiple functions of the enzyme in plastids. *Plant Cell Physiol.* **56** (2): 346-57.
- Seddon, J.M., Ajani, U.A., Sperduto, R.D., Hiller, R., Blair, N., Burton, T.C., Farber, M.D., Gragoudas, E.S., Haller, J., Miller, D.T., Yannuzzi, L.A. & Willett, W.** (1994) Dietary carotenoids, vitamins A, C, and E, and advanced age-related macular degeneration. Eye Disease Case-Control Study Group. *JAMA.* **272** (18): 1413-20.
- Seed World.** (2018) *KASP or HRM?* [Online] Available from: www.seedworld.com/kasp-or-hrm.
- Seifert, G.J., Xue, H. & Acet, T.** (2014) The *Arabidopsis thaliana* FASCICLIN LIKE ARABINOGALACTAN PROTEIN 4 gene acts synergistically with abscisic acid signalling to control root growth. *Ann Bot.* **114** (6): 1125-33.
- Seifi, A., Gao, D., Zheng, Z., Pavan, S., Faino, L., Visser, R.G.F., Wolters, A.M.A. & Bai, Y.** (2014) Genetics and molecular mechanisms of resistance to powdery mildews in tomato (*Solanum lycopersicum*) and its wild relatives. *Eur J Plant Pathol.* **138** (3): 641-65.
- Seo, H.S., Lee, S., Singh, D., Park, M.K., Kim, Y.S., Shin, H.W., Cho, S.A. & Lee, C.H.** (2018) Evaluating the Headspace Volatolome, Primary Metabolites, and Aroma Characteristics of *Koji* Fermented with *Bacillus amyloliquefaciens* and *Aspergillus oryzae*. *J Microbiol Biotechnol.* **28** (8): 1260-9.
- Seo, M. & Koshiba, T.** (2002) Complex regulation of ABA biosynthesis in plants. *Trends Plant Sci.* **7** (1): 41-8.
- Seong, E.S., Yoo, J.H., Lee, J.G., Kim, H.Y., Hwang, I.S., Heo, K., Lim, D.J., Lee, D.K., Sacks, E.J. & Yu, C.Y.** (2013) Transient overexpression of the *Miscanthus sinensis* glucose-6-phosphate isomerase gene (*MsGPI*) in *Nicotiana benthamiana* enhances expression of genes related to antioxidant metabolism. *Plant Omics.* **6** (6): 408-14.
- Sethuraman, S. & Madavalappil, K.P.** (2010) *A process for isolation of lutein and zeaxanthin crystals from plant sources*. European patent EP2246327A9.

- Shammai, A., Petreikov, M., Yeselson, Y., Faigenboim, A., Moy-Komemi, M., Cohen, S., Cohen, D., Besaulov, E., Efrati, A., Houminer, N., Bar, M., Ast, T., Schuldiner, M., Klemens, P.A.W., Neuhaus, E., Baxter, C.J., Rickett, D., Bonnet, J., White, R., Giovannoni, J.J., Levin, I. & Schaffer, A.** (2018) Natural genetic variation for expression of a SWEET transporter among wild species of *Solanum lycopersicum* (tomato) determines the hexose composition of ripening tomato fruit. *Plant J.* **96** (2): 343-57.
- Shao, W. & Espenshade, P.J.** (2014) Sterol regulatory element-binding protein (SREBP) cleavage regulates Golgi-to-endoplasmic reticulum recycling of SREBP cleavage-activating protein (SCAP). *J Biol Chem.* **289** (11): 7547-57.
- Sharma, D.K., Andersen, S.B., Ottosen, C.O. & Rosenqvist, E.** (2015) Wheat cultivars selected for high F_v/F_m under heat stress maintain high photosynthesis, total chlorophyll, stomatal conductance, transpiration and dry matter. *Physiol Plant.* **153** (2): 284-98.
- Shimada, T.L., Hayashi, M. & Hara-Nishimura, I.** (2018) Membrane Dynamics and Multiple Functions of Oil Bodies in Seeds and Leaves. *Plant Physiol.* **176** (1): 199-207.
- Shumbe, L., Bott, R. & Havaux, M.** (2014) Dihydroactinidiolide, a high light-induced β -carotene derivative that can regulate gene expression and photoacclimation in Arabidopsis. *Mol Plant.* **7** (7): 1248-51.
- Siefermann, D. & Yamamoto, H.Y.** (1975) Properties of NADPH and oxygen-dependent zeaxanthin epoxidation in isolated chloroplasts. *Arch Biochem Biophys.* **171** (1): 70-7.
- Silletti, M.F., Petrozza, A., Stigliani, A.L., Giorio, G., Cellini, F., D'Ambrosio, C. & Carriero, F.** (2013) An increase of lycopene content in tomato fruit is associated with a novel Cyc-B allele isolated through TILLING technology. *Mol Breeding.* **31** (3): 665-674.
- Simons, M.J.P. & Verhulst, S.** (2011) Zebra finch females prefer males with redder bills independent of song rate—a meta-analysis. *Behav Ecol.* **22** (4): 755-62.
- Singh, A. & Pandey, G.K.** (2016) How Phospholipase C Regulates Stress Tolerance and Development in Plants? *J Cell Signal.* **1**: 132.
- Singh, A.K., Singh, M.K. & Singh, R.J.** (2013) The Economics of marigold flowers in Eastern Uttar Pradesh. *J Rural Agric Res.* **13** (2): 75-8.
- Singh, D., Barrow, C.J., Mathur, A.S., Tuli, D.K. & Puri, M.** (2015) Optimization of zeaxanthin and β -carotene extraction from *Chlorella saccharophila* isolated from New Zealand marine waters. *Biocatal Agric Biotechnol.* **4** (2): 166-73.
- Singh, D., Puri, M., Wilkens, S., Mathur, A.S., Tuli, D.K. & Barrow, C.J.** (2013) Characterization of a new zeaxanthin producing strain of *Chlorella saccharophila* isolated from New Zealand marine waters. *Bioresour Technol.* **143**: 308-14.
- Singh, J., Freeling, M. & Lisch, D.** (2008) A Position Effect on the Heritability of Epigenetic Silencing. *PLoS Genet.* **4** (10): e1000216.
- Sivasubramanian, K. & Ganeshkumar, M.** (2004) Influence of vermishash on the biological productivity of marigold. *Madras Agric J.* **91** (4-6): 221-5.
- Slimestad, R. & Verheul, M.J.** (2005) Seasonal variations in the level of plant constituents in greenhouse production of cherry tomatoes. *J Agric Food Chem.* **53** (8): 3114-9.
- Smith, W., Assink, J., Klein, R., Mitchell, P., Klaver, C.C., Klein, B.E., Hofman, A., Jensen, S., Wang, J.J. & de Jong, P.T.** (2001) Risk factors for age-related macular degeneration: Pooled findings from three continents. *Ophthalmology.* **108** (4): 697-704.
- Snellen, E.L., Verbeek, A.L., Van Den Hoogen, G.W., Cruysberg, J.R. & Hoyng, C.B.** (2002) Neovascular age-related macular degeneration and its relationship to antioxidant intake. *Acta Ophthalmol Scand.* **80** (4): 368-71.
- Snodderly, D.M.** (1995) Evidence for protection against age-related macular degeneration by carotenoids and antioxidant vitamins. *Am J Clin Nutr.* **62** (6 Suppl): 1448S-61S.

- Snodderly, D.M., Auran, J.D. & Delori, F.C.** (1984) The macular pigment. II. Spatial distribution in primate retinas. *Invest Ophthalmol Vis Sci.* **25** (6): 674-85.
- Soleh, M.A., Ariyanti, M., Dewi, I.R. & Kadapi, M.** (2018) Chlorophyll fluorescence and stomatal conductance of ten sugarcane varieties under waterlogging and fluctuation light intensity. *Emir J Food Agr.* **30** (11): 935-40.
- Sommer, A., Tielsch, J.M., Katz, J., Quigley, H.A., Gottsch, J.D., Javitt, J.C., Martone, J.F., Royall, R.M., Witt, K.A. & Ezrine, S.** (1991) Racial differences in the cause-specific prevalence of blindness in east Baltimore. *N Engl J Med.* **325** (20): 1412-7.
- Sommerburg, O., Keunen, J.E.E., Bird, A.C. & van Kuijk, F.J.G.M.** (1998) Fruits and vegetables that are sources for lutein and zeaxanthin: the macular pigment in human eyes. *Br J Ophthalmol.* **82** (8): 907-10.
- Sonawane, P.D., Heinig, U., Panda, S., Gilboa, N.S., Yona, M., Kumar, S.P., Alkan, N., Unger, T., Bocobza, S., Pliner, M., Malitsky, S., Tkachev, M., Meir, S., Rogachev, I. & Aharoni, A.** (2018) Short-chain dehydrogenase/reductase governs steroidal specialized metabolites structural diversity and toxicity in the genus *Solanum*. *Proc Natl Acad Sci U S A.* **115** (23): E5419-28.
- Sonawane, P.D., Pollier, J., Panda, S., Szymanski, J., Massalha, H., Yona, M., Unger, T., Malitsky, S., Arendt, P., Pauwels, L., Almekias-Siegl, E., Rogachev, I., Meir, S., Cárdenas, P.D., Masri, A., Petrikov, M., Schaller, H., Schaffer, A.A., Kamble, A., Giri, A.P., Goossens, A. & Aharoni, A.** (2016) Plant cholesterol biosynthetic pathway overlaps with phytosterol metabolism. *Nat Plants.* **22** (3): 16205.
- Soukup, M., Widmer, E. & Lukáč, T.** (1990) Technical Procedures for the Syntheses of Carotenoids and Related Compounds from 6-Oxo-isophorone: Syntheses of (3*R*,3'*R*)-Zeaxanthin. Part II. *Helv Chim Acta.* **73** (4): 868-73.
- Sowbhagya, H.B., Sampathu, S.R. & Krishnamurthy, N.** (2004) Natural Colorant from Marigold-Chemistry and Technology. *Food Rev Int.* **20** (1): 33-50.
- Sowbhagya, H.B., Sushma, S.B., Rastogi, N.K. & Naidu, M.M.** (2013) Effect of pretreatments on extraction of pigment from marigold flower. *J Food Sci Technol.* **50** (1): 122-8.
- Sowmya, R. & Sachindra, N.M.** (2015) Carotenoid production by *Formosa* sp. KMW, a marine bacterium of Flavobacteriaceae family: Influence of culture conditions and nutrient composition. *Biocatal Agric Biotechnol.* **4** (4): 559-67.
- Speirs, J., Lee, E., Holt, K., Yong-Duk, K., Steele Scott, N., Loveys, B. & Schuch, W.** (1998) Genetic manipulation of alcohol dehydrogenase levels in ripening tomato fruit affects the balance of some flavor aldehydes and alcohols. *Plant Physiol.* **117** (3): 1047-58.
- Stam, M., Mol, J.N.M. & Mkoote, J.** (1997) Review Article: The Silence of Genes in Transgenic Plants. *Ann. Bot.* **79** (1): 3-12.
- Stankovic, I.** (2004) *Zeaxanthin. Chemical and Technical Assessment (CTA)*. 63rd JECFA. Available from: <http://www.fao.org/fileadmin/templates/agns/pdf/jecfa/cta/63/Zeaxanthin.pdf>.
- Stein, S.E., Mirokhin, Y., Tchekhovskoi, D. & Mallard, G.** (2012) NIST/EPA/NIH Mass Spectral Database (NIST 11) and NIST Mass Spectral Search Program (Version 2.0g). The NIST Mass Spectrometry Data Center, Gaithersburg, MD.
- Stepansky, A. & Leustek, T.** (2006) Histidine biosynthesis in plants. *Amino Acids.* **30** (2): 127-42.
- Steuer, B., Stuhlfauth, T. & Fock, H.P.** (1988) The efficiency of water use in water stressed plants is increased due to ABA induced stomatal closure. *Photosynth Res.* **18** (3): 327-36.
- Stigliani, A.L., Giorio, G. & D'Ambrosio, C.** (2011) Characterization of P450 carotenoid beta- and epsilon-hydroxylases of tomato and transcriptional regulation of xanthophyll biosynthesis in -root, leaf, petal and fruit. *Plant Cell Physiol.* **52** (5): 851-65.
- Stotz, H.U., Spence, B. & Wang, Y.** (2009) A defensin from tomato with dual function in defense and development. *Plant Mol Biol.* **71** (1-2): 131-43.

- Strack, D. & Fester, T.** (2006) Isoprenoid metabolism and plastid reorganization in arbuscular mycorrhizal roots. *New Phytol.* **172** (1): 22-34.
- Stransfeld, L., Eriksson, S., Adamski, N.M., Breuninger, H. & Lenhard, M.** (2010) KLUH/CYP78A5 promotes organ growth without affecting the size of the early primordium. *Plant Signal Behav.* **5** (8): 982-4.
- Strati, I.F., Gogou, E. & Oreopoulou, V.** (2015) Enzyme and high pressure assisted extraction of carotenoids from tomato waste. *Food Bioprod Process.* **94**: 668-74.
- Su, L., Diretto, G., Purgatto, E., Danoun, S., Zouine, M., Li, Z., Roustan, J.P., Bouzayen, M., Giuliano, G. & Chervin, C.** (2015) Carotenoid accumulation during tomato fruit ripening is modulated by the auxin-ethylene balance. *BMC Plant Biol.* **15**: 114.
- Sui, N., Li, M., Zhao, S.J., Li, F., Liang, H. & Meng, Q.W.** (2007) Overexpression of glycerol-3-phosphate acyltransferase gene improves chilling tolerance in tomato. *Planta.* **226** (5): 1097-108.
- Sujak, A., Gabrielska, J., Grudzinski, W., Borc, R., Mazurek, P. & Gruszecki, W.** (1999) Lutein and zeaxanthin as protectors of lipid membranes against oxidative damage: The structural aspects. *Arch Biochem Biophys.* **371** (2): 301-7.
- Sun, T., Yuan, H., Cao, H., Yazdani, M., Tadmor, Y. & Li, L.** (2018) Carotenoid Metabolism in Plants: The Role of Plastids. *Mol Plant.* **11** (1): 58-74.
- Sun, X., Shu, J., Ali Mohamed, A.M., Deng, X., Zhi, X., Bai, J., Cui, Y., Lu, X., Du, Y., Wang, X., Huang, Z., Guo, Y., Liu, L. & Li, J.** (2019) Identification and Characterization of *El* (*Elongated Internode*) Gene in Tomato (*Solanum lycopersicum*). *Int J Mol Sci.* **20** (9): 2204.
- Sutter, R.P.** (1975) Mutations affecting sexual development in *Phycomyces blakesleeana*. *Proc Natl Acad Sci U S A.* **72** (1): 127-30.
- Takahashi, H., Watanabe, A., Tanaka, A., Hashida, S.N., Kawai-Yamada, M., Sonoike, K. & Uchimiya, H.** (2006) Chloroplast NAD kinase is essential for energy transduction through the xanthophyll cycle in photosynthesis. *Plant Cell Physiol.* **47**: 1678-82.
- Takahashi, I., Kojima, S., Sakaguchi, N., Umeda-Hara, C. & Umeda, M.** (2010) Two *Arabidopsis* cyclin A3s possess G1 cyclin-like features. *Plant Cell Rep.* **29** (4): 307-15.
- Takaichi, S., Mochimaru, M., Uchida, H., Murakami, A., Hirose, E., Maoka, T., Tsuchiya, T. & Mimuro, M.** (2012) Opposite chirality of α -carotene in unusual cyanobacteria with unique chlorophylls, *Acaryochloris* and *Prochlorococcus*. *Plant Cell Physiol.* **53** (11): 1881-8.
- Takami, T., Shibata, M., Kobayashi, Y. & Shikanai, T.** (2010) De novo biosynthesis of fatty acids plays critical roles in the response of the photosynthetic machinery to low temperature in *Arabidopsis*. *Plant Cell Physiol.* **51** (8): 1265-75.
- Takayama, M., Koike, S., Kusano, M., Matsukura, C., Saito, K., Ariizumi, T. & Ezura, H.** (2015) Tomato Glutamate Decarboxylase Genes SIGAD2 and SIGAD3 Play Key Roles in Regulating γ -Aminobutyric Acid Levels in Tomato (*Solanum lycopersicum*). *Plant Cell Physiol.* **56** (8): 1533-45.
- Takemiya, A., Sugiyama, N., Fujimoto, H., Tsutsumi, T., Yamauchi, S., Hiyama, A., Tada, Y., Christie, J.M. & Shimazaki, K.** (2013) Phosphorylation of BLUS1 kinase by phototropins is a primary step in stomatal opening. *Nat Commun.* **4**: 2094.
- Takita, Y., Ichimiya, M., Hamamoto, Y. & Muto, M.** (2016) A case of carotenemia associated with ingestion of nutrient supplements. *J Dermatol.* **33** (2): 132-4.
- Talwar, D., Ha, T.K., Cooney, J., Brownlee, C. & O'Reilly, D.S.** (1998) A routine method for the simultaneous measurement of retinol, alpha-tocopherol and five carotenoids in human plasma by reverse phase HPLC. *Clin Chim Acta.* **270** (2): 85-100.
- Tam, J.P., Wang, S., Wong, K.H. & Tan, W.L.** (2015) Antimicrobial Peptides from Plants. *Pharmaceuticals (Basel).* **8** (4): 711-57.

- Tan, X., Cao, K., Liu, F., Li, Y., Li, P., Gao, C., Ding, Y., Lan, Z., Shi, Z., Rui, Q., Feng, Y., Liu, Y., Zhao, Y., Wu, C., Zhang, Q., Li, Y., Jiang, L. & Bao, Y.** (2016) *Arabidopsis* COG Complex Subunits COG3 and COG8 Modulate Golgi Morphology, Vesicle Trafficking Homeostasis and Are Essential for Pollen Tube Growth. *PLoS Genet.* **12** (7): e1006140.
- Tang, W., Wang, Y., Zhang, J., Cai, Y. & He, Z.** (2019) Biosynthetic Pathway of Carotenoids in *Rhodotorula* and Strategies for Enhanced Their Production. *J Microbiol Biotechnol.* **29** (4): 507-17.
- Tanvetyanon, T. & Bepler, G.** (2008) Beta-carotene in multivitamins and the possible risk of lung cancer among smokers versus former smokers: a meta-analysis and evaluation of national brands. *Cancer.* **113** (1): 150-7.
- Tark-Dame, M., Weber, B., de Sain, M., Anggoro, D.T., Bader, R., Walmsley, A., Oka, R. & Stam, M.** (2018) Generating Transgenic Plants with Single-copy Insertions Using BIBAC-GW Binary Vector. *J Vis Exp.* (133): e57295.
- Tähtiharju, S. & Palva, T.** (2001) Antisense inhibition of protein phosphatase 2C accelerates cold acclimation in *Arabidopsis thaliana*. *Plant J.* **26** (4): 461-70.
- Tenhaken, R.** (2015) Cell wall remodeling under abiotic stress. *Front Plant Sci.* **5**: 771.
- Tetali, S.D.** (2018) Terpenes and isoprenoids: a wealth of compounds for global use. *Planta.* **249** (1): 1-8.
- Thawornwiriyanun, P., Tanasupawat, S., Dechsakulwatana, C., Techkarnjanaruk, S. & Suntornsuk, W.** (2012) Identification of Newly Zeaxanthin-Producing Bacteria Isolated from Sponges in the Gulf of Thailand and their Zeaxanthin Production. *Appl Biochem Biotechnol.* **167** (8): 2357-68.
- Thompson, A.J., Jackson, A.C., Parker, R.A., Morpeth, D.R., Burbidge, A. & Taylor, I.B.** (2000) Abscisic acid biosynthesis in tomato: regulation of zeaxanthin epoxidase and 9-cis-epoxycarotenoid dioxygenase mRNAs by light/dark cycles, water stress and abscisic acid. *Plant Mol Biol.* **42** (6): 833-45.
- Tian, L., Magallanes-Lundback, M., Musetti, V. & DellaPenna, D.** (2003) Functional analysis of beta- and epsilon-ring carotenoid hydroxylases in *Arabidopsis*. *Plant Cell.* **15** (6): 1320-32.
- Tian, L., Musetti, V., Kim, J., Magallanes-Lundback, M. & DellaPenna, D.** (2004) The *Arabidopsis* LUT1 locus encodes a member of the cytochrome p450 family that is required for carotenoid epsilon-ring hydroxylation activity. *Proc Natl Acad Sci U S A.* **101** (1): 402-7.
- Tissier, A.F., Marillonnet, S., Klimyuk, V., Patel, K., Torres, M.A., Murphy, G. & Jones, J.D.** (1999) Multiple independent defective suppressor-mutator transposon insertions in *Arabidopsis*: a tool for functional genomics. *Plant Cell.* **11** (10): 1841-52.
- Todd, J., Post-Beittenmiller, D. & Jaworski, J.G.** (1999) KCS1 encodes a fatty acid elongase 3-ketoacyl-CoA synthase affecting wax biosynthesis in *Arabidopsis thaliana*. *Plant J.* **17** (2): 119-30.
- Tomato Genetics Resource Center (TGRC).** (n.d.) <https://tgrc.ucdavis.edu/>.
- Topuz, A. & Ozdemir, F.** (2003) Influences of γ -irradiation and storage on the carotenoids of sun-dried and dehydrated paprika. *J Agric Food Chem.* **51** (17): 4972-7.
- Torregrosa-Crespo, J., Montero, Z., Fuentes, J.L., Reig García-Galbis, M., Garbayo, I., Vílchez, C. & Martínez-Espinosa, R.M.** (2018) Exploring the Valuable Carotenoids for the Large-Scale Production by Marine Microorganisms. *Mar Drugs.* **16** (6): pii: E203.
- Torres-Cardona, M.D. & Vizcarra-Gonzales, D.** (2010) *Micronized carotenoid preparation as immunostimulant for crustaceans*. International patent WO2010094986A1.
- Torii, K.U.** (2004) Leucine-rich repeat receptor kinases in plants: structure, function, and signal transduction pathways. *Int Rev Cytol.* **234**: 1-46.
- Toyomizu, M., Sato, K., Taroda, H., Kato, T. & Akiba, Y.** (2001) Effects of dietary *Spirulina* on meat colour in muscle of broiler chickens. *Br Poult Sci.* **42** (2): 197-202.
- Tóth, T.N., Chukhutsina, V., Domonkos, I., Knoppová, J., Komenda, J., Kis, M., Lénárt, Z., Garab, G., Kovács, L., Gombos, Z. & Van Amerongen, H.** (2015) Carotenoids are essential for the assembly of cyanobacterial photosynthetic complexes. *Biochim Biophys Acta.* **1847** (10): 1153-65.

- Trapnell, C., Roberts, A., Goff, L., Pertea, G., Kim, D., Kelly, D.R., Pimentel, H., Salzberg, S.L., Rinn, J.L. & Pachter, L.** (2012) Differential gene and transcript expression analysis of RNA-seq experiments with TopHat and Cufflinks. *Nat Protoc.* **7** (3): 562-78.
- Trenkamp, S., Martin, W. & Tietjen, K.** (2004) Specific and differential inhibition of very-long-chain fatty acid elongases from *Arabidopsis thaliana* by different herbicides. *Proc Natl Acad Sci U S A.* **101** (32): 11903-8.
- Trevithick-Sutton, C.C., Foote, C.S., Collins, M. & Trevithick, J.R.** (2006) The retinal carotenoids zeaxanthin and lutein scavenge superoxide and hydroxyl radicals: a chemiluminescence and ESR study. *Mol Vis.* **12**: 1127-35.
- Tripathi, A.K., Pareek, A. & Singla-Pareek, S.L.** (2016) A NAP-Family Histone Chaperone Functions in Abiotic Stress Response and Adaptation. *Plant Physiol.* **171** (4): 2854-68.
- Tsao, R., Peterson, C.J. & Coats, J.R.** (2002) Glucosinolate breakdown products as insect fumigants and their effect on carbon dioxide emission of insects. *BMC Ecol.* **2**: 5.
- Tsay, Y.F., Chiu, C.C., Tsai, C.B., Ho, C.H. & Hsu, P.K.** (2007) Nitrate transporters and peptide transporters. *FEBS Lett.* **581** (12): 2290-300.
- Uematsu, K., Suzuki, N., Iwamae, T., Inui M. & Yukawa, H.** (2012) Increased fructose 1,6-bisphosphate aldolase in plastids enhances growth and photosynthesis of tobacco plants. *J Exp Bot.* **63** (8): 3001-9.
- Um, T.Y., Lee, S., Kim, J.K., Jang, G. & Choi, Y.D.** (2018) CHLORIDE CHANNEL 1 promotes drought tolerance in rice, leading to increased grain yield. *Plant Biotechnol Rep.* **12** (4): 283-93.
- Updike, A.A. & Schwartz, S.J.** (2003) Thermal Processing of Vegetables Increases *Cis* Isomers of Lutein and Zeaxanthin. *J Agric Food Chem.* **51** (21): 6184-90.
- Valberg, A.** (2005) *Light Vision Color*. Chippenham: Antony Rowe Ltd, p. 118.
- Van Eerden, F.J., Melo, M.N., Frederix, P.W.J.M., Periole, X. & Marrink, S.J.** (2017) Exchange pathways of plastoquinone and plastoquinol in the photosystem II complex. *Nat Commun.* **10** (8): 15214.
- Van Rossum, G.** (1995) Python tutorial, Technical Report CS-R9526. Centrum voor Wiskunde en Informatica (CWI), Amsterdam.
- Vanhercke, T., Divi, U.K., El Tahchy, A., Liu, Q., Mitchell, M., Taylor, M.C., Eastmond, P.J., Bryant, F., Mechanicos, A., Blundell, C., Zhi, Y., Belide, S., Shrestha, P., Zhou, X.R., Ral, J.P., White, R.G., Green, A., Singh, S.P. & Petrie, J.R.** (2017) Step changes in leaf oil accumulation via iterative metabolic engineering. *Metab Eng.* **39**: 237-46.
- Vasav, A.P. & Barvkar, V.T.** (2019) Phylogenomic analysis of cytochrome P450 multigene family and their differential expression analysis in *Solanum lycopersicum* L. suggested tissue specific promoters. *BMC Genomics.* **20** (1): 116.
- Veley, K.M., Maksaev, G., Frick, E.M., January, E., Kloepper, S.C. & Haswell, E.S.** (2014) *Arabidopsis* MSL10 has a regulated cell death signaling activity that is separable from its mechanosensitive ion channel activity. *Plant Cell.* **26** (7): 3115-31.
- Velten, J., Cakir, C., Youn, E., Chen, J. & Cazzonelli, C.I.** (2012) Transgene silencing and transgene-derived siRNA production in tobacco plants homozygous for an introduced *AtMYB90* construct. *PLoS One.* **7** (2): e30141.
- Venancio, T.M. & Aravind, L.** (2010) CYSTM, a novel cysteine-rich transmembrane module with a role in stress tolerance across eukaryotes. *Bioinformatics.* **26** (2): 149-52.
- Vicuna, D.** (2005) *The role of peroxidases in the development of plants and their responses to abiotic stresses*. Doctoral thesis. Dublin Institute of Technology.
- Viljevac, M., Dugalic, K., Mihaljevic, I., Simic, D., Sudar, R., Jurkovic, Z. & Lepedus, D.** (2013) Chlorophyll content, photosynthetic efficiency and genetic markers in two sour cherry (*Prunus cerasus* L.) genotypes under drought stress. *Acta Bot Croat.* **72** (2): 221-35.

- Villanueva, J., Canals, F., Prat, S., Ludevid, D., Querol, E. & Avilés, F.X.** (1998) Characterization of the wound-induced metalloprotease inhibitor from potato. cDNA sequence, induction of gene expression, subcellular immunolocalization and potential roles of the C-terminal propeptide. *FEBS Lett.* **440** (1-2): 175-82.
- Vincze, T., Posfai, J. & Roberts, R.J.** (2003) NEBcutter: a program to cleave DNA with restriction enzymes. *Nucleic Acids Res.* **31** (12): 3688-91.
- Vingerling, J.R., Dielemans, I., Hofman, A., Grobbee, D.E., Hijmering, M., Kramer, C.F. & de Jong, P.T.** (1995) The prevalence of age-related maculopathy in the Rotterdam Study. *Ophthalmology.* **102** (2): 205-10.
- Vishwanathan, R., Iannaccone, A., Scott, T.M., Kritchevsky, S.B., Jennings, B.J., Carboni, G., Forma, G., Satterfield, S., Harris, T., Johnson, K.C., Schalch, W., Renzi, L.M., Rosano, C. & Johnson, E.J.** (2014) Macular pigment optical density is related to cognitive function in older people. *Age Ageing.* **43** (2): 271-5.
- Vogel, J.T., Tan, B.C., McCarty, D.R. & Klee, H.J.** (2008) The carotenoid cleavage dioxygenase 1 enzyme has broad substrate specificity, cleaving multiple carotenoids at two different bond positions. *J Biol Chem.* **283** (17): 11364-73.
- Volpi e Silva, N. & Patron, N.J.** (2017) CRISPR-based tools for plant genome engineering. *Emerg Top Life.* **1**: 135-49.
- Von Lintig, J. & Vogt, K.** (2004) Vitamin A Formation in Animals: Molecular Identification and Functional Characterization of Carotene Cleaving Enzymes. *J Nutr.* **134** (1): 251S-6S.
- Voorrips, L.E., Goldbohm, R.A., Brants, H.A., van Poppel, G.A., Sturmans, F., Hermus, R.J. & van den Brandt, P.A.** (2000) A prospective cohort study on antioxidant and folate intake and male lung cancer risk. *Cancer Epidemiol Biomarkers Prev.* **9** (4): 357-65.
- Vosman, B., Kashaninia, A., Van't Westende, W., Meijer-Dekens, F., van Eekelen, H., Visser, R.G.F., de Vos, R.C.H. & Voorrips, R.E.** (2019) QTL mapping of insect resistance components of *Solanum galapagense*. *Theor Appl Genet.* **132** (2): 531-41.
- Vosman, B., Van't Westende, W.P.C., Henken, B., van Eekelen, H.D.L.M., de Vos, R.C.H. & Voorrips, R.E.** (2018) Broad spectrum insect resistance and metabolites in close relatives of the cultivated tomato. *Euphytica.* **214** (3): 46.
- Vu, H.T., Robman, L., Hodge, A., McCarty, C.A. & Taylor, H.R.** (2006) Lutein and zeaxanthin and the risk of cataract: the Melbourne visual impairment project. *Invest Ophthalmol Vis Sci.* **47** (9): 3783-6.
- Wandell, B.A.** (1995) *Foundations of Vision*. 1st ed. Massachusetts: Sinauer Associates Inc.
- Wang, H., Fan, W., Li, H., Yang, J., Huang, J. & Zhang, P.** (2013) Functional characterization of Dihydroflavonol-4-reductase in anthocyanin biosynthesis of purple sweet potato underlies the direct evidence of anthocyanins function against abiotic stresses. *PLoS One.* **8** (11): e78484.
- Wang, J., Liu, S., Li, C., Wang, T., Zhang, P. & Chen, K.** (2017a) PnLRR-RLK27, a novel leucine-rich repeats receptor-like protein kinase from the Antarctic moss *Pohlia nutans*, positively regulates salinity and oxidation-stress tolerance. *PLoS One.* **12** (2): e0172869.
- Wang, J.J., Foran, S., Smith, W. & Mitchell, P.** (2003) Risk of age-related macular degeneration in eyes with macular drusen or hyperpigmentation: the Blue Mountains Eye Study cohort. *Arch Ophthalmol.* **121** (5): 658-63.
- Wang, J.J., Mitchell, P., Smith, W. & Cumming, R.G.** (1998) Bilateral involvement by age related maculopathy lesions in a population. *Br J Ophthalmol.* **82** (7): 743-7.
- Wang, L., Li, Q.T., Lei, Q., Feng, C., Zheng, X., Zhou, F., Li, L., Liu, X., Wang, Z. & Kong, J.** (2017b) Ectopically expressing MdPIP1;3, an aquaporin gene, increased fruit size and enhanced drought tolerance of transgenic tomatoes. *BMC Plant Biol.* **17** (1): 246.

- Wang, W., Connor, S.L., Johnson, E.J., Klein, M.L., Hughes, S. & Connor, W.E.** (2007) Effect of dietary lutein and zeaxanthin on plasma carotenoids and their transport in lipoproteins in age-related macular degeneration. *Am J Clin Nutr.* **85** (3): 762-9.
- Wang, X., Cnops, G., Vanderhaeghen, R., De Block, S., Van Montagu, M. & Van Lijsebettens, M.** (2001) AtCSLD3, a cellulose synthase-like gene important for root hair growth in *Arabidopsis*. *Plant Physiol.* **126** (2): 575-86.
- Wang, Y., Hu, X.J., Zou, X.D., Wu, X.H., Ye, Z.Q. & Wu, Y.D.** (2015) WDSPdb: a database for WD40-repeat proteins. *Nucleic Acids Res.* **43** (Database issue): D339-44.
- Wang, Y., Liu, K., Liao, H., Zhuang, C., Ma, H. & Yan, X.** (2008) The plant WNK gene family and regulation of flowering time in *Arabidopsis*. *Plant Biol (Stuttg).* **10** (5): 548-62.
- Wang, Y., Qiao, L., Bai, J., Wang, P., Duan, W., Yuan, S., Yuan, G., Zhang, F., Zhang, L. & Zhao, C.** (2017c) Genome-wide characterization of JASMONATE-ZIM DOMAIN transcription repressors in wheat (*Triticum aestivum* L.). *BMC Genomics.* **18** (1): 152.
- Wang, Y., Yang, L., Chen, X., Ye, T., Zhong, B., Liu, R., Wu, Y. & Chan, Z.** (2016) Major latex protein-like protein 43 (MLP43) functions as a positive regulator during abscisic acid responses and confers drought tolerance in *Arabidopsis thaliana*. *J Exp Bot.* **67** (1): 421-34.
- Wass, M.N., Kelley, L.A. & Sternberg, M.J.** (2010) 3DLigandSite: predicting ligand-binding sites using similar structures. *Nucleic Acids Res.* **38** (Web Server issue): W469-73.
- Weber, E., Engler, C., Gruetzner, R., Werner, S. & Marillonnet, S.** (2011) A modular cloning system for standardized assembly of multigene constructs. *PLoS One.* **6** (2): e16765.
- Weichert, H., Kolbe, A., Kraus, A., Wasternack, C. & Feussner, I.** (2002) Metabolic profiling of oxylipins in germinating cucumber seedlings - lipoxygenase-dependent degradation of triacylglycerols and biosynthesis of volatile aldehydes. *Planta.* **215** (4): 612-9.
- Wellburn, A.R.** (1994) The Spectral Determination of Chlorophylls a and b, as well as Total Carotenoids, Using Various Solvents with Spectrophotometers of Different Resolution. *J Plant Physiol.* **144** (3): 307-13.
- Weller, P. & Breithaupt, D.E.** (2003) Identification and Quantification of Zeaxanthin Esters in Plants Using Liquid Chromatography–Mass Spectrometry. *J Agric Food Chem.* **51** (24): 7044-9.
- Wen, X., Hempel, J., Schweiggert, R.M., Ni, Y. & Carle, R.** (2017) Carotenoids and Carotenoid Esters of Red and Yellow Physalis (*Physalis alkekengi* L. and *P. pubescens* L.) Fruits and Calyces. *J Agric Food Chem.* **65** (30): 6140-51.
- Whittle, S.J. & Casselton, P.J.** (1975) The chloroplast pigments of the algal classes *Eustigmatophyceae* and *Xanthophyceae*. I. *Eustigmatophyceae*. *Br Phycol J.* **10** (2): 179-91.
- Wickham, H.** (2011) The Split-Apply-Combine Strategy for Data Analysis. *J Stat Softw.* **40** (1): 1-29.
- Wickham, H.** (2016) ggplot2: Elegant Graphics for Data Analysis. Springer-Verlag New York.
- Wickham, H. & Bryan, J.** (2018) readxl: Read Excel Files. R package version 1.2.0. Available from: <https://CRAN.R-project.org/package=readxl>.
- Wickham, H., François, R., Henry, L. & Müller, K.** (2018) dplyr: A Grammar of Data Manipulation. R package version 0.7.8. Available from: <https://CRAN.R-project.org/package=dplyr>.
- Widmer, E., Soukup, M., Zell, R., Broger, E., Wagner, H.P. & Imfeld, M.** (1990) Technical Procedures for the Syntheses of Carotenoids and Related Compounds from 6-Oxo-isophorone: Syntheses of (3R,3'R)-Zeaxanthin. Part I. *Helv Chim Acta.* **73** (4): 861-7.
- Wightman, R. & Turner, S.** (2010) Trafficking of the plant cellulose synthase complex. *Plant Physiol.* **153** (2): 427-32.
- Wittig, G. & Pommer, H.** (1959) Ger. Pat. 954,247.

- Wong, W.L., Su, X., Li, X., Cheung, C.M.G., Klein, R., Cheng, C. & Wong, T.Y.** (2014) Global prevalence of age-related macular degeneration and disease burden projection for 2020 and 2040: a systematic review and meta-analysis. *Lancet Glob Health.* **2** (2): 106-16.
- Wu, H.C., Bulgakov, V.P. & Jinn, T.L.** (2018) Pectin Methyltransferases: Cell Wall Remodeling Proteins Are Required for Plant Response to Heat Stress. *Front Plant Sci.* **9**: 1612.
- Wu, J., Cho, E., Willett, W.C., Sastry, S.M. & Schaumberg, D.A.** (2015) Intakes of Lutein, Zeaxanthin, and Other Carotenoids and Age-Related Macular Degeneration During 2 Decades of Prospective Follow-up. *JAMA Ophthalmol.* **133** (12): 1415-24.
- Wu, J., Liu, S., He, Y., Guan, X., Zhu, X., Cheng, L., Wang, J. & Lu, G.** (2012) Genome-wide analysis of SAUR gene family in *Solanaceae* species. *Gene.* **509** (1): 38-50.
- Wurtzel, E.T., Valdez, G. & Matthews, P.D.** (1997) Variation in expression of carotenoid genes in transformed *E. coli* strains. *Biores JI.* **1**: 1-11.
- Xiao, Y., Huang, X., Shen, Y. & Huang, Z.** (2013) A novel wheat α -amylase inhibitor gene, TaHPS, significantly improves the salt and drought tolerance of transgenic *Arabidopsis*. *Physiol Plant.* **148** (2): 273-83.
- Xiong, Y.C., Xing, G.M., Li, F.M., Wang, S.M., Fan, X.W., Li, Z.X. & Wang, Y.F.** (2006) Abscisic acid promotes accumulation of toxin ODAP in relation to free spermine level in grass pea seedlings (*Lathyrus sativus* L.). *Plant Physiol Biochem.* **44** (2-3): 161-9.
- Xu, L., Weathers, P.J., Xiong, X.R. & Liu, C.Z.** (2009) Microalgal bioreactors: Challenges and opportunities. *Eng Life Sci.* **9** (3): 178-89.
- Xu, L., Zeisler, V., Schreiber, L., Gao, J., Hu, K., Wen, J., Yi, B., Shen, J., Ma, C., Tu, J. & Fu, T.** (2017) Overexpression of the Novel *Arabidopsis* Gene At5g02890 Alters Inflorescence Stem Wax Composition and Affects Phytohormone Homeostasis. *Front Plant Sci.* **8**: 68.
- Xu, R.** (2014) Genome-wide analysis and identification of stress-responsive genes of the CCCH zinc finger family in *Solanum lycopersicum*. *Mol Genet Genomics.* **289** (5): 965-79.
- Yabuuchi, E., Kaneko, T., Yano, I., Ido, Y., Moss, C.W. & Miyoshi, N.** (1983) *Sphingobacterium* gen. nov., *Sphingobacterium spiritivorum* comb. nov., *Sphingobacterium multivorum* comb. nov., *Sphingobacterium mizutae* sp. nov., and *Flavobacterium indologenes* sp. nov.: glucose nonfermenting Gram-negative rod in CDC groups 11k-2 and 11b. *Int J Syst Bacteriol.* **33**: 580-98.
- Yabuzaki, J.** (2017) Carotenoids Database: structures, chemical fingerprints and distribution among organisms. *Database (Oxford).* **2017** (1).
- Yamaguchi-Shinozaki, K. & Shinozaki, K.** (1993) Characterization of the expression of a desiccation-responsive rd29 gene of *Arabidopsis thaliana* and analysis of its promoter in transgenic plants. *Mol Gen Genet.* **236** (2-3): 331-40.
- Yates, C.M., Filippis, I., Kelley, L.A. & Sternberg, M.J.** (2014) SuSPect: enhanced prediction of single amino acid variant (SAV) phenotype using network features. *J Mol Biol.* **426** (14): 2692-701.
- Ye, J., Coulouris, G., Zaretskaya, I., Cutcutache, I., Rozen, S. & Madden, T.L.** (2012) Primer-BLAST: a tool to design target-specific primers for polymerase chain reaction. *BMC Bioinformatics.* **13**: 134.
- Ye, X., Al-Babili, S., Klöti, A., Zhang, J., Lucca, P., Beyer, P. & Potrykus, I.** (2000) Engineering the provitamin A (beta-carotene) biosynthetic pathway into (carotenoid-free) rice endosperm. *Science.* **287** (5451): 303-5.
- Yen, H.C., Shelton, B.A., Howard, L.R., Lee, S., Vrebalov, J. & Giovannoni, J.J.** (1997) The tomato high-pigment (hp) locus maps to chromosome 2 and influences plastome copy number and fruit quality. *Theor Appl Genet.* **95** (7): 1069-79.
- Yeum, K.J., Shang, F., Schalch, W., Russell, R.M. & Taylor, A.** (1999) Fat-soluble nutrient concentrations in different layers of human cataractous lens. *Curr Eye Res.* **19** (6): 502-5.
- Yilmaz, E.** (2001) Oxylipin Pathway in the Biosynthesis of Fresh Tomato Volatiles. *Turkish J Biol.* **25**: 351-60.

- Yoda, H., Hiroi, Y. & Sano, H.** (2006) Polyamine oxidase is one of the key elements for oxidative burst to induce programmed cell death in tobacco cultured cells. *Plant Physiol.* **142** (1): 193-206.
- Yu, B., Wang, J., Suter, P.M., Russell, R.M., Grusak, M.A., Wang, Y., Wang, Z., Yin, S. & Tang, G.** (2012) *Spirulina* is an effective dietary source of zeaxanthin to humans. *Br J Nutr.* **108** (4): 611-9.
- Yu, J., Zhou, Y., Tanaka, I. & Yao, M.** (2010) Roll: a new algorithm for the detection of protein pockets and cavities with a rolling probe sphere. *Bioinformatics.* **26** (1): 46-52.
- Yun, J., Kim, Y.S., Jung, J.H., Seo, P.J. & Park, C.M.** (2012) The AT-hook motif-containing protein AHL22 regulates flowering initiation by modifying FLOWERING LOCUS T chromatin in *Arabidopsis*. *J Biol Chem.* **287** (19): 15307-16.
- Zanfini, A., Dreassi, E., la Rosa, C., D'Addario, C. & Corti, P.** (2007) Quantitative Variations of the Main Carotenoids in Italian Tomatoes in Relation to Geographic Location, Harvest Time, Varieties and Ripening Stage. *Ital J Food Sci.* **19**: 181-90.
- Zang, L., Zheng, T., Chu, Y., Ding, C., Zhang, W., Huang, Q. & Su, X.** (2015) Genome-Wide Analysis of the Fasciclin-Like Arabinogalactan Protein Gene Family Reveals Differential Expression Patterns, Localization, and Salt Stress Response in *Populus*. *Front Plant Sci.* **6**: 1140.
- Zervas, D., Pacanaro, A. & Fraser, P.D.** (2007) BioSynLab Version 1.3. Department of Computer Science and School of Biological Sciences, Royal Holloway University of London.
- Zhang, D. & Aravind, L.** (2010) Identification of Novel Families and Classification of the C2 domain Superfamily Elucidate the Origin and Evolution of Membrane Targeting Activities in Eukaryotes. *Gene.* **469** (1-2): 18-30.
- Zhang, J., Zhao, J., Xu, Y., Liang, J., Chang, P., Yan, F., Li, M., Liang, Y. & Zou, Z.** (2015) Genome-Wide Association Mapping for Tomato Volatiles Positively Contributing to Tomato Flavor. *Front Plant Sci.* **6**: 1042.
- Zhang, S., Hunter, D.J., Forman, M.R., Rosner, B.A., Speizer, F.E., Colditz, G.A., Manson, J.E., Hankinson, S.E. & Willett, W.C.** (1999) Dietary carotenoids and vitamins A, C, and E and risk of breast cancer. *J Natl Cancer Inst.* **91** (6): 547-56.
- Zhang, X., Fowler, S.G., Cheng, H., Lou, Y., Rhee, S.Y., Stockinger, E.J. & Thomashow, M.F.** (2004) Freezing-sensitive tomato has a functional CBF cold response pathway, but a CBF regulon that differs from that of freezing-tolerant *Arabidopsis*. *Plant J.* **39** (6): 905-19.
- Zhang, Y., Liu, Z., Sun, J., Xue, C. & Mao, X.** (2018) Biotechnological production of zeaxanthin by microorganisms. *Trends Food Sci Technol.* **71**: 225-34.
- Zhao, J., Favero, D.S., Qiu, J., Roalson, E.H. & Neff, M.M.** (2014) Insights into the evolution and diversification of the AT-hook Motif Nuclear Localized gene family in land plants. *BMC Plant Biol.* **14**: 266.
- Zhong, R., Morrison, W.H., Himmelsbach, D.S., Poole, F.L. & Ye, Z.H.** (2000) Essential role of caffeoyl coenzyme A O-methyltransferase in lignin biosynthesis in woody poplar plants. *Plant Physiol.* **124** (2): 563-78.
- Zhu, H. & Kranz, R.G.** (2012) A nitrogen-regulated glutamine amidotransferase (GAT1_2.1) represses shoot branching in *Arabidopsis*. *Plant Physiol.* **160** (4): 1770-80.
- Zhu, M., Chen, G., Dong, T., Wang, L., Zhang, J., Zhao, Z. & Hu, Z.** (2015) *SIDEAD31*, a Putative DEAD-Box RNA Helicase Gene, Regulates Salt and Drought Tolerance and Stress-Related Genes in Tomato. *PLoS One.* **10** (8): e0133849.
- Zhuo, C., Liang, L., Zhao, Y., Guo, Z. & Lu, S.** (2018) A cold responsive ethylene responsive factor from *Medicago falcata* confers cold tolerance by up-regulation of polyamine turnover, antioxidant protection, and proline accumulation. *Plant Cell Environ.* **41** (9): 2021-32.
- Zimmer, J.P. & Hammond, B.R.** (2007) Possible influences of lutein and zeaxanthin on the developing retina. *Clin Ophthalmol.* **1** (1): 25-35.

Zou, Y., Chintamanani, S., He, P., Fukushige, H., Yu, L., Shao, M., Zhu, L., Hildebrand, D.F., Tang, X. & Zhou, J.M. (2016) A gain-of-function mutation in Msl10 triggers cell death and wound-induced hyperaccumulation of jasmonic acid in *Arabidopsis*. *J Integr Plant Biol.* **58** (6): 600-9.